The University of Nottingham

UNITED KINGDOM · CHINA · MALAYSIA

# Cardiac development in the chick embryo with reference to conduction and structure using a myosin heavy chain knock down model and global RNA sequencing in an outflow tract banded model

**Matthew Parnall**

**Thesis submitted to the University of Nottingham for the degree of Doctor of Philosophy**

**April 2017**

**Abstract**

In the developing embryo the heart is the first organ to develop and thus supply the rest of the developing embryo with a good blood supply. Regulation of cardiogenesis in these early stages of development is key as any dysregulation will result in defects in the heart. Dysregulation of sarcomeric proteins has been associated with a range of cardiomyopathies and septal defects. This demonstrates the importance of structure on development. However, structural genes have not been linked to conduction disorders in the heart. Myosin heavy chain genes (*MYH*) encode sarcomeric structural proteins (MHC). Previous work by Rutland *et al.* (2011) showed that alpha myosin heavy chain (αMHC), beta myosin heavy chain (βMHC) and embryonic myosin heavy chain (eMHC) are necessary for correct $Ca^{2+}$ transients, with eMHC also required for a normal action potential and normal intracellular $K^{+}$. The thesis uses a chick model to analyse the effect of structure on the conduction system.

The first part of the thesis utilises antisense oligonucleotide morpholino technology for gene knockdown (KD) of the mRNA of αMCH, βMHC and eMHC proteins to analyse the effect on structure and conduction in the heart. Cultures of atrial and ventricular KD HH29 cells showed no differences in beating rate, though 2 out of 9 samples of *αMYH* and *eMYH* culture failed to form beating syncytiums, compared to all controls that did. The structural maturity of KD cultures was assessed through Z-disc integrity by immunocytochemistry. Decreased maturity of both the atria and ventricular culture was found KDs. Expression of selected conduction genes was also assed with the pace maker cell potassium channel *HCN4* showing decreased levels at the sinus venosus region by *in situ* hybridisation and significant decreases by RT-qPCR in whole chick heart embryos at HH20. The decrease in expression of such genes could be caused by disruption to internal cell architecture that organises expression of proteins at the cell membrane. Structure at the Z-disc, which show immaturity in KD hearts, is key for this process.

Altered haemodynamics and cardiomyopathy is known to effect internal heart structure and the next phase of the project utilised an out flow tract banding (OFT-banding) technique that has been shown previously to alter haemodynamics, effect heart

structure and show features of cardiomyopathy. Global sequencing was carried out in order to assess the effect that OFT-banding may have on the conduction system in HH29 chick embryos. In order to carry out global gene expression on OFT-banded hearts, a library preparation method was optimised that removed excess haemoglobin from the hearts and an >99% reduction in all embryonic globin genes was seen, this then allowed detailed gene analysis even of low read genes by RNA sequencing. Sequencing revealed differential expression of calcium sequestering genes in what appears to be a conductive cardioprotective mechanism to maintain coordinated contraction. Interestingly, sequencing also revealed a gene profile that would be expected to alter AMPK signalling that could lead to a multitude of disorders or affects such glycogen storage cardiomyopathy or increased inhibition of myosin expression.

**Acknowledgements**

Firstly, I would like to thank the British Heart foundation for providing funding for my project. Without this vital charity so much currently know would remain undiscovered. I would like to thank my principal supervisor, Dr. Siobhan Loughna for her continuous support over my Ph.D. Her belief in me strove me to keep going, not just in the lab, but also in my personal life, and I consider her as much a friend as she is my boss. I would also like to thank my secondary supervisor Dr. Catrin Rutland who would always be there whenever I needed her. Thanks also are extended Dr. Sunir Malla and Dr. Fei Sang – working on the RNA sequencing project alongside Sunir, though at the time stressful, ranks amongst my most satisfying experiences of the last 4 years. I would also like to thank Prof. David Brook and his laboratory (Tushar Ghosh, Ami Ketley, Anna Wilsdon and Kerry Setchfield,), Prof. Sablitzky, Dr. Margaret Pratten, and Dr. Sally Wheatley.

All of my colleagues in the lab; Chrys, James, Amelia, Nicola, Sophie, Omar, and others I'm sure I've missed, have made my time at work enjoyable over the past 2 years. My medical students Josh and Amandeep were a pleasure to teach and won't be forgotten.

Lastly, I would like to thank mother, favther and little (lil') Sarah for their unconditional love. Lil' Sarah is my one inspiration and the reason I'm here. The courage she shows every day living with congenital heart disease puts my 'allnighters' in the lab to shame and I will keep working because of you.

**Declaration**

Outflow tract banding (OFT-banding) was performed by Dr. Pang. The apoptosis study on OFT-banded hearts was also performed in collaboration with Dr. Pang. The RNA sequencing procedure was performed in collaboration with Dr Sunir Malla within the Deep Sequencing Department using the NextSeq500. The initial bioinformatics studies were performed in collaboration Dr Fei Sang from the Deep Sequencing Department, School of Life Sciences, University of Nottingham.

**Table of Contents**

Chapter 1 Introduction ..... 1

1.1 Cardiac development ..... 1

1.1.1 Embryonic heart development in chick and staging comparison with human 1

1.1.2 The primitive heart tube ..... 2

1.1.3 Looping of the primitive heart tube ..... 3

1.1.4 Chamber specification ..... 3

1.1.4.1 Looping and chamber specification: Heart fields, inner and outward curvature and cell lineage ..... 3

1.1.4.2 Atrial septation ..... 6

1.1.4.3 Ventricular septation and trabeculation ..... 8

1.1.5 Valve formation ..... 9

1.1.6 Outflow tract ..... 10

1.1.7 Formation of the conduction system and heart fields ..... 11

1.1.8 Formation of the sinus venosus pace making region ..... 11

1.1.9 Shift of electrical activation and the mature conduction pattern ..... 14

1.1.10 Neural crest cells ..... 16

1.2 The sarcomere and myofibrillogenesis ..... 16

1.2.1 The mature sarcomere ..... 16

1.2.1.1 Cardiac Myosin heavy chain ..... 17

1.2.2 Myofibrillogenesis ..... 20

1.2.3 Maturity scale ..... 22

1.2.4 Disorders of myosin heavy chain ..... 23

1.3 Contraction, conduction, impulse generation and important channels ..... 25

1.3.1 Action potential and the PQRST wave ..... 25

1.4 Morpholino treatment of αMYH, βMYC and eMYH ..... 30

1.4.1 Congenital heart defects of genes involved in generation or transmission of the action potential ..... 31

1.5 Haemodynamics and Outflow tract banding ..... 33

1.5.1 Haemodynamic stress in cardiac development ..... 33

1.5.2 Maladaptive Cardiac Remodeling in response to stress ..... 34

1.5.3 Cardiomyopathy ..... 35

1.5.3.1 Dilated cardiomyopathy ..... 37

1.5.3.2 Hypertrophic cardiomyopathy ..... 37

1.5.3.3 Arrhythmogenic right ventricular cardiomyopathy ..... 38

1.5.3.4 Left ventricular non-compaction cardiomyopathy ..... 38

1.5.3.5 Restrictive cardiomyopathy ..... 39

1.5.3.6 Clinical significance of fetal cardiomyopathy in utero ..... 39

1.5.4 Surgical intervention in embryonic animal model to induce cardiac phenotypes ..... 40

1.5.4.1 The OFT-banding technique and hemodynamic response ..... 42

1.5.4.2 OFT-banded effect on heart the myocardium ..... 42

1.6 The chick as a model ..... 43

1.7 Project Aims ..... 44

1.7.1 Main Hypothesis ..... 45

Chapter 2 Materials and Methods ..... 46

2.1 Egg incubation and harvesting, and ethics and welfare ..... 46

2.2 Knock down project ..... 46

1.1.1 Pluronic gel and in ovo morpholino application ..... 46

2.2.1 Morpholino design ..... 47

2.2.2 Assessment of morpholino up take ..... 48

2.2.2.1 In ovo assessment ..... 48

2.2.2.2 Colonies in cell culture assessment ..... 48

2.3 Western method ..... 49

1.1.2 Western blot for assessment of knock down ..... 49

2.3.1 Bradford assay ..... 49

2.3.2 Preparing SDS PAGE gel ..... 50

2.3.3 Western procedure ..... 50

2.3.4 Analysis ..... 51

2.3.5 GAPDH as a control ..... 52

2.4 Cell culture ..... 52

2.4.1 Optimisations ..... 52

2.4.2 Cell culture Protocol ..... 54

2.4.3 Cell culture knockdown ..... 56

2.4.4 Optimisation: cell culture maintenance media for reduction of cell cycle 56

2.5 Immunofluorescence of cultured cells ..... 57

2.5.1 Key optimisation ..... 57

2.5.2 Protocol ..... 57

2.5.3 Analysis ..... 58

2.6 Riboprobe design and preparation of probe template for in situ hybridisation 58

2.6.1 Primer design for in situ hybridisation riboprobes ..... 58

2.6.2 RNA isolation ..... 59

2.6.3 cDNA generation ..... 59

2.6.4 Generation of probe template by end point PCR ..... 61

2.6.5 Resolve primer products on agarose gel ..... 61

2.6.6 Purification of PCR product ..... 61

2.6.7 ligation ..... 62
2.6.8 Transformation and selection ..... 62
2.6.8.1 Optimisation ..... 62
2.6.8.2 Transformation and selection protocol ..... 63
2.6.8.3 Inoculation and plasmid preparation (midiprep) ..... 63
2.6.9 Linearisation ..... 64
2.6.10 Riboprobe synthesis ..... 65
Optimisation of Purification ..... 66
2.6.10.1 Micro columns ..... 66
2.6.10.2 Gel purification ..... 66
2.6.10.3 Comparison of purification technique ..... 66
2.6.11 RNA gel and estimation of concentration ..... 67
2.6.12 RNA gel optimisation ..... 67
2.6.13 Native gel with RNA denaturing buffer ..... 68
2.7 Whole mount In situ hybridisation ..... 69
..... 69
2.7.1 Embryo collection and preparation ..... 69
2.7.2 In situ hybridisation protocol ..... 70
2.8 Quantitative PCR (RT-qPCR) ..... 72
2.8.1 Harvesting and RNA isolation for RT-qPCR ..... 72

2.8.2 cDNA First strand synthesis for RT-qPCR validation and all other analysis 72

2.8.3 Primer design and optimisation for RT-qPCR ..... 73

2.8.4 Exon/exon spanning/ or intron inclusion ..... 73

2.8.5 RT-qPCR product size ..... 74

2.8.6 Primer details ..... 74

2.8.7 End point PCR ..... 75

2.8.8 RT-qPCR standard curve ..... 75

2.8.9 Interpreting results and cDNA dilution for relative RT-qPCR ..... 77

2.8.10 Relative quantitation ..... 81

2.8.11 Expression equation ..... 81

Figure 2.6 Calculation of fold change ..... 82

2.8.12 Statistics ..... 82

2.9 Outflow tract banding project ..... 85

2.9.1 OFT banding ..... 85

Harvesting and RNA isolation ..... 86

2.9.2 Harvesting ..... 86

2.9.3 Optimisation ..... 86

2.9.4 Isolation protocol ..... 88

2.9.5 Globin depletion ..... 89

2.9.6 Oligonucleotide design ..... 89

2.9.7 Globin Depletion procedure ..... 90

2.9.8 preparation for RNA sequencing ..... 91

2.9.9 mRNA isolation and fragmentation ..... 91

2.9.10 First and second strand synthesis and purification ..... 92

2.9.11 Adaptor ligation ..... 93

2.9.12 PCR enrichment and RT-qPCR quantification ..... 94

2.10 RNA sequencing ..... 97

2.10.1 RNA sequencing Bioinformatics analysis ..... 101

2.10.2 Trimming and mapping against reference genome ..... 102

2.10.3 Mapping Quality (MAPQ) ..... 102

2.10.4 RPKM/FPKM and TPM Expression Values ..... 103

2.10.5 Overall variation between OFT-banded and SHAM, and gene differential expression ..... 104

2.10.6 RT-qPCR validation ..... 105

2.10.7 Apoptosis on OFT banded heart atria ..... 105

2.10.8 Apoptosis data gathering ..... 106

2.10.9 Analysis of data ..... 106

2.11 Immunocytochemistry for myosin structure analysis at HH29 ..... 107

2.11.1 Harvesting and sectioning ..... 107

2.11.2 Fluorescent immunohistochemistry ..... 107

Chapter 3 Myosin heavy chain knockdown - effect on sarcomere embryonic maturity, beating rate and conduction gene expression ..... 108

3.1 Introduction ..... 108

3.2 Aims ..... 109

3.3 Results ..... 109

3.3.1 Morpholino uptake by primary cardiomyocytes ..... 109

3.3.2 Protein reduction validation of knockdowns by western blot ..... 110

3.3.3 Bradford assay ..... 111

3.3.4 Western blot ..... 113

3.3.4.1 Antibody optimisation ..... 113

3.3.4.2 Standard control validation ..... 113

3.3.5 Knockdown hearts to pooled controls and standard control ..... 113

3.3.6 Sarcomere maturity scale and random sampling ..... 120

3.3.7 Knockdown of myosin heavy chain proteins leads to reduced sarcomere maturity in embryonic cardiomyocytes ..... 121

3.3.8 Ventricular and atrial cardiomyocyte KD colonies show insignificant reduction in size ..... 122

3.3.9 Atrial colonies were significantly smaller than ventricle colonies ..... 125

3.3.10 Atrial and ventricular cell beating rate ..... 126

3.3.11 Knockdown effect on ventricular culture beating rate ..... 126

3.3.12 Cardiomyocytes and beating spread across colonies until synchronisation in merged and separated colonies ..... 126

3.3.13 Conduction migration across fibroblasts between colonies ..... 127

3.3.14 Cell culture result relevance ..... 128

3.3.15 Confirmation of unknown gene expression in early chick embryonic development of conduction genes to potentially be analysed in knockdown embryos 129

3.3.15.1 KCNE1 ..... 129

3.3.15.2 CACNA1C and CACNA1D expression profile across early development ..... 130

3.3.16 In situ hybridisation: development of protocol for whole mounts from HH16 to early HH35 ..... 132

3.3.17 Expression profile spatially within the heart of key conduction genes across developmental stages by In situ Hybridisation ..... 134

3.3.17.1 Voltage gated calcium channel CACNA1D ..... 134

3.3.17.2 Voltage gated calcium channel CACNA1C transcripts ..... 135

3.3.17.3 Voltage gated calcium channel CACNA1C developmental expression 137

3.3.17.4 Gap junction connexin 42 (GJA5) ..... 139

3.3.17.5 GJA5 arterial heart expression shows potential developmental tracts 139

3.3.17.6 GJA5 developmental expression ..... 140

3.3.17.7 GJA1 ..... 143

3.3.17.7.1 GJA1 Developmental expression ..... 143

3.3.18 Expression study of conduction genes in knockdown hearts by whole mount in situ hybridisation ..... 145

3.3.18.1 HCN4 ..... 145

3.3.18.2 GJA5 ..... 147

3.3.18.3 TBX3 ..... 149

3.3.18.4 TBX18 ..... 150

3.3.18.5 CACNA1C ..... 152

3.3.19 RT-qPCR of KD hearts ..... 153

3.3.19.1 cDNA check for genomic contamination for KD RT-qPCR ..... 153

3.3.19.2 Reference gene verification ..... 154

3.3.19.3 Differentially regulated gene verification ..... 157

3.3.19.4 RT-qPCR expression of HCN4, GJA5, and TBX3 in KD hearts ... 158

1.2 Discussion ..... 160

3.3.20 Knockdown efficiency and Morpholinos ..... 160

3.3.21 A role for αMHC, βMCH and eMHC in cardiac sarcomere development 161

3.3.22 Conduction across myocyte cultures ..... 163

3.3.23 Expression profiles of conduction genes ..... 164

3.3.23.1 Voltage-dependent, Long type Calcium channel expression HH16-HH35 164

3.3.23.2 GJA5 and GJA1 HH16-HH35 ..... 166

3.3.24 GJA5 tracts ..... 167

3.3.24.1 Future experimentation ..... 167

3.3.25 Regulation of conduction genes in myosin KD groups, effects on conduction and relationship with structure ..... 168

3.3.26 Relevance of results ..... 172

3.3.26.1 Future experimentation ..... 173

Chapter 4 Optimisation and verification of RNA sequencing in OFT-banded model 174

4.1 Introduction ..... 174

4.1.1 Our OFT banded phenotype ..... 175

4.1.2 Group survival rate ..... 176

4.1.3 OFT banded heart external phenotype ..... 176

4.1.4 haemodynamic alteration results in cardiac malformations ..... 180

4.1.5 Proportional stereological analysis reveals thickened epicardium but normal proportions of other heart regions ..... 182

4.1.6 Stereology revealed enlarged OFT-banded hearts with changes in the chamber components..... 184

4.1.6.1 Fibrosis in the OFT banded heart..... 186

4.1.7 Haemoglobin mRNA removal ..... 187

4.2 Specific Aims..... 188

4.3 Results ..... 189

4.3.1 Genomic contamination check following RNA preparation on HH29 and HH35 whole OFT-banded hearts ..... 189

4.3.2 Model verification and optimisation and verification required for RT-qPCR 191

4.3.3 RT-qPCR Primer optimisation ..... 191

4.3.4 Determination of reverse transcriptase consistency ..... 193

4.3.5 RT-qPCR reference gene verification for OFT-banded, SHAM and UT control and validation that SHAM and OFT-banded hearts were not failing at HH29 195

4.3.6 Sequencing results of chosen RT-qPCR internal reference genes..... 197

4.3.7 Verification of control model group and RT-qPCR procedure..... 198

1.2.1.1 Gene regulation in SHAM and UT hearts..... 198

Multiple gene analysis: ..... 198

4.3.8 RT-qPCR reference gene verification for OFT-banded and control HH35 hearts 200

4.3.9 qPRC Inter-plate variation check ..... 202

4.3.10 Globin depletion effect on relative quantity and expression of mRNA 203

..... 204

4.3.11 Effect of globin depletion on RNA Integrity ..... 205

4.4 Globin depletion of hearts for RNA sequencing ..... 207

4.4.1 Sequencing count normalisation technique using FPKM comparison with TPM followed by principle component analysis ..... 211

4.4.2 Differentially regulated genes ..... 214

4.4.3 Comparison of RNA sequencing result with RT-qPCR for validation .. 218

4.5 Discussion ..... 223

4.5.1 Verification of OFT-banded and SHAM model with consistency of reference genes ..... 224

4.5.2 Optimisation of library preparation for mRNA sequencing with globin depletion ..... 227

4.5.3 OFT-banding hearts sequencing - differential regulation and validation 230

Chapter 5 Differential gene expression in OFT-banded hearts ..... 235

5.1 Introduction ..... 235

5.2 Specific Aims: ..... 237

5.3 Results ..... 238

5.3.1 Genomic contamination check on HH29 and HH35 atrial and ventricular samples used to establish pattern of expression..... 238

5.3.2 Conduction gene expression analysis in atria and ventricles at HH29 and HH35 by end-point PCR..... 239

5.3.3 Expression of ERNI and ENS-1 in the atria and ventricle at HH29 and HH35 by RT-qPCR..... 240

5.3.4 Normality and variance analysis of RT-qPCR data at HH35 differentially regulated genes ..... 243

5.3.5 A comparison of the differential expression at HH29 and HH35 in OFT-banded hearts by RT-qPCR. ..... 245

5.3.6 Gene transcript variants identified in OFT-banded hearts ..... 252

5.3.7 Study of TBX18 in the epicardial organ and atria ..... 257

5.3.8 Structure and apoptosis in OFT-banded hearts at a late stage of the banding process..... 259

5.3.8.1 Immunohistochemistry ..... 259

5.3.8.2 Apoptosis in control and OFT-banded HH29 atria ..... 261

..... 262

5.4 Discussion..... 264

5.4.1 PRKAG3 and AMPK signaling..... 266

5.5 Future work ..... 273

5.5.1 EF-hand proteins ..... 276

5.5.2 Apoptosis ..... 279

5.5.3 Histone Deacetylase 7 ..... **Error! Bookmark not defined.**

5.5.3.1 HDACs association with fetal gene program and possible causative gene Limb bud and heart development (LBH) ... **Error! Bookmark not defined.**

5.5.4 Auxilin ..... 280

5.5.5 Endogenous retrovirus (ENS-1) and Early response to neural induction (ERNI) 280

5.5.6 Possible link with epicardium ..... 283

5.5.7 ANKRD1 in OFT-banded hearts ..... 283

5.5.8 Cardio-protection ..... 284

5.5.9 Transcript variant and differentially regulated gene ontology highlight AMPK associated pathways ..... 285

5.5.10 Structural gene expression and effect on conduction ..... 285

5.5.11 Implications of OFT-banded gene profile on potential therapies ..... 286

Chapter 6 General discussion ..... 290

6.1 hypothesis and commonality between chapters ..... 296

6.2 Conclusions ..... 299

Chapter 7 Academic Achievements ..... 321

Chapter 8 Appendices ..... 322

8.1 Appendix A Optimised cell culture protocol ..... 322

8.2 Appendix B. Solutions optimised and made up in house ..... 331

8.3 Appendix C. Optimised In situ hybridisation protocol ..... 341

8.4 Appendix D. Method for the preparation of RNA from cells / tissue ..... 356

8.5 Appendix E. Linearisation and riboprobe synthesis..... 364

8.6 Appendix F Western Blot ..... 370

## Abbreviations

Three myosin heavy chain genes were used extensively in this thesis. The proteins that these genes code for are alpha (αMHC) beta (βMHC) and embryonic (eMHC) myosin heavy. However, inconsistencies exist in chick gene name using the National Center for Biotechnology Information data base. αMHC in the human is called the *MYH6* gene, however, on NCBI the chick gene for the αMHC nucleotide sequence shows up as *MYH7*. βMHC in the human is called the *MYH7* gene however, on NCBI the chick gene for the βMHC nucleotide sequence shows up as *MYH15*.

To avoid confusion and have consistency of terms, this thesis uses *αMYH* and *βMYH* gene abbreviations for αMHC and βMHC proteins respectively.

| | |
|---|---|
| ADP | Adenosine diphosphate |
| αMHC | Beta myosin heavy chain protein |
| *αMYH* | Alpha myosin heavy chain gene |
| ANOVA | Analysis of variance |
| APES | 3-aminopropyltriethoxysilane |
| AP | Action potential |
| ATP | Adenosine triphosphate |
| AV | Atrioventricular |
| AVC | Atrioventricular canal |
| ARVC | Arrthythmogenic right ventricular cardiomyopathy |
| βMHC | Beta myosin heavy chain protein |
| *βMYH* | Beta myosin heavy chain gene |

| | |
|---|---|
| BSA | Bovine serum albumin |
| CHD | Congenital heart defect |
| cDNA | Complementary deoxyribonucleic acid |
| DAB | 3,3 diaminobenzidine |
| DAPI | 4’,6-diamidino-2-phenylindole |
| DCM | Dilated cardiomyopathy |
| DEPC | Diethylpyrocarbonate |
| DSHB | Developmental society hybridoma bank |
| dNTPs | Deoxynucleotide mix |
| EC | Endocardial cushions |
| ECM | Extracellular matrix |
| eMHC | Embryonic myosin heavy chain protein |
| *eMYH* | Embryonic myosin heavy chain gene |
| EMT | Epithelial-mesenchymal-transformation |
| EtBr | Ethidium bromide |
| EPDCs | Epicardium-derived cells |
| EtOH | Ethanol |
| FITC | Fluorescein isothiocyanate |
| FPKM | Fragments Per Kilobase of transcript per Million mapped reads |
| *GAPDH* | Glyceraldehyde-3-phosphate dehydrogenase |
| HH | Hamburger and Hamilton |
| HCM | Hypertrophic cardiomyopathy |

| | |
|---|---|
| IFT | Inflow tract |
| ISH | *In situ* hybridization |
| ifcSEM | Standard error of mean |
| $I_f$ | Funny current |
| IVS | Intraventricular septum |
| KD | Knock down |
| LA | Left atria |
| LAL | Left atrial ligation |
| LB | Luria broth |
| LDHB | Lactate dehydrogenase |
| LV | Left ventricle |
| LVNC | Left ventricular non-compaction cardiomyopathy |
| MAPQ | Mapping quality score |
| MABTw | Maleic acid buffer containing Tween-20 |
| MHC | Myosin heavy chain |
| MMPs | Matrix metalloproteases |
| MV | Mitral valves |
| OFT | Outflow tract |
| PBS | Phosphate buffered saline |
| PBST | Phosphate buffered saline with 0.1% Tween |
| PCA | Principal component analysis |
| PC1 | Principal component 1 |

| | |
|---|---|
| PC2 | Principal component 2 |
| PCR | End point polymerase chain reaction |
| PFA | Paraformaldehyde |
| PHF | Primary heart field |
| PLN | Phospholamban |
| RT-qPCR | Real time quantitative PCR |
| RA | Right atrium |
| RNA | Ribonucleic acid |
| RPKM | Reads Per Kilobase of transcript per Million mapped reads |
| RT | Room temperature |
| RV | Right ventricle |
| SC | Standard control |
| SOC | Super optimal broth |
| S100A11 | S100 Calcium Binding Protein A11 gene |
| TAE | 1X-Tris-acetate-ethylenediaminetetraacetic acid |
| TBX20 | T-Box 20 |
| VSD | Ventricular septal defect |
| VVL | Vitelline vein ligation |

**List of Figures**


**Figure No.** Title **Page**

**Figure 1.1** The heart tube, looping, ballooning and chamber formation **5**

**Figure 1.2** Atrial septation **7**

**Figure 1.3** Ventricular septation **9**

**Figure 1.4** The outflow tract (OFT) **10**

**Figure 1.5** Pace maker development **13**

**Figure 1.6** The mature heart conduction system **15**

**Figure 1.7** The sarcomere **19**

**Figure 1.8** Stages of sarcomere development **21**

**Figure 1.9** The formation of myofibrils maturity scale **22**

**Figure 1.10**. Action potential for working cardiomyocytes in the ventricle **27**

**Figure 1.11** Action potential for pace maker cell **28**

**Figure 1.12** Action potentials in pace maker tissue through the heart and their effect on the PQRST wave **29**

**Figure 1.13** Phosphodiester backbone DNA/RNA and morpholino comparison **31**

**Figure 1.14** Haemodynamic forces on the cardiac muscle wall **34**

**Figure 1.15** OFT-banding position **41**

**Figure 2.1** Atrial and Ventricular separation **55**

**Figure 2.1** Gel purification leads to greater loss of riboprobe when compared to micro columns **66**

**Figure 2.2** *In situ* hybridisation Colour intensity optimisation **68**

**Figure 2.3** RT-qPCR high efficiency optimisation **77**

**Figure 2.4** RT-qPCR low $R^2$ optimisation **78**

**Figure 2.5** The dilution series used for RT-qPCR primer optimisation **79**

**Figure 2.6** Calculation of fold change **80**

**Figure 2.7** Genomic contamination check. **86**

**Figure 2.8** Workflow overview of Ultra Directional RNA Library Preparation for Illumina **94**

**Figure 2.9** A, Full adapter sequence which forms a loop structure at end of fragments **95**

**Figure 2.10** Double stranded cDNA fragments post library preparation ready for sequencing **96**

**Figure 2.11** Overview of sequencing by Illumina nextseq 500 part 1 **98**

**Figure 2.12** Overview of sequencing by Illumina nextseq 500 part 2 **99**

**Figure 2.12** Overview of sequencing analysis **100**

**Figure 3.1** Representative embryos and hearts from qualitative observation groups **109**

**Figure 3.2** Bradford assay experiment optimisation and restult **111**

**Figure 3.3** Western optimisation of βMHC and *GAPDH* antibodies **113**

**Figure 3.4** βMHC KD western blot **114**

**Figure 3.5** No difference in protein signal between controls **116**

**Figure 3.6** Reduction in protien signal in KDs **118**

**Figure 3.7** Representative images taken from cell culture at HH29 of developing sarcomere stages showing with α-actinin antibody **119**

**Figure 3.8** Representative colonies in atrial and ventricular cardiomyocytes at HH29 with α-actinin antibody **122**

**Figure 3.9** Sarcomere maturity is affected upon knockdown of MHC proteins at HH29 **123**

**Figure 3.10** Atrial colonies are significantly smaller to ventricular **124**

**Figure 3.11** Synchronously beating colonies **126**

**Figure 3.12** KCNE1 Expression profile with cDNA templates from HH12 – HH34 **128**

**Figure 3.13** Magnesium optimisation PCR at HH21 **129**

**Figure 3.14** CACNA1C and CACNA1D Expression profile with cDNA templates from HH11 – HH29 **130**

**Figure 3.15** CACNA1D at HH20 **132**

**Figure 3.16** CACNA1C HH20 expression **134**

**Figure 3.17** CACNA1C expression from HH16 to HH35 **136**

**Figure 3.18** Anterior heart external surface expresses tracts of GJA5 **139**

**Figure 3.19** GJA5 expression from HH16 to HH35 **140**

**Figure 3.20** GJA1 expression from HH16 to HH35 **142**

**Figure 3.21** HCN4 shows reduced signal in knockdown embryos at the sinus venosus at HH20 **144**

**Figure 3.22** GJA5 shows reduced signal in a subset of knockdown embryos in the atria and ventricle at HH20 **146**

**Figure 3.23** TBX3 shows weak signal at the atrioventricular junction (Avj) at HH20 **147**

**Figure 3.24** TBX18 shows no noticeable differentiation in KD groups at HH20 **149**

**Figure 3.25** CACNA1C expression signal appears unaltered in KD hearts at HH20 **152**

**Figure 3.26** KD cDNA shows no noticeable genomic contamination **152**

**Figure 3.27** HH20 reference gene stability across KD and control embryos **154**
**Figure 3.28** No differences between SC and UT in genes highlighted by KD **155**
**Figure 3.29** RT-qPCR analysis of key conduction genes on knockdown **157**
**Figure 4.1** OFT-banded hearts are enlarged with a rounded apex **177**
**Table 4.2** Analysis phenotypic summary of OFT banded to control chick embryonic hearts at HH26, HH29 and HH35 **178**
**Figure 4.3** OFT-banding results in a spectrum of cardiac developmental defects **180**
**Figure 4.4** Proportional stereological analysis revealed a thickened epicardium in the OFT-banded hearts **182**
**Figure 4.5** Stereological analysis of tissue types contributing to the left and right atrium and ventricles **184**
**Figure 4.6** Fibrosis not effected by OFT-banding **186**
**Figure 4.7** Genomic contamination check on OFT-banded, SHAM and UT HH29 and (A) and HH35 hearts (B) **190**
**Figure 4.8** RT-qPCR primer optimisation **192**
**Figure 4.9** RT-qPCR amplification plot showing the constant Cq of different cDNA synthesis reactions **194**
**Figure 4.10** HH29 reference gene stability across OFT-banded (OFT), SHAM and untreated (UT) controls **196**
**Figure 4.11** Verification of treatment control groups **199**
**Figure 4.12** Reference gene stability across HH35 OFT-banded (OFT), SHAM and untreated (UT) control hearts **201**
**Figure 4.13** Analysis of inter-plate variation **202**
**Figure 4.14** Relative quantity comparison of RNase treated (+RNase) and non-RNase treated (-RNase) samples **204**
**Figure 4.15** Normalised expression of GJA5 for RNase positive and untreated controls show no difference between groups **204**
**Figure 4.9** Relative expression of each heart for sequencing at HH29 (OFT-banded and SHAM) before and after globin depletion treatment **208**
**Figure 4.17** Relative expression of each globin depleted gene; HBAA, HBAD, HBB, HBG1, HBG2 and HBZ in pooled treated to untreated hearts **209**

**Figure 4.18** Comparison of sequencing analysis normalisation method effect on principle component analysis (PCA). **213**

**Figure 4.19** Sequencing PCA plot showing the variation between OFT-banded and SHAM samples and variation within sample groups **213**

**Figure 4.13** Technical replication **219**

**Figure 4.21** Biological replication **220**

**Figure 4.22** Expression analysis at HH29 to HH35 **221**

**Figure 5.1** Contamination check on HH29 and HH35 hearts atrial and ventricular samples

**Figure 5.2** Expression profile of conduction genes to show what region of the heart conduction genes are expressed at HH29 and HH35 **239**

**Figure 5.3** Expression of ENS-1 and ENRI in the atria compared to the ventricle at HH29 and HH35

**Figure 5.4** Spread of data shows that PVALB is normally distributed and parametric tests can be performed **243**

**Figure 5.5** Metabolic, structural, and differentiation gene expression in OFT-banded hearts compared to SHAM controls **248**

**Figure 5.6** Gene expression of conduction in OFT-banded hearts compared to sham controls **249**

**Figure 5.7** A direct comparison of the expression of genes of interest in HH29 and HH35 OFT-banded and SHA M control hearts **250**

**Figure 5.8** Protein network interactions as examined by STRING analysis tool **254**

**Figure 5.9** No noticeable differences seen between OFT-banded (A) and SHAM (B) for TBX18 in the pro-epicardial organ and atria at HH25 **257**

**Figure 5.10** Myosin structure in OFT and SHAM hearts **259**

**Figure 5.11** Apoptosis in the OFT-banded heart **261**

**Figure 5.12** Differentially expressed genes, showing known interactions which have been analysed in detail in this thesis **264**

**Figure 5.13** Glycogen synthesis pathway within cardiac and skeletal muscle **275**

**Figure 5.14** Mechanism for differentiation of stem cells derived from the neural crest

**Figure 5.15** Gene overview **290**

**Figure 6.1** Overview of thesis findings and how sections work together **299**

**List of tables**

**Table No.** Title **Page**

**Table 1.1** Chick, human and mouse developmental stages in the heart **3**

**Table 2.1** Trypsin concentration **53**

**Table 2.2** Primers pairs and annealing temperatures with amplicon size designed for riboprobes **59**

**Table 2.3** Probe purification and quantification **64**

**Table 2.4** Primers pairs and optimal conditions for RT-qPCR **82**

**Table 2.5** Oligonucleotides for globin depletion **89**

**Table 2.6** FPKM and TMP equation **103**

**Table 3.1** Standard control viability showing no significant differences between UT and SC **116**

**Table 3.2** Pooled controls and standard control only comparison to good and poor βMHC, showing βMHC to *GAPDH* and normalised relative protein expression **118**

**Table 3.3** Key optimisations for preparation for whole mount *in situ* hybridisation **131**

**Table 4.1** Analysis phenotypic summary of OFT banded to control chick embryonic hearts at HH26, HH29 and HH35 **178**

**Table 4.2** Consistency of cDNA synthesis reaction **193**

**Table 4.3** Sequencing results of internal reference genes **197**

**Table 4.4** RIN values of RNase treated and non-treated RNA **206**

**Table 4.5** Globin gene expression and reduction following depletion treatment **210**

**Table 4.6** Effect of TPM on gene expression fold change **212**

**Table 4.7** Sequencing result of significantly differentially down regulated genes **215**

**Table 4.8** Sequencing result of significantly differentially up regulated genes **216**

**Table 4.9** Fragment per kilobase per million (FPKM) of fetal gene program genes, genes later analyses by RT-qPCR and additional genes of biological interest **216**

**Table 4.10** mRNA sequencing and RT-qPCR differential expression at HH29 and RT-qPCR at HH35 **218**

**Table 5.1** Normal distribution of PVALB on HH35 hearts using Shapiro-wilk test **242**

**Table 5.2** RT-qPCR data at HH35 for PVALB OFT-banded against SHAM control hearts **243**

**Table 5.3** T-test result showing significant differences for RT-qPCR PVALB OFT-banded hearts delta Cq in comparison to SHAM controls at HH35 **244**

**Table 5.4** Fold change by RT-qPCR at HH29 and HH35 on genes of interest **246**

**Table 5.5** Statistically significant transcripts identified in OFT-banded hearts **252**

**Table 5.6** STRING analysis identified molecular pathways from significantly regulated gene and transcript variants from OFT-Banded hearts **255**

# Chapter 1 Introduction

## 1.1 Cardiac development

### 1.1.1 Embryonic heart development in chick and staging comparison with human

In the developing embryo the heart is the first organ to form and thus allow a good blood supply to the rest of the developing embryo. The heart develops from a linear tube followed by looping, ballooning and septation to eventually become a 4 chambered heart with a mature conduction system (Manner, 2000, Lindsey et al., 2014). From this point the valves and the coronary vasculature become fully developed to produce a mature heart (Christoffels and Moorman, 2009). In order to investigate heart development, a basic understanding of heart development is required and will now be explained. This thesis uses the chick as a model organism and the developmental staging system for the chick is defined by Hamburger and Hamilton (HH) staging (Hamburger and Hamilton, 1951), this is compared to days of human development in table 1.

**Table 1.1** Chick, human and mouse developmental stages in the heart. Human and mouse staging is based on days and chick is based on is Hamburger- Hamilton staging (HH) (Hamburger and Hamilton, 1951).

| Chick (HH) | Human (days) | Mouse (days) | heart development event |
|---|---|---|---|
| 9 | 21-22 | 9 | Paired heart tube Fusion |
| 10-24 | 22-41 | 9-12.5 | Cardiac looping |
| 14-24 | 28-41 | 9-12.5 | Atrial septation |
| 17-30 | 30-45 | 11.5-14.5 | Trabeculation and ventricular septation<br>Trabeculae appear in the primitive ventricle<br>(HH17-18)<br>Initiation of ventricular septation (HH23)<br>Complete ventricular septation (HH29/30) |
| 34-35 | 50-56 | 15 -16 | Mature conduction pattern<br>from apex to base seen |

### 1.1.2 The primitive heart tube

Mesodermal cells from the anterior of the primitive streak give rise to the primitive heart tube at HH9 (day 21-22 human)(Brand, 2003, Martinsen, 2005b). Primary heart field progenitor cells form a crescent at the midline, while secondary heart field cells are found medial and dorsal to the primary heart field cells (Risebro and Riley, 2006). The heart tube is divided in to two layers, the inner endocardium and outer myocardium. The layers are separated by the extracellular matrix (ECM) known as cardiac jelly (Markwald et al., 1977, Anderson et al., 2006).Cells from this initial heart tube from the primary heart field will develop into the left ventricle, atrioventricular

canal (AVC) and inflow tract (IFT) (Anderson et al., 2006). The addition of secondary heart field (SHF) cells to the poles elongates the heart tube and will eventually lead to looping (Anderson et al., 2006). The SHF leads to the structures of the outflow tract (OFT) and right ventricle (RV) (Anderson et al., 2006).

### 1.1.3 Looping of the primitive heart tube

The heart tube begins rightward looping 22 in the human (HH10) by the addition of secondary heart field (SHF) cells to the poles of the elongating heart tube (figure 1 (A)). These SHF progenitor cells originate in the pharyngeal mesoderm and progressively contribute to the poles. The looping morphogenesis gives rise to the myocardium, smooth muscle and endothelial cells (Kelly, 2012). Looping continues until about day 28 (HH24). Cells of the SHF are important for the conduction system as they will eventually develop in to the bundle branches as well as the right ventricle and outflow tract (Kelly, 2012, Garry and Olson, 2006).

Looping can be divided into the initial C-shape looping (HH10-12) and then S-shape looping (HH13-24) (Manner, 2009). It is during S-shaped looping that further structures such as the primitive OFT, primordia of great arteries (truncus arteriosus), and the primitive atria and sinus venosus are first observed (Manner, 2009).

### 1.1.4 Chamber specification

#### 1.1.4.1 Looping and chamber specification: Heart fields, inner and outward curvature and cell lineage

The initial primitive heart tube made up of its outer myocardium and inner endocardium together with linking ECM developed in to the looped S shape with outer and inner curvatures in order to align correctly for chamber specification (Martinsen, 2005b). The

forming atria and ventricular regions are now separated by the atrioventricular canal (AVC) region and proliferating cells continue to differentiate at the outer curvatures forming the working myocardium (i.e. not pace maker tissue), and thus the ballooning the atrial and ventricular appendages (Christoffels et al., 2000a).

Molecular regulation of the heart fields is thought to be independent of each other and conduction cell lineage has been shown to be brought about by suppression of working myocardiocyte differentiation (Christoffels et al., 2010). Figure 1 (B) shows the heart tube that is going through rightward looping leading to a ventral outer curvature and a dorsal inner curvature. The outer curvature will develop into atrial and ventricular cardiomyocytes (figure 1 blue areas), and the inner curvature will develop into the inflow and outflow tracts. Myocytes of the outer curvature (figure 1 gray areas) enlarge in volume and reinitiate proliferation and differentiation (Christoffels et al., 2010, Anderson et al., 2006). Myocytes of the outer curvature show an increase in conduction velocity that coincides with expression of gap junctions (connexins) such as Cx40 (Cx42 in chick) (Christoffels et al., 2010). Myocardium of the inner curvature remains poorly differentiated. This process is regulated by T-box transcription factors TBX2 and TBX3. These transcriptional repressors are found in the inner curvature. Interestingly, TBX2 and TBX3 are expressed in differentiating conduction cells and repress working cardiomyocyte formation (van den Berg and Moorman, 2009, Hoogaars et al., 2007). The majority of the atrial appendages expand leading to the left atrium (LA) and the remaining atrial appendage, together with the AVC, will lead to the future right atrium (RA). This takes place from HH14 – 18 (around 30 days in human) (Horsthuis et al., 2009).

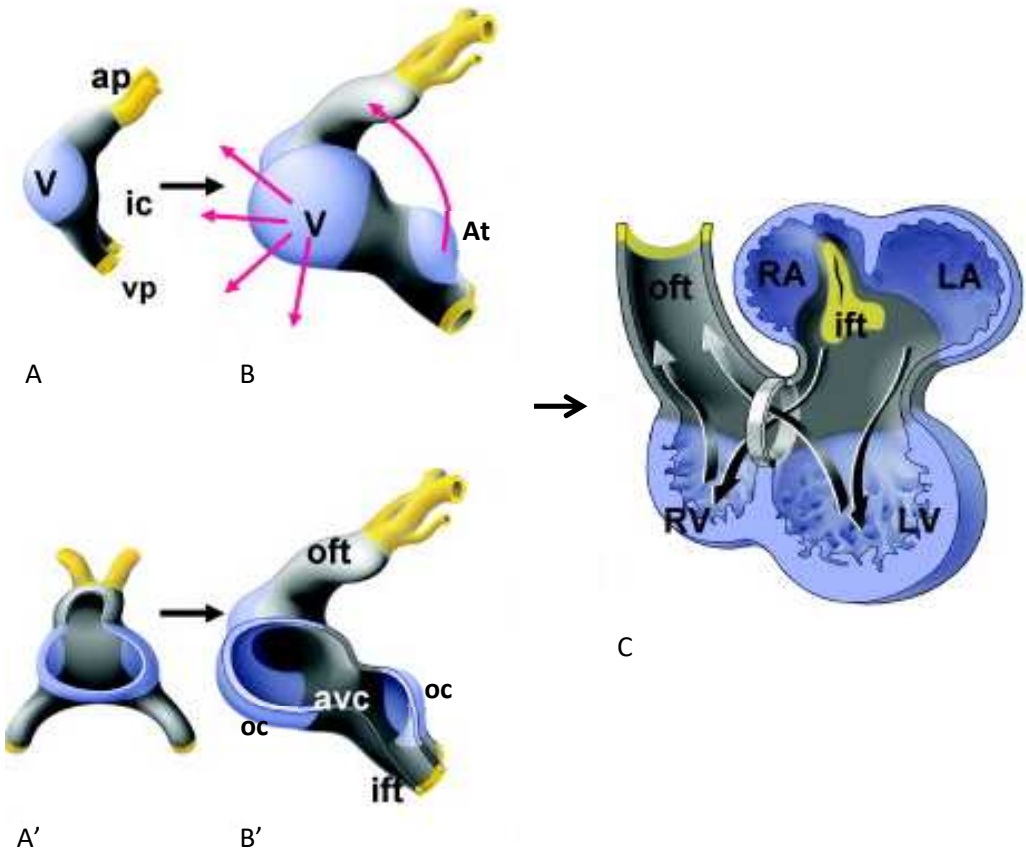



**Figure 1.1** The heart tube, looping, ballooning and chamber formation**.** A, (lateral) and A', (ventral) show the heart tube. Gray areas represent the primary tube, yellow shows arterial and venous extensions and blue shows the ballooning of atrial appendages and the forming ventricle. B, (external) and B' (internal) shows the looping heart. Ballooning of the ventricle is seen at the outer curvature and atrial ballooning appendages at the inner curvature. C, Frontal view of 4 chambered heart. Atrial appendages have balloon to left and right, and apical ventricle components have ballooned inlet and outlet portions. Ap, arterial pole; vp, venous pole; ic, inner curve; oc, outer curvature, V, ventricle; At, atrium; ift, inflow tract; avc, atrioventricular canal; oft, outflow tract. Source: adapted from Anderson (2006).

#### 1.1.4.2 Atrial septation

Septation of the atria is initiated during looping at about day 28 in human (HH13 chick), and continues to around day 42 (HH24), with the initiation of the septum primum from the primordial atrial that extends towards and fuses with the endocardial cushion in the AVC (figure 1.2 A) (Lamers and Moorman, 2002). The septum primum then undergoes apoptosis at specific sites to cause perforations at its cranial part to form the foramen secundum (opening between the atrial chambers) (Figure 1.2 B-D) (Lamers and Moorman, 2002). In the human day 42 (HH24 equivalent), the atria are septated by two septums, a second septum, the septum secumbum and the original septum primum. These structures overlap each other forming a valve opening called the foramen ovale that allows blood to still flow between chambers (figure 1.2 E-H) (Dunwoodie, 2007).

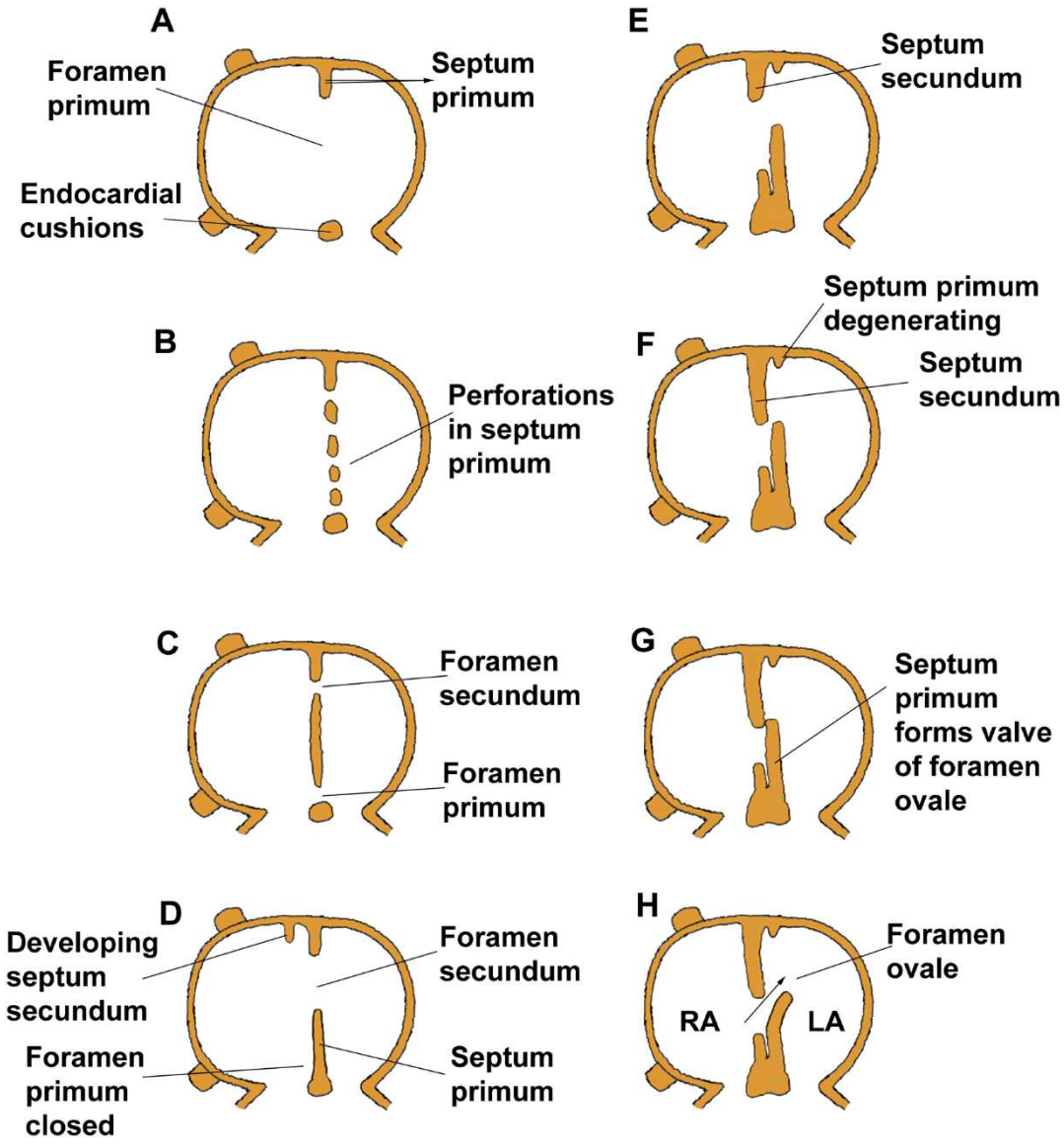



**Figure 1.2** Atrial septation. A, The muscular septum premium descends from the dorso-cranial atrial wall. B -C, The septum continues lengthening until fusing at the endocardial cushions when perforations occur eventually leading to the formation of the septum primum to form foramen secundum. D-E, The septum primum fuses with the endocardial cushions to close the foramen primum, with a new septum 'secundum' developing next to the septum primum. F-H, The septum secundum lengthens to close the foramen secundum and together with the septum primum ascending from the

endocardial cushions forms the foramen ovale, a valve that allows communication between the left and right atria. This valve fuses shortly after birth.

#### 1.1.4.3 Ventricular septation and trabeculation

The initiation of the interventricular septum, and ventricular trabeculation begins at about day 30 (HH17). The cardiac trabeculae are groups of linearly organized myocytes present in the left and right ventricles of adult hearts (Mamatha H, 2013, Samsa et al., 2013). These structures are considered to be responsible for generating contractile force in the embryonic myocardium (Samsa et al., 2013). In response to signalling from the endocardium to the myocardium, trabeculation is initiated from the myocardium. The column like groups of myocytes project out into the lumen by HH19-21 and as gestation proceeds they become compact at around the time of development of coronary circulation and septation completion (Samsa et al., 2013). The compact myocardium formation is key for the formation of the interventricular septum (IVS) where coalesced trabeculae now form the muscular portion of the IVS from the ventricle apex region. The septum extends towards the AVC endocardial cushions where fusion occurs. This replaces the interventricular foramen, however, this component of the septum is membranous rather than muscular and known as the septum membranaceum or membranous septa. By day 56 (HH35) a fully formed IVS is achieved (Figure 1.3 shows an overview of ventricular septation) (Martinsen, 2005a).

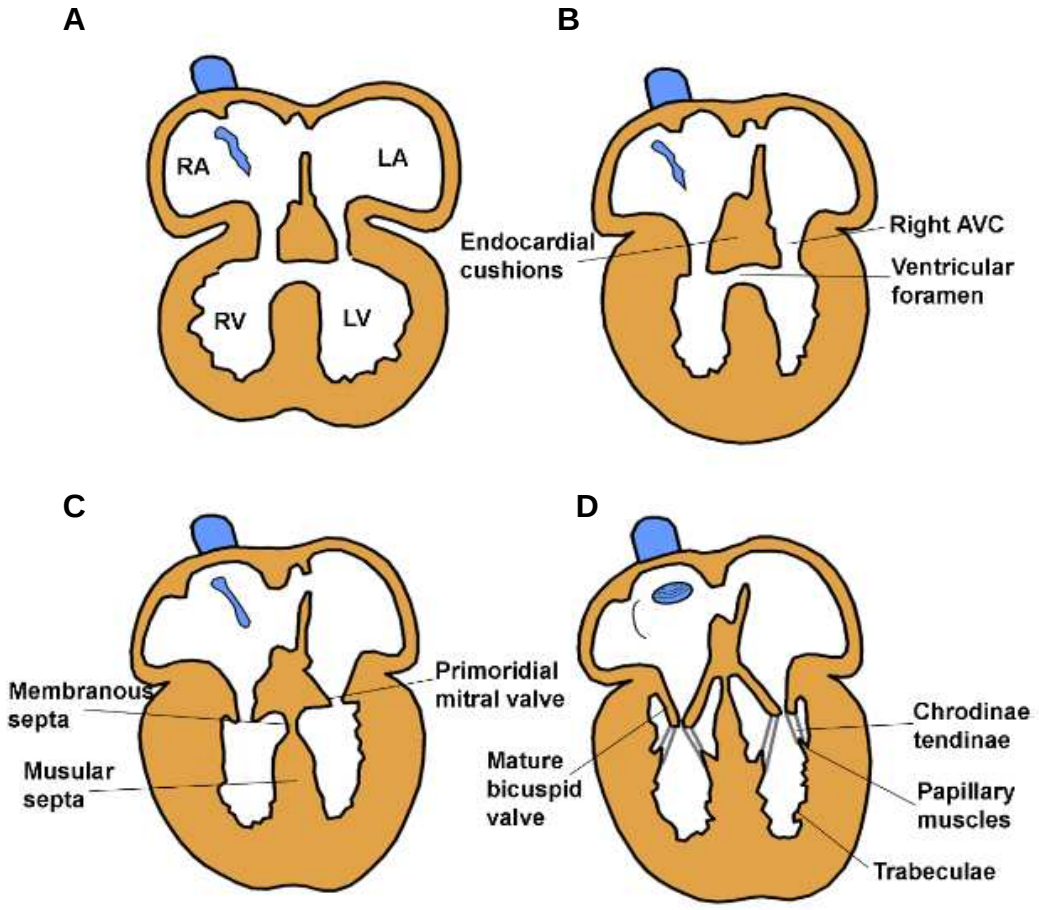



**Figure 1.3** Ventricular septation. A-B, The muscular portion of the IVS extends out towards the AVC. C, A membranous septa forms over the ventricular foramen separating the ventricle into two chambers. D, A fully formed septated ventricle. The compact myocardium that formed the septum is also important for forming the papillary muscles and remaining trabeculae.

### 1.1.5 Valve formation

After initial looping, about day 30 (HH17) there are expansions in the endocardial lining in the area connecting the atrium and common ventricle in a region known as the atrioventricular canal, and in the outflow tract (Person et al., 2005). These expansions

contain extracellular matrix (ECM) secretions known as cardiac jelly and form the cardiac cushions. Endocardial cells undergo epithelial-mesenchymal transition (EMT); these mesenchymal cells then penetrate the cushions remodelling them to eventually form valve structures and the beginnings of the membranous septa of the mature heart (von Gise and Pu, 2012). By around day 50 (HH34) valve formation is nearly complete (von Gise and Pu, 2012, Person et al., 2005).

### 1.1.6 Outflow tract

The aortic sac is connected to the ventricle via a single vessel at its arterial pole known as the outflow tract (OFT). It has a ‘dog leg’ bend structure as it leaves the heart that separates proximal from distal parts (figure 2) (Webb et al., 2003, Moorman et al., 2003). Progenitor cells from the second heart field lead to the elongation of the OFT leading to its completion by HH21 (day 32 human) (Webb et al., 2003) before the distal OFT is septated by the aorticopulmonary septum (Lin et al., 2012). The proximal OFT is septated in to right and left ventricle portions by the conal septum (Lamers et al., 1995, Van Den Hoff et al., 1999). This is formed by myocyte infux to right posterior and left anterior conal cushions within the OFT (Lamers et al., 1995, Van Den Hoff et al., 1999).

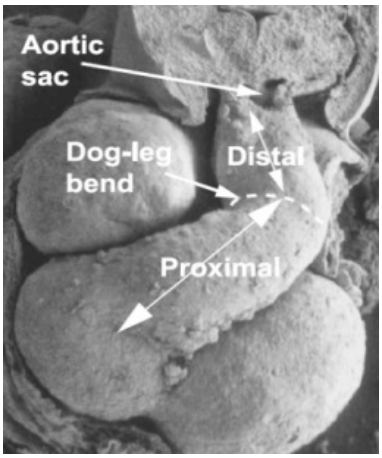



**Figure 1.4** The outflow tract (OFT). Ventral view of human embryo by Scanning electron microscope. Picture shows human embryo heart at day 36. The distinct ‘dog leg’ bend is seen to divide distal and proximal portions (Webb et al., 2003).

### 1.1.7 Formation of the conduction system and heart fields

In order to efficiently pump blood from the heart a coordinated conduction system is required as the heart is developing. In the chick, a primitive peristaltic contraction is initiated at HH10 with the heart tube, and this excitation evolves with heart development to an apex to base contraction by HH35 (see figure 1.5 for overview of this process) (Martinsen, 2005a).

### 1.1.8 Formation of the sinus venosus pace making region

The sinus venosus is a cavity at the venous pole which is supplied by the vitelline, umbilical and common cardinal veins and it opens into the primitive atrium (Martinsen, 2005a). The sinus venosus region of the heart is key in the development of the heart conduction system as it contributes to the sinoatrial node (SAN). Cells of the sinus venosus have been found to have a genetic lineage unique from the first and second heart field progenitor cells. Cells of the first and second heart field contribute to the primitive heart tube with cells of the second heart field contributing to the poles of the formed heart tube (Mommersteeg et al., 2010). However, both first and second heart field cells are positive for the transcription factor NKX2.5 and have the same lineage to the splanchnic mesoderm (Mommersteeg et al., 2010). The formation of the primitive heart tube at around HH10 coincides with the initiation of beating (Moreno-Rodriguez et al., 2006). It is shortly after this point, when the heart starts to loop that cells of the sinus venosus are progressively added at the venous pole (Moreno-Rodriguez et al., 2006) . Cells of the sinus venosus have been found to be NKX2.5 negative and TBX18 positive and traced to a lateral rim of the splanchnic mesoderm that become positioned ventral to the venous pole, often referred to as the ‘posterior heart field’ (Mommersteeg et al., 2010) and (Vicente-Steijn et al., 2010, Gittenberger-de Groot et al., 2007). These cells are positive for podoplanin, a coelomic and myocardial marker that has been shown to be needed for EMT, as podoplanin deficient mice have shown down regulation of Ras homolog gene family, member A (RhoA) (Mahtab et al., 2009). Interestingly, hypoplasia of the sinus venosus, and other sinus venosus derived myocardium, has been found when the EMT marker Ras is down

regulated (Mahtab et al., 2009). RhoA has been found necessary for EMT in the chick embryo (Tavares et al., 2006, Vicente-Steijn et al., 2010). This shows that migration of sinus venosus cells is important in the formation of the SAN, possibly involved in the initial sinus venosus-wide capacity to generate pacemaker signals then becoming confined to the definitive SAN (Vicente-Steijn et al., 2010). Proepicardial cells have also been found to be contributors to the early sinus venous region in the embryonic mouse heart (Katz et al., 2012).

The sinus venosus area has been shown to be HCN4 positive and to generate electrical potential that initiates beating. The area evolves with development eventually giving a right-sided activation pattern (Vicente-Steijn et al., 2010). Atria myocardia cells are repressed from becoming working cardiomyocytes by transcriptional repressor TBX3 at the developing nodal regions. Working cardiomyocytes are Cx42 positive and contract and propagate contraction in response to the HNC4 and TBX18 positive pace maker cells (Bakker et al., 2012).

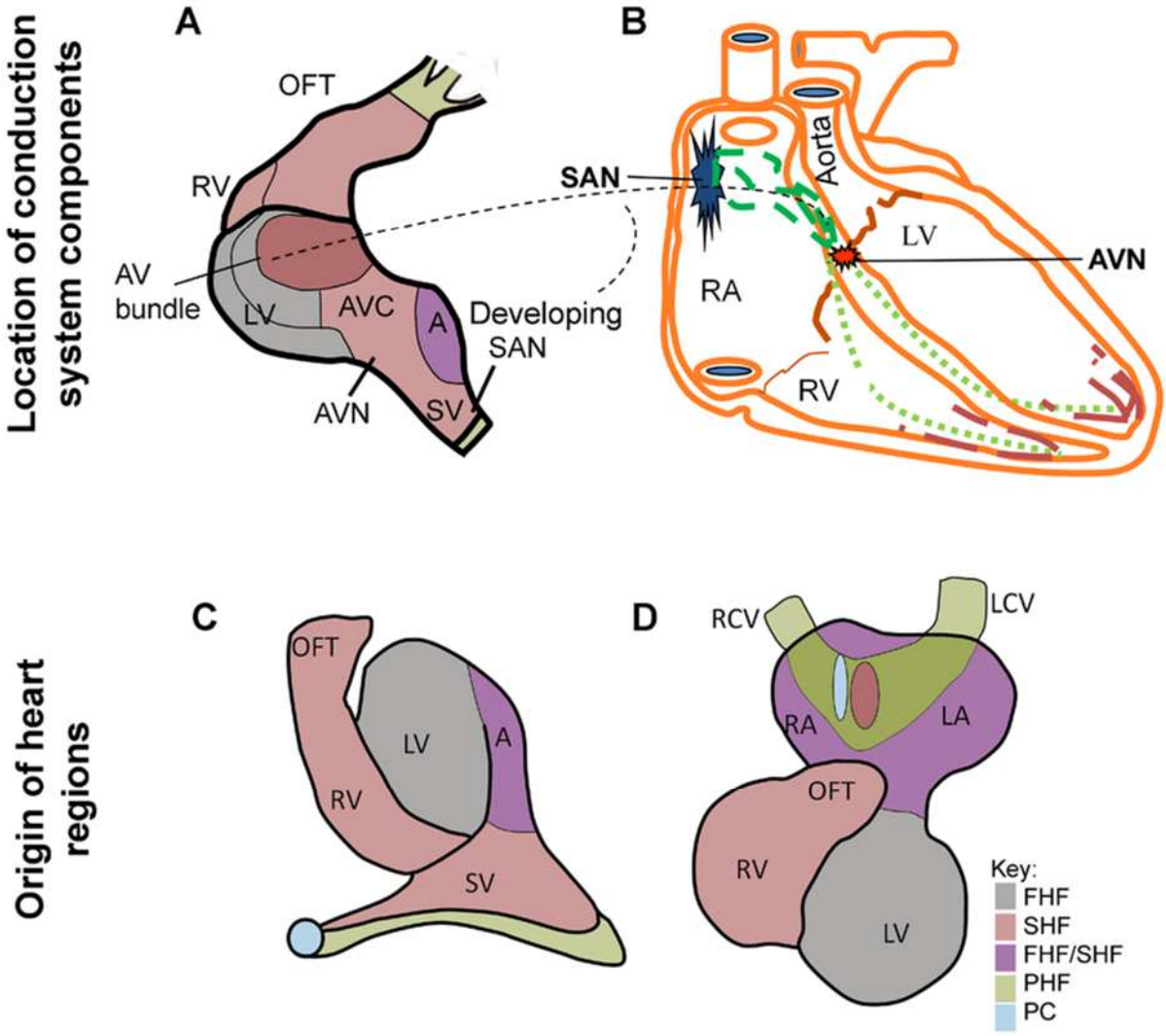



**Figure 1.5 Pace maker development** A, The looping heart shows the developing sinoatrial node (SAN) located in the inflow tract (IFT) and contributed to by the TBX18 positive posterior heart field (PHF). Cells of the AV bundle are located superiorly to the atrioventricular canal (AVC). B, shows a fully matured heart conduction system where dotted lines show where nodal areas in 'A' reside in the mature heart 'B'. C, Shows the chick embryo after continued looping from around HH10 (E8.5 in mouse) showing clearly the location of cell populations. The pace maker cells (PC – blue) are again seen in the IFT.D, The heart is shown at mid-gestation around HH30 (mouse E11.5) with the anterior atria cut away to show cell populations. The venous inflow to

the atria (green) via the cardinal veins (light green) can be seen. The sinoatrial node (blue) develops at the junction between the right cardinal vein myocardium (RCV; yellow, a PHF derived structure) and the right atrium (RA; a mixed FHF/SHF-derived structure). All dark pink areas represent lumen openings in the cut diagrams; FHF first/primary heart field; SHF, second heart field; PHF, posterior heart field; LA, left atrium; LCV, left cardinal vein; LV, left ventricle; OFT, outflow tract; RV, right ventricle; RA, right atrium.

### 1.1.9 Shift of electrical activation and the mature conduction pattern

The immature sino-atrial node has differentiated by HH10 (21 day human), and, located in the sinus venosus, it induces excitation in a wave across the heart from its initiation point (Gourdie et al., 2003, Boullin and Morgan, 2005). As development continues, more specialised conduction structures differentiate. This occurs when transcriptional repressors such as TBX3 repress working contractual cardiomyocyte differentiation and lead to pace maker cell differentiation (Boullin and Morgan, 2005). Pace making nodal cells accumulate to form the atrioventricular node (AVN) at a fibrous ring at the atrioventricular junction (Carlson, 2008). Expression of the fibrous ring starts at HH15, and its branches form along the developing interventricular septum and eventually forming the purkinje fibers at around HH35/36. The AVN and bundle branches are thought to originate from the same source with the AVN being formed at HH28/29. Lastly bundle branches become formed and functional at around HH35 (Arguello et al., 1988). Once the structures of the conduction system have developed, a mature conduction pattern from apex to base proceeds.

As described in section 1.1.4.3, trabeculae generate contractile force. They express Cx42 in contrast to the negative nodal pace maker regions. This is because the trabeculae are responsible for propagating depolarisation across the ventricular working cardiomyocytes and the connexin channel is involved in allowing this propagation. Before compaction of the ventricular myocardium, the thin non-compacted ventricular wall and forming trabeculae both expresses Cx42, however, as

the ventricular wall (and septum) thicken, expression becomes more specific the trabeculae and bundle branches and from HH35/36 to the purkinje fibres (Zhang et al., 2011a). The purkinje fibres are first recruited once chamber formation and an apex to base conduction pattern have been established and are derived from the trabeculae to allow efficient spreading of depolarisation across the ventricular working cardiomyocytes in the maturing and adult heart (Harris et al., 2006)

The SAN produces an action potential (AP) that is transmitted across the atrium leading to contraction; this is picked up by the AVN which delays the signal and allows blood from the atrial contraction to drain to the ventricles, and then transmits the AP down to the bundle of His (Boyett, 2009). This takes the AP to the left and right bundle branches and down to the heart apex where the purkinje fibres are activated by the AP, thus leading to coordinated contraction of the ventricles and blood is pumped out of the heart (Boyett, 2009) (Figure 1.6).

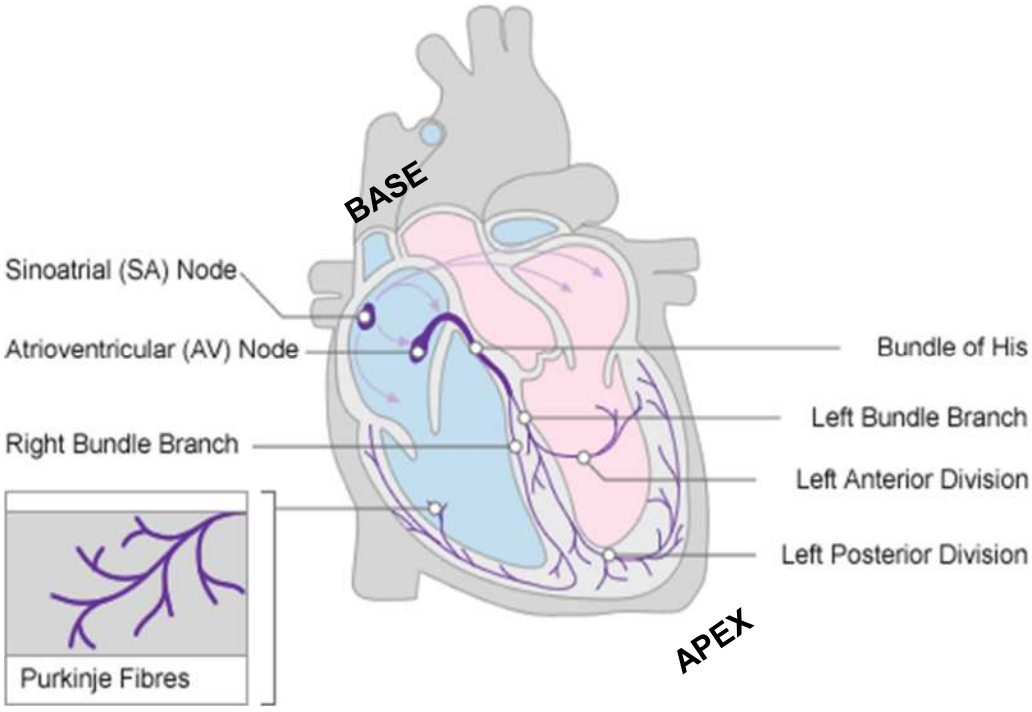



**Figure 1.6** The mature heart conduction system. The structures of the conduction system shown allow the action potential initiated at the sinoatrial node induce

contraction of the atria followed by contraction of the ventricle from apex to base. Source: Adapted from the University of Nottingham Learning Resources (2017).

### 1.1.10 Neural crest cells

Neural crest cells are found in the dorsal neural crest in the developing embryo and they are multipotent. Migration of these leads to the contribution to the parasympathetic nervous system (LE DOUARIN, 1982). Their contribution to the heart conduction system has been postulated following genetic lineage analysis in the mouse, where their contribution to cells of the His-Purkinje system was implicated. Little research has been continued in this field, however one study found ablation of the neural crest led to retarded apex to base conduction (Gurjarpadhye et al., 2007). This may suggest their involvement in the maturation of the His-Purkinje system.

## 1.2 The sarcomere and myofibrillogenesis

### 1.2.1 The mature sarcomere

Myocytes (muscle cells) contain chains of myofibrils (Figure 1.7 A). Cardiac myocytes are connected to each other via intercalated discs. The discs allow direct communication between cells via gap junction proteins such as Cx42 and Cx43 and allow the entire heart muscle to operate as a syncytium (Zhang and Shaw, 2014, Franke et al., 2006, Gutstein et al., 2003). Within the myofibrils, repeating sections called sarcomeres that align longitudinally (Figure 1.7 B.) (England and Loughna, 2013).The sarcomeres, which span between two Z-discs, are made up of contractile, accessory and scaffolding proteins and are responsible for the contractile ability of the cell. The sarcomere consists of thin actin (Figure 1.7 C) based filaments that attach at the Z line in the I band zone, and contractile thick filament myosin (Figure 1.7 D)

based filaments that overlap actin filaments across the A band and attach at the M line (Derrickson, 2006). The thin actin filament is bound to two accessory proteins tropomyosin and troponin that regulate contraction (contraction is described in section 1.3). Tropomyosin spans the actin filament and is bound to troponin. Troponin in turn has three polypeptides that work to regulate contraction: Troponin C ($Ca^{2+}$-binding), troponin I (bound to actin and inhibits contraction), and troponin T (tropomyosin-binding) (Figure 1.7 B) (England and Loughna, 2013). The contractile thick filament myosin proteins have two globular heavy chain heads, a heavy chain alpha helix body, with regulatory and essential light chains on the necks adjacent to the globular head region. The alpha helix body anchors to titin, whereas the globular heads allow binding to actin on contraction (Figure 7 D.) (Furst et al., 1988). The thick filament's (Figure 7. D) motor protein is myosin heavy chain (MHC) and it is this structural protein that forms the backbone of all muscle think filaments.

#### 1.2.1.1 Cardiac Myosin heavy chain

The thick filament's (Figure 7. D) motor protein is myosin heavy chain (MHC) and it is this structural protein that forms the backbone of all muscle think filaments. The MHCs contain a globular head that allows binding to thin actin filaments leading to contraction (Wells et al., 1996, Derrickson, 2006). Different isoforms of MHC exist in differing muscle types in order to carry out specific roles. The isoforms can have differing rates of actin-activation ATPase – this is perfectly demonstrated in the two main cardiac specific MHCs; αMHC and βMHC. In αMHC, $Ca^{2+}$ ATPase activity is three times that of βMHC (Wells et al., 1996). These two isoforms have been shown to be co-expressed in heart tube myocardium in chicken, mouse, rat, and human and become increasingly chamber specific with development, with αMHC in the atrium and βMHC in the ventricle and have been shown to be differentially regulated in response to haemodynamic overload (Somi et al., 2006, Lyons et al., 1990b, Wessels et al., 1991). However, in rodents αMCH becomes the dominant isoform throughout both chambers following birth ((Lyons et al., 1990b). Another structural myosin found in the developing heart is embryonic myosin heavy chain (eMHC coded by the e*MYH* gene), though less is known about this isoform. In chick heart e*MYH*, expression has been

shown across stages HH12-26 with eMHC protein expression found throughout the myocardium by immunocytochemistry (Rutland et al., 2011). The homologue of chick e*MYH*, *MYH*3, has been shown in the atria and ventricular myocardial walls at week 7 in human and E11.5 in mouse by *in situ* hybridisation (Rutland et al., 2011).

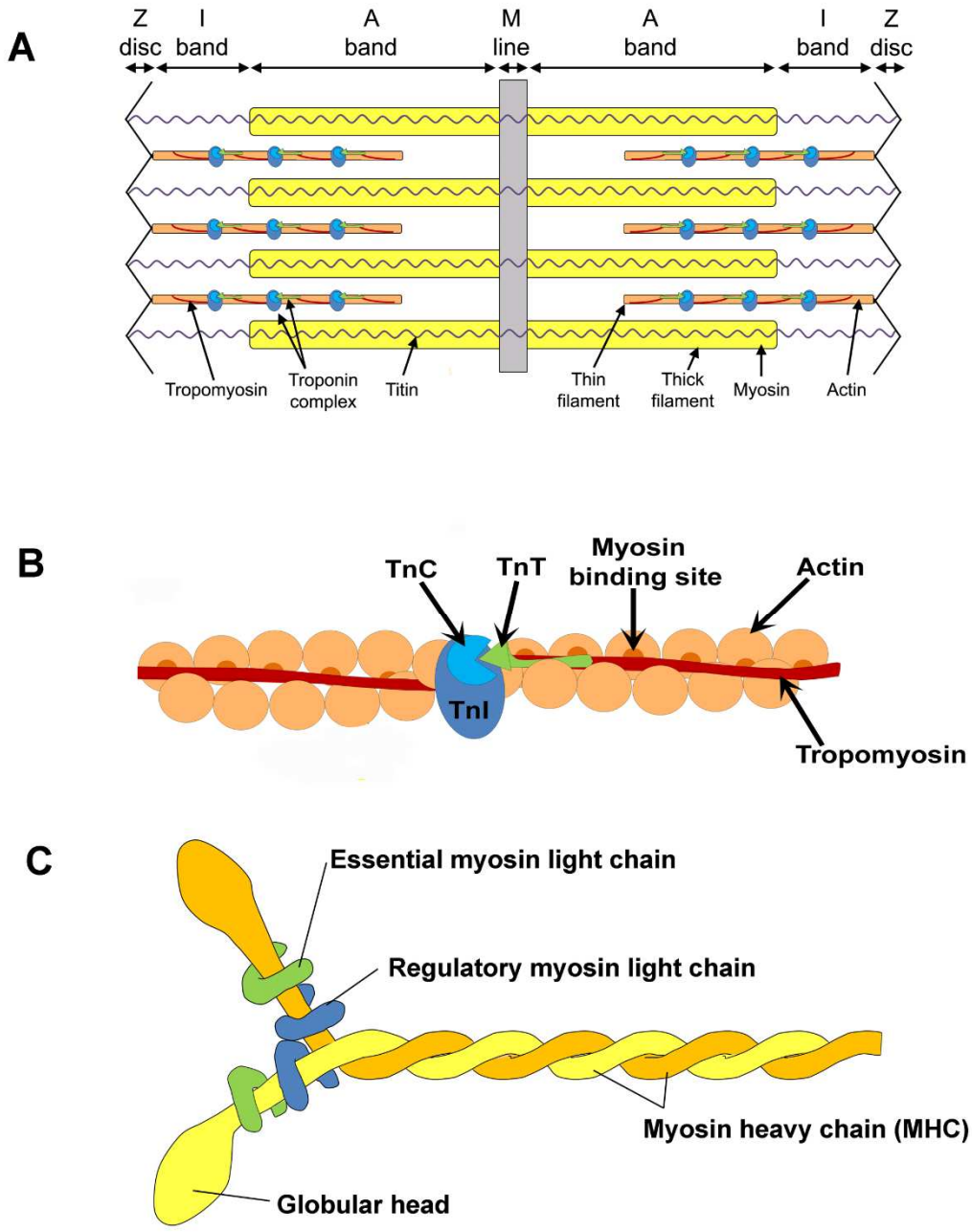



**Figure 1.7** The sarcomere. A, Fully formed sarcomere showing how thick and thin filaments align opposed to each other B, Enlarged thin actin filament showing the positions of tropomyosin and troponin C (TnC) troponin I (TnI) and troponin T (TnT) along the actin filament C, Enlarged think filament showing myosin heavy (MHC) and light chains; arrow indicates globular heads that bind to actin. Source: Adapted from Tortora & Derrickson 2001; England and Loughna 2013.

### 1.2.2 Myofibrillogenesis

Mature sarcomeres form in an organised step by step manner. Sarcomeric genes are first detected at HH5 (Colas et al., 2000). Analysis of the forming whole heart in the chick has backed up previous findings in avian cell culture that suggested myofibrils form over 3 steps in the 'premyofibril model' (Rhee et al., 1994, Du et al., 2008). The first step is the formation of premyofibrils (Figure 1.8 A). These primitive structures contain tightly packed α-actinin that surround non-muscle isoforms of myosin IIB and are found at the myocyte border. α-actinin is first detected around HH6 (Colas et al., 2000). Step 2 is the formation of nascent myofibrils where non-muscle myosin IIB starts to be replaced by myosin II that contains heavy (MHC) and light chain (MLC) myosin (Figure 1.8 B). The first MHC structures are detected around HH7, (Han et al., 1992). The maturation process continues into step 3 'mature myofibrils' where Z-bodies fuse into Z-bands and myosin II filaments into A-bands in a mature I-Z-I complex (Figure 1.8 C). Sarcomeric striations first become visible at HH9 shortly before beating is observed (Han et al., 1992). So, without myosin, structured I-Z-I complexes would not be expected to form correctly.

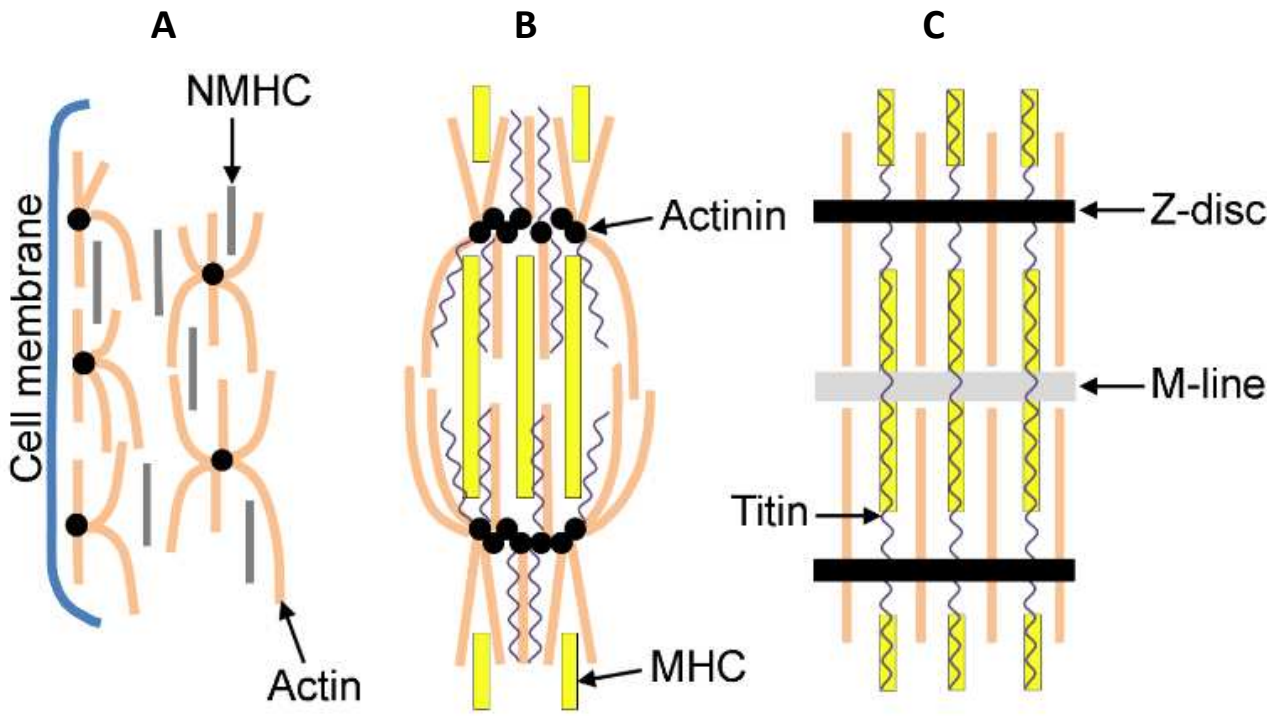



**Figure 1.8** Stages of sarcomere development. A, Premyofibrils. The sarcomeric protein α-actinin assembles at the periphery of the cell. It associates with actin monomers and assemble into Z-bodies. Between the forming Z-bodies nonmuscle myosin (NMHC) is scattered between them. B, Nascent myofibrils. The NMHC is replaced by muscle-type myosin II isoforms (MHC) and stabilizing proteins such as titin become incorporated into the myofibrils. C, Mature myofibrils. Z-bodies fuse into Z-bands and myosin II filaments into A-bands in a mature I-Z-I complex (England and Loughna, 2013).

### 1.2.3 Maturity scale

A maturity scale is used in the thesis based on the 3 levels of maturity, with the addition of a final level showing fully coordinated sarcomeres in alignment with each other over an enter colony in cell culture (Figure 8). This grading system is obtained using an α-actinin antibody to enable assessment across all stages of development. This is explained further in the methods where representative images of each stage can be seen.

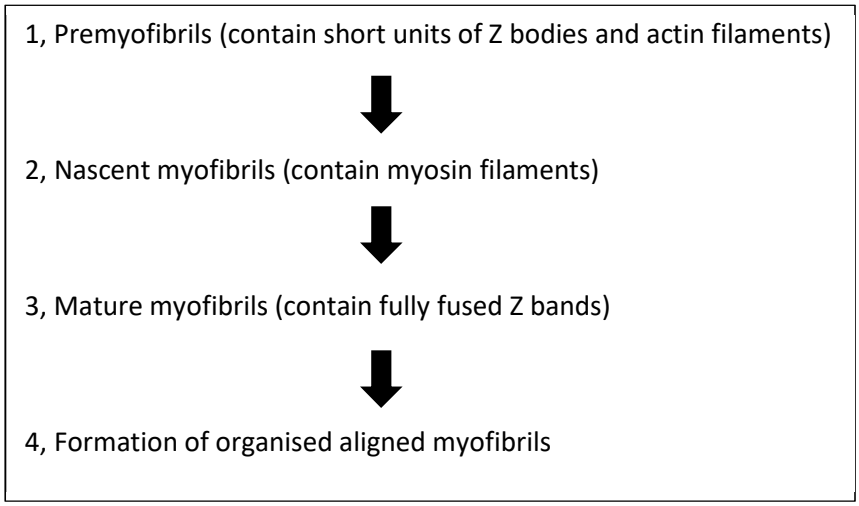



**Figure 1.9** The formation of myofibrils maturity scale. It can be seen that failure of one component will lead to deformations in the following step.

### 1.2.4 Disorders of myosin heavy chain

α*MYH*, β*MYH* and e*MYH* have been linked with a number of structural phenotypes. Knock down (KD) of α*MYH* previously in our lab in the chick embryo has led to disrupted atrial septum formation at HH19 (Rutland et al., 2009). The septum was either not formed at all, had restricted growth or had multiple septum's. A number of knock down hearts also featured ventricular trabeculae disruption (Rutland et al., 2009). In the human, a mutation to the αMHC gene *MYH*6 has been found in a large family with dominantly inherited atrial septal defects using microsatellite markers to identify genes followed by targeted sequencing (Ching et al., 2005). Mutation to *MYH*6 has also been seen in patients hypertrophic (HCM) and dilated cardiomyopathy (DCM). Work using mouse myoblast culture has revealed that cells transfected with *MYH*6 mutants led to significantly altered myofibril formation, be that disrupted or enhance depending on the mutation (Granados-Riveron et al., 2010). Mouse null *MYH*6 mutants displayed embryonic lethality and heterozygote mice had defects in cardiac contraction and relaxation (Jones et al., 1996).

Previous knock down work in our lab of chick β*MYH* has led to enlarged heart at HH19, but the atrial septa and other structures within the heart were found to be normal (Dr. Catrin Rutland and Siobhan Loughna, unpublished data). *MYH*7 (the human homologue of β*MYH*) has long been associated with both dilated and hypertrophic cardiomyopathy (Walsh et al., 2010, Tanjore et al., 2010), but more recently has also been found mutated in families with left ventricular non-compaction (LVNC) where some individuals were also found to have atria septal defect and/or Ebstein's anomaly of the tricuspid valve (Budde et al., 2007). Further mutations in *MYH*7 have been associated with Ebstein anomaly, where mutational analysis by targeted sequencing highlighted *MYH*7 in 6% of patients. Patients with mutated *MYH*7 also had LVNC, whereas patients without the *MYH*7 mutation had no such phenotype (Postma et al., 2011). To this authors knowledge gene deletion work in mouse has not been carried out for the β*MYH* gene.

Knock down of e*MYH* in the chick previously in our lab led to abnormal development of the atrial septa and trabeculae. Mutation to human *MYH*3 (the human homologue of e*MYH*) has been associated with Freeman-Sheldon and Sheldon-Hall syndromes and both of these conditions are associated with skeletal defects (Toydemir et al., 2006). To this authors knowledge gene delegation work in mouse has not been carried out for the e*MYH* gene.

Embryonic *MYH*, α*MYH* and βMHY isolated knockdown cells from the atrium all showed disrupted intracellular $Ca^{2+}$ levels in work done previously in our lab (Rutland et al., 2009), and e*MYH* KD showed increased duration of action potentials in both atrial and ventricular single cardiomyocytes and demonstrated increased resting membrane potential (RMP) from atrial and ventricular cells with decreased rapidly inactivating $K^+$ current normalised to the mean of the $I^{+K}$ control from atrial and ventricular cells (Rutland et al., 2009).

As mentioned earlier both α*MYH* and β*MYH* have been linked to cardiomyopathy. A transgenic mouse model expressing mainly β*MYH* over α*MYH* showed reduced contractile function and responded poorly when subjected to stress following coronary ligation showing a 20% enlargement compared to controls (Rutland et al., 2009). Another mouse model showed that in failing hearts a shift from αMHC to βMHC occurs (Harada et al., 1999). This suggests conservation of normal αMHC and βMHC levels is important for maintaining function. Cardiac myosin heavy chain gene expression has been shown to be important in both the cardiac conduction system and heart function in response to stress, and in the failing heart. It is for this reason that this thesis is split into two parts, that is, to see the effect of *MYH* knockdown on the conduction system, and to see the effect on gene expression, both structural and conduction, of induced haemodynamic stress on the developing heart.

## 1.3 Contraction, conduction, impulse generation and important channels

### 1.3.1 Action potential and the PQRST wave

The Action potential (AP)

An action potential is simply a wave of depolarisation caused by changes in membrane potential (Klabunde, 2011). With regard to the conduction system AP, within the heart there are 2 basic types of cardiomyocytes; pace making cells and contractile working cardiomyocytes. Both cell types can have distinct lineages and have different roles. Pace maker cells deliver spontaneous APs to the contractile cells in order for them to contract and pump blood out of the heart (Carmeliet, 2002).

Ventricular contractile working cardiomyocytes

For contraction of sarcomeres to occur in working cardiomyocytes, calcium ions ($Ca^{2+}$) must bind with troponin complex TnC on the thin actin filaments. The binding of $Ca^{2+}$ reveals actin biding sites to myosin by the movement of tropomyosin (Figure 1.3 B shows tropomyosin/troponin structure, this contraction phase is represented in deportation Figure 1.6 over phase 'B-C'). This binding action initiates movement as the thin actin filament moves fully in to the A band, thus bringing the Z lines closer together in contraction. Adenosine triphosphate (ATP) breakdown to ADP provides energy for release of the complex and allows the cycle to start over again. If $Ca^{2+}$ concentration is low then there will be a reduction in binding to troponin C (TnC). Less $Ca^{2+}$ TnC binding will result in weaker bonding of the troponin complex and tropomyosin will not be able to alter the actin configuration to allow myosin binding. Thus, contraction cannot take place or will be weak (Lehman et al., 1994). The $Ca^{2+}$

binds to TnC, leading to an increase in TnC and TnI interactions, whereas interactions between the remaining troponins with tropomyosin and actin decrease (Lehrer, 1994).

For intercellular $Ca^{2+}$ release and contraction to be initiated, cardiomyocytes must first be excited by an action potential. From a polarised resting membrane potential state (around -90 mv), initiation of contraction is started by influx of sodium ($Na^{+}$) through specific $Na^{+}$ channels and connexins, such as Cx42 (Figure 4a), leading to depolarisation of the cell (Figure 4b). At this early depolarisation stage, transverse tubules (T-Tubules) that extend into the sarcolemma allow an influx of $Ca^{2+}$ deep into the cell to initiate contraction. Inwardly rectifying Potassium ($K^{+}$) channels are also important as at negative membrane potentials they allow $K^{+}$ to leave the cell, until at depolarisation when current flow is very low. This together with long-type calcium channels ($Ca_v1.2$) that start to let $Ca^{2+}$ into the cell lead to the contraction plateau (Figure 4c). Following contraction, ATP phosphorylation of myosin binding heads allows $Ca^{2+}$ to be pumped back to the sarcoplasmic reticulum and also out of the cell (Luo and Rudy, 1991). Repolarisation is initiated by voltage gated $K^{+}$ channels, such as KCNE1, removing $K^{+}$, and as repolarisation continues $K^{+}$ also passes through the inward rectifier potassium channels. $Na^{+}$ also leaves the cell and the loss of positive charge leads to repolarisation (Figure 4d). On relaxation (polarisation), titin pulls the sarcomere back to its original formation (Luo and Rudy, 1991).

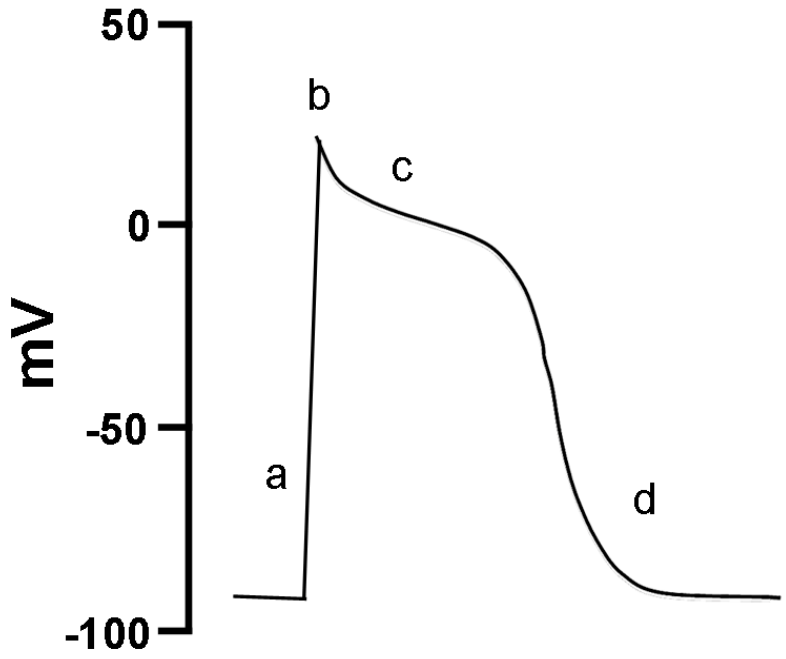



**Figure 1.10**. Action potential for working cardiomyocytes in the ventricle. (a) $Na^+$ enters the cell (b-c) The 'plateau', $Na^+$ channels close and $K^+$ leaves the cell, while $Ca^{2+}$ enters the cell maintaining contraction (d) $K^+$ and $Na^+$ leave the cell causing repolarisation. Source: adapted from (Klabunde, 2011).

Pacemaker cell in the sinoatrial node

In pacemaker cells, action potentials are generated slightly differently. These cells do not possess membrane resting potential and instead spontaneous depolarise (Klabunde, 2011). First a gradual polarisation to around -40 mV (threshold) is brought about by an influx of $K^+$ and $Na^+$ through hyperpolarisation activated cyclic nucleotide gated channels, such as HCN4, (Figure 5). From here, rather than a rapid depolarisation as seen in ventricular cardiomyocytes that utilise $Na^+$ current channels, depolarisation occurs more slowly initiated by long-type calcium channels such as Cav1.3 (Figure 5. B). Repolarisation is then brought about by removal of $K^+$ (Figure 5. C).

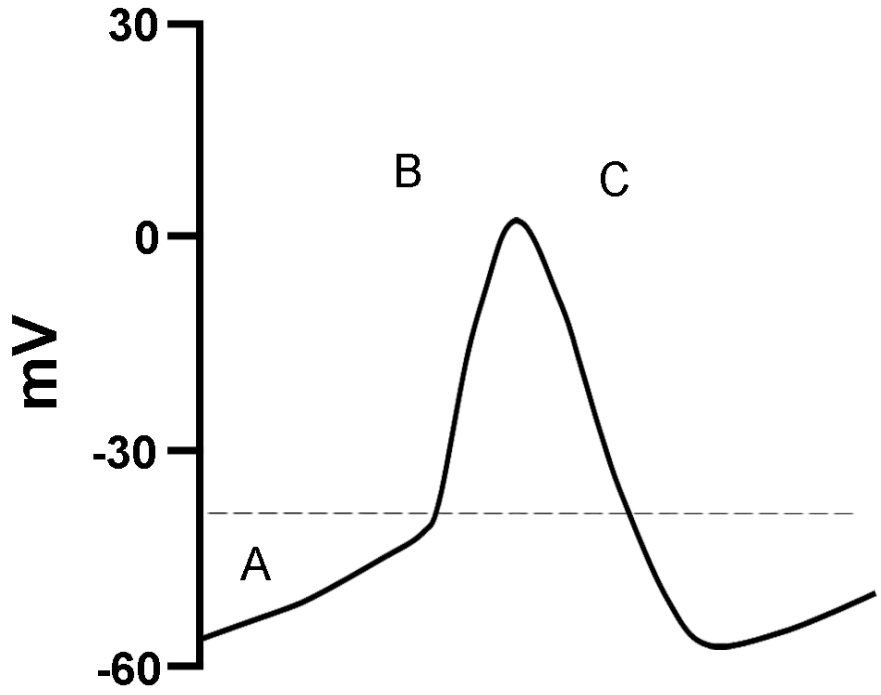



**Figure 1.11** Action potential for pace maker cell. Action potential A, $Na^+$ and $K^+$ enter the cell. B, $Ca^{2+}$ enters at threshold membrane potential (dotted line). C, $K^+$ and $Na^+$ leave the cell causing repolarisation. mV, millivolts. Source: Klabunde 2011.

Pacemaker cells and the PQRST wave

Pace maker cells that excite the heart from the SAN through to the purkinge fibers have subtle differences in there AP, with the natural AP duration becoming longer in each structure that carries the AP through the heart to the ventricular muscle. The AP given off from these cells is visualized in an electrocardiogram (ECG) PQRST wave (figure 6). This can be useful in deducing conduction phenotypes, as you could expect increased duration between S and T could be caused by faults in ventricular cardiomyocyte channels involved in maintaining the AP plateau, whereas increased duration between P and Q/R would be expected to be caused by faults in pacemaker

tissue. A bradycardia (low heart BPM) could be expected to be a fault with the SAN pace maker cells as it is these cells that have the fastest AP and set heart rate.

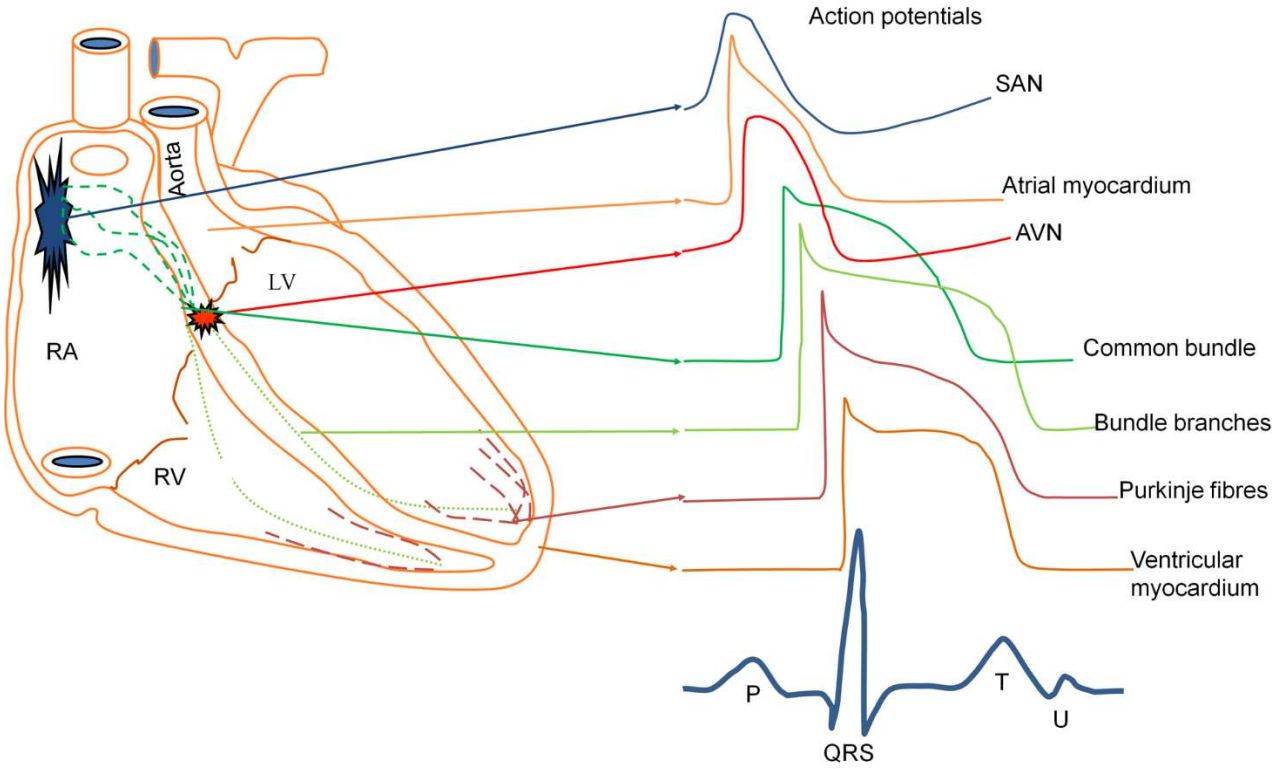



**Figure 1.12** Action potentials in pace maker tissue through the heart and their effect on the PQRST wave. P waves show depolarization in the atria, the PR interval shows the AP spreading to the ventricular cardiomyocytes, the QRR complex show depolarization in the ventricular cardiomyocytes and the T wave shows ventricular repolarisation. Sources adapted from (Mulroney, 2009, Hampton, 2013).

Excitation-contraction coupling

Following electrical stimulus, the sarcoplasmic reticulum (SR) and T tubules within cardiomyocytes initiate the muscle cells mechanical response (Bers, 2002). This occurs when APs reach T-tubules at the sarcomere membrane which then allows ions to penetrate deep into the myocyte sarcomere structure at the sarcomere Z-discs. They release $Ca^{2+}$ via L-type voltage gated channels such as $Ca_v1.2$ to Ryanodine 2 receptors (RyR2) on the SR (Bers, 2002). When $Ca^{2+}$ concentration is high enough for multiple RyR2 to be activated, the $Ca^{2+}$ stores within the SR are released into the sarcoplasm The $Ca^{2+}$ is then able bind to troponin C and initiate/maintain contraction (Cannell et al., 1995). Relaxation of contraction occurs after $Ca^{2+}$ calcium has been pumped out of the cytosol when concentrations of intracellular $Ca^{2+}$ are low (Bers, 2002). The AP in working contractile cardiomyocytes is passed from cell to cell via gap junction proteins such as Cx42 (*GJA5* gene) and so contraction travels out from the apex across the heart initiating contraction.

### 1.4 Morpholino treatment of *αMYH*, *βMYC* and *eMYH*

In this thesis 3 structural myosin heavy chain genes, α***MYH***, βMYC and e*MYH* will be targeted by morpholino treatment. Morpholinos are oligomers used for blocking translation of their specific target gene. They consist of 25 bases complimentary to their mRNA target (except in the case of the standard control morpholino that shows no/little binding energy to any potential (off)target mRNA). They contain a hexameric morpholino backbone, rather than the pentose ribose backbone seen in mRNA. They do not possess the negative charge usually seen in mRNA or other gene silencing iRNAs and so are not recognised enzymes or signaling proteins with a cell and thus can avoid the usual cell immune response. The non-ionic backbone is achieved by having phosphodiamidate inter-subunit linkages rather than the negatively-charged phosphodiester bonds seen in DNA/RNA (Figure 9) (Summerton, 2007). They bind to their target at just upstream or on the translational start site and sterically inhibit its

translation. Morpholinos can also be used to create splice variants as the morpholino can enter the nucleus and cause removal of specific exons with intron removal by affecting the normal intron removal process in pre-mRNA. However, this thesis only uses translation blocking (Moulton and Jiang, 2009).

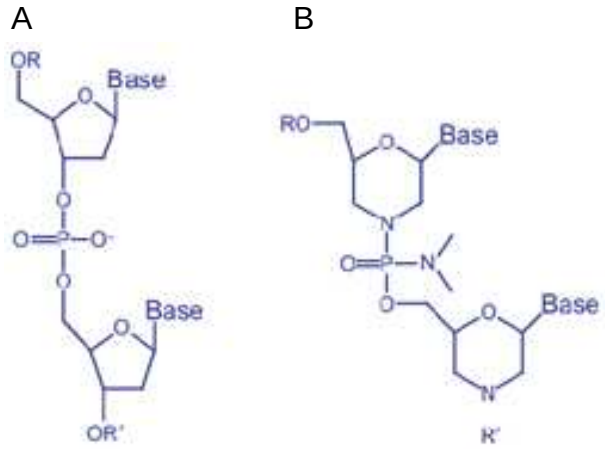



**Figure 1.13** Phosphodiester backbone DNA/RNA and morpholino comparison. A, shows the pentose ring negatively charged phosphodiester backbone seen in DNA/RNA. B, The morpholino contains hexameric morpholino backbone linked by uncharged phosphodiamidate inter-subunit linkages.

### 1.4.1 Congenital heart defects of genes involved in generation or transmission of the action potential

Calcium transients have previously been identified in αMHC, β*MYH* and e*MYH* KD, and significantly increased AP duration has been seen in e*MYH* KD (Rutland et al., 2011). It would be expected that genes involved in the generation and transmission of APs could be involved. Such genes have been identified in literature heart models or in congenital heart defects. The genes analysed in this thesis's KD project by in-situ hybridisation and RT-qPCR where chosen based on their potential effect on heart AP (see 1.3.1.) and their link to disorders.

Congenital conduction abnormalities have traditionally been associated with structural heart defects. However, cardiac conduction disorders have been found to be functional, that is, they have no obvious structural cause. These conduction disorders have been linked to familial clustering and therefore a hereditary basis (Wolf and Berul, 2006).

Two conduction channel genes are commonly linked to conduction disorders in the absence of known structural heart disease: Cx42 and HCN4. Cx42 is linked with AV block, and arrhythmias, and HCN4 with sick sinus syndrome (Wolf and Berul, 2006, Park and Fishman, 2011). Other conduction gene defects found include congenital long-QT syndrome, linked with mutation to KCNE1, while over-expression of fast gap junctions (Cx40 (human homologue of Cx42) and Cx43) have been shown to cause a thin bundle of His (Jay et al., 2004). Holt-Oram syndrome is a congenital disorder where sinus bradycardia and atrioventricular block have been seen, even when there is no observable structural phenotype detected, though absence in the right bundle branch is often observed (Park and Fishman, 2011, Christoffels et al., 2000b). The human connexin Cx40 has been shown to be down regulated with in patients with this condition (Park and Fishman, 2011, Christoffels et al., 2000b). Atrial fibrillation has also been shown to have Cx40 abnormally distributed and expressed and also linked this with increased dephosphorylation of Cx43 (Duffy and Wit, 2008). As the pace maker of funny current ($I_f$) in the SAN, HCN4 could be key. As well as being associated with patients of sick sinus syndrome, HCN4 knock out in animal models has led to an 85 % reduction in $I_f$ (Park and Fishman, 2011). This would be expected to disrupt/delay AP.

Long-type calcium channels have also been linked to congenital disorders. Patients with Timothy syndrome present with severe arrhythmias and Long QT interval, and have been found with substitution mutations in the CACNA1C gene (coding for $Ca_v1.2$) (Campuzano et al., 2010). It might be expected that incorrect function of a calcium channel responsible for maintaining contraction would cause alteration to the Q-T interval. CACNA1C is also linked to arrhythmias in Brugada syndrome where mutations to the gene have again been found (Antzelevitch et al., 2007).

## 1.5 Haemodynamics and Outflow tract banding

### 1.5.1 Haemodynamic stress in cardiac development

Haemodynamic force is the pressure on tissue exerted by blood flow and it is a key epigenetic factor that can alter development (Lindsey et al., 2014). The forces involved exert shear stress and stretch to the maturing cardiac wall (figure 10) triggering a biological response in signaling and endothelial cell organisation (Hove, 2006, Van der Heiden et al., 2006).

Peristaltic contractions commence at HH10 causing slow and irregular blood flow just as the heart starts looping (Yalcin et al., 2011). From HH17-23 flow becomes laminar through the AVC and OFT. The hearts inner curvature is under higher stress than the outer and it develops endocardial cushions, where as the outer curvature develops trabeculae in the ventricle (Yalcin et al., 2011). At this stage in the atria the propagation of AP is developing and shifting, and an increase in stress has been found to increase expression level of ion channels Cx42 and Nav1.5, this would be expected to affect the rate/direction at which cells become depolarised (Bressan et al., 2014). The same study showed that a decrease in pressure caused by atrial ligation (LAL) led to decreased conduction velocity (Bressan et al., 2014). By HH23, and through to HH30, when chamber septation is nearing completion, a plug flow is established through the heart i.e. flow is uniform with no back mixing. On completion of septation, the His-Purkinje system that is necessary for coordinating contraction in the ventricles becomes mature and a mature apex to base conduction pattern soon follows (Reckova et al., 2003). Increased hemodynamic load caused by OFT-banding has been seen to cause precocious emergence of the mature conduction pattern, whereas reduced load caused by left atrial LAL led to delay of the mature pattern (Reckova et al., 2003).

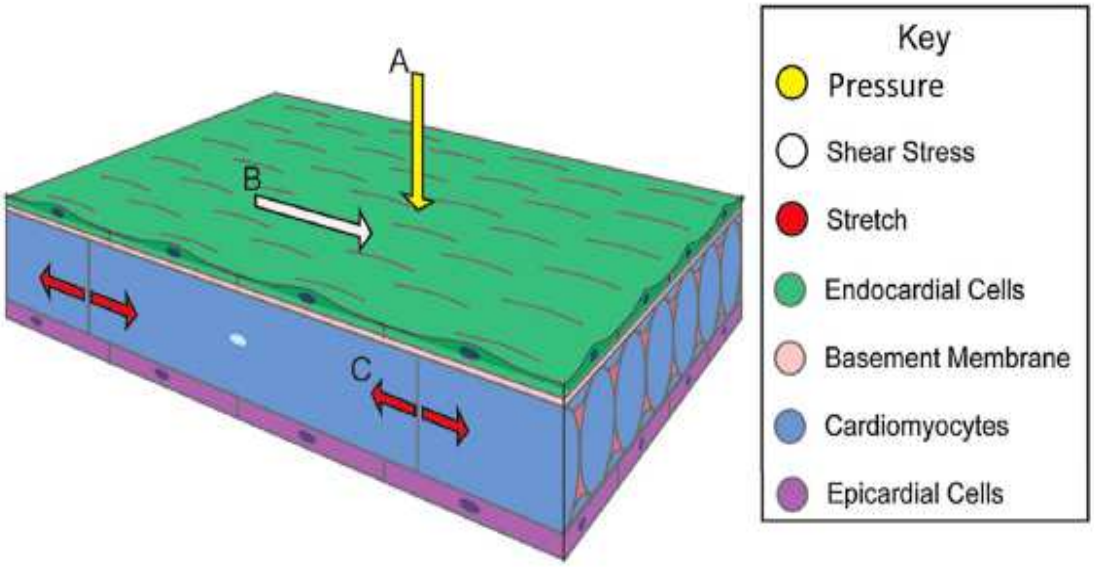



**Figure 1.14** Haemodynamic forces on the cardiac muscle wall. A, Pressure: the force perpendicular to the vessel wall. B, Shear stress: the frictional force parallel to the vessel wall. C, Stretch: stretch in the cardiac wall occurs with circumferential stress. Arrows indicate force vectors. Source: Lindsey et al., 2014.

### 1.5.2 Maladaptive Cardiac Remodeling in response to stress

The changes to cardiac wall stress explained in section 1.5.1 and depicted in figure 1.14, together with neurohormonal stimuli trigger a compensatory hypertrophic response in the heart. Pathological hypertrophy, that is, not hypertrophy from a normal physiological response, is brought about from stimuli such as genetic mutations, myocardial infarction, valve disorders or hypertension (McMullen and Jennings, 2007, Kehat and Molkentin, 2010). Hypertrophy can be classified as either concentric or eccentric (McMullen and Jennings, 2007). Induction of concentric hypertrophy is brought about by pressure overload from genetic mutation, myocardial infarction or hypertension, and leads to an increase in parallel contractile protein by an increase in myocyte width. This leads to left ventricular wall thickening with mild dilation (McMullen

and Jennings, 2007, Kehat and Molkentin, 2010). Eccentric hypertrophy results as a response to volume overload that increases series assemble of sarcomeric proteins that leads to lengthened myocytes, thus thinning of the left ventricular wall occurs and dilation is observed (McMullen and Jennings, 2007, Kehat and Molkentin, 2010). Pathological hypertrophy, though could possibly be caused by a single mutation, induces expression of many genes in response to the physiological phenotype. Genes of the fetal program, involved in extra cellular matrix remodeling and fibrosis are induced (Kehat and Molkentin, 2010). Genes induced of particular note encode for sarcomeric proteins and proteins involved in glucose and lipid metabolism (Lorell and Carabello, 2000). This demonstrates the complexities involved in the treatment of pathological hypertrophy, as what is initially a compensatory response to maintain cardiac output can lead to cardiomyopathy (McMullen and Jennings, 2007).

### 1.5.3 Cardiomyopathy

As outlined in section 1.5.2, the hearts maladaptive response to pathological stimulus in cardiovascular diseases is the cause of cardiomyopathy. Hearts displaying primary myocardium disease with mechanical or electrical dysfunction are defined as having cardiomyopathy. A key, but not invariable, identifier is ventricular hypertrophy or dilatation leading to heart failure (Maron et al., 2006). There are different forms of cardiomyopathy that are categorised as; dilated cardiomyopathy (DCM), hypertrophic cardiomyopathy (HCM), restrictive cardiomyopathy, arrhythmogenic right ventricular cardiomyopathy and left ventricular non-compaction cardiomyopathy (Harvey and Leinwand, 2011, McCartan et al., 2012, Morimoto, 2008, Towbin and Bowles, 2002).

The initial cause of cardiomyopathy can be a complex interaction a lifestyle, environmental and genetic factors (Seidman and Seidman, 2001). Though many single gene abnormalities have been highlighted as causative (highlighted below), there remains a significant proportion of patients presenting with cardiomyopathy that remain idiopathic (Seidman and Seidman, 2001). Treatment of cardiomyopathy that is unexplained has poor clinical outcomes (Seidman and Seidman, 2001, Ackerman et al., 2011). By studying the genetic makeup of heritable disorders, causative genes may be identified, and treatments be adjusted accordingly to the gene or genes

effected. Cardiomyopathy type can also be misdiagnosed. Infiltrative diseases (deposition of abnormal substances) such as glycogen storage disease can represent anatomical phenotypes of hypertrophic, dilated and restrictive cardiomyopathy, however it's treatment should be based on its often-missed physiological phenotype specific to the gene/s effected (Seward and Casaclang-Verzosa, 2010). This highlights the importance of genetic analysis and testing in the future treatment of the disease.

Familial (inherited) cardiomyopathy is found in 8-11% in the fetus and in 3% of newborns with cardiovascular disease (Pedra et al., 2002, Allan et al., 1985) and is caused by single gene disorders, such as metabolic disorders or chromosome abnormalities in the majority of cases (Pedra et al., 2002). Mutations in effected genes can be haploinsufficient resulting in less functional protein or mutations that cause proteins to function incorrectly (Seidman and Seidman, 2001).

Genes involved in force generation and structure are often important. Myosin mutations are prevalent in cardiomyopathies, particularly those of the heavy chain around the myosin head domain at the interface with actin and the ATP binding pocket (Meyer et al., 2013, Seidman and Seidman, 2001). The structural myosin heavy chain β*MYH* is shown to be mutated in 10 % of patients with familial cardiomyopathy out of a sample size of 54 in one study (Villard et al., 2005). Many studies have reported defects to β*MYH* to be linked to hypertrophic cardiomyopathy (Greber-Platzer et al., 2001, Seidman and Seidman, 2001, Meyer et al., 2013), however it is has also been linked with dilated cardiomyopathy along with other structural/force generating genes troponin T and C (TNNT1/2 and TNNC1/2) and amino-terminal-interacting partner cardiac ankyrin-repeat protein (CARP) (Schonberger and Seidman, 2001, Meyer et al., 2013). A gene involved in calcium regulation from these structures, phospholamban (PLN), is implicated with arrhythmogenic phenotypes in patients with dilated cardiomyopathy and arrhythmogenic right ventricular cardiomyopathy (van der Zwaag et al., 2012). Though both hypertrophic and dilated cardiomyopathy are both linked with the same genes, it is not clear if both morphologies are linked with disruption to the same physiological pathway, but of differing severity, i.e. dilated cardiomyopathy could be a more severe phenotype, or, if two distinct pathological pathways are affected in each phenotype. Metabolism errors account for 5% of genetic

paediatric cardiomyopathy, with gene enzymatic defects leading to the disorder (Cox, 2007). Genes effecting glycogen metabolism such as alpha-glucosidase (GAA) are implicated (Fukuda et al., 2007, Cox, 2007). It could be that in many cases of hypertrophic and dilated cardiomyopathy that the cause of the disease is actually a metabolic pathway, such as that in glycogen storage disease and expression of sarcomeric proteins may or may not be affected as part of a compensatory response.

#### 1.5.3.1 Dilated cardiomyopathy

Dilated cardiomyopathy (DCM) is found relatively commonly in around 1 in 2500 people in the USA and 20-25% DMC is familial (Maron et al., 2006). It leads to heart failure where it is the third most common cause and requires heart transplantation (Maron et al., 2006). It is characterised by thinning of ventricular walls with enlargement of the ventricle overall and demonstrates impaired systolic function (Harvey and Leinwand, 2011, Towbin, 2014a). Genetically DCM can be a dominant or recessive mutation, though dominant is more common, and is often X-chromosome linked (Harvey and Leinwand, 2011, Towbin, 2014a). Genes involved/inked tend to be structural such as cytoskeletal protein lamin, or sarcomeric protein βMHC (Parvari and Levitas, 2012, Teekakirikul et al., 2013).

#### 1.5.3.2 Hypertrophic cardiomyopathy

The most common inherited cardiomyopathy, Hypertrophic cardiomyopathy (HCM) is caused by autosomal dominant mutations in around 1 in 500 people and mainly effect young people (Towbin, 2014a, Maron et al., 2006). HCM demonstrates an increase in heart tissue mass, asymmetrical thickening of the anterior left ventricle wall and interventricular septum, and some dilation of the ventricles is also sometimes observed (Maron et al., 2006). At a Histological level, myocytes are found not only enlarged, but also disorganised, and increased fibrosis is present (Harvey and

Leinwand, 2011). Continued HCM without treatment will lead to dilation of the ventricles, where thinning of the left ventricle wall is seen and eventual heart failure (Teekakirikul et al., 2013). Sarcomeric proteins such as αMHC and βMHC have been linked with HCM (Teekakirikul et al., 2013, Maron and Maron, 2013).

#### 1.5.3.3 Arrhythmogenic right ventricular cardiomyopathy

Arrhythmogenic right ventricular cardiomyopathy (ARVC) is a relatively rare condition effecting around 1:5000 and predominately effects adults (Basso et al., 2009, Towbin, 2014a). An increase in fibrous fatty tissue in the heart wall is seen predominantly in the right ventricle and in the left at later stages (Towbin, 2014a, Basso et al., 2009). No sarcomeric proteins have previously been linked to ARVC, however cell adhesion proteins have been – where mutations to desmosomal proteins have been shown to have a knock-on effect on ion channels at the cell boundary. Gap junction and sodium channel protein impairment leads to impaired electrical impulse conduction and thereby leads to arrhythmias (Harvey and Leinwand, 2011).

#### 1.5.3.4 Left ventricular non-compaction cardiomyopathy

Once considered to be very rare, left ventricular non-compaction cardiomyopathy (LVNC) is becoming increasingly discovered with deter diagnosis (Belanger et al., 2008). Original population estimates put LVNC to effect 0.014 % of the population, however more recent work proposes up to 5 %, and out of systolic heart failure patient's prevalence ranged from 12 -19 % (Belanger et al., 2008). The predominant theory of its cause is by a halt in myocardial compaction in the embryo resulting in two distinct layers of compacted outer, and inner spongy myocardium (Towbin, 2014a). With the non-compacted inner layer containing excessively deep ventricular trabeculae and inter-trabecular recesses (Towbin, 2014a). Patients displayed both impaired systolic and diastolic function together with arrhythmias and conduction block in some cases (Towbin, 2014a). Sarcomeric genes such as β*MYH* and TNNT2 are once again often found muted in LVNC.

#### 1.5.3.5 Restrictive cardiomyopathy

Restrictive cardiomyopathy (RCM) is the least common of all cardiomyopathies, but often proves fatal (Harvey and Leinwand, 2011). RCM is an inherited autosomal dominant disorder that leads to impaired filling of the ventricles and therefore reduced diastolic ventricular volume (Teekakirikul et al., 2013, Cahill et al., 2013). Systolic function is relatively normal and no change to ventricular wall thickness is apparent (Teekakirikul et al., 2013, Cahill et al., 2013). RCM also leads to arrhythmias, heart block and sudden cardiac death (Teekakirikul et al., 2013, Cahill et al., 2013). Mutations to the sarcomeric structural protein cardiac troponin I gene has been found to be the main cause of RCM, however patients have also been found with alterations to β*MYH* and the MYL genes (Kaski et al., 2008, Karam et al., 2008, Caleshu et al., 2011).

#### 1.5.3.6 Clinical significance of fetal cardiomyopathy in utero

In the fetus cardiomyopathy is rare and usually fatal (Mongiovi et al., 2010). In a review of fetal cardiomyopathy, HCM was found in 35% of all cases with the other cases being of a non-hypertropic cardiomyopathy (NHCM) phenotype, however, considerable phenotypic overlap was seen, and most fetuses cases of fetal cardiomyopathy display endocardial fibroelastosis in the left ventricle (Weber et al., 2014, Vogel et al., 2011). Currently, the main method for fetal diagnosis is echocardiographic imaging where Doppler imaging can be used to assess cardiac haemodynamics (Zhang et al., 2016). However, etiology remains difficult and increasingly DNA microarray and whole genome sequencing have been used for diagnosis, particularly in families with a history of familial cardiomyopathy, and he identification of further genes that are markers or causative of differing types of cardiomyopathy would aid this process.

### 1.5.4 Surgical intervention in embryonic animal model to induce cardiac phenotypes

By performing surgical manipulation in key areas of the embryonic heart haemodynamic alteration can occur with resultant effects similar to that seen in congenital heart defects and cardiomyopathy. Three main surgical manipulation methods are currently used in the embryo; outflow tract banding (OFT-banding), left atrial ligation (LAL) and vitelline vein ligation (VVL). The OFT-banding model increases haemodynamic load by constriction of the OFT, thus shear stress and high blood pressure is generated in the heart (Sedmera et al., 1999, Lindsey et al., 2014). This project utilizes the OFT-banding model in order to gain a genetic profile of the altered haemodynamic model and is depicted in figure 11. The VVL model reduces haemodynamic load by reducing venous inflow and induces a model to study placental infarction (Hogers et al., 1999). LAL again leads to a reduction in haemodynamic load to induce a model of left heart hypoplasia by reducing blood flow to the left ventricle (Tobita and Keller, 2000). Our laboratory method for OFT-banding follows the method of Sedmera with the addition of an extra knot on the tied sultue. This enabled the initial knot to not be ‘too tight’, but to restrict with growth. The second knot then ensured that the initial relatively lose knot did not slip out of place.

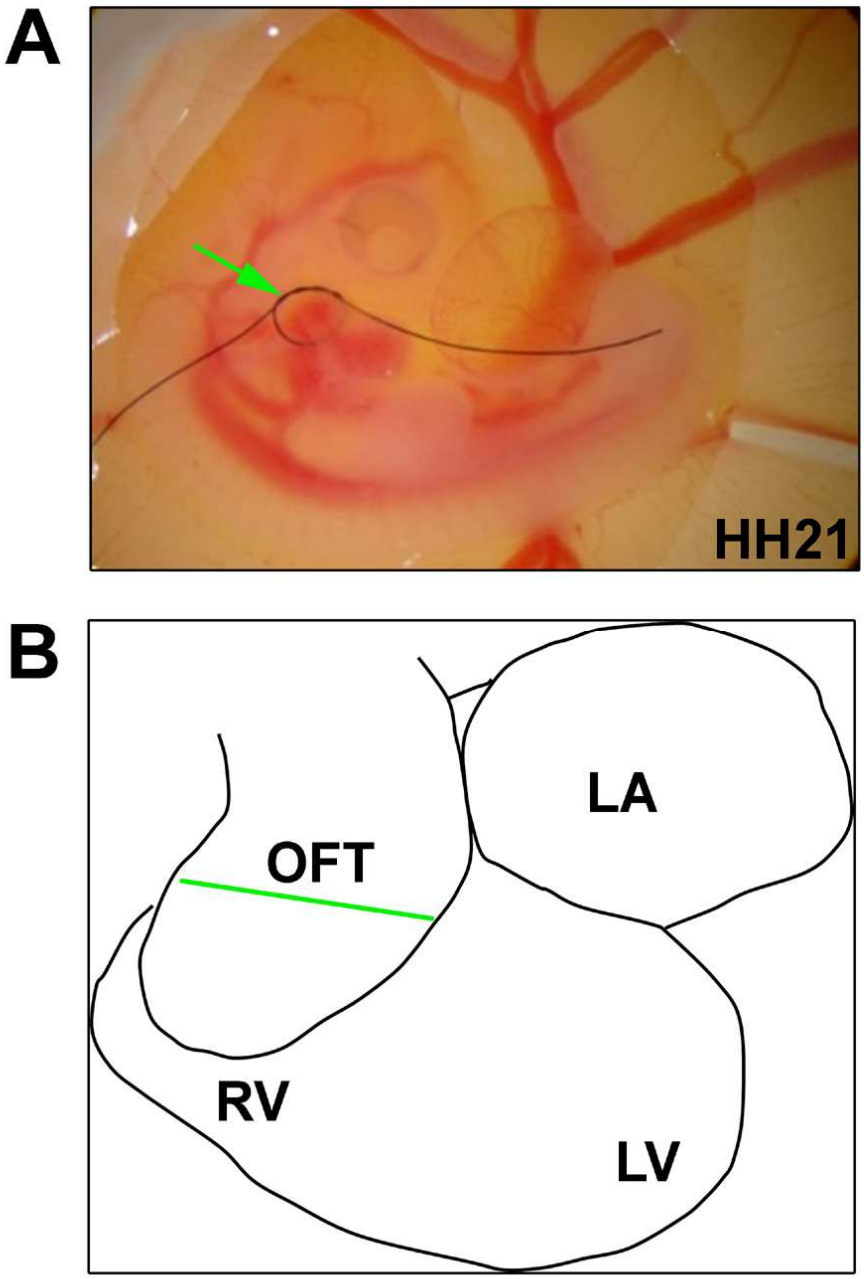



**Figure 1.15** OFT-banding position. A, experimental photo in the chick embryo at HH21 where the arrow indicates the location of the tied double knott suture. B, schematic diagram showing position of suture around the OFT (green line). OFT, out flow tract; RV, right ventricle; LV, left ventricle; LA, left atrium. Source: loughna lab stock photo and adapted from Lindsey et al., (2014).

### 1.5.4.1 The OFT-banding technique and hemodynamic response

The OFT-banding technique used in the thesis was performed by Dr. Pang. The technique consisted of a double overhand knot tied to a snug, but not overly tight fit to the OFT, as seen in figure 11 at HH21. This technique was adapted from the original technique first performed by Sedmera (Sedmera et al., 1999).

Extensive previous literature has shown alteration of haemodynamics in our OFT-banded model. Following banding at HH21 embryos showed a constant pressure increase from HH24 – HH34. Peak systolic pressure rose by 35% and end diastolic ventricular pressure by 11% (Clark et al., 1989, Tobita et al., 2002). Blood flow velocity at the OFT is was found increased by 120% at HH24 and sustained until HH29 (McQuinn et al., 2007). Interestingly, no alteration in heart rate or cardiac output/ejection fraction is found with the model, suggesting that the heart adapts so that cardiac function preserved and failure is not induced (McQuinn et al., 2007, Clark et al., 1989).

### 1.5.4.2 OFT-banded effect on heart the myocardium

As indicated above (section 1.5.4.1), the heart responds to the increased haemodynamic load in order to maintain function. This response is seen as dilation of whole heart (Clark et al., 1989, Tobita et al., 2002, Buffinton et al., 2013). Thickening of the compact myocardium in the heart ventricles at their apex region was seen along with an increase in the ventricular lumen at HH29 (Clark et al., 1989, Tobita et al., 2002). However, myocardium thickness when measured later in the model at HH36 was found to be significantly decreased when compared to controls (Tomanek et al., 1999). The dilation is proposed to be brought about by myocyte hyperplasia as the ratios of DNA to protein and myocyte area are found to be comparable in both controls and OFT-banded hearts (Clark et al., 1989). Myofiber patterning was found to have accelerated development in OFT-banded hearts. the expected pattern is for myofibers to be arranged in circumferential direction until HH27, then a longitudinal orientation is seen to HH36, however OFT-banded hearts show longitudinal orientation prior to HH27 (Tobita et al., 2005). It might be expected that these changes in myocardial

architecture will affect the conduction system. Optical mapping has shown precocious conduction system maturation in OFT-banded hearts, and, at a molecular level, upregulation of the working contractual cardiomyocyte conduction genes GJA5 and endothelin-converting enzyme 1 (ECE1) (Reckova et al., 2003, Hall et al., 2004).

## 1.6 The chick as a model

The chick embryo is a frequently used model system to study cardiac development. This is down to its genome being highly conserved compared to the human (Wallis et al., 2004) and its development pattern in the heart being very similar, with both chick and human hearts developing from a linier heart tube to a 4 chambered heart. Having said this, some changes in morphology are present. In atrial septation, the septum secondum does not form in the chick. Instead the septum primum grows inferiorly from the atria's cranio-dorsal wall and closes shortly after hatching (Wallis et al., 2004).

The chick model is easy to manipulate experimentally as it is easily accessible with a stationary developing pattern at early stages. So techniques like our morpholino treatment can be applied directly and consistently to the embryo, and similarly for our surgical manipulation model. This is demonstrated in previous models of haemodynamic manipulation in the embryo where the chick model has always been used. These studies were able to then directly measure blood flow and heart rate during development. The embryos are also easily grown to specific stages (Kain et al., 2014) at set timeframes and require little care other than maintenance of 37ºC and 60% humidity (Manner, 2000).

One drawback is that new gene silencing techniques such as clustered regularly interspaced short palindromic repeats (CRISPR) or transcription activator-like effector nucleases (TALEN) have not yet been achievable in the chick.

## 1.7 Project Aims

Sarcomere myosin heavy chain proteins are known to be important in muscle development (Agbulut et al., 2003). The myosin heavy chain proteins alpha (αMHC) beta (βMHC) and embryonic (eMHC) have been found to be expressed embryonically in the developing chick heart and are known to be involved in fundamental aspects of cardiogenesis (Rutland et al., 2009, Rutland et al., 2011). Further, they have also been associated with CHD's (Ching et al., 2005, Granados-Riveron et al., 2010, Budde et al., 2007). Additional, previous work using gene knockdown of αMHC, βMHC and eMHC in the chick embryo led to anomalies in $Ca^{+2}$ transients and, in the case of eMHC, increased duration of action potentials (Rutland et al., 2011). However, an understanding of how these proteins are involved in cardiogenesis and the formation of CHD's, and if they affect signaling of the conduction system, is unknown.

This thesis is split into two parts, but both were designed to place stress on the hearts. The first main aim is to investigate the effect of morpholino KD of αMHC, βMHC and eMHC on sarcomere maturity and selected conduction gene expression in the chick embryo at HH20. The chick embryo presents a useful model organism for gene knockdown models as it allows access to the embryo as it is developing. This permits the direct application of morpholino (MO) RNA oligonucleotidies, to permit gene-specific knockdown (KD) and hence the resultant phenotypes to be studied. This chapter's aim is to use MOs in order to study the effect of alpha myosin heavy chain (αMHC), beta myosin heavy chain (βMHC) and embryonic myosin heavy chain (eMHC) on the developing cardiac conduction system and impulse conduction through the working myocardium.

The second main aim of the thesis uses a chick embryo model of outflow tract constriction called OFT-banding. OFT-banding has been shown to cause significant heart enlargement, altered myosin expression and altered haemodynamics in the literature (Tobita et al., 2002, Clark et al., 1989, McQuinn et al., 2007). However, global gene expression on these whole hearts has not been previously studied. The stage chosen for this global gene expression profile is HH29, with initial banding taking place at HH20. This is when the conduction system is at a crucial stage of its development

(when the SAN had just located to the right atrium). In order to achieve this, library preparations to enable effective global sequencing were optimised. Obtaining the gene profile will enable greater insight as to the effects of OFT-banding in the developing heart, particularly with reference to the conduction system, and structural and metabolic genes that can affect conduction and the overall OFT-banded anatomical phenotype. As this thesis is split in to multiple parts, so separate results sections that include their own introduction, and aims were used.

### 1.7.1 Main Hypothesis

Alteration in heart structural genes or structure itself induced by gene expression manipulation or physical stress will have no effect on the cardiac conduction system.

# Chapter 2 Materials and Methods

## 2.1 Egg incubation and harvesting, and ethics and welfare

Fertilized white leghorn chicken eggs (*Gallus gallus*; Henry Stewart, Lincolnshire, UK) were incubated at 37 °C with constant rotation in a humidified atmosphere until they reached the required age (Bellairs and Osmond, 2005). A small window was made on the blunt-end shell. 3 ml (more than 3 ml led to increased death rate) of albumin was carefully drawn from the egg. This centralised the embryo and allowed removal of the chorioallantoic membrane which separates the embryo from the extra-embryonic membranes. The embryo can then be easily staged (Animal work was performed in accordance with national (UK home office) and institutional regulations and ethical guidelines). Embryo harvesting post HH2O was carried out by decapitation in ovo, pre HH2O by cutting chorioallantoic membrane. The Hamburger and Hamilton (HH) staging system was used to stage the developing embryos(Hamburger and Hamilton, 1992).

## 2.2 Knock down project

### 1.1.1 Pluronic gel and in ovo morpholino application

In order for effective cell delivery, morpholinos were applied with the delivery agent F127 pluronic gel (BASF Corp., Germany). Pluronic gel at the correct concentration forms a viscus gel at body/incubation temperature. This allows the morpholino to be applied directly over the heart without run off and enables constant semi-targeted delivery of the knock down agent. Correct concentration of pluronic gel is key to the KD procedure as too thin would lead to run off and too think would hinder delivery. 15 % pluronic gel gives the correct viscosity at our desired temperature (Khattak et al., 2005). To achieve this, 30 % stocks were made in Hanks' Balanced Salt Solution (HBSS). Accuracy is key at this step and stocks were prepared at 30 % w/w, so for a 25 ml stock solution, 17.5 g of HBSS is added to 7.5 g of pluronic gel powder using an

Analytical Balance Lab digital scale. Only relatively small volumes can be made as pluronic gel powder has a high volume when not dissolved and only dissolves slowly due to its viscus nature. To dissolve the powder the mix is placed at 4 °C side on, on a rotating platform for 48 hours. This allows the mixture to dissolve whilst not introducing bubbles. Morpholino application was performed at HH10/11 (about 48 hours of incubation). Both experimental and control morpholinos were diluted 1 : 1 with the pre-prepared pluronic gel mix. This gave a final concentration of 500 µM morpholino and 15% pluronic gel. Morpholino/pluronic gel solution were kept on ice to prevent thermogelation of the pluronic gel. The next key step is application of the morpholino. Morpholin must be applied directly over the heart. At HH10/11 the heart is visible (though barely discernible) as a very light flashing grey dot. This is identified by using an SV11 stereomicroscope (Zeiss, Germany). Once identified the morpholino can be applied. The eggs were then resealed using masking tape and were reincubated with no rotation until they reach HH2O (80 – 85) hours of development).

### 2.2.1 Morpholino design

Antisense oligonucleotide morpholinos targeting the ATG translational start site were designed against myosin heavy chain alpha (α*MYH*) (5'-TGGCTATCTAGCAGAACGCAAGGCA-3'); myosin heavy chain beta (β*MYH*) (5'-TATCGTAGTCATCATGCTAATTTATA-3') and myosin heavy chain embryonic (e*MYH*) 5'-GTTCATATCGCGTAACGCAAGGCA-3') by Dr. Catrin Rutand (GeneTools LLC, USA) (Rutland et al., 2011, Rutland et al., 2009). This allows morpholinos to bind to mRNA at the start site and thus translation cannot be initiated (knock down (KD)). A GeneTools standard control (SC) morpholino designed to the mutated human *β-globin* gene (5'-CCTCTTACCTCAGTTACAATTTATA-3'; GeneTools), as well as untreated (UT) controls were used to ensure no off-target effects of the treatment were apparent. Morpholinos are tagged at their 5' end with a fluorescein tag in order to be able to detect morpholino uptake by the embryo on excitation (494 nm). Sequence homology was checked by NCBI BLAST with morpholinos found to be specific to their target gene.

### 2.2.2 Assessment of morpholino up take

#### 2.2.2.1 In ovo assessment

At HH20 (for *in situ* hybridisation experiments), embryos were harvested *in ovo* by cutting around the chorioallantoic membrane and *placed* into a petri dish with ice cold phosphate buffered saline (PBS) (Thermo Scientific, UK). The chrioallantoic membrane was removed as it gives fluorescence owing to 5'-fluorescein morpholino application technique. Positive morpholino uptake was confirmed in each experimental and SC embryo by detection and qualitative assessment of the fluorescence intensity in the heart using a SV11 stereomicroscope (Zeiss, Germany). A numbering system from 1 - 5 was used to grade moropholino uptake, with 5 being good and 1 being poor. Hearts given 4-5 were used for KD experiments. In results section 2.4.1 western blott analysis shows the difference in protein level between 2-3 graded embryos and 4-5.

#### 2.2.2.2 Colonies in cell culture assessment

Individual colonies were assessed for morpholino uptake by a Leica DMIRE2 inverted microscope at 494 nm. Positive colonies fluoresced bright green. Only colonies graded 4-5 were considered KD colonies.

## 2.3 Western method

In order to assess protein reduction in knockdowns western blot analysis was performed

### 1.1.2 Western blot for assessment of knock down

Embryos were harvested at HH20 and HH29. Hearts, and HH29 liver for negative control samples, were removed and washed in ice cold PBS, snap frozen in liquid nitrogen and stored at -80. For protein extraction hearts were thawed and kept on ice until lysis treatment. 30 µl of Tris EDTA lysis buffer (see full protocol in appendices for recipe) was used per HH20 heart and 200 µl was used for HH29 heart and liver. Tissue was homogenised using needle homogenisation. For HH20 just a 0.5 mm needle was used, but for HH29 a stepped procedure was used from 0.8 to 0.6 to 0.5 mm. Once totally homogenised samples were centrifuged at 10 000 x g for 20 minutes at 4 °C. Supernatant was then transferred to a fresh Eppendorf. Samples were placed in -20 after taking necessary volumes for protein concentration determination via Bradford assay.

### 2.3.1 Bradford assay

Initial optimisations on the volume of sample to add to the Bradford assay were carried out using 3, 4 and 8 µl. Following this, 5 µl was always used as this gave a result midway on the standard curve. The 5 µl was made up to 800 µl with $dH_2O$ and known concentrations of BSA standards were added at 1.5, 2, 4, 6, 8 and 10 µl, plus a 0 µl blank. 200 µl protein assay dye (Biorad) was added to each sample and they were vortexed gently and incubated for in the dark for 10 minutes. Samples were analysed using a spectrometer at A 595, a standard curve was obtained, and concentration of samples was estimated. All samples were adjusted to 1 µg/µl so that the same concentration and volume could be added to each well of the SDS PAGE gel.

### 2.3.2 Preparing SDS PAGE gel

Initially gels were made in house, however for all later westerns including the experimental westerns pre-cast gels were used (4–20% Biorad). For the initial gels, each gel was made individually on the day of the experiment. The separation gel was made up of $dH_2O$ (2.3 ml), SDS 10 % w/v (1 ml), 30 % (w/v) acrylamide:bisacrylamide 29:1 (4.2 ml) (Protogel) and Tris-HCl 0.5 M 8.8pH per gel for a final concentration of 12.6 % and a pH of 8.8. The stacking gel was $dH_2O$ (4.5 ml), SDS 10 % w/v (1 ml), 30 % (w/v) acrylamide:bisacrylamide (29:1) (2 ml) and Tris-HCl 0.5 M pH 8.8 (2.5 ml) per gel for a final concentration of 12.6 % and pH of 8.8. Glass plates to house the gel were prepared on a biorad rack in lock plates and checked for leaks. The separating and stacking solutions were polymerised by addition of 10 % w/v ammonium persulfate (100 µl), and tetramethylethylenediamine (10 µl). The separating gel was pipetted between the pre-prepared glass plates that will hold the gel, to the top of the shutter gates (approx 3.3 ml). Water was pipetted on top. Following polymerisation, the water was poured off and the slides dried with filter paper. The stacking solution was then pipetted in to top and comb inserted, ensuring no air enters gel. Following polymerisation (about 30 mins) the comb was removed.

### 2.3.3 Western procedure

The gel was then placed in the tank supplied by Biorad and filled with running buffer (Tris base (18g/l) glycine (86.4 g/l, and SDS (6 g/l) to the fill line (around 2/3 of the tank). Samples were prepared for loading by mixing with 6X SDS sample buffer (Thermo Scientific) for a final dilution of 1X i.e. 1 µl SDS buffer with 5 µl sample (for 5 µg total protein) and heated to 95°C. Samples were vortexed and spun before and after the heating step and centrifuged for 1 minute at 13000 rpm. Samples were loaded into gel wells along with 1µl of marker ladder (Biorad) in lane 1 and the gel was run for 1.25 hours. The next step was gel transfer. The gel was removed from the tank and the removed from its case and placed in transfer buffer (see appendices). Pre-cast gels require case to be cracked open at the edges, whereas made up gels come apart

easily. The gel was then loaded into the transfer case. Transfer case order: (- charge side) pad, filter, gel, nitrocellulose membrane, filter pad (+ charge side), The case was then placed in the tank with an ice pack, filled with transfer buffer and run at 100 V for 60 minutes. Protein transfer was checked with Ponceaus stain. The membrane was washed with Tris buffered saline tween (TBST) then blocked in 5 % BSA solution in TBST for 1 hour on a shaker. Following blocking the membrane was placed in a sealed bag containing the primary antibody solution: 5 % BSA solution in TBST, the βMHC mouse antibody HV11 (DSHB) = 1:1000, and *GAPDH* rabbit polyclonal antibody (Abcam) = 1:1000. Mixes were taped to a flat surface on a shaking platform overnight protected from light at 4 °C. Following overnight incubation the blots were washed with 3 rinses and 3 5 minute washes followed by further 3 15 minute washes in TBST then incubated in secondary antibodies. Secondary antibodies were anti-mouse IRDye 800CW green (Li-cor 926-3225) and anti-rabbit IRDye 680RD red (925-68071 Li-cor). They were diluted 1:10000 in 5 % BSA TBST solution. The sealed bags were again placed on a flat surface and incubated at 37 °C on rotating platform in the dark. The wash process as per the primary antibody was repeated for the secondary with the edition of a final rinse in $H_2O$. The gel was kept moist and taken to be scanned using a GS710 imaging densitometer (BioRad). Images were obtained and band intensities quantified by odyssey image studio.

### 2.3.4 Analysis

Intensities of the βMHC band were compared to *GAPDH* to normalise for variation in protein level. The equation is: βMHC / *GAPDH*. These results were pooled to give a mean reduction in βMHC signal. However some variation existed in the data because some blots showed less of an overall difference between the βMHC and *GAPDH* bands. To remedy this inter-plate variation, results from all βMHC to *GAPDH* values on one blot were normalised against the pooled control βMHC to *GAPDH* values from the same blot. The equation is: normalised KD / normalised controls. This gave very similar results to the standard βMHC / *GAPDH* comparison, but as KDs were compared to controls on the same bolt, variation was reduced. This is shown in the

results section as ‘normalised relative protein expression’. Statistics were carried out on these values. Two sample T-tests assuming unequal variences were used and variance was checked using SD, SE and 95 % confidence interval. Equality of variance between samples was tested by an F-test. Both Excel (Microsoft) and SPSS (IBM) were used.

### 2.3.5 *GAPDH* as a control

Glyceraldehyde 3-phosphate dehydrogenase (*GAPDH*) is a glycolysis enzyme that catalyses the conversion of glyceraldehyde 3-phosphate to 1,3-bisphosphoglycerate producing 1 NADH, and thus is highly and stably expressed in nearly all tissue (Tarze et al., 2007). *GAPDH* is a common reference gene for chick heart western blots (Rutland et al., 2011, Rutland et al., 2009). We have analysed its stability at mRNA level by RT-qPCR (see section 3.3.19.3) and found the enzyme to be stability expressed across controls (UT and SC) and all KD groups (βMHC, αMHC and eMHC). On a western blot gel *GAPDH* is resolved around 36 kDa.

## 2.4 Cell culture

### 2.4.1 Optimisations

Cell culture was optimised to achieve beating colonies on glass cover slips that could be knocked down and analysed by immunocytochemistry. The first optimisation involved the cell seeding density onto a 24 well plate (Nunclon UK). Initial density used was 0.05 X $10^6$. This yielded poor sparse colonies with dead cells lifting off of the plate surface. Density was increased to 2.75 X$10^6$. This gave strong colonies with little detachment. In order to perform immunocytochemistry it was necessary to grow the cells on removable glass coverslips (Agar Scientific). For this the optimal seeding surface was tested. Conditions were: 1, Collagen coating; 2, Fibronectin coating; 3, Collagen and fibronectin; 4, No coating – just glass slide. All coverslips were sterilized by 70 % ethanol and dried in a tissue culture hood. Fibronectin (Sigma-Alrich) was

diluted to 5 µg/ml in PBS. Type I collagen (Santa Cruz) was diluted to 500 µg/ml in 0.02 M acetic acid. Coverslips were inserted into a 24 well plate and then totally covered with solution (non-coating wells were left blank). 24 well plates were then placed at 37°C in a tissue culture incubator for 1 hour. Wells were washed with PBS for 5 minutes X3 and dried at R/T in a tissue culture hood for at least 1 hour. Following this cell seeding took place. Results showed that optimal cell growth took place on the glass coverslip with no coating. Therefore, untreated glass coverslips were used for the project. The final major optimisation was trypsin concentration. Trypsin is required for cell dissociation and was found to be a key step in varying the type of cell mass cultured (Sigma-Aldrich). Concentration was varied from 0.1 X to 10 X (table 2.1). It was found that 0.1 X returned floating masses of cells that were so large they would dis-attach from the slide surface. 1 X returned individual colonies that could beat independently of each other. 10 X returned a thin layer of cells that would beat as one mass. This project uses 1 X to obtain independent colonies as greater amounts of information will be able to be gained with individual colonies than with one single beating layer.

**Table 2.1** Trypsin concentration for the dissociation of cell culture harvested at HH29 and at a cell density of 2.75 $X10^6$

| Trypsin concentration | Dissociation state of cell mass |
|---|---|
| 0.1 X | One cell mass |
| 0.5 X | Mass starting to break up |
| 1 X | Separate colonies that join up after 48 - 72 hours |
| 5 X | Colonies joined together |
| 10 X* | Mostly Single cell layer with some build up in places |
| *10 X stock solution is 0.5 % trypsin | |

### 2.4.2 Cell culture Protocol

In a laminar flow hood eggs were swabbed with 70 % EtOH, and HH29 embryos were removed into ice cold HBSS and hearts were isolated. Hearts were separated into atrial and ventricular sections by cutting out the valve region between chambers (figure 2.1). Heart sections where then placed in horse serum/HBSS 1:1 on ice until all hearts were isolated. When ready for the trypsination step, hearts were washed with HBSS X3 before being placed into 1X trypsin HBSS solution and incubated at 37°C in a cell culture incubator for 30 minutes with agitation every 5 minutes. Hearts where totally submerged, usually about of 2 ml solution. Following incubation cells were triturated

for further dissociation using syringe/pipette tips without sharp edges. The trypsin was neutralised by adding 15 ml of pre-warmed growth medium (see appendix A for details) and centrifuged at 1500 rpm for 5 mins. The supernatant was discarded and the pellet was re-suspended in 1 ml pre-warmed growth medium (10 %). Cell density was assessed via a haemocytometer and 20 µl of 2.75 X $10^6$ cell solution was pipetted onto the center of the pre-warmed coverslip in the 24 well plate. The plate was incubated for 3 hours at 37°C in a cell culture incubator. Following this time, 1 ml of pre-warmed growth medium (5 %) was carefully pipetted into the wells and the plate was re incubated.

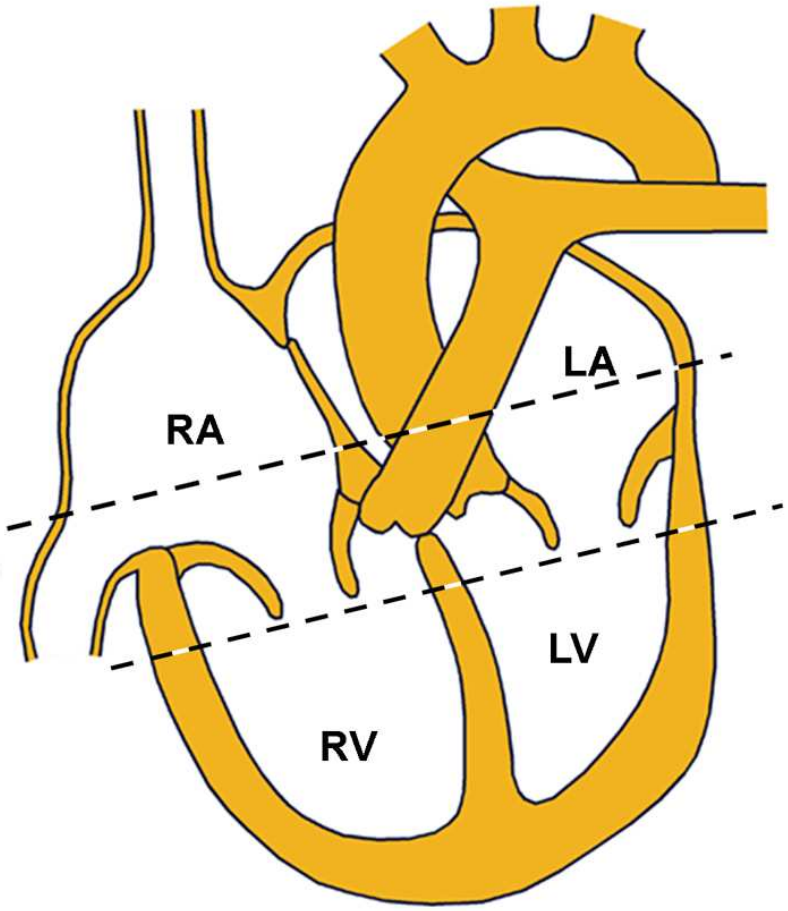



**Figure 2.1 Atrial and Ventricular separation**. The valve region of the heart was removed by two transverse cuts (dotted line) to leave atrial and ventricular halves. The center valve region was discarded, and atrial and ventricle regions used for cell culture.

### 2.4.3 Cell culture knockdown

Prepared morpholino was added to fresh growth media (GM) at 20 mM. The 250 µl morpholino GM solution was added to wells with 3 µl of endoporter delivery agent. Wells were then made up to 500 µl with GM.

### 2.4.4 Optimisation: cell culture maintenance media for reduction of cell cycle

In order to continuingly test the existing knocked down cell colonies without fibroblast overgrowth, a maintenance medium was developed containing 0.01 mM Cytosine Arabinoside (Sigma UK) and growth medium minus glutamine. Cytosine Arabinoside has been shown to decrease the rate of progression of cells into the S phase of cell cycle (Humphries and Coffin, 1976). The idea behind this was that knockdown colonies could be tested for longer periods of time. Though optimisations appeared to be successful, with colonies showing clear observed reduction in size following addition of maintenance media compared to normal growth media, this technique was never followed up on as the direction of my research altered.

## 2.5 Immunofluorescence of cultured cells

In order to assess the structure of sarcomeres in cultured cells Immunofluorescence was performed.

### 2.5.1 Key optimisation

One key optimisation was the finding that PBS tended to lift the cardiomyocytes from the glass cover slip. Cells in large colonies were more inclined to become detached before fixation. To remedy this, HBSS with $Ca^{2+}$ and $Mg^{2+}$ (Thermos Fisher) was used instead of the traditional PBS in solutions used in this protocol eg. in washes and PFA. This protected the cells from lifting

### 2.5.2 Protocol

(For full detailed optimised protocol please see appendices)

A 24 well plate was pre-preparred for washes with HBSS $Ca^{2+}$ & $Mg^{2+}$ and pre-warmed to 37 °C. Coverslips from cell culture were carefully removed from the initial 24 well plate and placed into the new pre-prepared wash plate. This new plate will not contain traces of morpholino like the original culture plate would. One more very gentle wash was carried out to the wells before proceeding to fixation in 2 % PFA for 30 minutes at R/T. This was followed by 2 washes in wash solution (HBSS plus 0.5 % BSA). Triton X-100 (0.1 – 0.2% v/v HBSS with 0.5 % BSA was then added to wells for 20 minutes followed by another 2 washes in was solution. A separate blocking was unnecessary as BSA blocks potential protein interactions. Primary antibody alpha-actinin (Alpha actinin mouse-anti sarcomeric (Sigma UK A7811)) was added at 1:100 in 0.1 % BSA and incubated with wells at 4°C O/N protected from light. Following incubation, the antibody solution was removed and wells were washed with wash solution 3 times before adding the secondary antibody (633 anti-Mouse (Invitrogen A21052)) at 1:100 for 60 minutes protected from light on rocking slowly platform at R/T. Finally, the

antibody solution was removed followed by 3 washes with wash solution. 27.

The final wash was gently removed from individual wells one at a time for mounting. Coverslips were removed and placed onto 12 µl of vectashield (+DAPI) centrally on glass slide. 31. Slides were placed in dark at 4°C to store, or at least 1 hour before analysis (vectrashiled hardens at 4°C negating the need to apply nail varnish).

### 2.5.3 Analysis

Images were acquired using Leica DMIRE2 inverted microscope using DAPI 480 nm (blue) for nuclei, FITC 530 nm excitation (green) for morpholino, and Alexa Fluor 633 nm (far red) for alpha actinin detection.

## 2.6 Riboprobe design and preparation of probe template for *in situ* hybridisation

### 2.6.1 Primer design for *in situ* hybridisation riboprobes

For riboprobe primer design, the key consideration is the properties of the primer product. Primers were designed with amplicon size ranging in from 490-1010 bp (information of each gene is detailed in Table 2.3.) Primers can be designed to gene isomer of interest or conversely to attach to all isomers, but unless stated otherwise, all probes were designed to pick up all variants in the heart. To ensure appropriate genes were targeted NCBI BLAST is used. Often designing probe sequence at the 3' UTR region ensures isomer specificity, but this is not always the case. A key step to probe design is to estimate the annealing temperature. For this M-fold software (The RNA Institute) was used. Probes were designed to anneal at around 65 ºC. As well as annealing temperature, maximum self-complimentary and pair complimentary energy was checked (information of each gene is detailed in (Table 2.1.) Each gene was amplified by end point polymerase chain reaction by 35 cycles as described in section

2.16 and was checked by gel electrophoresis for genomic contamination. PCR clean up then took place and templates were subcloned into pGEMT-easy vector (Promega, UK) followed by linearization (Section 2.2.3.1), riboprobe synthesis (Section 2.2.4.2) and purification (Section 2.2.4.3).

### 2.6.2 RNA isolation

Explained in detail in sequencing method section (2.3.2.3).

### 2.6.3 cDNA generation

Explained in detail in RT-qPCR method section (2.2.8).

**Table 2.12** Primers pairs and annealing temperatures with amplicon size designed for riboprobes

| Gene name | Accession number | Forward primer | Reverse primer | Size (bps) | Primer PCR annealing temperature (°C) |
|---|---|---|---|---|---|
| HCN4 | XM_425050 | 5’-ATGGTGAATGACTGCCACAC-3 | 5’-ATGTGCCGCTTCATGTGC-3’ | 515 | 58 |
| CX42 | XM_015295951 | 5’GTCCGCCCCACAGGTAGAAA3’ | 5’GTCCCACGGGCTGAGAACTTCA3’ | 528 | 62 |
| CX43 | NM_204586 | 5’AGATATGCCTACCACCGCTC-3’ | 5’-ATGGTACCTTGGCATGTGGA-3’ | 783 | 57 |
| CAV1.2 (T1 &t2) | NC_006088 | 5'-GTGGTCAGCGTTTCTCTCATC-3' | 5'-AGGTTGAGACAGTGAAGAGGG'3' | 508 | 62 |
| CAV1.2 (T1 only) | XM_004937946.1/ ENSGALT00000021261.5 | 5'-CTAACAACAGGTTCCGTGTCC -3' | 5'-GTATGCGGTCATCTTCAGAGC-3' | 212 | 61 |
| TBX18 | NM_204955.2 | 5’-CTGCGTTCCCTGAGATTAC-3’ | 5’-TTGCCAGGTCGATCTCAC-3’ | 963 | 62 |
| TBX3 | NM_204453 | 5’-TAATGCTCTCCACCACCACA-3’ 1 | 5’-TCTGCTGGCTTGATGATTTG -3’ | 1001 | 57.8 |
| KCNE1 | NC_006088 | 5’ CTCCAAGCTGCTTCAAGACC 3’ | 5’TATGCTCGGCTGCTCTACTG 3’ | 313 | 57 |

### 2.6.4 Generation of probe template by end point PCR

End point polymerase chain reaction (PCR) was performed using Red Taq® DNA polymerase (Sigma Aldrich). PCR reactions were conducted in 20 µl reaction mixtures comprising of 1X PCR buffer, 250 µM deoxynucleotide mix (dNTPs), 0.25 µM of each forward and reverse primer, 0.05U of DNA polymerase and 1 µl of cDNA made up to a 20 µl volume with DEPC $H_2O$. The PCR reaction was carried out using a T100 thermal cycler (Bio-Rad laboratories Inc., USA). The cycling programme's initial denaturation and DNA polymerase activation step is 95 ºC for 3 minutes. This was followed by 34 cycles of 95 ºC for 30 seconds, and 30 seconds annealing temperature for each gene designed (see Table 2.2 for all genes in the project). The extension step was 72 ºC for 1 minute. The cycling program was ended by a final extension step of 72 ºC of 5 minutes.

### 2.6.5 Resolve primer products on agarose gel

A 1–1.5% agarose gel (Sigma Aldrich) was made with 1X-Tris-acetate-ethylenediaminetetraacetic acid (TAE) buffer and 0.1 µg/ml ethidium bromide (EtBr). 1.5% gels were used to resolve smaller sequences whereas less viscus gels were used for larger sequences. 5 µl (small volumes were used so that yields taken for PCR clean up were larger) of amplified PCR product was loaded onto the gel, alongside with 1 Kb plus ladder (Invitrogen) and run at 150 V for 25 minutes. The gel was visualized and photographed under UV light using GeneGenius Bioimaging System (Syngene, UK).

### 2.6.6 Purification of PCR product

Amplified PCR products were purified with GenElute ™ PCR Clean-Up Kit according to manufacturers' instructions (Sigma Aldrich). Filtered columns were prepared by

adding 0.5 ml column preparation solution followed by centrifugeation at 12,000 x *g* for 1 min. 5 volumes of binding solution was added to the PCR products. The mixture was transferred to a column and centrifuged at 12,000 x *g* for 2 minutes. PCR products bound to the silica membrane in the column were washed with wash solution containing ethanol. To elute DNA, 35 µl pre-heated 65 ºC autoclaved milliQ $dH_2O$ was added and incubated for 5 minutes at R/T followed by centrifugation at 15,000 rpm for 2 minutes. DNA concentration was checked by NanoDrop 2000c UV/IV spectrophotometer at 260 nm absorbance (Thermo Fisher Scientific).

### 2.6.7 ligation

Cloning procedure started with the PCR amplicons were ligated into 1 µl of pGEM-T Easy vector (50ng/µl) (Promega, UK) at either a 3 : 1 or 1 : 3 ratio of PCR product : vector catalyzed by 1 µl of 100u T4 ligase (NEB) in 5 µl of 2X rapid ligation buffer. The mixture was made up to 10 µl as final volume with water and left at 16 ºC overnight.

### 2.6.8 Transformation and selection

#### 2.6.8.1 Optimisation

The transformation and selection process required key optimisation to gain transfected single colonies. Initial optimisations yielded an overgrowth on selective agar plates and single colonies could not be obtained. Two optimisations were introduced that obtained clear selectable colonies. The first was dilution of the SOC plasmid. The solution was tested in a range of dilutions from initial concentrated resuspensions of just 300 µl following pelleting to 1:25 dilutions. It was found that a 1:20 dilution yielded the best colonies. The second optimisation was to vary ampicillin concentration in the selective media. 50 µg/ml and 100 µg/ml were both tested with 100 µg/ml yielding better results.

#### 2.6.8.2 Transformation and selection protocol

2 µl of the ligation mix was added to 30 µl 5α-high efficiency competent E.coli cells (NEB, UK). The solution was gently mixed by flicking. It was incubated on ice for 25-30 minutes then cells were subjected to heat shock for 2 minutes at exactly 42ºC in a water bath. This was followed by immediate incubation on ice for 2 minutes. 950 µl of super optimal broth (SOC) was then added and the competent cell/DNA mixture was incubated for a further 1 hour at 37 ºC. A 1 : 20 dilution of the mixture was made and 200 µl was used to plate out on the McConkey Agar containing 100 µg/ml ampicillin (in aseptic conditions) using a spreader. The plates were air-dried for few minutes with agar facing down and were then incubated for 16-24 hours at 37 ºC. Individual white colonies containing the insert were checked by end point PCR for the band of interest. This followed the same procedure as a normal PCR, however, it required an additional 15 minute at 95 ºC to lyse the bacteria.

#### 2.6.8.3 Inoculation and plasmid preparation (midiprep)

A single white colony positive for the band of interest was picked from the plate and used to inoculate a 5 ml starter culture in Luria broth (LB) with 0.1mg/ml ampicillin. It was incubated overnight at 37 ºC whilst shaking. A volume of 0.625 ml starting culture was made up to 50 ml (a 1:80 dilution) with LB media and was grown at 37 ºC shaking overnight. Once an optical density of 80 was obtained by spectrophotometer (Bio-rad) plasmid DNA was extracted using a plasmid Midi kit (Sigma Aldrich, UK). At this point 50 % glycerol stocks were also made of each gene.

Cells were harvested by centrifugation at 5000 x g for 8 minutes. The pellet was firstly homogenised with 1.2 ml resuspension solution followed by 1.2 µl lysis solution with gentle inversion for 4-5 minutes. 1.6 ml neutralising solution was added to the mixture when the solution became clear and viscous. It was then pelleted down by centrifugation at 15,000 x g for 15 minutes. Clear lysate was transferred to column

followed by centrifugation at 5000 x g for 2 minutes. The bound plasmid DNA was washed to remove contaminating bacterial components. They were finally eluted in 600 µl pre-warmed RNase free $H_2O$. The $H_2O$ elution (pre-heated to 65 ºC) was incubated on the fliter for 10 minutes before centrifugation at 4000 xg for 5 minutes. Yield was checked by NanoDrop 2000c UV/IV spectrophotometer and if below 250 ng/µl samples were concentrated by sodium acetate precipitation (explained in section 2.2.4.1 below). Template sequence was checked by sequencing (DNA sequencing department, University of Nottingham) using T7 specific primer. This was important not just to confirm the riboprobe had been cloned, but also for plasmid insertion orientation, enabling identification of the sense and antisense probe for riboprobe synthesis.

### 2.6.9 Linearisation

Plasmid DNA was linearised using the following steps: 15 µg of plasmid DNA, 7.5 µl NEB cut smart buffer, 1 µl specific restriction enzymes NcoII or PvuII and SpeI (NEB, UK) in 19 µl diluent and made up to 75 µl with DEPC-treated $H_2O$. Reactions were left at 37 ºC for 1.5 hours. All genes were linearised with NcoII,SpeI , PvuII or EcoRV (only used wth T3 vector)(Table 2.4). Following the reaction, purification of the linearised product was performed. 425 µl of DEPC-treated $H_2O$ was added to bring the volume up to 500 µl, with an equal volume of phenol/chloroform/isoamyl alcohol, pH 7 (Amresco) added for DNA extraction. The samples were mixed thoughly and centrifuged at 11,000 x g for 10 minutes at R/T. DNA was precipitated by the addition of 1/10 volume of 3M sodium acetate, pH 5.2 and 2 volumes of absolute ethanol. The mixture was inverted multiple times and incubated at -20 ºC overnight. DNA precipitate was collected by centrifugation at 17,500 x g for 15 minutes at 4ºC, washed twice with 70% DEPC-ethanol and finally suspended in 11 µl DEPC-treated $H_2O$. The concentration of DNA was determined by NanoDrop 2000c UV/IV spectrophotometer at 260 nm absorbance (Thermo Fisher Scientific) and samples were stored at -20 ºC.

### 2.6.10 Riboprobe synthesis

Synthesis of single stranded DIG-labelled RNA probes was performed using a DIG RNA Labelling Mix by in vitro transcription with SP6 or T7 RNA polymerases. The reactions were set up on ice in the following process: 6 µl of 5x buffer, 3 µl of 100mM DTT, 1 µl of 30 U RNase inhibitor (RNasin - Promega, UK), 3 µg linearized plasmid DNA, 3 µl 10x DIG RNA labelling mix (Roche Diagnostics Ltd, UK), 3 µl of (30 U-60 U) SP6 or T7 RNA polymerase (Promega, UK) and made up to final volume of 33.6 µl with sterile RNase free water. Reactions were incubated at 37 ºC for 2.5 hours. Table 2.2 give probe details. The full riboprobe synthesis and purification procedure can be found in appendix E.

**Table 2.3** Probe purification and quantification

| **Probe** | **Antisense:** Enzyme/RNA polymerase | **Sense:** Enzyme/RNA polymerase |
|---|---|---|
| *HCN4* | SpeI/T7 | NcoI/Sp6 |
| *CX42* | SpeI/T7 | NcoI/Sp6 |
| *CX43* | SpeI/T7 | NcoI/Sp6 |
| *CAV 1.2* | NcoI/Sp6 | SpeI/T7 |
| *TBX18* | EcoRV/T7 | NcoI/Sp6 |
| *TBX3* | PvuII/Sp6 | SpeI/T7 |
| *GAPDH* | NcoI/Sp6 | SpeI/T7 |

Optimisation of Purification

#### 2.6.10.1 Micro columns

Purification of riboprobes using ProbeQuant G-50 micro columns (Illustra) was carried out according to manufacturer's instructions. Firstly, the column was prepared by vortexing to re-suspend the resin. The cap was then loosened by one quarter turn, and the bottom closure was removed prior to the placement in the collection tube. The column was spun for 1 minute at 735 x g. The column was then placed in a new microcentrifuge tube. The DIG labelling reaction mix of 33.6 µl was applied to the top centre of the resin (being sure not to touch the sides), and the column was centrifuged at 735 x *g* for 2 minutes for elution. 2.5 µl was kept for gel analysis then 20 µl of post hybridisation buffer was added to each sample and probes were stored at -80ºC.

#### 2.6.10.2 Gel purification

A native gel with optimised denaturing sample buffer (as described below in section 2.2.4.4.2) was used to resolve bands. Probes were cut from the gel under minimal UV light and extracted in a stepwise manner following manufactures instructions using a GeneElute Gel Extraction Kit (Sigma-Aldrich). Purified probe samples were eluted in 30 µl RNase free $H_2O$.

#### 2.6.10.3 Comparison of purification technique

To determine the optimal purification procedure in terms of yield, samples from gel and column purification were run alongside each other on a further gel (Figure 2.1). Each sample came from the same riboprobe synthesis reaction so riboprobe yeild should be identical in both wells. The gel revealed that gel purification led to loss in ribobrobe amount when compared to the column purified sample. Therefore column purification was used in this project for all synthesized riboprobes.

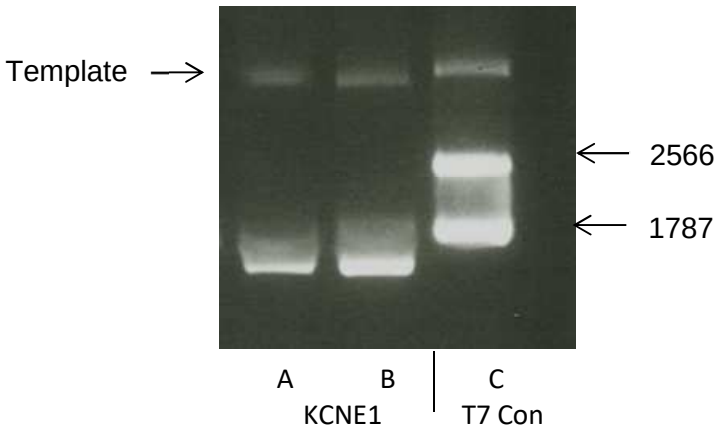



**Figure 2.1** Gel purification leads to greater loss of riboprobe when compared to micro columns. A, Shows KCNE1 gel purification. B, Shows microcolum purification. C, Shows the T7 control that was synthesised alongside KCNE1 at the same concentration. The control denotes band size with the upper band at 2566 and the lower at 1787.

### 2.6.11 RNA gel and estimation of concentration

### 2.6.12 RNA gel optimisation

Initial gels used for optimisation were full MOPs denaturing gels used with a bought in RNA sample denaturing buffer (thermos Fisher). However, gels yielded no bands. The denaturing buffer was then made up to include both deionized formamide and formaldehyde. This new buffer now yielded strong bands in expected positions in both denaturing gels and native gels. For ease of use, from this point on native gels with the made up denaturing buffer were used (see appendix B for full buffer and denaturing gel details).

### 2.6.13 Native gel with RNA denaturing buffer

An aliquot of riboprobe (2.5 µl) and a positive control T7 (2.5 µl) was electrophoresed on the 1% agarose gel to check the size and integrity of the riboprobe synthesized. Reaction was set up as follows: 2.5 µl of riboprobe or T7 control, 7.5 µl denaturing buffer, 2.5 µl EtBr and 2 µl 6X Gel loading dye buffer (NEB, UK). The samples were put at 67 ºC for 8 minutes, snap cooled on ice and then instantly pipetted in to the gel. This allowed partial denaturation of probes with little secondary structure. The buffer was pre-cooled 1X TAE running buffer and the gel was run at 70V for 1.5 hours. The T7 control probe allowed accurate estimation of band size, and comparison of DNA template band and riboprobe band allowed rough estimation of riboprobe yield (see figure 2.1).

## 2.7 Whole mount *In situ* hybridisation

The in situ hybridization process was optimised. Initial attempts yielded over stained embryos that were impossible to use. Clean embryos were obtained by increasing formaldehyde concentration and salt concentration was decreased in the washes (Figure 2.1) (all optimised solutions are show in appendices B and C). Following this initial optimisation, individual gene concentration and hybridisation temperature were optimised. From early (HH16) to later development (HH35) the proteinase K and fixation steps were also optimised to ensure penetration and signal accuracy. In the following protocol, when a range is given this is so adjustment can be made accordingly due to tissue size/structure.

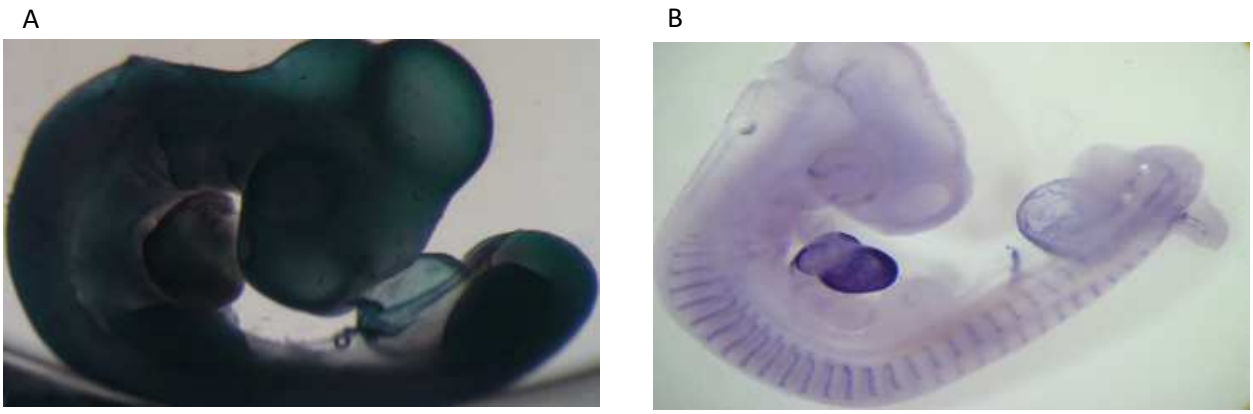



**Figure 2.2** *In situ* hybridisation Colour intensity optimisation. A, Overstained background embryo before wash optimisations. B, Clean background upon optimised *in situ* hybridisation.

### 2.7.1 Embryo collection and preparation

All embryos were dissected with autoclaved sterile forceps and placed in ice-cold DEPC-treated PBSt. Whole HH20 and HH25 embryos were de-membraned and a hole was made at the base of the hind brain as this area can accumulate BM purple during

the colour reaction step. This was not done for HH16 whole embryos, where because of their delicate nature, de-membraning was carried out after fixation. At HH29 whole hearts where isolated from the embryos and at HH35 the isolated whole heart was bisected by a frontal cut separating the heart into anterior and posterior hearts. All embryo's/hearts were fixed in 4% PFA at 4ºC overnight. Embryos were washed with DEPC-treated PBS with 0.1% Tween (PBSt), followed by dehydration of a graded methanol series (Sigma Aldrich, UK).The methanol series was a key step as early optimisations led to dehydrated shrunken embryos. Because of this two additional steps and 3 repeats in each step were utilized. The solutions were pre-made and at 4ºC, however, the dehydrations were carried out at room temperature on a slow rocker plate. For each change of solution, 1/3 was always retained from the previous repeat/step. This ensured embryos remained covered with solution whilst also providing a very gentle gradient into each step. Each repeat was 15 – 30 minutes depending on the stage of the embryo. Each step was carried out in X3 PBSt /methanol (%): Step 1, 75/25; Step 2, 50/50; Step 3, 75/25; Step 4, 5/95, Step 5, 100/0. Embryos/ hearts could then be stored at -20ºC for a maximum of two weeks before *in situ* hybridization.

### 2.7.2 *In situ* hybridisation protocol

Embryos or hearts were hydrated with a graded series of methanol made up with DEPC PBSt in the exact reverse of the dehydration reaction. If not already in one, embryos were transferred to a 24 well plate for the proteinase K step 0.02mg/ml of proteinase K (Sigma Aldrich, UK) in DEPC-PBSt was added for 17 minutes – 2 hours (depending on toughness of tissue).The proteinase K reaction is stopped by treating wells with 2mg/ml glycine (Fisher Scientific, UK) 5 – 30 minutes X2 followed by a rinse wash in PBSt and two 5 – 30 minute PBSt washes. Embryos/hearts were then re-fixed in 4% PFA (Sigma Aldrich, UK) for 20 – 45 minutes at R/T followed by another X3 5 – 30 minute minutes DEPC-PBSt washes. Embryos/hearts were then washed with 75 % hybe buffer (see appendix C for details) in PBSt. This step lasts until embryos sink. Hybridisation solution without probe was added to the wells for a pre-hybridisation

step. This mix contained 0.1 % CHAPS and the 24 well plate was incubated in a hybridisation oven at 65 °C for 3 - 6 hours. In order to keep evaporation to a minimum in the pre-hybridisation and the subsequent hybridisation step, the 24 well plate was placed inside a hydration chamber, sealed, and then placed inside the hybridisation oven on its rocker plate. Following pre-hybridisation, the mix was replaced with an identical solution that this time contains the probe. Each probe was optimised to find the correct concentration, but generally 4 µl probe in 750 µl worked well (this is an estimated 1-2 µg/ml). Incubations were at least 16 hours and up to three days and were at the optimised temperature (normally 65 °C).

Following hybridisation was the wash step. This contained a range of washes, each one becoming progressively more stringent: 1$^{st}$ wash, 50/50 post-hybe/d$H_2O$ for 15 minutes to 1 hour X2; 2$^{nd}$ wash, SSCx2 for 15 - 30 minutes X3; 3$^{rd}$ wash, SSCx0.2 for 15 -30 minutes X4 4;$^{th}$ wash, (this was not a stringent wash, instead its purpose was to slowly introduce MABt) SSCx1 in 50 % MABt for 10 – 30 minutes X1 (see appendix C for details and preparation of washes). The next step was 100 % MABt for 10 – 30 minutes followed by RNase digestion. RNase treatment (100 µg/ml) (Sigma Aldrich, UK) was performed on sections to remove of non-hybridized single stranded RNA probe for 30 minutes to 1.25 hours at 37 ºC with agitation every 10 minutes. Wells were washed by MABTw X3 for 10 minute to 1 hour. Embryos/hearts were blocked with 2% Boehringer Blocking reagent ™ (Roche) in MAB with 20% sheep serum (Sigma Aldrich, UK) for at least 3 hours at R/T. The antisense RNA probe was labelled with an anti-digoxigenin-alkaline phosphatase (AP) Fab fragment (Roche) at 1 : 5000 /4000 (depending on expression) in 1% Boehringer Blocking reagent and 5 % sheep serum overnight at 4 ºC. Wells were washed with MABt for 45 mins X7 and left overnight in a final MABt step at 4 °C on a rocking platform.

Embryos were equilibrated with BCL (colour development) buffer III containing 5mM levamisole (Sigma Aldrich) for three times 15 minutes each at R/T. mRNA signal was detected by incubating the wells in fresh BM purple AP substrate (Roche) to BCL buffer III in a 1 : 1 ratio (can be higher ratio). The plate was kept in the dark on a rocker plate for the colour development from 1 hour to 8 hours. After 8 hours the reaction was stopped (or stopped earlier due to saturation) and wells were washed in PBSt 3 times for 5 - 15 minutes. From here the reaction can be re-applied the next day or

permanently fixed with 4% PFA for 15 minutes at R/T. Pictures were taken before fixation in 100 % glycerol. A dilution series into 100 % was used to be sure not to shrink the embryos/hearts.

## 2.8 Quantitative PCR (RT-qPCR)

### 2.8.1 Harvesting and RNA isolation for RT-qPCR

Embryos were harvested and placed in ice cold Diethylpyrocarbonate (DEPC)-PBS (Sigma Aldrich, UK). Decapitation was performed in ovo in accordance with institutional and UK Home Office guidelines. Hearts were dissected from the embryo using sterile autoclaved forceps and were then placed in RNase free micro-centrifuge tubes (3 hearts per tube). The heart tissues were snap frozen in liquid nitrogen and stored at -80 ºC.

The original RNA isolation protocol was re-optimised for RT-qPCR and RNA sequencing. These techniques require negligible levels of gDNA and low levels of contaminants. (Please see optimised method in the RNA sequencing section 2.3.2 and)

### 2.8.2 cDNA First strand synthesis for RT-qPCR validation and all other analysis

The original cDNA synthesis protocol was re-optimised for RT-qPCR with changes made to reverse transcriptase and hexomers. Reverse transcription reactions were performed using SuperScript® II Reverse Transcriptase (Invitrogen, UK) following manufacturer's instructions in either 10 or 20 µl reactions. This protocol is based on 20 µl. Even amounts of RNA were added to each reaction (normally 1 µg, but if not possible, the same amount of the lower concentration was always added to each reaction (superscript II has a 1 ng – 5 ng range)) into a RNase-free tube with 50 ng (1.25 µM) hexamers and 0.5 mM dNTPs. The mixture was made up to a total volume of 10.5 µl using RNase free $H_2O$ if needed (depended on concentration of starting

RNA) (Invitrogen, UK). The mixture was heated to 65 ºC for 5 minutes and cooled on ice instantly (adding straight to ice reduces secondary structure formation). 4 µl of 5X reverse transcriptase buffer (Invitrogen, UK), 2 µl of 0.1 mM 1,4-Dithiothreitol (DTT) (Invitrogen, UK) and 0.5 µl of RNase free $H_2O$ (Invitrogen , UK) were added and mixed well. 0.5 µl of RNase OUT (Invitrogen, UK) was added and the mixture was incubated at 25 ºC for 2 minutes. 1 µl superscript II enzyme (Invitrogen, UK) was added to the mixture to give a final total volume of 20 µl. The reaction was heated to 25 ºC for 10 minutes and then to 42 ºC for 50 minutes. The mixture was finally heated to 70 ºC for 15 minutes to deactivate the enzyme and stored at -20 ºC. The cDNA reaction was tested for consistency by RT-qPCR, where the SuperScript II reaction was shown to be highly reproducible (results section 5.2.3).

### 2.8.3 Primer design and optimisation for RT-qPCR

The entire qPRC process was optimised from the designing and optimisation of all primer pairs to the RT-qPCR procedure itself. For Quantitative PCR (RT-qPCR) primer pairs, genes and splice variants were found in NCBI gene and primers were designed using the NCBI design tool to incorporate all known splice variants whilst not potentially on any SNP sites. Primers where checked using NCBI blast tool for 'Reference RNA sequencing' sequences. Ref RNA seq must be used as most primers are designed spanning exon boundaries. Primer design for RT-qPCR differs to that of end-point PCR primers as there are strict parameters that must be adhered to.

### 2.8.4 Exon/exon spanning/ or intron inclusion

Though all RNA was treated to remove gDNA (see section 2.2.8.1), primers were designed either on exon/exon boundaries or including introns >1000 bp. This ensures that no amplification of gDNA can take place. Exon/exon boundary primers were always designed unless impossible to do so because of primer parameters or splice variants. In these cases intron inclusion primers were designed instead. Exon/exon boundary primers have the advantage of not being limited to introns of >1000 bp (taq polymerase synthesizes at 1000 bp / min). Another advantage is that they will only

bind to their specific sequence i.e. they will not bind at all to gDNA or splice variants that are not its target, thus PCR efficiencies can be improved as all primers are available for synthesis of the intended sequence. In instances when it was impossible to design primer pairs at exon/exon boundaries or including introns, e.g. in small genes with no introns like ENS-1 and ERNI, an RT- (cDNA synthesis reaction with reverse transcriptase not added) was always run in the RT-qPCR as a negative control. In order for results to be valid, the RT- Cq must be negligible and could not be within 10 cycles of the experimental samples (10 cycles = 1024 fold). Additionally, primers were not designed on areas of low complexity, as this can increase the chance of gDNA binding.

### 2.8.5 RT-qPCR product size

Fragments were designed to be 90 – 210 bp. Fragment length is key as too short and it would be hard to distinguish the product from potential primer dimers in the RT-qPCR melt curve. Too large a fragment size can lead to inefficiencies as the larger synthesis time is more likely to be inhibited from artifacts left over from cDNA synthesis. This can be a particular issue with low expressing genes where high amounts of template were used in the RT-qPCR reaction. Another reason is that longer fragments are more likely to be effected by fragmentation, and so inaccuracies could occur if RT-qPCR is carried out post fragmentation (Sedlackova et al., 2013).

### 2.8.6 Primer details

Primers were designed to a Tm of 62 °C (+/- 1 °C). Tm is the theoretical temperature at which half of the primer is dissociated from its compliment and is defined by primer length and GC content. GC content was 50 – 60 % and primers were made up of 20 – 24 nucleotides. Higher Tm and annealing temperature lead to increased specificity and decreased dimer formation. For RT-qPCR, optimised annealing temperature is commonly the same as the theoretical Tm, as it is vital that genuine signal is clear whilst background from dimers is minimal. To reduce dimer formation, 3’ end heterodimers had low complimentary energies ($\Delta G < -3$), with a maximum of 2 GCs at

the 3’ end (over last 5 bp). This prevented dimer extension by DNA polymerase. For other dimer formations ΔG <-9 was acceptable. Primers with secondary structure with low free energy close to primer annealing temperature were not considered e.g. a ΔG of -10 at 55 °C is not permitted, but a ΔG of -30 at 5 °C is acceptable. IDT Oligo Analyser 3.1 was used to check all energies. Product secondary structure was also checked using mfold online software.

### 2.8.7 End point PCR

End point PCR was carried out over a temperature range using cDNA from the same developmental stage as that of the eventual experimental samples. Initial PCRs used 10 temperature points with -5 Tm in the center of the range. However, after experience with many RT-qPCR primers the temperature was increased and range reduced. Annealing temperatures used were 64°C, 62°C and 60°C (62°C being the theoretical Tm of all primer pairs). Depending on the expression of the gene, fewer cycles were used so that the reaction did not reach end point and a true comparison between temperatures could be sort by agarose gel analysis. The annealing temperature with a clear single specific product band and no/minimal primer dimers was used for RT-qPCR optimisations. If primer pairs subsequently could not be optimised at this temperature, then the same experiment can be repeated by RT-qPCR to accurately determine melting temperature. However, our technique of temperature optimisation by endpoint PCR yielded good results at RT-qPCR and confirmed expression for all primer pairs.

### 2.8.8 RT-qPCR standard curve

In order to perform relative quantitation RT-qPCR it is necessary to assess the amplification efficiency of primer pairs. This is because quantitation is a relative measure, and so gene of interest and reference genes must have the same efficiency

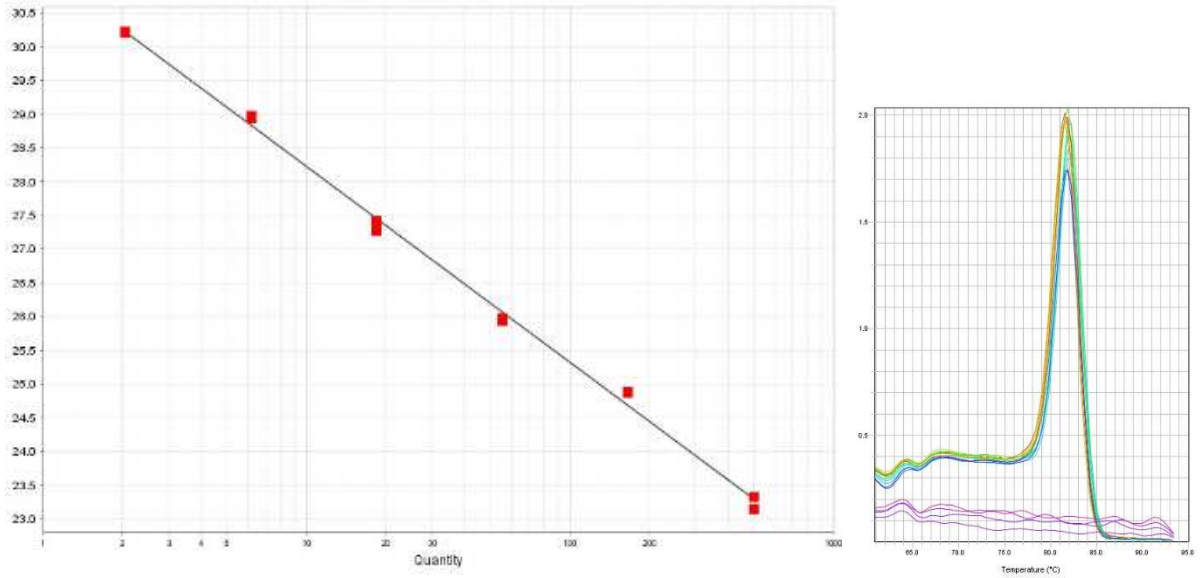
or close efficiencies with known differences to allow for correction. All three reference genes used in this project had efficiencies of 100 – 105% and all genes of interest had efficiencies of 95 – 110%. Results must also be consistent at each concentration with $R^2$ values 0.98 or above. To assess efficiencies a dilution curve is generated by RT-qPCR so that the increases in concentration can be compared to expected increases i.e. a 10 fold series dilution should have Cq values 3.3 cycles apart ($2^{\Delta\Delta CT}$, so $2^{3.3}$ = 10) if 100% efficient amplification is seen. In order to gain a good efficiency, optimal conditions for the primer set must be established. Universal SYBR green (Biorad) must be used under specific buffer conditions. It comes in a 2X mix containing $MgCl_2$, dNTPs, Taq polymerase, enhancers, stabilizers and reference dye Rox. This mix is diluted 1:1 for a final 1X mix in the RT-qPCR reaction. Because of this there are only three variants that can be manipulated to find optimal synthesis conditions; 1, template concentration; 2, primer concentration; 3, annealing temperature. For annealing temperature, 62°C was used across all primers, but template concentration and, to a lesser extent, primer concentration was varied (Tqable 2.3). The PCR was performed using 96 well plates (MicroAmp; Applied Biosystems; Cat No. N801-0560) covered with optical adhesive films (Applied Biosystems; Cat No. 4313663). The instrument used was the Applied Biosystems 7500 Fast Real-time PCR system under the following thermal cycling conditions: a single heat-denaturing step at 95 °C for 25 seconds, followed by 40 cycles of denaturation, annealing and extension at 95 °C for 20 seconds and 62 °C for 1 minute (annealing and extension both carried out at 62 °C). Reaction volumes were 20 µl and each well was run in duplicate for optimisations (but triplicate for relative RT-qPCR) (duplicate and triplicate SD <0.02). Each 20 µl PCR reaction mixture consisted of 10 µl of iTaq™ universal SYBR® Green supermix (1X), 0.5 - 0.75 µl (0.25 - 375 nM respectively) of primer pairs and varied amount of diluted cDNA template based on the individual gene. Following the PCR reaction, a melt curve was performed. The melt curve was run from 65 °C to 95 °C using 0.5 °C increments. As the temperature increases structures present dissociate and no longer generate SYBR/dsDNA signal. This information can be used to elucidate structures present, of which three are possible; 1, dimer formation; 2, intermediate specific product dissociation (rarely seen); 3, specific product.

### 2.8.9 Interpreting results and cDNA dilution for relative RT-qPCR

High efficiencies are caused for the most part by inhibition of the polymerase reaction at high template concentrations (Figure 2.2 shows high efficiency in MYL1). This is caused by artefacts and solvents left over from RNA preparation and cDNA synthesis. As the template volume reduces at each dilution, so to do the inhibitors and thus the reaction proceeds normally in more dilute samples. This gives the impression of higher than 100 % efficiency as more dilute samples come in earlier than expected compared to the less dilute e.g. in a 1:10 dilution, each step should be 3.32 cycles apart. If an early dilution is inhibited it will come in at a late Cq; if the next dilution is not inhibited it will come in at an earlier than expected Cq when compared to the earlier dilution, so less than 3.32 cycles. It is possible that primer dimers could also cause high efficiency, however this was rarely the case, as can be seen in Figure 2.2 no primer dimers were present with the high efficiency seen. Generally speaking, primer dimers were not an issue as end point PCR was performed before RT-qPCR. If off target bands were present, then primers were redesigned before proceeding to RT-qPCR. Conversely, it is possible that if primer concentration is too low for high template concentration, which would again make the reaction appear over efficient through the dilutions. However, this very rarely happened in this study. Figure 2.3 B shows MYL1 run at a lower starting template concentration. The new dilution now starts where the previous optimisation showed no inhibition, around dilution 3, and now has good efficiency and $R^2$. High efficiency is also seen in Figure 2.3 A, but this time the result is inconsistent as half of the dilutions Cq values were coming in near or over 35 Cq. This happens when template concentration is too low and the polymerise reaction can not take place consistently. This type of inconsistency could also cause low efficiency, however it will always lead to a poor $R^2$ and so is easily identifiable. Increasing template volume allows the reaction to perform consistnty over the dilution range and thus a good $R^2$ and efficiency is gained (Figure 2.3 B). If starting template volume is already high, then the dilution factor can be reduced instead, e.g. from 1:3 to 1:2. Low efficiency was much less of a problem as primers were always designed to strict parameters and pipetting was always consistent and accurate with calibrated pipettes. Low efficiency can also be caused by contamination that is large enough to effect all samples in the

dilution series; this was never the case in this study. To ensure that contamination was not a major problem RNA purity was checked post first strand cDNA synthesis by NanoDrop 2000c UV/IV spectrophotometer (Thermo Fisher Scientific) at 260 nm absorbance for RNA. A260/280 ratios were 1.90 – 2.20 and A260/230 ratios were 2.0 – 2.20. RNA quality was assessed by RIN values (see result 5.2.2.2). If it was RNA that was also used for RNA sequencing, then concentration was assessed via qubit assay (Thermo Fisher Scientific). This gave accurate concentration readings as second strand synthesis includes a purification step removing excess nucleotides and hexamers that interfere with concentration estimation. The template dilution for relative RT-qPCR was a point mid-way on the dynamic range of the standard curve. Generally, the dilution factor used was 1:330 (figure 2.4). The dilution used was 1:3. This was changed from the initial optimisations that were 1:10, however this dilution could only be used with very high expression genes and so was changed to a more practical dilution for our cDNA of 1:3.

A




B

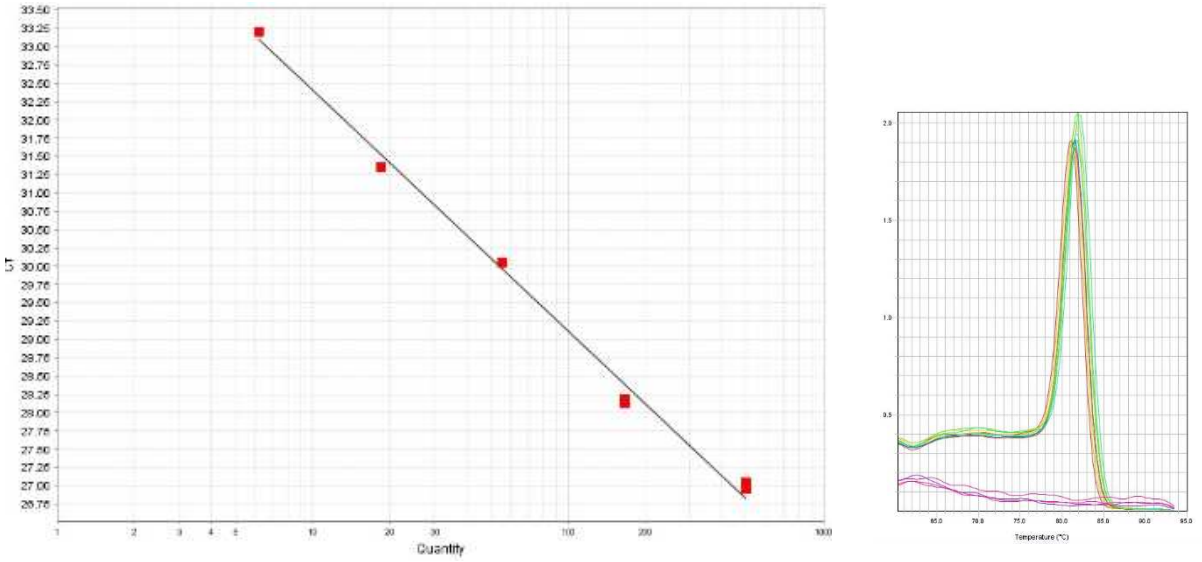
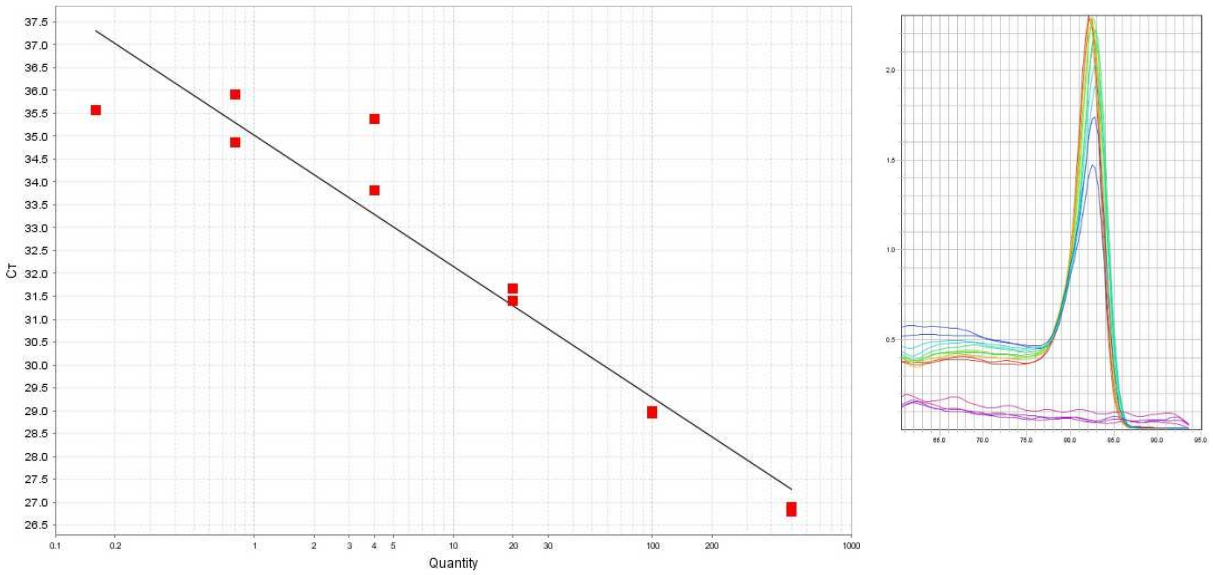



**Figure 2.3** RT-qPCR high efficiency optimisation. A, High efficiency (120 % of MYL gene) caused by inhibition at high concentration B, Rectified efficiency (102 r2 = 0.995) by decreasing starting concentration. No dimers present.

A




B

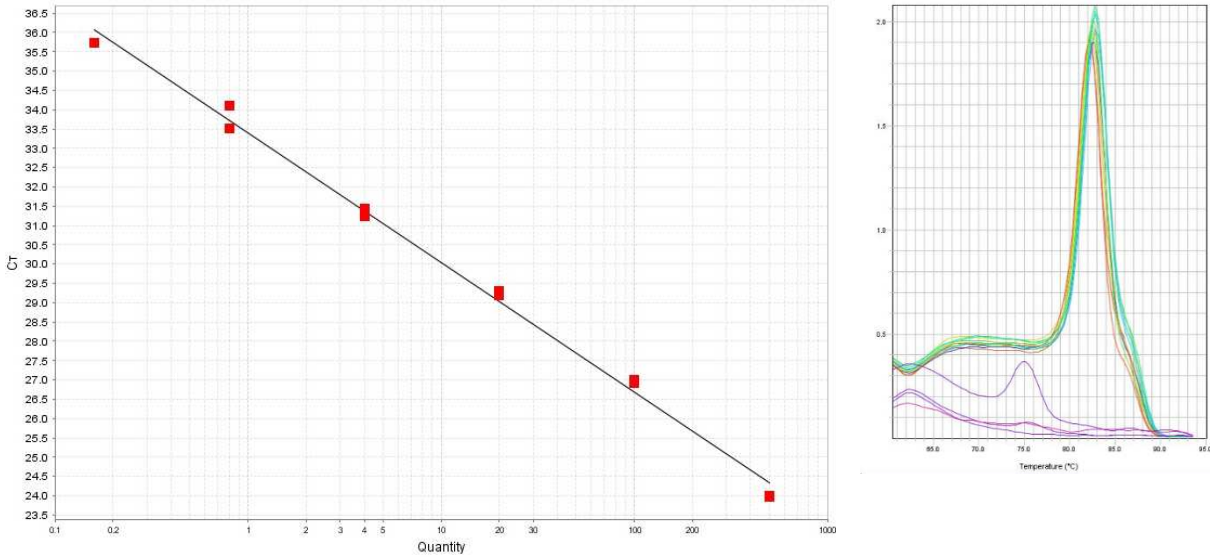



**Figure 2.4** RT-qPCR low $R^2$ optimisation. A, High efficiency and low $R^2$ (115 %, R2 = 0.927 of *PRKAG3* gene) this time caused by low concentration giving inconsistencies. B Rectified efficiency (99 % $R^2$ = 0.995) by increasing starting concentration. No significant dimers present.

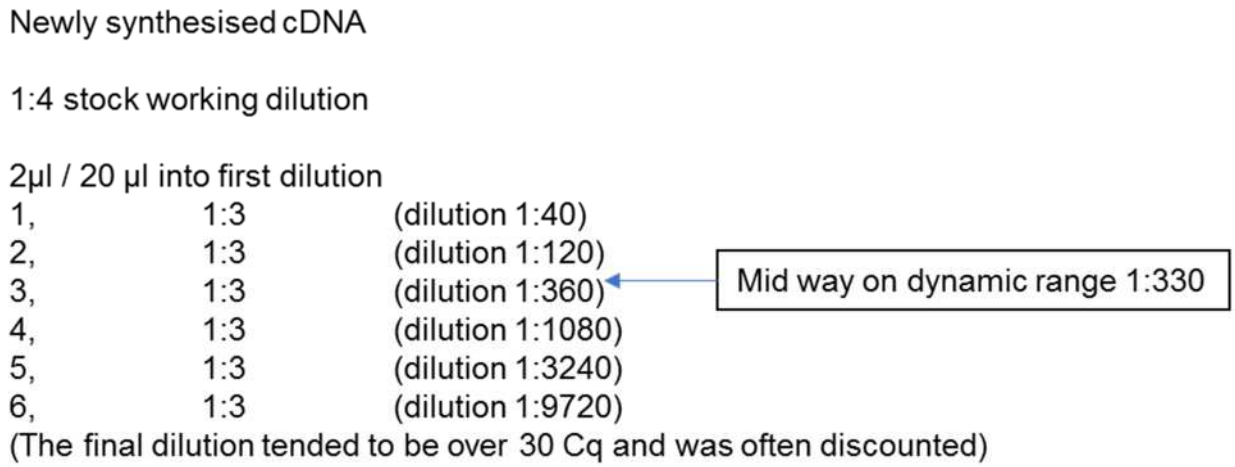



**Figure 2.5** The dilution series used for RT-qPCR primer optimisation. Brackets show the final dilution in each sample.

### 2.8.10 Relative quantitation

Quantitative assessment of gene expression by RT-qPCR was carried out in the optimised conditions for each gene. The same protocol was followed as for RT-qPCR optimisation, but now at the set template dilution (normally 1:330), primer concentration and annealing temperature (normally 62 °C).

### 2.8.11 Expression equation

The threshold cycle number for product detection (Δ T value) was used to calculate the relative gene expression using reference genes (*GAPDH*, and *EEF1A1* or *TBP*) using the Pfafll method (Figure 2.5) (Pfaffl, 2001). The Pfafll method takes the ΔΔCt and adjusts it for efficiency. This is because the ΔΔCt is a relative method that assumes that both primer sets have the same efficiencies, though our efficiencies were all very similar.

$$\text{Fold Change} = \frac{\text{Efficiency}_{\text{target}}^{\text{deltaCt}_{\text{target}}\,(\text{control-sample})}}{\text{Efficiency}_{\text{reference}}^{\text{deltaCt}_{\text{reference}}\,(\text{control-sample})}}$$

**Figure 2.6 Calculation of fold change**. The fold change equationis based on the ΔΔCt, but adjusted for primer pair efficiencies (Pfaffl, 2001).

### 2.8.12 Statistics

Statistics were carried out on normalized change in Cq values between OFT-banded and SHAM. It was checked that all data conformed to parametric principles by shapiro-wilk test, and variance between samples by F-test. A confidence interval of 95 % was checked as was standard error. Independent T-test assuming equal or unequal variances (depending on data) were carried out on individual genes. Genes with $p<0.05$ were considered significant.

**Table 2.4** Primer pairs and optimal conditions for RT-qPCR

| Gene | Forward sequence/Reverse sequence | Volume of cDNA (n/20µl) dilution ratio (n:n) | Primer volume (µl) (concentration (µM) | Annealing temperature (°C) | Efficiency (%) | $R^2$ |
|---|---|---|---|---|---|---|
| HBB | AAGCCGTGAAGAACCTGGACAA | | | | | |
| | CAAATTGGCAGGCAGGAGTGAAA | 2 (1:330) | 0.5 (0.25 uM) | 62 | 99 | .99 |
| HBG1 | GGGGAAGCCGTGAAGAACCT | | | | | |
| | GTCGGGGTGAAGTCCTTGGT | 2 (1:330) | 0.75 (0.375 uM) | 62 | 109 | .99 |
| HBG2 | TGTGGACCCCGAGAACTTCA | | | | | |
| | CAAATTGGCAGGCAGGAGTGAAA | 2 (1:330) | 1 (0.5 uM) | 60 | 107 | .98 |
| HBZ | TGGTCACGGCTCCAAGGTCC | | | | | |
| | ACGCAGCATGAACTTCTGGGGT | 2 (1:330) | 0.75 (0.375 uM) | 62 | 97 | .99 |
| | TGACCAGGTCCGTGGCCATG | | | | | |
| HBAD | ACAGCAGACACGGCAGACAGG | 2 (1:330) | 0.75 (0.375 uM) | 62 | 102 | .98 |
| | GTATGGCGCCGAGACCCTGG | | | | | |
| HBAA | TGTGGGCATGGAGGTCGCTG | 4 (1:165) | 0.75 (0.375 uM) | 62 | 101 | .99 |
| | GTCCGCCCCACAGGTAGAAA | | | | | |
| GJA5 | GTCCCACGGGCTGAGAACTTCA | 2 (1:330) | 0.75 (0.375 uM) | 62 | 103 | .99 |
| PRKAG3 | TCAACATCCTGCACCGCTACT | | | | | |
| | GGCGTCGAAGAGGCTATCACTT | 2 (1:330) | 0.75 (0.375 uM) | 62 | 109 | .98 |
| LDHB | ATCCTCGGCAAGGGTCTTTGT | | | | | |
| | CCACAATCTTGGAGTTGGCTGT | 2 (1:330) | 0.75 (0.375 uM) | 62 | 106 | .99 |
| HDAC7 | AGAACCCCAAGGCCATCCAG | | | | | |
| | GTTTTCACCATGCGCTTGCC | 2 (1:330) | 0.75 (0.375 uM) | 62 | 110 | .99 |
| GAPDH (exon/exon) | GGGTGGTGCTAAGCGTGTTATC | | | | | |
| | ACCCTCCACAATGCCAAAGTTG | 4 (1:165) | 0.75 (0.375 uM) | 62 | 100 | .99 |
| GAPDH (Intron) | AGACGGTGGATGGCCCCTCT | | | | | |
| | ACGGCAGGTCAGGTCAACA | 2 (1:330) | 0.75 (0.375 uM) | 62 | 100 | 1 |
| EEF1A1 | GCTCTAACATGCCCTGGTTCAAG | | | | | |
| | GAAACTGGTGTCCTGAAGCCA | 2 (1:330) | 0.75 (0.375 uM) | 62 | 104 | .98 |
| NOS3 | ACCTACCAGAGCGAGAACGG | | | | 107 | |
| | CTGCCAGAAGCTGCGGAAT | 6 (1:109) | 0.75 (0.375 uM) | 62 | | .98 |

| Gene | Forward sequence/Reverse sequence | Volume of cDNA (n/20µl) dilution ratio (n:n) | Primer volume (µl) (concentration (µM) | Annealing temperature (°C) | Efficiency (%) | $R^2$ |
|---|---|---|---|---|---|---|
| | GGAAACTGCGTGACTGGACA | | | | | |
| MYL1 | ACTCAGAGGTGTTGGGTGGTG | 2 (1:330) | 0.5 (0.25 uM) | 62 | 96 | .99 |
| | GCATCTTCGACAAGAACGCTGA | | | | | |
| TNNC2 | CCCTTACTGCACACCCTCCAT | 2 (1:330) | 0.75 (0.375 uM) | 62 | 102 | .99 |
| | ATGGCGTAGTCGGCAGGATAC | | | | | |
| ENS-1 | CGATCTTCCTGGAGAGGTGCT | 2 (1:330) | 1 (0.5 uM) | 60 | 104 | .98 |
| | TTCACCGCAACAGTGGAGACT | | | | | |
| ERNI | GTAGAGGAGGATCGGAAGGC | 2 (1:330) | 0.75 (0.375 uM) | 62 | 108 | .99 |
| | GGCGATGACTGACGTGCTCA | | | | | |
| PVALB | TCAACCCCACCATCTCAAAGAACT | 2 (1:330) | 0.75 (0.375 uM) | 62 | 97 | .98 |
| | GAGACAACCTCAAGCTCTCCAAG | | | | | |
| S100A11 | GCGGGGTCCTTCTGATTCTTTG | 4 (1:165) | 0.75 (0.375 uM) | 62 | 107 | .99 |
| | CACCAAACCTGAACTGGATGCC | | | | | |
| DNAJC6 | AGTGGGACCTTTACCTGCCAA | 2 (1:330) | 0.75 (0.375 uM) | 62 | 104 | .98 |
| | GATGTGCCAGCCAGAGAGACAA | | | | | |
| TBX3 | CAGCCTCCAGCCTCTTCATTTTC | 2 (1:330) | 0.75 (0.375 uM) | 62 | 102 | .98 |
| | CCGGGGAGACGTGGATGAGA | | | | | |
| TBX18 | GGCTTTACCGGGGACAGATCATC | 2 (1:330) | 0.75 (0.375 uM) | 62 | 111 | .99 |
| TBP | TGGTCAAACTCCCCAGCTCTTC | | | | | |
| HCN4 | TTCGGGCACGAAGTGCAATG | 2 (1:330) | 0.75 (0.375 uM) | 62 | 104 | .99 |
| | TGAGCGAGCCCCTCCGAGAG GCCAATGGTGCCCTCCCGAA | 2 (1:330) | 0.75 (0.375 uM) | 62 | 101 | .99 |
| | | | | | | |

## 2.9 Outflow tract banding project

### 2.9.1 OFT banding

The banding procedure was carried out and optimised by Dr. Pang. Embryos were incubated to HH21 (approximately 4 days 4 hours of development) then taking for OFT banding treatment. A small window was made on the blunt end of the shell and the underlying inner shell membrane was removed to expose the embryo for staging. Any embryos that showed haemorrhage upon surgical manipulation or displayed obvious structural malformations or developmental retardation were excluded from the studies.

A swaged needle with 3/8 circle spatula advanced micro-point double needle attached to 10-0 suture with the length of 13 mm (W1770 Ethilon, Johnson Johnson) was used for the procedure. The needle body was grasped in the holders on its flattened area approximately one-third of its length away from the suture material. The needle was passed between the mid-portion of the OFT and the primitive atrium in ventral-dorsal direction in ovo with slight pronation of the wrist. Force was applied in the natural curve of the curvature of the needle by rotating the wrist. When the needle emerged from the opposite site of the OFT, it was retrieved from the other end by grasping approximately one-third from needle tip and was pulled through following the natural arc of the needle. Suture was also be pushed through on the other end.

A loop was formed in the suture and the end of the suture was passed through the loop to make a first overhand knot. The end of suture was then passed through the loop again to make a secure double overhand knot. A completed knot should be snug surrounding the OFT, but not tight. Excess suture on one end was trimmed but not to the extent of causing slippage of the knot. The window was then sealed with masking tape, and the eggs were reincubated with no rotation to HH29 (a further 3 days 4 hours) or HH35 (another 5 days 4 hours).

Three groups of embryos were studied; 1, UT group, in which no interventions were performed; 2, sham group in which a 10-0 nylon suture was passed under the OFT

but not tightened and was removed immediately; 3, outflow tract banding (OFT-banded) group, in which a 10-0 nylon suture was passed under the OFT and tied in a double knot around the OFT as described above. The OFT-banding procedure was performed using SV11 stereomicroscope (Zeiss, Germany).

Harvesting and RNA isolation

### 2.9.2 Harvesting

HH29 or HH35 embryos were harvested and placed in ice cold Diethylpyrocarbonate (DEPC)-PBS (Sigma Aldrich, UK). Decapitation was performed *in ovo* in accordance with institutional and UK Home Office guidelines. The hearts were dissected from the embryo using sterile autoclaved forceps and were then placed in RNase free micro-centrifuge tubes. The heart tissue was snap frozen in liquid nitrogen and stored at -80 $^{o}$C.

### 2.9.3 Optimisation

The RNA isolation method was optimised to ensure gDNA and contaminants were removed and samples were of sufficient purity. This is important as contaminants can interfere with polymerase reactions during RT-qPCR or RNA sequencing by synthesis. It was also important to determine that large enough RNA yields could be gained from HH2O hearts.

To test for gDNA contamination, *GAPDH* primers were designed to contain a 100 bp intron so that cDNA generated from the RNA could be tested. If gDNA was present, a band would appear 140 bp higher than expected. Initial optimisations yielded results with gDNA contamination in negative control samples (RT-; cDNA reaction with no reverse transcriptase added) following end point PCR at 40 cycles and subsequent agarose gel electrophoresis (Figure 2.6A).

To address this, two modifications were made. Firstly, the phenol/chloroform step was altered in order to separate RNA from DNA. The new step used phenol/chloroform solution of lower pH than the original protocol (from pH 7 to 5.2). This causes the more acidic DNA to partition at the interphase, whilst the aqueous phase now mostly contains RNA. Secondly, the time period of DNase treatment was increased from 10 to 15 mins and the solutions were held and mixed gentle and continuously between fingers for the time period. This removed the gDNA (Figure 2.7B). To ensure purity an addition chloroform step was added following phenol/chloroform treatment in order to remove phenol. At the end of preparation two addition washes in RNase free 70 % ethanol were added and the ethanol was evaporated before pellet resuspension. RNA was checked with NanoDrop 2000c UV/IV spectrophotometer where RNA yields were 250 – 400 ng/µl for HH 29 whole hearts and 120 – 220 ng/µl for HH2O. A260/280 ratios were 1.90 – 2.20 and A260/230 ratios were 2.0 – 2.20.

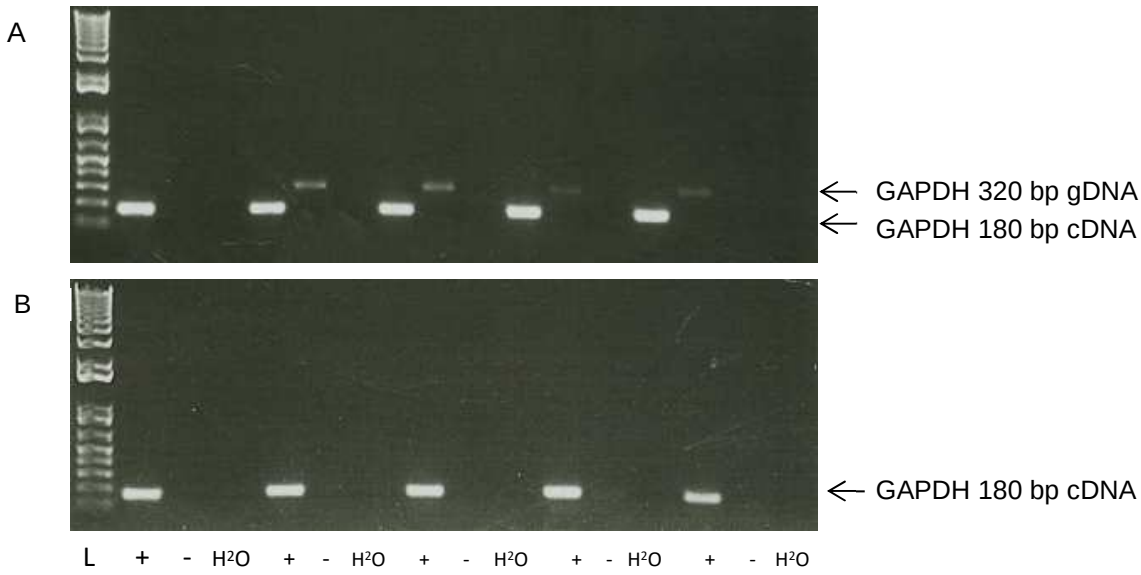



**Figure 2.7** Genomic contamination check. A, Initial optimisation returned amplification of gDNA in RT- negative controls. B, Following re-optimisation gDNA was no longer present in any sample. L, 1 KD plus ladder; +, reverse transcriptase positive; -, reverse transcriptase negative; $H_2O$, no cDNA template added.

### 2.9.4 Isolation protocol

Heart tissue was homogenized in 1 ml of ice-cold monophasic lysis reagent, Tri-Reagent (Sigma Aldrich, UK) using 23G followed by 25G needles. The homogenates were incubated for 5 minutes at R/T to permit complete dissociation of nucleoprotein complexes. To separate into three phases (1, Top phase containing mainly RNA, 2, interphase containing mainly DNA and 3, low phase containing protiens, and importantly RNases) 0.2 ml of 1-bromo-3-chloro-propane (Sigma Aldrich, UK) was added and vigorously mixed. Vigorous overtaxing was used as vortexing can sheer double stranded DNA. Single stranded DNA would cause the subsequent DNase step to be less efficient. The mixture was incubated for 3 minutes at R/T and was centrifuged at 10,000 x g for 15 minutes at 4 °C to separate the mixture into the phases. The upper aqueous phase was transferred to new 2 ml RNase-free tube, avoiding the contamination of the DNA in interphase and proteins in lower phase. For the precipitation of RNA from the aqueous phase to occur, pre-cooled (-20 °C) reagents of 0.25 ml 2M sodium acetate, pH 4 and 0.7 ml 100% isopropanol (Fisher Scientific UK Ltd., UK) were added. They were thoroughly mixed by over taxing and stored at -20 °C for at least 3 hours.

RNA Precipitate was collected by centrifugation at 17,500 x g for 15 minutes at 4 °C. The translucent/white RNA pellet that formed was then washed twice in 70% DEPC-ethanol and was re-suspended in 87.5 µl DEPC-treated water at 62 ºC for 1 - 5 minutes (until dissolved). 10 µl RDD buffer was added followed by 2.5 µl DNase I (Qiagen, UK) into each RNA sample and they were incubated for 15 minutes at R/T. 400ul of DEPC-ddH2O was added to bring the volume to 500 µl and an equal volume (500 µl) of phenol/chloroform/isoamyl alcohol, pH 5.2 (Amresco) was added for RNA extraction. The sample was vigorously mixed and centrifuged at 11,000 x g for 10 minutes at 12ºC. Again, the upper aqueous phase was transferred to new RNase-free tubes and was brought up to a 500 µl of DEPC-treated water. Removal of phenol was performed by purification with an equivalent volume of chloroform (Fisher Scientific, UK) (phenol can inhibit enzymatic reactions) followed by centrifugation at 11,000 x g for 10 minutes at R/T. The upper aqueous phase was transferred to a fresh tube. Pure RNA was

precipitated with the addition of a 1/10 volume of 3M sodium acetate, pH 5.2 and 2 volumes of absolute ethanol. The mixture was mixed by overtaxing and followed by -20 ºC incubation overnight. The precipitated RNA was collected by centrifugation at 17,500 x g for 15 minutes at 4°C, the pellet was washed twice with 70% RNase free ethanol in DEPC $H_2O$ and was finally re-suspended in 50ul DEPC-treated waterby heating to 60°C for 1 minute and gentle vortexing. The concentration of RNA was measured by NanoDrop 2000c UV/IV spectrophotometer at 260 nm absorbance (Thermo Fisher Scientific). RNA samples were stored at -80 ºC.

### 2.9.5 Globin depletion

Globin depletion was performed via enzymatic methods on hybridised RNA : DNA complexes. Before the procedure could be carried out, specific oligonucleotides had to be designed for each globin gene.

### 2.9.6 Oligonucleotide design

Oligonucleotides (oligos) were designed against globin genes to be depleted: HBAA, HBAD, HBB, HBG1, HBG2 and HBZ. Oigos must be close to the poly-A tail to enable the gene to be removed. This leaves little scope for oligo design, however it is important that oligos have good binding to their target sequence and so a compromise between being close to the 3’ end and being far enough away to produce good oligos had to be found. It was also important that the remaining regions did not contain RT-qPCR primer pair sites. Oligos were designed to be around 30 nucleotides to allow specific binding (checked by NCBI BLAST) and oligo Tm 60 - 70°C; it was impossible to get the same temperature due to limitations of the design region. Primer secondary structure was minimal. Secondary structure energy was performed using IDT analysis tools. Table 2.4 shows oligo sequence and properties.

### 2.9.7 Globin Depletion procedure

The designed oligos (1.5 µl of 10x) were mixed with 3 µl of 5x hybridization buffer and 3 µg of RNA and were made up to a total volume 15 µl with nuclease free water on each RNA sample. The mixture was heated to 95 °C for 2 minutes and cooled down at 5 °C intervals for 50 sec each step and finally to 50°C, with 1.5 minutes at 65°C and 60°C (the closest temperatures to all oligos annealing temperature) for oligo hybridisation to occur. Following the 60 °C step samples were placed straight to ice to help reduce secondary structure formation. Hybridised RNA : DNA was degraded by RNase H digestion for 15 minutes at 37 °C. DNase I digestion was carried out for 10 minutes at 37 °C to degrade the DNA probes. Globin-depleted total RNA were quantified by Qubit Fluorometric assay (Thermo Fisher Scientific). Globin depleted RNA with RIN above 7.0 was taken forward for cDNA library preparation.

**Table 2.5** Oligonucleotides for globin depletion

| Gene | Oligonucleotide sequence | Tm (°C) |
|---|---|---|
| HBAA | CAT CTCATT TGG CTG CTG GCT GCT GGA GGG | |
| | | 66.9 |
| HBAD | TGT ACT TCT CAG CCA GCA CAG CAG ACA CGG | |
| | | 66.2 |
| HBB | TTA CAG CCC AGC AGA CCC CGA GGA TGC CAG | |
| | | 69.3 |
| HBG1 | CTG TGT CCT GCT CTG GGA GCT CAG TGG TAC | |
| | | 65.9 |
| HBG2 | TGT CAC AAG CTG TCA GCT CCG GAG CAT | |
| | | 65.4 |
| HBZ | CTC AGT CAG AAC CGC GGA AAT GCT GGA CAG | |
| | | 61.7 |

### 2.9.8 preparation for RNA sequencing

cDNA library preparation was generated according to manufacturers' instructions of NEBNext Ultra Directional RNA Library Prep Kit for Illumina (New England Biolabs Inc.(NEB UK #E7420S/L)). (Section 2.3.4.1 – 2.3.4.4). A basic overview is shown in Figure 2.7.

In the directional cDNA generation process, the first strand is given unique non complimentary regions to the end of its adaptors; this allows for strand identification during sequencing. Though, manufacturer's instructions were followed, understanding of library preparation and sequencing is vital in order to be able to interpret the results, and hence are given below

### 2.9.9 mRNA isolation and fragmentation

Complete mRNA which contains a poly(A) tail was isolated from total RNA of each sample ($n$ = 3 of OFT-banded hearts and $n$ = 3 of shams) using poly-T oligonucleotide separation (Figure 2.7 A). 15 µl of NEBNext oligo d(T) 25 beads were prepared by washing with 100 µl of 2X RNA binding buffer and placement on a magnetic rack - supernatant was removed (repeated X1). Once washed, 50 µl of 2X binding buffer was added to the beads.

The 50 µl eluted mRNA from the purification columns after globin depletion treatment was added to the beads (100 µl total). The reaction mixture was heated to 65 ºC for 5 minutes to denature the RNA and was cooled to 4 ºC. The tubes were incubated at R/T for 5 minutes to facilitate the binding of mRNA to the beads. They were then placed in the magnetic rack at R/T for 2 minutes to separate the poly-A mRNA bound to the beads from the solution. Unbound RNA in the supernatant was removed, followed by wash step 1: Tubes were removed from the rack and well mixed (gently pipetted up and down at least 6 times) with 200 µl wash buffer, before being placed back on the magnetic rack for 2 minutes for separation. Supernatant was again removed (2 washing steps were carried out to ensure that all non-poly (A) tail RNA was removed).

50 µl of elution buffer was added and the tubes and mixed well (gently pipetted up and down at least 6 times) Tubes were then heated to 80 ºC for 2 minutes and decreased to 25 ºC to elute poly-A mRNA from the beads.

The washing process was then repeated: Re-binding of mRNA to the beads was facilitated by adding 50 µl binding buffer to each tube and mixing well (gently pipetted up and down at least 6 times) and incubated for 5 minutes then wash step 1 was repeated. Following the repeat of the wash step, one further wash step was carried out, but this time using elution buffer at R/T (elution buffer at R/T does not remove bound mRNA). 200 µl elution buffer is used and well mixed (gently pipetted up and down at least 6 times) followed by 2 minutes on the magnetic rack. All supernatant was then removed with a 10 µl pipette tip. This removal of all supernatant was repeated after a further centrifugation to ensure all supernatant was removed as it interferes with subsequent fragmentation.

Finally tubes were removed from magnetic rack for the next step which was elution, fragmentation and random primer attachment. The purified mRNA was eluted from the beads in 12 µl of the First Strand Synthesis Reaction Buffer (NEB, UK) and fragmentation by heat was achieved by incubation at 94 ºC for 15 minutes (Figure 2.7 B). The elution/fragmentation mix also contained Random Primers (2x) (NEB, UK) in order to hybridize with the fragmented RNA at random sites (Figure 2.7 B). Following incubation, samples were placed back on the magnetic rack and 10 µl was carefully and quickly pipetted out and transferred to a new tube and placed on ice.

### 2.9.10 First and second strand synthesis and purification

Actinomycin D (0.2 µg/µl) (NEB, UK), 0.5 µl murine RNase inhibitor (NEB, UK) and 1 µl Superscript® II Reverse transcriptase (NEB, UK) were added to the fragmented and primed mRNA (Actinomycin D reduces self-priming of the antisense strand). The first single stranded cDNA was synthesized following thermal cycling conditions: 25 ºC for 10 minutes, 42 ºC for 50 minutes and 70 ºC for 15 minutes (Figure 2.7 C). Second strand cDNA was synthesized by adding 8 µl 10x second strand buffer (containing dUTP mix) and 4 µl second strand synthesis enzyme mix (80 µl total) and incubated

for 1 hour 16 ºC (Figure 2.7 D). The enzyme mix contained RNase H and DNA polymerase and ligase, so RNA strand degradation and second strand DNA synthesis are completed in this step. The incorporation of uracil into the second strand (original sense) allows this strand to be selectively removed later for directional sequencing.
From this point on, library preparation and subsequent sequencing was performed in collaboration with Dr Sunir Malla from Deep Sequencing School of Life Sciences for the main part with a pre set-up Biomek Automated robot using standard 96 well plates when possible.

### 2.9.11 Adaptor ligation

The cDNA was purified following second strand synthesis using 1.8X Agencourt AMPure XP beads (Figure 2.7 E). Each double stranded cDNA library was treated with 10x End Repair Reaction Buffer and End Prep Enzyme Mix to generate blunt and 5'-phosphorylated dA-tailed ends with thermal cycling conditions based on manufacturer's instructions (Section 2.13.2) (Figure 2.7 F). dA-tailed cDNA libraries were ligated to a specific adaptor from the NEBNext Multiplex kit. Ligated cDNA transcripts are composed of a connecting structural loop containing a U with complementary dT overhangs that allow the ligation and structural formation. Following a complimentary region, the adapter contains non complimentary regions at its ends, it is this that causes a kink and the loop structure at the end of the ligated strands (NEB, UK) (Figure 2.7 G, and Adapter and structure shown in Figure 2.8). The second strand containing dUTP from the double stranded cDNA and the loop containing a U were removed by treatment with Uracil-Specific Excision Reagent (USER) Enzyme (NEB, UK) to open up the loop and make just the first strand with its specific adaptors available as a substrate for PCR enrichment (Figure 2.7 H).

### 2.9.12 PCR enrichment and RT-qPCR quantification

PCR enrichment incorporates the P5 and P7 primers (sequences and complimentary binding sequences on adapters shown in Figure 2.8) that are specific to the Illumina flow cell and thus allow attachment and sequencing. Barcodes are incorporated in to the P7 index primer for heart identification in multiplexing. Enrichment also increases concentration for efficient sequencing. The P7 index primer is complimentary for only the 3' end of the first strand (original antisense strand) and also incorporates the barcode. Once the second strand has been synthesised, the P5 primer can now anneal to the 3' end of that strand to synthesis the first strand. Thus double stranded cDNA is once again created, but now strand specific identification is possible (Figure 2.9)

It is important that PCR cycles at this point were kept to a minimum as excessive copies of a transcript lead to high levels of sequencing the same duplicated transcript (we used 12 cycles); this is known as PCR duplication error (Ebbert et al., 2016). These duplicates were removed from the data analysis post sequencing, however it is undesirable as duplicates can often be hard to identify, thus duplicated reads can be counted and lead to erroneous expression results (Ebbert et al., 2016). This is overcome in part by paired end sequencing that allows better identification of duplicates for removal (Head et al., 2014, Ebbert et al., 2016). Paired end sequencing is made possible as we ligated adaptors to both ends of the antisense strand. Amplification bias can also be an issue in PCR enrichment with GC rich transcripts; this is partially overcome by increasing the denaturation time (Head et al., 2014). We used 30 seconds as the NEB high fidelity DNA polymerase and buffer component has been shown to give even amplification of transcripts at low denaturisation times (Naesens et al., 2013).

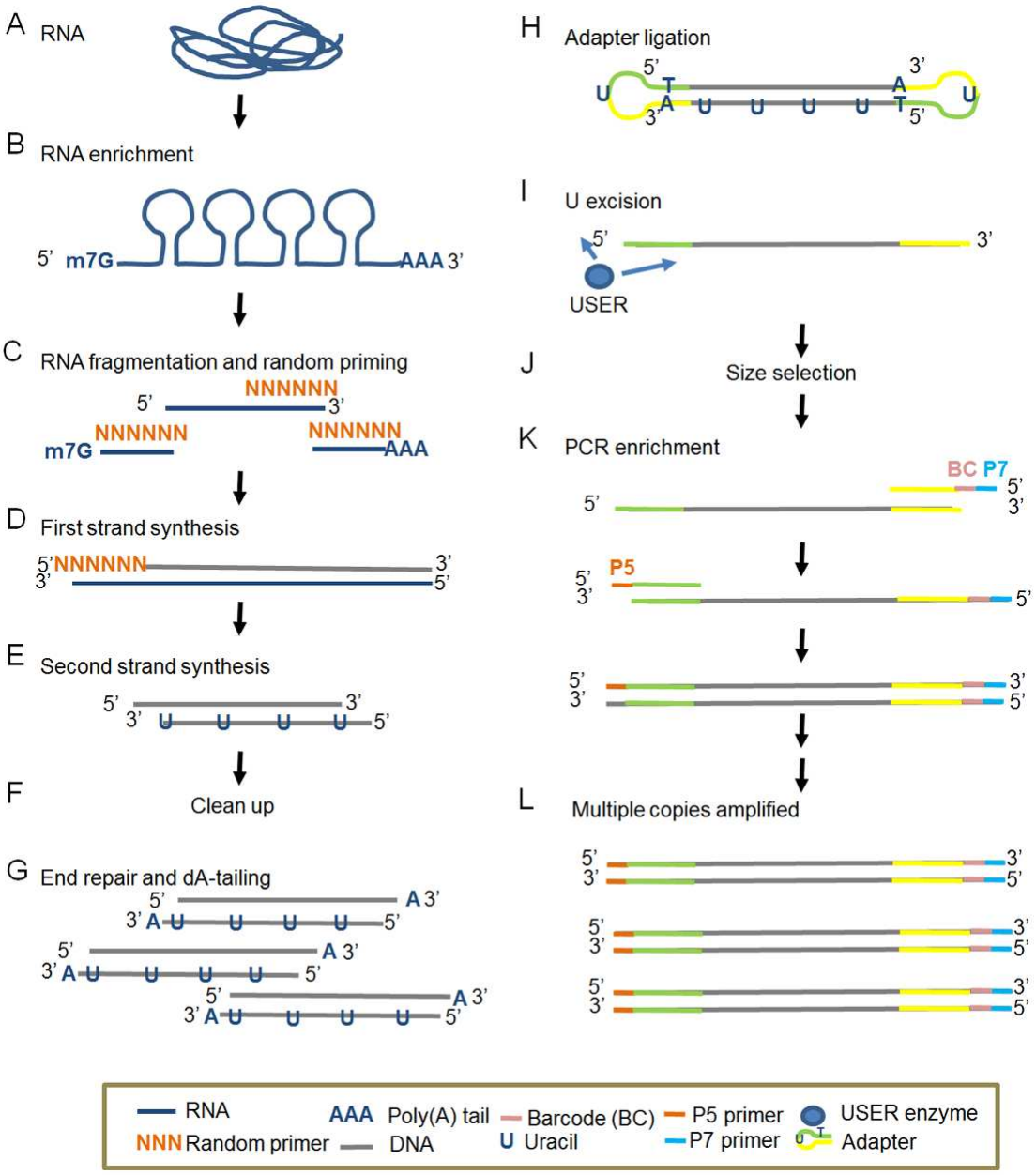



**Figure 2.8** Workflow overview of Ultra Directional RNA Library Preparation for Illumina A, mRNA isolation. B, Fragmentation at random sites. C-D, cDNA second strand synthesis. F-G, End repair to allow adaptor ligation. H, Removal of second strand and opening of adaptor loop by USER enzyme. I-J, Following size selection, PRC enrichment incorporates P7 and P5 primers, bar codes and retains strand specific information for sequencing (picture adapted from illumina online methods).

A,

Adapter

GATCGGAAGAGCACACGTCTGAACTCCAGTC-U-ACACTCTTTCCCTACACGACGCTCTTCCGATC

B,

Adapter structure

5’ /ACACTCTTTCCCTACACGACGCTCTTCCGATC*T 3’

U | | | | | | | | | | | | <-Ligated to library fragments

3’ \-CTGACCTCAAGTCTGCACACGAGAAGGCTAG-P 5’

C,

Structure with uracil removed

5’ ACACTCTTTCCCTACACGACGCTCTTCCGATC*T------

| | | | | | | | | | | |

3’ CTGACCTCAAGTCTGCACACGAGAAGGCTAG--------

D,

P7 Index primer

(P7) CAAGCAGAAGACGGCATACGAGAT***CGTGAT***GTGACTGGAGTTCAGACGTGTGCTCTTCCGATC

P5 Universal primer

(P5) AATGATACGGCGACCACCGAGATCT-ACACTCTTTCCCTACACGACGCTCTTCCGATC

**Figure 2.9** A, Full adapter sequence which forms a loop structure at end of fragments (B-C). Primers (D) are specific for adaptor sequences (matching colours correspond to binding regions). P7 is specific to the non-complimentary region at the

3’ end of the first strand so will synthesis the second strand. P5 then binds to the 3’. end of the second strand.

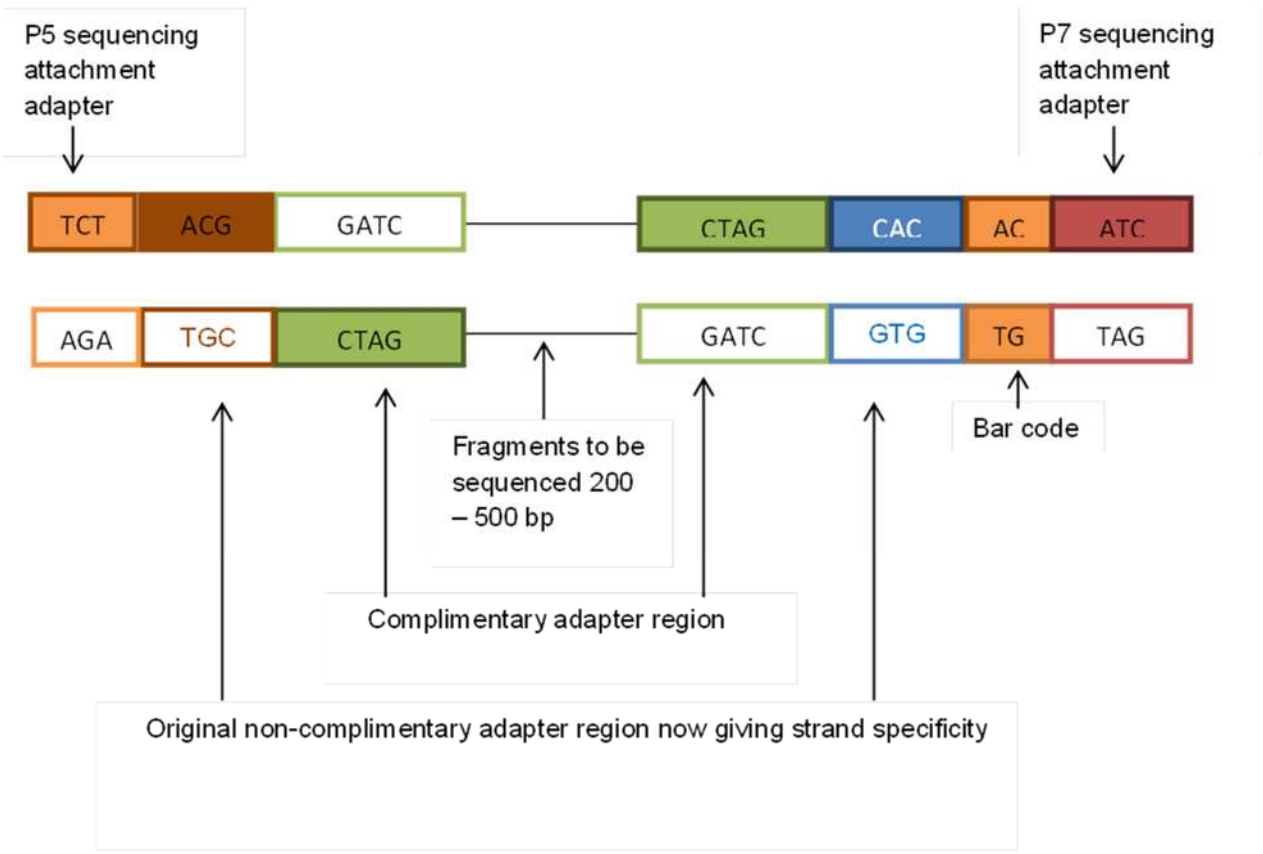



**Figure 2.10** Double stranded cDNA fragments post library preparation ready for sequencing.

## 2.10 RNA sequencing

Barcoded libraries were sequenced on the Illumina NextSeq 500 platform at the Deep Sequencing department in School of Life Sciences, University of Nottingham. Eight tenths of a full high output sequencing run were performed according to manufacturer’s instructions. 40 million total reads came from 2 flow cell reads with each read having 75bp paired-end reads (so 2 x 75 reads). Sequencing will now be very briefly described, again so that a true understanding of results can be sort. The prepared cDNA libraries from each heart were denatured, the denatured cDNA is added to the sequencer along with a new flow cell and the fragments were applied to

the flow cell (Figure 2.11 A (Figure 2.11 and 2.12 show over view)). The fragments attach to complimentary adapters on the flow cell and a reverse strand is synthesised from this. The first strand is washed away and the newly synthesised strand now bends over and attaches to the complimentary flow cell at the strands 3' end (Figure 2.11 B). From here the complimentary strand is synthesised until both reverse and forward strand are attached to the flow cell; this is called bridge amplification. This process happens many times and thus a single fragment is amplified many times. It is this amplification that makes the sequencing process so reliable, as a single fragment is read many times enabling any errors to be detected (Sims et al., 2014). Following amplification, the reverse strand is washed away and 3' end of the remaining strand are blocked to ensure no further annealing to the flow cell. Sequencing of the forward strand commences (Figure 2.12 C). Sequencing proceeds by synthesis (from P7 in Figure 2.9) with each nucleotide having its own unique excitation frequency. Following sequencing the product is washed away and the index site is sequenced for sample (heart) identification (Figure 2.12 D). 3' blocking is removed and the strand anneals to the first strand adapter on the flow cell to enable paired end sequencing. The sequencing process is then repeated for this strand.

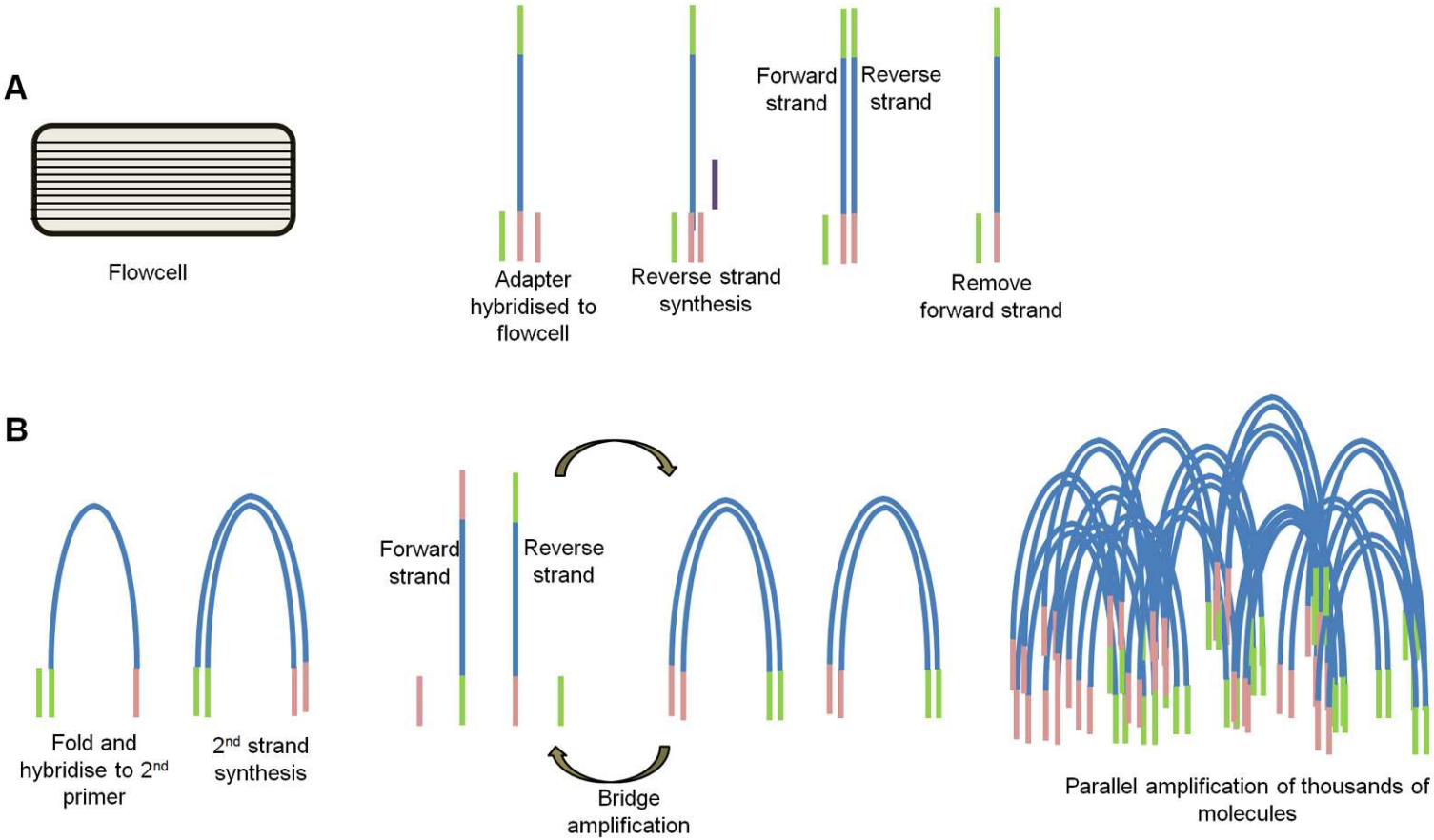



**Figure 2.11** Overview of sequencing by Illumina nextseq 500 part 1. Full description is in text. A, Adapters anneal to flow cell and a reverse strand is synthesised. B, The complimentary strand is synthesised amplified (picture adapted from illumina online methods).

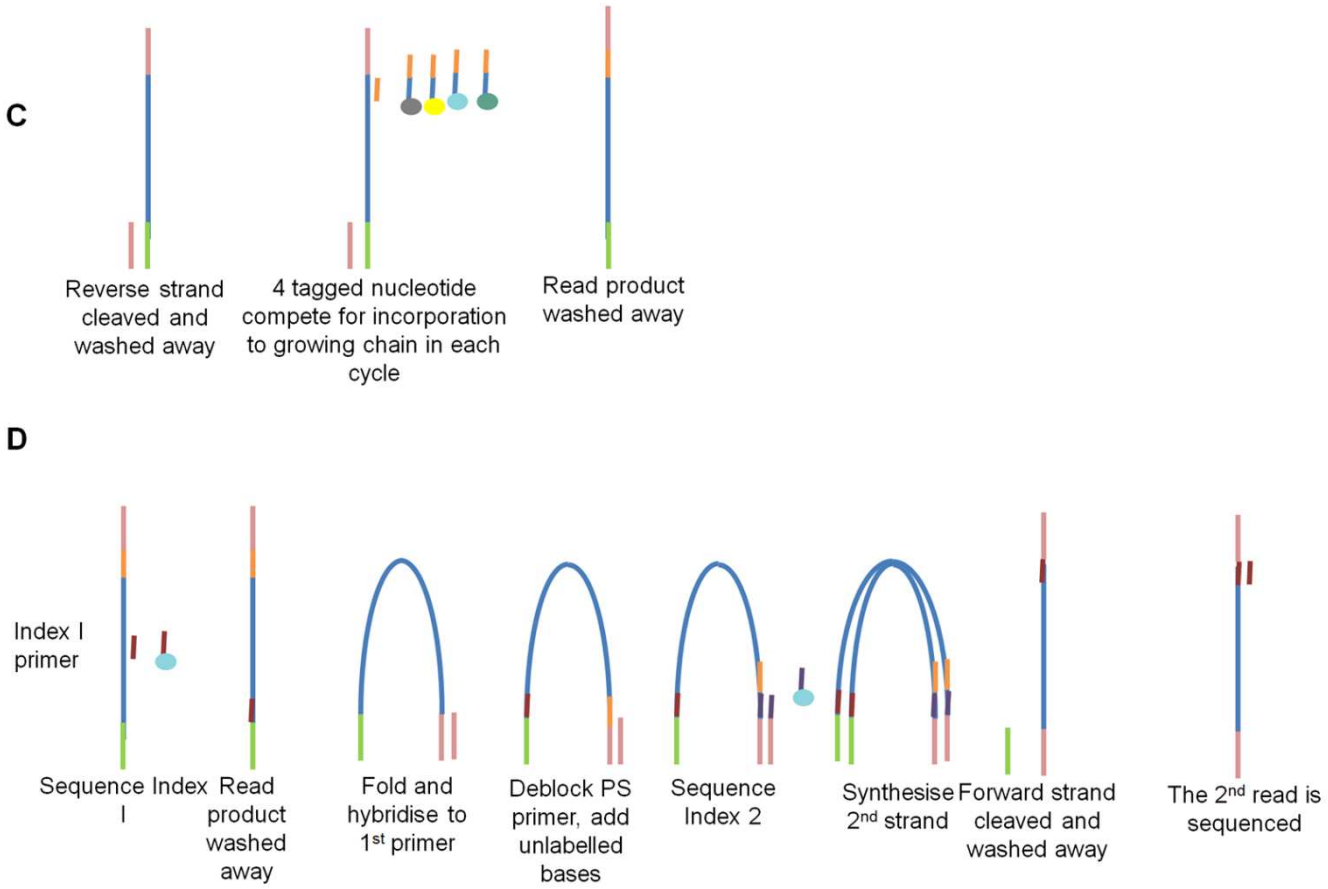



**Figure 2.12** Overview of sequencing by Illumina nextseq 500 part 2. Full description is in text. C The forward strand is sequenced. D, Paired end sequencing takes place and the reverse strand in sequenced (picture adapted from illumina online methods).

### 2.10.1 RNA sequencing Bioinformatics analysis

Bioinformatics analysis of RNA sequencing data was performed in collaboration with Dr Fei Sang from Deep Sequencing, School of Life Sciences. Fei performed the initial bioinformatics of trimming mapping and MAPQ and his protocols for these steps are provided. Comparison of FPKM, TPM and verification of overall differences by PCA was carried out by me. An overview of the process is shown in Figure 2.11.

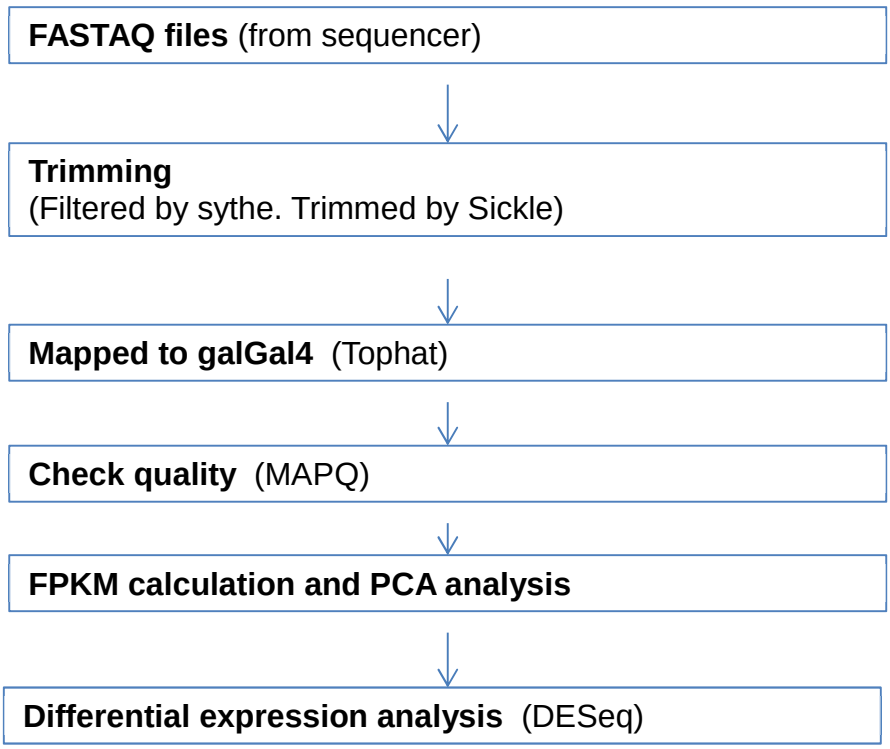



**Figure 2.12** Overview of sequencing analysis.

### 2.10.2 Trimming and mapping against reference genome

Bases and qualities output were first generated in sequencing output files (compressed FASTAQ files). Trimming was performed to filter reads for adapter and low quality bases. First, raw reads that aligned against adaptor sequences were filtered using Sythe (https://github.com/vsbuffalo/scythe). Reads with a low sequencing score were then trimmed using Sickle (https://github.com/najoshi/sickle). The chicken reference genome was downloaded from the UCSC database (http://genome.ucsc.edu) Nov. 2011 (ICGSC Gallus_gallus-4.0/galGal4). Reads were mapped to the galGal4 reference genome in the context of known gene exon coordinates by tophat mapping tool (https://ccb.jhu.edu/software/tophat/index.shtml). This generated sequence alignments for each sample in BAM format (the standard format of recording RNA sequencing alignment results). Read alignments were recorded against the reference genome in three ways; unique, primary and all. 'Uniquely' mapped reads are reads that map to only a single location, and there are no significant hits to any other reference genome location. 'Primary' mapped reads record the best mapping position of each read, regardless of whether they map uniquely. Primary mapped reads are shown in Bam files. 'All' mapped reads are when every single significant mapping position is recorded against the reference genome, therefore there can be a multiple recording for each gene (protocol communicated by Dr Fei Sang).

### 2.10.3 Mapping Quality (MAPQ)

Both primary and unique mapped read alignments (47-90 x $10^6$) were filtered based on their mapping quality score (MAPQ). MAPQ is a probabilistic metric of the accuracy of the read mapping. Low mapping quality implies low base quality of the read. This is attributed to incorrect observed read sequence which then leads to wrong alignment. In addition, low sensitivity of the alignment algorithm and the reads that fall in repetitive regions of the reference genome result in low mapping quality. In our case, RNA sequencing is a paired-end sequencing. Next generation sequencing (NGS) has a

limited read length and thus can lead to errors in overlapping gene identification. Paired end sequencing improves this as each end is matched allowing exact identification of gene and isoforms (Fullwood et al., 2009). By definition, MAPQ 10 equates 1 in 10 chance of a mapped read being incorrectly placed, MAPQ 20 means 1 in 100 chance of a mapped read being incorrectly placed and MAPQ 30 equals to 1 in 1000 chance of a mapped read being incorrectly placed. In our case, MAPQ is MAPQ 20. 'Htseq-count' was used to determine the number of uniquely aligned reads per gene to generate the read counts per gene (protocol communicated by Dr Fei Sang).

### 2.10.4 RPKM/FPKM and TPM Expression Values

Fragments per Kilobase of transcript per Million mapped reads (FPKM) expression values are based on the RPKM calculation from (Mortazavi et al., 2008). FPKM is a normalized read count (stranded/sense reads) for a given gene by taking sample sequencing depth and gene length into account. The read count of the exon-space of a gene is normalised against the total number of mapped reads (with rRNA and gobin genes originally excluded, plus reads not uniquely aligned and below MAPQ20 removed before analysis) in that particular alignment file, and against the total length of the gene's exon-space. The equation was also carried out by transcipts per kilobase per million (TPM) in order to confirm FPKM accuracy. A comparison of the two equations is shown in table 2.1 (this is explained in the discussion at the end of this section).

**Table 2.6** FPKM and TMP equation

| FPKM and TMP equation comparison | |
|---|---|
| **FPKM** | **TPM** |
| $\frac{\text{Reads / Kb (RPK)}}{\text{Total reads / } 10^6}$ | $\frac{\text{Reads / Kb (RPK)}}{\text{Sum RPK / } 10^6}$ |
| This is the transcripts per total number of reads | This is the transcripts per total number of transcripts |

### 2.10.5 Overall variation between OFT-banded and SHAM, and gene differential expression

In order to show that there were no differences overall between replicates and that there is variation between OFT-banded and SHAM, principal component analysis (PCA) was performed using r software. This procedure shows where the greatest overall differences between groups lies. It is a statistical process that uses an orthogonal transformation to convert a set of observations of possibly correlated variables into a set of values of linearly uncorrelated variables called principal components. Before PCA all ribosomal data was removed. For differential gene

expression, the DESeq package was employed for statistical analysis of FPKM values (Anders and Huber, 2010). This program implements a single analytical approach taking account of variance between and within groups in order to create a better model of the expression values using a *p*-value algorithm corrected for sequencing sample size and variance. Corrected *p*-values of <0.05 were set as the DESeq threshold. Genes with average FPKM values <1 were filtered from the raw data before statistical analysis.

### 2.10.6 RT-qPCR validation

Following the RNA sequencing result RT-qPCR was performed for each gene of interest and genes for validation. cDNA was generated for this as in section 2.2.6.2 for HH29, and HH35 for comparison. Primer design was the same as previously stated (see section 2.2.6.3). Primers for globin depletion and genes highlighted from RNA sequencing are shown in table 2.3.

### 2.10.7 Apoptosis on OFT banded heart atria

The study of Apoptosis was performed using ApopTag ® Peroxidase *In Situ* Apoptosis Detection Kit S7100 according to manufacturer's instructions (Millipore, USA) (performed by Dr. Pang). Following rehydration, Proteinase K (20 µg/ml) treatment permeabilised tissues for 15 minutes at R/T and slides were washed with $dH_2O$ To stop the reaction. Endogenous peroxidase activity was quenched by immersing the slides in 3.0% hydrogen peroxide in PBS for 10 minutes at R/T. Slides were incubated with equilibration buffer for 15 minutes. TdT enzyme was applied straight (at recommended working strength) onto sections and they were incubated at 37 ºC for 1 hour. Stop/wash buffer was applied onto each section to inactivate the enzyme for 10 minutes at R/T. Inactivation the enzyme proceeded by washing slides with PBS followed by application of anti-digoxigenin conjugate with incubation in a humidified chamber for 30 minutes at R/T. Again, sections were rinsed with PBS three times and

200 µl 0.05% 3,3 diaminobenzidine (DAB) with 0.03% hydrogen peroxide in PBS was applied to the sections. Slides were carefully monitored by microscopy during colour development and the reaction was stopped by immersing the slides with $dH_2O$. Non-apoptotic cells were counterstained with DAPI (1 : 500, Sigma Aldrich) for 15 minutes at R/T. A positive control was used throughout; heart tissues were pre-treated with DNase I before incubation with equilibration buffer. For the negative control, working strength TdT enzyme was substituted with PBS, with all other steps remaining identical.

### 2.10.8 Apoptosis data gathering

A total of 80 histological slides (each slide contains 25-30 tissue sections) were digitised using a slide scanner (Zeiss Axio Scan Z1, Imaging & Cytometry, University of York carried out by Dr Kar Lia Pang). Every section on each slide had to be marked using a permanent marker pen to enable section selection and a preview was taken for automatic tissue detection. These selections were refined manually. In order to obtain high resolution images of the whole HH29 hearts, tissues were divided into multiple small tiles or images. They were photographed with fluorescent imaging mode with a 20x objective for non-apoptotic cells and brightfield imaging mode for brown (DAB reactive) apoptotic cells. Focus was applied on every third tile. Z-stacking was also activated to obtain a single sharp plane image.

### 2.10.9 Analysis of data

Using ZEN software (Carl Zeiss Microscopy) tiles were aligned as a single virtual histological slide in.czi format. Brown (DAB reactive) apoptotic cells in the atria were counted manually, whereas the total number of non-apoptotic cells in each section was counted automatically using DAPI counterstain. Counting was performed by ImageJ software for automated cell imaging. Watershed was applied to separate the merged particles. The DAPI and DAB positive cells were then added together to get

a total cell count and the ratio of apoptotic cells to total cells was obtained for each heart atria. Unpaired student T-test was conducted to determine differences.

## 2.11 Immunocytochemistry for myosin structure analysis at HH29

### 2.11.1 Harvesting and sectioning

Upon harvesting, embryos were externally morphologically assessed for size and shape. Any embryos showing structural deformities or developmental delay were excluded. The embryos were harvested at HH29 and they were then fixed in 4% paraformaldehyde (PFA) (Sigma Aldrich, UK) overnight at 4°C. Embryos were washed in PBS and once with $dH_2O$ followed by a graded ethanol series (70%, 90% and 100% ethanol). Embryos were cleared using xylene and were paraffin-embedded. Heart serial sectioning took place at 8 µm in transverse orientation using a Leica DSC1 microtome (Leica, Germany). Sections were floated onto a 42°C water bath and were collected on 3-aminopropyltriethoxysilane (APES)-treated glass slides. The Positively-charged APES slides ensure firm adhesion of the sections to the slides. Sections were left overnight to dry out at 42°C on a hot plate.

### 2.11.2 Fluorescent immunohistochemistry

Following sectioning, the prepared slides were treated with 10 mM sodium citrate, pH 6.0 for 10 minutes for permeabilisation (Antigen retrieval). Permeabilisation was performed by microwaving for 10 minutes in 10 mM sodium citrate, pH 6.0. Sections were then processed for immunofluorescence. They were blocked in 10% goat serum in 1% BSA/PBS for 2 hours at R/T and then with the MF20 primary antibody at 1:50 overnight at 4 °C. After washing (3X in PBS), the secondary antibody (Alexa 647, 1: 100, Molecular Probes) was incubated for 1 hr at R/T. Finally nuclei were stained with DAPI (1: 1000, Sigma : D9542). The primary antibody MF20 is positive for all myosin heavy chains (Developmental Studies Hybridoma Bank (DSHB)). Images were acquired using Leica DMIRE2 inverted microscope.

# Chapter 3 Myosin heavy chain knockdown - effect on sarcomere embryonic maturity, beating rate and conduction gene expression

## 3.1 Introduction

Myosin heavy chain (MHC) proteins allow contraction to take place, but their effect on the development of electrical activation is yet to be elucidated. Previous work by Rutland *et al.* (2011) showed that alpha myosin heavy chain (αMHC), beta myosin heavy chain (βMHC) and embryonic myosin heavy chain (eMHC) **are** necessary for correct $Ca^{2+}$ transients, with eMHC also required for a normal action potential and normal intracellular $K^{+}$. This work used morpholino knockdown of the three afore mentioned myosin heavy chains in order to assess the effects. Mutations to the human homologues of αMHC and βMHC have also been found to cause congenital heart defects (CHD) (Ching et al., 2005, Budde et al., 2007), though the genetic cause of most CDHs, and indeed the conduction phenotype origins of myosin KD hearts remain unknown. The general aim of this chapter is to increase understanding of why myosin heavy chain proteins may be influencing the hearts conduction system. Morpholino knockdowns (KD) were used to look at the effect of KD to the myosin heavy chain proteins αMHC, βMHC and eMHC. Cell culture is then used to assess the effect on sarcomere maturity using immunocytochemistry, and observed beating rate. The second part of this section then goes on to assess the effect on gene expression of identified conduction markers with whole mount *in situ* hybridisation and RT-qPCR.

The heart is the first functional organ to form in vertebrates and it must beat spontaneously. In order to do this, it must have a well-coordinated contraction initiated by electrical stimulus. Rhythmical contraction of the heart commences at about HH11. The impulse is passed from the developing SAN region to the ventricle via the AV canal where the atrioventricular node (AVN) forms. Upon arrival at the AV canal the impulse slows, allowing ventricular filling prior to the impulse passing from the AVN to the ventricle, thus enabling contraction. Structural myosin's will be key to the

contraction process, and understanding how they may affect conduction and the genes of the conduction system could be key in the discovery of treatments of how to treat CHD, specifically those with conduction disorders. As heart contraction is initiated at around HH10/11, this is the time at which KD is administered in this thesis. The main stages of harvesting and analysis is then at HH20 and HH29. D over this timeframe should allow insight on myosin's role during early development of the conduction system as at HH20 cells that will become the sinoatrial node (SAN) are still yet to migrate from the sinus venosus and at HH29 when the SAN is located in its final position in the right atrium (Garcia-Frigola et al., 2003).

## 3.2 Aims

Specific Aims:

- To assess how αMHC, βMHC and eMHC KD effect the maturation and beating rate of the developing sarcomeres.

- To identify possible causes of $Ca^{+2}$ and abnormal AP previously seen in hearts with structural myosin gene KD by analysis of key conduction gene expression

## 3.3 Results

### 3.3.1 Morpholino uptake by primary cardiomyocytes

Initial morpholino uptake was assessed by qualitative observation in the heart before harvesting of embryo's to be analysed. A scale of 0 – 5 was invented, where 0 represented no noticeable uptake and 5 represented clear strong uptake. Hearts were taken from HH20 embryos and separated into two groups of good uptake (levels 4-5; Figure 3.1 A) and poor uptake (level 2-3; Figure 3.1 B). Though assessment is taken

with whole embryo, it is take up in the heart specifically that is qualitatively assessed. Embryos were then analysed by western blot to assess reduction in protein level.

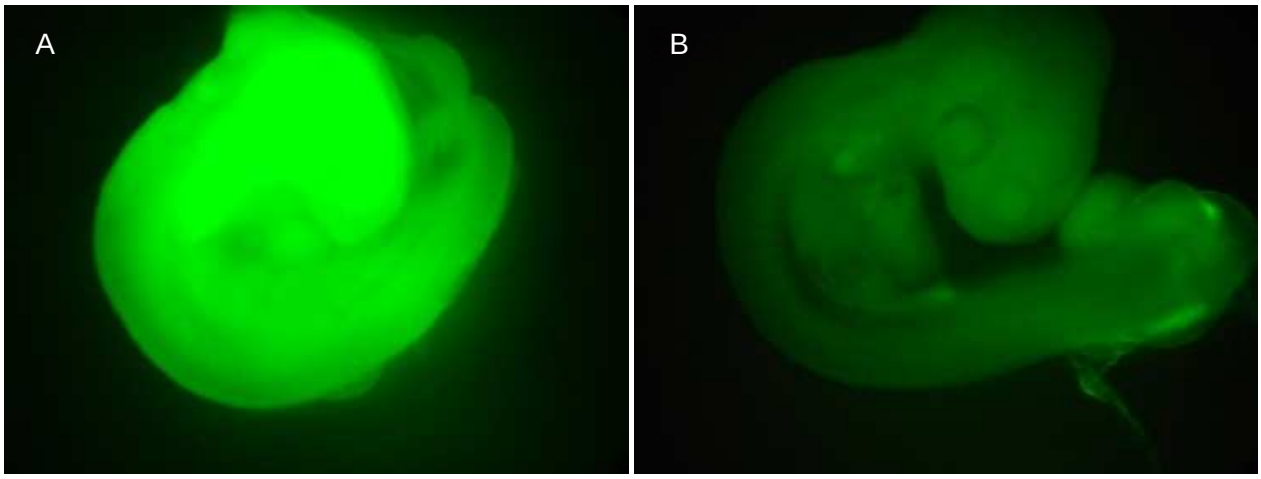



**Figure 3.1** Representative embryos and hearts from qualitative observation groups. A, represents strong uptake group (level 4-5). B, represents poor uptake group (level 2-3). Both A and B were embryos treated with standard control morpholino.

### 3.3.2 Protein reduction validation of knockdowns by western blot

Previously published data obtained from work in our lab preliminary to my PhD has demonstrated the significant reduction in protein of eMHC and αMHC following morpholino knockdown. eMHC was detected by EB165 primary antibody by DSHB and showed an 80% decrease ($p$ = 0.02) (Rutland et al., 2011). αMHC showed a 63 % reduction ($p$ = 0.034) using DSHB S58 primary antibody (Rutland et al., 2009). βMHC protein reduction is yet to be confirmed in our lab, so western blot analysis was carried out to determine knockdown was taking place.

HH20 isolated hearts from untreated (UT), standard control (SC) and beta myosin heavy (βMHC) chain KD were prepared for western blot analysis. The βMHC hearts were further divided based on morpholino uptake, with the sub groups of ‘good KD’ and ’poor KD’ as described in section 3.2.1. All groups had three biological samples, other than poor KD which had 2, and were tested via western blot three times. Even

concentrations of protein in even volumes were added to wells for analyses. This required a Bradford assay to be carried out in order to adjust stock concentration correctly.

### 3.3.3 Bradford assay

Protein concentration was unknown so initially a range of dilutions from differing samples was first tested using HH20 and HH29 hearts and HH29 liver. The re-suspended pellet was also tested for each sample. From the initial dilutions, it was seen that around 5 µl of any sample would give a concentration mid-range on the standard curve. Figure 3.2 A shows 5 µl dilutions of HH20 and HH29 heart with HH29 liver. The negligible amount of protein in the re-suspended pellet shows that the lysis procedure worked well. All samples were adjusted to 1 µg/µl so that equal concentrations and volumes could easily be added in the procedure (all samples shown in Figure 3.2 B).

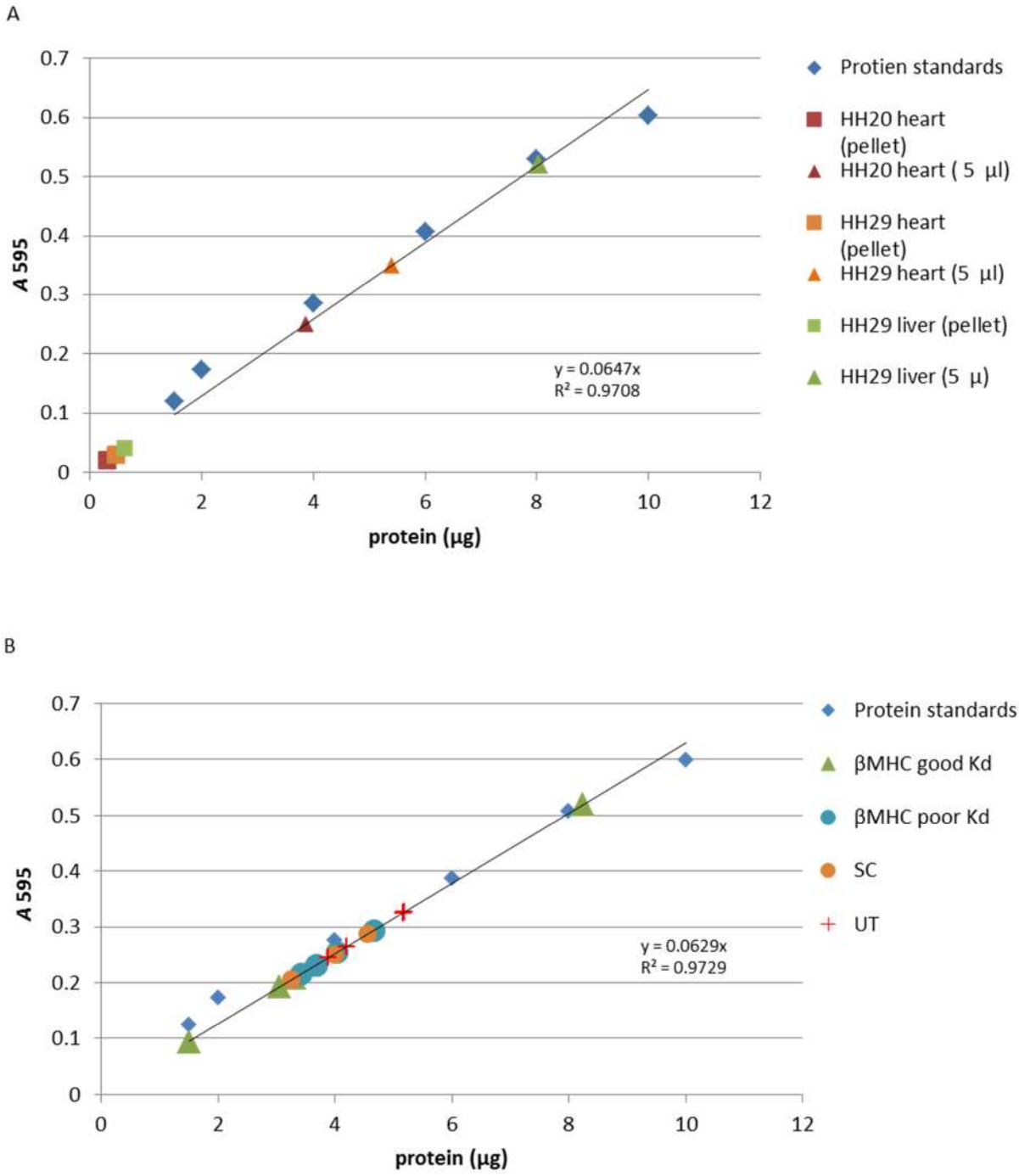



**Figure 3.2** Bradford assay experiment optimisation and restult. A, Bradford assay result showing 3 different samples within the range of the standard curve by using 5 µl of lysed protien solution. B, shows all of the single heart samples used for analysis of βMHC knockdown and SC validation. SC, standard control; UT, untreated.

### 3.3.4 Western blot

#### 3.3.4.1 Antibody optimisation

HH20 hearts positive for βMHC were compared to βMHC negative liver samples. 5 µg of heart tissue protein was used compared to 6 µg from liver samples. Two biological replicates of each group were used. Specific signal was seen at expected 220 kDa for βMHC and 36 kDa for GAPDH and no unspecific bands were seen (Figure 3.3).

#### 3.3.4.2 Standard control validation

Protein analysis (Figure 3.4 for blots) on untreated (UT) hearts compared to standard control (SC) revealed no significant differences with normalised relative protein optical density values being closely matched. Table 3.1 shows statistical analysis of data. No significant differences (>0.05) were found between groups and 95% confidence interval shows overlap. Figure 3.5 A, shows βMHC normalised to GAPDH, B, shows protein values of SC relative to UT. These results show that the SC hearts can be used as control hearts during experiments in this thesis.

### 3.3.5 Knockdown hearts to pooled controls and standard control

Protein analysis of good KD (figure 3.4 for blots) showed 66.38% reduction of βMHC using normalised signal relative to pooled controls. Table 3.2 shows statistical analysis of the data. Differences were significant when using pooled controls or SC separately (<0.0001), in fact, significance values were slightly better when using just SC. Figure 3.6 A, shows βMHC normalised to GAPDH, Figure 3.6 B, shows protein values of KD relative to pooled controls. ‘Poor KD’ hearts clearly showed less knockdown had occurred in comparison to ‘good KD’ hearts as can be seen in figure 3.4. They did however show a mean reduction of 41.8 % with a just significant *p*-value of $p = 0.049$. However on the final technical repeat one biological replicate had to be replaced. This heart showed zero reduction of βMHC and if included in the dataset poor KD protein reduction was not significant. It is clear from these results that hearts that showed

good clear morpholino uptake also show significant reduction in protein. However, harvested hearts that showed poor uptake showed inconsistencies and reduced KD. Therefore, only good KD (level 4-5 uptake) were used in this thesis.

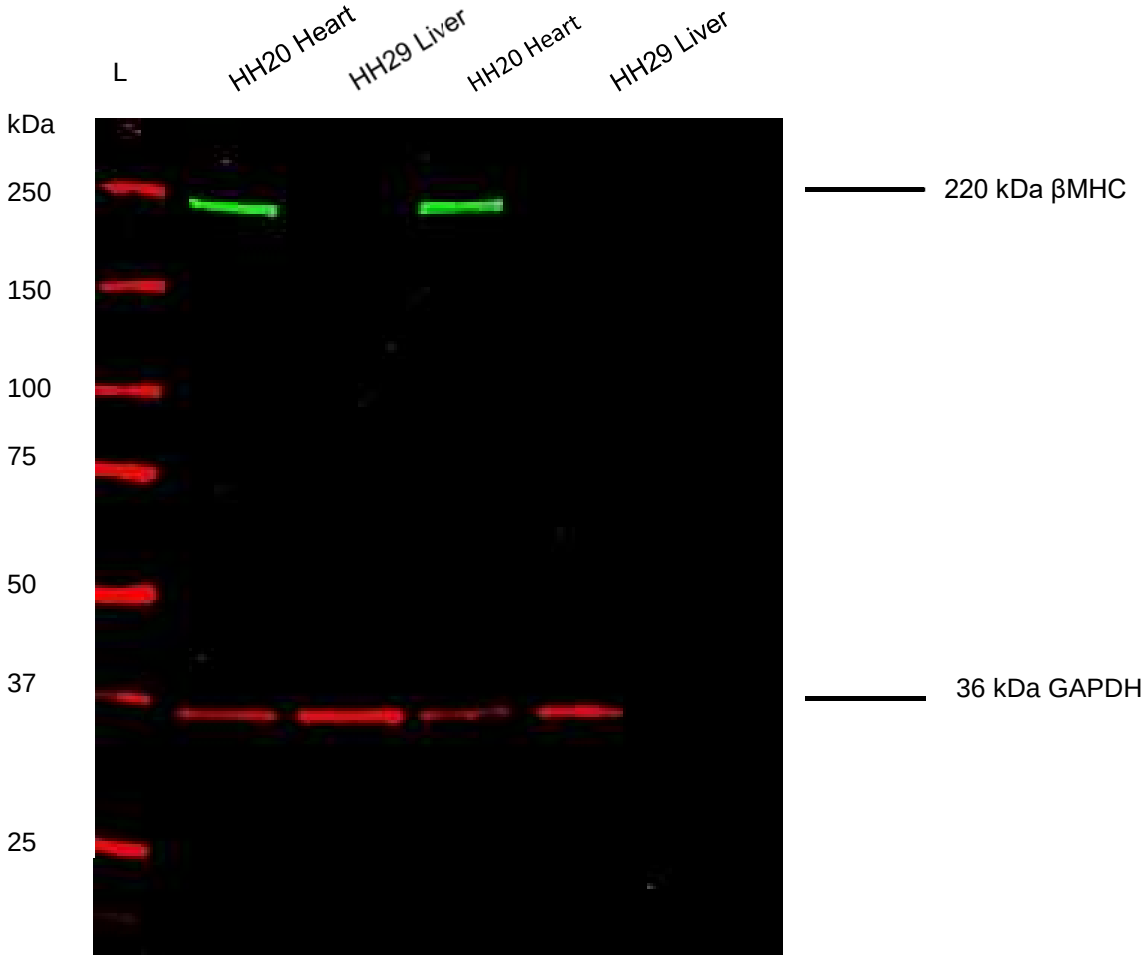



**Figure 3.3** Western optimisation of βMHC and GAPDH antibodies. HH20 hearts using 5 µg protein compared to negative control liver tissue 6 µg protein samples. Expected specific signal is seen in heart samples. No signal is seen in liver negative controls.

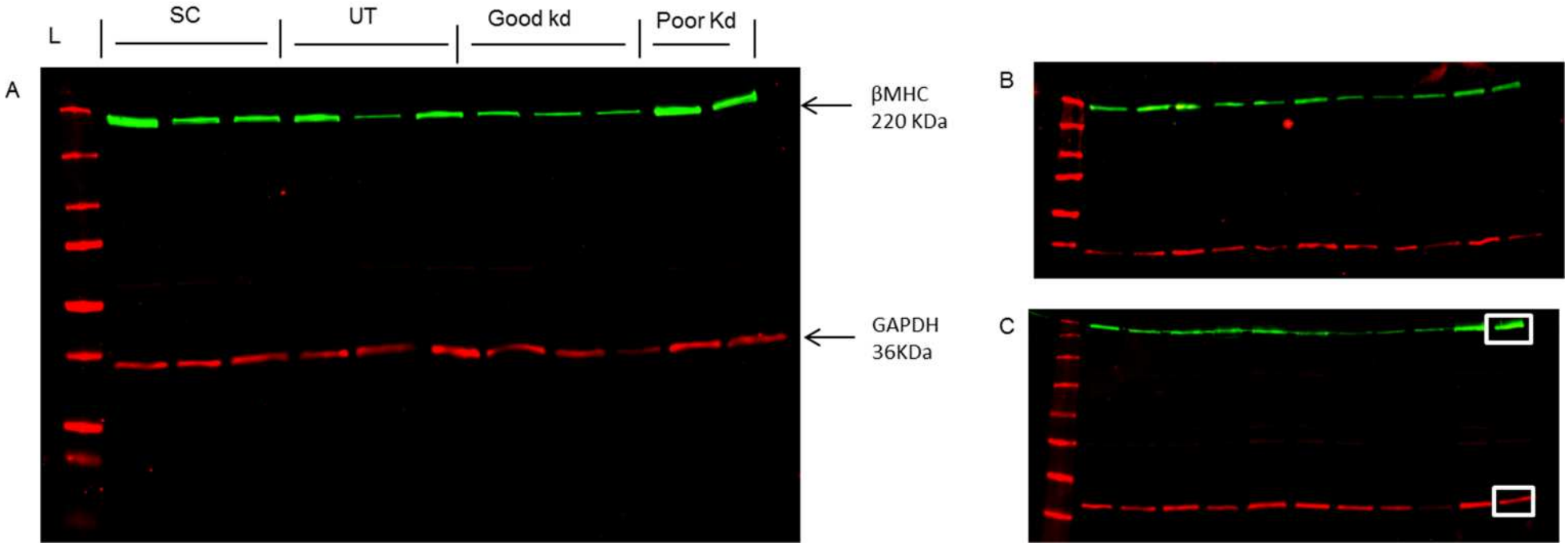
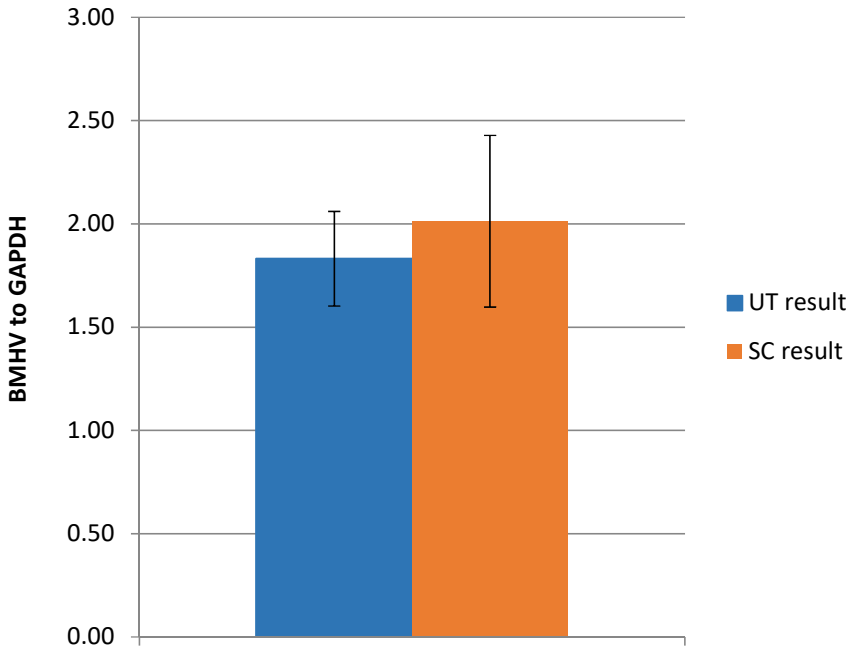



**Figure 3.4** βMHC KD western blot. A, First western blot showing βMHC to GAPDH for standard control (SC), untreated (UT), good KD and poor KD. B and C show repeated western results. Boxed area in C represents an additional biological replicate that was not on the previous two blots. Each well represents a single heart

**Table 3.1** Standard control viability showing no significant differences between UT and SC

| | **UT BMHC to GAPDH** | **SC BMHC to GAPDH** | **SC normalised relitive protien expression change (log2)** |
|---|---|---|---|
| | 1.78 | 1.19 | -0.38 |
| | 2.04 | 2.95 | 0.94 |
| | 0.80 | 1.75 | 0.18 |
| | 1.34 | 0.80 | -0.18 |
| | 1.01 | 0.82 | -0.15 |
| | 0.37 | 0.71 | -0.34 |
| | 4.64 | 5.45 | 0.88 |
| | 2.11 | 2.38 | -0.35 |
| | 2.39 | 2.07 | -0.55 |
| Mean | 1.83 | 2.01 | 0.01 |
| SD | 1.25 | 1.51 | 0.55 |
| SE | 0.42 | 0.50 | 0.18 |
| Difference (%) | **-** | **9.83** | **7.00** |
| **Significence (p-value, two way with unequal variences)** | | | **0.65000** |
| Margin of error (95 % confidence interval) | 0.81 | 0.99 | 0.36 |
| Upper bound | 2.65 | 3.00 | 0.37 |
| Lower bound | 1.02 | 1.03 | -0.35 |

A




B

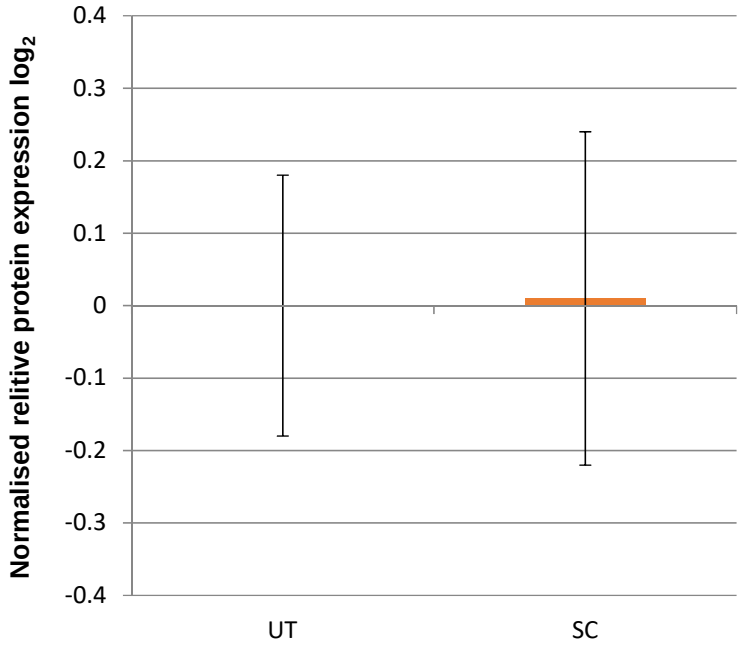



**Figure 3.5** No difference in protein signal between controls. A, Standard control to untreated βMHC normalised to GAPDH; B, Normalised relative protein expression of SC compared to UT showing no significant differences

**Table 3.2** Pooled controls and standard control only comparison to good and poor βMHC, showing βMHC to GAPDH and normalised relative protein expression.

| | Pooled controls (BMHV to GAPDH) | Pooled controls Normalised ($log^2$) | Good Kd (BMHV to GAPDH) | Good Kd normalised relitive protien expression ($log^2$) | Poor Kd (BMHV to GAPDH) | Poor Kd normalised relitive protien expression ($log^2$) |
|---|---|---|---|---|---|---|
| | 1.19 | -0.56 | 0.293235288 | -2.58 | 0.615469398 | -0.31 |
| | 2.95 | 0.75 | 0.286796746 | -2.61 | 0.694658868 | -0.67 |
| | 1.75 | 0.00 | 0.579525821 | -1.60 | 0.595939086 | -1.15 |
| | 1.78 | 0.02 | 0.085833333 | -3.29 | 2 | -1.01 |
| | 2.04 | 0.22 | 0.222562674 | -1.92 | 1.819248826 | -0.34 |
| | 0.80 | -1.13 | 0.801587302 | -0.41 | | |
| | 0.80 | -0.08 | 1.131926121 | -1.49 | | |
| | 0.82 | -0.04 | 0.959866221 | -1.73 | | |
| | 0.71 | -0.24 | 1.858333333 | -0.77 | | |
| | 1.34 | 0.68 | | | | |
| | 1.01 | 0.27 | | | | |
| | 0.37 | -1.20 | | | | |
| | 5.45 | 0.78 | | | | |
| | 2.38 | -0.42 | | | | |
| | 2.07 | -0.62 | | | | |
| | 4.64 | 0.55 | | | | |
| | 2.11 | -0.59 | | | | |
| | 2.39 | -0.41 | | | | |
| Mean | 1.92 | 0.00 | 0.69 | -1.82 | 1.15 | -0.70 |
| SD | 1.35 | 0.59 | 0.57 | 0.91 | 0.70 | 0.38 |
| SE | 0.32 | 0.14 | 0.19 | 0.30 | 0.31 | 0.17 |
| **Normalised Reduction** (%) | - | - | - | **66.38** | - | **41.80** |
| **Significence UT+SC** (*p*-value, two way with unequal variences) | - | | - | **0.00100** | - | **0.049*** |
| **Significence SC only** (*p*-value, two way with unequal variences) | - | - | - | **0.00060** | - | **0.031*** |
| Margin of error (95 % confidence interval) | 0.62 | 0.27 | 0.37 | 0.60 | 0.62 | 0.33 |
| Upper bound | 2.54 | 0.27 | 1.06 | -1.23 | 1.76 | -0.36 |
| Lower bound | 1.30 | -0.27 | 0.32 | -2.42 | 0.53 | -1.03 |
| Red = Standard contols | | | | | | |
| * Excluding last sample in 3rd western | | | | | | |

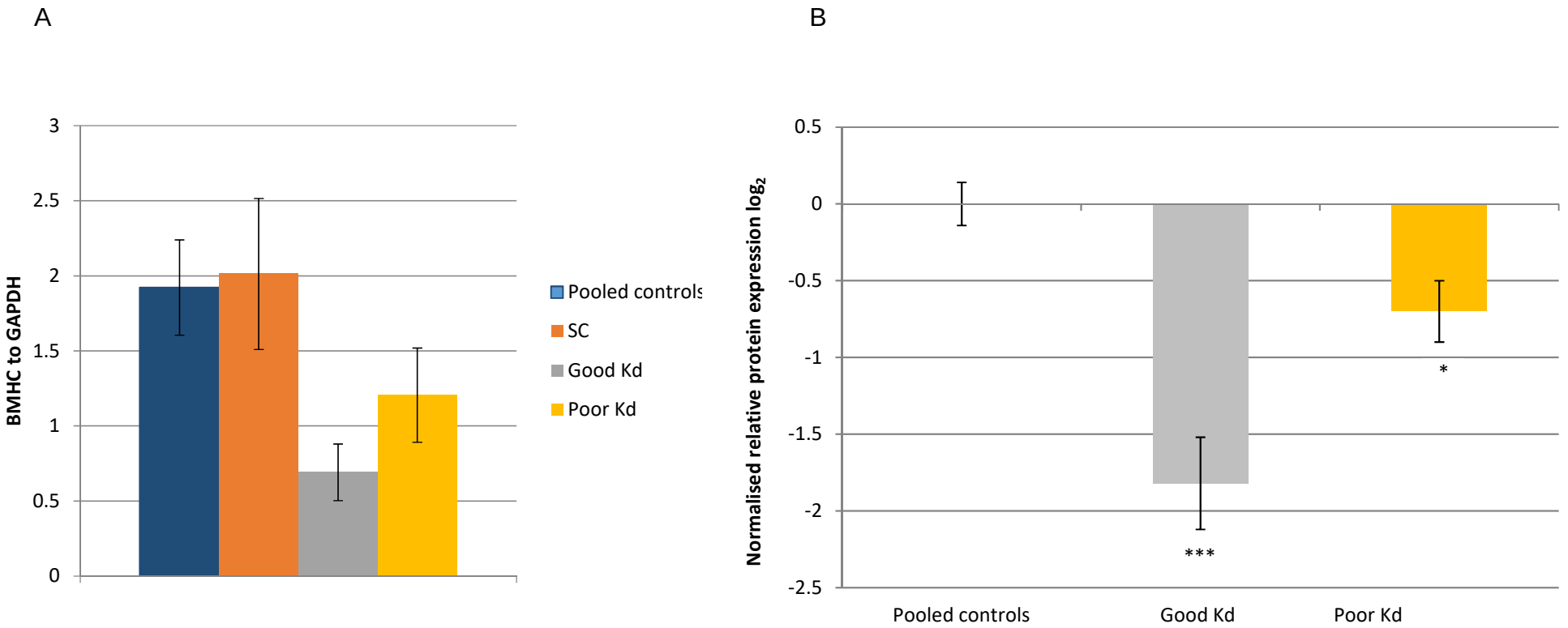



**Figure 3.6** Reduction in protien signal in KDs. A, Controls to KD samples βMHC normalised to GAPDH; B, Relative normalised protein expression. Both KD groups show significantly reduced protein (good KD <0.0001; poor KD <0.05), however, the poor KD group is only significant with the outlier biological repeat removed.

### 3.3.6 Sarcomere maturity scale and random sampling

Sarcomeres were categorised into developmental stages using a ‘maturity scale’. The scale was adapted from a previous study that described stages of sarcomeric assembly to form myofibrils, from the formation of premyofibrils followed by nascent myofibrils and finally mature myofibrils(Du et al., 2008). Our scale was based on this, but added a forth level for when formation of organised aligned myofibrils are seen. Therefore, our staging is based on 1 to 4, with 1 being the most immature and 4 being the most mature structures. Figure 3.7 shows these stages via immunocytochemistry with α-actinin showing the Z lines of sarcomeres.

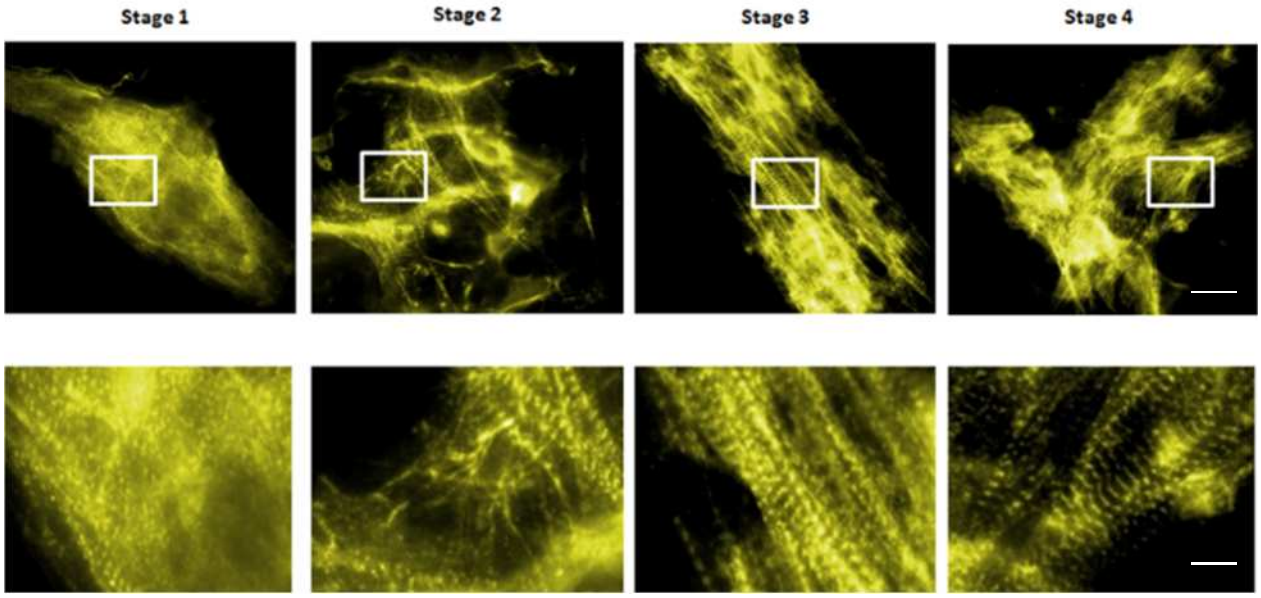



**Figure 3.7** Representative images taken from cell culture at HH29 of developing sarcomere stages showing with α-actinin antibody. Stage 1, Positive sarcomere structures not striated. Stage 2, Visible striated, but under developed sarcomeres. Stage 3, Full sarcomeres but not aligned to each other. Stage 4, Fully aligned sarcomeres. Lower panels are high magnification of boxed areas in upper panels. 100 µm for large images, 10 µm on focused boxed images

### 3.3.7 Knockdown of myosin heavy chain proteins leads to reduced sarcomere maturity in embryonic cardiomyocytes

In order to assess KD effect on sarcomere maturity immunocytochemistry was performed on cultured cells isolated from HH29 embryos. α-actinin antibody was used to show Z lines of sarcomeres. Analysis of sarcomere maturity was then assessed using the maturity scale just outlined in section 3.2.3. Statistics (were then used to determine differences on in-between groups maturity. Ventricular sarcomeres showed significantly reduced mean development against controls ($F(4, 36) = 8.479$ $p= 0.000$) (controls pooled from standard control MO and untreated as they show no significant differences $p= 0.964$). In comparison to the controls (development score 3.25), post hoc tests show a significant decrease in ventricular cardiomyocyte maturity upon eMHC (development score 2.1), αMHC (development score 2.5) and βMHC KD (development score 2.4) (n = 9 per group) (Figures 3.8 & 3.9). Embryonic MHC KD had a greater effect on sarcomere development in ventricular cardiomyocytes when compared with αMHC and βMHC KD, which both gave similar results on developmental level (Figures 3.8 & 3.9). In atrial cardiomyocyte cultures, significant reductions ($F(4, 40) = 3.044$ $p = 0 .028$) were also found against controls (development score 2.9) upon αMHC KD (development score 2.1) and βMHC KD (development score 2.3). However, eMHC KD had a smaller effect in atrial samples with mean scores of 2.4 (n = 9 total samples per treatment group, 18 total in controls) (Figure 3.8 & 3.9). A two way ANOVA examined the effect of KD and heart region (atria or ventricle) on maturity level. No significant interaction between effects of KD or heart region was found ($F (4, 88) =1.406$ $P= 0.240$).

### 3.3.8 Ventricular and atrial cardiomyocyte KD colonies show insignificant reduction in size

When compared to controls, eMHC displayed a 76.3% reduction in overall ventricular colony size, αMHC a 62% reduction and βMHC a 66% reduction. However, the large variation in colony size within controls precludes any significance. Nonparametric Kruskal-Willis tests show differences to be insignificant (X2 (3) = 2.291 P= 0.514).

All KDs showed insignificant reduction in atrial colony size against controls (X2 (3) = 1.973 P= 0.677). Nonparametric Kruskal-Willis was again used due to large variation of colony size. There was however a 16.6% decrease in size on βMHC KD when compared to controls, but values for αMHC and eMHC KD returned similar results to controls.

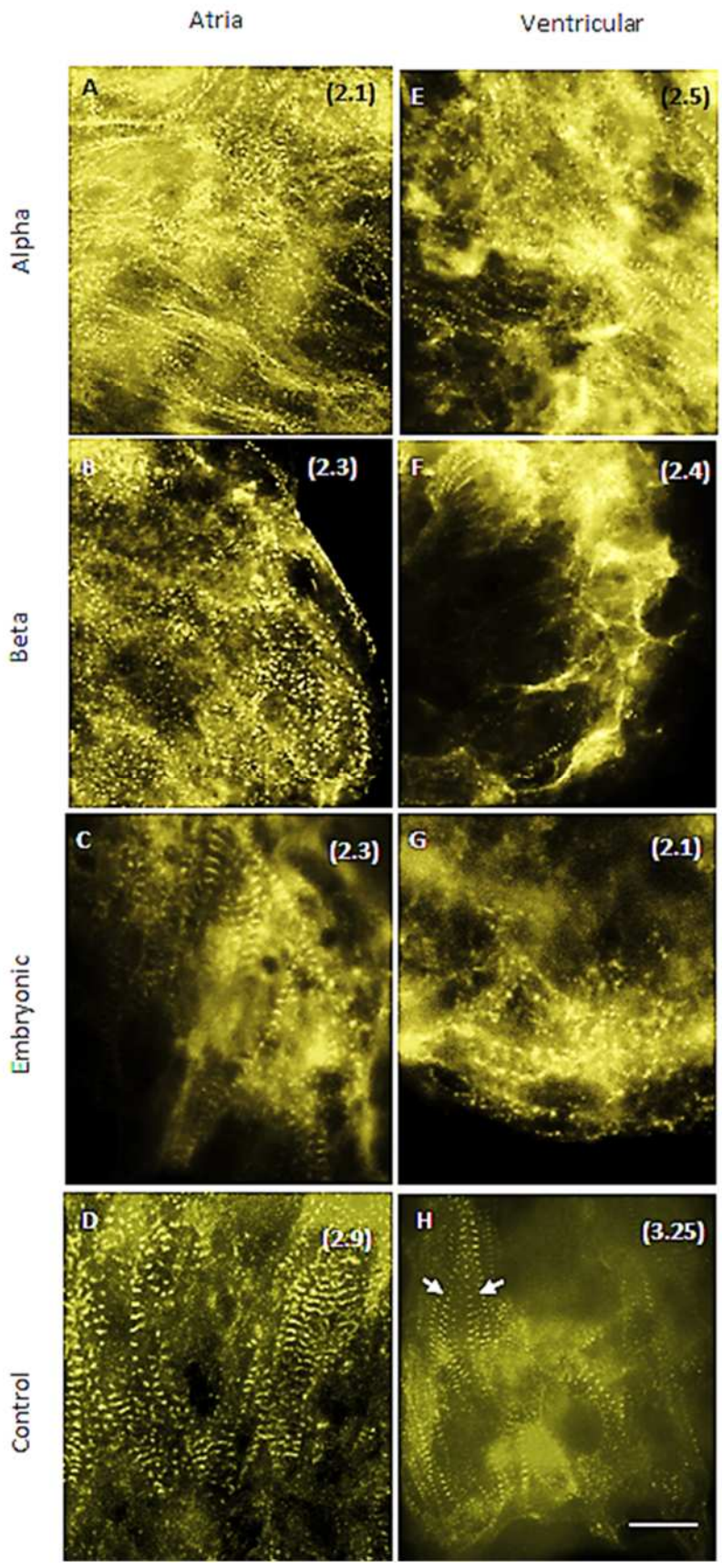



**Figure 3.8.** Representative colonies in atrial and ventricular cardiomyocytes at HH29 with α-actinin antibody.

**A-D** Atrial culture α**,** β, eMHC KD and controls respectively. **E - H:** Represent the average colony development found in ventricle culture α**,** β, eMHC KD and controls respectively. Mean development score denoted in brackets; arrows denote organised structures. Scale bar 20 µm.

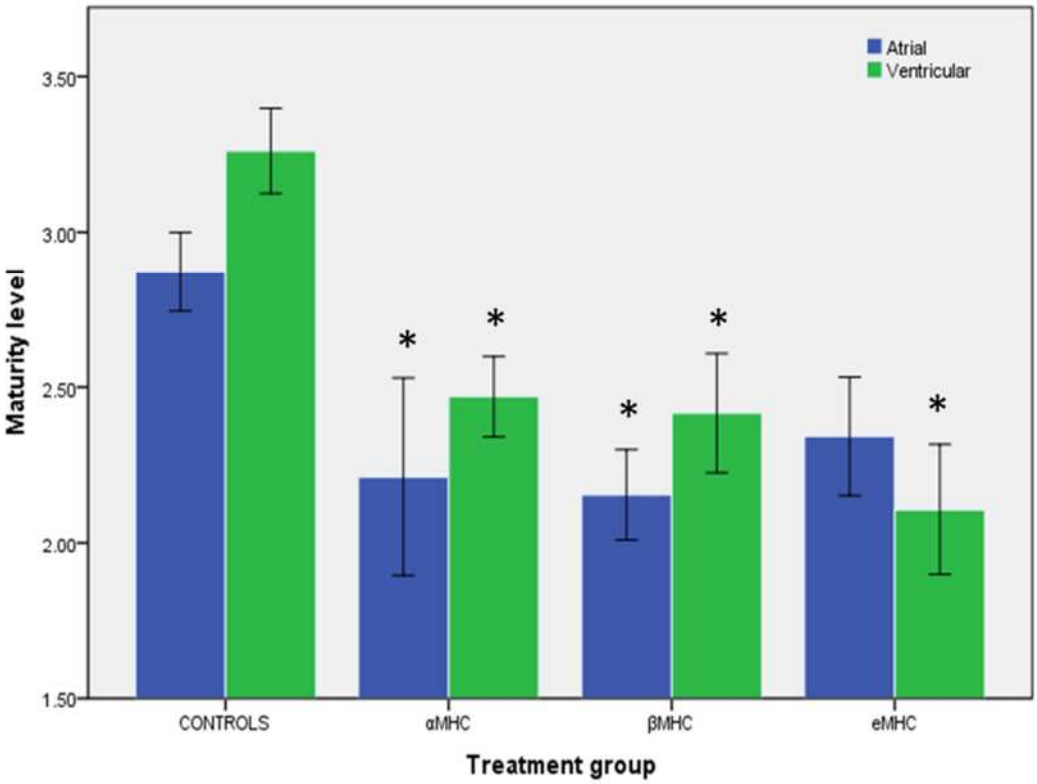



**Figure 3.9.** Sarcomere maturity is affected upon knockdown of MHC proteins at HH29. Maturity level in all treatment groups (KDs and controls) from atrial and ventricular samples (N = 9 wells per treatment group, 18 in pooled controls with cell density of 2.75 X $10^6$). *$p$<0.05. Error bars +/- 1 s.e.m.

### 3.3.9 Atrial colonies were significantly smaller than ventricle colonies

Overall atrial colony size was significantly smaller than overall ventricle colony size in control culture wells (n = 9 wells per group) (F (82) = 8.064 *p* = 0.006). Atrial mean size was 81715 μm$^2$ compared to 325917 μm2 for the ventricle. Figure 3.10 shows representative images. Both ventricular and atrial cells were seemed with the same cell density of 2.75 X 10$^6$.

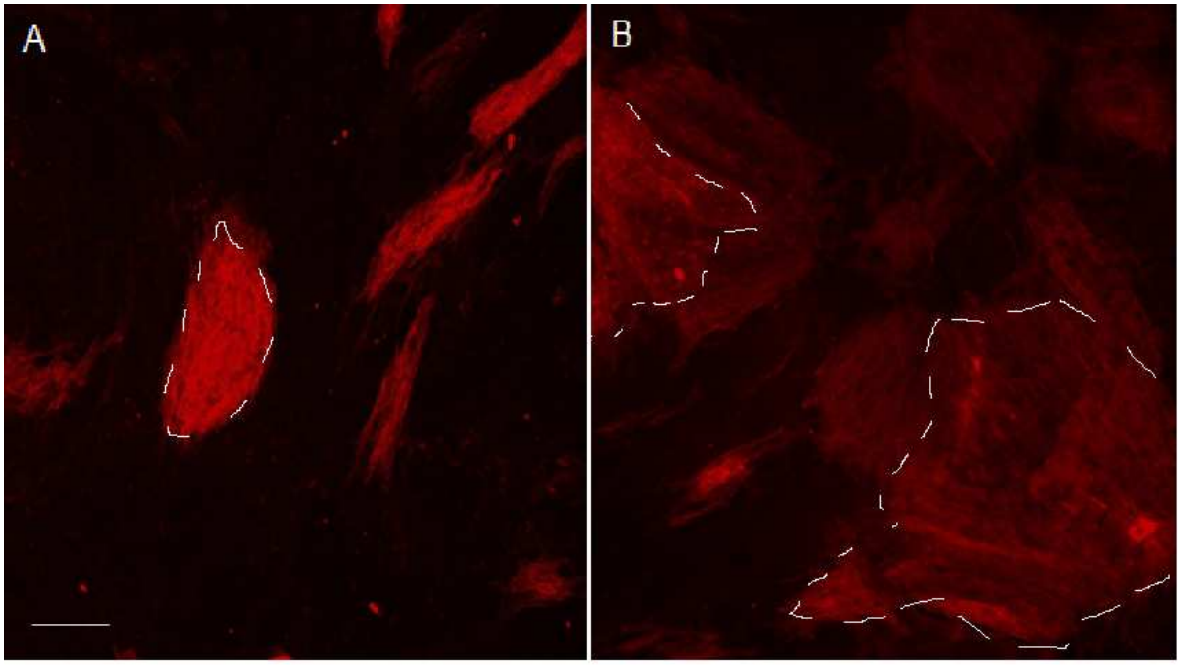



**Figure 3.10** Atrial colonies were significantly smaller to ventricular A, representative image of atrial colonies stained with α-actinin. B, Representative image of ventricular colonies stained with α-actinin. White dotted line represents colonies counted. Scale bar 200 μm.

### 3.3.10 Atrial and ventricular cell beating rate

Mean beats per minute (BPM) of all atrial colonies on day 1 after plating out from HH29 embryos was 106 BPM compared with 43 BPM for all ventricle colonies. Colonies in atrial only wells failed to beat 48 hours post plating out, whereas ventricle wells continued to beat strongly. This meant beating analysis of KD treatment could only be analysed in ventricular culture.

### 3.3.11 Knockdown effect on ventricular culture beating rate

Repeated measures ANOVA with Greenhouse-Geisser correction showed insignificant differences in beating rate across all KDs pre-to-post application of morpholino ($F(1.35, 20.3) = 2.244$ $p=0.144$). However, two out of nine eMHC KD wells failed to form synchronously beating syncytium's, as did two out of nine αMHC wells, compared to all controls wells which did form syncytiums.

### 3.3.12 Cardiomyocytes and beating spread across colonies until synchronisation in merged and separated colonies

Observation of wells showed separated beating colonies on day one after plating out. These colonies all beat independently of each other with differing rates. By day two, nearly all colonies had merged and beat synchronously forming syncytium's, with DAPI staining showing cardiomyocytes going through mitosis. Interestingly, colonies that were clearly separated from each other still beat synchronously. Colonies synchronised to the pace of the fastest colony i.e. when two colonies were found beating independently, one at 40 BPM, the other at 70 BPM, when the colonies started

to beat synchronously their rate was around 62 - 68 BPM. Taken from the faster colonies, this represents a 6.4 % decrease in rate after two days.

### 3.3.13 Conduction migration across fibroblasts between colonies

Colonies showed migration of synchronous beating across the separated colonies with conduction distances above 500 µm. Figure 3.11 Shows separated colonies that were beating synchronously with sarcomeres visualised by immunocytochemistry. The purple/pink stain shows up α-actinin in cardiomyocytes. This shows that the synchronously beating cardiomyocytes were totally isolated from each other with no link of cardiomyocytes present.

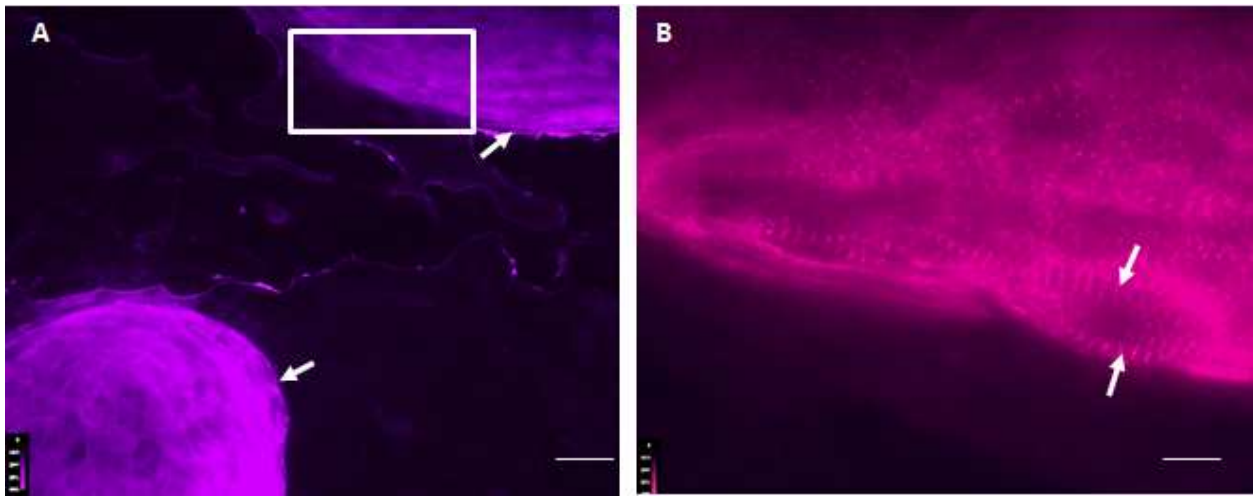



**Figure 3.11** Synchronously beating colonies. A, Separated colonies that beat simultaneously. Arrows denote separated colonies. B, From boxed area in panel A, a wall section of colony showing that cardiomyocytes do not extend out from colonies**.** Arrows show sarcomeric structures. A, Scale bar 100 µm; B, Scale bar 10 µm.

### 3.3.14 Cell culture result relevance

The cell culture experiment was utilised for multiple purposes. Firstly it allowed assessment of sarcomere maturity of KD compared to control wells by immunocytochemistry; were all cultured wells started from the same cell mass and were cultivated in identical conditions. Secondly it allowed the assessment of beating rate and spread of beating in of the cell mass in KD and control wells. Though this second aim of culture was only partly successful as atrial colonies failed to beat after around 48 hours of plating out, the information gained here can lead to future experiments were conditions can be altered to see if atrial culture can be maintained. Lastly, colony size was assessed were ventricular colonies were found insignificantly bigger than atrial. The variation in size in colonies lead to the insignificant value, and if a higher cut off point in colony size was used, than this variation would have been greatly reduced. With significant reductions found in sarcomere maturity in KD colonies, the next part of the project was to see if gene expression is altered by KD, particularly looking at genes of the conduction system.

Conduction gene expression I knockdown embryos

Previous findings by Rutland (Rutland et al., 2011, Rutland et al., 2009). demonstrated a conduction phenotype in myosin KD hearts. Our KD cultures revealed reduced sarcomere maturity on KD, however, no significant alteration in beating rate was seen. What was seen however was that two out of nine ventricular eMHC KD wells failed to form synchronously beating syncytium's, as did two out of nine ventricular αMHC wells, compared to all controls wells which did form syncytiums. This next section now looks at gene expression in KD embryos with an aim to identify expression in key cardiac conduction genes. Before KD gene expression experimentation, if it had not already beam established in the literature, gene expression of targets in the chick were assessed.

### 3.3.15 Confirmation of unknown gene expression in early chick embryonic development of conduction genes to potentially be analysed in knockdown embryos

#### *3.3.15.1 KCNE1*

Potassium voltage-gated channel subfamily E member 1 (KCNE1) has not previously been shown in the developing chick heart. KCNE1 shows expression by end point PCR in the chick heart across early developmental stages from just after heart tube formation and heart looping initiation at HH12 through to after septation of the heart at HH34 (Figure 3.12).

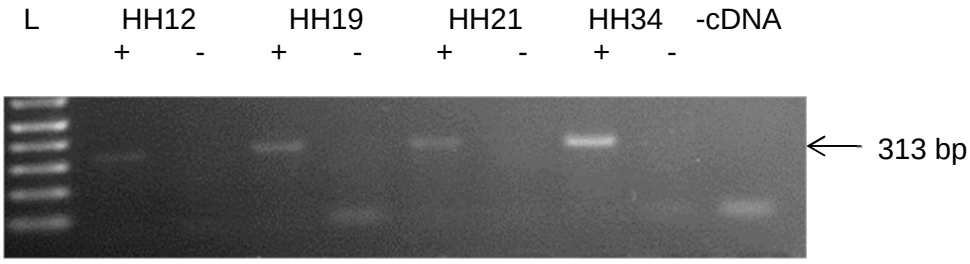



**Figure 3.12** *KCNE1* Expression profile with cDNA templates from HH12 – HH34. KCNE1 expression was shown at expected band size at HH12, 19, 21 and 34. L, 1 KD plus ladder; +, reverse transcriptase positive; -, reverse transcriptase negative. – cDNA, no template control.

To check that PCR binding and activity were working optimally, magnesium (Mg) concentration was altered in a range of 0.5 to 2.5 mM using cDNA from HH21. HH20/21 is the stage at which KD hearts were analysed so this is why only that stage was used (figure 3.13). Standard concentration was 1.5 mM, so 1.5 mM was used for

*GAPDH*. Altering concentration higher than standard made no difference to the band intensity. The PCR suggests that while present, expression may be low.

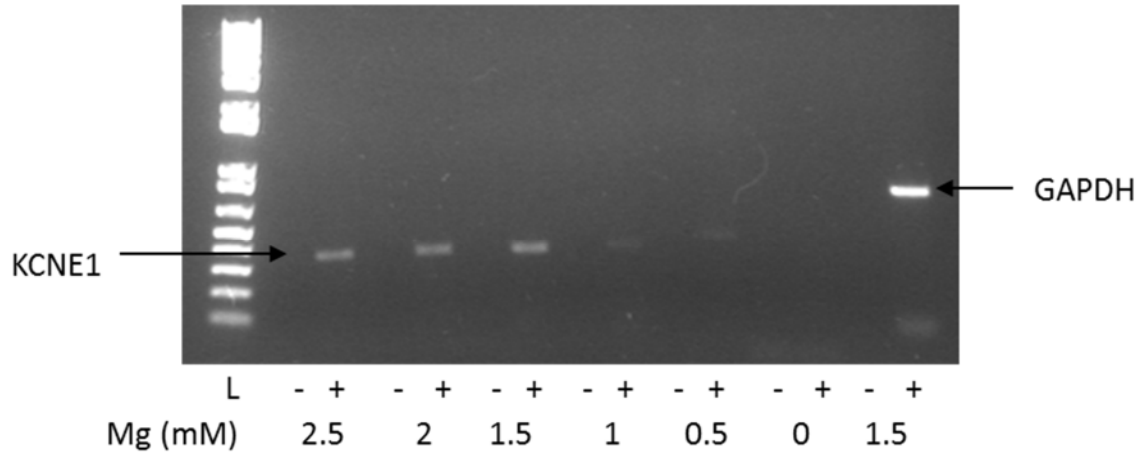



**Figure 3.13. Magnesium optimisation PCR at HH21**. *KCNE1* band (313 bp) intensity reached its highest point at standard Mg concentrations of 1.5 mM. GAPDH (lab stock 1 GAPDH 850 bp) shown at 1.5 mM Mg. L, 1 KD plus ladder; +, reverse transcriptase positive; -, reverse transcriptase negative.

#### 3.3.15.2 *CACNA1C* and *CACNA1D* expression profile across early development

Calcium channel, voltage-dependent, L type, alpha 1C subunit (*CACNA1C*) and 1D subunit (CACNA1D) have not previously been shown in the developing chick heart. *GAPDH* is used at HH20 was this is the main initial stage at which KD anaylsis will take place. Both genes show expression at HH12,19 and 29, with *CACNA1C* appearing to be the more highly expressed at HH20 based on qualitive observation of band intensity (Figure 3.43). HH29 is another key point in development where cells of the sinoatrial node have/ are in the process of locating itself in the left atrium.

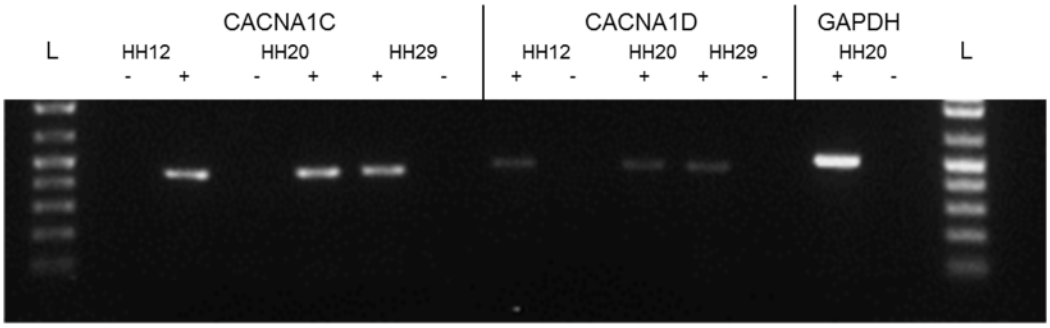



**Figure 3.14** *CACNA1C* and *CACNA1D* Expression profile with cDNA templates from HH11 – HH29. *CACNA1C* (415 bp) and *CACNA1D* (455 bp) expression was shown at expected band size at HH11, 20 and 29. L, 1 KD plus ladder; +, reverse transcriptase positive; -, reverse transcriptase negative.

Expression found in targeted genes now requires *In situ* hybridisation

These results confirm that *KCNE1*, *CACNA1C* and *CACNA1D* all show expression in the embryonic chick heart. This now means further analysis of these genes can take place. It would appear that *KCNE1* and *CACNA1D* may be lowly expressed at HH20/21, so expression analysis of these two genes may yield limited results.

The further analysis of these genes is by *in situ* hybridisation. The aim of the in-situs is to elucidate if gene expression is affected in knockdowns in a spatial manner. This is important as RT-qPCR cannot detect differences in ectopic expression, therefore in-situ hybridisation of whole mounts will allow the maximal information on expression to be obtained. Following in-situs, if an up or down regulation is seen/suspected, RT-qPCR will be carried out to confirm results. *In situ* hybridisation (ISH) requires individual gene optimisation in order to be successful. Optimisations were unsuccessful (no signal present) for *KCNE1* and so this gene is not used for in-situ analysis.

### 3.3.16 *In situ* hybridisation: development of protocol for whole mounts from HH16 to early HH35

*In situ* hybridisation across early and late stages required key optimisations of tissue in order to both retain embryo structural integrity and allow penetration of probe. *In situ* hybridisation was carried out at HH16, HH20, HH25, HH29, HH34. HH20 and HH25 used standard protocols with no need for optimisations. Table 3.3 shows alteration to whole-mount preparations. On the following *in situ* hybridisation experiments on *CACNA1C*, *GJA5* and *GJA1* the sense images were taken with a darker background than antisense as is was often impossible to make out the heart feature on a light background.

**Table 3.3** Key optimisations for preparation for whole mount *in situ* hybridisation

| **Developmental stage** | **Whole-mount preparations** |
|---|---|
| HH16 | Embryos were fixed before removal of chorioallantoic membrane. This stopped the embryos from pulling apart when harvesting. |
| HH25 | Whole mount embryos and isolated hearts were used at this stage to be sure that probe penetration was not an issue.<br><br>Isolated hearts: Remove heart from embryo and pierce chamber regions once to remove blood. |
| HH29<br><br>and<br><br>HH35 | Remove and bisect heart. Bisections were performed frontally separating anterior and posterior halves. The cut was made medially to the anterior outflow tracts and ran through to the apex. This ensured that maximal penetration of riboprobe was being attained. Images in this thesis show only the posterior portion. This is because it allows easy analysis of the full atria and ventricular chambers. |

### 3.3.17 Expression profile spatially within the heart of key conduction genes across developmental stages by *In situ* Hybridisation

*CACNA1C* and *CACNA1D* are voltage gated long acting cell membrane protein channels involved in $Ca^{2+}$ transport across the cell membrane. *GJA5* and *GJA1* code for are intracellular channels that allow ions to pass between cell membranes. Expression of these genes was analysed across different developmental stages development in an attempt to increase understanding of ion transport genes in the developing embryo. as it is currently poorly understood in the literature.

#### 3.3.17.1 Voltage gated calcium channel *CACNA1D*

Initial optimisations proved difficult with CACNA1D, possibly due to a potential low expression being hard to detect above background at HH20 (Figure 3.13), and it was decided to not continue analysis of this gene through developmental stages.

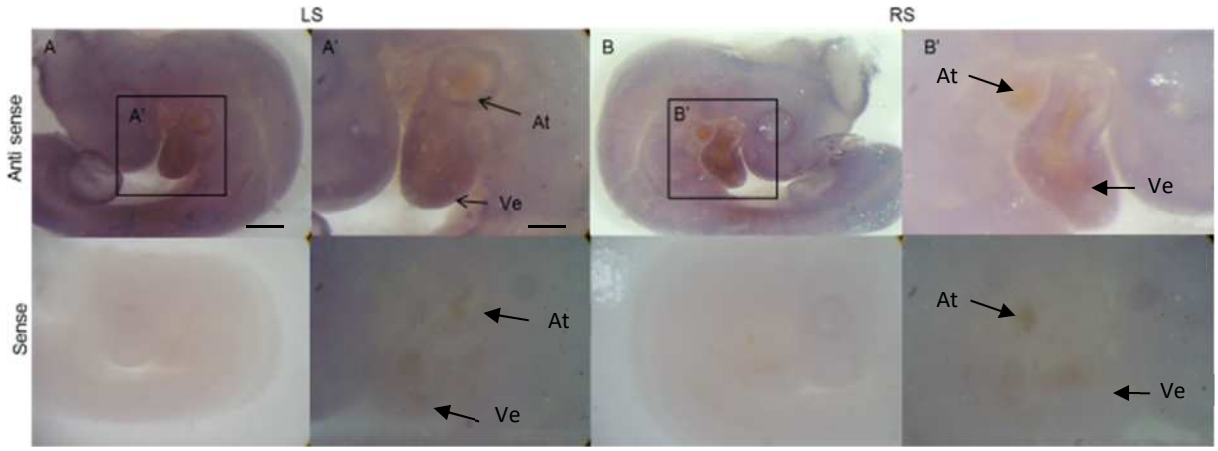



**Figure 3.15** *CACNA1D* at HH20. Weak expression is seen that is barely noticeable above background in the heart at the atrium border (At) and throughout ventricle (Ve). LS' left saggital; RS, right saggital. 1000 µm for whole embryo images, 500 µm on boxed images.

### 3.3.17.2 Voltage gated calcium channel *CACNA1C* transcripts

Two different probes designed for *CACNA1C*, one positive for both of the main known transcripts and another for just transcript 1 (see methods table 2.2). Analysis at HH20 showed weak expression of transcript 1 (Figure 3.16 A), again, barely noticeable above background. The probe positive for both transcripts however showed good expression (Figure 3.16 B). Because of this, only the probe for both transcripts was used to assess spatial expression across developmental stages.

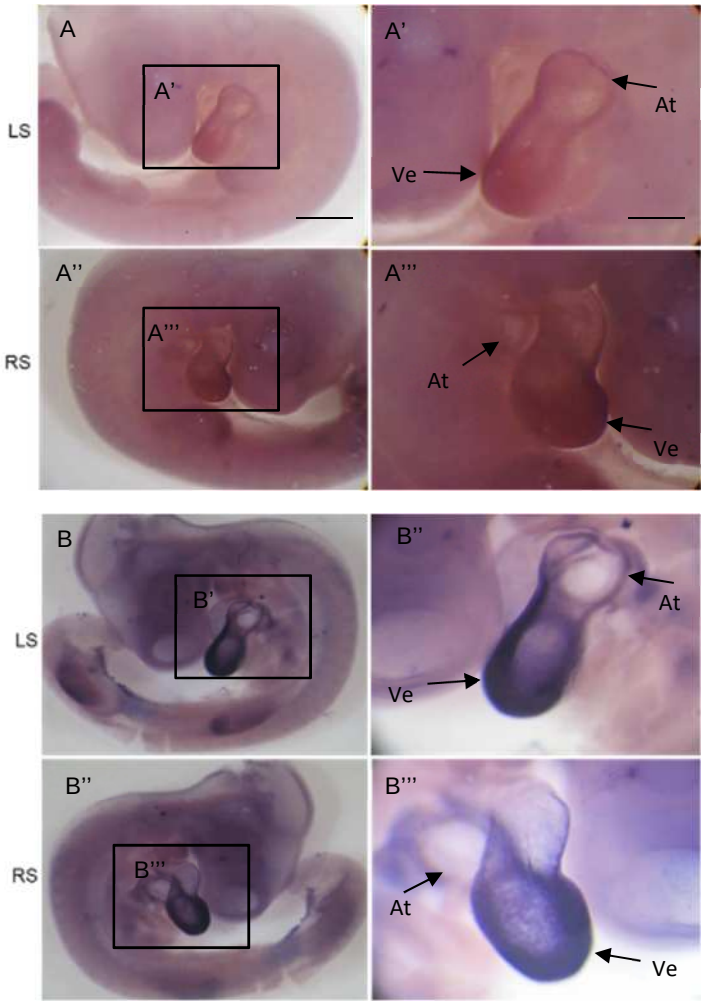



**Figure 3.16** ***CACNA1C*** **HH20 expression**. Transcript 1 was weakly expressed in the heart at HH20. The probe for transcript 1 and 2 together give strong signal. A, shows transcript 1 expression only just visible above. B, Shows clear expression of transcript 1 and 2 together at the boarder of the atrium and throughout the ventricle. Boxed area enlarged X2. LS, Left sagittal; RS, Right sagittal. 1000 µm for whole embryo images, 500 µm on boxed images.

#### 3.3.17.3 Voltage gated calcium channel *CACNA1C* developmental expression

Figure 3.17 shows the spatial expression pattern from HH16 to HH35. At HH16, weak, but broad expression was seen throughout the whole heart. At HH20 a clear pattern has been established throughout the ventricle, but not at all in the outflow tract. Expression in the atria was weak and mainly present in the border region. At HH25, the whole mount embryo pattern looks the same as at HH20, although expression was weaker. However, in HH25 isolated hearts, analysis reveals strong expression and shows for the first time a concentration of expression in the region of the developing interventricular septum. The right ventricle also appears to have increased expression compared to the left. HH29 and HH35 show similar expression patterns. Atrial expression was reduced to barely noticeable levels. Expression was strongest at the interventricular septum and right ventricle.

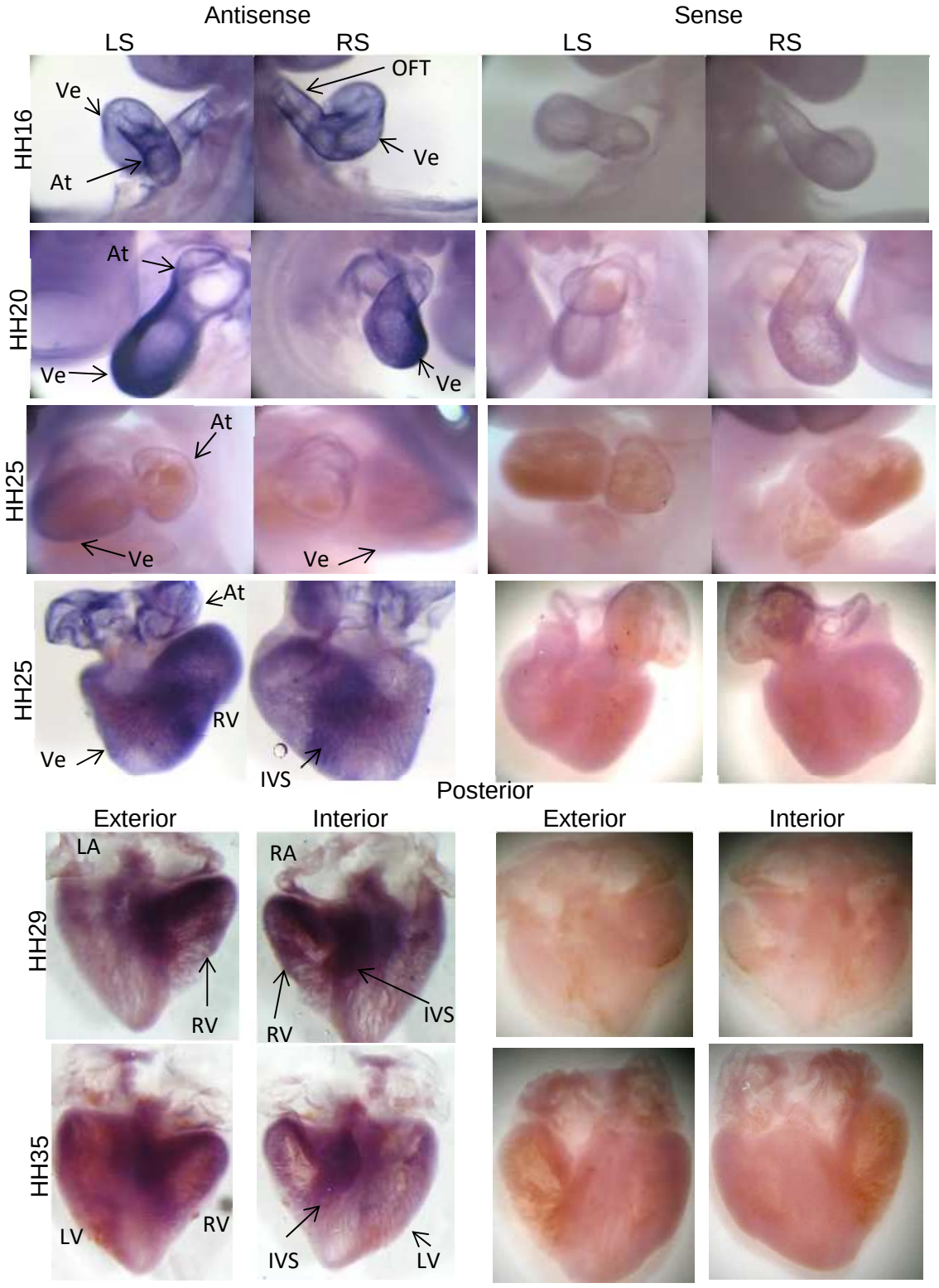



**Figure 3.17** *CACNA1C* expression from HH16 to HH35. At HH16 broad expression in developing atria (At), ventricle (Ve) and outflow tract (OFT) region was seen. At

HH20 expression was predominantly in the ventricle, with low levels at the atrial border (antisense n =5; sense n =3). At HH25 embryos show a similar, expression pattern to HH20 whole embryos. Individual hearts showed strong expression to the right ventricle (RV) and the interventricular septum (IVS) (antisense n = 2, sense = 1). HH29 and HH35 isolated hearts show little expression in the atria with strong ventricular expression; the strongest expression was seen in the right ventricle and the interventricular septum (antisense n=4, sense n=3). LS, left sagittal; RS, right sagittal.

#### 3.3.17.4 Gap junction connexin 42 (*GJA5*)

*GJA5* codes for ion channels that allow conduction signal to pass from cell to cell. *GJA5* expression was analysed to see if it would be affected by KD. The gene has been studied in the embryonic chick previously, so general developmental expression patterns were already known in the literature, however patterns at our particular stages remain relatively unknown.

#### 3.3.17.5 *GJA5* arterial heart expression shows potential developmental tracts

Though the general expression pattern of *GJA5* is known, an interesting pattern not previously reported was seen. Analysis of the anterior external surface at HH29 and HH35 revealed tract lines of *GJA5* being expressed proximal to the outflow tract in all hearts (n = 2 for at each stages) (Figure 3.18). These tract lines extend out in to the myocardium of the ventricle in a manner similar to the not yet developed coronary vascular system at HH29. The tract lines at HH35, when the preliminary coronary vessels had been established, appear weaker than HH29. No tracts were visible below or at HH25 (Figure 3.16).

#### 3.3.17.6 *GJA5* developmental expression

Figure 3.19 shows the spatial expression pattern from HH16 to HH35. At HH16 weak expression was seen in the ventricle particularly at the epicardium. At HH20 expression was strong throughout both the ventricle and atria, though expression in the atria was still weaker than ventricle. This pattern of strong expression throughout both chambers was then reciprocated at HH25, 29 and 35. Clear expression can be seen in trabeculae at HH35.

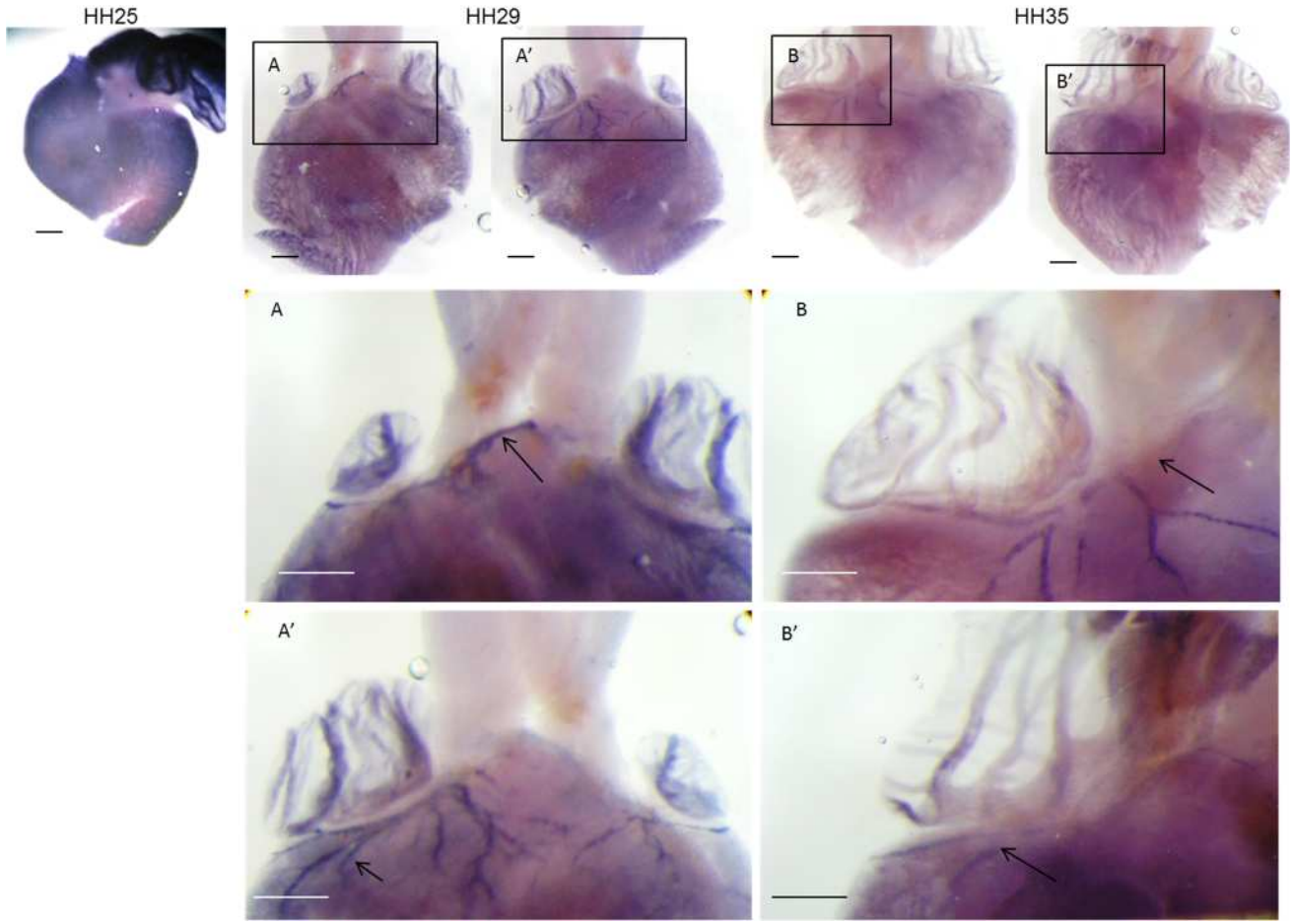



**Figure 3.18** Anterior heart external surface expresses tracts of *GJA5*. HH25 and earlier show no obvious tracts. HH29 shows tract line (arrow in A/A'). HH35 shows tract line network with apparent reduction compared to HH29 (arrow B/B'). All scale bars 500 µm. n=2 at each stage.

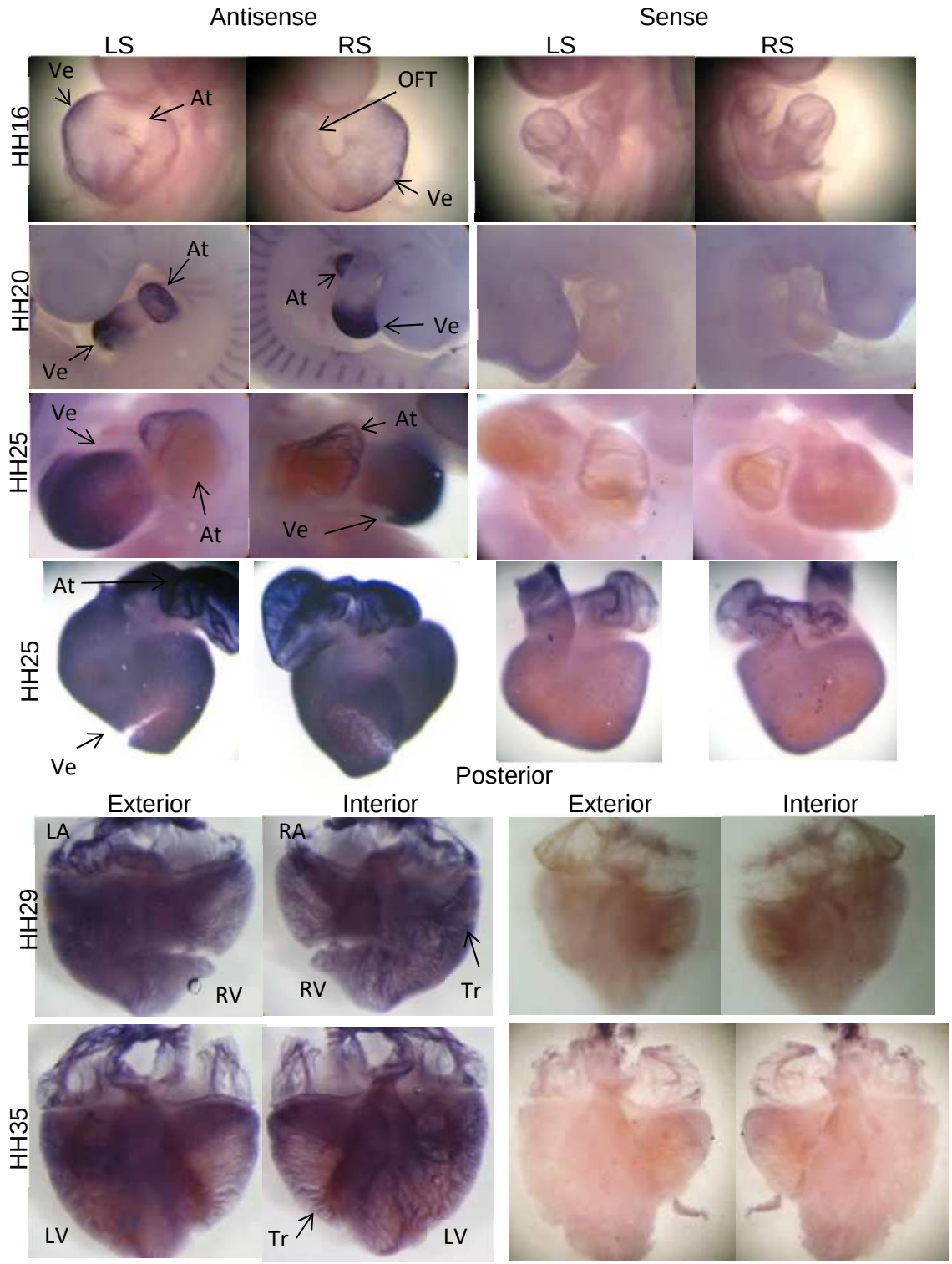



**Figure 3.19** *GJA5* expression from HH16 to HH35. At HH16 weak expression was seen in the ventricle (Ve). At HH20 expression was strong throughout both the

ventricle and atria (At), though expression in the atria was still weaker than ventricle (Antisense n =5; sense n =3 for both stages). This pattern of strong expression throughout both chambers was then reciprocated in the whole isolated hearts at HH25 (antisense n = 2, sense n =1), HH29 and HH35 posterior bisects (antisense n=4, sense n=3 for each stage). Clear expression was seen in trabeculae (Tr) at HH35. LS, left sagittal; RS, right sagittal.

#### *3.3.17.7 GJA1*

Similar to *GJA5*, *GJA1* codes for ion channels that allow conduction signal to pass from cell to cell. *GJA1* expression was analysed to see if it would be affected by KD. The gene has been studied in the embryonic chick previously, so general developmental expression patterns were already known in the literature, however patterns at our particular stages remain relatively unknown.

##### **3.3.17.7.1 *GJA1* Developmental expression**

Figure 3.20 shows the spatial expression pattern from HH16 to HH35. No noticeable expression was present at HH16, HH20 or HH25. At HH29 and HH35 a broad, but very weak expression similar to *GJA5* was in the ventricle and to a lesser extent the atrium was seen.

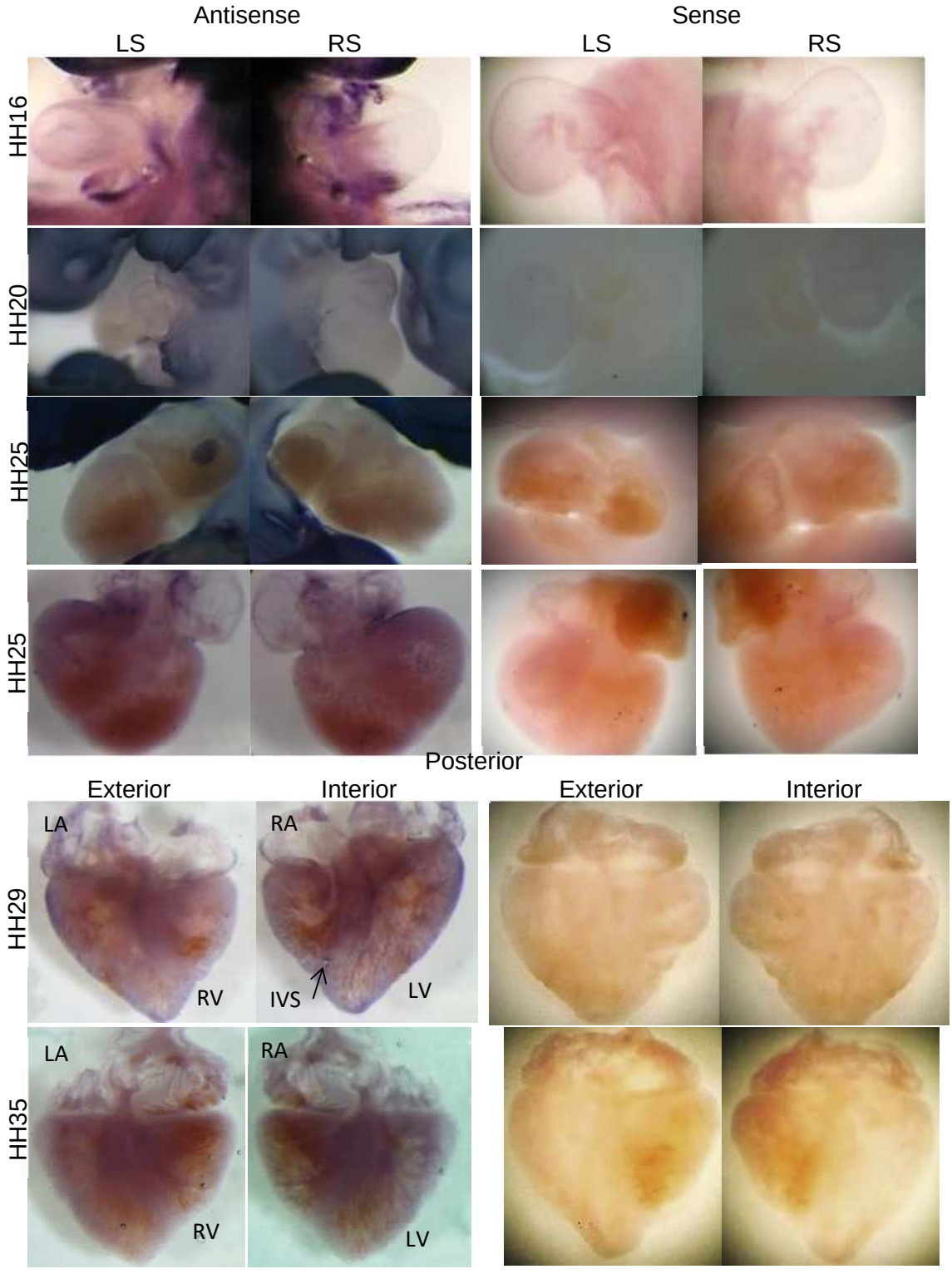



**Figure 3.20** *GJA1* expression from HH16 to HH35. At HH16 to HH25 no expression was seen (antisense n =4, sense n =2 for HH16 and HH20; antisense n =2, sense n =1 for HH25). Posterior bisects HH29 and 35 weak expression can be seen broadly in

the ventricle and very weakly in the atria (antisense n=4, sense n=3 for each stage). LS, left sagittal; RS, right sagittal.

### 3.3.18 Expression study of conduction genes in knockdown hearts by whole mount *in situ* hybridisation

To assess the effect of KD on key conduction gene expression, a combination of either/or or situ hybridisation and RT-qPCR was carried out on standard control (SC) and knocked down alpha myosin heavy chain (αMHC), beta myosin heavy chain (βMCH) and embryonic myosin heavy chain embryos (eMHC). The developmental stage assessed was HH20 when the cells that will become the sinoatrial node (SAN) are still yet to migrate from the sinus venosus (Garcia-Frigola et al., 2003). Genes assessed were Potassium/sodium hyperpolarization-activated cyclic nucleotide-gated channel 4 (*HCN4*), Gap junction alpha-5 protein (*GJA5*), Calcium channel, voltage-dependent, L type, alpha 1C subunit (*CACNA1C*), T-box transcription factor 18 (TBX18), and T-box transcription factor 3 (TBX3). Initial studies were by *in situ* hybridisation. Genes identified as potentially being up or down regulated were assessed further by RT-qPCR. Genes that were difficult to interpret because of low signal, such as TBX3, were also analysed by RT-qPCR as RT-qPCR has increased sensitivity and cDNA concentrations can be increased.

#### *3.3.18.1 HCN4*

*HCN4* is a specific marker for the cardiac conduction system in the action potential generating SAN (Liang et al., 2013). *HCN4* expression in standard control and untreated embryos showed an expression pattern consistent with literature at the sinus venosus (Garcia-Frigola et al., 2003). Knockdowns appear to show some differential expression by *in situ* hybridisation. αMHC and βMHC show reduced signal in a subset of embryos in the sinus venosus region, 2 out of 4 for αMHC and 3 out of 5 for βMCH. eMHC showed a slight, but consistent decrease in 5 out of 5 embryos (figure 3.21).

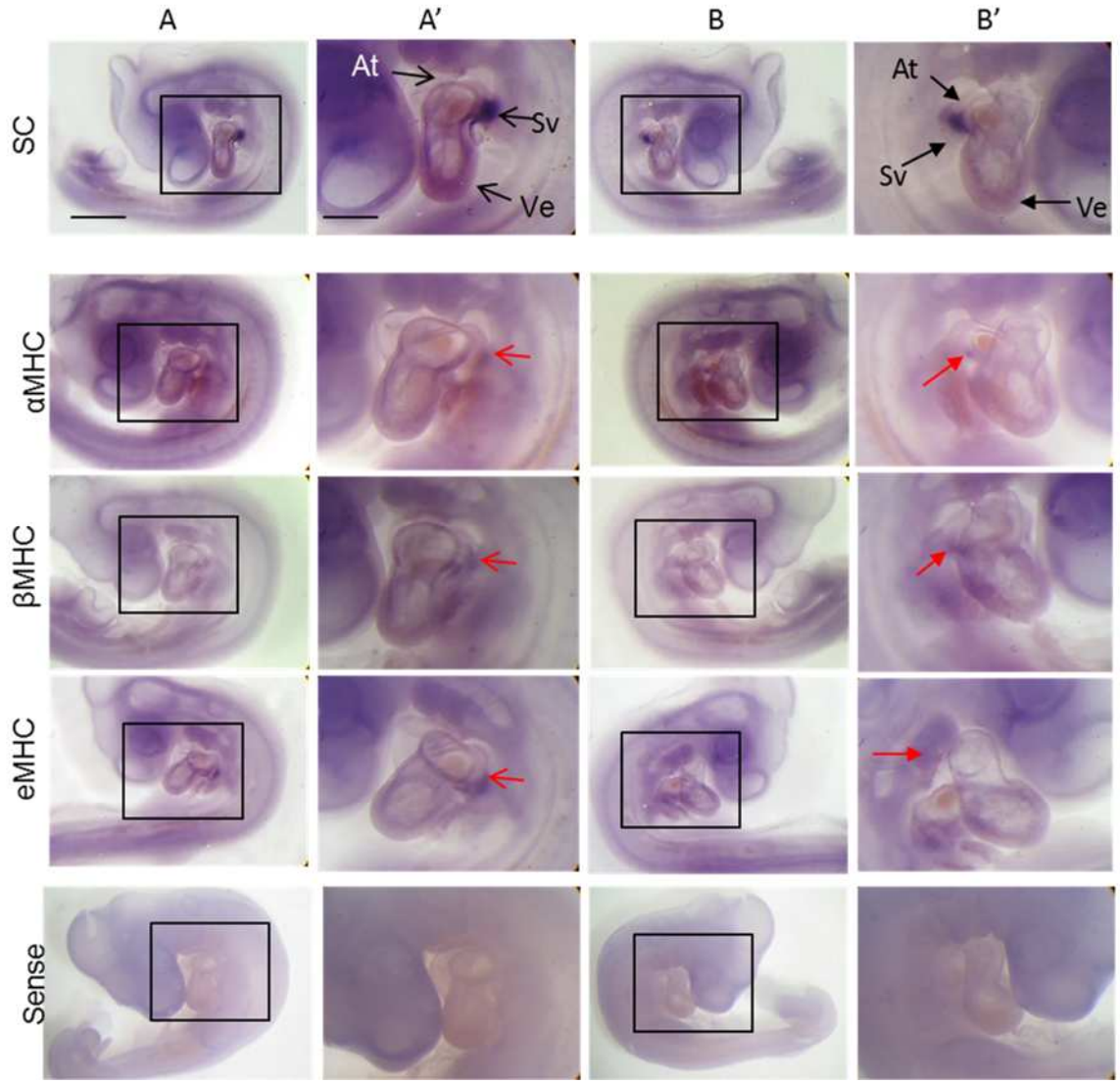



**Figure 3.21** *HCN4* shows reduced signal in knockdown embryos at the sinus venosus at HH20. Compared to standard controls (SC), αMHC and βMHC showed reduced expression in a subset of embryos at the sinus venosus in 2 out of 4 embryos for αMHC and 3 out of 5 for βMCH. eMHC showed slightly reduced signal in 5 out of 5 embryos. A, shows left side of heart, B shows right side. Black arrow indicates normal expression at sinus venosus in SC. Red arrow indicates reduction in signal at sinus venosus. At, Atrium; Ve, Ventricle; Sv, Sinus venosus. 1000 µm for whole embryo A and B images, 500 µm on A' and B' boxed images.

#### *3.3.18.2 GJA5*

*GJA5* is a known marker gene for the myocardium and is not present in the cardiac conduction system (Jansen et al., 2010).*GJA5* expression in controls is throughout the atrium, with strong expression at its borders from the inflow tract to the AV canal. Expression in the ventricle was strong distally at its apex, with gradual reduction superiorly until expression disappears completely before the AV canal and outflow tract where expression was absent. In comparison to the controls, results suggest that upon eMHC KD, decreased expression can be seen in 2 out of 7 embryos, most notably in the atria (red arrow) and possibly in the ventricle (green arrow). αMHC displayed a similar result, but in just 1 out of 5 embryos, and βMHC KD had results similar to controls (Figure 3.22).

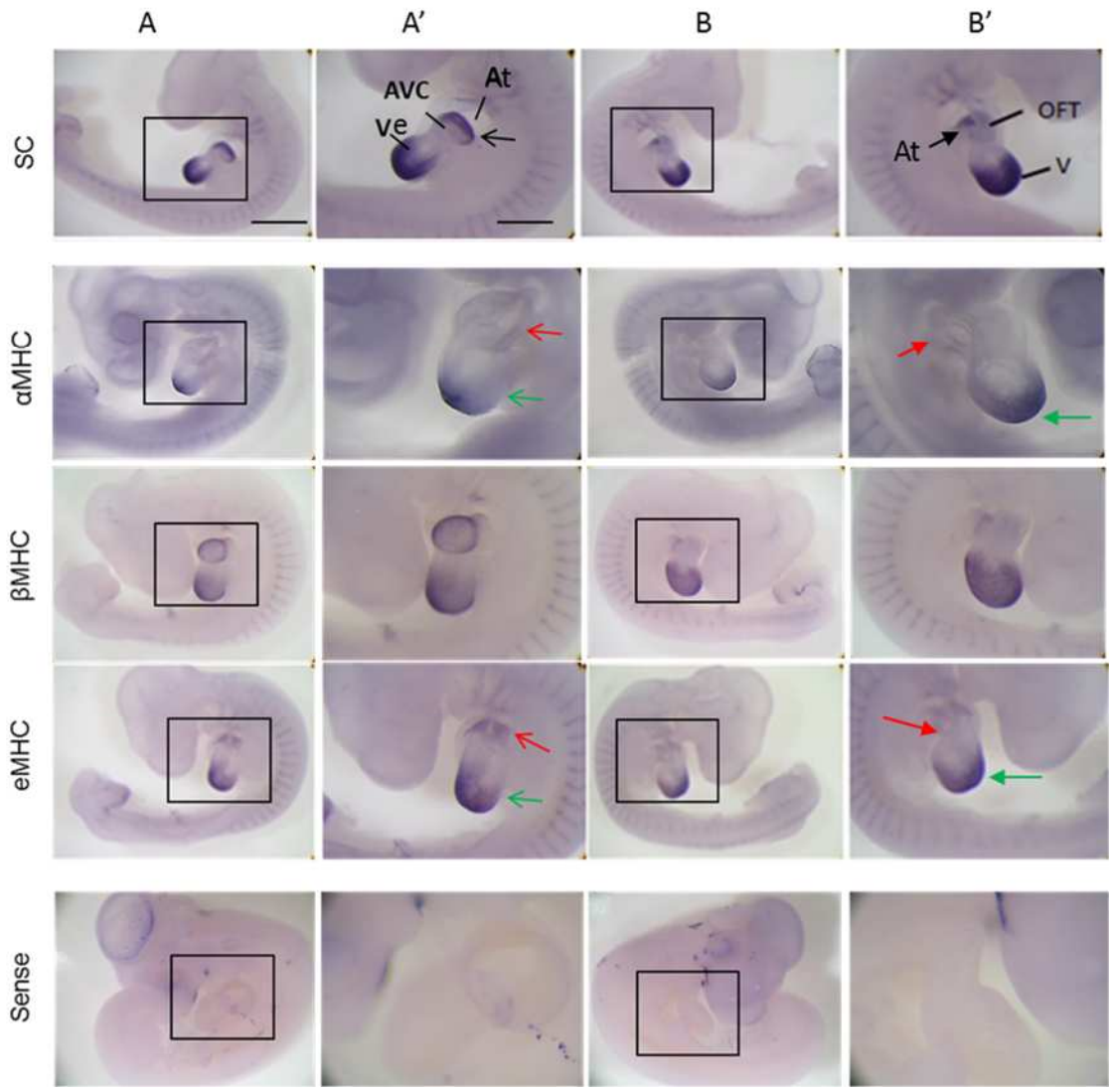



**Figure 3.22** *GJA5* shows reduced signal in a subset of knockdown embryos in the atria and ventricle at HH20. Compared to standard controls (SC), αMHC expression in 1 out of 5 embryos appeared to show a reduction in the atrium (red arrow) and ventricle (green arrow). eMHC appeared to show the same pattern in 2 out of 7 embryos. βMHC showed no apparent differences. Black arrow indicates normal expression in SCs. n = 3 for all groups A, shows left side of heart, B shows right side. Black arrow indicates normal expression at sinus venosus in SC. Red arrow indicates reduction in signal at sinus venosus. At, Atrium; Ve, Ventricle; AVC, atrial ventricular

canal; OFT, Outflow tract. 1000 µm for whole embryo A and B images, 500 µm on A' and B' boxed images.

#### *3.3.18.3 TBX3*

*TBX3* was assessed as it is a transcriptional repressor of myocardium tissue (Hoogaars et al., 2004). Initial *in situ* hybridisation optimisations showed *TBX3* to be very weakly expressed in the heart (Figure 3.23); expression was seen in the heart after extensive overstaining at the atrioventricular junction. Expression was strong in the otic vesicle, pharyngeal arches and limb buds as is consistent with literature (Hoogaars et al., 2007). Due to this weak heart staining, knockdown embryos were not analysed by *TBX3 in situ* hybridization. They were, however, analysed by *TBX3* RT-qPCR (see next Section 3.2.5.4).

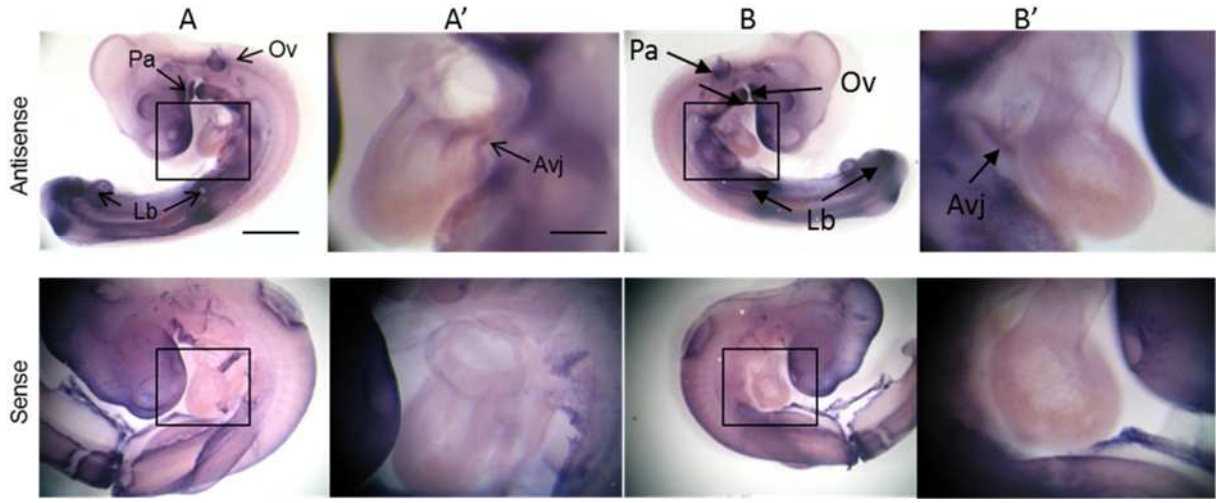



**Figure 3.23** *TBX3* shows weak signal at the atrioventricular junction (Avj) at HH20. Strong signal is seen in the otic vesicle (Ov), pharyngeal arches (Pa) and limb buds (Lb). This would suggest *TBX3* is expressed to only low levels at the AVJ at HH20. A, shows left side of heart, B shows right side. 1000 µm for whole embryo A and B images, 500 µm on A' and B' boxed images.

#### *3.3.18.4 TBX18*

*TBX18* was analysed as it is expressed at the sinus venosus alongside *HCN4* (Vicente-Steijn et al., 2010), and in the developing SAN at the head of the SAN (Wiese et al., 2009). Unlike *TBX3*, that represses working myocardium expression, *TBX18* is actually necessary for the formation of the SAN (Wiese et al., 2009). In-situ hybridisation revealed similar expression patterns in SC and all KD groups that corresponded to expected expression pattern in literature. Expression was at the sinus venosus, proepicardial organ and at the curvature of the AVJ. *TBX18* was also found in the migrating epicardium. (Figure 3.24)

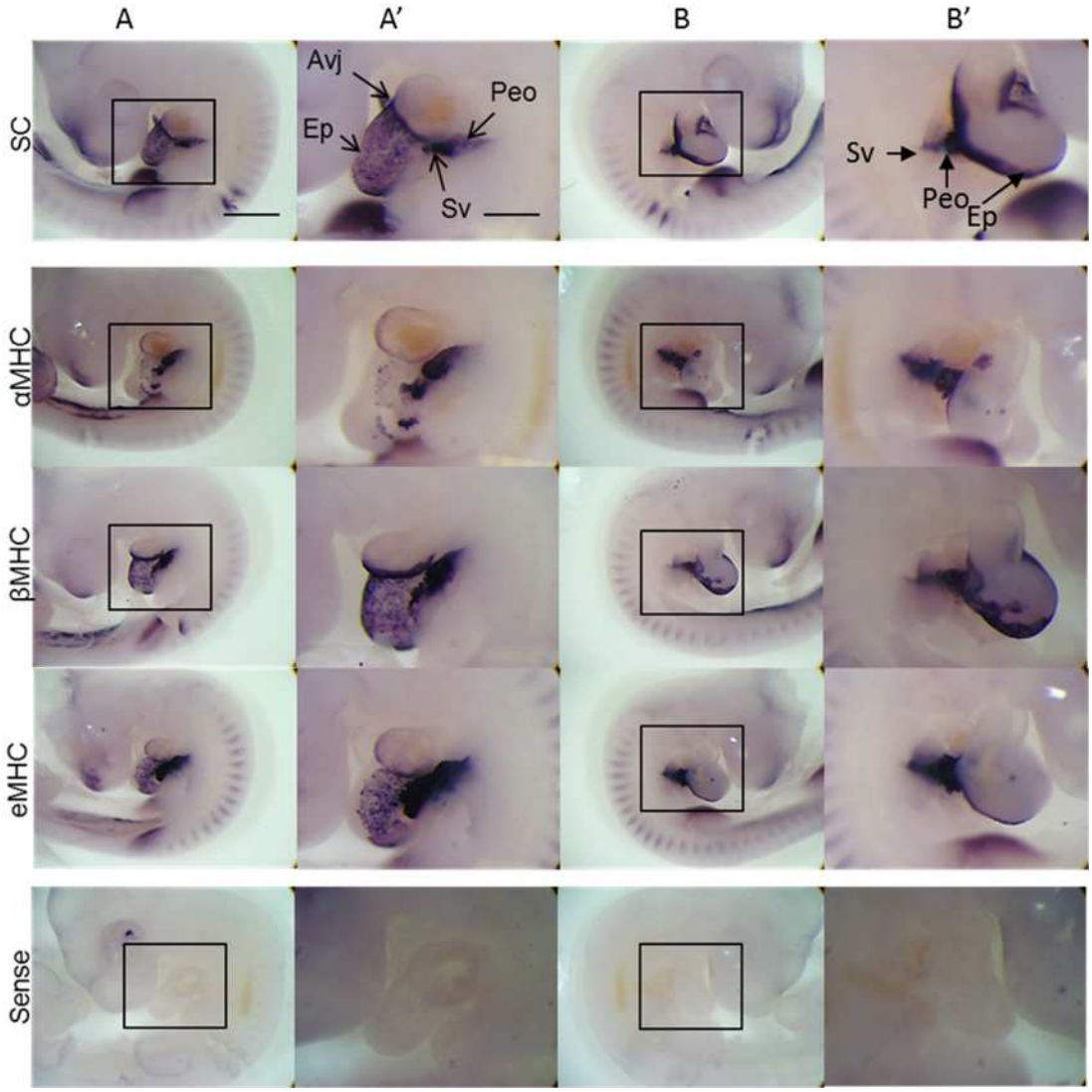



**Figure 3.24** *TBX18* shows no noticeable differentiation in KD groups at HH20. Strong expression signal at the proepicardial organ (Peo) and sinus venosus (Sv), as well as expression in the lower atria at the atrial ventricular junction (Avj) were seen. Expression is also seen throughout the developing epicardium (Ep). n = 3 for all groups. A, shows left side of heart, B shows right side. Avj, atrrio ventricular junction; Ep, epicardium; Peo, proepicardial organ, Sv, sinus venosus. 1000 µm for whole embryo A and B images, 500 µm on A' and B' boxed images.

### *3.3.18.5 CACNA1C*

CACNA1C was analysed as it is a $Ca^{+2}$ channel expressed in the cardiac conduction system at the I band (Hong et al., 2010), and may be affected by myosin structure. Expression is seen mainly in the ventricle, but also weakly seen in the atria with no noticeable differences in expression between knockdowns and controls. This corresponded to the literature that showed *CACNA1C* is mainly a ventricular channel (Hong et al., 2010).

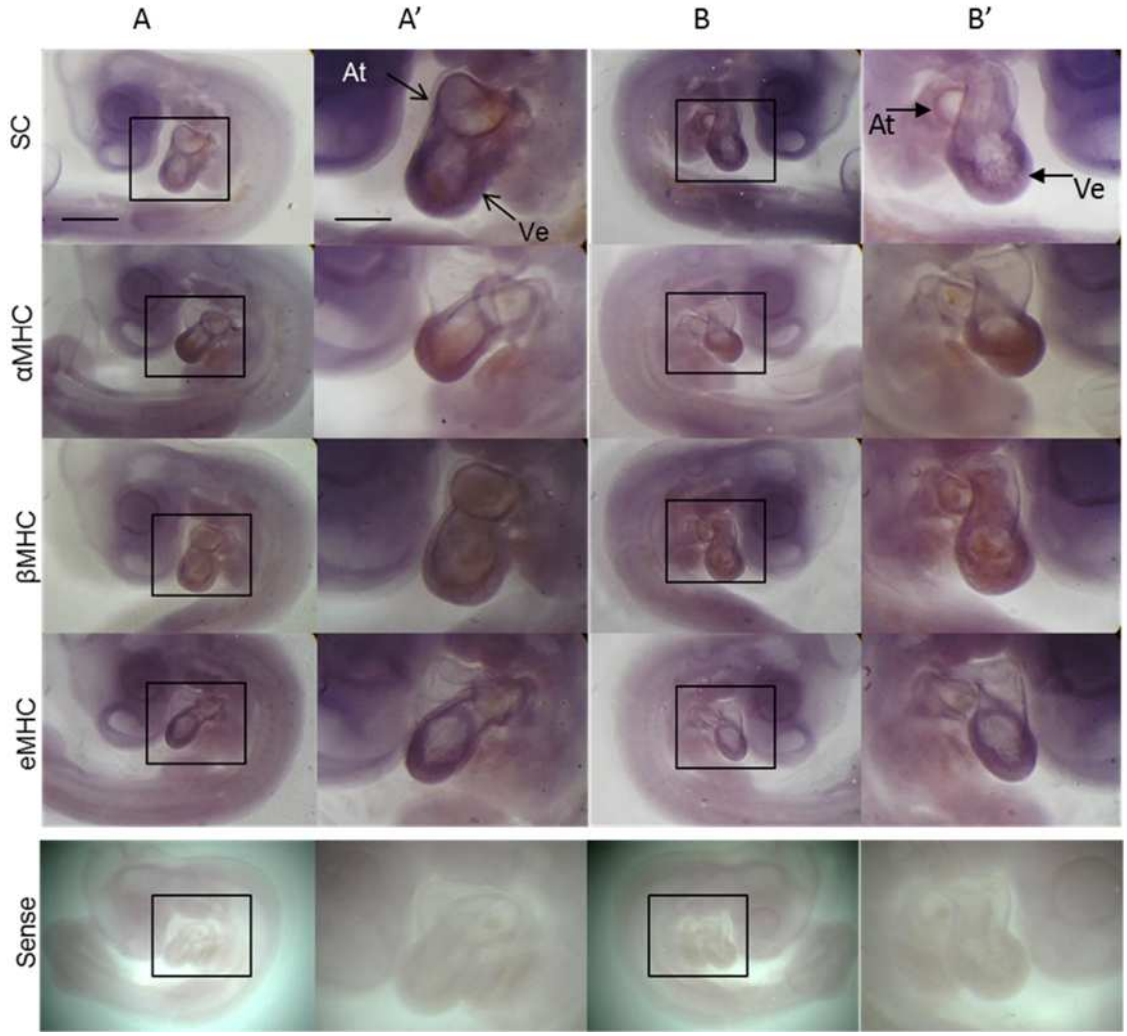



**Figure 3.25** *CACNA1C* expression signal appears unaltered in KD hearts at HH20. Expression is seen weakly in the atria toward it's outer surface and more broadly in the ventricle across all groups. n = 3 for all groups. At, atria; Ve, ventricle. A, shows

left side of heart, B shows right side. At, atrium; Ve, ventricle. 1000 µm for whole embryo A and B images, 500 µm on A' and B' boxed images.

### 3.3.19 RT-qPCR of KD hearts

Before genes highlighted from *in situ* hybridisation could be analysed, the RT-qPCR in the KD model had to be verified, that is; no genomic contamination, reference gene consistency and control verification.

#### 3.3.19.1 cDNA check for genomic contamination for KD RT-qPCR

RNA preparation to enable cDNA synthesis had concentrations of 800 – 1200 ng/µl, and 260/290 nm ratios from 190 – 215. End point PCR was performed on all cDNA synthesis reactions against Glyceraldehyde 3-phosphate dehydrogenase (*GAPDH*) in order to check for genomic contamination. The primer set for GAPDH (set 1) was designed to contain an intron of 200 bp. The cDNA samples synthesised and tested were KD hearts αMHC, βMHC, eMHC and controls SC and UT. The PCR was run over 40 cycles to ensure that low copy numbers of genomic DNA could give a band, and also to replicate the conditions of the RT-qPCR reaction that this cDNA is intended for. Upon gel electrophoresis, the expected 180 bp band was seen in the RT positive samples but with no noticeable bands in the non-reverse transcriptase controls (-) were seen (Figure 3.27); this shows genomic contamination in all samples is minimal.

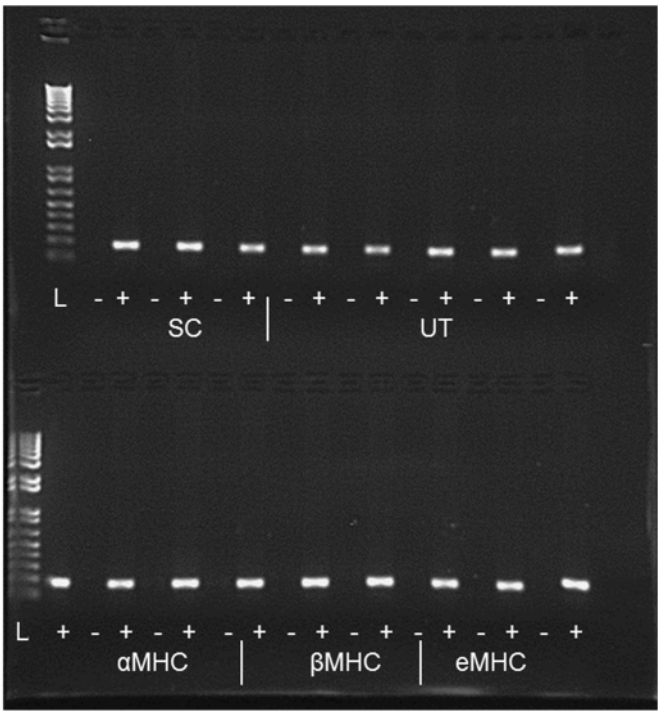



**Figure 3.26** KD cDNA shows no noticeable genomic contamination. End point PCR was performed using *GAPDH* gene-specific primers (40 cycles) on untreated (UT) and standard controls (SC) and for, αMHC, βMCH and eMHC KD hearts. A cDNA band of 180 bp was seen; a band of 320 bp would indicate gDNA (primers span 140 bp intron). L, 1 K plus ladder; +, reverse transcriptase positive; -, reverse transcriptase negative.

#### 3.3.19.2 Reference gene verification

Another key step for both the RT-qPCR procedure, but also to show that KD had no off target effects on standard cell housekeeping genes, was to verify reference genes for RT-qPCR. To enable normalised expression analysis at HH20, reference genes were assessed for their expression across treatment groups (αMHC, βMHC, eMHC, SC and UT). Reference genes tested by RT-qPCR were *GAPDH*, *EEF1A1* and *TBP* (more information on these genes can be found in the discussion of chapter 4) in optimised conditions. Relative quantity results revealed a pattern where all genes

showed consistent expression, but TBP appeared to be the most inconsistent gene out of the three. This can be seen in the relative quantity results in each embryo in figure 3.26 (A), this is to depict the consistency in gene expression across all embryos. This is important in order to see the expression of genes within each heart, then the individual gene results are shown in figure 3.26 (B). This was tested using three analysis algorithms: Gemorm, Bestkeeper and normFinder. These programs confirmed that *GAPDH* and *EEF1A1* had the most consistent expression, with results well within recommended values for constant expression. Values under 0.5 are deemed acceptable for reference gene stability, and both *GAPDH* and *EEF1A1* scored under 0.333 across all tests (Figure 3.26 B). *TBP* returned the most unstable results and so was discounted as a reference gene at. However, as can be seen from Figure 3.26 B, this gene also had consistent expression with its highest value at 0.337 by Best keeper. This shows that reference genes were stable at HH20, and also that the KD process has no effect on RT-qPCR reference gene expression

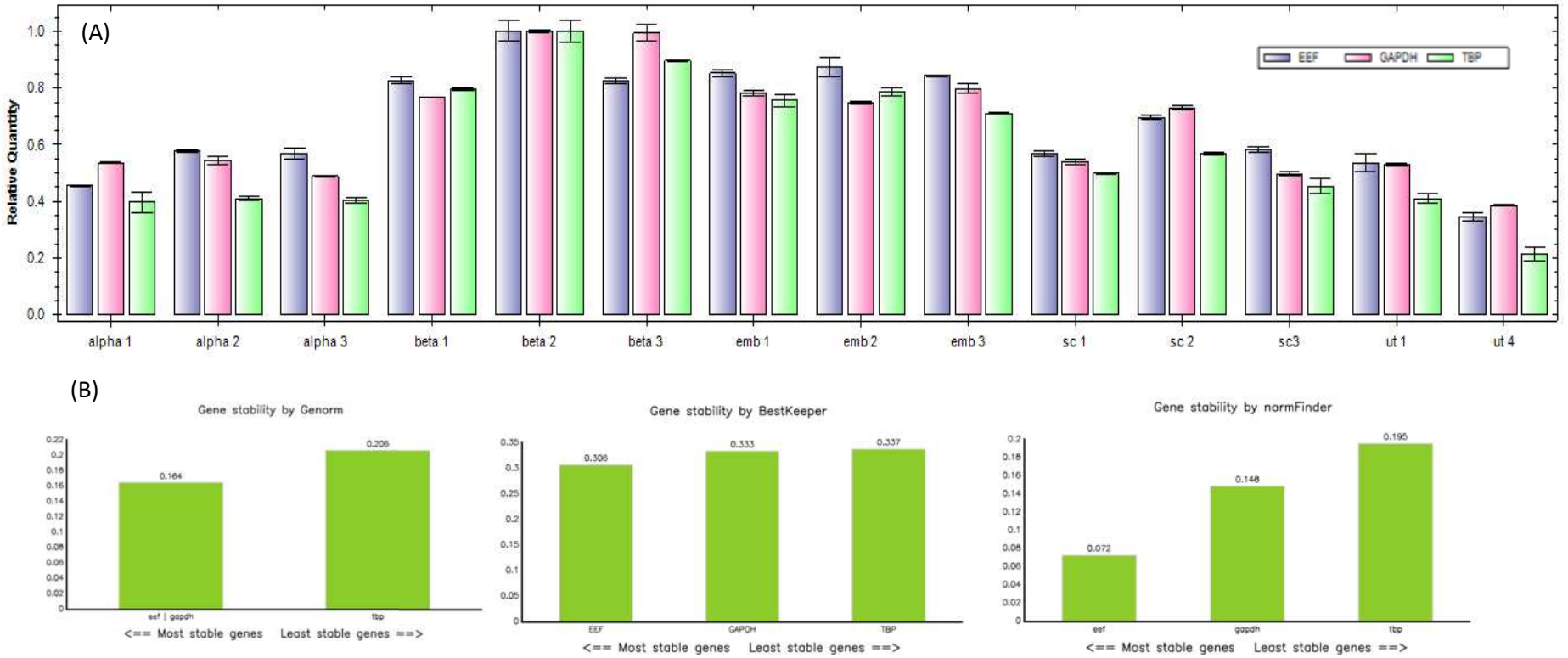



**Figure 3.27** HH20 reference gene stability across KD and control embryos. (A) Relative quantity across all samples shows consistency in gene expression across all embryos. (B) Analysis of relative quantity result by Genorm, BestKeeper and normFinder software packages, demonstrating *GAPDH* and *EEF1A1* to be the most stably expressed. n=3 KD and Sc, n=2 UT. Alpha, αMHC; beta, βMHC; emb, eMHC, standard control, SC; untreated (UT), ut.

### 3.3.19.3 Differentially regulated gene verification

Conduction gene analysis of KD hearts by RT-qPCR revealed one significantly down differentiated gene (see 3.4.5.1 next), *HCN4*, and one gene that showed an insignificant down regulation, *GJA5*. In order to verify that regulation of these genes is not affected by the morpholino application process or by the applied standard control (SC) MO itself, these genes were analysed by RT-qPCR in SC and untreated (UT) samples using *GAPDH* and *EEF1A1* as internal reference genes. No differences were observed between SC and UT groups for *HCN4* (t(4)=1.01, *p*=0.365) and GJA5 (t(4)=0.75, *p*=0.49) (figure 3.25). Figure 3.25 shows the RT-qPCR result in reference to zero to allow easy comparison to be seen between samples.

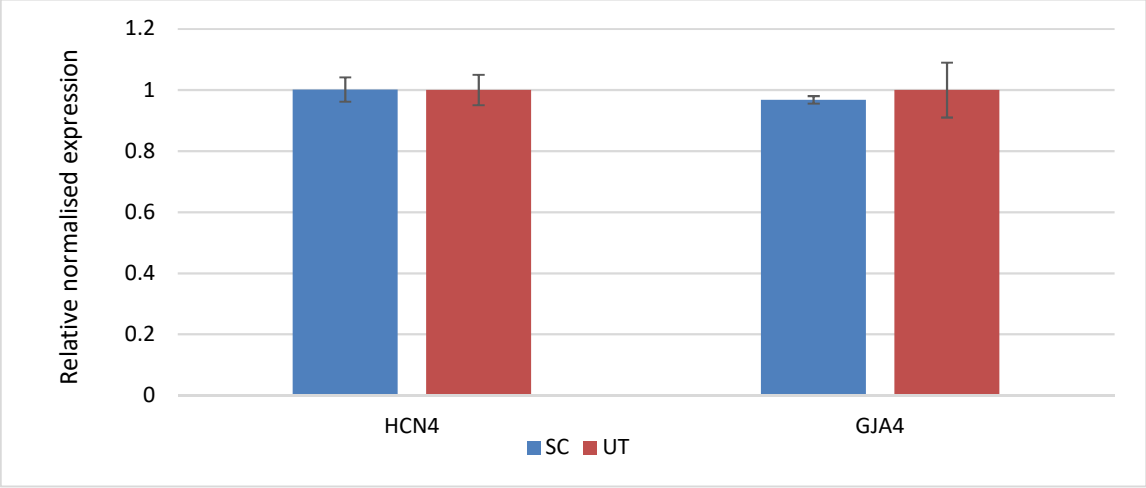



**Figure 3.28** No differences between SC and UT in genes highlighted by KD. Expression analysis of SC and UT reveals no differences between the control groups with clear overlap of error bars. Error bars represent 1 S.E. n = 3 pooled samples (each sample was 3 pooled hearts so total hearts n=9)

#### 3.3.19.4 RT-qPCR expression of HCN4, GJA5, and TBX3 in KD hearts

To see if the possible changes in mRNA expression highlighted through in-situ hybridisation were quantifiable as up or down regulations RT-qPCR was carried out. TBX3 is a transcription factor known to be key in sinoatrial node formation where it acts to repress myocardium gene *GJA5* (Hoogaars et al., 2004). So, even though *in situ* hybridisation experimentation revealed very low expression signal in the heart, RT-qPCR was still carried out to see how it related with possible down regulations in GJA5 and cardiac conduction gene HCN4. Each group contained 3 samples and each individual sample was made up of 3 pooled HH20 hearts. *HCN4* RT-qPCR analysis correlated its apparent reduction seen in *in situ* results, showing a significant decrease in HCN4 mRNA for eMHC and βMCH. eMHC showed a significant fold change reduction of -0.64 log2 ($t(4)=8.96 p=0.002$), βMCH showed a -0.53 log2 FC ($t(4)=8.67 p=0.002$). αMHC showed an insignificant decrease of -0.35 $\log_2$ FC (Figure 3.22). *GJA5* RT-qPCR analysis revealed no significant differences in any group, however a general down regulation was seen, particularly with eMHC that showed an insignificant -0.53 $\log_2$ fold change (Figure 3.22).

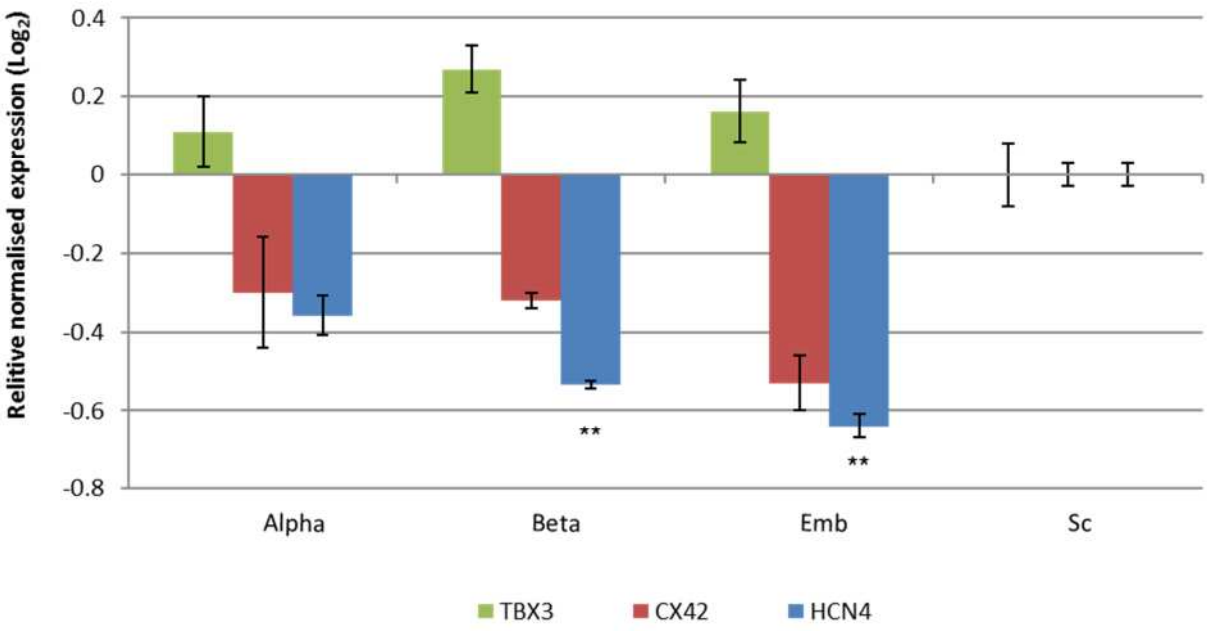



**Figure 3.29** RT-qPCR analysis of key conduction genes on knockdown. *TBX3* showed a small insignificant up regulation across all groups. *GJA5* showed an insignificant, but clear down regulation in all groups, αMHC, βMHC and eMHC showed a -0.30, 0.32 and -0.53 log2 FC respectively. *HCN4* showed insignificant down regulation in the αMHC KD (-0.35 log2 FC *p* =0.06) and significant downregulation in βMHC KD (-0.54 log2 FC, *p*=0.007) and eMHC (-0.64 log2 FC, p=0.002). Error bars represent 1 S.E

## 1.2 Discussion

The primary aim of this section was to is to increase understanding of why myosin heavy chain proteins may be influencing the hearts conduction system. Morpholino knockdowns (KD) were used to look at the effect of KD to the myosin heavy chain proteins αMHC, βMHC and eMHC. It was found that sarcomere maturity is affected and that a key component in generating SAN depolarisation, HCN4 is significantly down regulated. These findings can lead to follow up work, were links to structure and HNC4 can be investigated. Such avenues are discussed later in this discussion, but first the effectiveness of our knockdown model used to attain these results must be scrutinised.

### 3.3.20 Knockdown efficiency and Morpholinos

KD efficiency of morpholino was a primary concern of this project. Morpholinos (MOs) have been shown in the literature to have 100% KD efficiency (Sehnert et al., 2002, Nutt et al., 2001). However, this high efficiency was obtained in a zebra fish model that allows direct application of morpholino into single cells (Sehnert et al., 2002, Nutt et al., 2001). Our chick model necessitates application onto a developing embryo at a key stage in heart development as it is undergoing looping. This means the MO must be applied to the top of the developing heart area with pluronic gel delivery agent. Using this method, knockdown efficiencies have varied efficiencies from 33 to 83 % KD seen by western blot (England et al., 2016, Rutland et al., 2009). This project assessed how the level of qualitative observational florescence corresponded to KD, and found embryo hearts with average uptake (a uptake score of 2-3) gave inconsistent KD, whereas good uptake (uptake score 4-5) revealed a consistent and significant 66.38 reduction in protein by western analysis. Therefore, all hearts used in this project had an observational score of 4-5. MOs have recently been criticised as they have been found to have off-target effects (Kok et al., 2015). The study found that in zebra fish KD by MOs, 80% of the phenotype seen were not present in samples that had the gene of interest mutated. This led to the recommendation that genetically altered embryos/cells/animals should be used to ensure phenotypes are not caused

by off-target effects (Kok et al., 2015). This is particularly difficult in chick embryos however. To ensure thesis data was robust mRNA and protein levels were analysed in KD, SC and and UT embryos by RT-qPCR and western blot. The main gene highlighted in this thesis as being significantly down regulated in KDs, *HCN4*, and the gene that showed clear, but just insignificant down regulation, *GJA5*, where assed by RT-qPCR in standard control (SC) MO application compared to untreated (UT) hearts. No differences were found between SC and UT groups, thus showing that possible off target effects caused by the SC MO or the application procedure itself were apparent. Housekeeping genes *GAPDH*, *EEFA11* and *TBP* showed no differences across KD, SC and UT groups, and at a protein level the myosin targeted KD gene βMHC showed no differences between SC and UT groups. One concern dose still present itself however. Though all myosin MOs were specific for their target and checked by NCBI BLAST that they did not anneal to off target genes, individual MOs have been found to have differing individual effects on off target genes (Kok et al., 2015), particularly if the target is weakly expressed and excess MO is applied that does not find its specific target. One way to check this in the future would be to perform gene rescue using a transfected plasmid, where if an observed phenotype is reversed when targeted KD gene is re-expressed then we know the affected phenotype is not caused by off target effects.

### 3.3.21 A role for αMHC, βMCH and eMHC in cardiac sarcomere development

The fundamental structure of myosin in the sarcomere is identical across all species with cross-striated muscles (LoRusso et al., 1997). A study using embryonic Drosophila showed that organised sarcomeres fail to form in the absence of MHC1 expression and that development is associated with Z lines/Z discs i.e. Z-discs fail to form into organised I-Z-I complexes in MHC mutant embryos (Pashmforoush et al., 2004, Rui et al., 2010). To analyze sarcomere development at the Z-disc, immunocytochemistry using the α-actinin antibody that is specific to Z-discs was employed on cardiomyocyte colonies in culture. α-actinin is present at all stages of sarcomere development, but becomes increasingly structured with development. Our

data supports the MHC1 mutant data in the heart, where we have shown that αMHC, βMHC and eMHC were necessary for normal sarcomere development in our embryonic tissue culture. Results show cardiomyocyte maturity is significantly reduced in cultured ventricular and atrial HH29 hearts in αMHC and βMHC KDs, and in eMHC KD in the ventricle, and just out of significance in atria, when compared to controls. Though atrial eMHC KD had an insignificant reduction statistically, a maturity reduction in the atria was present (mean maturity score = 2.4 vs. controls 2.9). Mature structures have previously been seen by confocal microscopy in eMHC KD hearts, however, these studies were not quantifiably looking for mean differences against controls, and these studies did find poor myocardial tissue integrity (Rutland et al., 2011). Embryonic MHC has previously been shown to have a developmental role in skeletal muscle (Lyons et al., 1990a, Rui et al., 2010). Our data adds to this, showing that in the heart eMHC KD significantly reduced sarcomere maturity in the ventricle, and, though insignificantly, in the atria. Mutant *C. elegans* that do not express βMHC were also found to have disrupted muscle structure in the body wall muscle cells. Interestingly, double mutants of the aforementioned embryos plus sup-3 locus mutation showed that an increase in αMCH can compensate for the lack of β*MYH* expression, but this only happened after induction of the double mutant (Maruyama et al., 1989)**.** Whether or not any compensatory effect by myosin isoforms is taking place in our KD culture is unclear, however, what is clear is that correct expression both αMCH and β*MYH*, and e*MYH* is required in the developing heart for the normal development of sarcomeres.

Our results could suggest that at this stage of development in culture, eMHC is expressed to a greater extent in the ventricles. However, all atrial culture a displayed no beating two days post plating out, and colonies were significantly smaller than ventricle colonies. As the ventricle colonies contained a higher proportion of working cardiomyocytes than the atria, it might be expected that a gene involved in cardiomyogenesis will have a greater effect in the ventricle. At HH30, αMHC has been found to be mainly expressed in the atria, with lower expression levels in the ventricle, while βMHC has been found to be mainly expressed in the ventricle (Somi et al., 2006). Our data at HH29 show αMHC and βMHC KDs to have similar significant maturation reductions to each other in both atrial and ventricular cultures with no significant

interactions found between the two KD groups in relation to region of tissue (atrial or ventricular) ($F(4, 88) = 1.406$ $p = 0.240$). It could be expected that at HH29, KD of αMHC would have more of an effect in the atria, and KD of βMHC to have more of an effect in ventricular tissue. Previous data has shown that at the stage of primitive heart tube looping, αMHC and βMHC are expressed to similar levels broadly across the atrial and ventricular regions (Somi et al., 2006). It could be that in culture, atrial and ventricular cardiomyocytes take on a more primitive expression pattern, i.e. that of the looping primitive heart tube. Re-expression of fetal proteins such as alpha-smooth muscle actin has been seen in adult rat cardiomyocytes when cultured, but not observed normally in adult ventricular tissue (LoRusso et al., 1997, Eppenberger-Eberhardt et al., 1990).

As expected, mean BPM of atrial colonies (that contain the SAN) on day 1 was significantly quicker than in the ventricle. Knockdowns had no noticeable effect on beating rate or rhythm in ventricle samples, though 2 out of 9 wells in both eMHC and αMHC failed to form synchronously beating syncytiums. Work by Prof. David Brook (University of Nottingham) also found that αMHC led to abnormal/ failure to beat in culture (personal communication). Unfortunately, all atrial wells in this study stopped beating after day two of culture, so atrial KD results could not be obtained. The quiescence of beating found in all atrial cultures could have many causes. It could be that atrial cells require higher levels of potassium and calcium than ventricle tissue, as differences have been found in membrane action potential currents (Shrier and Clay, 1986). It has also been suggested that electromechanical uncoupling could be responsible for cessation of beating, once cells exhibit sarcomere recognition (Benardeau et al., 1997).

### 3.3.22 Conduction across myocyte cultures

As expected, initial separately beating colonies would merge and beat in a range close to that of the initial faster colony, just as in the heart conduction system - the heart beats to the rhythm of the fastest pacemaker, the SAN (K. G. Pal, 2016). An unexpected obseration was that colonies separated by fibroblasts had the ability to beat synchronously. Fibroblast cells are the largest cell population in the heart; they

are expressed at all stages of development and are known to proliferate well in culture (Souders et al., 2009). It has in previous studies been shown that fibroblast cells, not just cardiomyocytes, have the potential to conduct action potentials up to distances of 300 µm between cardiomyocytes, though a significant conduction delay was found to occur (Bakker et al., 2008). Our results support this; it was observed that action potentials pass through fibroblast tissue with distances travelled up to 600 um, distances previously only found using engineered fibroblast bridges (Bakker et al., 2008). Interestingly, culture that was filtered to remove excess fibroblasts returned poor beating results. These findings demonstrate the importance of fibroblast tissue in development and could even be a possible target for treatment post infarction.

### 3.3.23 Expression profiles of conduction genes

#### 3.3.23.1 Voltage-dependent, Long type Calcium channel expression HH16-HH35

Calcium channel, voltage-dependent, L type, alpha 1D subunit *CACNA1D* that encodes the atrial conduction cell channel protein Cav1.3 (Christel et al., 2012) showed very low expression signal. Firstly, band strength was very weak by endpoint RT-qPCR when compared to an endpoint *GAPDH* control reaction and *CACNA1C* from HH12 to HH29. Then in-situ hybridisation showed expression signal in the atria and ventricle that was barely noticeable above background. Because of this a full spatial expression profile or its analysis in myosin KD hearts was not performed on *CACNA1D*.

The *CACNA1C* gene expresses the $Ca_v1.2$ protein $Ca^{2+}$ channel. Expression has not previously been explored in the chick. Before performing the spatial expression profile, expression of the main 2 known transcripts were analysed in the heart. Two different probes were designed for *CACNA1C*, one positive for both of the main 2 known transcripts and another for just transcript 1 (*CACNA1C*-201 ENSGALT00000021261.5). Analysis at HH20 showed weak expression of transcript 1, again, barely noticeable above background. The probe positive for both transcripts

however showed good expression signal. Because of this, only the probe for both transcripts was used to assess spatial expression across developmental stages, and it could be that transcript 2 is the dominant transcript in the developing chick heart, though RT-qPCR was not carried out to confirm this.

We found that expression at HH16 was throughout the heart in both the ventricle and atria broadly. This is supported by early detection of CACNA1C in the mouse heart, where expression is shown 9.5 days post coitum (dpc) (Takemura et al., 2005). At HH20 expression became stronger in the ventricle, but was still present in the atria at its borders. The increased expression in the ventricle could be to accommodate for the establishment of base to apex propagation. This is backed up by multiple studies where *CACNA1C* is found to be mainly expressed in the ventricle (Boyett, 2009, Catterall et al., 2005). At HH25 a similar pattern is seen in the ventricle and atria, but it is also now becoming apparent that there is increasing expression in the area of the interventricular septum (IVS). The expression at the IVS continues and intensifies through to HH35 and this is likely because of complete formation of a IVS and bundle branches at HH35 (Martinsen, 2005a). Though expression remains strong at the IVS, generally *CACNA1C* expression appears to get weaker across HH29 and HH35 stages, particularly in the atria where colour detection was barely visible. At these later stages of development, the conduction pattern is nearing maturity at HH29 and is mature at HH35. It has previously been suggested that Cav1.2 channels are only upregulated at critical developmental stages and that down-regulation of Cav1.2 channels during these later stages may be effected by Fibroblast growth factor (Brillantes et al., 1994). Though this is the first time this has been seen, mouse data does show alterations in expression levels and expression sites during development and in the adult, and suggests this is due to earlier stages of development requiring more negative potentials to activate $Ca_v1.2$ channels (Takemura et al., 2005).

#### 3.3.23.2 *GJA5* and *GJA1* HH16-HH35

*GJA5* is a marker of the working myocardium and codes for the Cx42 connexin channel in the chick (mammalian homologue is Cx42) (Delorme et al., 1997). Connexins are responsible for the transfer of action potentials from cell to cell across the heart by transmitting $Na^{+}$ and $Ca^{+2}$ directly between cells (Jansen et al., 2010). Our in-situ hybridisation results at HH16 show expression, though relatively weak, in the ventricular region mainly at its borders. At HH20 expression is seen in the ventricle and atria, but remains stronger in the ventricle. Mouse data has shown that expression in the common ventricular chamber at 9.5-11.5 dpc and supports ore findings at HH16 – HH20 (Delorme et al., 1997). At the same developmental stages, we have no noticeable expression of GJA1. GJA1 codes for the Cx43 protein connexin channel. This agrees with current literature that suggests CX40/CX42 may provide the coupling between myocytes to compensate for the lack of CX43 (Coppen et al., 2003). CX43 -/- knock down neonatal mice have shown that other connexins such as Cx40 allow mutants to survive until birth (Reaume et al., 1995). However, literature in the mouse does show prominent CX43 expression in the ventricle at 10.5 dpc which becomes more intense at 12.5 dpc (Ruangvoravat and Lo, 1992). We show this expression is not apparent in the chick. From HH25 through to HH35, the established expression pattern of GJA5 in both the ventricle and atria is continued and expression is clearly visible in the trabeculae and IVS in bisected HH29 and HH35 hearts. This is consistent with investigations in a 9 week human heart and E15.5 mouse heart (Coppen et al., 2003). At HH25 weak GJA1 expression would appear to be becoming apparent broadly across both the atria and ventricle, though weak, this expression pattern resembled that GJA5. This pattern is then seen increasingly so at HH29 and HH35 and the IVS after HH29, and though remaining considerably weaker than GJA5 it's co expression with GJA5 is clear. This co-expression may be crucial to support a maturing/ matured conduction system to an apex to base pattern (Coppen et al., 2003). Our data correlates with observations in the adult human heart, where Cx43 is expressed in all cardiac chambers but predominates in the ventricles (Vozzi et al., 1999). Further supporting evidence is shown in 16 dpc rat hearts where Cx43 is

present in the ventricles, and with development, becomes more specific to the IVS (Van Kempen et al., 1996).

### 3.3.24 *GJA5* tracts

GJA5 was observed in track lines just beneath the atrioventricular sepal and outflow tract region. GJA5 in birds is known to form a Purkinje fiber network around coronary arteries (van Weerd and Christoffels, 2016), however, coronary vascularisation does not occur until HH32, and our tracts were seen extensively at HH29 (Ando et al., 2004). A coronary artery endothelial re-modeling zone in a post infarct mouse model has been shown to express GJA5 highly and these zones had an increase in smooth muscle (Miquerol et al., 2015). It could be that our expression of *GJA5* in the coronary artery zone could facilitate the formation of the coronary arteries by increasing differentiation signaling leading to arteriogenesis. *GJA5* has been shown to be expressed in arterial endothelial cells, but not veins in the chick (Buschmann et al., 2010), and this expression happens in response to shear stress following re-distribution of arterial flow and precludes arteriogenesis (Buschmann et al., 2010). Genetic ablation of *GJA5* resulted in reduced arteriogensis in the vitelline artery network (Buschmann et al., 2010). Whether not this effect is seen in the coronary arteries is unknown, and our reported tract lines are also not reported previously in the literature.

#### 3.3.24.1 Future experimentation

An examination of the formation of the coronary arteries in GJA5 knockdowns compared to control embryos, the hypothesis being that coronary artery formation will be disrupted in knockdown hearts. Also, to analyse the effect of shear stress on GJA5 tract and coronary artery formation, GJA5 in-situ hybridisation could be carried out on stress inducing OFT-banded hearts (see chapters 5 and 6) and compared to SHAM controls in bisected hearts at HH29 and HH35.

### 3.3.25 Regulation of conduction genes in myosin KD groups, effects on conduction and relationship with structure

*GJA5* showed a consistent down regulation, though insignificant, by RT-qPCR that backed up the subset of embryos that showed down regulation by in-situ hybridisation. All KD RT-qPCR results were based 3 experimental samples compared to 3 SC samples. Each sample was made up of 3 pooled hearts in order to give a consistent result with a high number of hearts i.e. 9 hearts were used per group in 3 pooled samples, without excessive labor time demands. The results show an insignificant relationship between structural myosin protein KD and reduced *GJA5* expression, with the greatest effect coming from eMHC KD. As mentioned, this result was based on a pooled sample of 9 hearts into three samples. It is possible this lead to a false negative in statistical analysis. Analysis of our experimental standard deviation and difference in effect between KD and control suggests that an n of at least 6 should be used (equation bases on power calculation as used in Kadam & Bhalerao paper) (Kadam and Bhalerao, 2010). Though 9 hearts were used in the experimental groups, the pooled nature to an n of three will reduce the power of the experiment meaning greater differences in effect would have to be shown for statistical significance. *GJA5* protein Cx42 is responsible for allowing the transfer of action potentials from the SAN across the heart by transmitting $Na^{+}$ and $Ca^{+2}$ directly between cells (Jansen et al., 2010). Expression is found in the chick in the atria and ventricle (Dhein, 2004). Reduction of this ion channel could result in retardation of the spreading action potential. It has been found previously that eMHC KD of chick atrial tissue led to a reduction of $Ca^{+2}$ transient frequency (Rutland et al., 2011), this would be in line with a reduction in Cx42. Our atrial cell culture all failed to beat, so the effect on beats per minute (BPM) could not be analysed in the atria, but it might be expected that this would cause a reduction in BPM or an arrhythmia. It has been found in GJA5 knockout mice that action potential patterns resemble that of the right bundle branches. This is likely because the impulse transmission from the SAN is interrupted (Saez et al., 2003). This effect has been found in the human inherited arrhythmia progressive familial heart block type I (PFHBI), where Cx40 (protein of GJA5 and human homologue of Cx42) has been associated. PFHBI is a bundle-branch disorder that may progress to complete heart

block with ECG traces showing broad QRS complexes (Makita et al., 2012). *TBX3* is a transcriptional repressor of working myocardium genes such as *GJA5* and thus its expression leads to specific areas of the cardiac conduction system like the cells of the sinoatrial node (SAN) or the developing SAN (Hoogaars et al., 2007, Bleeker et al., 1980). Our *TBX3* expression in the heart by in-situ hybridisation was at the atrioventricular junction where its expression was very weak when compared to expression in the wing buds; however, as a transcriptional repressor, small amounts/differences may have a large effect on targeted transcription (Hoogaars et al., 2004), and many genes implicated in congenital heart disease are indeed transcription factors (McNally and Svensson, 2009). By RT-qPCR, our *TBX3* expression shows slight and insignificant increases in expression in all 3 KD groups. As all 3 KD groups show similar results it could be that a relationship may exist between myosin KD and a small up regulation in *TBX3*, and so could lead to an increase in GJA5 down regulation. Interestingly, though *TBX3* represses working myocardium genes (Hoogaars et al., 2004), it's been shown to have no effect on genes of the cardiac conduction system such as *HCN4*, a sodium/potassium channel in the SAN (Hoogaars et al., 2007). *TBX3* is expressed alongside HCN4 in the developing SAN region in the atria, but it has been found that *TBX3* acts to suppress a working myocardium phenotype and has no effect on *HCN4*, or other cardiac conduction system genes (Hoogaars et al., 2007). We have found significant down regulation in *HCN4* in eMHC and βMHC KD, and near significant down regulation in αMHC KD. It is possible that due to immaturity of myosin structures, as observed in our KD cultures, a reduced HCN4 phenotype could have been observed. It has been shown in cardiomyocyte stem cells that less mature myosin structures observed at early stages of development were also correlated with reduced levels of HCN4 when compared to more mature cells (Lundy et al., 2013). A significant increase in action potential (AP) duration was published by Rutland *et al.* (2011) in eMHC KD. This increased AP duration could lead to bradycardia as seen in HCN4 mutants and knock outs (Yaniv et al., 2015). This makes sense when the AP is analysed, as depolarisation would be slowed if less $K^+/Na^+$ channels are available to depolarise the conduction cell, and in the SAN, and developing SAN, 70-80% of $I_f$ comes from HCN4 (Yaniv et al., 2015). Our eMHC KD showed the greatest down regulation in HCN4 and so would appear to

fit as an explanation to the formally observed AP phenotype. Unlike TBX3, that only represses working myocardium, TBX18 is a transcription factor shown to be necessary for the formation of the SAN. TBX18 positive progenitor cells have been found to migrate to the head of the SAN, express HCN4 and become pace maker cells (McNally and Svensson, 2009); while TBX18 homozygous knock out mice show reduced SAN head and disorganised SAN cells throughout (McNally and Svensson, 2009). Our KD embryos appear to show no differences compared to SC and so would have no knock-on effects on HCN4 positive conduction cells.

It could be that structural abnormalities within sarcomere architecture are the primary cause for the conduction phenotype previously seen in KDs, particularly as the down regulation of GJA5 was slight and it's questionable whether this would have any effect on conduction. Our KD colony immature Z-disc structure could lead to major disruption of $Ca^{2+}$ levels/distribution. Z-discs couple electrical activation via transverse tubules (T-tubules) (Orr et al., 2016), and T-tubules are responsible for the AP travelling along the sarcolemma (Orr et al., 2016, Hong et al., 2014). An important gene required for T-tubule formation and function in the heart is *BIN1* were it forms the inner membrane and stabilises at the t-tubule membrane (Hong et al., 2014). *BIN1* has been found down regulated in failing hearts leading to uncontrolled diffusion of $Ca^{2+}$ and $K^{+}$ ions and a prolonged AP (Hong et al., 2014). Disruption to Z discs in our immature sarcomeres maybe expected to disrupt T-tubules and therefore $Ca^{2+}$ transients. This has been seen in mutations to myosin light chain gene MYL4 that have led to disruption of sarcomeric structure and absent Z discs in zebra fish (Orr et al., 2016). The mutants also exhibited electrical abnormalities which were associated with T-tubule disruption, as T-tubules are located to Z-discs (Orr et al., 2016). Though T-tubules are found highly branched in cardiomyocytes, they are least developed in the SAN region (Meng et al., 1996), where *HCN4* is mainly expressed and the conduction signal in the heart is initiated. However, disruption to T-tubules may not be the only reason Z-disc disruption causes arrhythmias. The dystrophin (DMD) glycoprotein complex is expressed along with Nitric oxide synthases (NOS) in αMHC and βMHC rich tissue at sarcomere Z-discs (it is also expressed along the T-tubule membrane) (Meng et al., 1996, Masuda et al., 2009, Reilly et al., 2016). NOS has a critical role in

cardiomyocytes as it catalyses the production of nitric oxide (NO) which regulates $Ca^{2+}$ flux in both basal and high stress states and prevents arrhythmias (Reilly et al., 2016, Masuda et al., 2009, Meng et al., 1996). It has been shown in mice that repression of dystrophin expression leads to altered distribution of NOS localisation, which subsequently leads to reduced NO (Reilly et al., 2016). The model was induced by overexpression of mircoRNA miR-31 and had a conduction phenotype of shortened AP together with no rate-dependent adaptation of the action potential duration, thus the heart would not be able to respond correctly to stress (Reilly et al., 2016). This demonstrates that correct sarcomere structure is vital to maintain correctly coordinated contraction. CACNA1C is a $Ca^{+2}$ channel gene that is expressed at in the I-band and at T-tubules only in cardiac conduction cells and also at sarcomere membranes (Hong et al., 2010), and has been linked with arrhythmias such as 'sick sinus' syndrome characterized by severe bradycardia (Christel et al., 2012). If structural immaturity is the cause of *HCN4* down regulation, and other KD associated conduction phenotypes such as T-tubule disruption, it might also be expected to see similar down regulations in *CACNA1C* that were seen in *HCN4* or ectopic expression. Our in-situ hybridisation results revealed no apparent differences between SC and KD groups. However, *CACNA1C* is predominantly expressed in ventricular conduction cells (Hong et al., 2010), as seen in our expression profile at the IVS where the bundle braches lye, whereas *HCN4* is expressed in the atrial SAN/ developing SAN regions where the conduction signal is propagated (Hoogaars et al., 2007). So, it could be that we need to find a conduction protein linked to structure in the SAN region. As well as the ubiquitously expressed dystrophin previously mentioned, one such gene is conduction protein is Ankyrin-B (ANKB). Ankyrins are membrane organisers that underlie the cytoskeleton. They localise ion channels, such as *HCN4* in the case of ANKB, to the membranes of pace maker cells of the SAN (Yaniv et al., 2015). *ANKB* mutation/down regulation is associated with severe bradycardia and heart rate variability (Le Scouarnec et al., 2008), and is expressed in the SAN at the M line region in a striated pattern and at the cell membrane (Le Scouarnec et al., 2008). ANKB disruption and mutation has been shown to be correlated with a down regulation of *HCN4* (Verkerk and Wilders, 2014), and ANK is involved in sensing/responding to cardiac stress (Bennett and Healy, 2009). Our reduction in sarcomere maturity could be expected to

disrupt ANKB at the M line, or perhaps stress the heart, and so an effect on/down regulation of ANKB would be probable. This would then effect SAN membrane protein HCN4 leading to its down regulation and possibly our delayed AP phenotype. Ankyrin's involvement in cardiac stress has been shown in *ANKRD1*, an ankyrin repeat gene encoding the protein cardiac adriamycin-responsive protein (CARP). CARP is expressed at Intercalated discs (Jasnic-Savovic et al., 2015). CARP is induced upon stretch, injuries or hypertrophy (Miller et al., 2003b). The *ANKRD1* gene has also been implicated as being causative in human dilated cardiomyopathy (Duboscq-Bidot et al., 2009). To further investigate the effect of stress on the cardiac conduction system, rather than knocking down structural myosins, the next phase of the project was to induce stress on the heart in a technique called outflow tract banding (OFT-banding). This will allow analysis of the myosin and conduction genes in response to stress e.g. the expression of related genes at the Z line that could cause conduction phenotypes.

### 3.3.26 Relevance of results

The idea that alteration in one protein can have a knock-on effect on another is a feature of the "final common pathway of inherited cardiovascular diseases" hypothesis (Bowles et al., 2000, Towbin, 2014b). This had been used to hypothesize that HCN4 mutations that cause an arrhythmia phenotype, could also disturb downstream binding partners that cause left ventricular non-compaction cardiomyopathy (LVNC) affecting the sarcomere, Z-disk, cytoskeletal proteins, or signalling pathways (Towbin, 2014b). Indeed, HCN4 mutations have been found in families with bradycardia and left ventricular noncompaction cardiomyopathy, where the ion channel was hypothesised to be associated with structural abnormalities of the myocardium (Milano et al., 2014, Millat et al., 2015). However, to this authors knowledge, reduced HCN4 expression from a reduction in MHC and sarcomere maturation has not been previously been confirmed. It has been found that the time of arrest of the normal embryonic myocardial maturation determines the severity of the non-compaction cardiomyopathy phenotype (Floria et al., 2014). It is possible that reduced maturity of our sarcomeres could lead to a non-compaction phenotype, together with associated disruption to ion channels on the sarcomere membrane. Overall, we have found KD hearts to have affected

maturation and gene expression. Sarcomere maturity was found reduced in all KDs, though e*MYH* has less of an effect in the atrium. Cell cultures in the atrium failed to beat post 48 hours of plating out and ventricular cultures returned no significant differences in beating rate when compared to knockdowns. However, 2 out of 9 α*MYH* and e*MYH* failed to form beating sanctums compared to all the controls which did. The SAN gene HCN4 that allows depolarisation of the SAN was found significantly down regulated. It would be expected that less expression of this gene would alter the rate of depolarisation and affect the SAN action potential. What is causing this reduction is yet to be elucidated, but sarcomere structure would seem to be a likely candidate as HCN4 where disruption to the sarcomere membrane could be expected to affect membrane bound ion channels.

#### 3.3.26.1 Future experimentation

Investigate the effect of myosin knockdown/knockout/disruption and its reduction in sarcomere maturity on ANKB, dystrophin (DMD) and NOS by immunocytochemistry on sections through the atria. If disruption to expression, or differential expression is present, this could be the central mechanism governing the AP phenotype previously seen (Rutland et al., 2011), and our down regulation in SAN membrane sodium/potassium channel HCN4.

# Chapter 4 Optimisation and verification of RNA sequencing in OFT-banded model

## 4.1 Introduction

Structure and force generating proteins have been highly linked to cardiomyopathy, both dilated and hypertrophic. Data from the first part of this thesis, presented in chapter three, showed the effect of knockdown of structural/force generating myosin's in the heart leading to decreased sarcomere maturity. The reduced maturity could potentially be involved with conduction channel HCN4 expression by disruption to other structural/ force generating proteins that interact with HCN4 such as CARP. In this second part of the thesis, rather than knocking down structural/force generating genes in order to analyse the effects on the heart, the mechanical force placed on the heart itself is altered in order to assess its effect on gene expression. The outflow tract (OFT) banding technique (see section 1.5.4) is employed to alter haemodynamic load and recreate an environment similar to that of the cardiomyopic heart. As highlighted in section 1.5.3, cardiomyopathy is a maladaptive disease in response to a particular stressor, such as, in the case of familial cardiomyopathy, single gene mutations to myosins, ankyrins and tropomyosins etc. The OFT-banded model recreates conditions of stress similar to that seen in cardiomyopathy to allow analyses of maladaptive gene expression in response to haemodynamic stress. The overall of this chapter is to produce reliable RNA sequencing data that can identify genes of low reads. Though it is theorised that high abundance genes play the most important roles in particular organs (Ton et al., 2000), being able to analyse genes with low copy number is also important, as a very small amount of a regulator gene or transcription factor could have multiple knock on effects. Work carried out consisted of optimising RNA removal and library preparation for sequencing followed by verification of sequencing results by RT-qPCR. Before proceeding with this chapter, it is first necessary to present the anatomical and physiological data that defines our OFT-banded model.

### 4.1.1 Our OFT banded phenotype

The OFT procedure and other haemodynamic alteration models are detailed in the introduction section 1.5.4. However, it is important to show what phenotype the banding process has given in our lab. The procedure gave three groups of hearts; one, OFT hearts, two, SHAM controls, and three, untreated controls (UT). The SHAM control group comprises hearts that have the suture passed through the heart, but then removed. This is to test for changes due to the invasive nature of the procedure. The untreated controls are embryos incubated along with OFT banded hearts and SHAM controls, but remain untouched. No differences were found anatomically between SHAM and UT previously by Dr. Pang in house (see section 4.1.3 - 6), however, genetic analysis of cell viability housekeeping genes together with cardiomyopathy marker genes remained to be assessed between SHAM and UT. This is one of the key aims of this chapter, as the SHAM control must be genetically verified before sequencing comparison between SHAM and OFT banded hearts can be made.

The general features of the OFT banded heart compared to controls were that the hearts were nearly twice as large, however they were in the same proportion to controls with the exception of the epicardium which was significantly thickened. The general increase in size was due to increased lumen size in all atrial and ventricular chambers, with the exception of the unchanged right atrium. This significant increase in lumen is indicative of dilated cardiomyopathy. Significantly less trabeculae were also found. Additional observations were a laterally positioned ‘right sided’ outflow tract, rounder appearance at the apex, defective AV valve and incomplete IVS.

Phenotypes increased at HH35 when compared to HH29, however survival rates were very low. This would suggest that the heart is reaching failure point at around this developmental stage in OFT-banded hearts. For this reason, HH29 hearts were used for genetic analysis of the OFT-banded model.

(Full details of the phenotype are now presented in section 4.1.1-7. The section shows Dr. Pang’s original anatomical analysis and data gathering, though the actual statistical testing of stereological data was performed by me)

### 4.1.2 Group survival rate

Survival rate of OFT banded, SHAM and UT hearts was analysed. OFT banding was performed at HH21 and hearts were harvested at three different stages, HH26, HH29 and HH35. At HH26, the survival rates of the UT embryos (n=14), SHAM (n=18) were found to be 92.9% and 83% respectively ($p$=0.87, no significant differences). The survival rate was significantly lower in the OFT-banded embryos, 42.5% (n=40). At HH29, the survival rate was 76.5% and 70.5% for UT(n=68) and SHAM (n=88) respectively ($p$=0.71, no significant differences). The OFT-banded embryos (n=212) were had a survival rate of 36.3%. Upon harvesting at HH35, the UT embryos (n=30) and sham (n=28) showed a survival rate of 60% and 67.8% respectively ($p$=0.55, no significant differences). In contrast, the OFT-banded embryos (n=117) had a high mortality rate with just 11.1% of embryos surviving. Any embryos showing developmental retardation were excluded from the study. This showed that SHAM controls were variable when compared to UT controls and that the survival rate of OFT banded embryos decreased with development.

### 4.1.3 OFT banded heart external phenotype

Upon isolation of the heart from the embryo, the external features such as the size and shape of the heart and the position of the OFT were particularly studied. The UT and SHAM hearts all appeared to be normal across all stages examined (HH26 (n=16), HH29 (n=97) and HH35 (n=35); Table 3.1; Figure 3.2). Upon banding at HH21 and harvesting at HH26 (HH26), in 31.2% of the OFT-banded embryos, hearts appeared spherical (n=16) (Figure 3.2C). At this stage, the control hearts were still in the progress of acquiring the medial position of the OFT (Figure 3.2A,B). However, 94% of the banded hearts presented with a more lateral position of the OFT (Table 3.1; Figure 3.2C).

During harvesting at HH29 and HH35, the embryos presented more severe phenotypes at a higher higher rate. At these two stages, the OFT of the control hearts

has shifted to a medial position due to the growth of both atria (Figure 3.2D,E and G,H for HH29 and HH35 accordingly). However, the OFT was still laterally positioned in the banded hearts, and this was found in 95% (n=60) and 89% (n=9) of the OFT-banded hearts at HH29 and HH35 respectively (Table 3.1; Figure 3.2F and I for HH29 and HH35 respectively).

At HH29 and HH35 (when ventricular septation is complete), the normal hearts have a pointed apex (arrow in Figure 3.2D,E and G,H for HH29 and HH35 respectively). However, in OFT hearts a rounder apex was seen giving a spherical appearance (55% at HH29 (n=60) and 89% at HH35 (n=9); Table 3.1; Figure 3.2F & I accordingly). Additionally, a thickened epicardium was seen in a subset of OFT-banded hearts (denoted by double arrowhead in Figure 3.2F and I; Table 3.1).

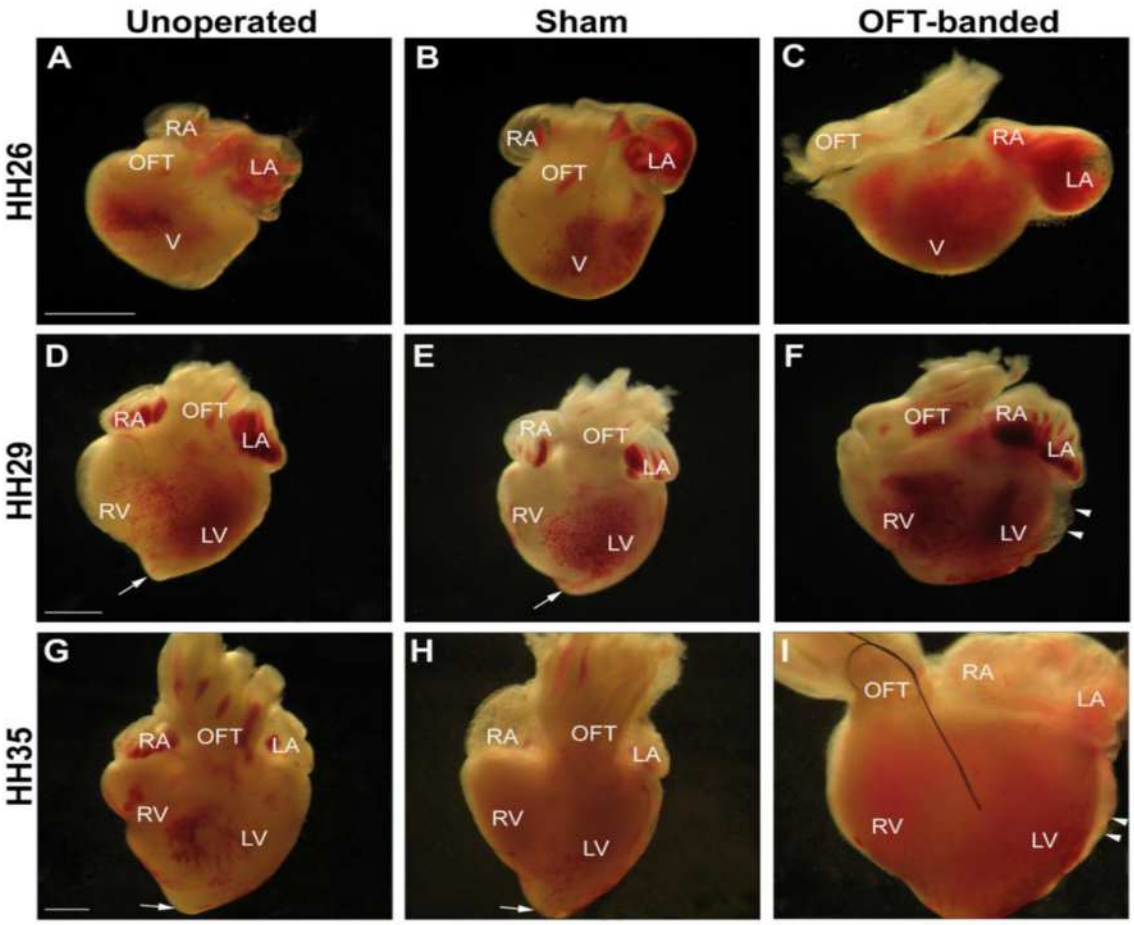



**Figure 4.1** OFT-banded hearts were enlarged with a rounded apex**.** (A-C) At HH26, the controls (UT and SHAM) were still in the progress of acquiring the medial position of the OFT (A,B). However, it can be seen that the outflow tract was laterally positioned at this stage in the banded hearts (C). (D-I) At HH29 and HH35, all controls displayed a normal external phenotype: the medial position of the outflow tract, a pointed apex (denoted by arrow) is present in both UT (D,G) and SHAM (E,H). However, the OFT-banded hearts exhibited a right-shifted position of the outflow tract with a rounded ventricular apex at HH29 (F) and HH35 (I). In addition, a thickened epicardium was seen in a subset of OFT-banded hearts at both stages (double arrow in F & I). The suture was still attached with the OFT upon harvesting at all stages (c,f,i). LA, left atrium; LV, left ventricle; OFT, outflow tract; RA, right atrium; RV, right ventricle; V, ventricle. Scale bar: 1000μm. (Source: Lougna lab, Dr Pang data).

**Table 4.1** Analysis phenotypic summary of OFT banded to control chick embryonic hearts at HH26, HH29 and HH35.

Assessment of the size of the heart and the heart shape was based on the qualitative analysis of gross morphological features.

Qualitative assessment of the interatrial and interventricular septum and epicardium was carried out on serial histological sections.

| Stage* | Embryo type ¤ | Heart morphology | | | | Total ext § | Septal defects | | | | Epicardial defects | | Total int § |
|---|---|---|---|---|---|---|---|---|---|---|---|---|---|
| | | Spherical shape | Normal | Lateral position of OFT | Normal | | ASD | Normal | VSD | Normal | Thickened epicardium | Normal | |
| HH21/26 | Control | 0 | 16 | 0 | 16 | 16 | 0 | 5 | NA | NA | 0 | 5 | 5 |
| | OFT-banded | 5 | 11 | 15 | 1 | 16 | 0 | 5 | NA | NA | 0 | 5 | 5 |
| HH21/29 | Control | 0 | 97 | 0 | 97 | 97 | 0 | 37 | 0 | 37 | 0 | 34 | 37 |
| | OFT-banded | 33 | 27 | 57 | 3 | 60 | 0 | 31 | 26 | 5 | 14 | 17 | 31 |
| HH21/35 | Control | 0 | 35 | 0 | 35 | 35 | 0 | 8 | 0 | 8 | 0 | 8 | 8 |
| | OFT-banded | 8 | 1 | 8 | 1 | 9 | 0 | 7 | 7 | 0 | 3 | 4 | 7 |

*****Stage of development when banding/harvesting performed.

¤ Control embryos include UT and sham.

§Total number of embryos analysed externally and internally.

ASD, atrial septal defect; ext, externally; int, internally; NA, not-applicable; OFT, outflow tract; VSD, ventricular septal defect

### 4.1.4 haemodynamic alteration results in cardiac malformations

Internal morphological assessment was carried out to assess if perturbation of haemodynamics gives rise to cardiac anomalies. Serial histological sections of the OFT-banded and SMAM were assessed at HH26, HH29 and HH35. Analysis revealed a membranous type of ventricle septal defect (VSD) and a defective epicardium in banded hearts. Additionally, a defective AV valve was found in OFT banded hearts. By HH29, the IVS forms by the merging and compaction of the ventricular trabeculae, it grows superiorly to fuse with the endocardial cushion dividing the ventricular chamber into left and right ventricles. In OFT banded hearts the membranous portion of the IVS that was derived from the endocardial cushion failed to fuse with myocardial crest of the IVS. This leaves an opening (as indicated by an asterisk) which led to a communication of both left and right ventricles at HH29 (*n*=26/31) (Figure 3.3Ad; Table 3.1) and HH35 (*n*=7/7) (Figure 3.3Af; Table 3.1). Investigation of atrial septation took place using histological analysis and was performed on serial sections at HH26. As the heart develops, a muscular septum (the primary atrial septum) grows from the atrial roof and fuses with the superior part of the endocardial cushion and is seen in all controls (*n*=5) (denoted by an arrow in Figure 3.3Aa; Table 3.1) and in the OFT-banded hearts (*n*=5) (Figure 3.3Ab; Table 3.1). Normal atrial septum was observed at later stages of HH29 and HH35 (Table 3.1). Additionally, an impaired epicardial development was seen in the OFT-banded embryos. Abnormal morphology and the blebbing of the epicardial surface was seen in the OFT-banded hearts (*n*=14/31) (as indicated by an arrowhead) at HH29 (Figure 3.3Bd; Table 3.1;) and HH35 (*n*=3/7) (Figure 3.3Bf; Table 3.1) in comparison to controls (Figure 3.3Bc and Figure 3.3Be respectively). However, this phenotype was not seen in all controls (Figure 3.3Ba; Table 3.1) and OFT-banded heart (Figure 3.3Bb; Table 3.1) at HH26.

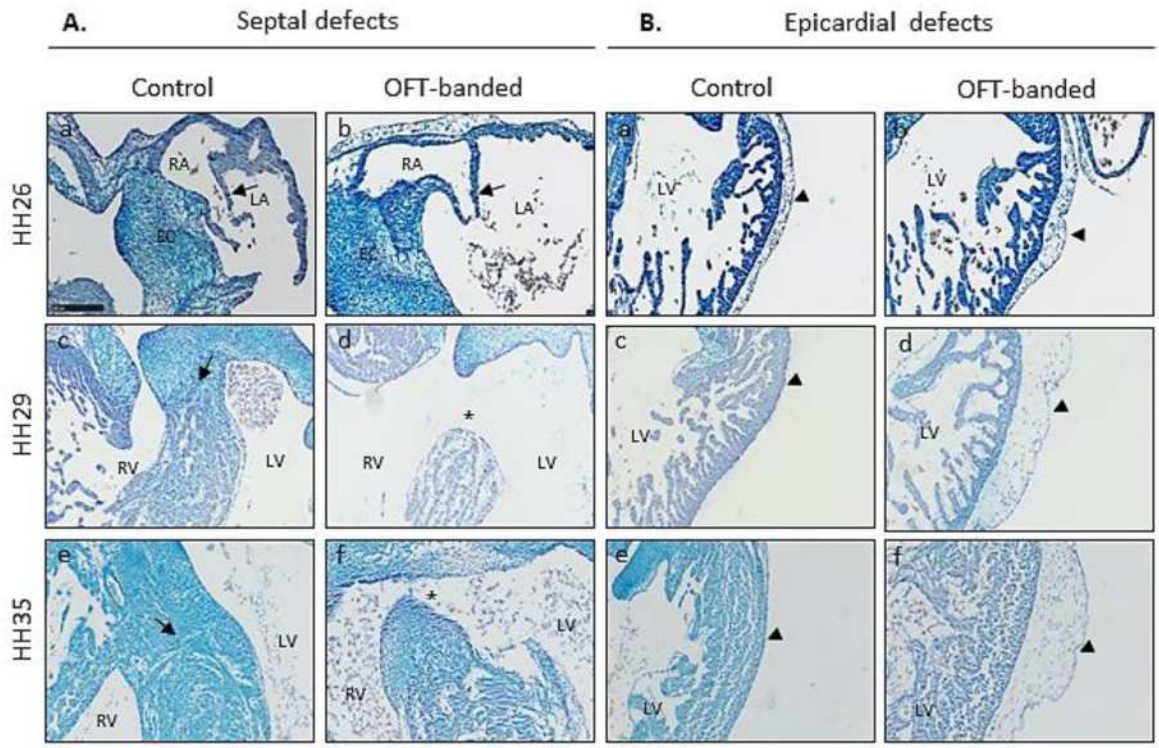



**Figure 4.3** OFT-banding results in a spectrum of cardiac developmental defects. A. OFT-banding results in the failure of ventricular septation, however atrial septation occurs normally. At HH26, the muscular atrial septum was fully fused with the endocardial cushion (denoted by an arrow) in both control (a) and OFT-banded embryos (b). At HH29 and HH35, the interventricular septum which grows in a superior direction has fused with the cushion in the control embryos (as indicated by an arrow) (c and e for HH29 and HH35 accordingly). However, this fails to occur in the OFT-banded hearts which created an opening between ventricular chambers (asterisk) at both HH29 (d) and HH35 (f). **B.** A normal thin epicardial layer (denoted by an arrowhead) was seen in controls at both HH29 (c) and HH35 (e) compared to a thickened epicardium with a blebbing appearance (arrowhead) in the OFT-banded hearts (d and f). However, this phenotype was not obvious at HH26, with a similar phenotype in control (a) and banded (b). EC, endocardial cushion; LA, left atrium; LV,

left ventricle; RA, right atrium; RV, right ventricle. An asterisk (*) denotes a presence of ventricular septal defect. Scale bar: 250μm.

### 4.1.5 Proportional stereological analysis reveals thickened epicardium but normal proportions of other heart regions

A 96-point grid was placed over every fourth 8 μm section throughout the HH21/29 embryonic hearts for stereological analysis. The point at which the grid hits an area is counted. Areas are, tissue; myocardium, lumen, trabeculae and ECM, and region; atria (contributed by RA and LA), and ventricles (contributed by RV and LV). The individual point that the grid hits at the region of dorsal mesenchymal protrusion (DMP), atrial septum and epicardium was included as well. For the control hearts (UT and sham; *n*=6 and *n*=6, respectively), a total of 4479 and 4437 points were counted for UT and sham respectively. 7868 points were counted for OFT-banded hearts (*n*=7). The total number of counts per region was divided by the total number of counts for that heart, giving a percentage of the proportion that each region contributed to the heart.

The percentage proportion of the atria, ventricle, dorsal mesenchymal protrusion (DMP), atrial septum and epicardium was not significantly different between the UT and sham group, so these were pooled into one group for analysis (*P*=0.636 for atrium, *P*=0.524 ventricle, *P*=0.922 for DMP*,* *P*=0.245 for atrial septum and *P*=0.373 for epicardium). When compared to the control group, the OFT-banded hearts mainly showed no significant differences in most of the regions analysed (*P*=0.569, 0.267, 0.33 and 0.72 for both atria, ventricle, DMP and atrial septum respectively; Figure 3.4). However, the epicardium was found proportionally thicker in the OFT-banded hearts, where the control groups presented 12.55±1.32% and the OFT-banded hearts showed 18.15±2.05%; an increase of 44.62% was seen (*P*=0.04; Figure 3.4). 107

This was in line with the thickened epicardium phenotype found in both the external and internal morphological assessments. Lastly, the OFT-banded hearts were found 1.8 times larger than the controls approximately.

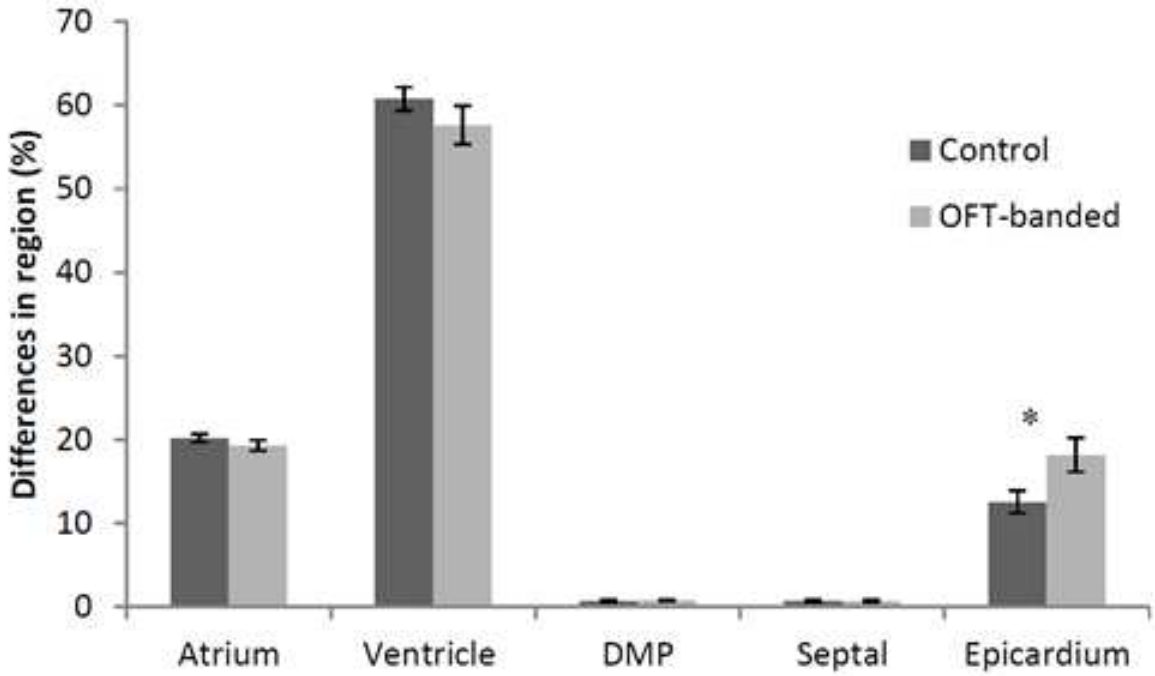



**Figure 4.4** Proportional stereological analysis revealed a thickened epicardium in the OFT-banded hearts**.** OFT banded heart epicardium was found proportionally thicker to that of control hearts, $p<0.05$. The atrium, ventricle, dorsal mesenchymal protrusion, atrial septum and epicardium contributing to each individual heart within each group showed no statistical differences ($n=12$ for controls and $n=7$ for OFT-banded hearts). Significant difference is indicated by an asterisk (*), when $p<0.05$. DMP, dorsal mesenchymal protrusion.

### 4.1.6 Stereology revealed enlarged OFT-banded hearts with changes in the chamber components

Stereological analysis took place to look at each tissue type contributing to the region within the heart, i.e. the percentage of the myocardium, lumen, trabeculae and ECM contributed to the right (RA) and left atrium (LA) and also to the right (RV) and left ventricle (LV) of the heart. When the UT and sham groups were compared, no significant differences were seen in any of the regions tested ($p$=0.064) and thus the two groups were pooled.

Upon analysis of the ventricular chambers, a significant reduction of the trabeculae was identified in both ventricular chambers of the OFT-banded hearts. Stereological analysis revealed the trabeculae of the RV in control hearts presented with 9.99±0.42% of the heart whereas the RV trabeculae in OFT-banded hearts accounted for 7.75±0.55%; a decrease of 22.4% was seen, $p$<0.01 (Figure 3.5). The decrease of the trabeculae was more prominent in the LV. It was found that the trabeculae of the LV in the control was 13.52±0.83%, while the OFT-banded hearts presented 8.53±0.37% LV trabeculae of the heart; a decrease of 36.9%, $p$<0.001 (Figure 3.5).

Consistent with this, a simultaneous increase of ventricular lumen was found in both right and left side of the heart in the banded hearts. Stereology revealed that 8.94±1.06% of the lumen of RV in controls whereas OFT-banded hearts accounted for 14.75±1.37% of the RV lumen, a 64.78% increase, $p$<0.01 (Figure 3.5). The LV lumen in both control and banded group were presented by 10.77±0.78% and 14.27±1.40% respectively, an increase of 32.5%, $p$<0.05 (Figure 3.5).

A thinner myocardium was found in the LV but not in the RV in OFT-banded hearts. The myocardium in the LV in the control contributed to 10.71±0.93% of the heart, whereas only 5.58±0.43% of the LV myocardium was found contributing to the banded heart, a decrease of 47.89%, $p$<0.001 (Figure 3.5). However, there was little change in the ventricular myocardium in RV of OFT-banded hearts, with 6.19±0.46% and 5.82±0.24% in control and banded hearts respectively, $p$=0.49; Figure 3.5.

With regards to the myocardium of the atrial chambers, the myocardium in RA in both controls and banded hearts were presented by 5.05±0.49% and 3.24±0.34% respectively, a decrease of 35.78%, $p$<0.01 (Figure 3.5). Similarly, a reduction of

27.48% was identified in the myocardium of the LA in banded hearts, in which the percentage of the LA myocardium in both controls and the banded hearts was 4.33±0.4% and 3.14±0.24% respectively, $p<0.05$ (Figure 3.5).

A significant increase of the LA lumen by 47.9% was found in the banded hearts ($p<0.01$), where the percentage contributing to the LA lumen of controls and banded hearts was 4.88±0.37% and 7.22±0.62% respectively (Figure 3.5). No changes where seen in the lumen of the RA, where 5.92±0.58% and 5.68±0.74% were identified in control and banded hearts respectively, $p=0.8$. ECM was found to be unchanged in both the RV and LV in the controls and the banded hearts. However, the number of counts was extremely low (200 point counts were desired; 13 points and 14 points were only counted for controls and banded hearts respectively) (Mayhew, 1991). Thus, statistical analyses could not be completed for ECM.

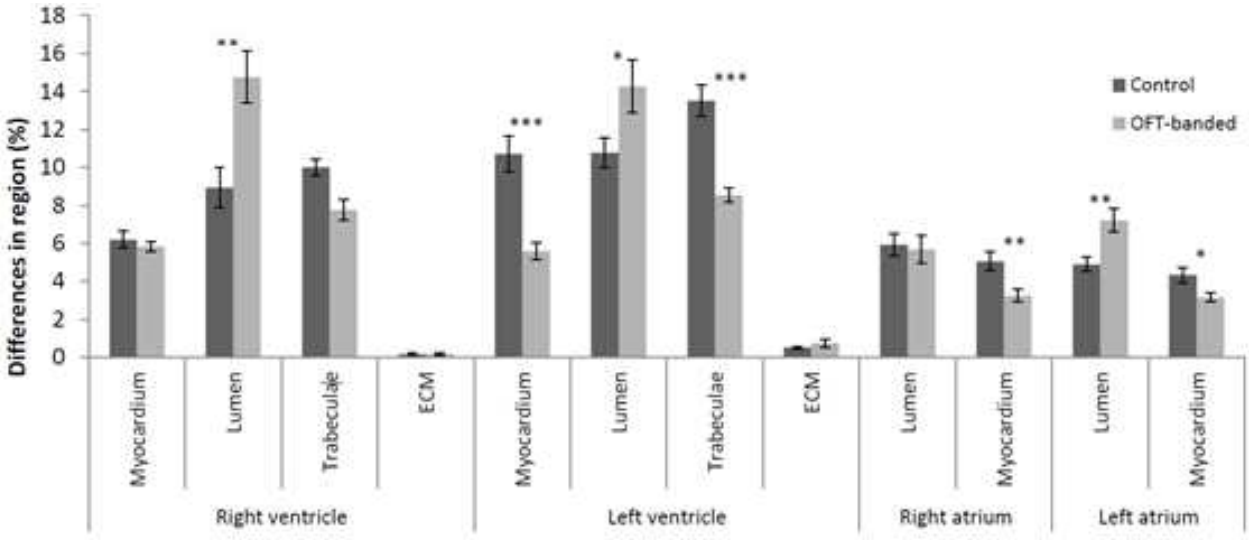



**Figure 4.5** Stereological analysis of tissue types contributing to the left and right atrium and ventricles**.** Reduced of trabeculation was found in both right and left ventricle of the OFT-banded hearts, with a concomitant increase of ventricular lumen in both chambers. Additionally, the myocardium was found thinner in the left ventricle but it appeared normal in the right ventricle. OFT-banded hearts showed an increase of the lumen and a decrease of myocardium in the left atrium. With the right atrium, only the

myocardium was found decreased but the lumen appeared to be normal in comparison to controls. ECM, extracellular matrix. Significant differences are indicated by a single asterisk (*) when $p<0.05$, double asterisks (**) when $p<0.01$ and three asterisks (***) when $p<0.001$. Error bars indicate s.e.m.

#### 4.1.6.1 Fibrosis in the OFT banded heart

Cardiac fibrosis is one of the main features seen in the adult hypertrophied hearts in response to the pressure-overloading (Creemers and Pinto, 2011). To investigate cardiac fibrosis, Masson's Trichrome staining was performed on OFT-banded and SHAM hearts (n=5 in each group) on HH35 serial sections. Black-blue staining indicates collagen deposition as seen in the positive control chick skin sample (Figure 4.6 E). Qualitative analysis was determined by the degree of black/blue staining. No fibrosis was observed in the myocardium of the atria (Figure .6 C) and ventricle (Figure 4.6 D) in both OFT-banded and SHAM hearts (Figure 6 A, B) when compared to the positive control.

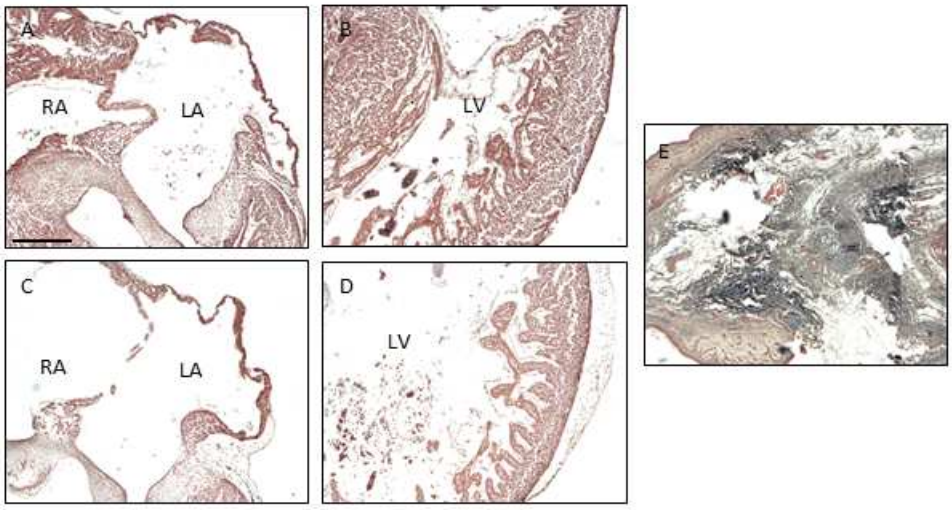



**Figure 4.6** Fibrosis not effected by OFT-banding. No change in deposition of collagen (black-blue staining) was seen in the atria (C) and the ventricle of OFT-banded hearts (D) compared to the atria (A) and ventricle (B) in the SHAM controls. Chick skin was used as a positive control (E). RA, right atrium; RV, right ventricle; LA, left atrium; LV, left ventricle. Scale bar: 150μm.

### 4.1.7 Haemoglobin mRNA removal

Another key aim of this chapter is to remove haemoglobin gene mRNA from samples as part of the library preparation procedure. Harvested hearts contain large amounts of blood due to the well perfused myocardium and the large volume of blood within the pumping chambers themselves. Though every effort was made to ensure hearts had the maximum blood ejected, harvested hearts will still contain large and differing amounts of blood. Blood is made up of 95-99% red blood cells with platelets and white blood cells making up the remaining.

Up to 76% of transcripts from sequenced tissue samples have been shown to be from reticulocytes in the human adult (Hitchen J, 2013, Mastrokolias et al., 2012). Array and sequencing studies have found deceased sensitivity with increased globin levels (Wu K, 2007, Shin et al., 2014). One array study showed having just 5% globin mRNA reduced sensitivity, while globin mRNA of more than 20% was shown to severely impact on results (Wu K, 2007). However, few studies exist using next generation sequencing on tissue that required, and subsequently was, globin depleted.

To ensure that low copy number reads will not be missed, and to ensure consistency among samples, a procedure to remove haemoglobin from samples was carried out. Globin depletion has been carried out previously on human, mouse/rat and porcine models, and has shown genes are detected at higher levels in globin depleted samples; further some genes of low copy number that previously were not detected could be after globin depletion (Choi et al., 2014, Mastrokolias et al., 2012, Wu K, 2007, Debey et al., 2006).

Within the literature, the rates of transcript deduction varied depending on species and kit used. Non-enzymatic methods utilizing biotin peptide nucleic acid (PNA) binding removes up to 95% of transcripts in the human, but only showed between 34% and 64% in porcine models (Choi et al., 2014, Mastrokolias et al., 2012). Another method using the Ribonuclease HI (RNase H) Affymetrix technique showed up to 94% reduction in porcine models when using uniquely designed DNA oligonucleotides (Choi et al., 2014).

Though established in other organisms, globin depletion has never been performed in the chick. However, evidence from the previous working models suggested that the RNase H method could be used. This involves the attachment of oligonucleotides (oligos) to the globin mRNA 3' end which can then be degraded with RNase, thus removing the polyadenylated tail. The subsequent polyadenylated selection step carried out prior to sequencing removes the selected globin mRNA. Chick and human haemoglobin DNA have relatively low sequence homology; for this reason, chick specific oligonucleotides were designed for each selected globin gene. Before the oligos could be designed, a profile of what haemoglobin genes were expressed in the embryonic chick was carried out.

## 4.2 Specific Aims

Haemodynamic alteration models have been used in the chick and other organisms in order to determine the effect altered blood flow has on stress within the heart (Clark et al., 1984, Sedmera et al., 1999, Tobita et al., 2002, Buffinton et al., 2013). Using OFT-banding as a model for altered haemodynamics, we aim for the first time to see the global embryonic gene expression in OFT-banded hearts. However, in order to use our model of OFT- banding to study the effect of abnormal blood flow on cardiac development, it is necessary to verify the model. Without extensive optimisation and verification of lab procedures and data handling techniques expression analysis would not be reliable.

Specific Aims:

- To demonstrate the OFT-banded model is working, i.e. is not causing the heart to fail at time of harvesting, and that the SHAM control shows no difference to the untreated control
- To optimise a library preparation procedure in order to perform detailed global gene analysis by RNA sequencing on OFT-banded hearts able to identify small

read genes; this necessitates optimisation of globin depletion in the chick embryo.

- To perform and analyse mRNA sequencing in order to show differential gene expression in OFT-banded hearts via next generation sequencing and verification via RT-qPCR.

## 4.3 Results

### 4.3.1 Genomic contamination check following RNA preparation on HH29 and HH35 whole OFT-banded hearts

The RNA preparations had concentrations of 800 – 1200 ng/µl, and 260/290 nm ratios from 190 – 215. RNA integrity showed high scores across all samples with RINs of 9.5 – 9.7 (Table 5.3 pre-depletion results). This demonstrates our optimised RNA purification procedure not only delivers high yields from small amounts of tissue, but it also consistently produces non-degraded RNA. End point PCR was performed on all cDNA synthesis reactions against Glyceraldehyde 3-phosphate dehydrogenase (*GAPDH*) in order to determine if genomic contamination was present. The cDNA samples synthesized and tested were HH29 OFT (X5), SMAM (X5) and UT (X4); a similar experiment was performed at HH35 except all groups hearts were n=4. The end point PCR was run over 40 cycles to ensure that low copy numbers of genomic DNA could give a band, and also to replicate the conditions of the RT-qPCR reaction that this cDNA is intended for. Upon gel electrophoresis, no noticeable bands were seen in the non-reverse transcriptase controls (-) across all samples (Figure 4.7); this demonstrates genomic contamination in all samples is minimal.

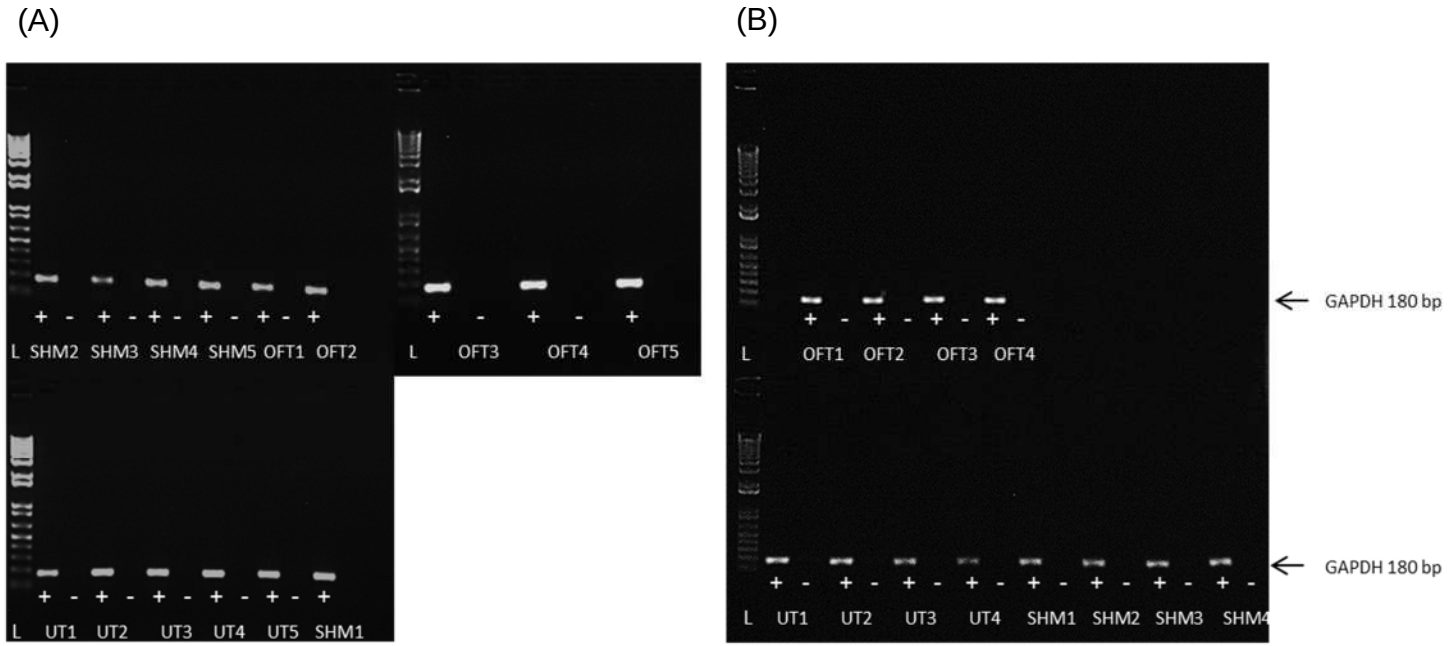



**Figure 4.7** Genomic contamination check on OFT-banded, SHAM and UT HH29 and (A) and HH35 hearts (B). End point PCR was performed using *GAPDH* gene-specific primers (40 cycles) on untreated (UT), sham (SHAM) and outflow tract banded (OFT) hearts. A cDNA band of 180 bp was seen in reverse transcriptase positive samples; no band was present in reverse transcriptase negative samples show no noticeable contamination is present. L, 1 KD plus ladder; +, reverse transcriptase positive; -, reverse transcriptase negative.

### 4.3.2 Model verification and optimisation and verification required for RT-qPCR

### 4.3.3 RT-qPCR Primer optimisation

In order to carry out RT-qPCR analysis, gene-specific primer pair optimisations needed to be carried out in order to assess efficiency. Before proceeding to RT-qPCR, endpoint PCR was carried out to check the annealing temperatures (64, 62 and 60°C) of the primers and also for excessive primer dimers. RT-qPCR dilution series $R^2$ values of >0.98 were attained for all primer pairs, efficiencies were between 95 and 110%, the Cqs were below 35, and primer dimers were negligible. Figure 5.2 shows these values for the three RT-qPCR reference genes *GAPDH*, *EEF1A1* and *TBP*. Full details of how the optimisation procedure was carried out and how to interpret standard curve results can be found in the methods section 2.8.8-12. All primers were designed and optimised in house and the whole procedure was optimised from scratch.

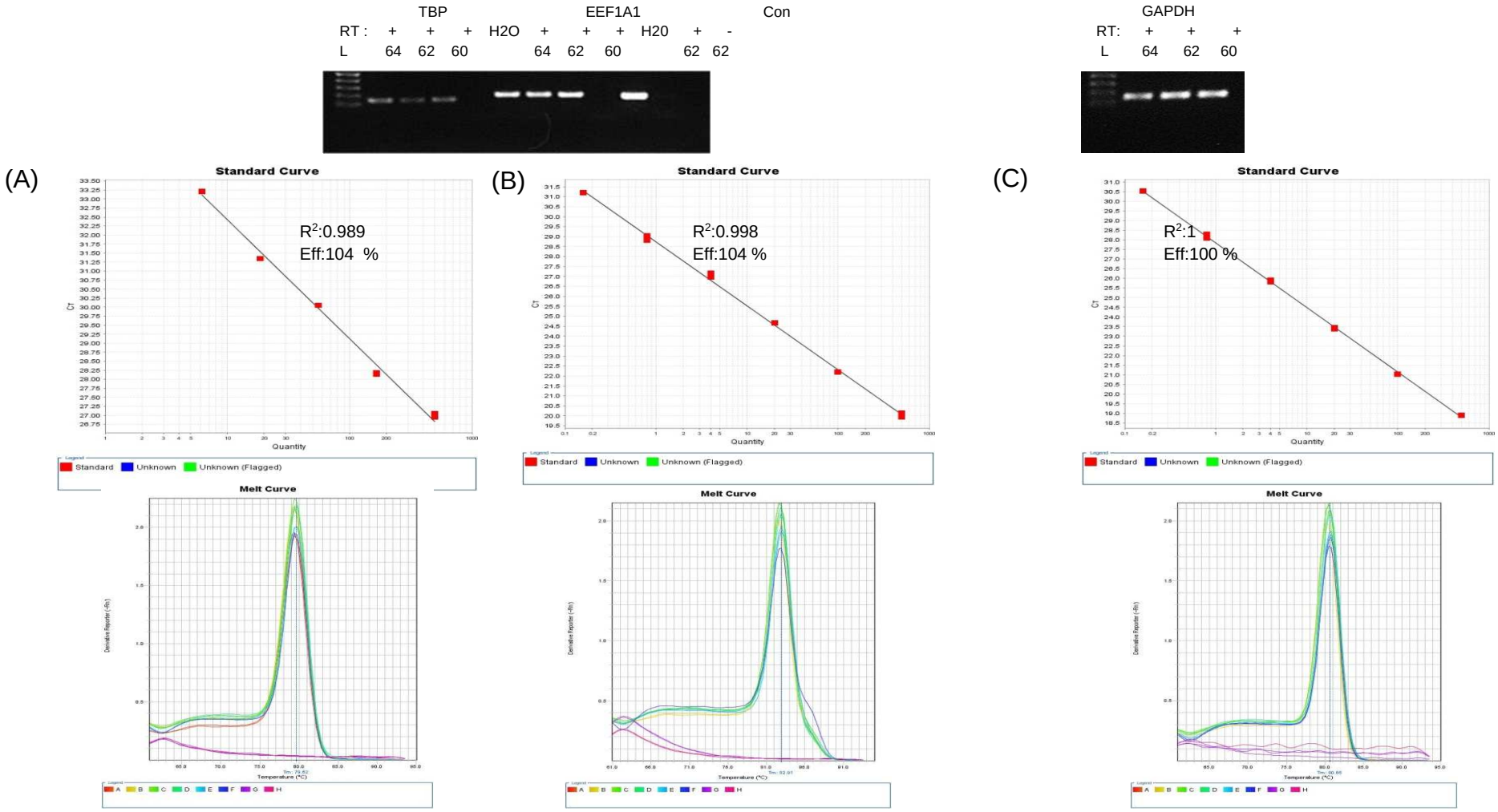



**Figure 4.8** RT-qPCR primer optimisation**.** Representative data for standard and melt curves, for gene-specific primers to reference genes (A) 179 bp *TBP* (B) 218 bp *EEF1A1* (C) 180 bp *GAPDH*. L, 1 KD plus ladder; +, reverse transcriptase positive; -, reverse transcriptase negative; Con, control (220 bp *GAPDH*); $H_2O$, water control; Eff, efficiency.

### 4.3.4 Determination of reverse transcriptase consistency

In order for library preparation for RNA sequencing and RT-qPCRs to be performed, consistency of reverse transcriptase was vital. Superscript II has been shown in the literature to be one of the most reliable transcriptases for library generation using RNA of low abundance (Levesque-Sergerie et al., 2007). Our results confirm this, with reproducibility of RT-qPCR results on cDNA repeats from both the same and different runs of cDNA synthesis. Table 4.2 and Figure 4.9 demonstrate that cDNA synthesis is consistent when the same RNA is used in different reactions on the same synthesis run (reaction 1 and repeat) and when the same RNA is used for synthesis on a different day (reaction 2).

**Table 4.2** Consistency of cDNA synthesis reaction

| DNA sample | Reaction 1 | | Reaction 1 repeat | | Reaction 2 | |
|---|---|---|---|---|---|---|
| | Mean Cq | Triplicate standard deviation | Mean Cq | Triplicate standard deviation | Mean Cq | Triplicate standard deviation |
| **Heart 1** | **13.76** | 0.007 | **13.71** | 0.018 | **13.74** | 0.035 |
| **Heart 2** | **13.70** | 0.043 | **13.59** | 0.059 | **13.54** | 0.070 |
| **Heart 3** | **13.81** | 0.031 | **13.85** | 0.207 | **13.86** | 0.021 |

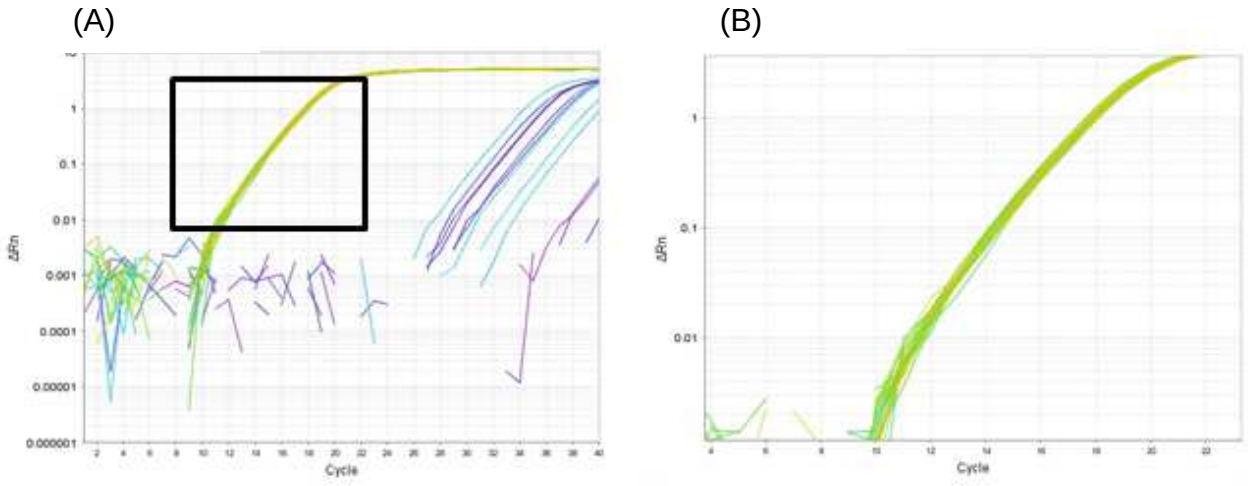
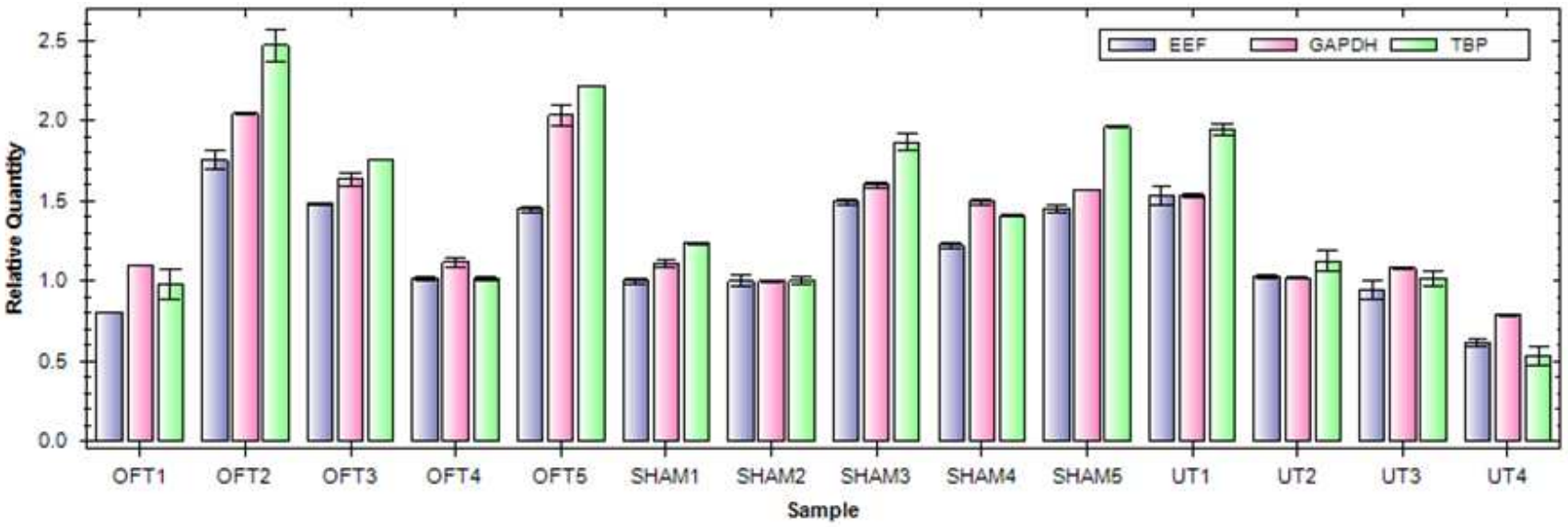



**Figure 4.9** RT-qPCR amplification plot showing the constant Cq of different cDNA synthesis reactions. (A) cDNA amplification with no reverse transcriptase is shown in blue, with *GAPDH* amplification in green/yellow. (B) The boxed area in A shows a close up of *GAPDH* threshold Cqs.

### 4.3.5 RT-qPCR reference gene verification for OFT-banded, SHAM and UT control and validation that SHAM and OFT-banded hearts were not failing at HH29

To enable normalised expression analysis at HH29, reference genes were assessed for their expression across treatment groups (OFT-banded, and SHAM and UT controls). Reference genes tested by RT-qPCR were *GAPDH*, *EEF1A1* and *TBP* (more information on these genes can be found in the discussion to this chapter) in optimised conditions. Relative quantity results revealed a pattern where TBP appeared to be the most inconsistent gene (Figure 4.10). This was tested using three analysis algorithms: Gemorm, Bestkeeper and normFinder. These programs confirmed that *GAPDH* and *EEF1A1* had consistent expression (i.e. expression was not more or less between groups), with results well within recommended values for constant expression. Values under 0.5 are deemed acceptable for reference gene stability, and both *GAPDH* and *EEF1A1* scored under 0.36 across all tests (Figure 4.10 B). TBP returned the most unstable results and so was discounted as a reference gene at HH29. However, as can be seen from Figure 4.10 B, this gene also had consistent expression with its highest value at 0.502 by Bestkeeper. This consistent expression in cell cycle marker genes expressed across all OFT, SHAM and UT groups not only shows that these genes can be used as reference genes in RT-qPCR, but also that show that the SHAM is a viable control and that OFT-banded hearts are not failing at HH29.

(A)




(B)

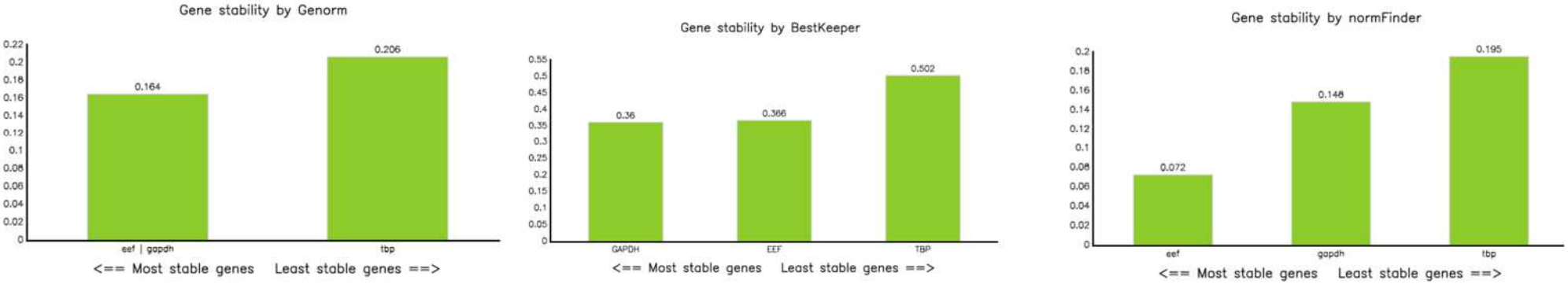



**Figure 4.10** HH29 reference gene stability across OFT-banded (OFT), SHAM and untreated (UT) controls. (A) Relative quantity across all samples; n=5 OFT and SHAM, n=4 UT. (B) Analysis of relative quantity result by Genorm, BestKeeper and normFinder software packages, demonstrating *GAPDH* and *EEF1A1* to be the most stably expressed

### 4.3.6 Sequencing results of chosen RT-qPCR internal reference genes

Final sequencing results confirmed that the reference genes were not affected by OFT-banding treatment. $Log_2$ FC values show no differences between OFT-banded and SHAM hearts (Table 4.3). These results were from genome sequencing carried out after optimisation, they are included here as they directly back up the initial RT-qPCR verification.

**Table 4.3** Sequencing results of internal reference genes

| Gene | Heart | FPKM | $Log_2$FC | *P*-value |
|---|---|---|---|---|
| ***EEF1A1*** | **OFT 6**<br>**OFT 11**<br>**OFT 17**<br><br>**SHAM 38**<br>**SHAM 42**<br>**SHAM 48** | **6046**<br>**5733**<br>**6009**<br><br>**6191**<br>**6471**<br>**6543** | **-0.04** | **0.9** |
| ***GAPDH*** | **OFT 6**<br>**OFT 11**<br>**OFT 17**<br><br>**SHAM 38**<br>**SHAM 42**<br>**SHAM 48** | **14188**<br>**13138**<br>**12395**<br><br>**13347**<br>**12907**<br>**12701** | **0.09** | **0.8** |
| ***TBP*** | **OFT 6**<br>**OFT 11**<br>**OFT 17**<br><br>**SHAM 38**<br>**SHAM 42**<br>**SHAM 48** | **46**<br>**54**<br>**51**<br><br>**51**<br>**49**<br>**49** | **0.07** | **0.7** |

### 4.3.7 Verification of control model group and RT-qPCR procedure

#### 1.2.1.1 Gene regulation in SHAM and UT hearts

To check that the SHAM control is a viable control, it was checked by RT-qPCR against UT hearts in two genes shown to be significantly differentially regulated in OFT-banded hearts that have links to cardiomyopathy. No differences where seen between SHAM and UT hearts for *DNAJC6* and *PVALB* ($F(2, 4) = 2$, $p = 0.27$; Wilk's $\Lambda = 0.421$, partial $\eta 2 = .579$); in the OFT-banded hearts these genes show significant down and up regulation respectively. Figure 4.11 shows RT-qPCR relative expression.

**Individual Gene comparison:**

SHAM vs. UT and SHAM vs. OFT-banded by T-Test:

*DNAJC6*; **SHAM vs. UT** = $t(4)=0.75, p=0.49$ **OFT vs SHAM** = $t(4)=2.7, p=0.05$

*PVALB*; **SHAM vs. UT** = $t(4)=0.77, p=0.48$ **OFT vs SHAM** = $t(4)=-3.6, p=0.02$

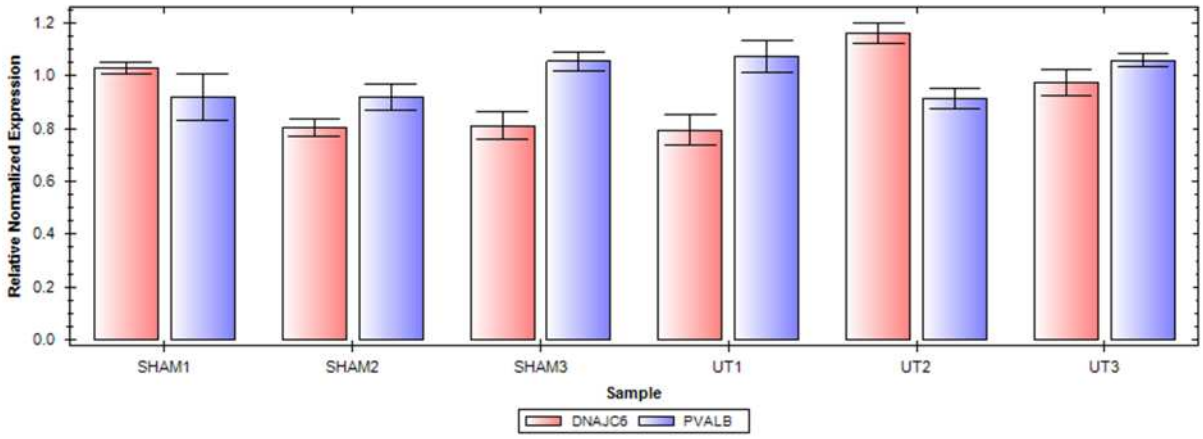
This direct comparison shows that differentially expressed genes in the OFT-banded hearts are not differentially regulated between control groups using the same statistical test.

**Multiple gene analysis:**

Over all differences were insignificant in SHAM vs. UT by one way MANOVA:

$F(2, 4) = 2$, $p = 0.27$; Wilk's $\Lambda = 0.421$, partial $\eta 2 = .579$

A




B

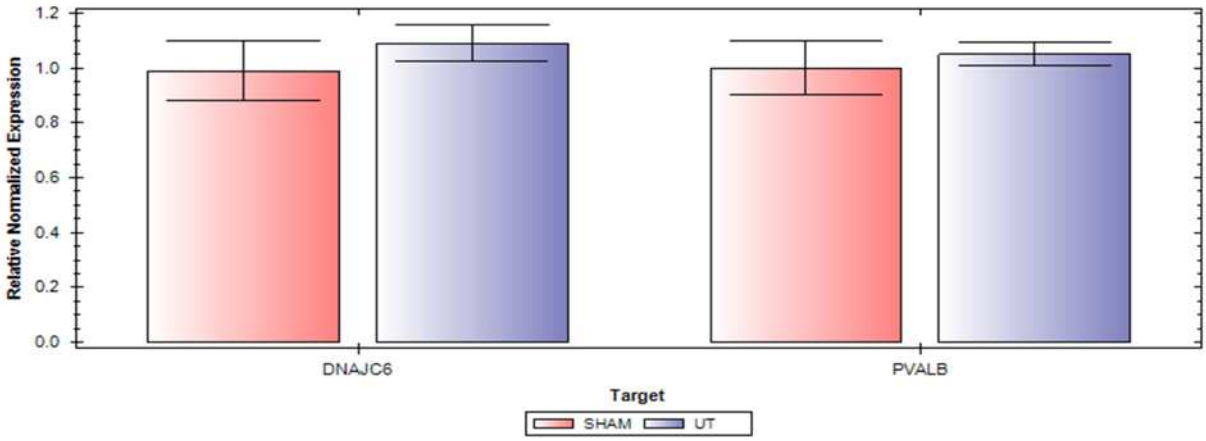
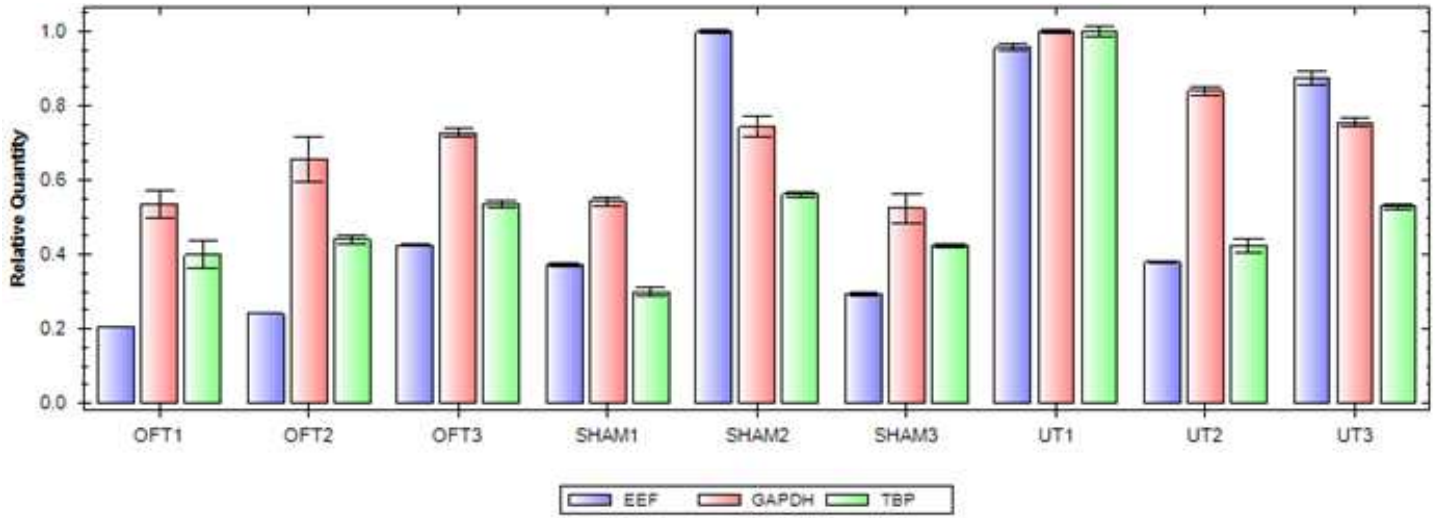



**Figure 4.11** Verification of treatment control groups. A, Relative expression across all SHAM and untreated (UT) samples. B. Relative normalised expression of *DNAJC6* and *PVALB* in SHAM and UT (SHAM used as control for comparison). SHAM and UT samples show no differences on genes found to be differentially regulated between SHAM and OFT-banded hearts.

### 4.3.8 RT-qPCR reference gene verification for OFT-banded and control HH35 hearts

In the next chapter of this thesis, RT-qPCR is carried out on HH35 hearts on genes identified with differential regulation at HH29. This necessitated reference gene verification at this later stage. At HH35 the OFT-banded model has reached a later stage of development and so gene expression may be different to HH29, particularly as we have increased death rate of OFT-banded hearts at HH35 (see section 4.1.2). Reference genes were assessed for their expression across treatment groups (OFT-banded, and SHAM and UT controls). Reference genes tested by RT-qPCR were *GAPDH*, *EEF1A1* and *TBP* in optimised conditions. Relative quantity results (Figure 4.12 A) revealed a pattern where *EEF1A1* appeared to be the most inconsistent gene. This was tested using three analysis algorithms: Gemorm, Bestkeeper and normFinder. These programs confirmed that *GAPDH* and *TBP* had consistent expression, with results well within recommended values for constant expression. Values under 0.5 are deemed acceptable for reference gene stability, and both *GAPDH* and *TBP* scored under 0.28 across all tests (Figure 4.12). *EEF1A1* returned the most unstable results and so was discounted as a reference gene at HH35.

A




B

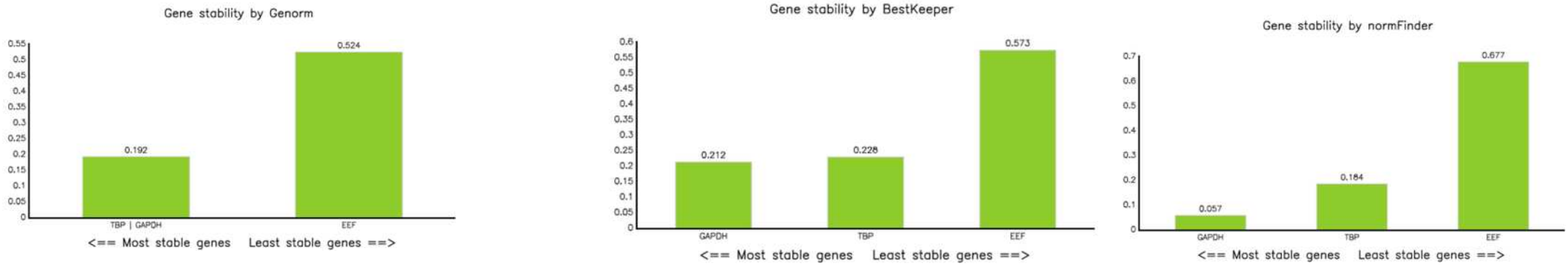
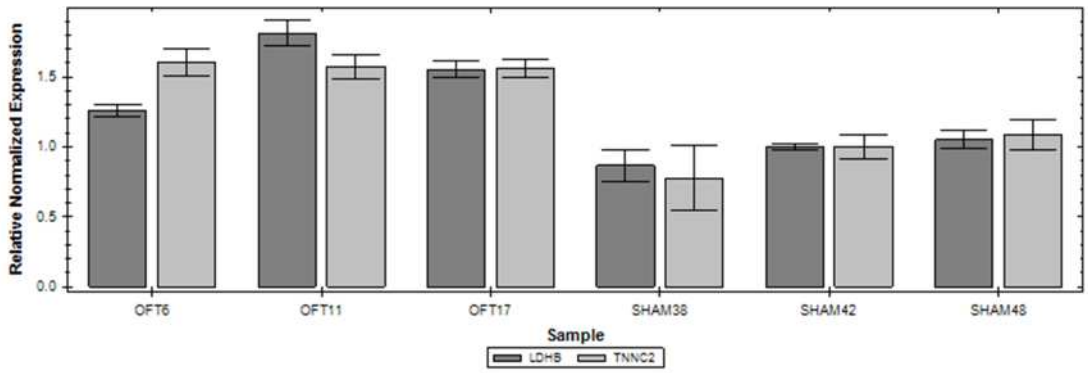



**Figure 4.12** Reference gene stability across HH35 OFT-banded (OFT), SHAM and untreated (UT) control hearts. (A) Relative quantity across all samples; n=3 for each group. (B) Analysis of relative quantity result by Genorm, BestKeeper and normFinder software packages, demonstrating *GAPDH* and *TBP* to be the most stably expressed.

### 4.3.9 qPRC Inter-plate variation check

To efficiently perform RT-qPCR analysis of differentially regulated genes in our model, it wass necessary to perform multiple RT-qPCRs using the same reference genes. To ensure this procedure was valid, reference genes were prepared on two different plates. One plate contained the reference genes (*GAPDH* and *EEF1A1*) and the genes of interest (*LDHB* and *TNNC2*), the other plate contained only reference genes. Analysis of gene regulation of target genes using reference genes on the same plate (Figure 4.13 A), or reference genes on a separate plate (Figure 4.13 B) made no difference to the levels of expression seen.

(A)




(B)

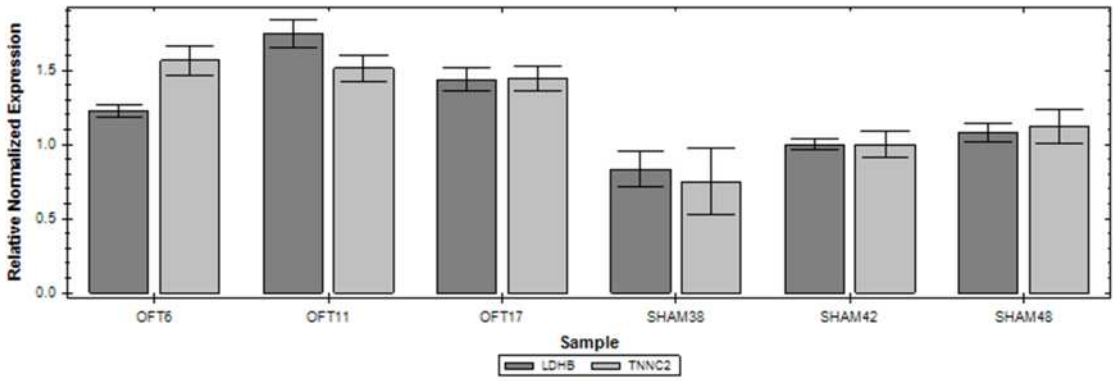



**Figure 4.13** Analysis of inter-plate variation. The reference (*GAPDH* and *EEF1A1*) and experimental (LDH5 and TNNC2) genes were analysed on the same (A) and separate (B) plates. OFT, OFT-banded.

Determine the effect globin depletion has on RNA quality and quantity

### 4.3.10 Globin depletion effect on relative quantity and expression of mRNA

In order to be able to sequence low read transcripts, globin mRNA was removed from total RNA. This is discussed at length in the discussion to this chapter (Choi et al., 2014, Mastrokolias et al., 2012). Before RNA sequencing was performed on globin depleted hearts, the effect of globin depletion (+RNase samples) on gene expression was assessed against non-treated (-RNase samples) using the gene *GJA5* and the reference genes *GAPDH* and *EEF1A1*. A general decrease in RNA is seen in globin depleted samples of around 1-fold (Figure 4.14). However, no differences in proportional gene expression were seen between treated and non-treated hearts when normalised against a reference genes, expression was consistent across GJA5 and two reference genes, *GAPDH* and *EEF1A1* ($t(4)=2.77, p=0.78$ for GJA5) (Figure 4.15).

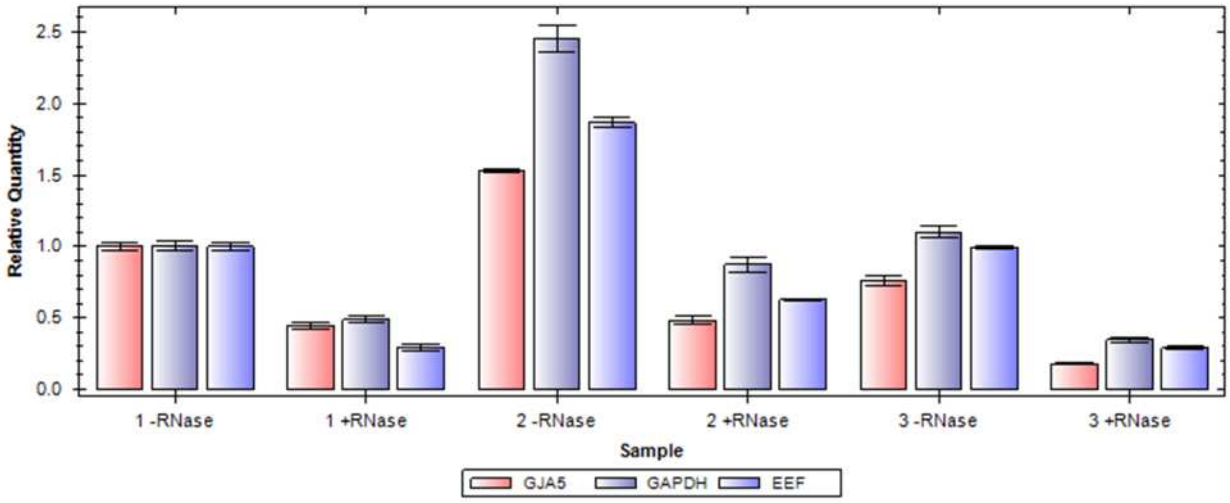



**Figure 4.14** Relative quantity comparison of RNase treated (+RNase) and non-RNase treated (-RNase) samples. A decrease in relative quantity was seen of around 1 fold. Numbers 1,2 and 3 represent the 3 hearts tested.

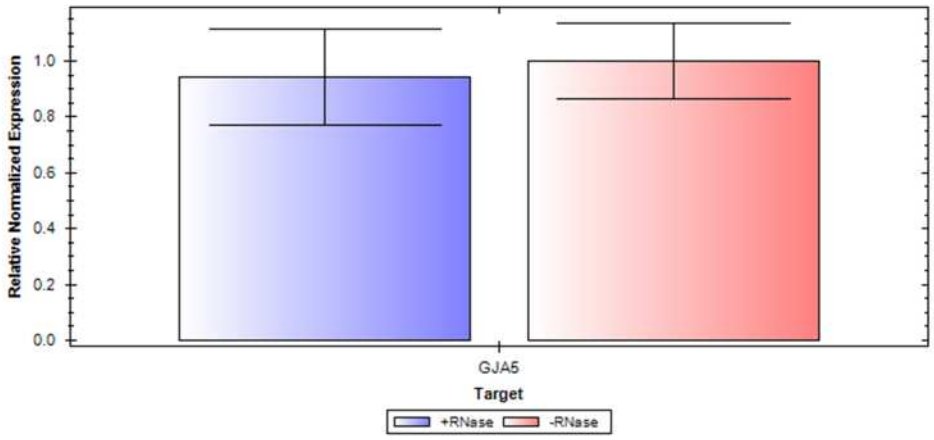



**Figure 4.15** Normalised expression of *GJA5* for RNase positive and untreated controls show no difference between groups. +RNase, treated; -RNase without RNase treatment. Differences were insignificant $t(4)=2.77, p=0.78$

### 4.3.11 Effect of globin depletion on RNA Integrity

RNA integrity following RNA preparation and subsequence storage at -80°C showed RIN values of 9.5 – 9.7. Globin depletion treatment (post RNase) generally lowered the RIN compared to before treatment (pre RNase); however, values still remained high enough and consistent enough for RNA sequencing to take place (Table 4.4). The top half of the table shows RIN values of RNA use for RT-qPCRs and preliminary studies. The bottom half shows the RNA that was used for RT-qPCR and for RNA sequencing.

**Table 4.4** RIN values of RNase treated and non-treated RNA

| Heart | RNA used for optimisations and RT-qPCR | |
|---|---|---|
| | **Pre-RNase H treatment**<br><br>**RIN** | **Post RNase H treatment**<br><br>**RIN** |
| **OFT 1a** | 9.6 | 8.4 |
| **OFT 2a** | 9.7 | 8.0 |
| **OFT 3a** | 9.6 | 8.6 |
| **SHAM 1a** | 9.5 | 6.5 |
| **SHAM 2a** | 9.6 | 6.7 |
| **SHAM 3a** | 9.5 | 8.0 |
| | **RNA used for RNA sequencing** | |
| | **Pre-RNase H treatment** | **Post RNase H treatment** |
| **OFT 1** | 7.4 | 7.2 |
| **OFT 2** | 7.1 | 7.3 |
| **OFT 3** | 7.8 | 6.9 |
| **SHAM 1** | 7.8 | 7.8 |
| **SHAM 2** | 7.8 | 7.4 |
| **SHAM 3** | 7.3 | 7.0 |

## 4.4 Globin depletion of hearts for RNA sequencing

Successful globin depletion treatment led to $\log_{10}$ fold changes of -10 to -20 of the targeted genes, as demonstrated by RT-qPCR (Figure 4.16 and 4.17). Globin depletion treatment was performed on selected globin genes (HBAA, HBAD, HBB, HBG1, HBG2 and HBZ; Table 4.5) and RNA sequencing confirmed the RT-qPCR result. Following globin depletion, hearts then passed to library preparation for RNA sequencing. Before globin depletion treatment, RT-qPCR was carried out on all globin genes in order to assess expression level at HH29 (Cq values shown in Table 4.5). After globin depletion and subsequent sequencing FPKM values were near zero for all depleted genes (Table 4.5)

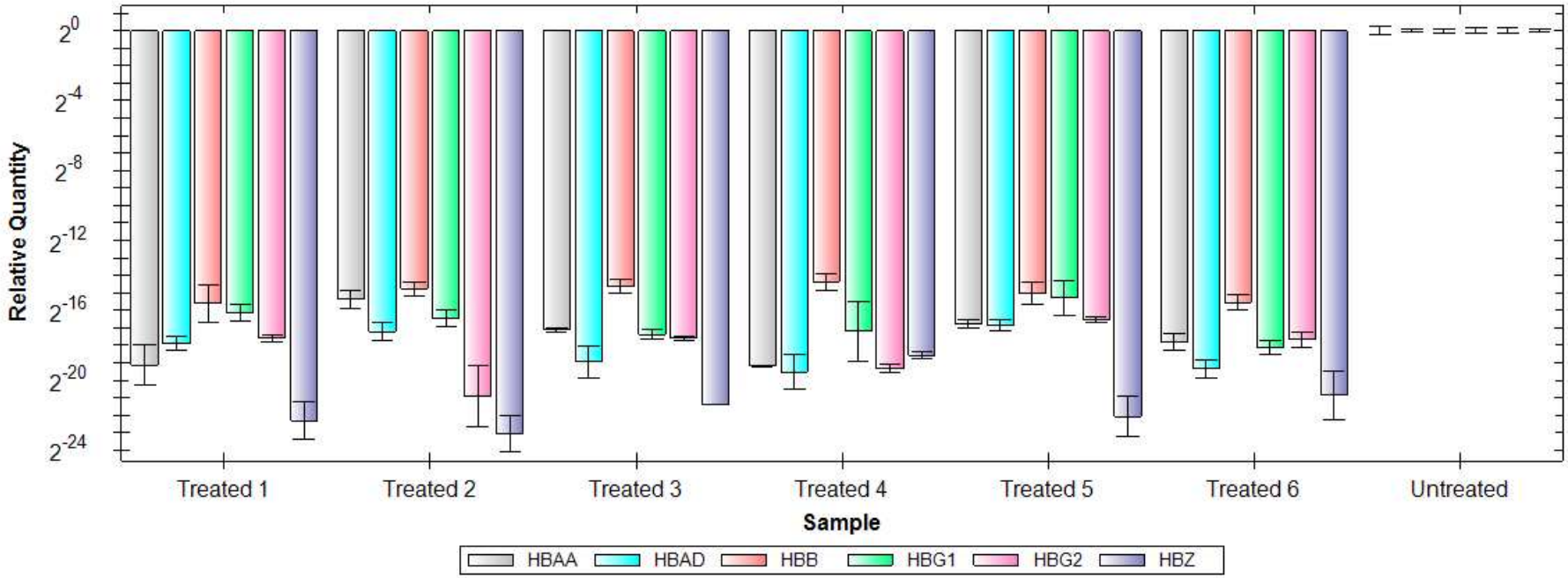



**Figure 4.16** Relative expression of each heart for sequencing at HH29 (OFT-banded and SHAM) before and after globin depletion treatment. Controls represent the 6 hearts before treatment pooled. Globin genes tested HBAA, HBAD, HBB, HBG1, HBG2 and HBZ. The cDNA was then used for RNA sequencing at HH29. Values are +/- s.e.m of mean treated and pooled untreated hearts. (n = 6 before and after treatment).

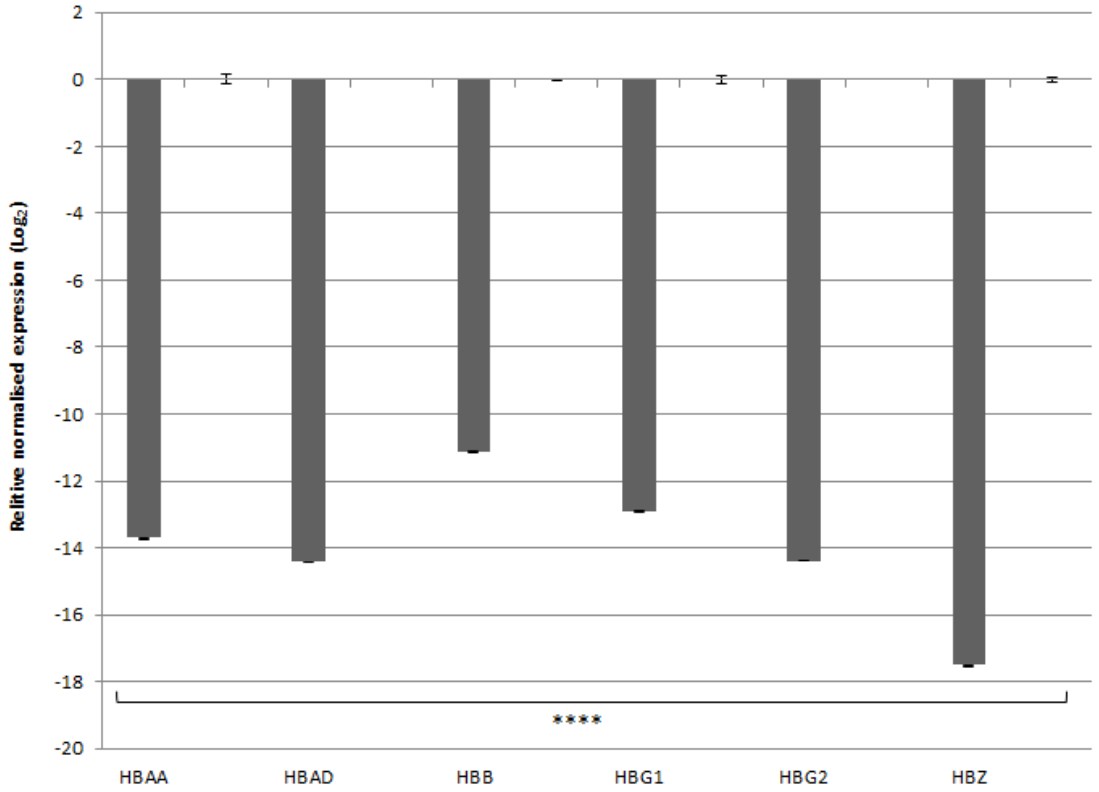



**Figure 4.17** Relative expression of each globin depleted gene; HBAA, HBAD, HBB, HBG1, HBG2 and HBZ in pooled treated to untreated hearts. Treatment samples significantly different to non-treated. Values are +/- s.e.m of mean treated and pooled untreated hearts. (n = 6 before and after treatment (****, <*p*0.0001).

**Table 4.5** Globin gene expression and reduction following depletion treatment.

| Gene name | RT-qPCR (Cq) (non RNase) | Post RNase depletion treatment | | |
|---|---|---|---|---|
| | | Relative fold change post globin depletion ($log_2$) | Reduction (%) | Sequencing mean FPKM |
| ***HBAA*** Haemoglobin α1 | 19.1 | 16 | >99.999 | <0.00 |
| ***HBAD*** Haemoglobin αD | 21.9 | 17 | >99.999 | 0.20 |
| ***HBZ*** Haemoglobin Z | 19.9 | 15 | >99.999 | <0.00 |
| ***HBB*** Haemoglobin β | 22.2 | 17 | >99.999 | 0.4 |
| ***HGB1*** Haemoglobin γ1 | 18.1 | 21 | >99.999 | Not in data set |
| *HBG2* Haemoglobin γ2 | 18.7 | 23 | >99.999 | 3 |
| ***HBE*** Haemoglobin ε | 26.8 | 0* | 0* | 12500* |

***HBE** **Not globin depleted**

RNA Sequencing on SHAM versus OFT-banded hearts

### 4.4.1 Sequencing count normalisation technique using FPKM comparison with TPM followed by principle component analysis

Normalisation of reads was carried out by fragments per kilobase per million (FPKM). Paired end sequencing uses FPKM as a standard normalised read count of a gene, taking the sample sequencing depth and gene length into account (Mortazavi et al., 2008). Transcripts per kilobase per million (TPM) was also used to see if the differences in the method effected our expression values. TPM normalizes against total transcripts rather than total reads. Overall variation of OFT-banded and SHAM hearts by principle component analysis was identical with both FPKM and TPM (Figure 4.18). To demonstrate what this means at an individual gene analysis level, table 4.6 shows a subset of genes (chosen as they represent a full spread of expression) with fold change values given for FPKM and TPM. No differences were seen between FPKM and TPM. As normalization by TPM had no effect on our gene abundance, FPKM values were taken forward for statistical analysis by DESeq. The final PCA plot showed that OFT-banded hearts all had similar overall expression and that this differed to that of SHAM hearts. The three SHAM hearts also showed similar overall expression (Figure 5.11 – heart numbers represent original harvesting numbers). The separation between the OFT-banded group and the control was predominately by the PC2 and less so by PC1. This indicates only a modest number of differentially expressed genes, and is in line with the small number of differentially expressed genes found in Tables 4.7 and 4.8 later in this result section.

**Table 4.6** Effect of TPM on gene expression fold change

| Gene | FPKM fold change | TPM fold change |
|---|---|---|
| ***ENS-1*** | 0.40 | 0.40 |
| ***TNNC2*** | 1.85 | 1.88 |
| ***PRKAG3*** | 0.65 | 0.65 |
| ***FUTIO*** | 0.95 | 0.94 |

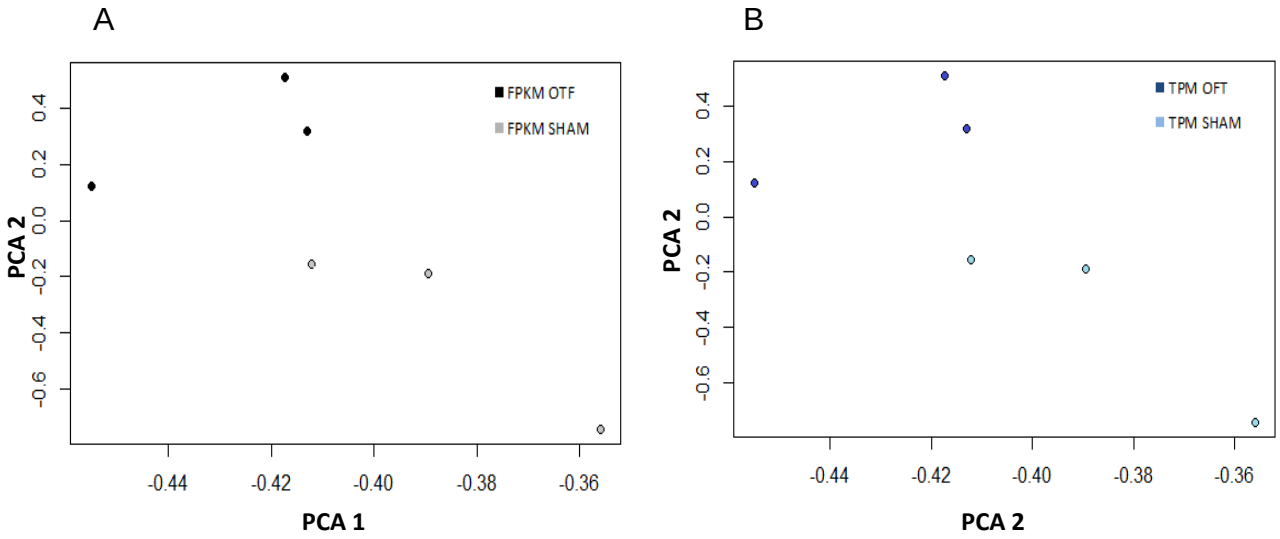



**Figure 4.18** Comparison of sequencing analysis normalisation method effect on principle component analysis (PCA). A; PCA of FPKM. B; PCA of TPM. Both (A) and (B) show almost identical variation

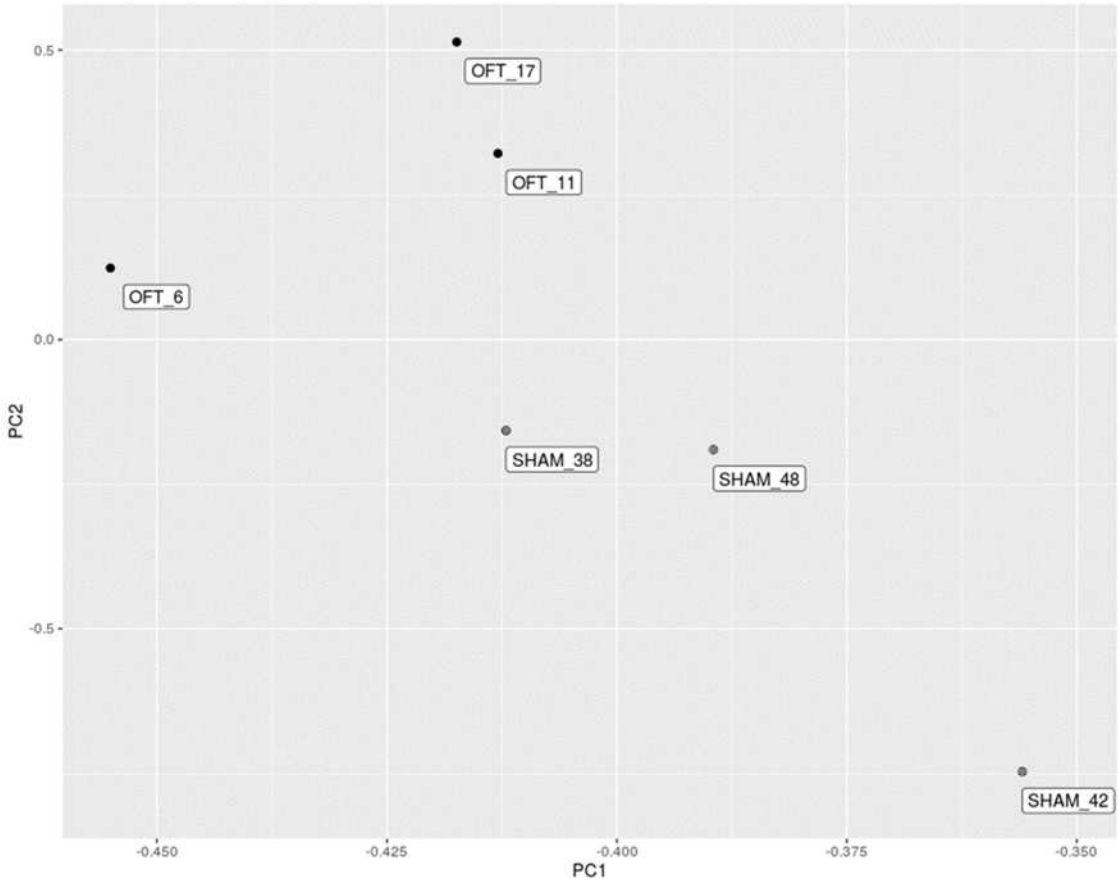



**Figure 4.19** Sequencing PCA plot showing the variation between OFT-banded and SHAM samples and variation within sample groups.

### 4.4.2 Differentially regulated genes

RNA sequencing was carried out on OFT-banded and SHAM hearts (n=3 for each group). Uniquely and correctly aligned sequence reads (47-90 x 106) with MAPQ values above 20 were generated for all the samples and were mapped against the galGal4 reference sequence genome, using refSeq gene annotations from UCSC database (http://genome.ucsc.edu Nov. 2011) (ICGSC Gallus_gallus-4.0/galGal4).

The fragment read count of the exon-space of a gene is normalised against the total number of mapped fragment reads (ribosomal RNA, reads which were not uniquely aligned and those below MAPQ 20 were excluded) in that particular alignment file and against the total length of the gene's exon-space.

Sequencing studies of large sample size will often have a differential regulation cut off of a 2 fold regulation change. This is because very small differences that would be biologically inconsequential can be significant in studies with large sample sizes. Our study uses three OFT-banded compared to three SHAM, so this effect would not be so apparent. Because of this, genes with consistent differential expression across all 3 repeats and a significance level of $p$ =<0.05 are considered biologically significant in this study, this is discussed further in this chapter's discussion.

Thirty genes were found to be statistically significantly regulated in the OFT-banded hearts compared to SHAM controls (Table 5.6 and 5.7). Principal component analysis showed that OFT-banded hearts all had similar overall expression and that this differed to that of SHAM hearts. The three SHAM hearts also showed similar overall expression (Figure 5.11). The separation between the OFT-banded group and the control was predominately by the PC2 and less so by PC1. This indicates only a modest number of differentially expressed genes, and is in line with the small number of differentially expressed genes found in Table 4.7 – 8.

Table 5.6 and 5.7 summarises the genes which were differentially expressed with corrected $\log_2$ fold change, ifcSEM (corrected standard error of mean) and $p$ adjusted values. Genes found significantly differentially regulated were indicative of a haemodynamic alteration phenotype. Genes generally display metabolic and

conduction system cardioprotective properties. Molecular pathways possibly implicated by data in this thesis are discussed at length in Chapter 6.

With regards to the genes which were normally reactivated and upregulated as part of the fetal gene programme in the adult heart in response to pathological insults (e.g. pressure overloading), NPPB, ACTA1 and PLN showed increased FPKM values in two of the banded hearts compared to controls (Song et al., 2012). Genes highlighted from the KD study as being affected by changes to structure and subsequently could affect conduction also show some changes. Also shown here are genes of biological interest that were RT-qPCRed. This took place as borderline insignificant genes found insignificant by the corrected DESeq method needed to be checked for false negative. However, all differences in these genes are insignificant. For this reason, FPKM values are shown in Table 4.9.

**Table 4.7** Sequencing result of significantly differentially down regulated genes

| Gene | Corrected $log_2$ fold change | lfcSEM | P-value | Corrected P-value |
|---|---|---|---|---|
| ***ENS-1*** | -0.91 | 0.16 | 1.41E-08 | 2.98E-05 |
| ***ERNI*** | -0.76 | 0.15 | 3.39E-07 | 4.79E-04 |
| *ADORA2B* | -0.74 | 0.18 | 4.89E-05 | 2.08E-02 |
| *ITPK1* | -0.68 | 0.17 | 6.07E-05 | 2.34E-02 |
| *GLRX* | -0.71 | 0.18 | 9.41E-05 | 3.33E-02 |
| *PDCD4* | -0.41 | 0.11 | 1.08E-04 | 3.52E-02 |
| *HBG1* | -0.68 | 0.18 | 1.65E-04 | 4.37E-02 |
| *PIAS2* | -0.36 | 0.10 | 1.75E-04 | 4.37E-02 |
| *TGM2* | -0.38 | 0.10 | 1.75E-04 | 4.37E-02 |
| *DNAJC6* | -0.48 | 0.13 | 1.87E-04 | 4.40E-02 |

| | | | | |
|---|---|---|---|---|
| *RAP1GAP2* | -0.57 | 0.15 | 2.14E-04 | 4.46E-02 |
| *H1F0* | -0.64 | 0.18 | 2.31E-04 | 4.46E-02 |
| *ARFGAP1* | -0.47 | 0.13 | 2.53E-04 | 4.46E-02 |
| ***LBH*** | 0.60 | 0.17 | 2.93E-04 | 4.86E-02 |
| *CDH8* | -0.60 | 0.16 | 2.98E-04 | 4.86E-02 |
| *GSTA4* | -0.65 | 0.18 | 3.21E-04 | 4.88E-02 |

**Table 4.8** Sequencing result of significantly differentially up regulated genes

| Gene | Corrected $log_2$ fold change | lfcSEM | P-value | Corrected P-value |
|---|---|---|---|---|
| *TIMM10* | 0.72 | 0.13 | 1.02E-08 | 2.98E-05 |
| *GBX2* | 0.83 | 0.17 | 7.80E-07 | 8.27E-04 |
| ***LDHB*** | 0.64 | 0.13 | 1.45E-06 | 1.23E-03 |
| ***TNNC2*** | 0.75 | 0.16 | 1.90E-06 | 1.34E-03 |
| *PNO1* | 0.59 | 0.13 | 5.97E-06 | 3.62E-03 |
| ***PVALB*** | 0.70 | 0.17 | 4.05E-05 | 1.91E-02 |
| ***MYL1*** | 0.54 | 0.15 | 2.05E-04 | 4.46E-02 |
| *IFNGR1* | 0.55 | 0.15 | 2.30E-04 | 4.46E-02 |
| *S100A11* | 0.52 | 0.14 | 2.47E-04 | 4.46E-02 |
| ***LBH*** | 0.60 | 0.17 | 2.93E-04 | 4.86E-02 |
| *LGALS1* | 0.64 | 0.18 | 3.22E-04 | 4.88E-02 |
| *LLPH* | 0.58 | 0.16 | 3.40E-04 | 4.97E-02 |

**Table 4.9** Fragment per kilobase per million (FPKM) of fetal gene program genes, genes later analyses by RT-qPCR and additional genes of biological interest

| Gene | OFT-Banded FPKM | | | | SHAM FPKM | | | |
|---|---|---|---|---|---|---|---|---|
| | 1 | 2 | 3 | Mean | 1 | 2 | 3 | Mean |
| ***NPPB*** | 2038 | 3662 | 7026 | **4242** | 2052 | 1916 | 1123 | **1697** |
| ***ACTA1*** | 2463 | 4681 | 5433 | **4192** | 3808 | 3216 | 3912 | **3645** |
| ***PLN*** | 613 | 617 | 740 | **656** | 472 | 618 | 451 | **513** |
| ***βMYH*** | 2410 | 2781 | 3227 | **2806** | 2183 | 3363 | 2158 | **2568** |
| ***αMYH*** | 263 | 229 | 283 | **258** | 365 | 316 | 218 | **300** |
| ***ANKRD 1*** | 29 | 27 | 197 | **84** | 23 | 20 | 11 | **18** |
| ***DMD*** | 10.9 | 10 | 12.5 | **11.1** | 14.2 | 14.1 | 12.8 | **13.7** |
| ***BIN1*** | 3.1 | 6.8 | 6.7 | **5.5** | 5.0 | 8.5 | 9.5 | **7.7** |
| ***NOS2*** | 6.2 | 8.1 | 7.3 | **7.2** | 6.8 | 8.4 | 9 | **8** |
| ***MYL4*** | 730 | 781 | 740 | **750** | 849 | 720 | 836 | **801** |
| ***PRKAG3*** | 8.81 | 8.58 | 8.47 | **8.62** | 11.36 | 12.97 | 15.33 | **13.22** |
| ***HDAC 7*** | 16.82 | 18.92 | 20.10 | **18.61** | 23.15 | 24.35 | 26.36 | **24.62** |
| ***STK11*** | 20.56 | 24.66 | 25.42 | **23.54** | 24.83 | 30.19 | 35.99 | **30.33** |
| ***TRPV4*** | 2.07 | 234 | 2.12 | **2.17** | 3.38 | 3.19 | 3.88 | **3.48** |
| ***PFKM*** | 33.06 | 45.17 | 38.69 | **38.97** | 47.97 | 62.12 | 54.64 | **54.91** |
| ***TBX3*** | 10.31 | 9.06 | 8.25 | **9.20** | 5.64 | 7.27 | 7.56 | **6.82** |
| ***S100A 1*** | 123.94 | 102.60 | 100 | **108.84** | 98.73 | 85.63 | 86.82 | **90.39** |
| ***GJA5*** | 199.18 | 212.10 | 169.55 | **193.61** | 211.60 | 230.84 | 255.97 | **230.80** |

### 4.4.3 Comparison of RNA sequencing result with RT-qPCR for validation

Sequencing results of 14 genes were repeated by RT-qPCR at HH29. RT-qPCR samples were from newly synthesised non-globin depletion and non-fragmented first strand cDNA from the same RNA used for sequencing. Genes covered the full expression range from sequencing with top differentially regulated up and down regulated genes as well as non-differentially regulated in order get a good range for comparison. Table 5.6 shows genes of biological interest by sequencing and RT-qPCR at HH29, and by RT-qPCR at HH35. HH29 expression is seen to been closely matched (Figure 4.20 (A)) and a direct statistically significant relationship is seen between sequencing and RT-qPCR $\log_2$ FC results ($r = 0.98$, $n = 14$, $p = <.01$) (Figure 4.20 (B)), this is also seen in new biological repeat samples (Figure 4.21). The relationship between techniques is near direct with a line m value of 0.95 showing that RT-qPCR (x axis) results have a slightly higher $\log_2$ FC than sequencing (y axis).

RT-qPCR results at HH35 show expression is closely matched with HH29 (Figure 4.22 (A)) and a direct statistically significant relationship is seen between HH29 and HH35. Some genes do show more or less differential expression at the later stage. This can clearly be seen in Figure B where individual genes sit above or below the trend line. The biological relevance of this is discussed in chapter 5.

**Table 4.10** mRNA sequencing and RT-qPCR differential expression at HH29 and RT-qPCR at HH35

| Gene | Sequencing HH29 | | | | RT-qPCR HH29 | | | | RT-qPCR HH35 | | | |
|---|---|---|---|---|---|---|---|---|---|---|---|---|
| | **Mean fold change** | **Mean $log_2$ Fold change (corrected)** | **S.E** | ***P* value (corrected)** | **Mean fold change** | **Mean $log_2$ Fold change** | **S.E** | ***P* value** | **Mean fold change** | **Mean $log_2$ Fold change** | **S.E** | ***P* value** |
| *PRKAG3* | 0.652 | **-0.46** | 0.13 | 0.06 | 0.68 | **-0.55** | 0.05 | <0.05 | 0.44 | **-1.18** | 0.04 | <0.05 |
| *LDHB* | 1.6 | **0.64** | 0.13 | <0.05 | 1.54 | **0.62** | 0.24 | <0.05 | 1.10 | **0.13** | 0.06 | 0.61 |
| *HDAC7* | 0.75 | **-0.37** | 0.09 | 0.06 | 0.7 | **-0.51** | 0.04 | 0.12 | 0.75 | **-0.41** | 0.04 | 0.22 |
| *MYL1* | 1.52 | **0.54** | 0.15 | <0.05 | 1.57 | **0.65** | 0.12 | 0.13 | 2.66 | **1.41** | 0.2 | <0.05 |
| *TNNC2* | 1.8 | **0.75** | 0.16 | <0.05 | 1.6 | **0.65** | 0.19 | <0.05 | 1.54 | **0.62** | 0.16 | 0.32 |
| *ENS-1* | 0.4 | **-0.91** | 0.16 | <0.05 | 0.39 | **-1.35** | 0.02 | <0.05 | 0.72 | **-0.47** | 0.16 | 0.63 |
| *ERNI* | 0.48 | **-0.76** | 0.15 | <0.05 | 0.47 | **-1.08** | 0.04 | <0.05 | 0.45 | **-1.15** | 0.10 | 0.22 |
| *PVALB* | 1.85 | **0.7** | 0.17 | <0.05 | 1.76 | **0.81** | 0.17 | <0.05 | 2.249 | **1.16** | 0.37 | <0.05 |
| *S100A11* | 1.49 | **0.52** | 0.14 | <0.05 | 1.6 | **0.67** | 0.07 | <0.05 | 2.11 | **1.07** | 0.179 | <0.05 |
| *DNAJC6* | 0.64 | **-0.48** | 0.13 | <0.05 | 0.59 | **-0.75** | 0.03 | <0.05 | 0.76 | **-0.41** | 0.07 | 0.15 |
| *TBX3* | 1.35 | **0.4** | 0.15 | 0.2 | 1.3 | **0.38** | 0.05 | 0.2 | 1.07 | **0.14** | 0.08 | 0.84 |

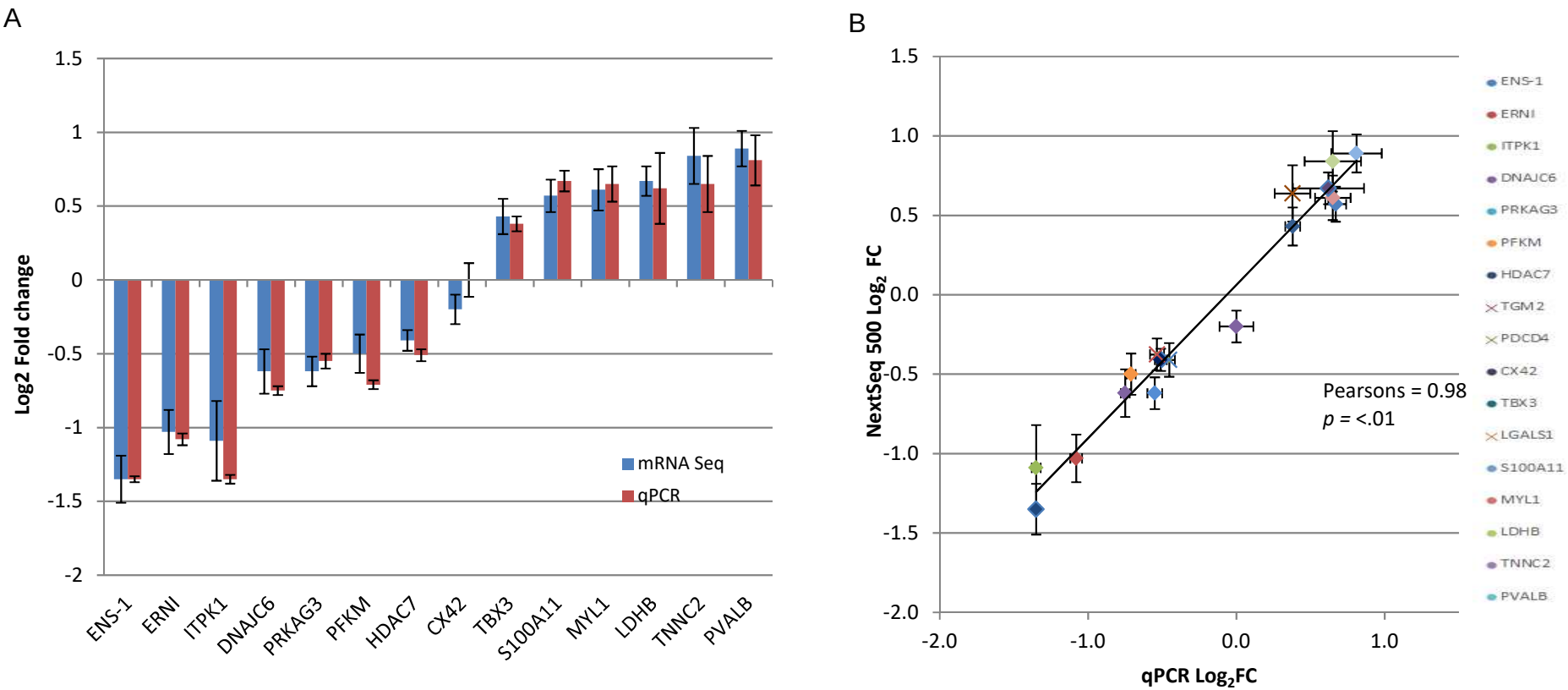



**Figure 4.20 Technical replication.** (A) Gene expression of all globin depleted and sequenced hearts by NextSeq 500, compared to same hearts non-globin depleted by RT-qPCR. No statistical differences shown between globin depleted sequenced and non-treated RT-qPCR samples s(t(26)=0.145, *p*= 0.88). (B) The relationship of expression between groups shows significant correlation (r = .98 (12) *p* = <.01).

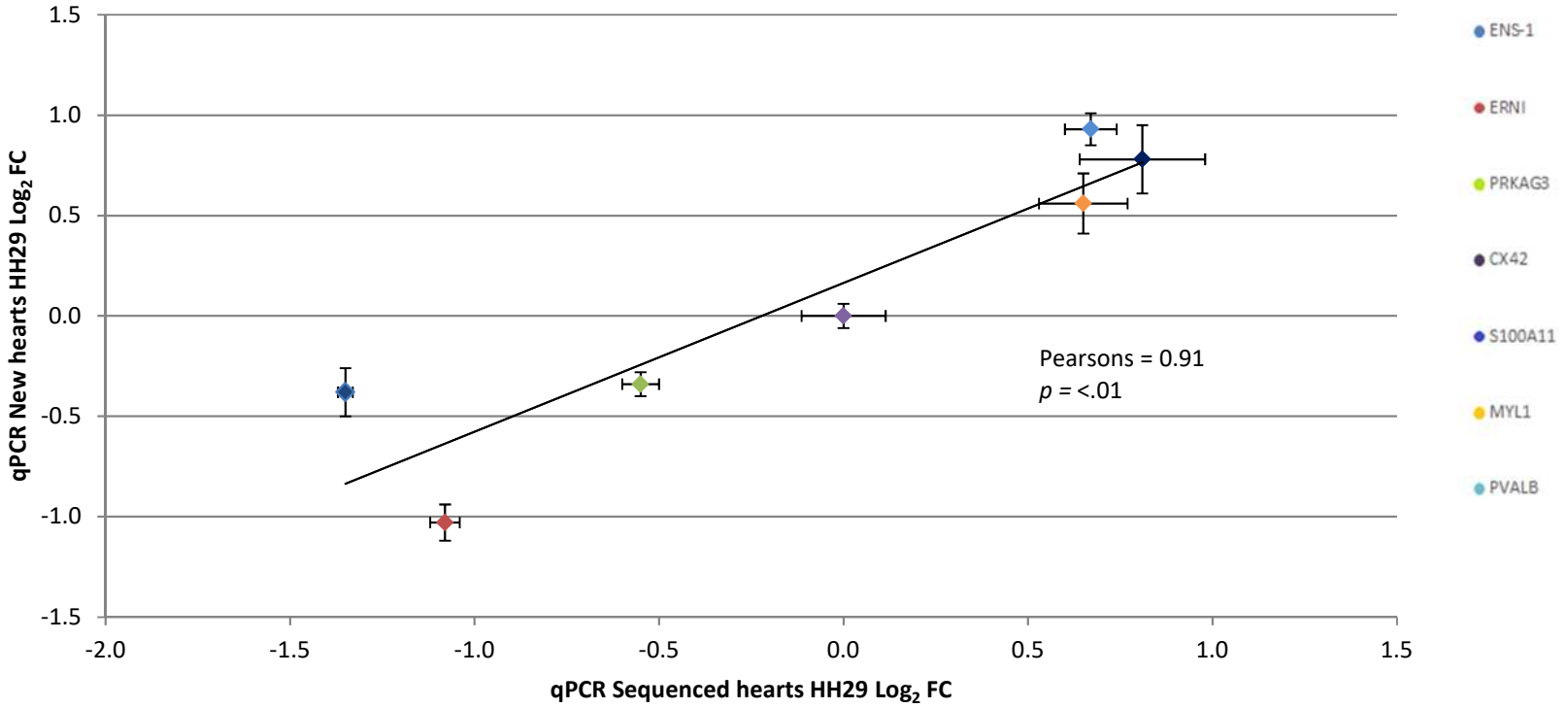



**Figure 4.21** Biological replication**.** Relationship of gene expression of sequenced hearts at HH29 (n = 3 OFT, n= 3 SHAM) and new biological replicants (n = 3 OFT, n= 3 SHAM) at HH29 by RT-qPCR. Statistically significant biological replication is shown (r = .91 (5), *p* = <.01).

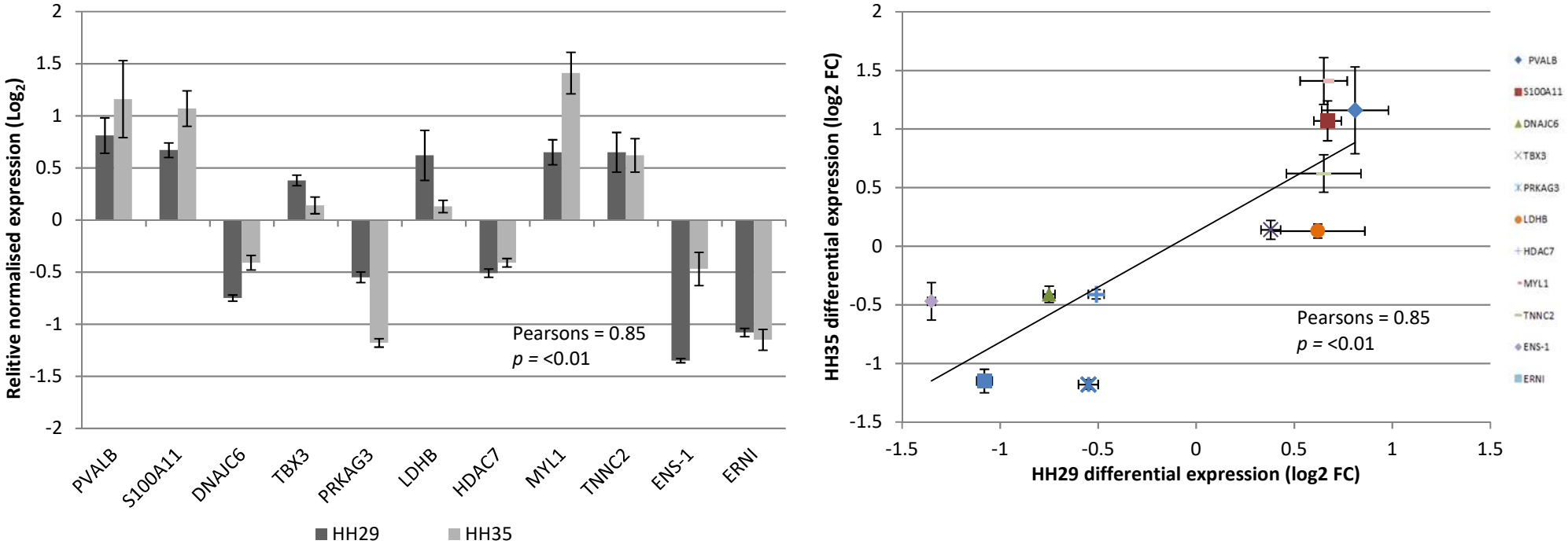



**Figure 4.22** Expression analysis at HH29 to HH35. (A) Gene expression comparisons by RT-qPCR from HH29 to HH35 in selected genes of interest. (B) A direct statically significant relationship is scene in expression of differentially regulated genes between HH29 and HH35 (r = .85 (9), *p* = .001).

## 4.5 Discussion

The primary aim of this section was to perform reliable and verified mRNA sequencing of OFT-banded hearts. The RNA sequencing method highlighted by Mortazavi *et al.* 2008 mapped low reads from small amounts of RNA using the illumina sequencing platform. Deep sequencing, when compared to microarrays, permits more information to be gained, allowing analysis of alternative splicing, non-coding RNA, unknown transcripts, small insertions and deletions, and has increased read depth and sensitivity. This has meant it has overtaken microarrays and has now become the gold standard technique for analysis of gene expression (Mortazavi et al., 2008, Wang et al., 2009).

The strand specific (directional) sequencing we employed will allow the analysis of sense and antisense overlapping transcripts. Strand specific RNA-seq is a relatively new concept and is important as it allows information to be gained on strand overlapping genes, this is achieved as only the sense strand of each gene cDNA is sequenced (Mills et al., 2013). Antisense transcription has mainly a regulatory function, but can also code for protein (Mills et al., 2013). In the human genome, currently, 25% of transcripts have been found to have an overlapping antisense transcripts (Wood et al., 2013). Our method of strand specific sequencing uses dUTP second-strand marking (see section 2.3.4.2 – 4) and has been shown to be the most reliable protocol in a review on literature based on specificity, library complexity, continuity and evenness of coverage, agreement with known annotations and expression profiling accuracy (Levin et al., 2010, Parkhomchuk et al., 2009).

The whole illumine RNA seq method was shown to be highly reliable with very little technical variation (Marioni et al., 2008). In order for us to exploit this technique and gain maximum information, the pre-processing of samples is of vital importance, as genetic information can be lost, and variation between samples can be introduced. Following harvesting of our OFT-banded hearts and SHAM controls, high yields of pure RNA of high integrity were gained via optimisation of RNA preparation techniques using tri-reagent separation, and DNA removal by DNase and purification phenol chloroform at pH5.2. cDNA was then generated and showed consistent expression

across multiple cDNA synthesis reactions. In this chapter we have proved reliability in our RNA purification and cDNA generation; this enables reliable results to be obtained from expression analysis. mRNA sequencing results were obtained showing differentially expressed genes from our OFT-banded model. These results also showed stable expression of housekeeping genes across SHAM and OFT-banded hearts. These results were then verified with qPCR proving that we have a reliable model without regulation of housekeeping genes, but with a differential profile for further analysis

### 4.5.1 Verification of OFT-banded and SHAM model with consistency of reference genes

Before any work on sequencing to identify differential expression could take place, first the OTF-banding model had to be verified terms of gene expression, ensuring the OFT-banded and SHAM hearts were not failing and that SHAM hearts showed no difference to untreated controls.

RT-qPCR reference gene verification

In order that RT-qPCRs could take place it was important that reference genes were assessed for consistency (Pfaffl, 2001). In our model, this took on increased significance for two reasons. Firstly, reference gene expression could be affected by heart failure. However, if consistency could be shown in these genes across OFT-banded, SHAM controls and untreated controls, it would prove that our model is viable and indicate that our phenotype is not down to failure of our OFT-banded hearts, but due to genuine differential regulation. Secondly, confirmation that SHAM controls were not affected by the SHAM procedure and are a suitable control for mRNA sequencing.

Three reference genes were chosen that have been used previously in the chick heart; *GAPDH*, *EEFA1A* and *TBP* (Brattelid et al., 2010). At HH29 RT-qPCR showed consistent expression across all groups in all three genes. However, of the three genes, TBP was the most inconsistent and was therefore excluded as a reference gene. This is shown in our eventual sequencing result where no differential regulation

is seen between OFT-banded and SHAM groups, with differential *p*-values of 0.9, 0.8 and 0.7 seen for *GAPDH*, *EEF1A1* and *TBP* respectively. At HH35, again, good consistency was seen; however, this time *EEF1A1* was clearly more inconsistent than *GAPDH* and *TBP*, so *EEF1A1* was excluded at HH35.

Simple observation of the Cq values across all groups show that they all have similar expression ratios; however, consistency assessment was carried out and compared between three algorithms: Genorm, Best keeper and NormFinder. Genorm assesses a stability measure 'M' value and uses pairwise correlations to assess the best two reference genes and exclude the most unstable (Vandesompele et al., 2002). Best keeper uses standard deviations and a coefficient of variance (Pfaffl et al., 2004), and NormFinder assesses gene stability coefficients (Andersen et al., 2004). The three algorithms were amalgamated into one software package called ref-finder (Xie et al., 2012). This software is R based to allow analysis of reference genes in both the individual algorithms and combined analysis in order to gain the most accurate result. Data obtained from ref-finder has been shown to correlate with that of the results when analysis is performed individually by the three software programs (De Spiegelaere et al., 2015). Ref-finder uses Cq values in its algorithm and assumes gene reaction efficiencies are at 100 %. Our *GAPDH*, *EEF1A1* and *TBP* genes are 100 %, 104% and 104% efficient respectively, so Ref-finder can be used as an effective tool for assessment of our RT-qPCR reference genes (De Spiegelaere et al., 2015).

Our eventual sequencing result showed that differential regulation of metabolism is an important factor, and with hindsight it may have been preferable to of not selected glycolytic enzyme Glyceraldehyde 3-phosphate dehydrogenase (*GAPDH*) as a reference gene. However previous models of heart failure have shown no alteration in *GAPDH* (Brattelid et al., 2010), and *GAPDH* has been used as a reference gene in previous heamodynamic banding studies in the chick heart (Hall et al., 2004). Our RT-qPCR data at HH29 and HH35 together with the sequencing result shows no differential expression in OFT-banded, SHAM and UT hearts and confirms our model hearts are not failing.

TATA-binding protein (*TBP*) has been shown to be stably expressed in post infarct heart failure and also across developmental stages of the heart in rat (Brattelid et al., 2010). We showed consistent expression of TBP at HH29 and HH35, though at HH29 it was excluded as there were more stably expressed genes found in *GAPDH* and *EFF1A1*.

Elongation factor 1-alpha 1 (*EEF1A1*) has been shown to be one of the most stably expressed reference genes in the human myocardium, even during end stage heart failure (Pilbrow et al., 2008), and proved to be a very stable gene for us at HH29. At HH35 a slight down regulation led to reduced stability scores – scoring over 0.5 in all algorithms, though its stability scores were still generally reasonable and all <1. However, as it was the least stable, *EEF1A1* was excluded as a reference gene at HH35. Analysis of multiple array data sets has highlighted *EEF1A1* as possibly being involved in dilated cardiomyopathy (DCM) (Camargo and Azuaje, 2008). The gene is involved in the enzymatic delivery of aminoacyl tRNAs to the ribosome and as such has been found by protein network analysis to have many links to other DCM differentially regulated genes. The array studies showed up regulation in the failing heart (Camargo and Azuaje, 2008, Barth et al., 2006). Our slight down regulation again still indicates that our hearts are not failing.

SHAM control verification

We have shown consistency of expression in housekeeping genes in UT and SHAM. The consistency is also repeated in genes found to be differentially regulated in OFT-banded hearts. That is, no differences overall were found in DNAJC6 and PVALB (differentially regulated genes in OFT-banded when compared to SHAM hearts) between UT and SHAM hearts ($F(2, 4) = 2$, $p = 0.27$; Wilk's $\Lambda = 0.421$, partial $\eta 2 = .579$), and in individual gene direct comparison by t-test with significance on OFT-banded hearts: DNAJC6; SHAM vs. UT = $t(4)=0.75, p=0.49$, OFT vs SHAM = $t(4)=2.7, p=0.05$; and PVALB; SHAM vs. UT = $t(4)=0.77, p=0.48$, OFT vs SHAM = $t(4)=-3.6, p=0.02$. The gene expression data, together with the previously identified survival/phenotypic analysis, as displayed in the introduction to this chapter, show that the SHAM control technique has no effect on the embryo compared to UT. Therefore,

the SHAM control was used as the control to OFT-banded hearts in mRNA sequencing and other all experiments in this thesis.

### 4.5.2 Optimisation of library preparation for mRNA sequencing with globin depletion

Removal of globin cDNA for next generation sequencing

Before oligonucleotides, that enable the globin depletion procedure, could be designed, gene expression in the chick embryo had to be deduced in order to know what genes had to be depleted. In the adult heart there are two main haemoglobin subunits that make up the haemoglobin heterotetramer – alpha and beta. Previous research into human and chicken haemoglobin genes has found that the alpha haemoglobin genes are more consistently expressed throughout embryonic development and in the adult than the more variable beta genes (Rincon-Arano et al., 2009). Embryonic gene expression differs from that of the adult, and studies have shown that expression of one subtype can down regulate another (Rincon-Arano et al., 2009). A subtype of the alpha gene, zeta haemoglobin (*HBZ*), has been shown embryonically in chick and human, but the expression level at HH29 was not clear (Chapman et al., 1980). Our RT-qPCR results show relatively high levels of expression, with a mean Cq of 19.9, compared to the adult alpha globin genes of *HBAA* and *HBAD* that had mean Cq values of 19.1 and 21.96 respectively. The beta globin genes potentially have more subtypes. Epsilon haemoglobin (HBE) is known to only be expressed in early embryonic development (Roninson and Ingram, 1982). Our RT-qPCR result showed relatively low expression levels of this subtype with a mean Cq of 26.8 compared to other beta globin genes *HBB*, *HBG1* and *HBG2* with mean values of 22.2, 18.1 and 18.7 respectively. The gamma haemoglobin genes *HBG1* and *HBG2* are known to be dominantly expressed throughout embryonic development (Chou et al., 2015, Roninson and Ingram, 1981), and as expected the results from this thesis showed these genes to be the predominant beta subunits. Beta

haemoglobin *HBB* is mainly expressed in the adult, but has been seen at low levels in the embryo (Choi and Engel, 1988). Our data shows that at HH29, *HBB* has already taken over from the embryonic HBE subtype. Our expression analysis revealed that both alpha subtypes are expressed at high levels, but the beta subunit *HBE* showed relatively weak expression. For this reason, the *HBE* gene did not undergo globin depletion treatment; however all other globin genes did. Following sequencing, FPKM levels close to zero were seen against all treated genes and the untreated *HBE* showed levels from 3000 - 300000 FPKM. This would suggest that HBE should have been treated as well, as although relative to the other globin genes its expression was very low, this is only in relative terms and the absolute expression level was still high. This demonstrates how highly expressed the globin genes are, as *HBE* was one of the most highly expressed genes in the data set and also shows large variation between samples. This reinforces the importance of removing excess globin mRNA, to allow consistent results to be obtained and to detect genes of low read depth.

Haemoglobin gene reduction

The levels of reduction we have attained are more than seen in previous models. Our treated samples showed expression levels around 0.00005 to that of before-treatment samples (around a 99.9999% reduction) across the six selected globin genes (near zero levels seen in sequencing result). This could be down to our optimising the oligo binding temperature. Previous studies just used the recommended Tm of their oligo's in the kit. Our custom oligo's had a Tm of 65 – 72°C. To ensure complete binding of all oligos we used a stepwise process from 95°C down to below all oligo Tm at 60°C. Following the final step at 60°C, samples were placed on ice. This would ensure complete unwinding of RNA secondary structures to allow oligo binding, with low re-formation of secondary structures to allow efficient action of RNase H in the subsequent step.

Globin depletion effect on RNA integrity and relative quantity

Few studies exist using next generation sequencing on tissue that required and subsequently was globin depleted. One study on human blood samples showed successful sequencing with increased sensitivity following globin depletion; however, the same study expressed concerns after finding RNA concentrations were reduced to around half that of non-treated samples (Shin et al., 2014). In array studies globin depletion treatment has been seen to cause slight decrease in general off target gene RNA and it has been surmised that this is down to a small degree of non-specific hybridization (Wu K, 2007, Choi et al., 2014). However, it could also be down to increased degradation of RNA by the process of the globin depletion (GD) treatment itself which requires heating and enzymatic degradation.

We have found a decrease in relative quantity of RNase H treated samples compared to non-RNase H added controls by RT-qPCR. Differences seen were around 1 Cqs (around a 2 fold or 1 $\log_2$ FC reduction); this is similar to previous next generation globin depleted studies (Shin et al., 2014). However, differences were constant across all samples and there was no change in expression values (delta delta Cq) between RNase H treated and non-treated controls. This is in line with a previous studiy that found there to be no reduction in gene detection levels following globin depletion treatment (Mastrokolias et al., 2012).

RNA integrity of globin depleted samples was tested in a preliminary study prior to sequencing. Initial results showed a drop in RIN number of 1.0 – 2.9, though RIN was still of an acceptable level of around 7 - 8. This reduction was more than seen in previously depleted samples used for next generation sequencing of 0.2 – 0.9 (Shin et al., 2014), and again, it was thought that this was down to our technique being more damaging. Sequencing studies with reductions in RIN of 0.5 – 1.5 have been seen (Mastrokolias et al., 2012). In these studies it was found that even in the samples with the lowest RIN, transcript reads were still greatly increased. The actual hearts we used for sequencing showed little to no decrease in RIN, with pre-treatment and globin depleted hearts showing a RIN of around 7. It could be that this improvement is down to a streamlining of the technique upon final sequencing when less time was spent in

the heated oligo hybridisation phase. This is now more in line with previous literature (Mastrokolias et al., 2012, Shin et al., 2014). Studies have shown that RNA RIN values of 6 – 9 show consistent expression by RT-qPCR and our RT-qPCR data correlates with this (Schroeder et al., 2006).

It was consistently observed in all previous published studies that there was a reduction in RNA yield following GD treatment, with one study showing as much as 78% total RNA being lost (Mastrokolias et al., 2012). Our RT-qPCR data also shows a reduction; however, the high integrity of the RNA ensures that the data we have acquired is reliable and consistent expression is seen for all genes. With good RNA integrity across all samples, we have shown for the first time a reduction of both embryonic and adult globin genes in the chick embryo. Previously globin depletion had neither been carried out in the embryo of any organism or in the chick at any stage.

The globlin depletion procedure carried out will facilitate the analysis s of low reads from mRNA sequencing as we have not only reduced excess transcripts that would reduce the number of reads throughout the transcriptome, but we have also maintained good RNA integrity and yield.

### 4.5.3 OFT-banding hearts sequencing - differential regulation and validation

Data analysis from sequencing can be carried out in differing ways and give differing results, so it was important to understand why these differences exist and what should be utilised and what should be avoided. Our sequencing analysis was carried out on fragments per kilobase per million (FPMK) values. This is the same algorithm as RPKM, but as our sequencing used paired end reads we use identified fragments rather than reads, as read values would not represent fragments if one of the paired reads were to fail. Before carrying FPKM analysis out, transcripts per million (TPM) values were also attained for comparison. The reason for this is that FPKM has been shown to give inconsistent comparison between samples (Wagner et al., 2012), and

said paper suggests using TPM as a more consistent measure. TPM normalises fragments to total transcripts and allows consistent comparison of gene expression proportions between hearts as each heart has the same number of total normalised reads. This could be particularly important if a gene is turned off in one heart, but is expressed in on other. Analysis of FPKM and TPM showed identical variation by principle component analysis (PCA), and gene non-corrected fold change values also showed no differences, therefore, FPKM values were used for the project. PCA allows heart gene expression to be represented by an individual point on a PCA plot and shows were variation lies between samples. When all hearts are plotted together it allows overall variation to be assessed between hearts. Before proceeding with DESeq analysis, the FPKM PCA plot was analysed to assess the overall data. It showed that all 3 OFT-banded and all 3 SHAM hearts had consistent expression within groups, and that groups showed overall variation between each other in PC2 and to a lesser extent PC1. This data proves that all 3 hearts in each group could be used in this study and FPKM values were subsequently analysed be DESeq.

To confirm our sequencing result, 14 genes were analysed by RT-qPCR. RT-qPCR is the most sensitive method of assessing gene expression (Bustin, 2000) and is the standard analysis method used to verify sequencing data (Griffith et al., 2010). Validation of sequencing and array studies is often performed in the literature, with Pearson product-moment correlation coefficients of >0.7 considered satisfactory for technical replication (Fang and Cui, 2011, Rockett and Hellmann, 2004, Allison et al., 2006). The 14 genes chosen for validation provided a good range of expression, from genes with maximum up and down regulation to genes that showed insignificant differences and no differences. Our RT-qPCR result backed up our sequencing with almost perfect repeatability ($r = 0.98$, $n = 14$, $p = <0.01$). This was vital for our study as only small fold changes were seen in our model with statistically significant genes analysed having $\log_2$ fold changes ranging from 0.5 – 2.5 (discussed below). All genes of interest highlighted by sequencing were RT-qPCRed, and their significance confirmed. Generally, RT-qPCR $\log_2$ FC was very slightly higher than sequencing $\log_2$ FC, as shown in Figure 5.12 (B), with line value m = 0.95 (RT-qPCR on x axis). This would be expected due to RT-qPCRs increased sensitivity (Bustin, 2000).

By performing RT-qPCR technical verification with non-globin depleted and non-fragmented first strand cDNA from the same RNA used for sequencing, we also answer important questions about the whole sequencing process, form library preparation, to accuracy of post sequencing analysis software. Our near perfect repeatability in 14 genes confirms that globin depletion has no effect on relative expression. Another important factor on our sequencing result is post sequencing analysis software used. Analysis software is constantly being updated, and what is considered the gold standard one year is out of date the next. Our sequencing analyses used Tophat for genome mapping to galGal4 for transcript assembly and DESeq to determine differential regulation. DESeq was shown to give good sensitivity and specificity in 2014 (Love et al., 2014), but a more recent paper showed DESeq to be, though very specific, very conservative in its sensitivity and gave many false negatives when compared to Edge R and RT-qPCR (Rajkumar et al., 2015). Another paper assessing differential regulation software also found DESeq to be very accurate in terms of false positives, with genes considered differentially regulated having adjusted *p* value threshold of <0.05 (Soneson and Delorenzi, 2013). However, in order to attain this, both experimental and control groups must have at least n=3, as our study did (Soneson and Delorenzi, 2013). A general review of all current software showed that true positive rate could fall to <40% when n=<3 if fold change is <2 ((Nicholas J. Schurch, 2015). This finding is of particular importance to us because many our significant differentially regulated genes have a FC <2, and again demonstrates the importance of our RT-qPCR technical variation (Nicholas J. Schurch, 2015). The inconsistency in the literature, in terms of what is the best differential expression software, also necessitates using another expression and analysis method, such as RT-qPCR, using the same RNA for technical verification. Because of potential false negatives, genes with *p*-values just outside the significance threshold (adjusted $p<0.05$) were included for RT-qPCR verification. Our very close correlation ($r = 0.98$, $n = 14$, $p = <0.01$) with a near direct relationship ($m = 0.95$) shows that our sequencing methods of analysis for fold change are acceptable. Individual gene regulation significance ($p=<0.05$) of sequencing is reflected by RT-qPCR. Interestingly, of the two genes used with near significant sequencing adjusted *p*-values of 0.06, one gene was found to be significant by RT-qPCR (*PRKAG3*), however the

other gene, (*HDAC7*) was still found to be insignificant. This data shows that our differentially significant genes identified by sequencing can be trusted, but also shows that some false negatives exist in the data in genes of near significance. With these genes, RT-qPCR is needed to confirm the significance of their differential regulation. RT-qPCR verification was carried out on an n of three for each group (OFT-banded and SHAM) as this repeated the number used for sequencing. However Analysis of our experimental standard deviation and difference in effect between OFT-banded and SHAM controls suggests that an n of at least 6 should be used (equation bases on power calculation as used in Kadam & Bhalerao paper) (Kadam and Bhalerao, 2010). With hindsight, RT-qPCR verification analysis on genes initially shown to be just outside of significance should have been carried out on an n=6 in RT-qPCR analysis, and it's possible that false negative results were given.

RT-qPCR results at HH35 allow greater interpretation of our gene regulation. HH35 harvesting, RNA preparation and first strand cDNA synthesis were carried out in an identical way to hearts at HH29. A direct significant relationship is seen between HH29 and HH35 with differential $\log_2$ FC seen at HH29 also seen at HH35 ($r = 0.85$, $n= 11$, $p = <0.01$). This shows that genes differentially regulated at HH29 are still showing differential regulation at later stages of development. A small number of genes show increased or decreased regulation at this later stage, these genes are discussed further in chapter 6.

Reactivation of the fetal gene program is one of the common features of the haemodynamically stressed heart during cardiac hypertrophy in the adult, and is thought to be a cardio-protective mechanism for the heart (Taegtmeyer et al., 2010, Ames et al., 2013). The hallmarks of the fetal gene program include upregulation of the atrial natriuretic peptide (NPPA), NPPB (Izumo et al., 1988), β-myosin heavy chain (Izumo et al., 1988, Mahdavi et al., 1984), skeletal α-actin (Schwartz et al., 1986), and phospholamban (PLN) (Song et al., 2012). Though no significant differential expression was found on these genes, our FPKM values did show increased values in three of the genes, NPPB, ACTA1 and PLN in two of the OFT-banded hearts (Table 5.6. in Section 5.2.4.1). Analysis on NPPA wasn't performed as NPPA doesn't exist in

chick. Genes found significantly regulated displayed metabolic and conduction system cardio-protective properties. These are discussed at length in Chapter 5.

We have shown the genetic viability of the OFT-banded model and produced mRNA, with excess haemoglobin transcripts removed, of good integrity and yield. This allowed mRNA sequencing to take place where small gene reads could be identified. The analysis used showed the results where genuine and reproducible, though with the possibility that some false negatives exist. We have produced a platform for the analysis of gene expression from tissue samples allowing the study of low reads with consistency across samples. Using directional sequencing we have gained information on both sense and antisense transcription. It is here where there could be improvements in the future. The standard NEB directional library preparation kit utilises Poly-A selection, as does our globin depletion treatment. This means that antisense products that are not poly-A-tailed, such as functionally important products that do not leave the nucleus and effect transcription are not sequenced. It has been found that over 24% of long non-coding RNA transcripts lack a poly A tail in the human (Cheng et al., 2005, Cui et al., 2010), and a study using HeLa cells showed that 6 million size selected, rRNA depleted, reads were obtained from the flow through of poly-A selection during a sequencing process (Yang et al., 2011). To fully utilise directional sequencing, library preparation without the poly-A-selection step would be preferable if it could be optimised to show sequencing reliability on par with the dUTP method. This is something that could be possible in the future. Recent research has shown that mRNA sequencing using ribo-zero (hybridisation style removal) demonstrates effective coverage uniformity, genome-based mapped reads, and consistently high quality quantification of transcripts (Zhao et al., 2014). Likewise, globin depletion kits utilising PNA hybridisation removal are available. As well as not needing poly-A-selection, these kits also have higher RNA yields due to no RNase treatment (Shin et al., 2014, Choi et al., 2014, Mastrokolias et al., 2012). If a system could be optimised to effectively use non-RNase based globin depletion and with rRNA removal not requiring poly-A-selection, then it would have the advantage of not only having less RNA degradation, but also being able to obtain all transcribed information.

# Chapter 5 Differential gene expression in OFT-banded hearts

## 5.1 Introduction

The last chapter confirmed that our OFT-banded model, that gives an anatomical phenotype resembling that of dilated cardiomyopathy, is not failing at HH29 or HH35. mRNA sequencing results were then gained and confirmed by RT-qPCR in technical and biological repeats. As mentioned in the main introduction, cardiomyopathy can often be misdiagnosed or be idiopathic. This is because the genetic causes of cardiomyopathy are still not fully understood. The main aim of this chapter is to elucidate reasons for the differential gene expression found during sequencing and/or RT-qPCR at HH29 and HH35 by looking for genes involved in mechanisms linked or potentially linked to dilated cardiomyopathy (see introduction section 1.5.3 for full description of the genetic bases of cardiomyopathies). Genes will be looked for that may be involved in the maladaptive cardiac remodeling response that may lead cardiomyopathy. These genes may initially be expressed to have a cardioprotective role in response to OFT-banding and this response will be elucidated by looking at the function of the corresponding protein, protein interactions and what effect up or down regulation at HH29 or HH35 would be expected to have. Specific attention will be paid to the genes involved in the conduction system, but metabolism, structure and differentiation will also to looked at. As identified in the previous chapter, we have down regulation of *PRKAG3* (gene coding the regulatory region of AMPK). This is a good example of a gene that could influence multiple processes, as AMPK can phosphorylate transcription factors such as p300, transcriptional repressors such as HDACs (Zhang et al., 2011b). Though the initial purpose of this project was to look at the conduction system and how structure may affect it, the combined effect of one gene on multiple molecular pathways made it necessary to look deeper into molecular regulation. This is vital as Familial dilated cardiomyopathy (DCM) causes a multitude of phenotypes. When compared to hypertrophic cardiomyopathy, DCM has a wider variety of mutations, both sarcomeric and non sarcomeric (Li and Hwang, 2015).

Knowledge genes identified could possibly aid the future treatment of dilated cardiomyopathy

Though molecular aspects have been looked at in the atria of previous OFT-banded models, our model of OFT-banding at HH20, when the primitive SAN is still located in the left side of the developing atrium, and harvesting at HH29, when the SAN has just located in the left atrium, but the conduction pattern is still maturing, should allow analysis of genes involved in the maturation process of the conduction system in whole hearts for the first time. OFT-banding has been seen to give rise to precocious development of mature apex to base conduction in the chick heart with mature patterns seen starting from HH29 in banded hearts compared to HH31 in controls (Reckova et al., 2003).

The choice of molecular pathway analysed is based on a number of factors. That is, how the heart develops and at what stage certain genes appear, particularly those of the conduction system, structural and force generating proteins, the metabolism behind these pathways, and also genes known to be involved in stress response. In the developing embryo, heart growth takes place by the proliferation of the cardiac myocytes (Olson and Schneider, 2003). Growth in the adult heart can occur in response to physiological and pathological stimuli presenting as cardiac hypertrophy, which is a major component of many cardiac diseases (Olson and Schneider, 2003, Park et al., 2011). Stress on the heart caused by conditions inducing pressure overload (altered haemodynamics) or extreme metabolic irregularities, have been seen to cause cardiac hypertrophy as an adaptive response to maintain cardiac output (Park et al., 2011, Kim et al., 2014). However, sustained stress can lead to maladaptive remodelling that progress to dilated cardiomyopathy (DCM) and heart failure (Park et al., 2011, Kim et al., 2014). Gene regulation during stress from induced pressure overload or in patients with cardiomyopathy has previously been studied in the adult heart (Song et al., 2012, Park et al., 2011). However, the effect of altered haemodynamics on global gene expression in the embryo at a developmental stage when cardiomyocytes and conduction cells are still undergoing proliferation has not been studied in the whole heart. When children present with cardiomyopathy, it is likely that the cause is an inherited genetic fault (Cirino and Ho, 2013); however, whether

the cause is associated with metabolic, structural or conduction based genes is rarely known (Eriksson et al., 2015, Evans et al., 2000, Choi et al., 2009).

OFT-banding is a model that has been used to induce pressure-overloaded/altered haemodynamics in the embryo and has been shown to give features of cardiomyopathy (Midgett and Rugonyi, 2014, Sedmera et al., 1999). Though measurement of the blood pressure was not performed on our OFT-banded model, as already detailed in the introduction, it has previously been published that OFT-banding produces a significant rise in blood pressure in the ventricles with no change in heart rate (Clark et al., 1989, Chivukula et al., 2016).

## 5.2 Specific Aims:

- To identify genes differentially regulated that implicate particular molecular pathways in the OFT-banded model, with particular reference to the conduction system

- To elucidate the functional relevance of these genes, be it responsive cardioprotective genes, or genes that may be causative of our anatomical phenotype or cardiac disorders

- Elucidate differentially regulated gene profile effect on the conduction system and how structure may be linked

- Assess the effect of OFT-banding on structure and functional characteristics
    - Fibrosis
    - Apoptosis

## 5.3 Results

### 5.3.1 Genomic contamination check on HH29 and HH35 atrial and ventricular samples used to establish pattern of expression

After sequencing identified differential gene regulation, additional OFT-banded hearts were used to generate cDNA at HH29 and HH35 in separate atrial and ventricular samples. This was to gain information on the location of expression within the heart across the two stages. RNA preparation to enable cDNA synthesis had concentrations of 800 – 1200 ng/µl, and 260/290 nm ratios from 190 – 215. End point PCR was performed on all cDNA synthesis reactions against Glyceraldehyde 3-phosphate dehydrogenase (*GAPDH*) in order to check for genomic contamination. The primer set for *GAPDH* (set 1) was designed to contain an intron of 200 bp. The cDNA samples synthesized and tested were HH29 and HH25 atria and ventricle. Each sample represented X3 pooled atria or ventricular samples. The PCR was run over 40 cycles to ensure that low copy numbers of genomic DNA could give a band, and also to replicate the conditions of the RT-qPCR reaction that this cDNA was intended for. Upon gel electrophoresis, the expected 180 bp band was seen in the RT positive samples but with no noticeable bands in the non-reverse transcriptase controls (-) were seen (Figure 5.1); this shows genomic contamination in all samples was minimal. Samples were poled n=3.

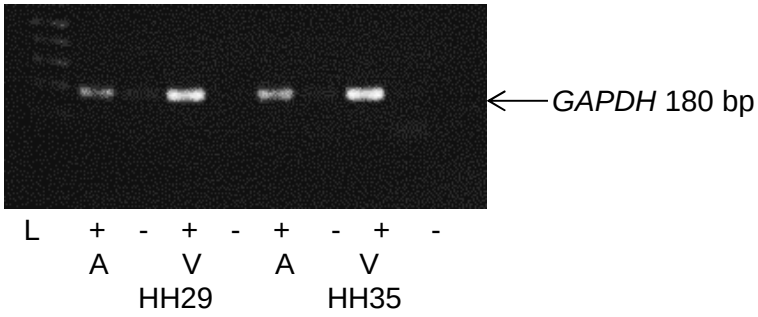



**Figure 5.1** Contamination check on HH29 and HH35 hearts atrial and ventricular samples. End point PCR was performed using *GAPDH* gene-specific primers (40 cycles) on HH29 and HH35 atrial (A) and ventricular (V) samples s. A cDNA band of 180 bp was seen; a b and of 380 bp would indicate gDNA (primers span 200 bp intron). L, 1 Kb plus ladder; +, reverse transcriptase positive; -, reverse transcriptase negative, n=3 (pooled).

### 5.3.2 Conduction gene expression analysis in atria and ventricles at HH29 and HH35 by end-point PCR

As the initial aim of my work was to concentrate on conduction in the heart, end point PCR expression profiling was carried out on separate atrial and ventricular hearts (pooled n=3). Conduction genes highlighted from sequencing of OFT-banded HH29 whole hearts (ENS-1, ERN1, PVALB, S100A11, TBX3 and DNAJC6). cDNA was generated from pooled atrial and ventricular (n=3 per group) regions at HH29 and HH35. The PCR was performed at 30 cycles in an attempt to see if expression level before endpoint could be estimated between samples. Expression in the atrial and ventricular regions for all genes was seen, and so genes will now be RT-qPCRed at HH35 using whole hearts OFT-banded and SHAM. Additionally, there appeared to be a possible reduction in expression in the atria at HH35 for ENS-1 and possibly also for ERNI (n=2 gels). To test this, these highlighted genes were carried forward to RT-qPCR analysis on the separated atrial ventricular samples (Figure 5.2).

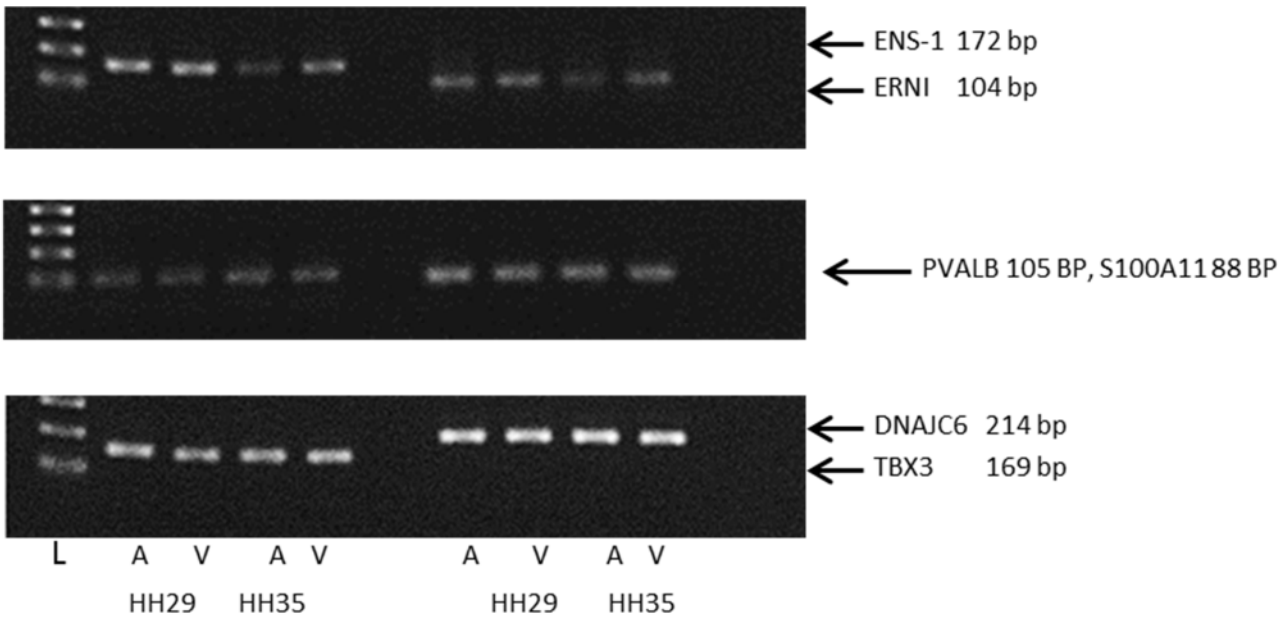



**Figure 5.2** Expression profile of conduction genes to show what region of the heart conduction genes are expressed at HH29 and HH35. End point PCR was performed using ENS-1, ERNI, PVALB, S100A11, DNAJC6 and TBX3 gene-specific primers (30 cycles) on HH29 and HH35 atria (A) and ventricle (V). Expression was seen in all samples. L, 1 Kb plus ladder, n=3 (pooled)

### 5.3.3 Expression of ERNI and ENS-1 in the atria and ventricle at HH29 and HH35 by RT-qPCR

Following the end point PCR results that suggested a possible reduction for ENS-1 in the atria at HH35 (see section 5.2.2), the two genes where assessed for expression by RT-qPCR using the same cDNA as used for the end point PCR. Delta Delta Cq values revealed a down regulation in the atria between HH29 and HH35 for ENS-1 and to a lesser extent in ENRI. ENS-1 normalised expression shows a 0.56 down regulation (S.E. 0.009); this represents a 44% reduction in expression in the atria between HH29 and HH35 (Figure 5.3). ERNI normalised expression shows a 0.61

down regulation (S.E 0.15) (Figure 5.3). This represents a 39% reduction; however, error bars show more variation than for ENS-1. No differences were found in the ventricle in either sample. Statistics were not carried out as only one cDNA sample of three pooled atria and ventricles per group was used (n= 3 pooled). However, the normalised data show a 44% difference and error bars do not overlap, this shows expression is reduced in the atria between HH29 and HH35 in the 3 pooled hearts used at HH29 and HH35 (Figure 5.3).

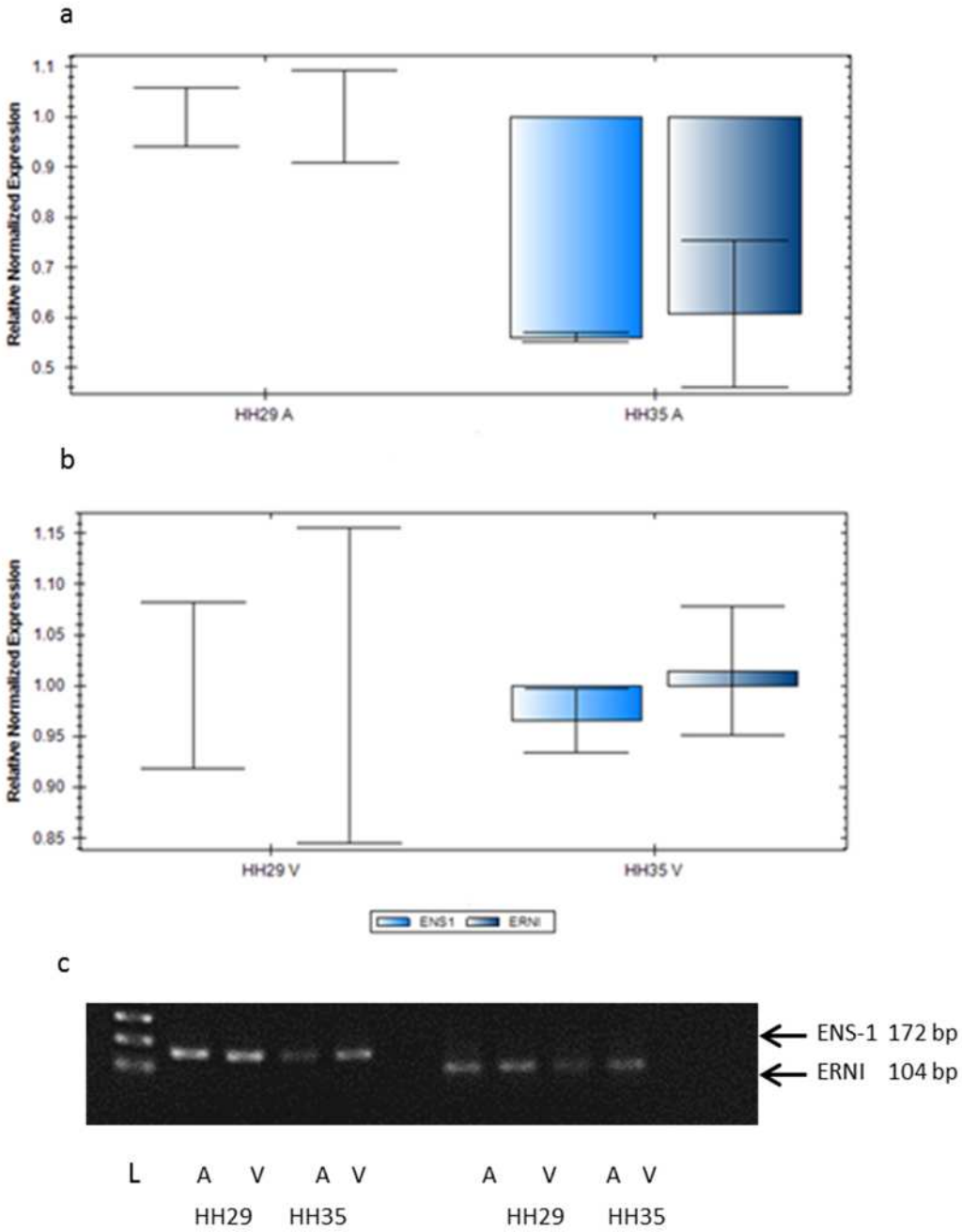



**Figure 5.3** Expression of ENS-1 and ENRI in the atria compared to the ventricle at HH29 and HH35. $Log_2$ FC of ENS-1 and ERNI at HH29 and HH35 shown, where HH35 hearts were normalised to HH29 hearts in the atrial and ventricular samples. **a**, atria (A) and **b**, ventricle (V). A reduction in expression is seen in the atria for ENS-1 and to a lesser extent ERNI, but no differences are seen in the ventricular samples. **c**, Original end point PCR using the same cDNA. n= 3 (pooled) for all samples for both RT-qPCR and endpoint PCR.

### 5.3.4 Normality and variance analysis of RT-qPCR data at HH35 differentially regulated genes

It was clear from observation of Delta Cq and standard deviation values (Table 5.2) that there was greater variation both within groups and between groups at HH35 than at HH29, possibly because small changes at HH29 may be exacerbated at HH35. To test that the data was parametric the Shapiro-wilk test was performed. The gene that showed the greatest variation was PVALB, so this gene is show in results. All data was shown to be normally distributed so parametric tests were used (Table 5.1 and Figure 5.4 for PVALB) Secondly, the spread of variation between samples was tested between OFT-banded and SHAM by performing an F-test on variance. This showed all samples can be used with assumed equal variance, with the exception PVALB. PVALB in OFT-banded hearts showed the greatest variation within and between OFT-banded and SHAM samples than any other gene (Table 5.2). The F-Test recommended unequal variances paired T-test to be used, so P-value shown for this gene at HH35 are based on this. However, even this gene passed the Laverne's test, suggesting that equal variances could be used on all (Table 5.3). Within sample variation is shown with 95% confidence interval. This showed that the upper and lower values of OFT and SHAM did not overlap and P-values can be trusted.

**Table 5.1** Normal distribution of PVALB on HH35 hearts using Shapiro-wilk test.

| Heart | Shapiro-Wilk | | |
|---|---|---|---|
| | Statistic | df | Sig. |
| OFT | 0.992 | 3 | 0.824 |
| SHAM | 0.957 | 3 | 0.600 |

df, degrees of freedom

Sig. , p-value

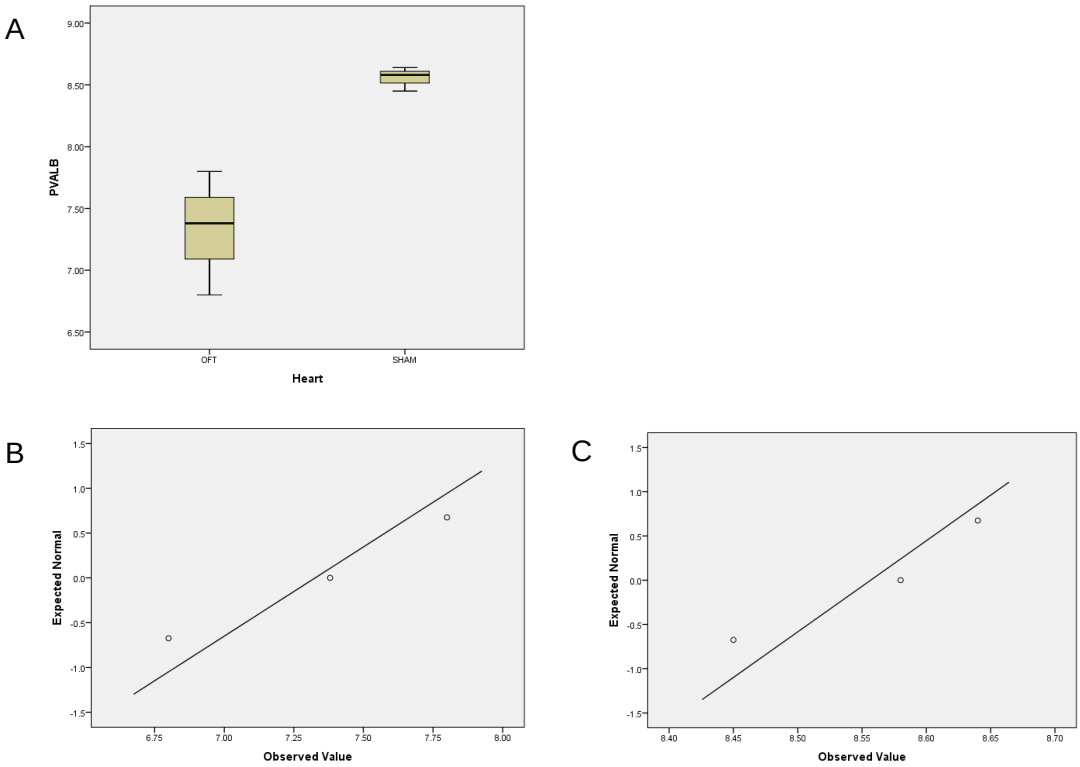



**Figure 5.4** Spread of data shows that PVALB is normally distributed and parametric tests can be performed. A, OFT-banded and SHAM box and whisker distribution. B, OFT to expected distribution. C, SHAM to expected distribution.

**Table 5.2** RT-qPCR data at HH35 for PVALB OFT-banded against SHAM control hearts.

| **Heart and statistical tests** | **PVALB Delta Cq** | |
|---|---|---|
| | **OFT** | **SHAM** |
| Heart 1 | 7.38 | 8.64 |
| Heart 2 | 6.80 | 8.58 |
| Heart 3 | 7.80 | 8.45 |
| **Mean** | **7.33** | **8.56** |
| **SD** | 0.502 | 0.095 |
| DeltaDetaCq | 1.23 | |
| **FC** | **2.24 (1.16 $\log_2$)** | |
| **P-value** ( unequal variance T-Test) | **0.047** | |
| SE | 0.29 | 0.05 |
| Variance | 0.25 | 0.01 |
| f-stat | 27.94 | |
| Sample size | 3 | 3 |
| Confidence coefficient | 1.96 | 1.96 |
| Margin of error (95% confidence internal) | 0.57 | 0.11 |
| Upper bound | **7.89** | **8.66** |

| | | |
|---|---|---|
| Lower bound | **6.76** | **8.45** |

OFT, OFT-banded; SD, standard deviation ; DDCq, Delta delta Cycle quantification ; FC, fold change ; SE, standard error ; F-stat .F distribution statistic for equality of variances

**Table 5.3** T-test result showing significant differences for RT-qPCR PVALB OFT-banded hearts delta Cq in comparison to SHAM controls at HH35.

| **PVALB** | Levene's Test for Equality of Variances | | t-test for Equality of Means | | | | | | |
|---|---|---|---|---|---|---|---|---|---|
| | F | Sig. | t | df | **Sig. (2-tailed)** | Mean Difference | Std. Error Difference | 95% Confidence Interval of the Difference | |
| | | | | | | | | Lower | Upper |
| Equal variances assumed | 3.406 | 0.139 | -4.166 | 4 | 0.014 | -1.23000 | 0.29528 | -2.04982 | -0.41018 |
| Equal variances not assumed | | | -4.166 | 2.15 | 0.047 | -1.23000 | 0.29528 | -2.41947 | -0.04053 |

F, critical figure; Sig, Significance; t, critical figure

### 5.3.5 A comparison of the differential expression at HH29 and HH35 in OFT-banded hearts by RT-qPCR.

A positive correlation of expression between RNA sequencing data and RT-qPCR of all genes analysed has been shown in Chapter 4. In this section, specific genes will be analysed, by RT-qPCR. All results of genes of interest are shown in Table 5.4. and are separated on gene function into conduction, and metabolic, structural and

differentiation. However, as deliberated in the discussion later, there is some cross over and relationships between genes.

Differential expression of metabolic and structural genes at HH29

From the top 30 significantly differentially expressed genes shown in Chapter 4 (see Table 4.7,8), genes were selected for analysis as being related to structure, metabolism of differentiation. These genes were: *PRKAG3, LDHB, HDAC7, MYL1, TNNC2, ENS-1,* and *ERNI* and all showed significant differential regulation by RT-qPCR (Figure 5.6 a) with the exception of HDAC7 and MYL1. Metabolic genes *PRKAG3* and *LDHB* showed mean differential regulation of -0.55 $log_2$ FC (SEM 0.05) and 0.62 $log_2$ FC (SEM 0.24) respectively. Structural genes *MYL1* and *TNNC2* were upregulated to similar levels, both showing a mean differential expression of 0.65 $log_2$ FC (SEM 0.12 and 0.19 respectively). *HDAC7*, a repressor of structural proteins is down regulated with a -0.51 $log_2$ FC (SEM 0.04). *ENS-1* and *ERNI* are involved in embryonic differentiation; both display similar levels of down regulation, with *ENS-1* showing a -1.35 $log_2$ FC (SEM 0.02) and *ENRI* showing a -1.08 $log_2$ FC (SEM 0.04).

Expression of conduction genes at HH29

From the top 30 significantly differentially expressed genes shown in Chapter 5 (see Table 5.6), genes were selected that had established conduction links within the literature. These genes were: *PVALB, S100A11* and *DNAJC6*, and all showed significant differential regulation by RT-qPCR (Figure 6.7a). $Ca^{+2}$ sequestering genes *PVALB* and *S100A11* both show up regulations of 0.81 (SEM 0.17) and 0.67 (SEM 0.07) $log_2$ FC respectively. Chaperone protein coding gene *DNAJC6*, linked with congenital heart block, displayed a down regulation with a -0.75 $log_2$ FC (SEM 0.03). Conduction lineage transcription factor gene *TBX3* was also included for further analysis as, though insignificant by sequencing, it showed consistently increased

FPKM values across all OFT-banded hearts (10.31, 9.06 and 8.25 FPKM) compared to SHAM (5.64, 7.27 and 7.56 FPKM) with a corrected $log_2$ FC of 0.4 (SEM 0.2). Quantitative-PCR of TBX3 again showed similar insignificant up regulation with a 0.38 $log_2$ FC (SEM 0.05).

Expression of non-conduction genes at HH29 compared to hearts HH35

Differential expression values at HH35 showed some changes to the original HH29 data (Figure 6.6 b). *PRKAG3* had a 54% increase in down regulation, from -0.55 to -1.18 mean $log_2$ FC from HH29 to HH35. *LDHB* showed a reduced differential upregulation from significant 0.62 to insignificant 0.13 mean $log^2$ FC. *MYL1* displayed a 54% increase in significant differential up regulation from 0.65 (at HH29) to 1.41 mean $log_2$ FC (at HH35). The structural gene *TNNC2* and structural regulator *HDAC7* showed no differences to HH29. *ENS-1* showed a decrease in differential down regulation of 54% from significant -1.35 to insignificant -0.47 mean $log_2$ FC; however *ERNI* displayed no differences. A direct comparison of the expression for all genes in HH29 and HH35 hearts is shown in Figure 5.8a – and Table 5.4).

Differential expression of conduction genes at HH35 compared to HH29 hearts

Conduction genes showed increases in differential expression for *PVALB* and *S100A11* (Figure 6.8 b for all genes). *PVALB* showed a 30% increase in significant differential up regulation from 0.81 to 1.16 $log_2$ FC. S100A11 gave a 37% increase in significant differential up regulation from 0.67 to 1.07 $log_2$ FC. In contrast, *DNAJC6* showed a decrease of 45% differential down regulation from -0.75 (significant) to -0.41 $log_2$ FC (insignificant). *TBX3* displayed a decrease of 66% to the insignificant up regulation at HH29, going from 0.38 to 0.13 $log_2$ FC. A direct comparison of the HH29 and HH35 RT-qPCR for all genes is shown in Fig 5.8b.

**Table 5.4** Fold change by RT-qPCR at HH29 and HH35 on genes of interest

| | Gene | HH29 | | | | HH35 | | | |
|---|---|---|---|---|---|---|---|---|---|
| | | **Mean fold change** | **Mean $Log_2$ Fold change** | **SEM** | ***p*-value** | **Mean fold change** | **Mean $Log_2$ Fold change** | **SEM** | ***p*-value** |
| **Genes involved in metabolism, structure and differentiation** | PRKAG3 | 0.68 | -0.55 | 0.05 | <0.05 | 0.44 | -1.18 | 0.04 | <0.05 |
| | LDHB | 1.54 | 0.62 | 0.24 | <0.05 | 1.10 | 0.13 | 0.06 | 0.62 |
| | HDAC7 | 0.7 | -0.51 | 0.04 | 0.12 | 0.75 | -0.410 | 0.04 | 0.27 |
| | MYL1 | 1.57 | 0.65 | 0.12 | 0.13 | 2.66 | 1.41 | 0.20 | <0.05 |
| | TNNC2 | 1.60 | 0.65 | 0.19 | <0.05 | 1.54 | 0.62 | 0.16 | 0.32 |
| | ENS-1 | 0.39 | -1.35 | 0.02 | <0.05 | 0.72 | -0.47 | 0.16 | 0.61 |
| | ERNI | 0.47 | -1.08 | 0.04 | <0.05 | 0.45 | -1.15 | 0.1 | 0.20 |
| **Genes directly involved in conduction** | PVALB | 1.76 | 0.81 | 0.17 | <0.05 | 2.24 | 1.16 | 0.37 | <0.05 |
| | S100A11 | 1.60 | 0.67 | 0.07 | <0.05 | 2.11 | 1.07 | 0.17 | <0.05 |
| | DNAJC6 | 0.59 | -0.75 | 0.03 | <0.05 | 0.75 | -0.41 | 0.08 | 0.17 |
| | TBX3 | 1.30 | 0.38 | 0.05 | 0.20 | 1.10 | 0.13 | 0.08 | 0.2 |

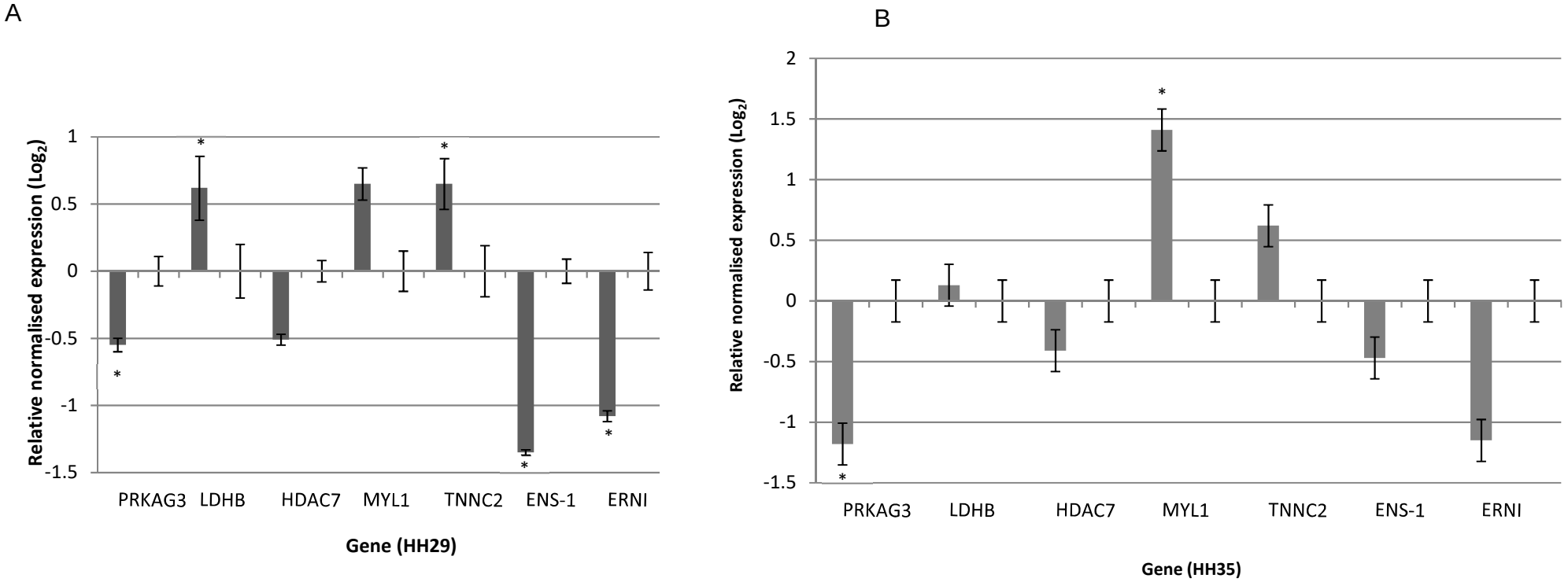



**Figure 5.5** Metabolic, structural, and differentiation gene expression in OFT-banded hearts compared to SHAM controls. **A** , HH29; **B**, HH35; *, $p<.05$. n = 3.

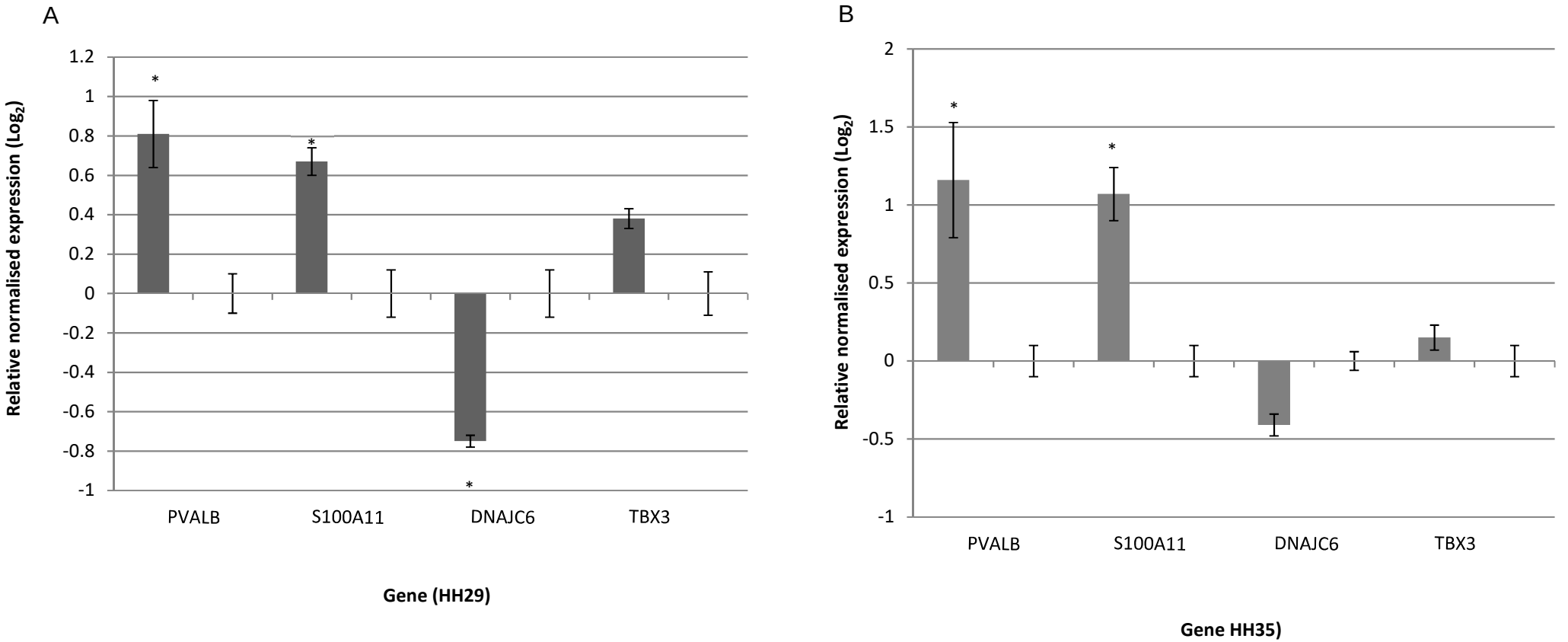



**Figure 5.6** Gene expression of conduction in OFT-banded hearts compared to sham controls. **A**, HH29; **B**, HH35; *, $p<.05$, n=3

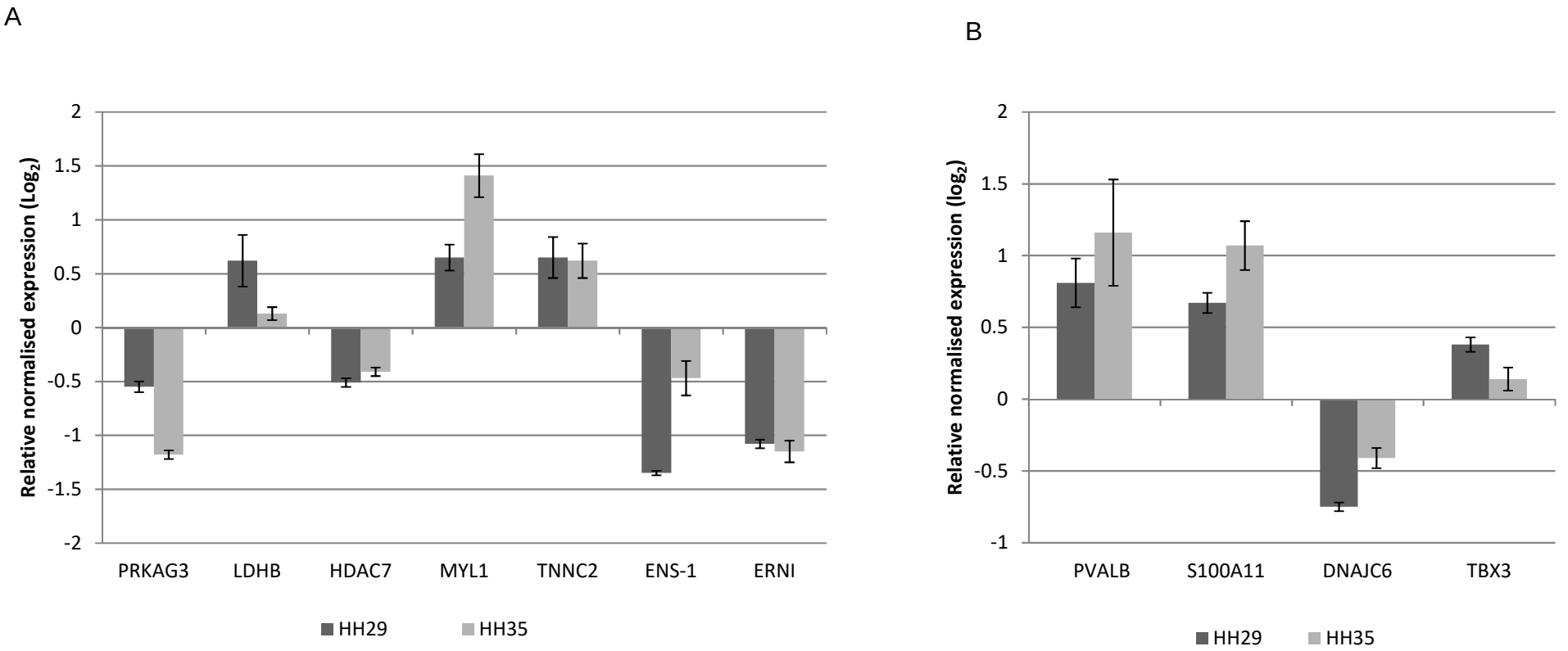



**Figure 5.7** A direct comparison of the expression of genes of interest in HH29 and HH35 OFT-banded and SHA M control hearts. **A**, Metabolic, structural and differentiation genes; **B**, Conduction genes. n=3

### 5.3.6 Gene transcript variants identified in OFT-banded hearts

As described in detail in the methods chapter, transcripts were sequenced from both ends. This allowed variation in gene transcript expression to be analysed. This analysis took place late in the project well after the initial study of differential gene expression had taken place. Table 6.5 lists statistically significant transcripts identified in OFT-banded hearts. Gene transcript variants were analysed following the initial differential gene regulation analysis. This was to see if OFT-banding would lead to any particular transcript differentiation and this data together with the initial gene regulation data will be used to help identify particular pathways that may be affected in our model. Our analysis of sequencing gene differentiation allowed genes to be identified that were linked to particular mechanisms/pathways. For example, a key finding appears to be in metabolism where a gene important in glycogen metabolism, PRGAG3 that encodes the regulatory region for AMPK, shows differential regulation. Using STRING functional protein association networks software, all significant (<0.05) differentially regulated gene transcripts (table 5.5) and genes already highlighted (table 4.7 and 4.8 in chapter 4) where analysed. The STRING diagram (figure 6.16) shows one added gene, PRKAA2, which is added to the diagram to show the relationship of AMPKs active site with its regulator *PRKAG3*, but this gene was not identified by sequencing and thus this gene was not included in the statistical analysis or the pathway table (table 5.6). Statistical analysis showed edges (possible relationships) were significantly different to expected normal values ($p$ = 0.00119) using medium confidence (figure 5.9).

**Table 5.5** Statistically significant transcripts identified in OFT-banded hearts.

| GeneName | Corrected $log_2$ fold change | lfcSE | *p*-value | Corrected *p* -value |
|---|---|---|---|---|
| *DNPEP* | 11.00 | 1.42 | 9.16E-15 | 7.82E-11 |
| *BUD31* | 10.92 | 1.45 | 5.75E-14 | 1.74E-10 |
| *HDAC8* | -10.77 | 1.43 | 6.13E-14 | 1.74E-10 |
| *TIMM23* | -9.61 | 1.51 | 1.91E-10 | 3.68E-07 |
| *PTPMT1* | 9.57 | 1.51 | 2.15E-10 | 3.68E-07 |
| *SNX21* | -9.39 | 1.51 | 5.04E-10 | 7.18E-07 |
| *EHD3* | -9.60 | 1.56 | 7.42E-10 | 9.05E-07 |
| *IPO9* | -2.48 | 0.43 | 8.60E-09 | 9.18E-06 |
| *WDR91* | -8.83 | 1.55 | 1.28E-08 | 1.22E-05 |
| *HGS* | -8.61 | 1.55 | 3.10E-08 | 2.64E-05 |
| *COPS7B* | 8.59 | 1.56 | 3.52E-08 | 2.74E-05 |
| *RABIF* | 8.59 | 1.58 | 5.46E-08 | 3.88E-05 |
| *DNAJC1* | 8.46 | 1.58 | 8.91E-08 | 5.50E-05 |
| *C22ORF39* | -8.40 | 1.57 | 9.02E-08 | 5.50E-05 |
| *PDRG1* | -1.43 | 0.27 | 1.40E-07 | 7.98E-05 |
| *RP11-529K1.3* | 1.75 | 0.34 | 1.96E-07 | 1.04E-04 |
| *ATP6V0E2* | 8.13 | 1.59 | 3.15E-07 | 1.50E-04 |
| *SPEG* | 8.14 | 1.59 | 3.05E-07 | 1.50E-04 |
| *ENSGALG00000026654* | 8.16 | 1.61 | 3.85E-07 | 1.73E-04 |
| *SLC29A1* | -8.36 | 1.65 | 4.07E-07 | 1.74E-04 |
| *GTF2F2* | 7.95 | 1.60 | 7.24E-07 | 2.94E-04 |
| *RNF34* | -7.96 | 1.64 | 1.27E-06 | 4.92E-04 |
| *MAFB* | 7.75 | 1.62 | 1.66E-06 | 6.17E-04 |
| *TOP1MT* | -7.95 | 1.67 | 1.80E-06 | 6.40E-04 |
| *SENP6* | -7.87 | 1.65 | 1.93E-06 | 6.59E-04 |
| *TNFRSF21* | 1.76 | 0.38 | 3.41E-06 | 1.12E-03 |
| *AGA* | 7.67 | 1.66 | 3.80E-06 | 1.20E-03 |
| *PPME1* | -7.73 | 1.68 | 4.18E-06 | 1.28E-03 |
| *UBE2L6* | 7.48 | 1.64 | 5.19E-06 | 1.53E-03 |
| *KLHDC1* | -7.46 | 1.64 | 5.50E-06 | 1.57E-03 |
| *CAP1* | -0.88 | 0.20 | 6.50E-06 | 1.73E-03 |
| *CYP51A1* | -7.60 | 1.68 | 6.53E-06 | 1.73E-03 |
| *UBR5* | -7.41 | 1.65 | 6.70E-06 | 1.73E-03 |
| *TLE4* | 4.64 | 1.03 | 7.35E-06 | 1.85E-03 |
| *FAIM* | 7.42 | 1.66 | 7.68E-06 | 1.87E-03 |
| *KPNA1* | 7.31 | 1.68 | 1.33E-05 | 3.15E-03 |

| | | | | |
|---|---|---|---|---|
| *LDHB* | 0.62 | 0.15 | 2.61E-05 | 6.02E-03 |
| *SFSWAP* | 7.02 | 1.68 | 2.91E-05 | 6.55E-03 |
| *ADGRG1* | -1.40 | 0.34 | 3.52E-05 | 7.72E-03 |
| *IPO13* | 6.88 | 1.70 | 5.09E-05 | 1.09E-02 |
| *PYGO1* | 6.87 | 1.71 | 6.06E-05 | 1.26E-02 |
| *TTC32* | 1.55 | 0.39 | 6.36E-05 | 1.29E-02 |
| *TULP3* | 6.89 | 1.76 | 9.07E-05 | 1.80E-02 |
| *TCEANC* | -6.65 | 1.71 | 1.02E-04 | 1.98E-02 |
| *TM9SF2* | -0.80 | 0.21 | 1.26E-04 | 2.39E-02 |
| *PPP1R21* | 6.66 | 1.75 | 1.44E-04 | 2.67E-02 |
| *ENKD1* | 6.73 | 1.78 | 1.57E-04 | 2.86E-02 |
| *RECQL5* | 6.47 | 1.73 | 1.77E-04 | 3.11E-02 |
| *SSFA2* | 4.42 | 1.18 | 1.78E-04 | 3.11E-02 |
| *FGFRL1* | -6.41 | 1.73 | 2.17E-04 | 3.71E-02 |
| *ENSGALG00000014375* | -6.47 | 1.76 | 2.28E-04 | 3.75E-02 |
| *GPX1* | -0.31 | 0.08 | 2.28E-04 | 3.75E-02 |
| *DGKG* | 4.12 | 1.13 | 2.80E-04 | 4.51E-02 |

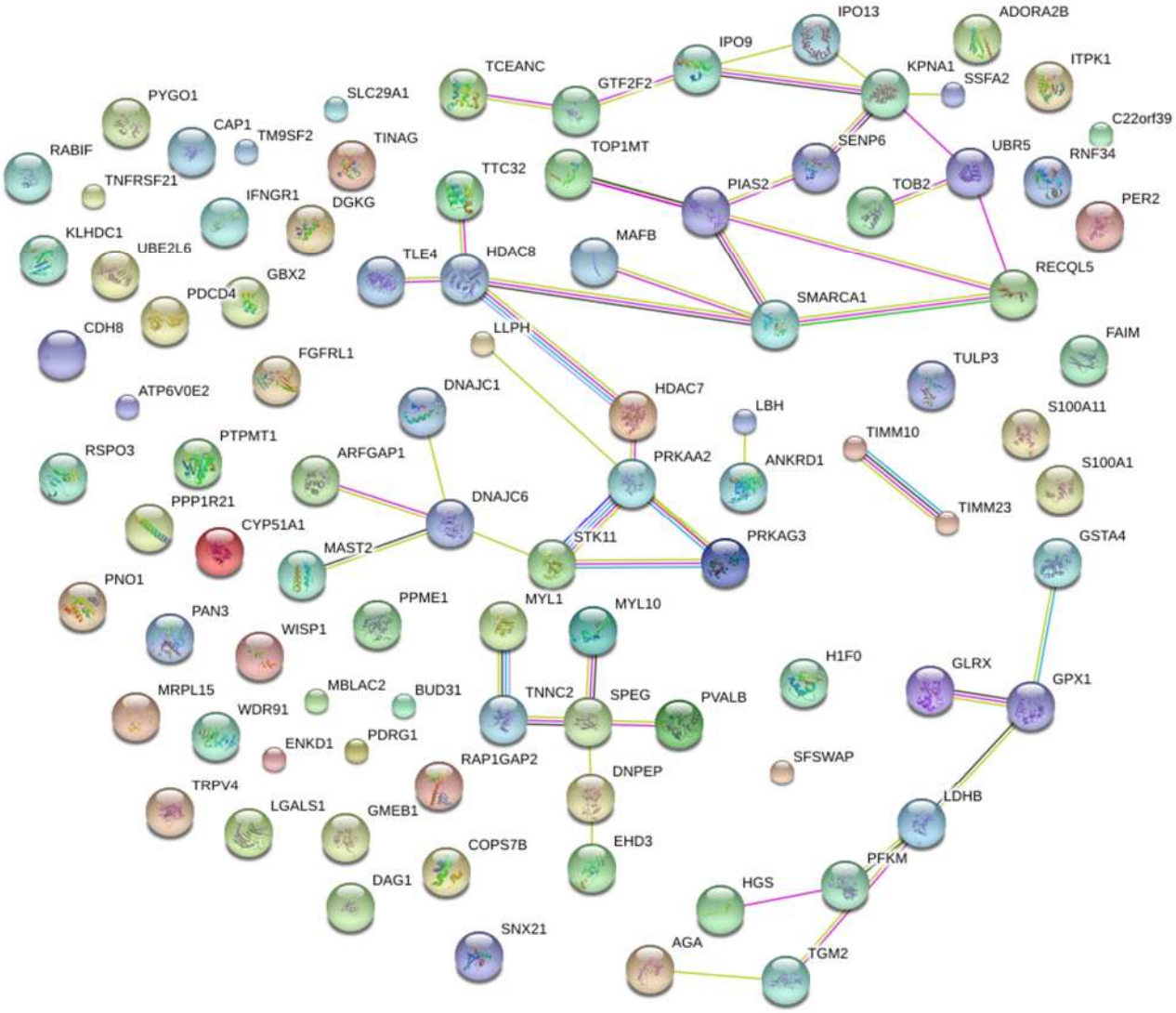



**Figure 5.8** Protein network interactions as examined by STRING analysis tool. Number of nodes: 88, Number of edges: 39, expected number of edges: 23. The network has significantly more interaction than expected (PPI enrichment *p*: 0.00119) with medium confidence.

**Table 5.6** STRING analysis identified molecular pathways from significantly regulated gene and transcript variants from OFT-Banded hearts

| DATABASE KNOWLEDGE | |
|---|---|
| annotated pathway (KEGG)<br>*Name: Endocytosis* | ARFGAP1 EHD3 HGS DNAJC6 [... and 175 other proteins] |
| annotated pathway (KEGG)<br>*Name: AMPK signaling pathway* | PRKAG3 STK11 PFKM [... and 115 other proteins] |
| annotated pathway (KEGG)<br>*Name: Alcoholism* | HDAC7 ADORA2B SLC29A1 [... and 119 other proteins] |
| annotated pathway (KEGG)<br>*Name: Ubiquitin mediated proteolysis* | UBE2L6 UBR5 PIAS2 [... and 126 other proteins] |
| curated pathway<br>*Catalysis: Activation of cytosolic AMPK by phosphorylation* | PRKAG3 STK11 [... and 9 other proteins] |
| curated complex (Gene Ontology)<br>*mitochondrial inner membrane presequence translocase complex* | TIMM10 TIMM23 [... and 7 other proteins] |
| annotated pathway (KEGG)<br>*Name: FoxO signaling pathway* | PRKAG3 STK11 [... and 116 other proteins] |
| curated pathway<br>*Pathway: Regulation of AMPK activity via LKB1* | PRKAG3 STK11 [... and 11 other proteins] |
| annotated pathway (KEGG)<br>*Name: Influenza A* | KPNA1 IFNGR1 [... and 147 other proteins] |
| annotated pathway (KEGG)<br>*Name: Herpes simplex infection* | PER2 IFNGR1 [... and 147 other proteins] |

[truncated after 10 items]

### 5.3.7 Study of TBX18 in the epicardial organ and atria

One of the aims of this project was to assess the conduction system in OFT-banded hearts. A key area in the development of the conduction system is the pro-epicardial organ (PEO), as cells of the conduction system have been traced to a genetic lineage from the PEO. A marker of these cells is TBX18. To examine potential ectopic expression of this key conduction gene, TBX18, whole mount *in situ* hybridisation was performed on HH25 OFT-banded and SHAM hearts. HH25 was used as cells of the forming conduction system are in migration in the atria/pro-epicardial organ at this time. Figure 6.9 shows no noticeable differences in TBX18 in the pro-epicardial organ or atria are apparent. However, a phenotype emerged in the epicardium surrounding the hearts. All OFT-banded hearts (n = 4) showed a reduction in this region compared to SHAM controls (n = 2) (the limb buds can be used as an internal control and no differences were seen in limb bud expression in Figure 5.10). This could be involved in vascular genesis (Wu et al., 2013), and off the back of this data a new PhD studentship was obtained vascularisation is now being studied.

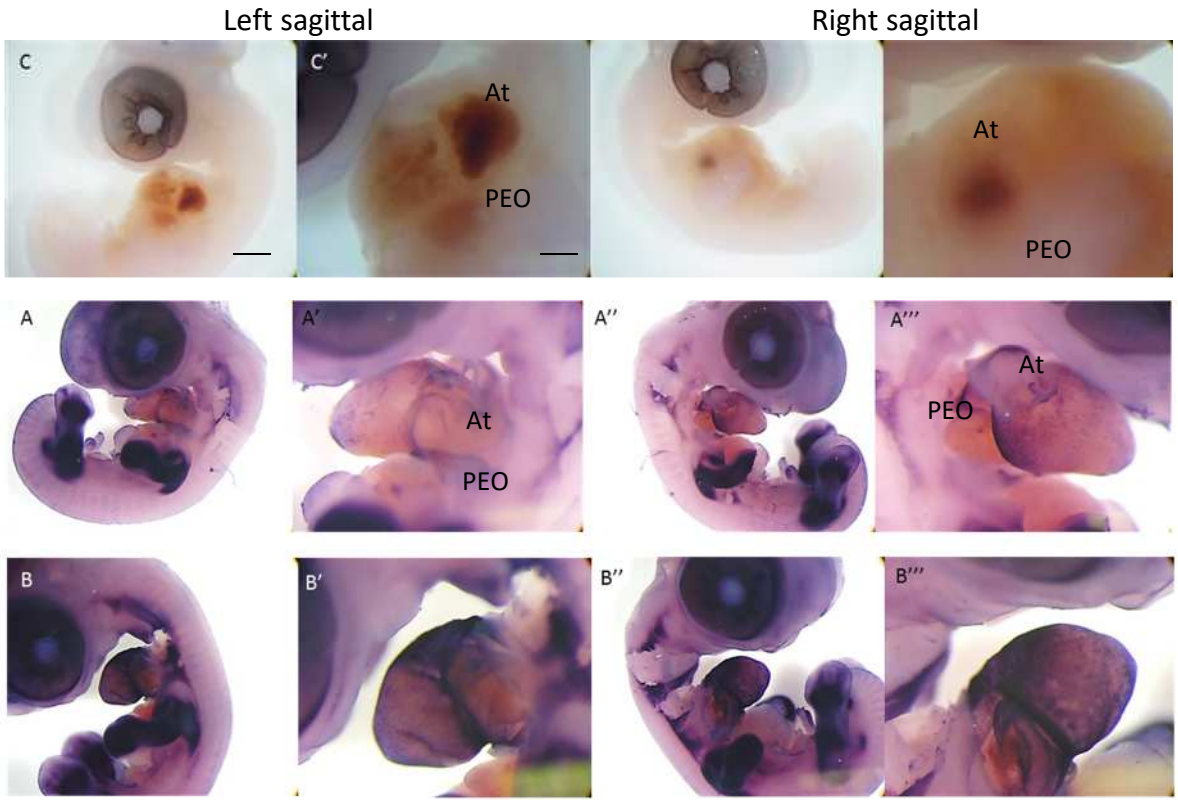



**Figure 5.9** No noticeable differences seen between OFT-banded (A) and SHAM (B) for TBX18 in the pro-epicardial organ and atria at HH25. C shows the sense negative control probe. At, Atria; PEO, pro-epicardial organ. 1000 µm for whole embryo images, 500 µm on focused images. n = 4

### 5.3.8 Structure and apoptosis in OFT-banded hearts at a late stage of the banding process

Altered hemodynamics might be expected to have adverse effects on the hearts in terms of myofilament structure, and cell death. To test this, OFT-banding hearts were harvested at the late stage of HH35 in order to put the maximum stress on the system.

#### 5.3.8.1 Immunohistochemistry

Immunostaining of HH35 serial sectioned hearts at 8 mm was performed on OFT-banded and SHAM hearts (n = 5 for both groups) using the MF20 (DSHB) antibody. This antibody recognizes all myosin heavy chain (MHC) isoforms by binding the meromyosin portion of the protein. Myofibrils appear relatively normal across both groups with no noticeable differences (Figure 5.11 A/B and A'/B'). The epicardial region in two out of five hearts appeared to show an increase in myosin stain intensity (Figure 6.10 A/B and A/B'''). No statistics were carried out due to low number of hearts.

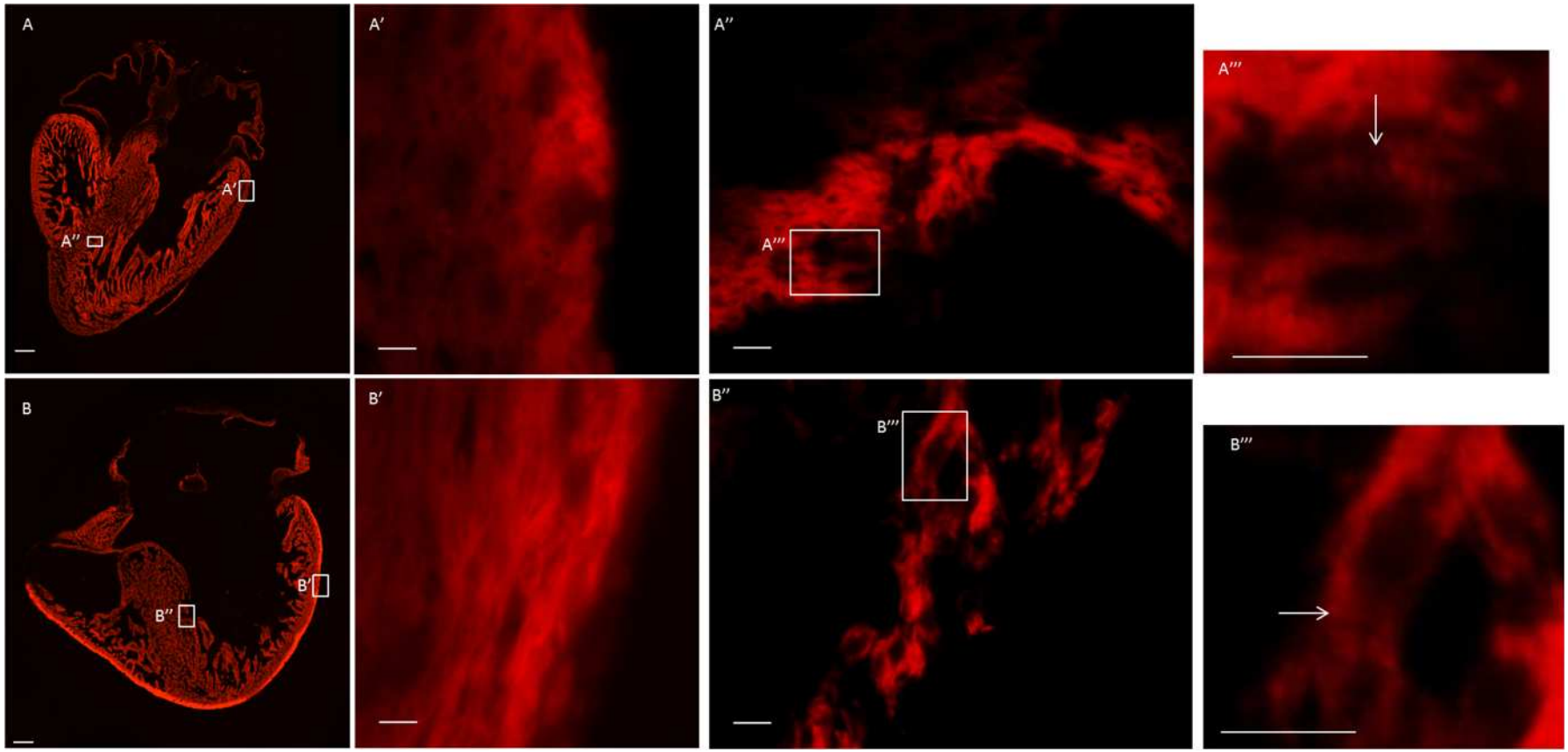



**Figure 5.10** Myosin structure in OFT and SHAM hearts. SHAM (A) and OFT-banded (B). A and A', and B and B' show epicardium with possible increase in myosin at epicardium in 2 out of 5 OFT hearts. Scale bar 10 µm. A'' and A''', and B'' and B''' shows some sarcomeric structures, (arrows) with no noticeable differences between OFT-banded hearts and SHAM. Scale bars, A,B - 250 µm; A',B' and A''B'' – 10 µm ; A'',B''' - 1 µm.

#### 5.3.8.2 Apoptosis in control and OFT-banded HH29 atria

Apoptosis was quantified in the chick heart by enzymatically labelling the free 3'-OH terminus of DNA with TdT. A total of 180,448 cells were identified as positive or negative for apoptosis in both RA and LA of sham and OFT-banded hearts (n=3 for each group). Cells positive for apoptosis were found scattered throughout the hearts and no clustering pattern was observed in both groups. The apoptotic cells counted in the right and left atrial region included the apoptotic cells in the myocardium and in the pectinate muscle. In the RA, the apoptosis accounted for 3.04±0.35% of the control hearts but 1.06±0.07% for the OFT-banded hearts, a decrease of 66.7% of apoptotic level was seen with the difference being significant, $p<0.01$ (arrow in Figure 6.12). In the LA, 2.26 ±0.39% cells were found apoptotic in sham and 0.85±0.09% cells were undergoing apoptosis in the banded hearts. A significant decrease of apoptotic cells by 62.3% was detected in the OFT-banded hearts in this region as well, $p<0.05$ (Figure 5.12).

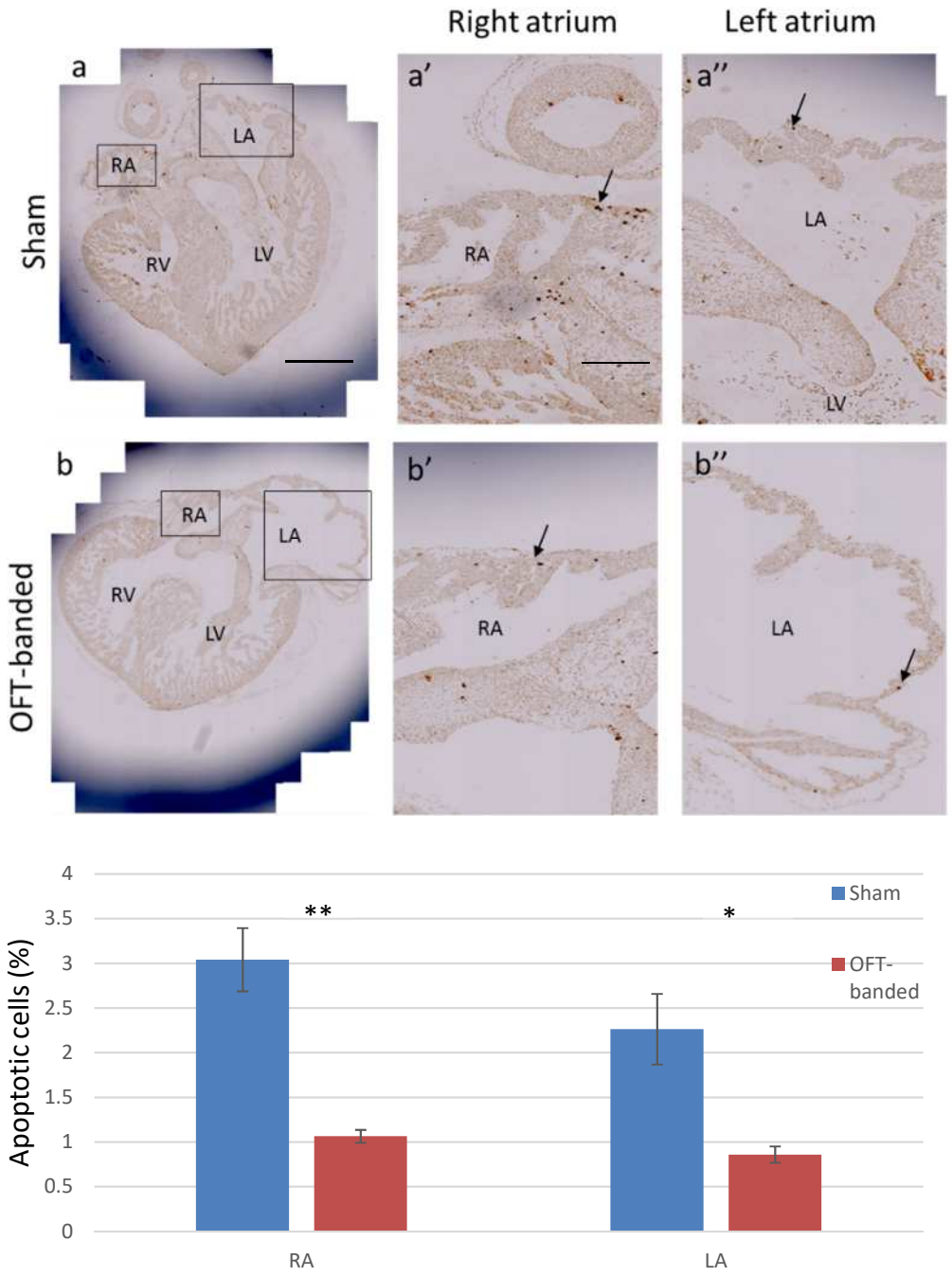



**Figure 5.11** Apoptosis in the OFT-banded heart. A, Apoptosis was decreased in both right and left atria upon OFT-banding. a, Apoptotic cells were identified and were found occurred in isolation in the myocardium of both right and left atria (as indicated by arrow in controls and in OFT-banded hearts. A decrease of apoptotic cells was revealed in both atria with $p<0.01$ in the right atrium and $p<0.05$ in left atria. Boxed

areas in a and b are shown in higher magnification in a',a'' and b,b'' respectively. LA, left atrium; RA, right atrium. Scale bar: 300 μm on whole heart, 150 μm on focussed. n = 3 for each group.

## 5.4 Discussion

RNA sequencing was performed to assess the effect on global gene expression of the OFT-banded model. From the global sequencing and RT-qPCR data at HH29, significantly regulated genes were identified. The primary aim of this chapter is to relate this expression to molecular pathways and potential function. Identified genes appear to relate to metabolism, structure, differentiation and conduction, and where differential expression was seen, genes were analysed further at HH35 by RT-qPCR. In general, these genes seem to present a pattern of cardio-protection, but some genes would also seem to point to a causative profile indicating glycogen storage cardiomyopathy. Of all the pathways/mechanisms implicated, the AMPK signalling pathway and EF-hand proteins seem to be highly effected. The possible implications of this will be discussed in this chapter. The RT-qPCR values at HH29 and HH35 for our genes of interest and gene interactions are shown in Figure 6.13. The genetic profile presented will now be discussed.

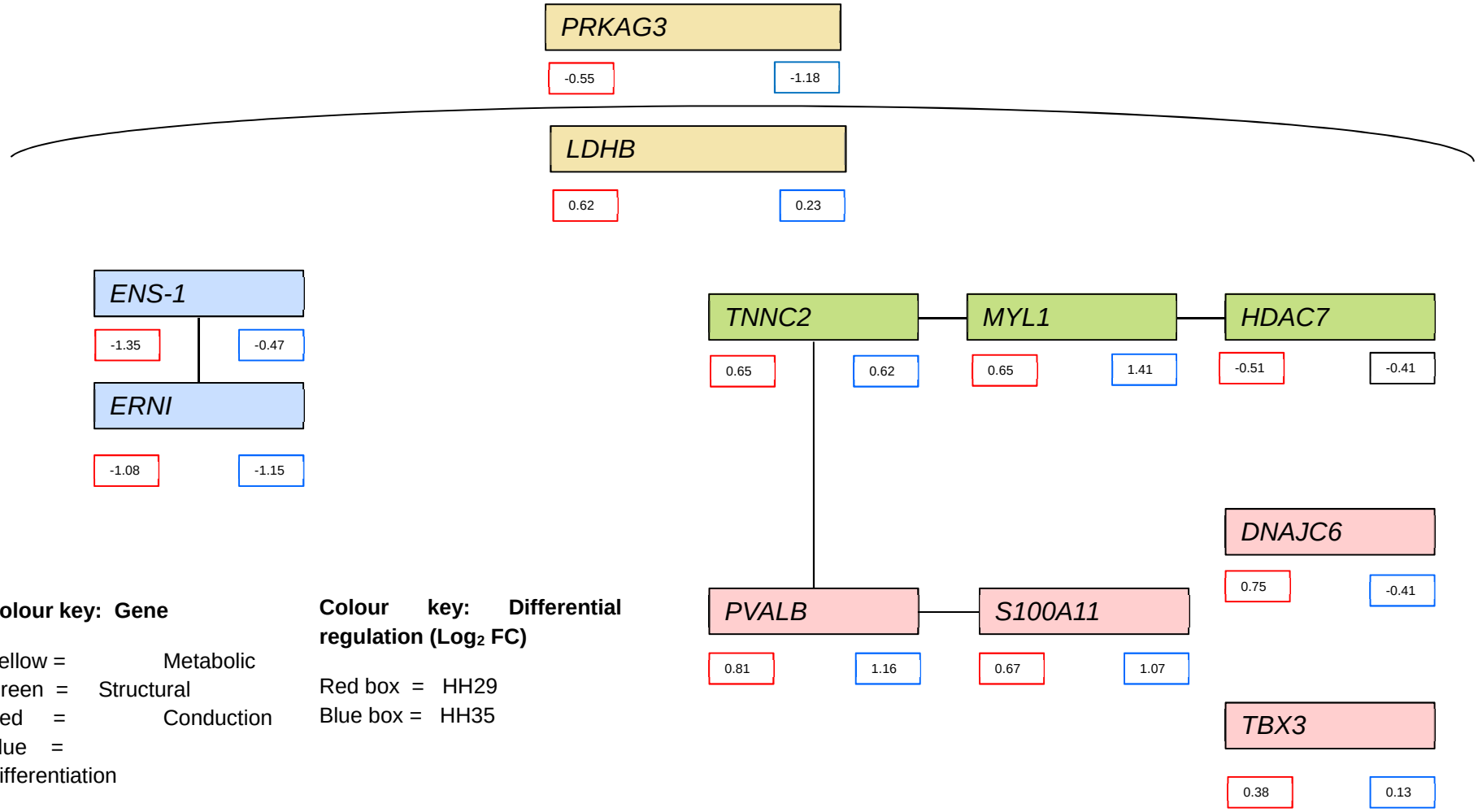



**Figure 5.12** Differentially expressed genes, showing known interactions which have been analysed in detail in this thesis. Small red box = HH29 expression, small blue box = HH35 expression (corrected $\log_2$ FC).

### 5.4.1 *PRKAG3* and AMPK signaling

*PRKAG3* - the sensory subunit of AMPK and its isoforms

A significant down regulation by RT-qPCR at HH29 which increased at HH35 (-0.55 $log_2$ FC at HH29 and increasing to -1.18 at HH35), of protein kinase AMP-activated non-catalytic subunit gamma 3 (*PRKAG3*), a regulator of the 5' AMP-activated protein kinase AMPK gene (Gralund et al 2010). The consequences of this could be far reaching as AMPK is a stress-activated regulatory kinase that is involved in regulation of a multitude of different genes and pathways (Zaha and Young, 2012). In order to gain a better understanding as to why this gene might be differentially expressed upon altered haemodynamics, and what effect this may have, it is important to understand its key interactions.

*PRKAG3* codes for a regulatory gamma subunit of 5' AMP-activated protein kinase (AMPK) (Xiao, Heath et al. 2007). The subunit senses levels of AMP/ADP/ATP and allows a conformational change that inhibits AMPK deactivation by blocking potential phosphorylases from AMPKs alpha subunit; thus keeping the enzyme activated - this is crucial in the heart where ATP demand is very high (Xiao, Heath et al. 2007). AMPK plays a key role in regulation of metabolism where in response to stress it will act on regulatory proteins involved in fatty acid oxidation, glucose uptake and glycogen synthesis - acting like a 'cellular fuel gauge and master metabolic regulator' for metabolism (Blair et al., 2001, Granlund et al., 2010, Xiao et al., 2007, Zaha and Young, 2012).

The PRKAG subunit has 3 main isoforms, *PRKAG1*, *PRKAG2* and *PRKAG3* (Milan et al., 2000). Importantly, our sequencing reveals that in the embryonic chick heart PRKAG2 is not expressed, with isoforms PRKAG1 and *PRKAG3* being expressed. PRKAG1 is known to be the dominant isoform of the subunit (Cheung et al., 2000); our sequencing data confirms this with FPKM values of 41 – 50 in controls, compared to 11 -15 FPKM for *PRKAG3* and 0 FPKM for *PRKAG2*. Though *PRKAG1* is known to be the dominant isoform, it is well documented that it is *PRKAG2* and *PRKAG3* that

show differential expression in cardiac and skeletal muscle disorders with *PRKAG1* being unaltered (Pinter et al., 2013, Milan et al., 2000).

Previously thought to be only in skeletal muscle (Yu et al., 2005, Granlund et al., 2011), we have shown *PRKAG3* is expressed in the embryonic chick heart at HH29 and HH35. Studies of *PRKAG* genes in the developing heart have identified a new transcript, termed *PRKAG* γ2-3B (Pinter et al., 2012). Interestingly, increased levels of this transcript are seen where levels of *PRKAG3* are low (Pinter et al., 2012), and an embryonic mouse study found that PRKAG γ2-3B levels increased with development, with corresponding decreasing levels of *PRKAG3* (Pinter et al., 2013). In the Human, this transcript has been found to increase with embryonic development to become the dominant regulator of AMPK in the adult heart, and it has been suggested that 'functional changes in AMPK containing γ2-3B may mediate *PRKAG2* cardiomyopathy' (*PRKAG2* mutation is found in cardiomyopathy and is discussed later) (Pinter et al., 2012). This suggests that when one transcript is not expressed, then another might be compensating, and that dysregulation in one, may mediate disruption in the other. Our data of all sequenced samples suggest that *PRKAG3* is expressed to regulate AMP/ATP sensitivity in the absence of *PRKAG2* in the embryonic heart. The sequence of PRKAG γ2-3B is not available in the chick galGal 4 database, thus no results were obtained for this gene from this RNA sequencing study.

Functional relevance of *PRKAG3* reduced expression

Expression analysis of *PRKAG3* at HH35 revealed a 54% increase in significant differential down regulation from -0.55 at HH29 to -1.18 at HH35 mean $log_2$ FC. This decrease in expression in OFT-banded hearts shows that the effect on metabolism increases at later developmental stages upon OFT-banding treatment. This may be expected, with greater variation between AMP and ATP levels, and a reduction in oxygen availability as the embryo becomes larger and the restricted outflow tract becomes proportionally smaller. Activation of *PRKAG3* in skeletal muscle increases

fatty acid oxidation, whereas knockout of this isoform has led to excessive triglyceride accumulation (Granlund et al., 2011, Barnes et al., 2004). So, our decrease in expression seen could suggest less reliance on oxidative metabolism, possibly due to impaired oxygen availability due to OFT-banding. This is correlated in part by the significant increase in lactate dehydrogenase B (LDHB) observed at HH29 in OFT-banded hearts; LDHB catalyses the interconversion of pyruvate and lactate in anaerobic glycolysis and has previously been linked to dilated cardiomyopathy (Hamada et al., 1992, Wang et al., 2013a).

We have shown a down regulation of the AMP/ADP/ATP regulator (PRKAG3) of AMPK. Interestingly our sequencing also shows that Serine/threonine kinase 11 (*STK11*) is down regulated (-0.25 DESeq corrected $\log_2$ FC (non-corrected value was -0.4 $\log_2$ FC). *STK11* acts like the on switch of AMPK (Proszkowiec-Weglarz et al., 2006), and though changes were insignificant, when taken together with a down regulation of *PRKAG3* it could be expected that function of AMPK will be affected.

There are currently no publications within the literature describing models of glycogen storage cardiomyopathy (and subsequent reduction in activity of PRKAG2 or *PRKAG3*) following haemodynamic stress. Previous studies have focussed on creating transgenic mice to model gene mutations or knockout mice of PRKAG2 in order to induce a phenotype of increased stress and glycogen storage (Arad et al., 2003, Patel et al., 2003, Arad et al., 2005). However, upon altering the haemodynamics (banding of the thoracic aorta) in the glycogen synthase kinase-3 (GSK-3) knockout neonatal mouse, the β-adrenergic response was analysed (Zhou et al., 2010). This is of particular interest as GSK-3, like AMPK, is a regulator of Glycogen Synthase (GS) (Zhou et al 2010; Gralund et al 2010). When activated, GSK-3 phosphorylates GS making it inactive and unable to synthesize glycogen (Zhou et al 2010). Activated AMPK also phosphorylates GS, with the same effect of reduced glycogen synthesis (see Figure 6.14 for potential mechanism) (Halse et al., 2003, Granlund et al., 2010). Zhou and colleagues showed that when *GSK-3* was knocked out, haemodynamic alteration led to hypertrophy that quickly developed into ventricular dilation and contraction dysfunction (Zhou et al., 2010). This was not present in WT animals. It would be expected that knockout of *GSK-3* would lead to

increased glycogen storage to account for the phenotype; however, muscle glycogen increases compared to WT were relatively slight and not enough to induce the cardiomyopathy phenotype seen. This suggests an alternative mechanism is at play; another function of GSK-3 is its involvement in a positive feedback loop that enhances β-adrenergic response, with knockout or GSK-3 inhibited WT, animals producing markedly impaired β-adrenergic response (Zhou et al., 2010). GSK-3 regulates and increases cAMP levels independently of epinephrine activation of Beta-adrenergic receptors, so reduced GSK-3 expression leads to a reduced cAMP production, with knock on effects on contractibility and possibly hypertrophy (Zhou et al., 2010). This could be particularly important as beta-adrenergic desensitisation caused by continuously raised levels of epinephrine, that would be seen in times of stress, has been linked to cardiac dysfunction and eventual heart failure (Mielcarek et al., 2014, Sucharov et al., 2011). (see figure 5.13 for possible mechanism involved in glycogen storage).

AMPK has also been linked to β-adrenergic response, where AMPK is activated by β-adrenergic signalling (Jorgensen et al., 2006, Pulinilkunnil et al., 2011, Wang et al., 2016, Mellor et al., 2016). A decrease in activity of AMPK and subsequent increase in glycogen synthase activity could lead to less ATP generation from glycolysis. Acting in a similar way to the GSK-3 positive feedback loop, this could inhibit cAMP signalling as cAMP is generated from ATP and thus lead to cardiac dysfunction.

AMPK can have unexpected results in terms of glycogen storage; as although activation of AMPK would be expected to result in a decrease in glycogen, increases have also been observed (Steinberg and Kemp, 2009, Aschenbach et al., 2002). This is likely because of stimuli, such as AICAR-stimulated glucose uptake, that are able to overcome the inhibitory effect of AMPK by producing an increase in the concentration of intracellular Glucose 6-phosphate (G-6-P) in the liver which allosterically activates GS independent of phosphorylation (Aschenbach et al., 2002, Steinberg and Kemp, 2009).

What purpose *PRKAG3* reduction serves and how it affects AMPK is something that could be debated. The direction this thesis takes is that it would lead to a decreased

action of the key inhibitor of glycogen synthase which could be causative of many metabolic problems (discussed in detail in section 6.3.2.1). AMPK activation is already being tested for treatment of heart disease, where drugs such as nucleoside 5-aminoimidazole-4-carboxyamide-1-beta-D-ribofuranoside (AICAR) that activate AMPK have been found to have cardio-protective effects in animal models (Zaha and Young, 2012).

Association with cardiomyopathy and AMPK potential effect on signaling pathways and expression

There are 4 main types of cardiomyopathy; hypertrophic, dilated, restrictive and arrhythmogenic right ventricular dysplasia. All share similar features of altered gene expression whilst at the same time displaying unique phenotypic characteristics. Excess glycogen storage has been presented in the past as a general symptom of cardiomyopathy, however, some studies suggest hearts displaying glycogen storage cardiomyopathy have their own unique characteristics (Blair et al., 2001, Wolf et al., 2008). Glycogen-Storage Cardiomyopathy generally does not show fibrosis or the structural disarray of sarcomeres usually seen in HCM (Semsarian et al., 2002); however it does still have an enlarged ventricle that becomes dilated due to the increased storage of glycogen. This is consistent with our phenotype where immunohistochemistry of myosin by MF20 shows no obvious disruption of sarcomeres, Masons Trichrome staining showed no fibrosis, and a dilated left ventricle are seen (data for fibrosis and phenotypic analysis of hearts carried out by Dr Pang).

Interestingly, Glycogen-Storage Cardiomyopathy presents the unique conduction phenotype of pre-excitation (Wolf et al., 2008). Pre-excitation, known as Wolff Parkinson White syndrome, presents a conduction phenotype where a shortened PR interval (<120 msec), a widened QRS (>100 msec), an abnormal initial QRS vector delta wave and a supraventricular tachycardia are seen (Wolf, Arad et al. 2008). This results in early ventricular depolarization that occurs through accessory pathways (bundles of Kent) that bypass the AV node to the ventricle (Wolf, Arad et al. 2008).

PRKAG2 has been implicated as the causative gene in familial hypertrophic cardiomyopathy (HCM) in two families (Blair et al., 2001). Interestingly, although HCM, dilated ventricles were also seen (as with our OFT-banded hearts) across all subjects as in with our OFT-banded hearts. The families had inconsistent mutations in expected cardiomyopathy marker fetal gene program genes such as alpha and beta myosin heavy chain or cardiac myosin-binding protein C (*MYBPC3*) i.e. not all family members presenting a cardiomyopathy phenotype had mutations in the same cardiomyopathy marker genes. This is often the case with cardiomyopathy and it complicates potential treatments/therapies (Scheffold et al., 2011). One consistency found in all family members with the cardiomyopathy phenotype was mutation to PRKAG2. This suggested that an inability to efficiently use/respond to AMP/ADP/ATP levels may be the central cause of the cardiomyopathy phenotype (Blair et al., 2001). Cardiomyopathy induced by PRKAG2 mutation is known as glycogen-Storage Cardiomyopathy (Arad et al., 2005). Though relatively few studies exist, glycogen-storage cardiomyopathy has been shown to lead to a dilated cardiomyopathy phenotype (Blair et al., 2001, Gollob, 2008).

AMPK has also been shown to directly phosphorylate HDAC class II enzymes leading to nuclear export and cytoplasmic retention (Zhao et al., 2011, Seto and Yoshida, 2014). Additionally, HDAC class II enzyme phosphorylation by β-adrenergic target PKA has also been observed (Lehmann et al., 2014). This could account for the inconstant expression of cardiomyopathy markers as disruption to HDAC phosphorylation would disrupt expression of the fetal gene program that is usually up regulated in cardiomyopathy. HDACs are inhibitors of expression (Backs and Olson, 2006). Their general mode of repression is, as the name suggests, by deacetylation of chromatin that leads to its compression and thus represses transcription, but they can also bind directly to transcription factors (Backs and Olson, 2006). Class IIa HDACs are signal transducers that shutter between cytoplasm and nucleus and are known to be repressors in molecular pathways governing cardiomyopathy (Lee et al., 2016).

We have down regulation of HDAC7 in our OFT-banded hearts, though just insignificant ($p$=0.06) (4.4.7 for possibility of false negatives), and it is possible this could be a response to AMPK regulation, where a possible reduction in HDACs phosphorylation by as less active AMPK could lead to less repression of HDACs which would lead to less gene expression in cardiomyopathy marker genes, a reduction in HDAC expression could counter this effect. To clarify, our possible decrease in AMPK activity could lead to less expression of fetal gene program genes because HDACs may not be being removed from the nucleus, but less expression of HDACs would lead to increased expression as there would be less HDACs to repress expression. A key target for class IIa HDACs is myocyte enhancer factor-2 (MEF2) (Dressel et al., 2001). Though expression is unaltered in OFT-banded hearts, HDAC7 directly inhibits the MEF2 protein activity by binding at HDAC7's repression domain 1 (Dressel et al., 2001). MEF2, and other MEF proteins, are transcription factors that promote expression of key fetal cardiac genes involved in contractility such as; MYL1 (0.54), MYL2 (0.2), TNNC1 (0.75) and TNNT2 (0.36) (parenthesis show our sequencing increased corrected $Log_2$ FC) (Dressel et al., 2001, Dirkx et al., 2013). These genes resemble our differentially up regulated gene profile following OFT-banding. Forced expression of MEF2 has been seen to lead to intolerance to pressure overload, ventricular dilation and contractile dysfunction (Dirkx et al., 2013). We have significant left ventricular dilation in our model, so it could be that MEF2 is a component of hemodynamic alteration response and expression of the fetal gene program. HDACs act in response to β-Adrenergic receptor signaling and intracellular $Ca^{2+}$, where increased expression in fetal genes is seen in response to β-Adrenergic stimulation (Mielcarek et al., 2014). Genes associated with β-Adrenergic response such as AMPK may be involved in regulation in OFT-banded hearts. When HDACs bind calcium/calmodulin-dependent protein kinase (CaMK) they become phosphorylated and are removed from the nucleus and thus repression on transcription of fetal genes is removed (Backs and Olson, 2006). Mutant HDACs without regulatory phosphorylation sites showed reduced hypertrophy in response to adrenergic agonists (Mielcarek et al., 2014, Zhang et al., 2002). Inhibition/ removal of HDACs has been seen to have a cardioprotective effect where inflammation is actually reduced (Lee et al., 2016, Lkhagva et al., 2015). Though this is converse to the chronic up regulatory

effect of the fetal gene program, which would be expected to cause hypertrophy, a link to metabolism may be cardioprotective. Cardiomyopathy in diabetes mellitus rats shows dilated left ventricle, larger heart-size-to-body-weight ratio, increased QT intervals, abnormal fatty acid signalling and a decrease in AMPK phosphorylation (Lee et al., 2016). Inhibition of HDACs led to an increased phosphorylation of AMPK, and a reduction in the other aforementioned phenotypes (Lee et al., 2016). Their cardiomyopathy model resembles our phenotype of enlarged heart, dilated left ventricle and possible decrease to AMPK activity. Phosphorylation and activation of AMPK by down regulation of HDACs could help to correct reduced activity of AMPK that is potentially being brought about in our model by down regulation of *PRKAG3* and STK11. Genes usually associated with cardiomyopathy, such as structural genes α*MYH*, which normally show downregulation, and β*MYH*, which normally show up regulation (Blair et al., 2001), were not significantly altered in our model; though a small down regulation was found in α*MYH* and a small up regulation was in (β*MYH*). The possible cardioprotective effect of AMPK is also highlighted in conduction system maturation latter in this discussion.

To summarise, the down regulation of *PRKAG3* and to an extent STK11 in our OFT-banded hearts will would be expected to effect on AMPK, with a likely reduction in AMPK activity, and therefore have an effect many metabolic and signalling processes (see figure 5.13 for possible mechanism involved in glycogen storage). This could be causative of our enlarged dilated left ventricle by both glycogen storage and possibly HDAC disruption, and could also have involvement in contractibility by affecting the β-adrenergic response.

## 5.5 Future work

To ascertain our cardiomyopathy phenotype, glycogen and AMP/ATP assays could be carried out. This would prove if we have a glycogen storage cardiomyopathy phenotype. Additionally, phosphorylation of AMPK could be tested by western blot in order to elucidate the practical effect of *PRKAG3* and STK11 down regulation on the ratio of phosphorylated to un-phosphorylated AMPK.

Conduction system maturation

Our aim to identify genes differentially regulated with particular reference to the conduction system came about because of precocious development of conduction seen in OFT banding models where an apex to base conduction pattern appears earlier than in controls (Reckova et al., 2003). Genes that lead to conduction system differentiation over that of cardiomyocyte maybe involved in this. Our increase in expression of TBX3 at HH29 (0.38 $log_2$ FC [SEM 0.05]), but not at HH35 (0.13 $log_2$ FC [SEM 0,08]) could also indicate precocious conduction system development as TBX3 is required for the differentiation of conduction cells, where it out-competes TBX5, sending cells down a conduction lineage pathway (van Weerd and Christoffels, 2016, Hoogaars et al., 2004). Another gene shown to bind and directly inhibit TBX5 is the Limb bud and heart development (LBH) transcription cofactor (Briegel et al., 2005). Our sequencing shows significant up regulation of this gene (0.60 $log_2$ FC [SEM 0.17]). LBH overexpression in mice also lead to impaired pulmonary outflow tract valvulogenesis, cardiac septation, inflow tract morphogenesis, abnormalities in ventricular cardiomyocyte growth and ventricular cardiomyopathy (Briegel et al., 2005). Our OFT-banding induced significant up regulation in this gene and has physiological effects similar to those seen in the LBH overexpression mice. It could be that heart cells are being forced down a more conduction cell route, rather than a TBX5 uninhibited functional working cardiomyocyte route. Further work to elucidate effects could be done with in-situ hybridisation on sections for LBH along with known conduction and functional cardiomyocyte marker genes. This thesis does report findings on a conduction marker, TBX18 *in situ*. However, the initial reason for this was to look at expression in the pro-epicardial organ and only whole mount embryos were assed, where the only phenotype visible was that there was reduced expression in the epicardium. So, it could in fact be possible that LBH is a gene involved in causing our phenotype with features of dilated cardiomyopathy, as with LBH overexpressing mice that showed cardiomyopathy (Briegel et al., 2005); and it could be that the AMPK/HDAC acts in response to try and regulate force generating fetal gene program genes such *as MYL1, MYL2, TNNC1* etc.

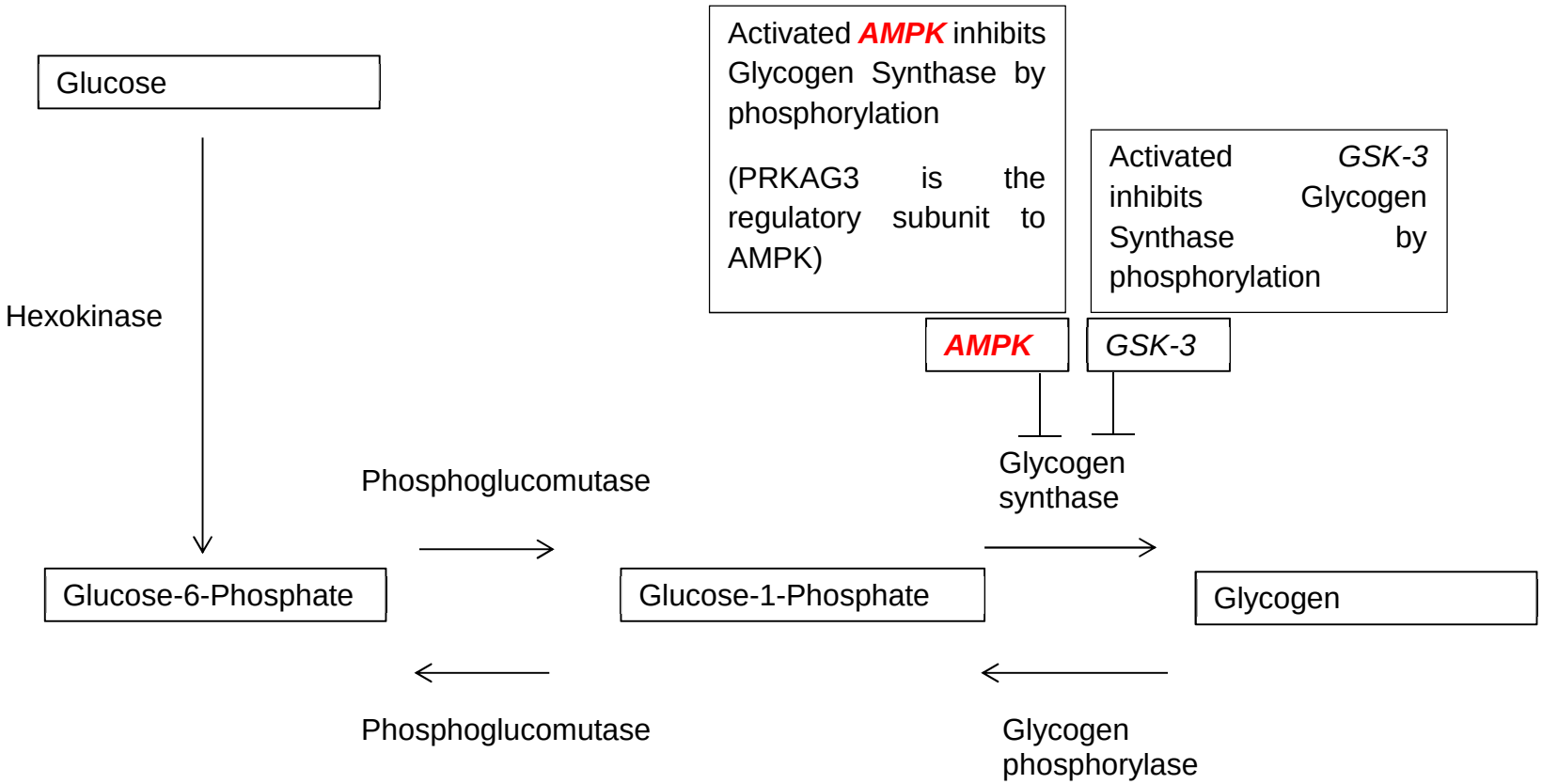



**Figure 5.13** Glycogen synthesis pathway within cardiac and skeletal muscle. AMPK acts to regulate synthesis by phosphorylation of a serine residue on glycogen synthase (GS) – thus inactivating the enzyme. GSK-3 mirrors AMPKs function but binds to a different serine residue on GS (Source: Matthew Parnall 2017 with mechanism adapted from (Voet, 2004).

### 5.5.1 EF-hand proteins

Conduction abnormalities such as delayed repolarisation are commonly seen in both hypertrophic and dilated cardiomyopathy (Reckova et al., 2003), and calcium binding genes are known to be linked to these phenotypes (Reckova et al., 2003). Our results show a general up regulation in $Ca^{2+}$ sequestering EF-hand proteins. The EF-hand motif is a high affinity $Ca^{2+}$ binding helix-loop-helix structure that is present in a number of structural and buffering proteins (Lewit-Bentley and Rety, 2000), and binding of $Ca^{2+}$ can cause conformational change as seen in TNNC2 (Wang et al., 2013b). We have seen significant up regulation EF-hand structural proteins MYL10, MYL1 and TNNC2, intercellular membrane protein S100A11 and cytoplasmic protein PVALB.

Force generating proteins

The fetal gene program gene *MYL10*, *MYL1* and *TNNC2* proteins are all involved in force generation and all showed significant up regulation to a similar degree, with 0.65, 0.67 and 0.75 for MLY1, MYL10 $Log_2$ FC and TNNC2 respectively. An increase in these proteins could be expected as part of the hearts initial response to stress in attempt to maintain cardiac output (Zelis and Mason, 1970). These genes have already been mentioned in this discussion in the AMPK section, as their expression is increased by MEF2, which is itself inhibited by HDAC expression and activation which could explain their up regulation. TNNC2, a fast-skeletal isoform of troponin C, is a regulator of contraction that releases inhibition of the troponin complex following $Ca^{+}$ binding, as such, an increase should increase calcium sensitivity of the contractile units of the heart. The protein interacts with PVALB, where during relaxation $Ca^{+}$ is carried away from troponin C. PVALB is also up regulated and is discussed in the AMPK section. The fast twitch skeletal TNNC2 gene has been linked to muscular diseases (Gupta et al., 2014), but unlike its slow isoform TNNC1, TNNC2 has not previously been linked with dilated cardiomyopathy or stress in the heart (Baryshnikova et al., 2008). The myosin light chain 1 (MYL1) is also a fast skeletal

isoform. Mice with upregulated phenotypes for fast twitch fiber types (including MYL1 up regulation) have been found to develop dilated cardiomyopathy (Petchey et al., 2014). The mice in the aforementioned study had the phenotype induced by Prospero-related homeobox factor 1 (Prox1) knock out. Our sequenced OFT-banded hearts show an insignificant down regulation in this gene. To this authors knowledge, MYL10 has not been implicated in cardiomyopathy or stress models, however, it has be found expressed highly in developing skeletal muscle during early growth in the chicken (Xue et al., 2017), and so would seem to be a gene that reacts to enable increased force generation.

Parvalbumin

Parvalbumin (*PVALB*) showed significant up regulation at HH29 and increased up regulation at HH35 (0.81 [SEM 0.17] and 1.16 [SEM 0.37] $log_2$ FC respectively). PVALB is found in myocyte cytoplasm in all chambers of the heart (Vongvatcharanon et al., 2008). It has high affinity to $Ca^{2+}$, and interacts with TNNC2 by removing $Ca^{2+}$ and returning it to the sarcoplasmic reticulum, thus allowing repolarisation (Cheung et al., 2000, Vongvatcharanon et al., 2008). Its expression is increased in organisms where the heart is under high stress e.g. birds that require higher cardiac output than larger mammals, and have increased levels of PVALB (Mutryn et al., 2015). It had previously been thought that PVALB was only expressed in fast conducting skeletal muscle; however, it has now been seen by immunochemistry in pig and rabbit heart (Vongvatcharanon et al., 2008), and our sequencing confirms this in the embryonic chick heart with FPKM values of 17 – 20 in controls.

Abnormalities in repolarization of the ventricular myocardium, such as longer QT uncoupled from heart rate and independent of ejection fraction, that lead to arrhythmias have been seen in DCM (Reckova et al., 2003). PVALB has an action that is not dependent on ATP (Wang et al., 2013b). This therefore means that its action may not be altered by the disruption in metabolism that is seen in our model and in cardiomyopathy in general. This could make PVALB a good therapeutic target in

cardiomyopathy identified as having metabolic disruption. The upregulation of *PVALB* would speed up repolarisation, thus stopping the delay seen in DCM and help prevent eventual diastolic heart failure. This cardioprotective feature would maintain the heart rate during haemodynamic alteration. It has been shown that OFT-banding does not cause an alteration in heart rate (Steinberg and Kemp, 2009), and this could be because of the up regulation of cardioprotective genes such as PVALB.

*PVALBs* increased differential expression at HH35 corresponds to the increase seen in *MYL1* and *PRKAG3*, and suggests an increase in expression is required over time upon altered haemodynamics. As *PVALB* has such a key role in repolarisation, and we have seen large increases with an increasing phenotype, it could be that this EF-hand protein is a key cardioprotective regulator of heart rate and thus cardiac output in the embryonic hemodynamically altered heart.

*S100A11*

*S100A11* shows a significant upregulation in OFT-banded hearts (0.67 $\log_2$ FC [SEM 0.07] at HH29 increasing to 1.07 $\log_2$ FC [SEM 0.17] at HH35). S100A11 is co-expressed with S100A1 on internal cell membranes and at Z-discs in cardiomyocytes (Arcuri et al., 2002). *S100A1* shows an up regulation in our sequencing of 0.3 $\log_2$ FC; however, its regulation is statically insignificant. When taken together with the *S100A11* data at HH29, and increased differential regulation of *S100A11* at HH35 it seems clear something is going on with this $Ca^{2+}$ binding protein. Little is currently known about the functional relevance of S100A11, however it has been found to be upregulated following β-adrenergic stimulation in the rat heart (Inamoto et al., 2000). Knockout of the S100A11 isomer, S100A1, has been directly linked to reduced left ventricular contractility following thoracic aortic constriction (Du et al., 2002). This would again suggest a cardioprotective effect to maintain functional contractility of S100A11 and S100A1.

### 5.5.2 Apoptosis

Though cardio myopathy is linked to increased apoptosis (Narula et al., 2000), the results in this thesis show a significant decrease. Shear stress has been linked with a decrease though, with a proposed mechanism of protein kinase B (Akt) phosphorylation of p300 histone acetyltransferase (HAT) that is required for transcriptional cofactor activation (Chen et al., 2008). Akt is activated by a mechanosensory complex induced by PECAM in response to shear stress and the subsequently activated p300 is known to reduce apoptosis (Tan et al., 2008). AMPK has been found to phosphorylate and deactivate P300 in human cultured heart endothelial cells (Zhang et al., 2011b), our potentially less active AMPK could then potentially lead to less inhibition of P300 and thus a decrease apoptosis. AMPK has been found to be a key regulator of cell survival or death in response to stress (Hwang et al., 2010); in a mouse lung cell study, activation of AMPK led to cell cycle arrest and induction of apoptosis (Hwang et al., 2010). So, if activation leads to apoptosis, a proposed deactivation could reduce apoptosis. Another differentially regulated gene in from this thesis sequencing data, S100A11, has also been implicated in reduced apoptosis studies. Suppression by siRNA has been seen to lead to apoptosis, whereas over expression has inhibited apoptosis (Kanamori et al., 2004). The increase in *S100A11* expression observed in OFT-banded hearts corresponds to this and also supports our decrease in apoptosis. This reduction could have a cardioprotective effect in reducing hypertrophy in OFT-banded hearts.

### 5.5.3 Auxilin

Auxilin (*DNAJC6*) is a chaperon protein involved in un-coating of clatherin during endocytosis (Koutras and Braun, 2014). We show significant down regulation at HH29 (-0.75 $Log_2$ FC [SEM 0.03]) and similar levels at HH35 (-0.41 $log_2$ FC [0.08]). This gene has recently been associated with abnormal $Ca^2$+ homeostasis with rhythm disorders and atria ventricular ectopias (Meisgen and Hedlund, 2015). However, little is understood about its action in the heart, as previous studies have focused on its role in juvenile Parkinsons, with expression known to be in the brain (Meisgen and Hedlund, 2015, Koutras and Braun, 2014). It is found in the heart co-localised with clatherin (Koutras and Braun, 2014) so again it would seem it plays a role in endocytosis. Table 6.5 later in this discussion highlights endocytosis as being effected in our model.

### 5.5.4 Endogenous retrovirus (*ENS-1*) and Early response to neural induction (*ERNI*)

*ENS-1* and *ERNI* are of viral origin and are expressed in embryonic stem cells of the neural crest in the cytoplasm and nucleus; as development progresses they become increasingly expressed just in the nucleus (Nakamura et al., 2006). *ENS-1* encodes a protein identical to *ERNI*, but *ENS-1* starts with long viral repeat section and has a different locus (Blanc et al., 2014). Multipotent neural crest cells have been detected in the conduction system of the heart into late development (Dowaki et al., 2000). Our RT-qPCR result of HH29 against HH35 atria and ventricle would suggest that differentiation of the atria proceeds before the ventricle as ENS-1 and to a lesser extent ERNI is decreased in the atria but not in the ventricle at HH35. Ablation of neural crest cells led to a retardation of apex to base conduction pattern (Gurjarpadhye et al., 2007), suggesting that these cells are vital for the timing of differentiation. Our sequencing and RT-qPCR reveal down regulation of these genes in OFT-banded hearts. *ENS-1* shows -1.35 log2 FC (SEM 0.02) at HH29 and -0.47 log2 FC (SEM 0.16) at HH35 with *ERNI* showing similar levels, but less of a reduction at HH35. A down regulation of these genes could be expected to lead to increased differentiation.

This may have an effect on the previously seen precocious conduction system was seen upon OFT banding (Reckova et al., 2003) . This is perhaps supported by our expression profile where decreasing levels where seen in *ENS-1* compared to *ERNI* at HH35 – thus more differentiation would be expected. A mechanism of differentiation is proposed to be regulated by the transcription factor *SOX2* (Gurjarpadhye et al., 2007, Papanayotou et al., 2008). In the proposed mechanism, activation of SOX2 by brahma (BRM) and geminin (GEM) at the N2 enhancer site will lead to neural stem cells maintaining their progenitor identity (see Figure 5.15 for potential mechanism). Our down regulation of ENS-1 / ERNI could lead to less SOX2 inhibition, as they recruit HP1γ the the N2 enhancer blocking its activity, and thus greater differentiation. Our results from sequencing of SOX2 and its downstream targets, DKK1 and cMYC do support this, but they only show very small levels of up regulation (Figure 5.15).

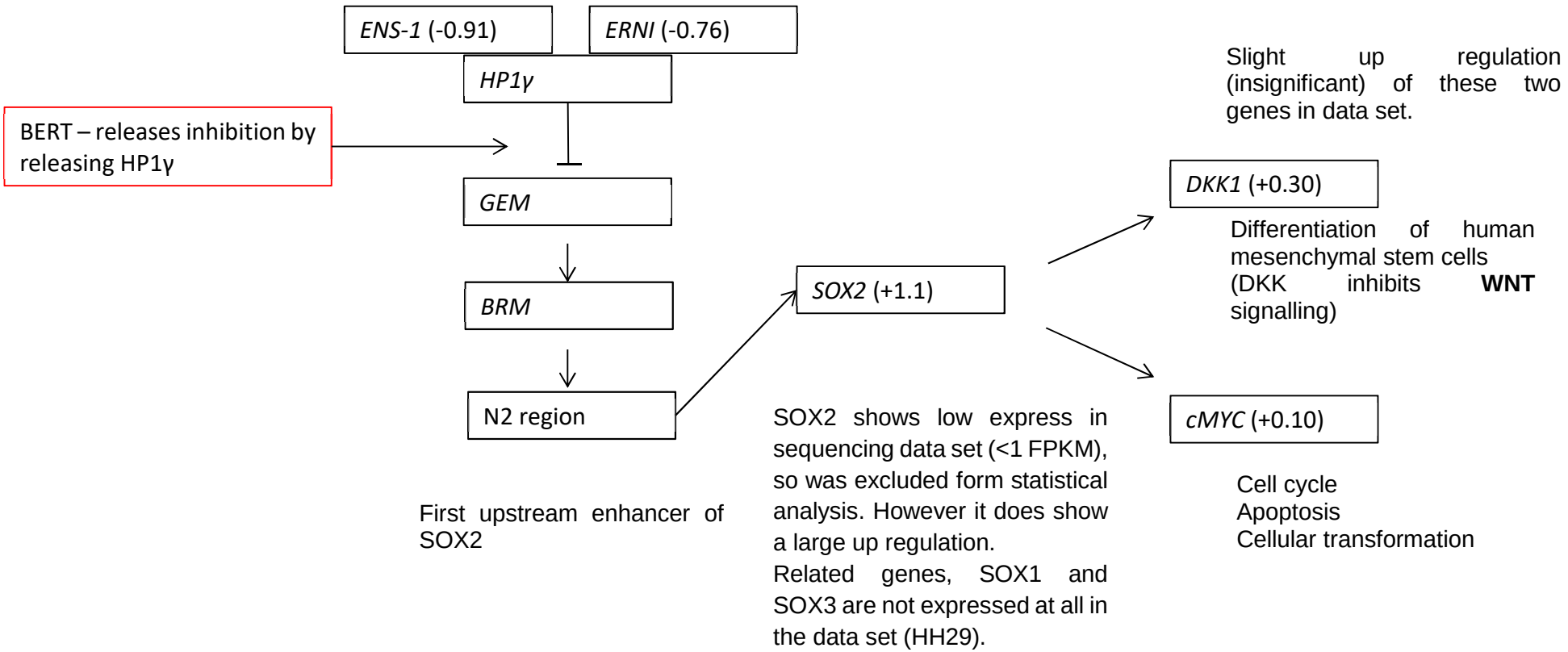



**Figure 5.14** Mechanism for differentiation of stem cells derived from the neural crest. ENS-1/ ERNI when bound to HP1γ inhibit SOX2 transcription. Inhibition is released by BERT, which then leads to transcription of SOX2 targets DKK1 and cMYC leading to differentiation. Brackets denote $\log_2$ FC from HH29 sequencing. Mechanism adapted from Papanayotou et. al. (2008).

### 5.5.5 Possible link with epicardium

A possible increase in myosin at the epicardium was seen in 2 out of 5 OFT-banded hearts at HH35. An increase in overall myosin brought about by increased αMHC in cells derived from the porcine epicardium has been seen previously (Duboscq-Bidot et al., 2009). It was found that these cells had faster rates of stretch activation and force redevelopment when compared to cells derived from the endocardium. It perhaps be expected then to see increased MHC signal at the epicardium in all hearts. Any additional increase in MHC at the epicardium could be to try to further improve force development, as in our OFT-banded hearts to maintain cardiac output. However, further experiments with more hearts would be needed to confirm this. Also at the epicardium, a reduction in *TBX18* was visibly seen in OFT-banded hearts compared to SHAMS. This data was used to gain a further research grant to investigate vascularisation and particularly coronary vessel formation, as TBX18 has been found to be a key gene involved with the development of the epicardium and coronary vessels (Chen et al., 2014).

### 5.5.6 *ANKRD1* in OFT-banded hearts

In the knockdown chapter of this thesis, Ankyrin proteins were highlighted as possibly being important players in terms of reacting to stress and effecting conduction gene expression. *ANKRD1* has been found to be up regulated in haemodynamically altered hearts using transverse aortic constriction (TAC), and *ANKRD1* was found to be required for hypertrophy in these hearts as silencing of *ANKRD1* with short hairpin RNAs inhibited hypertrophy (Chen et al., 2014). ANKRD1 has also been implicated as a causative gene in human dilated cardiomyopathy, with patients showing mutations for *ANKRD1* having increased hypertrophy (Duboscq-Bidot et al., 2009). The results from sequencing reveal *ANKRD1* to have no differential regulation at all between OFT-banded and SHAM statistically, with a *p*-value of 0.35. However, analysis of the FPKM values reveals something maybe going on. FPMK values for OFT-banded are: 29.13,

27.41 and 197.97; mean: 84.84. FPKM values for SHAM were: 23.08, 19.91, and 11.65, mean: 18.21. All OFT-banded hearts clearly have higher expression of *ANKRD1* when compared to SHAM. However, it is impossible to get significance when there is such variation within the OFT-banded samples. When the high OFT banded FPKM result is removed (197.97), the increased expression of ANKRD1 has a very close to significant *p*-value of 0.06, this is with just n=2, and power calculations showed an n of 6 should be used to avoid false negatives. Interestingly, *ANKRD1* expression has been shown to be affected by AMPK (Wang et al., 2015). When the heart is placed under stress, a normal response of AMPK is to phosphorylate the transcriptional co-activator Yes-associated protein (YAP) (Wang et al., 2015). This leads to YAP leaving the nucleus and thus *ANKRD1* expression is reduced (Wang et al., 2015). Our possible reduction in AMPK activation could lead to YAP accumulation in the nucleus causing increased expression of *ANKRD1*.

### 5.5.7 Cardio-protection

The majority of differentially regulated genes analysed, with the possible exception of a few genes - particularly *PRKAG3*, appear to give cardio-protective qualities. As our model is inducing a phenotype on embryonic hearts, it could be expected then that gene expression will be to try and correct for the increased stress placed on the system. There were many genes in the top 200 differentially regulated genes that would appear to be cardio-protective such as Phospholamban (*PLN*) (mechanism involving PLN shown in Figure 6.12) that were not analysed as they were outside of corrected significance. PLN deletion mutation has been linked to dilated cardiomyopathy with enlargement of the left ventricle and ventricular arrhythmias (Karakikes et al., 2015). Our OFT-banded PLN showed an up regulation of 0.35 $\log^2$ (RT-qPCR not carried out for PLN). Therapeutic opportunities could arise from these cardio-protective genes, as if hearts presenting cardiomyopathy could be induced to express these genes a reduction in phenotype may be seen.

### 5.5.8 Transcript variant and differentially regulated gene ontology highlight AMPK associated pathways

As described in detail in the methods chapter, transcripts were sequenced from both ends. This allowed variation in gene transcript expression to be analysed. This analysis took place after the initial study of differential gene expression had taken place, but reassuringly transcripts identified belonged to pathways already highlighted by differential gene expression. STRING functional protein association networks were used for analysis (figure 6.16 and table 6.5). Genes taken for STRING analysis were all significant genes ($p$ = <0.05) from differentially regulated genes and transcript variant results. Taken together, analysis allowed identification of potential molecular pathways implicated from sequencing results. STRING results must be viewed with caution however, as a relationship between 2 genes identified by STRING does not necessarily mean the 2 genes are functionally related - they could simply be mentioned in the same journal paper. However the STRING results identify the main molecular pathway implicated in all sequencing results is the AMPK signaling pathway, with *PRKAG3* involved in 4 of the top 10 molecular pathways identified (table 6.5). Interestingly, if PRKAA2 (the catalytic subunit of AMPK that is regulated by *PRKAG3*) is included in the pathway/database analysis, hypertrophic cardiomyopathy is also identified. This backs up the interactions already identified in this thesis showing our model has an effect on energy metabolism, and, is a possible, but yet to be proved, model for cardiomyopathy /glycogen storage cardiomyopathy.

### 5.5.9 Structural gene expression and effect on conduction

As already highlighted in chapter 4, we do not have significant differentiation of fetal gene program genes such as βMHY (Taegtmeyer et al., 2010, Ames et al., 2013), and other structural genes. However analysis of sequencing FPKM levels at HH29 does show small differences in some expected genes. It could be that at later stages of development these small differences become more prominent with a heart becoming

increasing enlarged to the point of failure. The KD project (see chapter 3) highlighted structural genes and their effect on conduction genes possibly brought about by Z-disc disruption. Sequencing shows small (insignificantly in all cases talked about here, see table 5.7 in chapter 5) up regulation to βMHY and down regulation to α*MYH*, as is often seen in cardiomyopathy and cardiac dieses/failure (Krenz and Robbins, 2004, Nakao et al., 1997). The structural gene dystrophin (*DMD*) expressed at the Z-discs in βMHY and α*MYH* tissue shows a down regulation in all OFT-banded hearts. This gene is in turn expressed with Nitric oxide synthase (*NOS*) that also shows a down regulation in the data set. NOS catalyses Nitric oxide (NO) which regulates $Ca^{2+}$ flux in both basal and high stress states and prevents arrhythmias (Reilly et al., 2016, Masuda et al., 2009). If the expression pattern seen here continues and increases with development of the OFT-banded hearts, conduction phenotypes could be expected to develop, as, as was noted in the KD chapter 3, repression of dystrophin expression leads to altered distribution of NOS localisation, which subsequently leads to reduced NO (Reilly et al., 2016). This subsequently led to shortened AP together with no rate-dependent adaptation of the action potential duration, thus the heart would not be able to respond correctly to stress (Reilly et al., 2016). Their phenotype was brought about by over expression of mircoRNA miR-31. Short reads cannot be analysed by conventional RNA sequencing so no information can be gained on this in our sequencing, but, in our case, it is likely that alteration of structural gene expression in response to pressure overload would be causative of the effect. This chain of events started by disruption/down regulation of *DMD* could be the reason arrhythmias are seen in dilated cardiomyopathy in patents with muscular dystrophy, however, before continuing any research in this key area, analysis of the highlighted genes at HH35, as well as RT-qPCR analysis with n=6 to avoid false negatives at HH29 is necessary to see if significant differential expression exists.

### 5.5.10 Implications of OFT-banded gene profile on potential therapies

A mechanism is shown in Figure 5.16 where 3 genes highlighted in this study as being significantly differentially regulated at HH29 and increasingly so and HH35 in OFT-banded hearts are linked to the same inhibition step in terms of their effect on the

heart. That is, the reduction of the potential negative effect of *PRKAG3* and beneficial effects of both *PVALB* and *S1001A1* could be gained by manipulation of protein phosphatase (PP1) inhibition. Research on PP1 in hamster models has shown improved contractility and reduced chamber size on PP1 inhibition which in turn then does not inhibit *PLN* (Yamada et al., 2006). A drug currently under trial for heart failure called Carfostin utilises this by delivering protein phosphatase-1 inhibitor-1 (I-1) to the heart (Therapeutics, 2016). This drug could be ideally suited for the treatment of glycogen storage cardiomyopathy as an inhibited glycogen synthase will synthesize less glycogen and strengthen contraction, but it isn't yet being used for this purpose. The improved calcium cycling during diastole by reduction of inhibition on SERCA should not worsen any effect of pre-excitation often seen in glycogen storage cardiomyopathy as ryanodine receptors that initiate contraction are not affected, and over expression of I-1 has not been found to cause any debilitating effects (Wittkopper et al., 2011). This therapy is somewhat controversial though as some data suggest I -1 should be therapeutically reinforced and some suggest it should be inhibited (Wittkopper et al., 2011). It is possible that this is down to different genes being affected in individual cases of cardiomyopathy, for instance glycogen storage cardiomyopathy has its specific gene profile. This shows the importance of gene testing for cardiomyopathy to get the correct treatment, rather just looking at external phenotypes, e.g testing a patient for *PRKAG3* mutation.

There could be a potential for future gene therapy work on identified genes of interest. Adeno-associated viral vectors (AAV) have been used successfully in the mouse neonate and been shown to have long lasting effects and lead to correction of mutated genes (Waddington et al., 2004). Directly targeting the specific genes highlighted from sequencing data that the I-1 treatment could be correcting/reinforcing. For instance, *PRKAG3* could be delivered to the heart via AAV. It is possible that this single gene could reverse the cardiomyopathic phenotype. If this could be administered straight after birth or even during fetal development then lasting correction could be gained (Wittkopper et al., 2011, David and Peebles, 2008). Indeed, a postnatal study in the mouse found that suppression of a PRKAG2 transgene lead to lower glycogen content and recovery of the cardiomyopathy phenotype seen (Wolf et al., 2008). Clearly gene

therapy for cardiomyopathy has the potential to be the most effective treatment available and further work on animal and animal culture models with selected genes is needed.

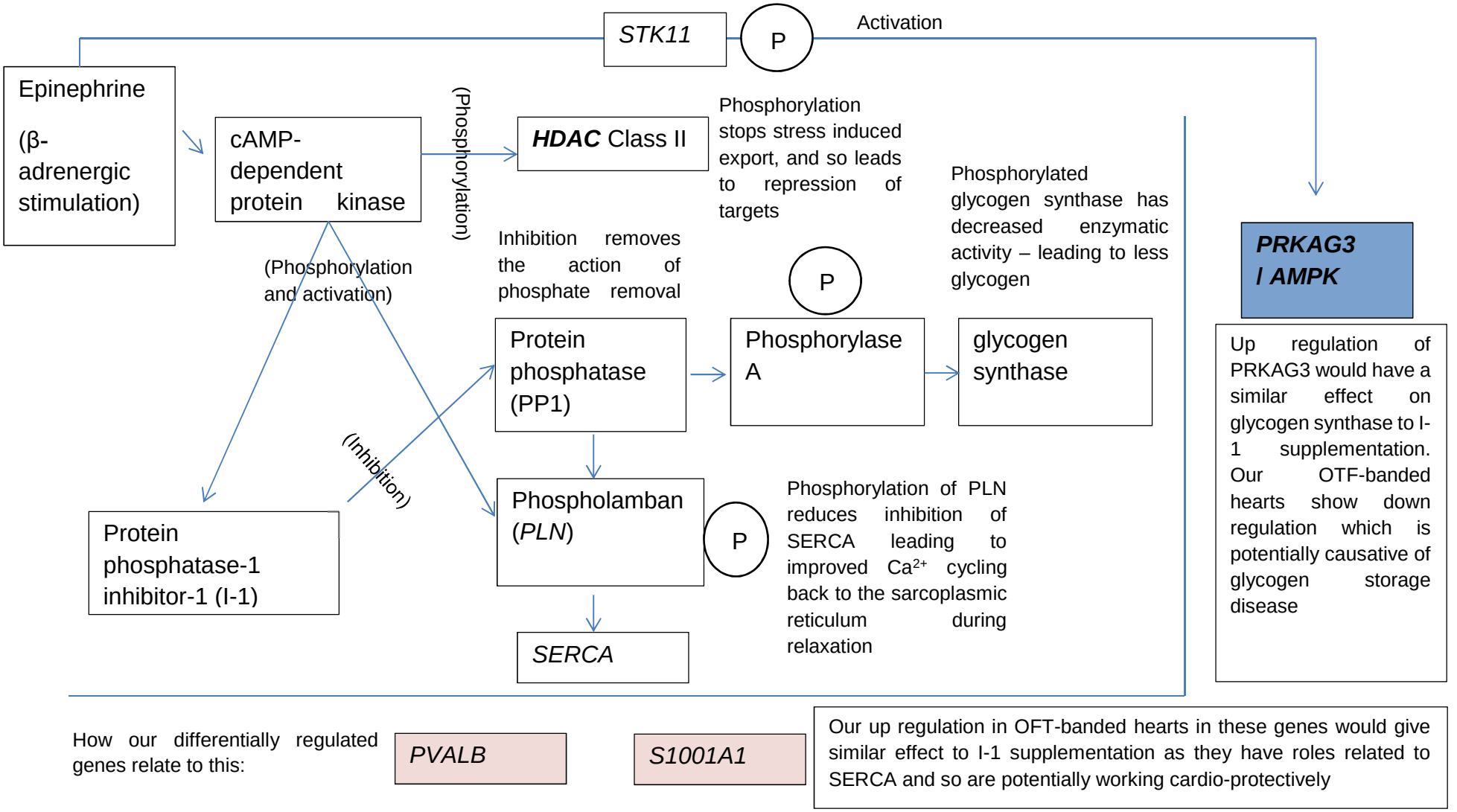



**Figure 5.15** Gene overview. Links in our differentially regulated genes and involvement to possible gene therapy targets highlighted in our study, *PRKAG3*, *PVALB* and *S1001A1*, in stimulatory regulation pathways of contractility and glycogen storage/breakdown.

# Chapter 6 General discussion

A huge amount of time and effort on this project has gone into optimisation procedures. Be that depleting globin from samples to allow sequencing of OFT-banded hearts, setting up and optimising analysis techniques in the lab such as in-situ hybridisation and RT-qPCR, or growing beating colonies of cardiomyocytes on glass slides. With these techniques and model systems in place, data was obtained across the 2 aspects of this thesis, that is, how conduction and structure are related in the myosin KD model and in an OFT-banded model.

Structural heart defects and abnormal heart hemodynamics are known to effect conduction (Schonberger and Seidman, 2001, Messina et al., 1997). A study of 193 human fetuses identified as having cardiac abnormalities analysed structural and arrhythmia disorders (Eronen, 1997). It found that 67% of fetuses identified with structural defects were fatal, whereas only6 5% identified with arrhythmias alone were fatal; however, when structural and arrhythmia defects were present together, 75% of cases were fatal (Eronen, 1997). This demonstrates the importance of understanding the interaction of structure and conduction. The aim of our study of myosin heavy chain structural protein KD, and alteration in haemodynamics, is to try and elucidate molecular mechanisms involved in the model systems, particularly with respect to the conduction system. This originated from previous studies in our laboratory and the literature, where myosin KD has led to unexplained $Ca^{+2}$ transients and action potentials in the chick heart (Rutland et al., 2011), and altered haemodynamics and conduction abnormalities are associated with cardiomyopathy (Clark et al., 1989). Further, hemodynamic alteration models have shown severe cardiac malformations such as, ventricular septal defect, precious conduction patterns and heart enlargement brought about by increased stress and myocardial stiffness (Reckova et al., 2003, Chivukula et al., 2016, Sedmera et al., 1999, Tomanek et al., 1999, Miller et al., 2003a). Sequencing of OFT-banded hearts showed that alteration of haemodynamics via pressure-overloading resulted in differential regulation of conduction, regulatory,

transport and metabolic genes; however, this thesis focuses its attention on conduction, and genetic pathways that may influence conduction.

In the adult, cardiac contractility is dependent on the expression of 2 myosin heavy chain (MHC) genes – fast twitch alpha myosin heavy chain (αMHC) and slow twitch beta myosin heavy chain (βMHC) (van Rooij et al., 2007). Though both are present in the developing embryo, αMHC is up-regulated postnatally whereas βMHC is upregulated embryonically (van Rooij et al., 2007). Postnatally βMHC is greatly reduced in the atrium, becoming mainly expressed in the ventricle, whereas αMHC is mainly found in the atrium (van Rooij et al., 2007, Rutland et al., 2009, Rutland et al., 2011, van Rooij et al., 2009). This would appear to correlate with findings in this thesis where α*MYH* KD was found to have the lowest effect on differential gene expression in embryonic hearts, and β*MYH* KD effected the structure of embryonic atrial cultures. However, what was also clear was that both αMHC and βMHC are necessary for normal development of sarcomeres in the atria and ventricles of the developing chick embryo, as KD of both led to immature sarcomere structure at the Z-disc. Interestingly, the cardiac myosin heavy chain genes have been found to have a regulatory effect on each other. The genes encoding αMHC and βMHC have been found to have miRNA expressed from their intronic regions (van Rooij et al., 2009, van Rooij et al., 2007). That is, the expression of one has an effect on the other. Though this is a new area of research and much is yet to be known about intron regulation, it has been found that expression of the α*MYH* intron coding for the microRNA miRNA-208, when coupled with haemodynamic stress, led to increased expression of βMHC in the post-natal mouse (van Rooij et al., 2009). Patients with human dilated cardiomyopathy identified with high levels of βMHC were also found to have raised levels of miRNA-208 (Satoh et al., 2010). Whether or not these miRNA are expressed embryonically is yet to be clarified, however, with regard to our KD project it is reassuring to know these regulatory areas are expressed via myosin gene intons, and thus would not be effected by our morpholino which function via post-transcriptional KD. Our sequencing of hemodynamically altered OFT-banded hearts unfortunately was not able to assess levels of miR-208 as it was not included in the data set. Of the miRNA that were present in the data set, FPKM levels were very low, from 0 – 1 FPKM and so would

have been below threshold for analysis. In the future, if miRNA like miR-208 were to be analysed by sequencing, it would require a targeted sequencing approach using microRNA sequencing (miRNA-seq) that allows short reads to be analysed. More recently embryonic myosin heavy chain (eMHC) has been shown to be vital for embryonic development. The human gene for eMHC, *MYH*3, is expressed during fetal development, but not after birth (Rutland et al., 2011). In the chick, expression in the developmental heart has been confirmed (Rutland et al., 2011). KD of all 3 myosins (αMHC, βMHC and eMHC) led to disrupted intracellular $Ca^{2+}$ levels and an increased duration of action potential (AP) was seen eMHC KDs (Rutland et al., 2011). Our KD of αMHC, βMHC and eMHC revealed immature sarcomeres across all groups in atrial and ventricular cultured colonies and shows the importance of all three myosin heavy chain genes in the development of the heart. How KD of these myosin genes could affect the expression of conduction genes was investigated by targeting the analysis of genes that could possibly cause the previously observed $Ca^{2+}$ transients and increased AP duration. HCN4, a potassium/sodium hyperpolarization-activated cyclic nucleotide-gated channel was found to be significantly down regulated in eMHC KD and, though to a lesser extent, also in βMHC KDs. This could account for a possible increased AP duration as potentially less potassium/sodium would be present to depolarise the cell. What is causing this down regulation remains unclear; however, a link between structure and membrane conduction channels may be present. One gene known to organise membrane conduction channels is ankyrin gene ANKB, and ANB disruption has been correlated with a down regulation of HCN4 (Bennett and Healy, 2009). ANKB expression is at the M-line in the SAN region and so an immature sarcomere structure could be expected to disrupt ANKB and therefore lead to the down regulation of membrane conduction channels such as *HCN4*.

Our structural abnormalities within sarcomere architecture could be the primary cause for the conduction phenotype previously seen in KDs. The disruption/immaturity of the sarcomere Z-discs in KDs would be expected to affect key structures at the Z-disc involved in sarcomere contractility. T-tubules and dystrophin are located to Z-discs (Orr et al., 2016, Reilly et al., 2016), and these structures have been found to affect

AP travelling along the sarcolemma across the heart, and $Ca^{2+}$ flux in basal and stress conditions in to myocytes respectively (Orr et al., 2016, Masuda et al., 2009, Meng et al., 1996). The knockdown experiment stressed the heart by reducing contractile element expression. Myosin heavy chain expression has also been altered by stressing the heart mechanically in models that alter heamodynamics (Tobita et al., 2005), where haemodynamic load was found to moderate myofiber architecture. One such haemodynamic alteration model used OFT-banding and found this led to a precocious conduction phenotype where an apex to base conduction pattern was seen early in banded hearts (Reckova et al., 2003). OFT-banded models already exist in the chick and have been shown to alter haemodynamics by increasing blood velocity and ventricular blood pressure and thus impose higher shear stress on the heart (Chivukula et al., 2016, Sedmera et al., 1999, Tomanek et al., 1999, Miller et al., 2003a). Though other models exist, never before has whole genome analysis been carried out on whole hearts in the developing chick embryo at a stage when the SAN has just formed and the conduction shift from immature to apex to base is about taking place. The OFT-banding procedure in our lab was optimised, and initial anatomical phenotype defined, by Dr. Pang, and though I have successfully performed the technique, for consistency, Dr. Pang performed all OFT-banding on hearts used in this thesis. Our OFT-banded phenotype was defined via stereological analysis, and showed an increase of ventricular lumen and thinner myocardium in the left chamber; this effect was also seen in the left atrium (Dr. Pang, Personal communication). This dilatation of the left ventricle was significant; however, an insignificantly increased lumen was also present in the right ventricle. Trabeculae were significantly reduced in both ventricles and the epicardium was thickened throughout (Dr. Pang, Personal communication). Reduced apoptosis was seen in the ventricle, which corresponds to the slight decrease I observed in the atria. A phenotype was also present in the mitral valve region where smaller and dysmorphic mitral valve primordia were seen (Dr. Pang, Personal communication). An aberrant expression of a shear stress responsive genes and extracellular matrix markers were also observed in the endocardial cushions (Dr. Pang, Personal communication). Together, these data suggest that altering the blood flow can have an effect on a range of structures in the developing heart.

Upon whole genome analysis, our OFT-banded model highlighted a number of $Ca^{2+}$ sequestering EF-hand genes involved in conduction and contractility in the heart. Two key genes, parvalbumin (*PVALB*) and S100 calcium-binding protein A11 (*S100A11*) showed significant up regulations in OFT-banded hearts at HH29 and increasingly so at HH35. *PVALB*, found in myocyte cytoplasm is involved with returning $Ca^{2+}$ to the sarcoplasmic reticulum following contraction and thus allowing repolarisation (Cheung et al., 2000, Vongvatcharanon et al., 2008). It has been found up regulated in high stress animal systems (Mutryn et al., 2015). S100A11 is expressed at internal cell membranes and at z-discs (Arcuri et al., 2002). S100A11 is co-expressed with S100A1 and this gene also showed an up regulation, though insignificant in our OFT-banded hearts. S100A1 has been linked with reduced left ventricular contractility following aortic constriction (Du et al., 2002). As highlighted in the discussion of Chapter 5, our induced hemodynamic alteration model has brought a differential expression pattern that appears to deliver cardio-protection against the physiological alteration. The PVALB and the S100 genes represent this. Their over expression would be expected to increase heart rate by decreasing repolarisation time. However, an unaltered heartbeat is usually seen in OFT-banded models in the literature, where cardiac output has also been found unaltered (Steinberg and Kemp, 2009, McQuinn et al., 2007, Tobita et al., 2002, Clark et al., 1989). Bradycardia and delayed repolarisation are often seen in dilated cardiomyopathy (Reckova et al., 2003), and it is likely that our increased expression of *PVALB* and the S100 genes is to counter-act the potential slower beating rate of our dilated heart OFT-banded hearts.

Genes usually associated with cardiomyopathy, such as structural genes α*MYH*, which normally show downregulation, and β*MYH*, which normally show up regulation (Blair et al., 2001), were not significantly altered in our model; though a small down regulation was found in α*MYH* and a small up regulation was in β*MYH*. Another structural gene associated with α*MYH* and β*MYH* that also showed small down regulation is dystrophin (DMD), and an enzyme dystrophin is in complex with, Nitric oxide synthase (*NOS*) showed a similar down regulation. Values were insignificant because of variation between samples, and power analysis showed that n=6 should be used in order to avoid false positives. Though insignificant by sequencing, further

work by RT-qPCR should be carried out with an n=6. Down regulation of NOS has been seen to lead to shortened AP together with no rate-dependent adaptation of the action potential duration, thus altered response to stress and arrhythmias could be induced (Reilly et al., 2016). It could be that at later stages of the OFT-banded model a more prevalent differential regulation of these genes exists, as would be expected as the heart adapts to the increased stress, so RT-qPCRs could be carried out at HH29 and HH35. Analysis of these structurally associated proteins would also be informative in the myosin heavy chain KD embryos, as disruption to these proteins could be causative the conduction disruption seen. Analysis of protein and/or expression on sections through the heart by immunocytochemistry and *in situ* hybridisation, followed by RT-qPCR quantitation if necessary could be used.

Whether our model is inducing the early stages of cardiomyopathy is yet to be proven. This thesis proposes that our model could be inducing the early stages of glycogen storage cardiomyopathy, as our heart's anatomical phenotype resembles that of glycogen storage cardiomyopathy, with no fibrosis and a dilated left ventricle. The regulatory subunit of key metabolic control enzyme AMPK in our chick hearts, *PRKAG3*, is significantly down regulated at HH29 and to a greater extent at HH35. Mutation to the regulatory units of AMPK has been found to be causative of glycogen storage cardiomyopathy (Blair et al., 2001). Glycogen storage cardiomyopathy has previously been induced by mutations to the adult mouse AMPK regulator PRKAG2 (Wolf et al., 2008), but to this authors knowledge never has it been seen/proposed to be induced by changes to haemodynamics. In future studies, glycogen content within our hearts must be measured, but if increased, our OFT-banded hearts will be an invaluable model for the study of glycogen storage cardiomyopathy.

## 6.1 hypothesis and commonality between chapters

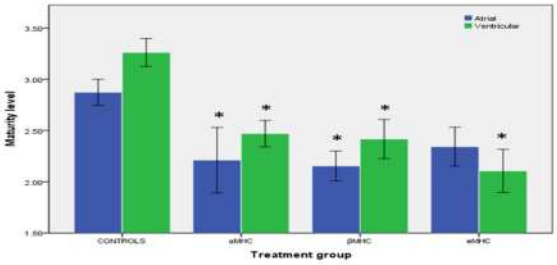
The main thesis hypothesis of ‘’Alteration in heart structural genes or structure itself induced by gene expression manipulation or physical stress will have no effect on the cardiac conduction system’’ can be rejected as KD led to down regulation of key SAN depolarising current gene *HCN4*, and OFT-banding led to up regulation of conduction genes, such as the $Ca^{2+}$ sequestering *S100A11* and *PVALB* genes.

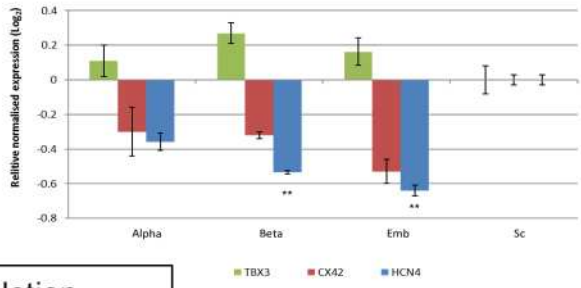
Each section of this thesis answered different questions (see figure 6.1 for overview). The first part was the knock-down project that analysed the effect of myosin heavy chain knock down in the developing chick embryo. A reduction in sarcomere maturity was found along with significant reduction in the ion channel *HCN4*. The reduced ion channel expression could be involved in the conduction phenotype previously seen in myosin heavy chain KDs. Reasons for the down regulation of this gene, though only hypothesised, are based on findings that proteins bound together can be affected by their binding partners and that the structure of the membrane to which they are bound may be altered by the reduced maturity of sarcomeres. Indeed, channelopathies have been associated with myocardial structural abnormalities such as dilated cardiomyopathy and a similar affect could be happening with *HCN4* (Towbin, 2014b). Backing this up, it has been seen that mutations to *HCN4* are found in patients with non-compaction cardiomyopathy where *HCN4* is associate with structural abnormalities of the myocardium, and (Towbin, 2014b, Milano et al., 2014). It would seem likely then that sarcomere maturity may have an effect ion channel expression, though as previously stated, follow up work is required. The effect of sarcomere structure and its knock-on effects brings us on to the next part of the thesis where the OFT-banding model was used to stress the sarcomere rather than knocking down its structural components. The induction of a dilated cardiomyopathy like phenotype that followed allowed global genetic analysis with RNA sequencing. Sequencing revealed a differentially regulated gene profile of 30 significantly regulated genes. This project focused and pathways that can have a multitude of effects, including the conduction system. It was found that $Ca^{2+}$ sequestering genes, such as *S100A11* and *PVALB* were up regulated. This would be expected to increase hearts rate, so, it is likely a

cardioprotective response by the heart to try to maintain heart rate. A metabolic pathway would appear to be affected also as the regulatory unit (*PRKAG3*) of the metabolic master switch AMPK is down regulated. The effect of this can be theorised by looking at genes/pathway interactions from the differentially regulated gene profile. This implicates the AMPK signaling pathway. Disruption to AMPK activity/associated pathways could be causative of glycogen storage cardiomyopathy where the heart starts to fail because of glycogen build up and responds with overexpression of certain cardiomyopathy markers. It is also possible that it could have a cardioprotective function, as less activation of AMPK could lead to less phosphorylation and there-for less removal of HDACs from the nucleus. This could lead to less expression of genes like myosin heavy chain. It is possible this could be in a response to limit over expression of myosin genes often seen cardiomyopathy such as β*MYH*. Again, as previously mentioned, future work with our OFT-banded model is now needed to elucidate if increased glycogen storage is taking place or if HDACs are reduced in the nucleus.

Knockdown project

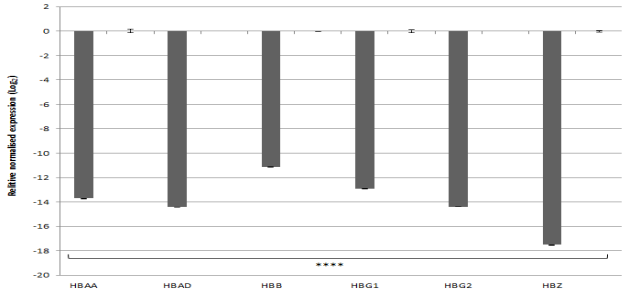
Significant reduction found in sarcomere maturity. This reduction in structural maturity may be linked to phenotypes such as channelopathies and non-compaction cardiomyopathy. Ion channel membrane protein HCN4 is seen significantly down regulated




Library preparation –globin depletion

To gain reliable results for low reads via mRNA sequencing, library preparation had to be optimised. This included depletion of 6 haemoglobin genes that were identified with high expression in the chick embryo. mRNA from these genes was removed with expression levels of around 0.0005% to that of before treatment




OFT banding mRNA sequencing

Sequencing revealed differentially regulated genes. $Ca^{2+}$ sequestering genes show up regulation with a hypothesised cardioprotective effect to maintain heart rate. It would also appear that AMPK signalling could be affected, this could lead to a multitude of effects from glycogen storage to reduction in myosin expression

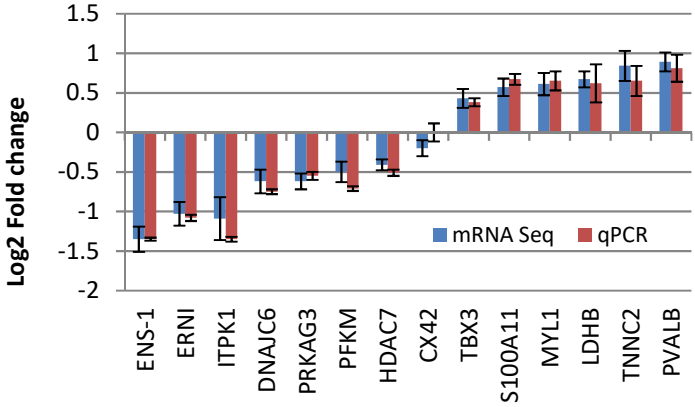



**Figure 6.1** Overview of thesis findings and how sections work together.

## 6.2 Conclusions

The maturity of sarcomere structure is affected by myosin heavy chain gene KD in the embryonic chick heart. This shows that correct expression of both αMHC and βMHC, and also eMHC is necessary to form mature sarcomere structure in the embryo. Knock down also lead to reductions in membrane ion channels. The reduced maturity of sarcomeres could be having an effect on the expression of the membrane ion channels, potentially by the disruption of organiser proteins, and could also potentially disrupt key structures located at the sarcomere Z-disc that are needed for AP generation and transmission of the signal. This suggests the correct expression of key structural proteins is required not just for cardiac structure, but also for conduction gene expression. Further, the optimisation of the library preparation processes for low read sequencing in OFT-banded hearts allowed the identification of differentially regulated genes in the stressed heart. The majority of these genes appear have a cardioprotective function. Calcium sequestering proteins are up regulated and potentially their over expression could maintain cardiac output. Therapies that would induce the same action of these genes have the potential to aid in the treatment of cardiomyopathies and now require further investigation. Of particular interest was the differential expression of the regulatory subunit of metabolic control enzyme AMPK that could potentially induce glycogen storage cardiomyopathy in our OFT-banded hearts. In conclusion, understanding how blood flow can affect the developing heart might provide insights into the causes of many structural and conduction defects which currently have an unknown etiology.

## References


ACKERMAN, M. J., PRIORI, S. G., WILLEMS, S., BERUL, C., BRUGADA, R., CALKINS, H., CAMM, A. J., ELLINOR, P. T., GOLLOB, M., HAMILTON, R., HERSHBERGER, R. E., JUDGE, D. P., LE MAREC, H., MCKENNA, W. J., SCHULZE-BAHR, E., SEMSARIAN, C., TOWBIN, J. A., WATKINS, H., WILDE, A., WOLPERT, C. & ZIPES, D. P. 2011. HRS/EHRA expert consensus statement on the state of genetic testing for the channelopathies and cardiomyopathies this document was developed as a partnership between the Heart Rhythm Society (HRS) and the European Heart Rhythm Association (EHRA). *Heart Rhythm,* 8**,** 1308-39.

ALLAN, L. D., CRAWFORD, D. C., ANDERSON, R. H. & TYNAN, M. 1985. Spectrum of congenital heart disease detected echocardiographically in prenatal life. *Br Heart J,* 54**,** 523-6.

ALLISON, D. B., CUI, X., PAGE, G. P. & SABRIPOUR, M. 2006. Microarray data analysis: from disarray to consolidation and consensus. *Nat Rev Genet,* 7**,** 55-65.

AMES, E. G., LAWSON, M. J., MACKEY, A. J. & HOLMES, J. W. 2013. Sequencing of mRNA identifies re-expression of fetal splice variants in cardiac hypertrophy. *J Mol Cell Cardiol,* 62**,** 99-107.

ANDERS, S. & HUBER, W. 2010. Differential expression analysis for sequence count data. *Genome Biol,* 11**,** R106.

ANDERSEN, C. L., JENSEN, J. L. & ORNTOFT, T. F. 2004. Normalization of real-time quantitative reverse transcription-PCR data: a model-based variance estimation approach to identify genes suited for normalization, applied to bladder and colon cancer data sets. *Cancer Res,* 64**,** 5245-50.

ANDERSON, R. H., BROWN, N. A. & MOORMAN, A. F. 2006. Development and structures of the venous pole of the heart. *Dev Dyn,* 235**,** 2-9.

ANDO, K., NAKAJIMA, Y., YAMAGISHI, T., YAMAMOTO, S. & NAKAMURA, H. 2004. Development of proximal coronary arteries in quail embryonic heart: multiple capillaries penetrating the aortic sinus fuse to form main coronary trunk. *Circ Res,* 94**,** 346-52.

ANTZELEVITCH, C., POLLEVICK, G. D., CORDEIRO, J. M., CASIS, O., SANGUINETTI, M. C., AIZAWA, Y., GUERCHICOFF, A., PFEIFFER, R., OLIVA, A., WOLLNIK, B., GELBER, P., BONAROS, E. P., JR., BURASHNIKOV, E., WU, Y., SARGENT, J. D., SCHICKEL, S., OBERHEIDEN, R., BHATIA, A., HSU, L. F., HAISSAGUERRE, M., SCHIMPF, R., BORGGREFE, M. & WOLPERT, C. 2007. Loss-of-function mutations in the cardiac calcium channel underlie a new clinical entity characterized by ST-segment elevation, short QT intervals, and sudden cardiac death. *Circulation,* 115**,** 442-9.

ARAD, M., MARON, B. J., GORHAM, J. M., JOHNSON, W. H., JR., SAUL, J. P., PEREZ-ATAYDE, A. R., SPIRITO, P., WRIGHT, G. B., KANTER, R. J., SEIDMAN, C. E. & SEIDMAN, J. G. 2005. Glycogen storage diseases presenting as hypertrophic cardiomyopathy. *N Engl J Med,* 352**,** 362-72.

ARAD, M., MOSKOWITZ, I. P., PATEL, V. V., AHMAD, F., PEREZ-ATAYDE, A. R., SAWYER, D. B., WALTER, M., LI, G. H., BURGON, P. G., MAGUIRE, C. T., STAPLETON, D., SCHMITT, J. P., GUO, X. X., PIZARD, A., KUPERSHMIDT, S., RODEN, D. M., BERUL, C. I., SEIDMAN, C. E. & SEIDMAN, J. G. 2003. Transgenic mice overexpressing mutant PRKAG2 define the cause of Wolff-Parkinson-White syndrome in glycogen storage cardiomyopathy. *Circulation,* 107**,** 2850-2856.

ARCURI, C., GIAMBANCO, I., BIANCHI, R. & DONATO, R. 2002. Subcellular localization of S100A11 (S100C, calgizzarin) in developing and adult avian skeletal muscles. *Biochim Biophys Acta,* 1600**,** 84-94.

ARGUELLO, C., ALANIS, J. & VALENZUELA, B. 1988. The early development of the atrioventricular node and bundle of His in the embryonic chick heart. An electrophysiological and morphological study. *Development,* 102**,** 623-37.

ASCHENBACH, W. G., HIRSHMAN, M. F., FUJII, N., SAKAMOTO, K., HOWLETT, K. F. & GOODYEAR, L. J. 2002. Effect of AICAR treatment on glycogen metabolism in skeletal muscle. *Diabetes,* 51**,** 567-73.

BACKS, J. & OLSON, E. N. 2006. Control of cardiac growth by histone acetylation/deacetylation. *Circ Res,* 98**,** 15-24.

BAKKER, M. L., BOINK, G. J., BOUKENS, B. J., VERKERK, A. O., VAN DEN BOOGAARD, M., DEN HAAN, A. D., HOOGAARS, W. M., BUERMANS, H. P., DE BAKKER, J. M., SEPPEN, J., TAN, H. L., MOORMAN, A. F., T HOEN, P. A. & CHRISTOFFELS, V. M. 2012. T-box transcription factor TBX3 reprogrammes mature cardiac myocytes into pacemaker-like cells. *Cardiovasc Res,* 94**,** 439-49.

BAKKER, M. L., BOUKENS, B. J., MOMMERSTEEG, M. T., BRONS, J. F., WAKKER, V., MOORMAN, A. F. & CHRISTOFFELS, V. M. 2008. Transcription factor TBX3 is required for the specification of the atrioventricular conduction system. *Circ Res,* 102**,** 1340-9.

BARNES, B. R., MARKLUND, S., STEILER, T. L., WALTER, M., HJALM, G., AMARGER, V., MAHLAPUU, M., LENG, Y., JOHANSSON, C., GALUSKA, D., LINDGREN, K., ABRINK, M., STAPLETON, D., ZIERATH, J. R. & ANDERSSON, L. 2004. The 5'-AMP-activated protein kinase gamma3 isoform has a key role in carbohydrate and lipid metabolism in glycolytic skeletal muscle. *J Biol Chem,* 279**,** 38441-7.

BARTH, A. S., KUNER, R., BUNESS, A., RUSCHHAUPT, M., MERK, S., ZWERMANN, L., KAAB, S., KREUZER, E., STEINBECK, G., MANSMANN, U., POUSTKA, A., NABAUER, M. & SULTMANN, H. 2006. Identification of a common gene expression signature in dilated cardiomyopathy across independent microarray studies. *J Am Coll Cardiol,* 48**,** 1610-7.

BARYSHNIKOVA, O. K., ROBERTSON, I. M., MERCIER, P. & SYKES, B. D. 2008. The dilated cardiomyopathy G159D mutation in cardiac troponin C weakens the anchoring interaction with troponin I. *Biochemistry,* 47**,** 10950-60.

BASSO, C., CORRADO, D., MARCUS, F. I., NAVA, A. & THIENE, G. 2009. Arrhythmogenic right ventricular cardiomyopathy. *Lancet,* 373**,** 1289-300.

BELANGER, A. R., MILLER, M. A., DONTHIREDDI, U. R., NAJOVITS, A. J. & GOLDMAN, M. E. 2008. New classification scheme of left ventricular noncompaction and correlation with ventricular performance. *Am J Cardiol,* 102**,** 92-6.

BELLAIRS, R. & OSMOND, M. 2005. *The Atlas of Chick Development*, Elsevier.

BENARDEAU, A., HATEM, S. N., RUCKER-MARTIN, C., TESSIER, S., DINANIAN, S., SAMUEL, J. L., CORABOEUF, E. & MERCADIER, J. J. 1997. Primary culture of human atrial myocytes is associated with the appearance of structural and functional characteristics of immature myocardium. *J Mol Cell Cardiol,* 29**,** 1307-20.

BENNETT, V. & HEALY, J. 2009. Membrane domains based on ankyrin and spectrin associated with cell-cell interactions. *Cold Spring Harb Perspect Biol,* 1**,** a003012.

BERS, D. M. 2002. Cardiac excitation-contraction coupling. *Nature,* 415**,** 198-205.

BLAIR, E., REDWOOD, C., ASHRAFIAN, H., OLIVEIRA, M., BROXHOLME, J., KERR, B., SALMON, A., OSTMAN-SMITH, I. & WATKINS, H. 2001. Mutations in the gamma(2) subunit of AMP-activated protein kinase cause familial hypertrophic cardiomyopathy: evidence for the central role of energy compromise in disease pathogenesis. *Hum Mol Genet,* 10**,** 1215-20.

BLANC, S., RUGGIERO, F., BIROT, A. M., ACLOQUE, H., DECIMO, D., LERAT, E., OHLMANN, T., SAMARUT, J. & MEY, A. 2014. Subcellular localization of ENS-1/ERNI in chick embryonic stem cells. *PLoS One,* 9**,** e92039.

BLEEKER, W. K., MACKAAY, A. J., MASSON-PEVET, M., BOUMAN, L. N. & BECKER, A. E. 1980. Functional and morphological organization of the rabbit sinus node. *Circ Res,* 46**,** 11-22.

BOULLIN, J. & MORGAN, J. M. 2005. The development of cardiac rhythm. *Heart,* 91**,** 874-5.

BOWLES, N. E., BOWLES, K. R. & TOWBIN, J. A. 2000. The "final common pathway" hypothesis and inherited cardiovascular disease. The role of cytoskeletal proteins in dilated cardiomyopathy. *Herz,* 25**,** 168-75.

BOYETT, M. R. 2009. 'And the beat goes on.' The cardiac conduction system: the wiring system of the heart. *Exp Physiol,* 94**,** 1035-49.

BRAND, T. 2003. Heart development: molecular insights into cardiac specification and early morphogenesis. *Dev Biol,* 258**,** 1-19.

BRATTELID, T., WINER, L. H., LEVY, F. O., LIESTOL, K., SEJERSTED, O. M. & ANDERSSON, K. B. 2010. Reference gene alternatives to Gapdh in rodent and human heart failure gene expression studies. *BMC Mol Biol,* 11**,** 22.

BRESSAN, M. C., LOUIE, J. D. & MIKAWA, T. 2014. Hemodynamic forces regulate developmental patterning of atrial conduction. *PLoS One,* 9**,** e115207.

BRIEGEL, K. J., BALDWIN, H. S., EPSTEIN, J. A. & JOYNER, A. L. 2005. Congenital heart disease reminiscent of partial trisomy 2p syndrome in mice transgenic for the transcription factor Lbh. *Development,* 132**,** 3305-16.

BRILLANTES, A. M., BEZPROZVANNAYA, S. & MARKS, A. R. 1994. Developmental and tissue-specific regulation of rabbit skeletal and cardiac muscle calcium channels involved in excitation-contraction coupling. *Circ Res,* 75**,** 503-10.

BUDDE, B. S., BINNER, P., WALDMULLER, S., HOHNE, W., BLANKENFELDT, W., HASSFELD, S., BROMSEN, J., DERMINTZOGLOU, A., WIECZOREK, M., MAY, E., KIRST, E., SELIGNOW, C., RACKEBRANDT, K., MULLER, M., GOODY, R. S., VOSBERG, H. P., NURNBERG, P. & SCHEFFOLD, T. 2007. Noncompaction of the ventricular myocardium is associated with a de novo mutation in the beta-myosin heavy chain gene. *PLoS One,* 2**,** e1362.

BUFFINTON, C. M., FAAS, D. & SEDMERA, D. 2013. Stress and strain adaptation in load-dependent remodeling of the embryonic left ventricle. *Biomech Model Mechanobiol,* 12**,** 1037-51.

BUSCHMANN, I., PRIES, A., STYP-REKOWSKA, B., HILLMEISTER, P., LOUFRANI, L., HENRION, D., SHI, Y., DUELSNER, A., HOEFER, I., GATZKE, N., WANG, H., LEHMANN, K., ULM, L., RITTER, Z., HAUFF, P., HLUSHCHUK, R., DJONOV, V., VAN VEEN, T. & LE NOBLE, F. 2010. Pulsatile shear and Gja5 modulate arterial identity and remodeling events during flow-driven arteriogenesis. *Development,* 137**,** 2187-96.

BUSTIN, S. A. 2000. Absolute quantification of mRNA using real-time reverse transcription polymerase chain reaction assays. *J Mol Endocrinol,* 25**,** 169-93.

CAHILL, T. J., ASHRAFIAN, H. & WATKINS, H. 2013. Genetic cardiomyopathies causing heart failure. *Circ Res,* 113**,** 660-75.

CALESHU, C., SAKHUJA, R., NUSSBAUM, R. L., SCHILLER, N. B., URSELL, P. C., ENG, C., DE MARCO, T., MCGLOTHLIN, D., BURCHARD, E. G. & RAME, J. E. 2011. Furthering the Link Between the Sarcomere and Primary Cardiomyopathies: Restrictive Cardiomyopathy Associated With Multiple Mutations in Genes Previously Associated With Hypertrophic or Dilated Cardiomyopathy. *American Journal of Medical Genetics Part A,* 155a**,** 2229-2235.

CAMARGO, A. & AZUAJE, F. 2008. Identification of dilated cardiomyopathy signature genes through gene expression and network data integration. *Genomics,* 92**,** 404-13.

CAMPUZANO, O., BELTRAN-ALVAREZ, P., IGLESIAS, A., SCORNIK, F., PEREZ, G. & BRUGADA, R. 2010. Genetics and cardiac channelopathies. *Genet Med,* 12**,** 260-7.

CANNELL, M. B., CHENG, H. & LEDERER, W. J. 1995. The control of calcium release in heart muscle. *Science,* 268**,** 1045-9.

CARLSON, B. M. 2008. *Human Embryology and Developmental Biology*, Elsevier.

CARMELIET, E., VEREECKE, J 2002. *Cardiac Cellular Electrophysiology*, Springer.

CATTERALL, W. A., GOLDIN, A. L. & WAXMAN, S. G. 2005. International Union of Pharmacology. XLVII. Nomenclature and structure-function relationships of voltage-gated sodium channels. *Pharmacol Rev,* 57**,** 397-409.

CHAPMAN, B. S., TOBIN, A. J. & HOOD, L. E. 1980. Complete amino acid sequences of the major early embryonic alpha-like globins of the chicken. *J Biol Chem,* 255**,** 9051-9.

CHEN, C., SHEN, L., CAO, S., LI, X., XUAN, W., ZHANG, J., HUANG, X., BIN, J., XU, D., LI, G., KITAKAZE, M. & LIAO, Y. 2014. Cytosolic CARP promotes angiotensin II- or pressure overload-induced cardiomyocyte hypertrophy through calcineurin accumulation. *PLoS One,* 9**,** e104040.

CHEN, W., BACANAMWO, M. & HARRISON, D. G. 2008. Activation of p300 histone acetyltransferase activity is an early endothelial response to laminar shear stress and is essential for stimulation of endothelial nitric-oxide synthase mRNA transcription. *J Biol Chem,* 283**,** 16293-8.

CHENG, J., KAPRANOV, P., DRENKOW, J., DIKE, S., BRUBAKER, S., PATEL, S., LONG, J., STERN, D., TAMMANA, H., HELT, G., SEMENTCHENKO, V., PICCOLBONI, A., BEKIRANOV, S., BAILEY, D. K., GANESH, M., GHOSH, S., BELL, I., GERHARD, D. S. & GINGERAS, T. R. 2005. Transcriptional maps of 10 human chromosomes at 5-nucleotide resolution. *Science,* 308**,** 1149-54.

CHEUNG, P. C., SALT, I. P., DAVIES, S. P., HARDIE, D. G. & CARLING, D. 2000. Characterization of AMP-activated protein kinase gamma-subunit isoforms and their role in AMP binding. *Biochem J,* 346 Pt 3**,** 659-69.

CHING, Y. H., GHOSH, T. K., CROSS, S. J., PACKHAM, E. A., HONEYMAN, L., LOUGHNA, S., ROBINSON, T. E., DEARLOVE, A. M., RIBAS, G., BONSER, A. J., THOMAS, N. R., SCOTTER, A. J., CAVES, L. S., TYRRELL, G. P., NEWBURY-ECOB, R. A., MUNNICH, A., BONNET, D. & BROOK, J. D. 2005. Mutation in myosin heavy chain 6 causes atrial septal defect. *Nat.Genet.,* 37**,** 423-428.

CHIVUKULA, V. K., GOENEZEN, S., LIU, A. & RUGONYI, S. 2016. Effect of Outflow Tract Banding on Embryonic Cardiac Hemodynamics. *J Cardiovasc Dev Dis,* 3.

CHOI, I., BAO, H., KOMMADATH, A., HOSSEINI, A., SUN, X., MENG, Y., STOTHARD, P., PLASTOW, G. S., TUGGLE, C. K., REECY, J. M., FRITZ-WATERS, E., ABRAMS, S. M., LUNNEY, J. K. & GUAN LE, L. 2014. Increasing gene discovery and coverage using RNA-seq of globin RNA reduced porcine blood samples. *BMC Genomics,* 15**,** 954.

CHOI, O. R. & ENGEL, J. D. 1988. Developmental regulation of beta-globin gene switching. *Cell,* 55**,** 17-26.

CHOI, Y. H., COWAN, D. B., MORAN, A. M., COLAN, S. D., STAMM, C., TAKEUCHI, K., FRIEHS, I., DEL NIDO, P. J. & MCGOWAN, F. X., JR. 2009. Myocyte apoptosis occurs early during the development of pressure-overload hypertrophy in infant myocardium. *J Thorac Cardiovasc Surg,* 137**,** 1356-62, 1362 e1-3.

CHOU, Y. C., CHEN, R. L., LAI, Z. S., SONG, J. S., CHAO, Y. S. & SHEN, C. K. 2015. Pharmacological Induction of Human Fetal Globin Gene in Hydroxyurea-Resistant Primary Adult Erythroid Cells. *Mol Cell Biol,* 35**,** 2541-53.

CHRISTEL, C. J., CARDONA, N., MESIRCA, P., HERRMANN, S., HOFMANN, F., STRIESSNIG, J., LUDWIG, A., MANGONI, M. E. & LEE, A. 2012. Distinct localization and modulation of Cav1.2 and Cav1.3 L-type Ca2+ channels in mouse sinoatrial node. *J Physiol,* 590**,** 6327-42.

CHRISTOFFELS, V. M., HABETS, P. E., FRANCO, D., CAMPIONE, M., DE JONG, F., LAMERS, W. H., BAO, Z. Z., PALMER, S., BIBEN, C., HARVEY, R. P. & MOORMAN, A. F. 2000a. Chamber formation and morphogenesis in the developing mammalian heart. *Dev.Biol.,* 223**,** 266-278.

CHRISTOFFELS, V. M., KEIJSER, A. G., HOUWELING, A. C., CLOUT, D. E. & MOORMAN, A. F. 2000b. Patterning the embryonic heart: identification of five mouse Iroquois homeobox genes in the developing heart. *Dev.Biol.,* 224**,** 263-274.

CHRISTOFFELS, V. M. & MOORMAN, A. F. 2009. Development of the cardiac conduction system: why are some regions of the heart more arrhythmogenic than others? *Circ Arrhythm Electrophysiol,* 2**,** 195-207.

CHRISTOFFELS, V. M., SMITS, G. J., KISPERT, A. & MOORMAN, A. F. 2010. Development of the pacemaker tissues of the heart. *Circ Res,* 106**,** 240-54.

CIRINO, A. L. & HO, C. Y. 2013. Genetic testing for inherited heart disease. *Circulation,* 128**,** e4-8.

CLARK, E. B., HU, N., FROMMELT, P., VANDEKIEFT, G. K., DUMMETT, J. L. & TOMANEK, R. J. 1989. Effect of increased pressure on ventricular growth in stage 21 chick embryos. *Am J Physiol,* 257**,** H55-61.

CLARK, E. B., HU, N. & ROSENQUIST, G. C. 1984. Effect of conotruncal constriction on aortic-mitral valve continuity in the stage 18, 21 and 24 chick embryo. *Am J Cardiol,* 53**,** 324-7.

COLAS, J. F., LAWSON, A. & SCHOENWOLF, G. C. 2000. Evidence that translation of smooth muscle alpha-actin mRNA is delayed in the chick promyocardium until fusion of the bilateral heart-forming regions. *Dev Dyn,* 218**,** 316-30.

COPPEN, S. R., KABA, R. A., HALLIDAY, D., DUPONT, E., SKEPPER, J. N., ELNEIL, S. & SEVERS, N. J. 2003. Comparison of connexin expression patterns in the developing mouse heart and human foetal heart. *Mol Cell Biochem,* 242**,** 121-7.

COX, G. F. 2007. Diagnostic Approaches to Pediatric Cardiomyopathy of Metabolic Genetic Etiologies and Their Relation to Therapy. *Prog Pediatr Cardiol,* 24**,** 15-25.

CREEMERS, E. E. & PINTO, Y. M. 2011. Molecular mechanisms that control interstitial fibrosis in the pressure-overloaded heart. *Cardiovasc Res,* 89**,** 265-72.

CUI, P., LIN, Q., DING, F., XIN, C., GONG, W., ZHANG, L., GENG, J., ZHANG, B., YU, X., YANG, J., HU, S. & YU, J. 2010. A comparison between ribo-minus RNA-sequencing and polyA-selected RNA-sequencing. *Genomics,* 96**,** 259-65.

DAVID, A. L. & PEEBLES, D. 2008. Gene therapy for the fetus: is there a future? *Best Pract Res Clin Obstet Gynaecol,* 22**,** 203-18.

DE SPIEGELAERE, W., DERN-WIELOCH, J., WEIGEL, R., SCHUMACHER, V., SCHORLE, H., NETTERSHEIM, D., BERGMANN, M., BREHM, R., KLIESCH, S., VANDEKERCKHOVE, L. & FINK, C. 2015. Reference gene validation for RT-qPCR, a note on different available software packages. *PLoS One,* 10**,** e0122515.

DEBEY, S., ZANDER, T., BRORS, B., POPOV, A., EILS, R. & SCHULTZE, J. L. 2006. A highly standardized, robust, and cost-effective method for genome-wide transcriptome analysis of peripheral blood applicable to large-scale clinical trials. *Genomics,* 87**,** 653-64.

DELORME, B., DAHL, E., JARRY-GUICHARD, T., BRIAND, J. P., WILLECKE, K., GROS, D. & THEVENIAU-RUISSY, M. 1997. Expression pattern of connexin gene products at the early developmental stages of the mouse cardiovascular system. *Circ Res,* 81**,** 423-37.

DERRICKSON, G. J. T. B. H. 2006. *Principles of Anatomy and Physiology* Wiley.

DHEIN, S. 2004. Pharmacology of gap junctions in the cardiovascular system. *Cardiovasc Res,* 62**,** 287-98.

DIRKX, E., DA COSTA MARTINS, P. A. & DE WINDT, L. J. 2013. Regulation of fetal gene expression in heart failure. *Biochim Biophys Acta,* 1832**,** 2414-24.

DOWAKI, S., KIJIMA, H., KASHIWAGI, H., OHTANI, Y., TOBITA, K., TSUKUI, M., TANAKA, Y., TAZAWA, K., MATSUBAYASHI, H., TSUCHIDA, T., NAKAMURA, M., UEYAMA, Y., TANAKA, M., TAJIMA, T. & MAKUUCHI, H. 2000. CEA immunohistochemical localization is correlated with growth and metastasis of human gallbladder carcinoma. *Int J Oncol,* 16**,** 49-53.

DRESSEL, U., BAILEY, P. J., WANG, S. C., DOWNES, M., EVANS, R. M. & MUSCAT, G. E. 2001. A dynamic role for HDAC7 in MEF2-mediated muscle differentiation. *J Biol Chem,* 276**,** 17007-13.

DU, A., SANGER, J. M. & SANGER, J. W. 2008. Cardiac myofibrillogenesis inside intact embryonic hearts. *Dev Biol,* 318**,** 236-46.

DU, X. J., COLE, T. J., TENIS, N., GAO, X. M., KONTGEN, F., KEMP, B. E. & HEIERHORST, J. 2002. Impaired cardiac contractility response to hemodynamic stress in S100A1-deficient mice. *Mol Cell Biol,* 22**,** 2821-9.

DUBOSCQ-BIDOT, L., CHARRON, P., RUPPERT, V., FAUCHIER, L., RICHTER, A., TAVAZZI, L., ARBUSTINI, E., WICHTER, T., MAISCH, B., KOMAJDA, M., ISNARD, R., VILLARD, E. & NETWORK, E. H. F. 2009.

Mutations in the ANKRD1 gene encoding CARP are responsible for human dilated cardiomyopathy. *Eur Heart J,* 30**,** 2128-36.

DUFFY, H. S. & WIT, A. L. 2008. Is there a role for remodeled connexins in AF? No simple answers. *J Mol Cell Cardiol,* 44**,** 4-13.

DUNWOODIE, S. L. 2007. Combinatorial signaling in the heart orchestrates cardiac induction, lineage specification and chamber formation. *Semin Cell Dev Biol,* 18**,** 54-66.

EBBERT, M. T., WADSWORTH, M. E., STALEY, L. A., HOYT, K. L., PICKETT, B., MILLER, J., DUCE, J., ALZHEIMER'S DISEASE NEUROIMAGING, I., KAUWE, J. S. & RIDGE, P. G. 2016. Evaluating the necessity of PCR duplicate removal from next-generation sequencing data and a comparison of approaches. *BMC Bioinformatics,* 17 Suppl 7**,** 239.

ENGLAND, J. & LOUGHNA, S. 2013. Heavy and light roles: myosin in the morphogenesis of the heart. *Cell Mol Life Sci,* 70**,** 1221-39.

ENGLAND, J., PANG, K. L., PARNALL, M., HAIG, M. I. & LOUGHNA, S. 2016. Cardiac troponin T is necessary for normal development in the embryonic chick heart. *J Anat*.

EPPENBERGER-EBERHARDT, M., FLAMME, I., KURER, V. & EPPENBERGER, H. M. 1990. Reexpression of alpha-smooth muscle actin isoform in cultured adult rat cardiomyocytes. *Dev Biol,* 139**,** 269-78.

ERIKSSON, J., BOLGER, A. F., EBBERS, T. & CARLHALL, C. J. 2015. Left ventricular hemodynamic forces are altered in patients with dilated cardiomyopathy. *Journal of Cardiovascular Magnetic Resonance,* 17**,** 1-2.

ERONEN, M. 1997. Outcome of fetuses with heart disease diagnosed in utero. *Arch Dis Child Fetal Neonatal Ed,* 77**,** F41-6.

EVANS, C. C., PENA, J. R., PHILLIPS, R. M., MUTHUCHAMY, M., WIECZOREK, D. F., SOLARO, R. J. & WOLSKA, B. M. 2000. Altered hemodynamics in transgenic mice harboring mutant tropomyosin linked to hypertrophic cardiomyopathy. *Am J Physiol Heart Circ Physiol,* 279**,** H2414-23.

FANG, Z. & CUI, X. 2011. Design and validation issues in RNA-seq experiments. *Brief Bioinform,* 12**,** 280-7.

FLORIA, M., TINICA, G. & GRECU, M. 2014. Left ventricular non-compaction -challenges and controversies. *Maedica (Buchar),* 9**,** 282-8.

FRANKE, W. W., BORRMANN, C. M., GRUND, C. & PIEPERHOFF, S. 2006. The area composita of adhering junctions connecting heart muscle cells of vertebrates. I. Molecular definition in intercalated disks of cardiomyocytes by immunoelectron microscopy of desmosomal proteins. *Eur J Cell Biol,* 85**,** 69-82.

FUKUDA, T., ROBERTS, A., PLOTZ, P. H. & RABEN, N. 2007. Acid alpha-glucosidase deficiency (Pompe disease). *Curr Neurol Neurosci Rep,* 7**,** 71-7.

FULLWOOD, M. J., WEI, C. L., LIU, E. T. & RUAN, Y. 2009. Next-generation DNA sequencing of paired-end tags (PET) for transcriptome and genome analyses. *Genome Res,* 19**,** 521-32.

FURST, D. O., OSBORN, M., NAVE, R. & WEBER, K. 1988. The organization of titin filaments in the half-sarcomere revealed by monoclonal antibodies in immunoelectron microscopy: a map of ten nonrepetitive epitopes starting at the Z line extends close to the M line. *J Cell Biol,* 106**,** 1563-72.

GARCIA-FRIGOLA, C., SHI, Y. & EVANS, S. M. 2003. Expression of the hyperpolarization-activated cyclic nucleotide-gated cation channel HCN4 during mouse heart development. *Gene Expr Patterns,* 3**,** 777-83.

GARRY, D. J. & OLSON, E. N. 2006. A common progenitor at the heart of development. *Cell,* 127**,** 1101-4.

GITTENBERGER-DE GROOT, A. C., MAHTAB, E. A., HAHURIJ, N. D., WISSE, L. J., DERUITER, M. C., WIJFFELS, M. C. & POELMANN, R. E. 2007. Nkx2.5-negative myocardium of the posterior heart

field and its correlation with podoplanin expression in cells from the developing cardiac pacemaking and conduction system. *Anat Rec (Hoboken),* 290**,** 115-22.

GOLLOB, M. H. 2008. Modulating phenotypic expression of the PRKAG2 cardiac syndrome. *Circulation,* 117**,** 134-5.

GOURDIE, R. G., HARRIS, B. S., BOND, J., JUSTUS, C., HEWETT, K. W., O'BRIEN, T. X., THOMPSON, R. P. & SEDMERA, D. 2003. Development of the cardiac pacemaking and conduction system. *Birth Defects Res C Embryo Today,* 69**,** 46-57.

GRANADOS-RIVERON, J. T., GHOSH, T. K., POPE, M., BU'LOCK, F., THORNBOROUGH, C., EASON, J., KIRK, E. P., FATKIN, D., FENELEY, M. P., HARVEY, R. P., ARMOUR, J. A. & DAVID BROOK, J. 2010. Alpha-cardiac myosin heavy chain (MYH6) mutations affecting myofibril formation are associated with congenital heart defects. *Hum Mol Genet,* 19**,** 4007-16.

GRANLUND, A., JENSEN-WAERN, M. & ESSEN-GUSTAVSSON, B. 2011. The influence of the PRKAG3 mutation on glycogen, enzyme activities and fibre types in different skeletal muscles of exercise trained pigs. *Acta Vet Scand,* 53**,** 20.

GRANLUND, A., KOTOVA, O., BENZIANE, B., GALUSKA, D., JENSEN-WAERN, M., CHIBALIN, A. V. & ESSEN-GUSTAVSSON, B. 2010. Effects of exercise on muscle glycogen synthesis signalling and enzyme activities in pigs carrying the PRKAG3 mutation. *Exp Physiol,* 95**,** 541-9.

GREBER-PLATZER, S., MARX, M., FLEISCHMANN, C., SUPPAN, C., DOBNER, M. & WIMMER, M. 2001. Beta-myosin heavy chain gene mutations and hypertrophic cardiomyopathy in Austrian children. *J Mol Cell Cardiol,* 33**,** 141-8.

GRIFFITH, M., GRIFFITH, O. L., MWENIFUMBO, J., GOYA, R., MORRISSY, A. S., MORIN, R. D., CORBETT, R., TANG, M. J., HOU, Y. C., PUGH, T. J., ROBERTSON, G., CHITTARANJAN, S., ALLY, A., ASANO, J. K., CHAN, S. Y., LI, H. I., MCDONALD, H., TEAGUE, K., ZHAO, Y., ZENG, T., DELANEY, A., HIRST, M., MORIN, G. B., JONES, S. J., TAI, I. T. & MARRA, M. A. 2010. Alternative expression analysis by RNA sequencing. *Nat Methods,* 7**,** 843-7.

GUPTA, S., KIM, S. M., WANG, Y., DINASARAPU, A. R. & SUBRAMANIAM, S. 2014. Statistical insights into major human muscular diseases. *Hum Mol Genet,* 23**,** 3772-8.

GURJARPADHYE, A., HEWETT, K. W., JUSTUS, C., WEN, X., STADT, H., KIRBY, M. L., SEDMERA, D. & GOURDIE, R. G. 2007. Cardiac neural crest ablation inhibits compaction and electrical function of conduction system bundles. *Am J Physiol Heart Circ Physiol,* 292**,** H1291-300.

GUTSTEIN, D. E., LIU, F. Y., MEYERS, M. B., CHOO, A. & FISHMAN, G. I. 2003. The organization of adherens junctions and desmosomes at the cardiac intercalated disc is independent of gap junctions. *J Cell Sci,* 116**,** 875-85.

HALL, C. E., HURTADO, R., HEWETT, K. W., SHULIMOVICH, M., POMA, C. P., RECKOVA, M., JUSTUS, C., PENNISI, D. J., TOBITA, K., SEDMERA, D., GOURDIE, R. G. & MIKAWA, T. 2004. Hemodynamic-dependent patterning of endothelin converting enzyme 1 expression and differentiation of impulse-conducting Purkinje fibers in the embryonic heart. *Development,* 131**,** 581-92.

HALSE, R., FRYER, L. G., MCCORMACK, J. G., CARLING, D. & YEAMAN, S. J. 2003. Regulation of glycogen synthase by glucose and glycogen: a possible role for AMP-activated protein kinase. *Diabetes,* 52**,** 9-15.

HAMADA, M., SUZUKI, M., OHTANI, T., KAWAKAMI, H., KOBAYASHI, T., OKAYAMA, H., ABE, M., MATSUOKA, H., SUMIMOTO, T. & HIWADA, K. 1992. Does Hypertrophic Cardiomyopathy Change into Dilated Cardiomyopathy-Like Features? *In:* YASUDA, H. & KAWAGUCHI, H. (eds.) *New Aspects in the Treatment of Failing Heart.* Tokyo: Springer Japan.

HAMBURGER, V. & HAMILTON, H. L. 1951. A Series of Normal Stages in the Development of the Chick Embryo. *J.Exp.Morphol.,* 88**,** 49-49.

HAMBURGER, V. & HAMILTON, H. L. 1992. A series of normal stages in the development of the chick embryo. 1951. *Dev Dyn,* 195**,** 231-72.

HAMPTON, J. R. 2013. *The ECG made easy*, churchill and livingstone.

HAN, Y., DENNIS, J. E., COHEN-GOULD, L., BADER, D. M. & FISCHMAN, D. A. 1992. Expression of sarcomeric myosin in the presumptive myocardium of chicken embryos occurs within six hours of myocyte commitment. *Dev Dyn,* 193**,** 257-65.

HARADA, K., SUGAYA, T., MURAKAMI, K., YAZAKI, Y. & KOMURO, I. 1999. Angiotensin II type 1A receptor knockout mice display less left ventricular remodeling and improved survival after myocardial infarction. *Circulation,* 100**,** 2093-9.

HARRIS, B. S., SPRUILL, L., EDMONSON, A. M., RACKLEY, M. S., BENSON, D. W., O'BRIEN, T. X. & GOURDIE, R. G. 2006. Differentiation of cardiac Purkinje fibers requires precise spatiotemporal regulation of Nkx2-5 expression. *Dev Dyn,* 235**,** 38-49.

HARVEY, P. A. & LEINWAND, L. A. 2011. The cell biology of disease: cellular mechanisms of cardiomyopathy. *J Cell Biol,* 194**,** 355-65.

HEAD, S. R., KOMORI, H. K., LAMERE, S. A., WHISENANT, T., VAN NIEUWERBURGH, F., SALOMON, D. R. & ORDOUKHANIAN, P. 2014. Library construction for next-generation sequencing: overviews and challenges. *Biotechniques,* 56**,** 61-4, 66, 68, passim.

HITCHEN J, S. R., KHANNA A 2013. Rapid and Efficient Methods for Preparing Globin- and rRNA-Depleted Directional RNA-Seq Libraries. *Journal of Biomolecular Techniques,* 24(Suppl)**,** S43-S44.

HOGERS, B., DERUITER, M. C., GITTENBERGER-DE GROOT, A. C. & POELMANN, R. E. 1999. Extraembryonic venous obstructions lead to cardiovascular malformations and can be embryolethal. *Cardiovasc.Res.,* 41**,** 87-99.

HONG, T., YANG, H., ZHANG, S. S., CHO, H. C., KALASHNIKOVA, M., SUN, B., ZHANG, H., BHARGAVA, A., GRABE, M., OLGIN, J., GORELIK, J., MARBAN, E., JAN, L. Y. & SHAW, R. M. 2014. Cardiac BIN1 folds T-tubule membrane, controlling ion flux and limiting arrhythmia. *Nat Med,* 20**,** 624-32.

HONG, T. T., SMYTH, J. W., GAO, D., CHU, K. Y., VOGAN, J. M., FONG, T. S., JENSEN, B. C., COLECRAFT, H. M. & SHAW, R. M. 2010. BIN1 localizes the L-type calcium channel to cardiac T-tubules. *PLoS Biol,* 8**,** e1000312.

HOOGAARS, W. M., ENGEL, A., BRONS, J. F., VERKERK, A. O., DE LANGE, F. J., WONG, L. Y., BAKKER, M. L., CLOUT, D. E., WAKKER, V., BARNETT, P., RAVESLOOT, J. H., MOORMAN, A. F., VERHEIJCK, E. E. & CHRISTOFFELS, V. M. 2007. TBX3 controls the sinoatrial node gene program and imposes pacemaker function on the atria. *Genes Dev,* 21**,** 1098-112.

HOOGAARS, W. M., TESSARI, A., MOORMAN, A. F., DE BOER, P. A., HAGOORT, J., SOUFAN, A. T., CAMPIONE, M. & CHRISTOFFELS, V. M. 2004. The transcriptional repressor TBX3 delineates the developing central conduction system of the heart. *Cardiovasc Res,* 62**,** 489-99.

HORSTHUIS, T., CHRISTOFFELS, V. M., ANDERSON, R. H. & MOORMAN, A. F. 2009. Can recent insights into cardiac development improve our understanding of congenitally malformed hearts? *Clin Anat,* 22**,** 4-20.

HOVE, J. R. 2006. Quantifying cardiovascular flow dynamics during early development. *Pediatr Res,* 60**,** 6-13.

HUMPHRIES, E. H. & COFFIN, J. M. 1976. Rate of virus-specific RNA synthesis in synchronized chicken embryo fibroblasts infected with avian leukosis virus. *J Virol,* 17**,** 393-401.

HWANG, S. K., PIAO, L., LIM, H. T., MINAI-TEHRANI, A., YU, K. N., HA, Y. C., CHAE, C. H., LEE, K. H., BECK, G. R., PARK, J. & CHO, M. H. 2010. Suppression of lung tumorigenesis by leucine zipper/EF hand-containing transmembrane-1. *PLoS One,* 5.

INAMOTO, S., MURAO, S., YOKOYAMA, M., KITAZAWA, S. & MAEDA, S. 2000. Isoproterenol-induced myocardial injury resulting in altered S100A4 and S100A11 protein expression in the rat. *Pathol Int,* 50**,** 480-5.

IZUMO, S., NADAL-GINARD, B. & MAHDAVI, V. 1988. Protooncogene induction and reprogramming of cardiac gene expression produced by pressure overload. *Proc Natl Acad Sci U S A,* 85**,** 339-43.

JANSEN, J. A., VAN VEEN, T. A., DE BAKKER, J. M. & VAN RIJEN, H. V. 2010. Cardiac connexins and impulse propagation. *J Mol Cell Cardiol,* 48**,** 76-82.

JASNIC-SAVOVIC, J., NESTOROVIC, A., SAVIC, S., KARASEK, S., VITULO, N., VALLE, G., FAULKNER, G., RADOJKOVIC, D. & KOJIC, S. 2015. Profiling of skeletal muscle Ankrd2 protein in human cardiac tissue and neonatal rat cardiomyocytes. *Histochem Cell Biol,* 143**,** 583-97.

JAY, P. Y., HARRIS, B. S., MAGUIRE, C. T., BUERGER, A., WAKIMOTO, H., TANAKA, M., KUPERSHMIDT, S., RODEN, D. M., SCHULTHEISS, T. M., O'BRIEN, T. X., GOURDIE, R. G., BERUL, C. I. & IZUMO, S. 2004. Nkx2-5 mutation causes anatomic hypoplasia of the cardiac conduction system. *J Clin Invest,* 113**,** 1130-7.

JONES, W. K., GRUPP, I. L., DOETSCHMAN, T., GRUPP, G., OSINSKA, H., HEWETT, T. E., BOIVIN, G., GULICK, J., NG, W. A. & ROBBINS, J. 1996. Ablation of the murine alpha myosin heavy chain gene leads to dosage effects and functional deficits in the heart. *J Clin Invest,* 98**,** 1906-17.

JORGENSEN, S. B., RICHTER, E. A. & WOJTASZEWSKI, J. F. 2006. Role of AMPK in skeletal muscle metabolic regulation and adaptation in relation to exercise. *J Physiol,* 574**,** 17-31.

K. G. PAL, N. N. 2016. *Comprehensive Textbook of Medical Physiology*, Jp Medical Ltd; Com edition.

KADAM, P. & BHALERAO, S. 2010. Sample size calculation. *Int J Ayurveda Res,* 1**,** 55-7.

KAIN, K. H., MILLER, J. W. I., JONES-PARIS, C. R., THOMASON, R. T., LEWIS, J. D., BADER, D. M., BARNETT, J. V. & ZIJLSTRA, A. 2014. The Chick Embryo as an Expanding Experimental Model for Cancer and Cardiovascular Research. *Developmental Dynamics,* 243**,** 216-228.

KANAMORI, T., TAKAKURA, K., MANDAI, M., KARIYA, M., FUKUHARA, K., SAKAGUCHI, M., HUH, N. H., SAITO, K., SAKURAI, T., FUJITA, J. & FUJII, S. 2004. Increased expression of calcium-binding protein S100 in human uterine smooth muscle tumours. *Mol Hum Reprod,* 10**,** 735-42.

KARAKIKES, I., STILLITANO, F., NONNENMACHER, M., TZIMAS, C., SANOUDOU, D., TERMGLINCHAN, V., KONG, C. W., RUSHING, S., HANSEN, J., CEHOLSKI, D., KOLOKATHIS, F., KREMASTINOS, D., KATOULIS, A., REN, L., COHEN, N., GHO, J. M., TSIAPRAS, D., VINK, A., WU, J. C., ASSELBERGS, F. W., LI, R. A., HULOT, J. S., KRANIAS, E. G. & HAJJAR, R. J. 2015. Correction of human phospholamban R14del mutation associated with cardiomyopathy using targeted nucleases and combination therapy. *Nat Commun,* 6**,** 6955.

KARAM, S., RABOISSON, M. J., DUCREUX, C., CHALABREYSSE, L., MILLAT, G., BOZIO, A. & BOUVAGNET, P. 2008. A de novo mutation of the beta cardiac myosin heavy chain gene in an infantile restrictive cardiomyopathy. *Congenit Heart Dis,* 3**,** 138-43.

KASKI, J. P., SYRRIS, P., BURCH, M., ESTEBAN, M. T. T., FENTON, M., CHRISTIANSEN, M., ANDERSEN, P. S., SEBIRE, N., ASHWORTH, M., DEANFIELD, J. E., MCKENNA, W. J. & ELLIOTT, P. M. 2008. Idiopathic restrictive cardiomyopathy in children is caused by mutations in cardiac sarcomere protein genes. *Heart,* 94**,** 1478-1484.

KATZ, T. C., SINGH, M. K., DEGENHARDT, K., RIVERA-FELICIANO, J., JOHNSON, R. L., EPSTEIN, J. A. & TABIN, C. J. 2012. Distinct compartments of the proepicardial organ give rise to coronary vascular endothelial cells. *Dev Cell,* 22**,** 639-50.

KEHAT, I. & MOLKENTIN, J. D. 2010. Molecular Pathways Underlying Cardiac Remodeling During Pathophysiological Stimulation. *Circulation,* 122**,** 2727-2735.

KELLY, R. G. 2012. The second heart field. *Curr Top Dev Biol,* 100**,** 33-65.

KHATTAK, S. F., BHATIA, S. R. & ROBERTS, S. C. 2005. Pluronic F127 as a cell encapsulation material: utilization of membrane-stabilizing agents. *Tissue Eng,* 11**,** 974-83.

KIM, T., KIM, J. O., OH, J. G., HONG, S. E. & KIM DO, H. 2014. Pressure-overload cardiac hypertrophy is associated with distinct alternative splicing due to altered expression of splicing factors. *Mol Cells,* 37**,** 81-7.

KLABUNDE, R. 2011. *Cardiovascular Physiology Concepts*, Wolters Kluwer Health.

KOK, F. O., SHIN, M., NI, C. W., GUPTA, A., GROSSE, A. S., VAN IMPEL, A., KIRCHMAIER, B. C., PETERSON-MADURO, J., KOURKOULIS, G., MALE, I., DESANTIS, D. F., SHEPPARD-TINDELL, S., EBARASI, L.,

BETSHOLTZ, C., SCHULTE-MERKER, S., WOLFE, S. A. & LAWSON, N. D. 2015. Reverse genetic screening reveals poor correlation between Morpholino-induced and mutant phenotypes in zebrafish. *Dev Cell,* 32**,** 97-108.

KOUTRAS, C. & BRAUN, J. E. 2014. J protein mutations and resulting proteostasis collapse. *Front Cell Neurosci,* 8**,** 191.

KRENZ, M. & ROBBINS, J. 2004. Impact of beta-myosin heavy chain expression on cardiac function during stress. *J Am Coll Cardiol,* 44**,** 2390-7.

LAMERS, W. H. & MOORMAN, A. F. 2002. Cardiac septation: a late contribution of the embryonic primary myocardium to heart morphogenesis. *Circ Res,* 91**,** 93-103.

LAMERS, W. H., VIRAGH, S., WESSELS, A., MOORMAN, A. F. & ANDERSON, R. H. 1995. Formation of the tricuspid valve in the human heart. *Circulation,* 91**,** 111-121.

LE DOUARIN, N. 1982. *The Neural Crest*, Cambridge University Press.

LE SCOUARNEC, S., BHASIN, N., VIEYRES, C., HUND, T. J., CUNHA, S. R., KOVAL, O., MARIONNEAU, C., CHEN, B., WU, Y., DEMOLOMBE, S., SONG, L. S., LE MAREC, H., PROBST, V., SCHOTT, J. J., ANDERSON, M. E. & MOHLER, P. J. 2008. Dysfunction in ankyrin-B-dependent ion channel and transporter targeting causes human sinus node disease. *Proc Natl Acad Sci U S A,* 105**,** 15617-22.

LEE, T. I., KAO, Y. H., TSAI, W. C., CHUNG, C. C., CHEN, Y. C. & CHEN, Y. J. 2016. HDAC Inhibition Modulates Cardiac PPARs and Fatty Acid Metabolism in Diabetic Cardiomyopathy. *PPAR Res,* 2016**,** 5938740.

LEHMAN, W., CRAIG, R. & VIBERT, P. 1994. Ca(2+)-induced tropomyosin movement in Limulus thin filaments revealed by three-dimensional reconstruction. *Nature,* 368**,** 65-7.

LEHMANN, L. H., WORST, B. C., STANMORE, D. A. & BACKS, J. 2014. Histone deacetylase signaling in cardioprotection. *Cell Mol Life Sci,* 71**,** 1673-90.

LEHRER, S. S. 1994. The regulatory switch of the muscle thin filament: Ca2+ or myosin heads? *J Muscle Res Cell Motil,* 15**,** 232-6.

LEVESQUE-SERGERIE, J. P., DUQUETTE, M., THIBAULT, C., DELBECCHI, L. & BISSONNETTE, N. 2007. Detection limits of several commercial reverse transcriptase enzymes: impact on the low- and high-abundance transcript levels assessed by quantitative RT-PCR. *BMC Mol Biol,* 8**,** 93.

LEVIN, J. Z., YASSOUR, M., ADICONIS, X., NUSBAUM, C., THOMPSON, D. A., FRIEDMAN, N., GNIRKE, A. & REGEV, A. 2010. Comprehensive comparative analysis of strand-specific RNA sequencing methods. *Nat Methods,* 7**,** 709-15.

LEWIT-BENTLEY, A. & RETY, S. 2000. EF-hand calcium-binding proteins. *Curr Opin Struct Biol,* 10**,** 637-43.

LI, M. X. & HWANG, P. M. 2015. Structure and function of cardiac troponin C (TNNC1): Implications for heart failure, cardiomyopathies, and troponin modulating drugs. *Gene,* 571**,** 153-66.

LIANG, X., WANG, G., LIN, L., LOWE, J., ZHANG, Q., BU, L., CHEN, Y., CHEN, J., SUN, Y. & EVANS, S. M. 2013. HCN4 dynamically marks the first heart field and conduction system precursors. *Circ Res,* 113**,** 399-407.

LIN, C. J., LIN, C. Y., CHEN, C. H., ZHOU, B. & CHANG, C. P. 2012. Partitioning the heart: mechanisms of cardiac septation and valve development. *Development,* 139**,** 3277-99.

LINDSEY, S. E., BUTCHER, J. T. & YALCIN, H. C. 2014. Mechanical regulation of cardiac development. *Front Physiol,* 5**,** 318.

LKHAGVA, B., LIN, Y. K., KAO, Y. H., CHAZO, T. F., CHUNG, C. C., CHEN, S. A. & CHEN, Y. J. 2015. Novel Histone Deacetylase Inhibitor Modulates Cardiac Peroxisome Proliferator-Activated Receptors and Inflammatory Cytokines in Heart Failure. *Pharmacology,* 96**,** 184-91.

LORELL, B. H. & CARABELLO, B. A. 2000. Left ventricular hypertrophy - Pathogenesis, detection, and prognosis. *Circulation,* 102**,** 470-479.

LORUSSO, S. M., RHEE, D., SANGER, J. M. & SANGER, J. W. 1997. Premyofibrils in spreading adult cardiomyocytes in tissue culture: evidence for reexpression of the embryonic program for myofibrillogenesis in adult cells. *Cell Motil Cytoskeleton,* 37**,** 183-98.

LOVE, M. I., HUBER, W. & ANDERS, S. 2014. Moderated estimation of fold change and dispersion for RNA-seq data with DESeq2. *Genome Biol,* 15**,** 550.

LUNDY, S. D., ZHU, W. Z., REGNIER, M. & LAFLAMME, M. A. 2013. Structural and functional maturation of cardiomyocytes derived from human pluripotent stem cells. *Stem Cells Dev,* 22**,** 1991-2002.

LUO, C. H. & RUDY, Y. 1991. A model of the ventricular cardiac action potential. Depolarization, repolarization, and their interaction. *Circ Res,* 68**,** 1501-26.

LYONS, G. E., ONTELL, M., COX, R., SASSOON, D. & BUCKINGHAM, M. 1990a. The expression of myosin genes in developing skeletal muscle in the mouse embryo. *J.Cell Biol.,* 111**,** 1465-1476.

LYONS, G. E., SCHIAFFINO, S., SASSOON, D., BARTON, P. & BUCKINGHAM, M. 1990b. Developmental regulation of myosin gene expression in mouse cardiac muscle. *J.Cell Biol.,* 111**,** 2427-2436.

MAHDAVI, V., LOMPRE, A. M., CHAMBERS, A. P. & NADAL-GINARD, B. 1984. Cardiac myosin heavy chain isozymic transitions during development and under pathological conditions are regulated at the level of mRNA availability. *Eur Heart J,* 5 Suppl F**,** 181-91.

MAHTAB, E. A., VICENTE-STEIJN, R., HAHURIJ, N. D., JONGBLOED, M. R., WISSE, L. J., DERUITER, M. C., UHRIN, P., ZAUJEC, J., BINDER, B. R., SCHALIJ, M. J., POELMANN, R. E. & GITTENBERGER-DE GROOT, A. C. 2009. Podoplanin deficient mice show a RhoA-related hypoplasia of the sinus venosus myocardium including the sinoatrial node. *Dev Dyn,* 238**,** 183-93.

MAKITA, N., SEKI, A., SUMITOMO, N., CHKOURKO, H., FUKUHARA, S., WATANABE, H., SHIMIZU, W., BEZZINA, C. R., HASDEMIR, C., MUGISHIMA, H., MAKIYAMA, T., BARUTEAU, A., BARON, E., HORIE, M., HAGIWARA, N., WILDE, A. A., PROBST, V., LE MAREC, H., RODEN, D. M., MOCHIZUKI, N., SCHOTT, J. J. & DELMAR, M. 2012. A connexin40 mutation associated with a malignant variant of progressive familial heart block type I. *Circ Arrhythm Electrophysiol,* 5**,** 163-72.

MAMATHA H, D. S., ANTONY SYLVAN D' SOUZA, PRASANNA LC, AND SUHANI SUMALATH 2013. A Morphometric Study on the Septomarginal Trabeculae in South Indian Cadavers. *Journal of Medical and Health Sciences*.

MANNER, J. 2000. Cardiac looping in the chick embryo: a morphological review with special reference to terminological and biomechanical aspects of the looping process. *Anat Rec,* 259**,** 248-62.

MANNER, J. 2009. The anatomy of cardiac looping: a step towards the understanding of the morphogenesis of several forms of congenital cardiac malformations. *Clin Anat,* 22**,** 21-35.

MARIONI, J. C., MASON, C. E., MANE, S. M., STEPHENS, M. & GILAD, Y. 2008. RNA-seq: an assessment of technical reproducibility and comparison with gene expression arrays. *Genome Res,* 18**,** 1509-17.

MARKWALD, R. R., FITZHARRIS, T. P. & MANASEK, F. J. 1977. Structural development of endocardial cushions. *Am.J.Anat.,* 148**,** 85-119.

MARON, B. J. & MARON, M. S. 2013. Hypertrophic cardiomyopathy. *Lancet,* 381**,** 242-55.

MARON, B. J., TOWBIN, J. A., THIENE, G., ANTZELEVITCH, C., CORRADO, D., ARNETT, D., MOSS, A. J., SEIDMAN, C. E. & YOUNG, J. B. 2006. Contemporary definitions and classification of the cardiomyopathies: an American Heart Association Scientific Statement from the Council on Clinical Cardiology, Heart Failure and Transplantation Committee; Quality of Care and Outcomes Research and Functional Genomics and Translational Biology Interdisciplinary Working Groups; and Council on Epidemiology and Prevention. *Circulation,* 113**,** 1807-1816.

MARTINSEN, B. J. 2005a. Reference guide to the stages of chick heart embryology. *Dev Dyn,* 233**,** 1217-37.

MARTINSEN, B. J. L., J. L. 2005b. *Handbook of Cardiac Anatomy, Physiology, and Devices*, Springer.

MARUYAMA, I. N., MILLER, D. M. & BRENNER, S. 1989. Myosin heavy chain gene amplification as a suppressor mutation in Caenorhabditis elegans. *Mol Gen Genet,* 219**,** 113-8.

MASTROKOLIAS, A., DEN DUNNEN, J. T., VAN OMMEN, G. B., T HOEN, P. A. & VAN ROON-MOM, W. M. 2012. Increased sensitivity of next generation sequencing-based expression profiling after globin reduction in human blood RNA. *BMC Genomics,* 13**,** 28.

MASUDA, S., HAYASHI, T., HASHIMOTO, T. & TAGUCHI, S. 2009. Correlation of dystrophin-glycoprotein complex and focal adhesion complex with myosin heavy chain isoforms in rat skeletal muscle. *Acta Physiol (Oxf),* 195**,** 483-94.

MCCARTAN, C., MASON, R., JAYASINGHE, S. R. & GRIFFITHS, L. R. 2012. Cardiomyopathy classification: ongoing debate in the genomics era. *Biochem Res Int,* 2012**,** 796926.

MCMULLEN, J. R. & JENNINGS, G. L. 2007. Differences between pathological and physiological cardiac hypertrophy: Novel therapeutic strategies to treat heart failure. *Clinical and Experimental Pharmacology and Physiology,* 34**,** 255-262.

MCNALLY, E. M. & SVENSSON, E. C. 2009. Setting the pace: TBX3 and TBX18 in cardiac conduction system development. *Circ Res,* 104**,** 285-7.

MCQUINN, T. C., BRATOEVA, M., DEALMEIDA, A., REMOND, M., THOMPSON, R. P. & SEDMERA, D. 2007. High-frequency ultrasonographic imaging of avian cardiovascular development. *Dev Dyn,* 236**,** 3503-13.

MEISGEN, S. & HEDLUND, M. 2015. Auxilin Is a Novel Susceptibility Gene for Congenital Heart Block Modulating Cardiac Function.

MELLOR, K. M., UPASNA VARMA, STEVENS, E. & DELBRIDGE3, L. M. 2016. Cardiomyocyte Glucose Handling is Influenced by β-adrenergic and AMPK Regulation of Glycogen and Autophagy in Metabolic Stress Settings. *The FASEB Journal,* 30.

MENG, H., LEDDY, J. J., FRANK, J., HOLLAND, P. & TUANA, B. S. 1996. The association of cardiac dystrophin with myofibrils/Z-disc regions in cardiac muscle suggests a novel role in the contractile apparatus. *J Biol Chem,* 271**,** 12364-71.

MESSINA, D. N., SPEER, M. C., PERICAK-VANCE, M. A. & MCNALLY, E. M. 1997. Linkage of familial dilated cardiomyopathy with conduction defect and muscular dystrophy to chromosome 6q23. *Am J Hum Genet,* 61**,** 909-17.

MEYER, T., RUPPERT, V., ACKERMANN, S., RICHTER, A., PERROT, A., SPERLING, S. R., POSCH, M. G., MAISCH, B., PANKUWEIT, S. & GERMAN COMPETENCE NETWORK HEART, F. 2013. Novel mutations in the sarcomeric protein myopalladin in patients with dilated cardiomyopathy. *Eur J Hum Genet,* 21**,** 294-300.

MIDGETT, M. & RUGONYI, S. 2014. Congenital heart malformations induced by hemodynamic altering surgical interventions. *Front Physiol,* 5**,** 287.

MIELCAREK, M., BONDULICH, M. K., INUABASI, L., FRANKLIN, S. A., MULLER, T. & BATES, G. P. 2014. The Huntington's disease-related cardiomyopathy prevents a hypertrophic response in the R6/2 mouse model. *PLoS One,* 9**,** e108961.

MILAN, D., JEON, J. T., LOOFT, C., AMARGER, V., ROBIC, A., THELANDER, M., ROGEL-GAILLARD, C., PAUL, S., IANNUCCELLI, N., RASK, L., RONNE, H., LUNDSTROM, K., REINSCH, N., GELLIN, J., KALM, E., ROY, P. L., CHARDON, P. & ANDERSSON, L. 2000. A mutation in PRKAG3 associated with excess glycogen content in pig skeletal muscle. *Science,* 288**,** 1248-51.

MILANO, A., VERMEER, A. M., LODDER, E. M., BARC, J., VERKERK, A. O., POSTMA, A. V., VAN DER BILT, I. A., BAARS, M. J., VAN HAELST, P. L., CALISKAN, K., HOEDEMAEKERS, Y. M., LE SCOUARNEC, S., REDON, R., PINTO, Y. M., CHRISTIAANS, I., WILDE, A. A. & BEZZINA, C. R. 2014. HCN4 mutations in multiple families with bradycardia and left ventricular noncompaction cardiomyopathy. *J Am Coll Cardiol,* 64**,** 745-56.

MILLAT, G., JANIN, A., DE TAURIAC, O., ROUX, A. & DAUPHIN, C. 2015. HCN4 mutation as a molecular explanation on patients with bradycardia and non-compaction cardiomyopathy. *Eur J Med Genet,* 58**,** 439-42.

MILLER, C. E., WONG, C. L. & SEDMERA, D. 2003a. Pressure overload alters stress-strain properties of the developing chick heart. *Am J Physiol Heart Circ Physiol,* 285**,** H1849-56.

MILLER, M. K., BANG, M. L., WITT, C. C., LABEIT, D., TROMBITAS, C., WATANABE, K., GRANZIER, H., MCELHINNY, A. S., GREGORIO, C. C. & LABEIT, S. 2003b. The muscle ankyrin repeat proteins: CARP, ankrd2/Arpp and DARP as a family of titin filament-based stress response molecules. *J Mol Biol,* 333**,** 951-64.

MILLS, J. D., KAWAHARA, Y. & JANITZ, M. 2013. Strand-Specific RNA-Seq Provides Greater Resolution of Transcriptome Profiling. *Curr Genomics,* 14**,** 173-81.

MIQUEROL, L., THIREAU, J., BIDEAUX, P., STURNY, R., RICHARD, S. & KELLY, R. G. 2015. Endothelial plasticity drives arterial remodeling within the endocardium after myocardial infarction. *Circ Res,* 116**,** 1765-71.

MOMMERSTEEG, M. T., DOMINGUEZ, J. N., WIESE, C., NORDEN, J., DE GIER-DE VRIES, C., BURCH, J. B., KISPERT, A., BROWN, N. A., MOORMAN, A. F. & CHRISTOFFELS, V. M. 2010. The sinus venosus progenitors separate and diversify from the first and second heart fields early in development. *Cardiovasc Res,* 87**,** 92-101.

MONGIOVI, M., FESSLOVA, V., FAZIO, G., BARBARO, G. & PIPITONE, S. 2010. Diagnosis and prognosis of fetal cardiomyopathies: a review. *Curr Pharm Des,* 16**,** 2929-34.

MOORMAN, A., WEBB, S., BROWN, N. A., LAMERS, W. & ANDERSON, R. H. 2003. Development of the heart: (1) formation of the cardiac chambers and arterial trunks. *Heart,* 89**,** 806-14.

MORENO-RODRIGUEZ, R. A., KRUG, E. L., REYES, L., VILLAVICENCIO, L., MJAATVEDT, C. H. & MARKWALD, R. R. 2006. Bidirectional fusion of the heart-forming fields in the developing chick embryo. *Dev Dyn,* 235**,** 191-202.

MORIMOTO, S. 2008. Sarcomeric proteins and inherited cardiomyopathies. *Cardiovasc Res,* 77**,** 659-66.

MORTAZAVI, A., WILLIAMS, B. A., MCCUE, K., SCHAEFFER, L. & WOLD, B. 2008. Mapping and quantifying mammalian transcriptomes by RNA-Seq. *Nat Meth,* 5**,** 621-628.

MOULTON, J. D. & JIANG, S. 2009. Gene knockdowns in adult animals: PPMOs and vivo-morpholinos. *Molecules,* 14**,** 1304-23.

MULRONEY, S. E. 2009. *Netter's Essential Physiology*, Elsevier.

MUTRYN, M. F., BRANNICK, E. M., FU, W., LEE, W. R. & ABASHT, B. 2015. Characterization of a novel chicken muscle disorder through differential gene expression and pathway analysis using RNA-sequencing. *BMC Genomics,* 16**,** 399.

NAESENS, L., GUDDAT, L. W., KEOUGH, D. T., VAN KUILENBURG, A. B., MEIJER, J., VANDE VOORDE, J. & BALZARINI, J. 2013. Role of human hypoxanthine guanine phosphoribosyltransferase in activation of the antiviral agent T-705 (favipiravir). *Mol Pharmacol,* 84**,** 615-29.

NAKAMURA, T., COLBERT, M. C. & ROBBINS, J. 2006. Neural crest cells retain multipotential characteristics in the developing valves and label the cardiac conduction system. *Circ Res,* 98**,** 1547-54.

NAKAO, K., MINOBE, W., RODEN, R., BRISTOW, M. R. & LEINWAND, L. A. 1997. Myosin heavy chain gene expression in human heart failure. *J Clin Invest,* 100**,** 2362-70.

NARULA, J., KOLODGIE, F. D. & VIRMANI, R. 2000. Apoptosis and cardiomyopathy. *Curr Opin Cardiol,* 15**,** 183-8.

NICHOLAS J. SCHURCH, P. S., MAREK GIERLIŃSKI, CHRISTIAN COLE, ALEXANDER SHERSTNEV, VIJENDER SINGH, NICOLA WROBEL, KARIM GHARBI, GORDON G. SIMPSON, TOM OWEN-HUGHES, MARK BLAXTER, GEOFFREY J. BARTON 2015. Evaluation of tools for differential gene expression analysis by RNA-seq on a 48 biological replicate experiment. *Cornel University library*.

NUTT, S. L., BRONCHAIN, O. J., HARTLEY, K. O. & AMAYA, E. 2001. Comparison of morpholino based translational inhibition during the development of Xenopus laevis and Xenopus tropicalis. *Genesis.,* 30**,** 110-113.

OLSON, E. N. & SCHNEIDER, M. D. 2003. Sizing up the heart: development redux in disease. *Genes Dev,* 17**,** 1937-56.

ORR, N., ARNAOUT, R., GULA, L. J., SPEARS, D. A., LEONG-SIT, P., LI, Q., TARHUNI, W., REISCHAUER, S., CHAUHAN, V. S., BORKOVICH, M., UPPAL, S., ADLER, A., COUGHLIN, S. R., STAINIER, D. Y. & GOLLOB, M. H. 2016. A mutation in the atrial-specific myosin light chain gene (MYL4) causes familial atrial fibrillation. *Nat Commun,* 7**,** 11303.

PAPANAYOTOU, C., MEY, A., BIROT, A. M., SAKA, Y., BOAST, S., SMITH, J. C., SAMARUT, J. & STERN, C. D. 2008. A mechanism regulating the onset of Sox2 expression in the embryonic neural plate. *PLoS Biol,* 6**,** e2.

PARK, D. S. & FISHMAN, G. I. 2011. The cardiac conduction system. *Circulation,* 123**,** 904-15.

PARK, J. Y., LI, W., ZHENG, D., ZHAI, P., ZHAO, Y., MATSUDA, T., VATNER, S. F., SADOSHIMA, J. & TIAN, B. 2011. Comparative analysis of mRNA isoform expression in cardiac hypertrophy and development reveals multiple post-transcriptional regulatory modules. *PLoS One,* 6**,** e22391.

PARKHOMCHUK, D., BORODINA, T., AMSTISLAVSKIY, V., BANARU, M., HALLEN, L., KROBITSCH, S., LEHRACH, H. & SOLDATOV, A. 2009. Transcriptome analysis by strand-specific sequencing of complementary DNA. *Nucleic Acids Res,* 37**,** e123.

PARVARI, R. & LEVITAS, A. 2012. The mutations associated with dilated cardiomyopathy. *Biochem Res Int,* 2012**,** 639250.

PASHMFOROUSH, M., LU, J. T., CHEN, H., AMAND, T. S., KONDO, R., PRADERVAND, S., EVANS, S. M., CLARK, B., FERAMISCO, J. R., GILES, W., HO, S. Y., BENSON, D. W., SILBERBACH, M., SHOU, W. & CHIEN, K. R. 2004. Nkx2-5 pathways and congenital heart disease; loss of ventricular myocyte lineage specification leads to progressive cardiomyopathy and complete heart block. *Cell,* 117**,** 373-86.

PATEL, V. V., ARAD, M., MOSKOWITZ, I. P., MAGUIRE, C. T., BRANCO, D., SEIDMAN, J. G., SEIDMAN, C. E. & BERUL, C. I. 2003. Electrophysiologic characterization and postnatal development of ventricular pre-excitation in a mouse model of cardiac hypertrophy and Wolff-Parkinson-White syndrome. *J Am Coll Cardiol,* 42**,** 942-51.

PEDRA, S. R., SMALLHORN, J. F., RYAN, G., CHITAYAT, D., TAYLOR, G. P., KHAN, R., ABDOLELL, M. & HORNBERGER, L. K. 2002. Fetal cardiomyopathies: pathogenic mechanisms, hemodynamic findings, and clinical outcome. *Circulation,* 106**,** 585-91.

PERSON, A. D., KLEWER, S. E. & RUNYAN, R. B. 2005. Cell biology of cardiac cushion development. *Int Rev Cytol,* 243**,** 287-335.

PETCHEY, L. K., RISEBRO, C. A., VIEIRA, J. M., ROBERTS, T., BRYSON, J. B., GREENSMITH, L., LYTHGOE, M. F. & RILEY, P. R. 2014. Loss of Prox1 in striated muscle causes slow to fast skeletal muscle fiber conversion and dilated cardiomyopathy. *Proc Natl Acad Sci U S A,* 111**,** 9515-20.

PFAFFL, M. W. 2001. A new mathematical model for relative quantification in real-time RT-PCR. *Nucleic Acids Res,* 29**,** e45.

PFAFFL, M. W., TICHOPAD, A., PRGOMET, C. & NEUVIANS, T. P. 2004. Determination of stable housekeeping genes, differentially regulated target genes and sample integrity: BestKeeper--Excel-based tool using pair-wise correlations. *Biotechnol Lett,* 26**,** 509-15.

PILBROW, A. P., ELLMERS, L. J., BLACK, M. A., MORAVEC, C. S., SWEET, W. E., TROUGHTON, R. W., RICHARDS, A. M., FRAMPTON, C. M. & CAMERON, V. A. 2008. Genomic selection of reference genes for real-time PCR in human myocardium. *BMC Med Genomics,* 1**,** 64.

PINTER, K., GRIGNANI, R. T., CZIBIK, G., FARZA, H., WATKINS, H. & REDWOOD, C. 2012. Embryonic expression of AMPK gamma subunits and the identification of a novel gamma2 transcript variant in adult heart. *J Mol Cell Cardiol,* 53**,** 342-9.

PINTER, K., GRIGNANI, R. T., WATKINS, H. & REDWOOD, C. 2013. Localisation of AMPK gamma subunits in cardiac and skeletal muscles. *J Muscle Res Cell Motil,* 34**,** 369-78.

POSTMA, A. V., VAN ENGELEN, K., VAN DE MEERAKKER, J., RAHMAN, T., PROBST, S., BAARS, M. J., BAUER, U., PICKARDT, T., SPERLING, S. R., BERGER, F., MOORMAN, A. F., MULDER, B. J., THIERFELDER, L., KEAVNEY, B., GOODSHIP, J. & KLAASSEN, S. 2011. Mutations in the sarcomere gene MYH7 in Ebstein anomaly. *Circ Cardiovasc Genet,* 4**,** 43-50.

PROSZKOWIEC-WEGLARZ, M., RICHARDS, M. P., RAMACHANDRAN, R. & MCMURTRY, J. P. 2006. Characterization of the AMP-activated protein kinase pathway in chickens. *Comp Biochem Physiol B Biochem Mol Biol,* 143**,** 92-106.

PULINILKUNNIL, T., HE, H., KONG, D., ASAKURA, K., PERONI, O. D., LEE, A. & KAHN, B. B. 2011. Adrenergic regulation of AMP-activated protein kinase in brown adipose tissue in vivo. *J Biol Chem,* 286**,** 8798-809.

RAJKUMAR, A. P., QVIST, P., LAZARUS, R., LESCAI, F., JU, J., NYEGAARD, M., MORS, O., BORGLUM, A. D., LI, Q. & CHRISTENSEN, J. H. 2015. Experimental validation of methods for differential gene expression analysis and sample pooling in RNA-seq. *BMC Genomics,* 16**,** 548.

RECKOVA, M., ROSENGARTEN, C., DEALMEIDA, A., STANLEY, C. P., WESSELS, A., GOURDIE, R. G., THOMPSON, R. P. & SEDMERA, D. 2003. Hemodynamics Is a Key Epigenetic Factor in Development of the Cardiac Conduction System. *Circulation Research,* 93**,** 77-85.

REILLY, S. N., LIU, X., CARNICER, R., RECALDE, A., MUSZKIEWICZ, A., JAYARAM, R., CARENA, M. C., WIJESURENDRA, R., STEFANINI, M., SURDO, N. C., LOMAS, O., RATNATUNGA, C., SAYEED, R., KRASOPOULOS, G., RAJAKUMAR, T., BUENO-OROVIO, A., VERHEULE, S., FULGA, T. A., RODRIGUEZ, B., SCHOTTEN, U. & CASADEI, B. 2016. Up-regulation of miR-31 in human atrial fibrillation begets the arrhythmia by depleting dystrophin and neuronal nitric oxide synthase. *Sci Transl Med,* 8**,** 340ra74.

RHEE, D., SANGER, J. M. & SANGER, J. W. 1994. The premyofibril: evidence for its role in myofibrillogenesis. *Cell Motil Cytoskeleton,* 28**,** 1-24.

RINCON-ARANO, H., GUERRERO, G., VALDES-QUEZADA, C. & RECILLAS-TARGA, F. 2009. Chicken alpha-globin switching depends on autonomous silencing of the embryonic pi globin gene by epigenetics mechanisms. *J Cell Biochem,* 108**,** 675-87.

RISEBRO, C. A. & RILEY, P. R. 2006. Formation of the ventricles. *ScientificWorldJournal,* 6**,** 1862-80.

ROCKETT, J. C. & HELLMANN, G. M. 2004. Confirming microarray data--is it really necessary? *Genomics,* 83**,** 541-9.

RONINSON, I. B. & INGRAM, V. M. 1981. cDNA sequence of a new chicken embryonic rho-globin. *Proc Natl Acad Sci U S A,* 78**,** 4782-5.

RONINSON, I. B. & INGRAM, V. M. 1982. Gene evolution in the chicken beta-globin cluster. *Cell,* 28**,** 515-21.

RUANGVORAVAT, C. P. & LO, C. W. 1992. Connexin 43 expression in the mouse embryo: localization of transcripts within developmentally significant domains. *Dev Dyn,* 194**,** 261-81.

RUI, Y., BAI, J. & PERRIMON, N. 2010. Sarcomere formation occurs by the assembly of multiple latent protein complexes. *PLoS Genet,* 6**,** e1001208.

RUTLAND, C., WARNER, L., THORPE, A., ALIBHAI, A., ROBINSON, T., SHAW, B., LAYFIELD, R., BROOK, J. D. & LOUGHNA, S. 2009. Knockdown of alpha myosin heavy chain disrupts the cytoskeleton and leads to multiple defects during chick cardiogenesis. *J Anat,* 214**,** 905-15.

RUTLAND, C. S., POLO-PARADA, L., EHLER, E., ALIBHAI, A., THORPE, A., SUREN, S., EMES, R. D., PATEL, B. & LOUGHNA, S. 2011. Knockdown of embryonic myosin heavy chain reveals an essential role in the morphology and function of the developing heart. *Development,* 138**,** 3955-66.

SAEZ, J. C., BERTHOUD, V. M., BRANES, M. C., MARTINEZ, A. D. & BEYER, E. C. 2003. Plasma membrane channels formed by connexins: their regulation and functions. *Physiol Rev,* 83**,** 1359-400.

SAMSA, L. A., YANG, B. & LIU, J. 2013. Embryonic cardiac chamber maturation: Trabeculation, conduction, and cardiomyocyte proliferation. *Am J Med Genet C Semin Med Genet,* 163C**,** 157-68.

SATOH, M., MINAMI, Y., TAKAHASHI, Y., TABUCHI, T. & NAKAMURA, M. 2010. Expression of microRNA-208 is associated with adverse clinical outcomes in human dilated cardiomyopathy. *J Card Fail,* 16**,** 404-10.

SCHEFFOLD, T., WALDMULLER, S. & BORISOV, K. 2011. A case of familial hypertrophic cardiomyopathy emphasizes the importance of parallel screening of multiple disease genes. *Clin Res Cardiol,* 100**,** 627-8.

SCHONBERGER, J. & SEIDMAN, C. E. 2001. Many roads lead to a broken heart: the genetics of dilated cardiomyopathy. *Am.J.Hum.Genet.,* 69**,** 249-260.

SCHROEDER, A., MUELLER, O., STOCKER, S., SALOWSKY, R., LEIBER, M., GASSMANN, M., LIGHTFOOT, S., MENZEL, W., GRANZOW, M. & RAGG, T. 2006. The RIN: an RNA integrity number for assigning integrity values to RNA measurements. *BMC Mol Biol,* 7**,** 3.

SCHWARTZ, K., DE LA BASTIE, D., BOUVERET, P., OLIVIERO, P., ALONSO, S. & BUCKINGHAM, M. 1986. Alpha-skeletal muscle actin mRNA's accumulate in hypertrophied adult rat hearts. *Circ Res,* 59**,** 551-5.

SEDLACKOVA, T., REPISKA, G., CELEC, P., SZEMES, T. & MINARIK, G. 2013. Fragmentation of DNA affects the accuracy of the DNA quantitation by the commonly used methods. *Biol Proced Online,* 15**,** 5.

SEDMERA, D., PEXIEDER, T., RYCHTEROVA, V., HU, N. & CLARK, E. B. 1999. Remodeling of chick embryonic ventricular myoarchitecture under experimentally changed loading conditions. *Anat Rec,* 254**,** 238-52.

SEHNERT, A. J., HUQ, A., WEINSTEIN, B. M., WALKER, C., FISHMAN, M. & STAINIER, D. Y. R. 2002. Cardiac troponin T is essential in sarcomere assembly and cardiac contractility. *Nat Genet,* 31**,** 106-110.

SEIDMAN, J. G. & SEIDMAN, C. 2001. The genetic basis for cardiomyopathy: from mutation identification to mechanistic paradigms. *Cell,* 104**,** 557-567.

SEMSARIAN, C., AHMAD, I., GIEWAT, M., GEORGAKOPOULOS, D., SCHMITT, J. P., MCCONNELL, B. K., REIKEN, S., MENDE, U., MARKS, A. R., KASS, D. A., SEIDMAN, C. E. & SEIDMAN, J. G. 2002. The L-type calcium channel inhibitor diltiazem prevents cardiomyopathy in a mouse model. *J Clin Invest,* 109**,** 1013-20.

SETO, E. & YOSHIDA, M. 2014. Erasers of histone acetylation: the histone deacetylase enzymes. *Cold Spring Harb Perspect Biol,* 6**,** a018713.

SEWARD, J. B. & CASACLANG-VERZOSA, G. 2010. Infiltrative cardiovascular diseases: cardiomyopathies that look alike. *J Am Coll Cardiol,* 55**,** 1769-79.

SHIN, H., SHANNON, C. P., FISHBANE, N., RUAN, J., ZHOU, M., BALSHAW, R., WILSON-MCMANUS, J. E., NG, R. T., MCMANUS, B. M. & TEBBUTT, S. J. 2014. Variation in RNA-Seq transcriptome profiles of peripheral whole blood from healthy individuals with and without globin depletion. *PLoS One,* 9**,** e91041.

SHRIER, A. & CLAY, J. R. 1986. Repolarization currents in embryonic chick atrial heart cell aggregates. *Biophys J,* 50**,** 861-74.

SIMS, D., SUDBERY, I., ILOTT, N. E., HEGER, A. & PONTING, C. P. 2014. Sequencing depth and coverage: key considerations in genomic analyses. *Nat Rev Genet,* 15**,** 121-32.

SOMI, S., KLEIN, A. T., HOUWELING, A. C., RUIJTER, J. M., BUFFING, A. A., MOORMAN, A. F. & VAN DEN HOFF, M. J. 2006. Atrial and ventricular myosin heavy-chain expression in the developing chicken heart: strengths and limitations of non-radioactive in situ hybridization. *J.Histochem.Cytochem.,* 54**,** 649-664.

SONESON, C. & DELORENZI, M. 2013. A comparison of methods for differential expression analysis of RNA-seq data. *BMC Bioinformatics,* 14**,** 91.

SONG, H. K., HONG, S. E., KIM, T. & KIM, D. H. 2012. Deep RNA sequencing reveals novel cardiac transcriptomic signatures for physiological and pathological hypertrophy. *PLoS One,* 7**,** e35552.

SOUDERS, C. A., BOWERS, S. L. & BAUDINO, T. A. 2009. Cardiac fibroblast: the renaissance cell. *Circ Res,* 105**,** 1164-76.

STEINBERG, G. R. & KEMP, B. E. 2009. AMPK in Health and Disease. *Physiol Rev,* 89**,** 1025-78.

SUCHAROV, C. C., DOCKSTADER, K., NUNLEY, K., MCKINSEY, T. A. & BRISTOW, M. 2011. beta-Adrenergic receptor stimulation and activation of protein kinase A protect against alpha1-adrenergic-mediated phosphorylation of protein kinase D and histone deacetylase 5. *J Card Fail,* 17**,** 592-600.

SUMMERTON, J. E. 2007. Morpholino, siRNA, and S-DNA compared: impact of structure and mechanism of action on off-target effects and sequence specificity. *Curr Top Med Chem,* 7**,** 651-60.

TAEGTMEYER, H., SEN, S. & VELA, D. 2010. Return to the fetal gene program: a suggested metabolic link to gene expression in the heart. *Ann N Y Acad Sci,* 1188**,** 191-8.

TAKEMURA, H., YASUI, K., OPTHOF, T., NIWA, N., HORIBA, M., SHIMIZU, A., LEE, J. K., HONJO, H., KAMIYA, K., UEDA, Y. & KODAMA, I. 2005. Subtype switching of L-Type Ca 2+ channel from Cav1.3 to Cav1.2 in embryonic murine ventricle. *Circ J,* 69**,** 1405-11.

TAN, H. L., VAN DER WAL, A. C., CAMPIAN, M. E., KRUYSWIJK, H. H., TEN HOVE JANSEN, B., VAN DOORN, D. J., OSKAM, H. J., BECKER, A. E. & WILDE, A. A. 2008. Nodoventricular accessory pathways in PRKAG2-dependent familial preexcitation syndrome reveal a disorder in cardiac development. *Circ Arrhythm Electrophysiol,* 1**,** 276-81.

TANJORE, R., RANGARAJU, A., VADAPALLI, S., REMERSU, S., NARSIMHAN, C. & NALLARI, P. 2010. Genetic variations of beta-MYH7 in hypertrophic cardiomyopathy and dilated cardiomyopathy. *Indian J Hum Genet,* 16**,** 67-71.

TARZE, A., DENIAUD, A., LE BRAS, M., MAILLIER, E., MOLLE, D., LAROCHETTE, N., ZAMZAMI, N., JAN, G., KROEMER, G. & BRENNER, C. 2007. GAPDH, a novel regulator of the pro-apoptotic mitochondrial membrane permeabilization. *Oncogene,* 26**,** 2606-20.

TAVARES, A. L., MERCADO-PIMENTEL, M. E., RUNYAN, R. B. & KITTEN, G. T. 2006. TGF beta-mediated RhoA expression is necessary for epithelial-mesenchymal transition in the embryonic chick heart. *Dev Dyn,* 235**,** 1589-98.

TEEKAKIRIKUL, P., KELLY, M. A., REHM, H. L., LAKDAWALA, N. K. & FUNKE, B. H. 2013. Inherited cardiomyopathies: molecular genetics and clinical genetic testing in the postgenomic era. *J Mol Diagn,* 15**,** 158-70.

THERAPEUTICS, N. 2016. *NanoCor Therapeutics Announces FDA Acceptance of Investigational New Drug (IND) for Carfostin* [Online]. Available: http://www.prnewswire.com/news-releases/nanocor-therapeutics-announces-fda-acceptance-of-investigational-new-drug-ind-for-carfostin-300254307.html [Accessed].

TOBITA, K., GARRISON, J. B., LIU, L. J., TINNEY, J. P. & KELLER, B. B. 2005. Three-dimensional myofiber architecture of the embryonic left ventricle during normal development and altered mechanical loads. *Anat Rec A Discov Mol Cell Evol Biol,* 283**,** 193-201.

TOBITA, K. & KELLER, B. B. 2000. Right and left ventricular wall deformation patterns in normal and left heart hypoplasia chick embryos. *Am J Physiol Heart Circ Physiol,* 279**,** H959-69.

TOBITA, K., SCHRODER, E. A., TINNEY, J. P., GARRISON, J. B. & KELLER, B. B. 2002. Regional passive ventricular stress-strain relations during development of altered loads in chick embryo. *Am J Physiol Heart Circ Physiol,* 282**,** H2386-96.

TOMANEK, R. J., HU, N., PHAN, B. & CLARK, E. B. 1999. Rate of coronary vascularization during embryonic chicken development is influenced by the rate of myocardial growth. *Cardiovasc Res,* 41**,** 663-71.

TON, C., HWANG, D. M., DEMPSEY, A. A., TANG, H. C., YOON, J., LIM, M., MABLY, J. D., FISHMAN, M. C. & LIEW, C. C. 2000. Identification, characterization, and mapping of expressed sequence tags from an embryonic zebrafish heart cDNA library. *Genome Res,* 10**,** 1915-27.

TOWBIN, J. A. 2014a. Inherited cardiomyopathies. *Circ J,* 78**,** 2347-56.

TOWBIN, J. A. 2014b. Ion channel dysfunction associated with arrhythmia, ventricular noncompaction, and mitral valve prolapse: a new overlapping phenotype. *J Am Coll Cardiol,* 64**,** 768-71.

TOWBIN, J. A. & BOWLES, N. E. 2002. The failing heart. *Nature,* 415**,** 227-33.

TOYDEMIR, R. M., RUTHERFORD, A., WHITBY, F. G., JORDE, L. B., CAREY, J. C. & BAMSHAD, M. J. 2006. Mutations in embryonic myosin heavy chain (MYH3) cause Freeman-Sheldon syndrome and Sheldon-Hall syndrome. *Nat.Genet.,* 38**,** 561-565.

VAN DEN BERG, G. & MOORMAN, A. F. 2009. Concepts of cardiac development in retrospect. *Pediatr Cardiol,* 30**,** 580-7.

VAN DEN HOFF, M. J., MOORMAN, A. F., RUIJTER, J. M., LAMERS, W. H., BENNINGTON, R. W., MARKWALD, R. R. & WESSELS, A. 1999. Myocardialization of the cardiac outflow tract. *Dev.Biol.,* 212**,** 477-490.

VAN DER HEIDEN, K., GROENENDIJK, B. C., HIERCK, B. P., HOGERS, B., KOERTEN, H. K., MOMMAAS, A. M., GITTENBERGER-DE GROOT, A. C. & POELMANN, R. E. 2006. Monocilia on chicken embryonic endocardium in low shear stress areas. *Dev Dyn,* 235**,** 19-28.

VAN DER ZWAAG, P. A., VAN RIJSINGEN, I. A., ASIMAKI, A., JONGBLOED, J. D., VAN VELDHUISEN, D. J., WIESFELD, A. C., COX, M. G., VAN LOCHEM, L. T., DE BOER, R. A., HOFSTRA, R. M., CHRISTIAANS, I., VAN SPAENDONCK-ZWARTS, K. Y., LEKANNE DIT DEPREZ, R. H., JUDGE, D. P., CALKINS, H., SUURMEIJER, A. J., HAUER, R. N., SAFFITZ, J. E., WILDE, A. A., VAN DEN BERG, M. P. & VAN TINTELEN, J. P. 2012. Phospholamban R14del mutation in patients diagnosed with dilated cardiomyopathy or arrhythmogenic right ventricular cardiomyopathy: evidence supporting the concept of arrhythmogenic cardiomyopathy. *Eur J Heart Fail,* 14**,** 1199-207.

VAN KEMPEN, M. J., VERMEULEN, J. L., MOORMAN, A. F., GROS, D., PAUL, D. L. & LAMERS, W. H. 1996. Developmental changes of connexin40 and connexin43 mRNA distribution patterns in the rat heart. *Cardiovasc Res,* 32**,** 886-900.

VAN ROOIJ, E., QUIAT, D., JOHNSON, B. A., SUTHERLAND, L. B., QI, X., RICHARDSON, J. A., KELM, R. J., JR. & OLSON, E. N. 2009. A family of microRNAs encoded by myosin genes governs myosin expression and muscle performance. *Dev Cell,* 17**,** 662-73.

VAN ROOIJ, E., SUTHERLAND, L. B., QI, X., RICHARDSON, J. A., HILL, J. & OLSON, E. N. 2007. Control of stress-dependent cardiac growth and gene expression by a microRNA. *Science,* 316**,** 575-9.

VAN WEERD, J. H. & CHRISTOFFELS, V. M. 2016. The formation and function of the cardiac conduction system. *Development,* 143**,** 197-210.

VANDESOMPELE, J., DE PRETER, K., PATTYN, F., POPPE, B., VAN ROY, N., DE PAEPE, A. & SPELEMAN, F. 2002. Accurate normalization of real-time quantitative RT-PCR data by geometric averaging of multiple internal control genes. *Genome Biol,* 3**,** RESEARCH0034.

VERKERK, A. O. & WILDERS, R. 2014. Pacemaker activity of the human sinoatrial node: effects of HCN4 mutations on the hyperpolarization-activated current. *Europace,* 16**,** 384-95.

VICENTE-STEIJN, R., KOLDITZ, D. P., MAHTAB, E. A., ASKAR, S. F., BAX, N. A., LM, V. D. G., WISSE, L. J., PASSIER, R., PIJNAPPELS, D. A., SCHALIJ, M. J., POELMANN, R. E., GITTENBERGER, D. E. G. A. C. & JONGBLOED, M. R. 2010. Electrical activation of sinus venosus myocardium and expression patterns of RhoA and Isl-1 in the chick embryo. *J Cardiovasc Electrophysiol,* 21**,** 1284-92.

VILLARD, E., DUBOSCQ-BIDOT, L., CHARRON, P., BENAICHE, A., CONRAADS, V., SYLVIUS, N. & KOMAJDA, M. 2005. Mutation screening in dilated cardiomyopathy: prominent role of the beta myosin heavy chain gene. *Eur Heart J,* 26**,** 794-803.

VOET, D. V. A. J. G. 2004. *Biochemistry 3rd edition*, John Wiley & Sons.

VOGEL, M., MCELHINNEY, D. B., WILKINS-HAUG, L. E., MARSHALL, A. C., BENSON, C. B., JURASZEK, A. L., SILVA, V., LOCK, J. E., MARX, G. R. & TWORETZKY, W. 2011. Aortic stenosis and severe mitral regurgitation in the fetus resulting in giant left atrium and hydrops: pathophysiology, outcomes, and preliminary experience with pre-natal cardiac intervention. *J Am Coll Cardiol,* 57**,** 348-55.

VON GISE, A. & PU, W. T. 2012. Endocardial and epicardial epithelial to mesenchymal transitions in heart development and disease. *Circ Res,* 110**,** 1628-45.

VONGVATCHARANON, S., VONGVATCHARANON, U. & BOONYOUNG, P. 2008. Immunohistochemical localization of parvalbumin calcium-binding protein in the heart tissues of various species. *Acta Histochem,* 110**,** 26-33.

VOZZI, C., DUPONT, E., COPPEN, S. R., YEH, H. I. & SEVERS, N. J. 1999. Chamber-related differences in connexin expression in the human heart. *J Mol Cell Cardiol,* 31**,** 991-1003.

WADDINGTON, S. N., KENNEA, N. L., BUCKLEY, S. M., GREGORY, L. G., THEMIS, M. & COUTELLE, C. 2004. Fetal and neonatal gene therapy: benefits and pitfalls. *Gene Ther,* 11 Suppl 1**,** S92-7.

WAGNER, G. P., KIN, K. & LYNCH, V. J. 2012. Measurement of mRNA abundance using RNA-seq data: RPKM measure is inconsistent among samples. *Theory Biosci,* 131**,** 281-5.

WALLIS, J. W., AERTS, J., GROENEN, M. A., CROOIJMANS, R. P., LAYMAN, D., GRAVES, T. A., SCHEER, D. E., KREMITZKI, C., FEDELE, M. J., MUDD, N. K., CARDENAS, M., HIGGINBOTHAM, J., CARTER, J., MCGRANE, R., GAIGE, T., MEAD, K., WALKER, J., ALBRACHT, D., DAVITO, J., YANG, S. P., LEONG, S., CHINWALLA, A., SEKHON, M., WYLIE, K., DODGSON, J., ROMANOV, M. N., CHENG, H., DE JONG, P. J., OSOEGAWA, K., NEFEDOV, M., ZHANG, H., MCPHERSON, J. D., KRZYWINSKI, M., SCHEIN, J., HILLIER, L., MARDIS, E. R., WILSON, R. K. & WARREN, W. C. 2004. A physical map of the chicken genome. *Nature,* 432**,** 761-4.

WALSH, R., RUTLAND, C., THOMAS, R. & LOUGHNA, S. 2010. Cardiomyopathy: a systematic review of disease-causing mutations in myosin heavy chain 7 and their phenotypic manifestations. *Cardiology,* 115**,** 49-60.

WANG, G., ZHAO, X., ZHONG, J., CAO, M., HE, Q., LIU, Z., LIN, Y., XU, Y. & ZHENG, Y. 2013a. Cloning and polymorphisms of yak lactate dehydrogenase B gene. *Int J Mol Sci,* 14**,** 11994-2003.

WANG, J., SONG, Y., LI, H., SHEN, Q., SHEN, J., AN, X., WU, J., ZHANG, J., WU, Y., XIAO, H. & ZHANG, Y. 2016. Exacerbated cardiac fibrosis induced by beta-adrenergic activation in old mice due to decreased AMPK activity. *Clin Exp Pharmacol Physiol*.

WANG, W., BARNABEI, M. S., ASP, M. L., HEINIS, F. I., ARDEN, E., DAVIS, J., BRAUNLIN, E., LI, Q., DAVIS, J. P., POTTER, J. D. & METZGER, J. M. 2013b. Noncanonical EF-hand motif strategically delays Ca2+ buffering to enhance cardiac performance. *Nat Med,* 19**,** 305-12.

WANG, W., XIAO, Z. D., LI, X., AZIZ, K. E., GAN, B., JOHNSON, R. L. & CHEN, J. 2015. AMPK modulates Hippo pathway activity to regulate energy homeostasis. *Nat Cell Biol,* 17**,** 490-9.

WANG, Z., GERSTEIN, M. & SNYDER, M. 2009. RNA-Seq: a revolutionary tool for transcriptomics. *Nat Rev Genet,* 10**,** 57-63.

WEBB, S., QAYYUM, S. R., ANDERSON, R. H., LAMERS, W. H. & RICHARDSON, M. K. 2003. Septation and separation within the outflow tract of the developing heart. *J Anat,* 202**,** 327-42.

WEBER, R., KANTOR, P., CHITAYAT, D., FRIEDBERG, M. K., GOLDING, F., MERTENS, L., NIELD, L. E., RYAN, G., SEED, M., YOO, S. J., MANLHIOT, C. & JAEGGI, E. 2014. Spectrum and outcome of primary cardiomyopathies diagnosed during fetal life. *JACC Heart Fail,* 2**,** 403-11.

WELLS, L., EDWARDS, K. A. & BERNSTEIN, S. I. 1996. Myosin heavy chain isoforms regulate muscle function but not myofibril assembly. *EMBO J,* 15**,** 4454-9.

WESSELS, A., VERMEULEN, J. L., VIRAGH, S., KALMAN, F., LAMERS, W. H. & MOORMAN, A. F. 1991. Spatial distribution of "tissue-specific" antigens in the developing human heart and skeletal muscle. II. An immunohistochemical analysis of myosin heavy chain isoform expression patterns in the embryonic heart. *Anat.Rec.,* 229**,** 355-368.

WIESE, C., GRIESKAMP, T., AIRIK, R., MOMMERSTEEG, M. T., GARDIWAL, A., DE GIER-DE VRIES, C., SCHUSTER-GOSSLER, K., MOORMAN, A. F., KISPERT, A. & CHRISTOFFELS, V. M. 2009. Formation of the sinus node head and differentiation of sinus node myocardium are independently regulated by TBX18 and TBX3. *Circ Res,* 104**,** 388-97.

WITTKOPPER, K., DOBREV, D., ESCHENHAGEN, T. & EL-ARMOUCHE, A. 2011. Phosphatase-1 inhibitor-1 in physiological and pathological beta-adrenoceptor signalling. *Cardiovasc Res,* 91**,** 392-401.

WOLF, C. M., ARAD, M., AHMAD, F., SANBE, A., BERNSTEIN, S. A., TOKA, O., KONNO, T., MORLEY, G., ROBBINS, J., SEIDMAN, J. G., SEIDMAN, C. E. & BERUL, C. I. 2008. Reversibility of PRKAG2 glycogen-storage cardiomyopathy and electrophysiological manifestations. *Circulation,* 117**,** 144-54.

WOLF, C. M. & BERUL, C. I. 2006. Inherited conduction system abnormalities--one group of diseases, many genes. *J Cardiovasc Electrophysiol,* 17**,** 446-55.

WOOD, E. J., CHIN-INMANU, K., JIA, H. & LIPOVICH, L. 2013. Sense-antisense gene pairs: sequence, transcription, and structure are not conserved between human and mouse. *Front Genet,* 4**,** 183.

WU K, M. G., MARTIN J, FINKELSTEIN D 2007. Globin reduction protocol: A method for processing whole blood RNA samples for improved array results. *Affymetrix Technical Note,* Available at: http://media. affymetrix.com:80/support/technical/technotes/blood2_technote.pdf.

WU, S. P., DONG, X. R., REGAN, J. N., SU, C. & MAJESKY, M. W. 2013. TBX18 regulates development of the epicardium and coronary vessels. *Dev Biol,* 383**,** 307-20.

XIAO, B., HEATH, R., SAIU, P., LEIPER, F. C., LEONE, P., JING, C., WALKER, P. A., HAIRE, L., ECCLESTON, J. F., DAVIS, C. T., MARTIN, S. R., CARLING, D. & GAMBLIN, S. J. 2007. Structural basis for AMP binding to mammalian AMP-activated protein kinase. *Nature,* 449**,** 496-500.

XIE, F., XIAO, P., CHEN, D., XU, L. & ZHANG, B. 2012. miRDeepFinder: a miRNA analysis tool for deep sequencing of plant small RNAs. *Plant Mol Biol*.

XUE, Q., ZHANG, G., LI, T., LING, J., ZHANG, X. & WANG, J. 2017. Transcriptomic profile of leg muscle during early growth in chicken. *PLoS One,* 12**,** e0173824.

YALCIN, H. C., SHEKHAR, A., MCQUINN, T. C. & BUTCHER, J. T. 2011. Hemodynamic patterning of the avian atrioventricular valve. *Dev Dyn,* 240**,** 23-35.

YAMADA, M., IKEDA, Y., YANO, M., YOSHIMURA, K., NISHINO, S., AOYAMA, H., WANG, L., AOKI, H. & MATSUZAKI, M. 2006. Inhibition of protein phosphatase 1 by inhibitor-2 gene delivery ameliorates heart failure progression in genetic cardiomyopathy. *FASEB J,* 20**,** 1197-9.

YANG, L., DUFF, M. O., GRAVELEY, B. R., CARMICHAEL, G. G. & CHEN, L. L. 2011. Genomewide characterization of non-polyadenylated RNAs. *Genome Biol,* 12**,** R16.

YANIV, Y., TSUTSUI, K. & LAKATTA, E. G. 2015. Potential effects of intrinsic heart pacemaker cell mechanisms on dysrhythmic cardiac action potential firing. *Front Physiol,* 6**,** 47.

YU, S. L., KIM, J. E., CHUNG, H. J., JUNG, K. C., LEE, Y. J., YOON, D. H., LEE, S. H., CHOI, I., BOTTEMA, C. D., SANG, B. C. & LEE, J. H. 2005. Molecular cloning and characterization of bovine PRKAG3 gene: structure, expression and single nucleotide polymorphism detection. *J Anim Breed Genet,* 122**,** 294-301.

ZAHA, V. G. & YOUNG, L. H. 2012. AMP-activated protein kinase regulation and biological actions in the heart. *Circ Res,* 111**,** 800-14.

ZELIS, R. & MASON, D. T. 1970. Compensatory mechanisms in congestive heart failure--the role of the peripheral resistance vessels. *N Engl J Med,* 282**,** 962-4.

ZHANG, C. L., MCKINSEY, T. A., CHANG, S., ANTOS, C. L., HILL, J. A. & OLSON, E. N. 2002. Class II histone deacetylases act as signal-responsive repressors of cardiac hypertrophy. *Cell,* 110**,** 479-88.

ZHANG, S. S., KIM, K. H., ROSEN, A., SMYTH, J. W., SAKUMA, R., DELGADO-OLGUIN, P., DAVIS, M., CHI, N. C., PUVIINDRAN, V., GABORIT, N., SUKONNIK, T., WYLIE, J. N., BRAND-ARZAMENDI, K., FARMAN, G. P., KIM, J., ROSE, R. A., MARSDEN, P. A., ZHU, Y., ZHOU, Y. Q., MIQUEROL, L., HENKELMAN, R. M., STAINIER, D. Y., SHAW, R. M., HUI, C. C., BRUNEAU, B. G. & BACKX, P. H. 2011a. Iroquois homeobox gene 3 establishes fast conduction in the cardiac His-Purkinje network. *Proc Natl Acad Sci U S A,* 108**,** 13576-81.

ZHANG, S. S. & SHAW, R. M. 2014. Trafficking highways to the intercalated disc: new insights unlocking the specificity of connexin 43 localization. *Cell Commun Adhes,* 21**,** 43-54.

ZHANG, Y., CAI, A. L., REN, W. D., GUO, Y. J., ZHANG, D. Y., SUN, W., WANG, Y., WANG, L., QIN, Y. & HUANG, L. P. 2016. Identification of fetal cardiac anatomy and hemodynamics: a novel enhanced screening protocol. *BMC Pregnancy Childbirth,* 16**,** 145.

ZHANG, Y., QIU, J., WANG, X., ZHANG, Y. & XIA, M. 2011b. AMP-activated protein kinase suppresses endothelial cell inflammation through phosphorylation of transcriptional coactivator p300. *Arterioscler Thromb Vasc Biol,* 31**,** 2897-908.

ZHAO, J. X., YUE, W. F., ZHU, M. J. & DU, M. 2011. AMP-activated protein kinase regulates beta-catenin transcription via histone deacetylase 5. *J Biol Chem,* 286**,** 16426-34.

ZHAO, W., HE, X., HOADLEY, K. A., PARKER, J. S., HAYES, D. N. & PEROU, C. M. 2014. Comparison of RNA-Seq by poly (A) capture, ribosomal RNA depletion, and DNA microarray for expression profiling. *BMC Genomics,* 15**,** 419.

ZHOU, J., LAL, H., CHEN, X., SHANG, X., SONG, J., LI, Y., KERKELA, R., DOBLE, B. W., MACAULAY, K., DECAUL, M., KOCH, W. J., FARBER, J., WOODGETT, J., GAO, E. & FORCE, T. 2010. GSK-3alpha directly regulates beta-adrenergic signaling and the response of the heart to hemodynamic stress in mice. *J Clin Invest,* 120**,** 2280-91.

# Chapter 7 Academic Achievements

## Publications:

1) KL Pang, M Parnall and S Loughna. Effect of altered haemodynamics on the developing mitral valve in chick embryonic heart. Journal of Molecular and Cellular Cardiology. Article under revision.

2) J England, KL Pang, M Parnall, M Haig and S Loughna. 2016. Cardiac troponin T is necessary for normal development in the embryonic chick heart. Journal of Anatomy, 229, 436-449.

## Conferences:

Attended The anatomical society winter conference in Birmingham 2014. Presented my research orally and won the 2nd best young researcher prize.

Attended the European society of cardiology's summer conference in Bordeaux and presented a poster of my reseach.

# Chapter 8 Appendices

## 8.1 Appendix A Optimised cell culture protocol

### Downstairs Fume hood

- If needed, place 2in wells in 24 well plate (in fume hood)
- Put 24 well plates in $CO^2$ incubator
- Put 1 aliquot of 10 % GM in $CO^2$ incubator
- Put 2 aliquots of 5 % GM $CO^2$ incubator (enough for all plates )
- Aliquot enough HBSS

### E34

laminar flow hood in E34 backroom,

- Put 2 aliquots of 10 % GM in E34 incubator
- Ice
- Transfer all eggs to E34 incubator
- Prepare 2 petri dishes with HBSS
- Prepare 5 ml horse serum in 5 ml HBSS on ice
- Rinse Heamocytometer with 70 % EtOH, then dd$H_2O$ and dry - all in fume hood

### E34

50 min

- Take out 6 eggs and quickly swab with 70 % EtOH)
- Crack all eggs, de-shell all
- Remove embryo with spoon into petri dish 1
- Take out heart and place in petri dish 2, remove all excess tissue and stab heart to remove blood
- Place heart in horse serum/ HBSS 1:1

- Do for all eggs

> When about half way through, take out **trypsin** as it should be R/T
>
> > 15 min before use, place in incubator to pre -warm for next step)

## E34

25 min

(1h 15

- Remove horse serum/HBSS
- Wash X2 with 5 ml HBSS
- Place in R/T trypsin solution 0.1 ml / embryo, so:
    - 1.2 ml for 12
    - 1.5 for 15
    - **2.5 ml for 24**
    - 2.7 ml for 27
    - 3 ml for >30
- Incubate at 37 C for 20 - 30 mins with agitation (swirl) every 5 mins
- At end of incubation triturate up and down to further dissociate material.
- Use syringe **without** sharp edges
- Pipette up and down **gently to avoid bubbles** until homogeneous mixture
- Neutralise trypsin **-** Add 15 ml pre warmed GM **(15 ml for 24 – 0.6 ml / embryo)** by slowly pouring through the cell strainer

## E33/ E34

7 min

(1h 22

- Match volume by sight to balance tube
- Centrifuge at 1500rpm for 5 minutes

- Adjust rpm and time yourself at 1500
- Remove supernatant and **re-suspend** pellet in **1ml pre-warmed 10 % GM**.
- **E34**

7 min

(1h 29

Count cells and determine viability with Haemocytometer

- Mix 15 ul cells mix with 15 ul **Trypan blue** (1:1)
- Settle/incubate at R/T for 5 mins

NOW Transfer to downstairs

- dd$H_20$ just on sides of cover slide so it sticks to haemocytometer
- Pipette 12 ul carefully up under slide

10 min

(1h 39

## Downstairs microscope

- Count cells in 2 squares – one corner and the centre (**measure of 0.1 ul**)
- Don't count cells on **top** and **left borders**
- **Divide total by 2** (for cell number $mm^2$)
- **Average against opposite well on haemocytometer**
- **Multiply by 10,000** (for amount in 1 ml)
- **Multiple by 2** (for amount in our original sample (we diluted 1:1))

Dilute cells to 2.75 X $10^6$ (2,750,000 or just 2.75 in my equation) and **–** submit **X** for your cell count in the following equation to work out how much pre-warmed GM to add:

$$\frac{X}{2.75} = \text{Final volume (ml)}$$

## Downstairs fume hood

- Make to correct volume
- Add 20ul to the centre of the **pre-warmed 24 well plate**

5 min

(1h 44

- Incubate for 3 - 3.5 hours (**no longer** than this) at 37C 5% $CO_2$.
- Flood wells with 1 ml of 5% GM after the incubation time

# Notes on solutions

- Prepare fume hood
  - Spray down with 70% EtOH
  - Spray down lids of all reagents

- Prepare (aliquot) – 50 m l
  When new, Aliquot:

  - Aliquot the Hyclone (FBS substitute) **into 50 ml** tubes (don't over fill as serum expands when frozen(9 – 10) **(E170 freezer)**
  - HBSS with $Ca^{2+}$ and $Mg^{2+}$ **50 ml (E168 fridge, stock in D floor)**
  - Horse serum **20 ml (E170)**
  -

All below in E170 freezer:

- Glutamine, 1 ml eppendorfs
- Trypsin EDTA, 1 ml eppendorf
- Strep/ Penicillin 1 ml eppendorf

Place remaining stocks of HBSS and GM (GM = FBS, GLN, P/S) in **D48 fridge**

- **Growth Medium**
  **(use within two weeks)**

*****MAKE 10% AND 6 % SERUM VERSIONS – SEE ADDITIONAL INFO*****

**450 ml** DMEM (Dulbecco's Modified Eagle Medium)

**50 ml** Hyclone ( FBS - Foetal bovine serum substitute )

**5ml** 200mM Glutamine (**add 1 ml per 100 ml solution**)

**1ml** Penicillin/Streptomycin. (**add 1 ml per 500 ml solution**)

- Make 50 ml aliquots (E168 fridge)

- Store at 4 C, use within two weeks

| **5 % VERSION (100 ml)** | **10 % VERSION (100 ml)** |
|---|---|
| Hyclone: 5 ml | Hyclone: 10 ml |
| P&S: 0.4 ml | P&S: 0.4 ml |
| Glutamine: 0.5 ml | Glutamine: 1 ml |
| DMEM: 95 ml | DMEM: 90 ml |

- **HBSS Horse Serum (1:1)**

1 Volume HBSS plus 1 Vol Horse Serum

- **Trypsin/EDTA (20 ml E170 freezer)**

For trypsin/EDTA, stock is X10 (0.5 % w/v)

**NOW WE USE 0.75 X IN HBSS (1.5 ml / 18.5 ml) or 0.0375 % w/v.**

---

❖ Remove all waist in Trigene (under sink E170) beaker

❖ GM colour observations:

- **Orange** = Acid (if orange change GM)
- **Pinkish**/ purple = normal
- **Purple** = Alkali

**Hyclone** (thermo scientific),

Bovine Growth serum supplemented calf

Triple 0.1 um sterile filtered

Cat no. SH30541.03

Lot no. AUE 34991

Bottle no. 500ml

Store at -10 or lower

**Trypsin** – EDTA solution X10

T4H4 – 100 ml

**L-Glutamine** 20 mM

100 ml

Lot RNBC5692

G7518

**Nunc 24 Well tissue culture plate:**

Scientific Laboratory Supplies Nottingham UK. **– Nunclon UK**

# Cell Culture Requirements

## From Stores

LH-SIG2012E DMEM 500ml. £2-26

LH-SIG2024E 200mM Glutamine 100ml £2-26

LH-SIG2025E HBSS 500ml. £2-48

LH-SIG2026E HBSS 500ml. £2-48

(with or without Phenol red – use without for diluting Morpholino)

LH-SIG2031E PEN/STREP 500ml £2-48

LH-SIG2017E DPBS **no** Ca or Mg 500ml. £2-26

Ca and Mg can interfere with cell adhesion: Follow the guideline below to choose appropriate PBS:

- Use DPBS without calcium/magnesium to wash cells if cells are to be trypsinized subsequently.

- Use DPBS containing calcium/magnesium, glucose and sodium pyruvate if cells are to be kept outside of incubator for a long period of time.

### SciQuest

VX31053028 DMEM-Phenol red 500ml £10-56

SH30541.03 Hyclone (thermo scientific), 500 ml

**Cytosine Arabinoside Solutions for non-glutamine maintenance media**

Sigma 100 mg (0.1 g) crystalline

If non separable, dissolve the **100 mg** in **5 ml GM** for 80 mM stock

Dilute to 0.01 mM final working solution, so,

Add **2.5 ul** stock to **19.9975 ml** of GM.

In 1 ml:

**100 mg** to **1 ml GM** = 400 mM

For 0.01 mM

Add **0.5 ul** to **19.9995 ml**

If crystal can be separated,

Weigh out **0.025 g** and add to **2.5 ml GM** for 41.6 mM stock

Dilute to 0.01 mM final working solution, so,

Add **5 ul** stock **to 19.995 ml of GM**.

Keep all at 4 C **wrapped in foil** with **sealing tape around the lid**

**Prepare all in FUME HOOD**

In 1 ml:

**25 mg** to **1 ml GM** = 100 mM

For 0.01 mM

Add **2 ul** to **19.998 ml**

Biochem/physiol Actions

Ara-C incorporates into DNA and inhibits DNA replication by forming cleavage complexes with topoisomerase I resulting in DNA fragmentation; does not inhibit RNA synthesis. Anti-leukemia agent

## 8.2 Appendix B. Solutions optimised and made up in house

**Making solutions from there solutes**

Most accurate way to make all solutions listed is to use w/w. This can also make solutions dissolve quicker, as the correct amount of solvent is added at the start rather than dissolving solute and topping up the solution and is un-effected by temperature.

**Do NOT autoclave (but mix with autoclaved DEPC and use autoclaved DEPC treated glassware):**

- Tris
- Denhardt's solution
- Tween
- Triton
- Hybridization (Hybe) Buffer
- NaOH

**Autoclave (together with DEPC):**

- EDTA
- PBS
- $H_2O$
- SSC
- CHAPS
- MAB

**Tween 20 Solution (Sigma P9416)**

- Use fume hood
- Add 100 ml of RNase free Tween 20 to 400 ml of DEPC treated water (1:5; 20%)
- Aliquot to 10 falcon tubes 50 ml.

Working Conc.

Just to make sure this is clear:

Tween working conc. is always 0.1 %

Tween stock is 20%

**PBST**

- In fume hood
- Add 2.5ml tween 20 (20%) to the 500 ml PBS
- Wrap in foil store at RT

**Glycine 50mg/ml (Fisher G0800/50; M.W. =75.07) (used to stop proteinase K reaction)**

**(working molarity is very low so use mg/ml as units)**

- Add 10 ml DEPC $H_2O$ to glassware
- Add 1 g glycine
- make up to 20 ml DEPC $H_2O$ (Use PBS for *in situ*)
- Dissolve
- Add 20 µl DEPC
- Shake and leave O/N
- Autoclave
- Aliquot in 2 ml

**Note**:

Most accurate way to make all solutions listed is to use w/w. This can also make solutions dissolve quicker, as the correct amount of solvent is added at the start rather than dissolving solute and topping up the solution and is un-effected by temperature.

e.g.

Glycine: 2.5g

PBS: 47.5g

Dissolve

Add 50 ul DEPC

Mix and leave overnight

Double autoclave

**CHAPS (Sigma C3023; M.W. =614.88) (Blocks interactions with Dig)**

**Stock 10%**

- Add 1 g CHAPS in autoclaved glassware
- Add 10 ml dd $H_2O$ and dissolve
- Add 10 µl DEPC. Leave O/N
- Autoclave
- Aliquot 0.5 ml
- Store in -20 $^oC$

**Working Conc.**

For 0.1% add 0.5 ml to 50 ml

For 0.3% add 1.5 ml to 50 ml

**Proteinase K stock 1 mg/ml (Sigma P6556)**

- Use ice in fume hood
- Add all 5 mg P. K to falcon tube
- Make up to 5 ml with PBSt or DEPC treated $H_2O$
- Split 400 µl to single use screw cap Eppendorfs
- Store at -20 $^oC$.

Working Conc.

400 µl in 20ml (20 µg/ml)

**PBST + Glycine (Fisher G/0800/50; M.W. =75.07)**

**Stock (50 mg/ml):**

- In fume hood
- Add 15ml PBST in falcon tubes
- Add 1 g glycine
- Dissolve
- Make up to 20 ml with PBST
- Store at -20 $^oC$

**Working Conc. 1 mg/ml**

Add 2 ml of glycerine stock to falcon tube and make up to 50 ml with PBST. Wrap in foil and store at 4 $^oC$.

**Heparin**

- With ice in fume hood
- Heparin: All 250 mg of in falcon tube
- Make up to 2.5 ml with DEPC treated $H_2O$ (final: 100 mg/ml)
- Dispense 250 µl into screw cup Eppendorfs
- Store at -20 $^oC$

**RNase A (Sigma R4875)**

**Stock 10 mg/ml**

- Dissolve all 100 mg RNase in 10 ml MABT in a flacon tube
- Aliquot to 500 µl
- Sore at -20 $^oC$ **Working Conc. 0.1 mg/ml**

E.g. add 100µl to 10ml MABT

Breaks down unbound RNA but can weaken signal. Last resort for ISH background.

**tRNA (Sigma 10109525001)**

**Stock 100 mg/ml**

- Use ice in fume hood
- Add all 500 mg into a falcon tube
- Make up to 5 ml with DEPC treated $H_2O$
- Dispense 500 µl in screw cup Eppendorfs
- Store at -20 $^oC$
-

**EDTA (Disodium EDTA; Fisher D/0700/53; M.W. = 372.24)**

**Stock 0.5 M**

- Add250 ml dd$H_2O$ in a bottle on stirrer
- Slowly add 93.05 g EDTA
- Adjust to pH 8.0 with NaOH
    - Adjust to over 8.0 pH and leave spinning. Once EDTA dissolves the pH will come down
- Make up to 500 ml with dd$H_2O$
- Add 0.5 ml DEPC treatment
- Autoclave
- 20% x 0.25 ml = 0.1% x 50 ml

**Pre-Hybe (100 ml)**

- Use treated conical flask in fume hood
- **Deionized Formamide**: Add 50 ml (50 % foramide in any hybe buffer)
- **SCC 20X**: Add 25 ml (25 % SSCx20)
- **Citric acid**: Add 0.92 ml of 1M stock (460 ul / 50 ml)
- **EDTA**: Add 1 ml 0.5 M stock (final: 5 mM) ( helps prevent DNA deplexes)
- **CHAPS**: add 1 ml from 10 % stock (final 0.1%)
- **tRNA:** Add 1 ml 100 mg/ml (final: 1mg/ml)

- **Heparin:** Add 50 µl 100 mg/µl (final: 50 ug/ml)
- **Tween:** Add 500 µl 20% stock
- **RNase free $H_2O$**: Add 20.5 ml (final vol. 100 ml)
- Mix and aliquot 12 ml in flacon tubes
- Store at -20 $^oC$

**Post-Hybe (300 ml)**

- Use treated conical flask in fume hood
- **Deionized Formamide**: Add 150 ml (50 % foramide in any hybe buffer)
- **SCC 20X**: Add 75 ml (10 % SSCx20)
- **Citric acid**: Add 2.76 ml of 1M stock (460 ul / 50 ml)
- **EDTA**: Add 3 ml 0.5 M stock (final: 5 mM) ( helps prevent DNA deplexes)
- **CHAPS**: add 3 ml from 10 % stock (final 0.1%)
- **Tween:** Add 1.5 20% stock
- **DEPC treated $H_2O$**: Add 64.74 ml (final vol. 100 ml)
- Mix and aliquot 12 ml in flacon tubes
- Store at -20 $^oC$
- **SSC 1L 20X**
- Add 175.32 g NaCl (3M)
- Add 88.23 g trisodium citrate dehydrate (0.3 M)
- Add 800 ml $ddH_2O$
- Check pH 7. Adjust with citric acid or HCl (usually no need at adjust)
- Make up to 1 L with $ddH_2O$
- Add 1ml of DEPC. Leave O/N
- Autoclave

**SSC 100 ml 20X stock**

- Add 17.53 g NaCl (3 M)
- Add 8.82 g trisodium citrate dehydrate (0.3 M)
- Add 80 ml $H_2O$
- Check pH 7. Adjust with citric acid or HCl
- Make up to 100 ml with $ddH_2O$

- Add 0.1 ml DEPC. Leave O/N
- Autoclave

**4% PFA/PBS**

**PBS**

- Add 4 tablets of PBS in 400 ml $ddH_2O$
- Add 0.4 ml of DEPC
- Shake until everything is dissolved and leave O/N
- Autoclave

**PFA**

- In fume hood
- Add 16 g of PFA
- Add 384 g DEPC treated PBS
- Mix at 65 $^oC$ until fully dissolved (treated spinner and glass wear)
- Add a few drops of NaOH to help dissolve
- Check pH 6.9-7.3 with pH paper
- Add more DEPC treated NaOH if needed

- Aliquot 10 ml in falcon tubes
- Store at -20 $^oC$

**2.5 M NaOH**

- Dissolve 100 g of NaOH in 1 L $ddH_2O$.
- Dissolve in ice in fume hood
- Add NaOH slowly in $ddH_2O$ as heat is generated
- (be careful - pellets will oxidise in the atmosphere)

**5 M NaCl (Fisher S3160/63; M.W. =58.44)**

- Dissolve 29.2 g of NaCl in 100 ml $ddH_2O$ or DEPC $ddH_2O$

**0.5 M MgCl**

– 10.165 g in 100 ml of $H_2O$
– Autoclave



**MAB (M.W. =116.07) 1X**

– 5.8 g Malic acid (0.1 M)
– Add 300 ml DEPC treated $H_2O$
– **NaCl:** 15ml of 5 M (or 30 ml NaCl 2.5 M). final 0.15M
– Adjust pH 7.5 by adding NaOH
    - Using 2.5 M NaOH will take around 30-40 ml
    - Be very careful as it is easy to go beond 7.5 pH
    - Use large magnetic spinner to ensure mixing when checking pH
– Make up to 500 ml $H_2O$ (does not have to be DEPC)
– Autoclave
– Store at 4 $^oC$

(1 liter is often more practical to make up)

**MABT**

– Add 2.5 ml Tween 20 (20%) in 500 ml MAB

**Sheep Serum (Sigma S3772)**

– Place sheep serum in heat bath for 30 min at 56 $^oC$ to inactivate antigen.
– Aliquot in 1.5 ml
– Store at -20 $^oC$.

***Working Conc.* 1:5 (20%) solution**

e.g. 1.3 ml in 6.5 ml (in what you use at the time)

If used in IHC must not be the same as the primary antibody, but can be the same as the secondary.

**Tris 1 M; pH 9.5**

- Add 24.228 g Tris in 100 ml DEPC treated $H_2O$
- Dissolve in RT
- Adjust pH to 9.5 using HCl (takes around 10 ml)
- Make up to 200 ml with DEPC treated $H_2O$
- Autoclave or filter (manufacturer states that tris can be autoclaved)

**Levamisole (Tetramisole hydrochloride; Sigma L9756-5g; M.W. =240.75)**

**Stock 100 mM**

- Use fume hood
- Add 0.48 g in 20 ml dd$H_2O$ (will not dissolve in colour reaction buffer)
- Store at -20 $^oC$ in 1 ml aliquots
-

**Working Conc. 5 mM**

- 1:20 in BCL
- E.g. 1 ml in 20 ml BCL
- Store at -20 $^oC$

**Blocking Buffer 2%**

- Add 2 g boehringer in 100 ml MAB (measure out w/w)
- Place on rotor at 80 $^oC$ until dissolved
- Autoclave
- Aliquot 10 ml
- Store at -20 $^oC$

**Solutions for RNA gels and RNA preps**

**MOPS (Fisher 327661000) Buffer**

**Stock 5X**

- Pour 50 ml DEPC treated $H_2O$ in a flacon and add:
- 10.45 g of MOPS (0.2 M; pH 7)
- 1.7 g of NaAc (50 mM)

- 0.46 g of EDTA (5 mM)
- Dissolve and filter into bottle
- Make up to 500 ml with DEPC treated $H_2O$
- Store at 4 $^oC$

**TAE Buffer (50X) (Appropriate for RNA gels and gel purification techniques as well as standard)**

- (Perform in fume hood)
- Add 750 ml DEPC $H_2O$ to a 1 litre DEPC treated bottle
- Add 242 g Tris (2 M)
- Add 100 ml EDTA stock solution (0.5 M (see below)) for 50 mMAdd**:** Slowly add 57.1 ml glacial acetic acid (17.4 stock M) for 1 M
  (Note: always add acid to the solution – never add another solution to concentrated acid)
- Make up to 1 L with DEPC $H_2O$

Working concentrations in Gel – 1 X TAE (20 ml in 1000ml)
Tris final: 40 mM
Acetate final:20 mM
EDTA final: 1mM

**RNA Sample Buffer (for RNA gel)**

- 1 ml deionized Formamide (64.5%)
- 350 µl 37% formaldehyde (22.5%)
- 200 µl MOPS buffer 5X (12%)

Aliquot in fume hood and place in ice in 100-70 µl then place in -20 $^oC$.

**Sodium acetate trihydrate (Sigma S8625; M.W. =136.08)**

- **3 M:** 81.65 g NaOAc to 200ml dd$H_2O$. pH 5.2 use glacial acetic acid

- **2 M:** 54.4 g NaOAc to 200ml dd$H_2O$. pH 4 use glacial acetic acid
- Add 0.2 ml DEPC. Leave O/N
- Autoclave

**Other**

**Sigma Primers 100 mM**

**Working Conc. 10 mM**

- Do a 1:10 dilution
- E.g. 20µl primers in 180 µl DEPC treated $H_2O$

## 8.3 Appendix C. Optimised *In situ* hybridisation protocol

### Sunday pre-treatment (HH25 – HH35)

**Cut after rehydration**
**Cut/ stab**

- **1, Keep hearts whole, but stab each chamber**
- **2, Make frontal (coronal) cut through heart to reveal chambers**
- **3, Cut hearts into atrial and ventral halves (de-membrane HH16)**

**Whole hearts follow exact protocol that follows; cut hearts must have modification on time.**

**Rehydrate HH25**

**IN 20 ML STERILIN – ALL EMBRYOS AT SAME TIME UNTILL PRE-HYDRIDISATION**

**1,** Select the embryos then rehydrate into PBST (0.1% **Tween20** in PBS) in the following gradient process at R/T on rocker:

***Embryos should sink, if not make washes longer**

| | |
|---|---|
| 95% MeOH + 5% PBSt | 10 -30' x 3 |
| 75% MeOH + 25% PBST | 10-30' X 3 |
| 50% MeOH + 50% PBST | 10- 30' X 3 |
| 25% MeOH + 75% PBST | 10-30' X 3 |
| 100% PBST | **3 x 10-30'** can leave O/N at **4 C** |

WHEN CHANGING SOLUTIONS, KEEP THE EMBRYO COMPLETELY COVERD IN OLD SOLUTION TO STOP EMBRYOS FLATTENING AND ALLOW MORE GRADUAL REHYDRATION

Make section cuts on Monday morning before start of insitu on hearts post HH29

## Day 1 (Monday)

**In wells – bisect hearts if necessary**

- Turn on C floor oven
- Take out glycine PBS to thaw
- Take out proteinase K on last wash
- Thaw P

Glycine:2 ml stock made up to 50 ml PBSt (50 mg/ml glycine stock E168 - 20)

- If not already present, add 0.1-0.3 % CHAPS to **Pre-hybe**.
- 0.1 - 0.3 ml of 10% stocks to 10 ml.

6, Wash 1x 10 - 50' 25% PBST + 75% Hybe buffer– Embryos must sink

**Digestion of cellular proteins** ! NO SHAKING! ! STOP IF DEGRADATION OBSERVED !

Treat with Proteinase K (0.02 – 0.04 mg/ml) for 17' – 2h RT

1. From 1mg/ml in PBST STOCK, add **400 ul single** use aliquot to **20 ml PBST** (0.02 mg/ml, on later embryos can increase up to 0.04 mg).

2. Incubate embryos at R/T **for 17' – 2h** BUT WATCH AND STOP IF DEGREDATION OCCURS

3. Stop the Proteinase K with **glycine** 2 mg/ml in PBST (PRE MADE)
   - First wash is rinse
   - Then **5 - 30'**
   - NOW PBSt only
     - Rinse
     - **5 - 30'**

4. Re-fix embryos in 4% PFA in PBS 30 - 45' RT.
5. Rinse X3 in PBST at R/T ALL.
   - First wash is rinse
   - Then **5 - 30'** on 2nd and **10 – 1.5'** for remaining wash
   - Now on rocker plate

- Thaw out CHAPS for hybe if not pre added

**TRANSFER EMBRYOS TO 24 WELL PLATE (RAPPED IN FOIL AND LABBLED), 2 - 3 PER WELL PLATE**
**TO PREVENT EVAPORATION PLACE FOIL DIRECTLY OVER WELLS THEN PLACE LID ON TOP**

7, Prehybridise in **1 mL Pre-**Hybe buffer. **3 – 6 h 66˚C** in incubator on C floor. KEEP PRE-HYBE ON ICE BEFORE INCUBATION

(can be O/N)

## TRANSFER PLATE TO C20 FLOOR INCUBATOR

8, Replace prehybe with prehybe buffer ALREADY MIXED WITH PROBE

- Turn incubator to 64 C (optimise: 58 – 67 C)
- Add **X ul** probe to **750 ul** Hybe **plus chaps** on ice (start with 4/750 and optimise
  up or down)
- **Mix up** and down with pipette and then cover embryos with the **750 ul.**
- Place in hydrated box wrapped in cling film inside incubator
- Incubate: 2 nights recommended, but one usually works fine. Try to get at least 16 hours though

Recommended is 0.1 ug – 1 ug / ml probe, another source stats 0.5 ug / ml as the max amount. We estimate 30 ug probe in 56 ul = 530 ng / ul.

Further source stats 1:1000 on brain tissue.

- IF GENE IS WEAKLY EXPRESSED INCREASE THE HYBRIDISATION TIME.
- For each 1 % **mismatched** base pairs, reduce hybridisation temp down from 65 C by 1 C if possible - Stringency washes must be matched accordingly.

**Make solutions on next page and pre-warm with plate**

## Day 1 pre-warm solutions

- Hybridisatation day. Prepare washes for tomorrow

1, Pre warm stringent washes (1-3 below) in incubator O/N !!! **DO NOT USE DEPC - JUST DDH$_2$O!!!**

- Will need to thaw 3 aliquots of CHAPS

**1,** 50/50 Hybe/ddH$_2$0 (conc. = ssc2.5 with 25 % formamide )

Post hybe 10 / H$_2$0 10 ml **Pre-warm 65 C (for 2 washe**

CHAPS 0.1% - add 200 ul in 20 ml

Adding up % solutions:
Solution1 = 5% x 100 ml / 100 = 5 (5 ml of the solution is 100 SSC)
Solution 2 = 15 % x 100 ml/ 100 = 15
Final solution = (20 ml (SSC) / 200 ml (total volume)) x100

**2,** SSCx2 5 ml SSCx20 / 45 ml ddH$_2$O (1 – 2 falcons)

CHAPS 0.1% - add 500 ul in 50 ml

**Pre-warm 65 C (for 3 washes)**

**3,** SSCx0.2 5 ml SSCx2 / 45 ml ddH$_2$O (1 – 2 falcons)

CHAPS 0.1% - add 500 ul in 50 ml

**Pre-warm 65 C (for 4 washes)**

**4** 50/50 SScx2/MABTw (conc. = ssc1)

5 ml SSCx2 / 5 ml MABT

**leave at R/T in E168 (1 wash)**

**Note:**
Formamide reduces the stability of double stranded polynucleotides i.e. reduces the temp that DNA denatures.
Each % formamide reduces binding temp by 0.74 $^{o}$C, so, if denaturisation starts at 75 $^{o}$C normally, then with 50 % formamide it will at 37 $^{o}$C. With 25 % around 56 $^{o}$C.

## Day 5

## Day Two (Tuesday)

**Wash – remove non-specific bound probe**

**Stringency washes**

(The lower the salt, higher the temp and longer the washes; the more DNA removed – so increase all to reduce background, or reduce all if signal low)

- Incubate wash solutions at 65 C for 1 hour
- Remove well plate and take to D. Brooks lab for washes
- Keep incubator to **65 C (58 – 67 C)**.
- THAW BLOCKING BUFFR AND SHEEP SERUM
- Turn on incubator in chick lab 37 C
- Turn on chick lab incubator to 37 C

**Wash 1**

- C20
- Turn on 37 c incubator
- Ensure small amount of fluid remains always in wells to prevent nonspecific binding
- Filter tips and DEPC no longer needed

1. Remove the Hybe containing the probe and put in another tube (this can be reused at least twice and may give lower backgrounds when reused, though never compare new to old).

2. The following washes are **all** done in the 55 - 65˚C in incubator with **agitation/ on rocker plate**. All the SSC solutions contain 0.1% Tween20.

- 1 ml in each well on short washes
- 2 ml on long washes

| | | |
|---|---|---|
| **1**, | 50/50 Hybe/ SScx2 (sscx2.5 conc.) | 2 x 15' – 1h |
| **2,** | 2x SSC | |
| **3,** | **0.2x SSC** | 4x15 30' |

**SSC and MABT (non stringent)**

- E161

3. Using the pre made **MABTw (0.1 % TWEEN)**. The following gradient washes are done at RT on shaker (horizontally, speed 5 (gentle)):

| | | |
|---|---|---|
| **1, 50/50** SScx2/MABTw (ssc1 conc.) | | 10 - 30' |
| **2,** 100% MABTw (make up RNase) | | 10 - 30' |

- Thaw sheep serum if needed - Thaw blocking buffer

**RNase (!Can slightly reduce genuine signal if left to long!)**

4. Add 100 ug/ml RNase in MABTw
   - 1 - 2ml per well

- 37 C for 30' – 1.25h in chick lab incubator
- Agitate every 5 - 10'

5. **Wash**
   - MABTw X3
     - Rinse
     - 5 - 15' at 37 C, 5' on rocker
     - 5' at 37 C, 10' – 1h on rocker

Make solution fresh:-

- 1.4 ml ss in 7 ml total vol
- 1.2 ml ss in 6 ml total vol
- 1 ml ss in 5 ml total vol

**Block**

- **E161**

  **ALL STOCKES OF BLOCKING SOLUTION ARE**

  **ALLREADY AT 2**

RNase - Make solution fresh:-

- Add 200 ul of 10 mg/ml stock
- To 20 ml MABTw

6. Block with 2% Boehringer B… S 20 % SHEEP SERUM (for **3h** (or more, m… O/N). RT gently shaking (horizontally).

To work out sheep serum amount (if not already added):

Divide starting volume by 0.8 to give the final volume – then make up to this amount with sheep serum

**Apply DIG antibody**

- **Centrifuge antibody at 5000 rpm for 3' and ONLT pipette from top**

7. Replace with antibody DIG 1:5000 in MAB Blocking buffer, anti-Dig-AP (alkaline phosphatase) Fab fragments are stored in the fridge) diluted in 1% Boehringer Blocking Reagent™ in MAB + 5 % ss.

   - 1 ml per well e.g. 6 wells = make up 6.450 ml etc…
     - 2900 ul MAB

**5 Wells**
2688 blocker
269 serum
2417 MAB
1.08 antibody
**MIX**

- 3225 ul 2% blocking solution (for 1 % w/v)
- 323 ul sheep serum (for 5 %)
- 1.29 Antibody
- MIX

| **10 Wells** |
|---|
| 5.25 blocker |
| 500 ul serum |
| 4.73 MABt |
| 2.6 ul antibody |
| **MIX** |

| **7 Wells** |
|---|
| 3760 blocker |
| 375 serum |
| 3390 MAB |
| 1.5 antibody |
| **MIX** |

- Shake for a few minutes RT then put in the fridge at 4 C O/N in fridge.
- CAN INCREASE TO **1:4000** IN WEAKLY EXPRESSED GEN

*(If you are in a real hurry you can do this for 3h RT shaking – the antibody solution must be prepared on day of use).*

## Day 3 (Wednesday)

(as usual, add 1 ml to embryos throughout)

1. Shake 30' RT. Remove the antibody solution, which can be reused *(only reuse antibody in Block + MAB if you are going to do so within a few days, it's hard to tell if it has been infected because it's **already turbid**).*

**Removal of unbound antibody**

2. Wash with MABTw RT.

- Can remove wash with same pipette tip as all well solutions are the same
- Use new for filling as you will be pipetting from working stock solution
- Place on rocker plate

- WASH 1. 15'
- WASH 2 – 5. 60'
- WASH 6. O/N at 4 C

## Day 4 (Thursday)

- Make up BCL Buffer from stocks

➢ **BCL Buffer III (50ml) made up from stocks (shown on left):**

| | | |
|---|---|---|
| 1M Tris-HCl (pH 9.5) | 5 ml | (for 0.1M) |
| 5M NaCl | 1 ml | (for 0.1M) |
| 0.5M $MgCl_2$ | 5 ml | (for 0.05M) |
| Tween20 (20%)<br>(Foil rapped) | 0.25 ml | (for 0.1M) |
| - MAKE UP TO 50 ml dd$H_20$ | | |

Make up **Levamisole** from 100 mM stock, 5mM working conc.

- 1 ml to 20 ml BCL for washes
- 0.5 ml to 1:1 puple /BCL

**Levamisole Stock**
In -20 E170 – see work folder
Stock: 100mM
Working Conc. : 5mM

**Levamisole in BCL foil equilibration**

5 wells = 900 ul in 17.5 ml total BCL

>7 well = 1.2 ml in 25 ml total BCL

**3.** Equilibrate wells with developing BCL buffer III + Levamisole

- 3x5’ RT

(for X-phos/NBT, 0.1M TrisHCl pH 8.2 for Fast Red).

4. For purple, now **replace** with developing buffer containing **BCL buffer + BM Purple™ 1:1**

    - Get Bottle to R/T
    - Invert once
    - *MAKE UP: BCL buffer + BM PurpleTM 1:1. Must be made on the day as BM purple is sensitive to light.*
    - *Add 1 ml to wells*

    *Check throughout day at start every 25 mins!*

    *(if you have tested your probes, you can leave it O/N in the fridge O/N, – works quicker when hotter)*.

    Develop at RT protected from light (in dark) until colour develops (in foil wrapped petri dish and placed on rocker plate).

**To check embryos…**

Check WT for stain

Replace back on rocker plate **(wrapped in foil)**

BM Purple for over-stain **OR** weakly expressing gene…

As with other solutions, but with **75 %** BM Purple

e.g.
**For 7525 ul**

- 5645 ul BM purple
- 375 Lev
- 1500 BCL

*(It could take from tens of minutes to hours depending on the strength of the signal. Rate of colour development can be altered by raising or lowering the temperature in the range 4˚C to 37˚C).*

**Eliminate background**

If background starts to appear before genuine signal, stop the reaction with PBST wash (see below) and then restart at stage 3. This only works if tissue is NOT over

stained. An O/N step may have to be used in PBST. This may need to be done multiple times to obtain true signal. Also can pause reaction to continue later.

**First pictures**

5. Take initial photos of embryos when reaction has taken place

**Stop colour reaction**

6. Stop reaction when colour reacts correct intensity and localisation by washing with:

   PBST 3x15'.

**Take Whole mount pictures**

7. Remove last PBST wash and replace with 50/50 PBST/Glycerol mix 15'
8. Finally add 500 ul 100 % Glycerol to wells
9. Leave o/n at R/T on rocker plate
10. Take pictures the following morning

**11**, To permanently stop the reaction either **re-fix** in:

- PFA ( at least 45' RT)
- or wash with 0.1M glycine-HCL pH 2.2 4x5'.

Store in PBS at 4 C

**Useful tips:**

- Can leave the embryo longer if purple colour can't be seen yet after leaving overnight at 4°C.
- Avoid developing too much colour due to increase possibility of high background (pink colour)

- If getting pink background? – might need to increase the temperature from 65° to 67°C.
- For embryos for ISH, sectioning might need to be performed at 20µM and usually purple colour needs to be over-developed as the colour might be washed off throughout processing.
- Optimisation will probably be required for all times and temperatures for different embryos
- Embryos may be stored at 4°C in 80 % Glycerol
- Young HH12 embryos might not need Proteinase K treatment
- If the procedure does not work, try pre-absorbing:
    - Try anti-DIG-AP fab fragments diluted to 1:5000, anti-fluorescein-AP fab fragments to 1:2000 in 2% anti-fluorescein-AP fab. Absorb about 1ml onto about 50µl of fixed, MeOH'd, rehydrated embryos/fry, 1h RT, then 4˚C O/N.)

**To section/ permanently store:**

- Overstain for 24 hours on rocker at R/T
- Stop reaction with PBSt 15 min X3
- Fix O/N on rocker at 4 C (can store embryos at 4 C)
- PBST (**15 min X 2** on all following steps unless stated otherwise) and **store at 4 C indefinitely**
- $H_2O$ (the following dilutions are with $H_2O$
- 25 % (**Ethanol**)
- 50 %
- 75 %
- 95 %
- 100% X3 (can store at -20)
- Xylene X3 (must be at room temperature)
- Xylene/wax X1
- Wax X2 (can store indefinitely)

- Pre-cut and mount the block correctly in the microtome machine. Make sections of 7- (**15**) - 20 mm thickness and put the resulting ribbons on paper. Meanwhile, preheat a microscope slide on a heating plate at 45 C.

- CRITICAL STEP Ribbons are easily blown away and lost, so try to avoid air movement near the ribbons.

- Add a large drop of 10% ethanol (approximately 1 ml) on the heated slide and allow the ribbons to float on top of it, with their shiny face down.

- CRITICAL STEP Avoid forming air bubbles underneath the ribbons, as these will damage the section.

- Wait for 5 min, and then remove the liquid. Blot excess liquid with a kim-wipe, but never touch the section directly. Leave the slides O/N on the heating plate at 45 1C.

- Counterstain with Contrast Red (see Box 4) to colour the nuclei pink, which contrasts the blue-coloured cytoplasm. Finish by mounting in Permount.

## 8.4 Appendix D. Method for the preparation of RNA from cells / tissue

- **Materials:**

1. RNase- and DNase-free pipette tips and tubes **(filtered)**
2. If doing 2 ml Trireagent, homogenise in competent cells tube – Fisher 35-2063; if do 1ml, or use **2ml centrifuge tubes** – are from stores or Starlab E1420-2000, **or found in bottom draw near photography microscope in E161**
3. **TriReagent - 4 C** (Ambion AM9738; Sigma T9424)
4. **1-bromo-3-chloro-propane (BCP) (SIGMA B9673) – secure cabinent -**
5. **2M** sodium acetate, **pH 4** (DEPC-treated, autoclaved)
6. **Isopropanol (Propan-2-ol), MOLECULAR GRADE BP2618.500 – secure cabinet**
7. 70% ethanol (made with DEPC-treated, autoclaved water **- 20 ml, 14 ml ETOH, 6 ml DEPC**)
8. DEPC-treated water (autoclaved)
9. **DNase I and RDD buffer from Qiagen – buffer 4 C, DNase -20**
10. phenol/chloroform/isoamyl alcohol **– Fridge door E161. Phenol is kept under another aqueous layer to prevent going off. If phenol has gone off it will be yellowish – use an aliquote taken from the stock solution on the protocol. AMRESCO 0966-100 ml pH 5 (see back page)**
11. **3M** sodium acetate (w or w/o 100mM Mg-acetate), **pH 5.2** (DEPC-treated, autoclaved)
12. Absolute ethanol – **Yellow hazardous chemicals cabinet E168**
13. **SDA DEPC $H_20$ – 1 %, 5 g SDS in 500 ml DEPC (SDS on shelf in E168)**

**ADDITIONAL:**

- **Use RNase free ethanol as RNase can reform after denaturisation**
- **RNase free water (BUY IN NON-DEPC)**

- ON WASHES, USE AT LEAST THE SAME VOLUME AS THE SOLUTION YOU ARE WASING OUT, I.E. 500UL ETOH TO WASH OUT 500UL PHENOL



**= Reagent**



= **Equipment**

= **Can stop and freez**

## Lysis/ Homogenise

*The following protocol shows stages where the sample is stored at either **-20** or **-80°C** at the bottom of each page allowing protocol to be split up if required – show in green.*

### For Tissue Extraction

**Pre cool:**
Eppendorf rack in -20
2M NaAc -20
Isopropanol -20
Centrifuge 4°C

Use the 2 ml RNA tubes throughout - makes wash steps easier (not disrupting pellet)

**Don't vortex until after DNase step! as DNase has low efficiency om single stranded DNA**

**1.** Get **tissue** on **dry ice** from -80

-

- **Add 1ml Tri-Reagent**

The volume of the tissue should not exceed 10% of the volume of the TRI Reagent – this will dissolve RNA and DNA in the tissue

2. Homogenise thoroughly by **NEDDLE HOMGENISE**

Suck up and down until homogenous then change needle

- 1, Needle 21 (0.8 green – not usually needed)
- 2, Needle 23 (0.6 blue)

  **Use above on hearts older than HH25, otherwise you can just use Needle 25 only**
- **3**, Needle 25 (0.5 yellow)

3, Put on ice until all hearts are homogenised, then:

4**, Incubate** the homogenates for **5 minutes** at room temperature to permit complete dissociation of nucleoprotein complexes

**3.** Add 0.2ml **(200 ul)** of **1-bromo-3-chloro-propane (BCP)** per millilitre of Tri-reagent.

**USE NEW TIP EACH TIP AS THEY CAN MELT!**

(0.2 ml / ml, so if 1 ml of Tri-reagent: 0.2ml of 1-bromo-3-chloro-propane (BCP)

BCP separates to phases – RNA (TOP PHASE), DNA (interphase) and proteins in lower phase. So endogenous RNase should all be removed here

**4.** Mix the samples by **vigorous shaking** or overtaxing until cloudy

- **THEN INCUBATE FOR 3 MINS at R/T** before centrifugation…

**5.** **Separate** the mixture into two phases by centrifuging

- **10,000g (no higher than this speed)** for **15** minutes at 4°C

1. **Transfer the upper aqueous phase** to fresh tube 2ml RNA tube

   - Pipet just below meniscus (No bubble at this step)

     - 450 + 30 ul

   - do not pipet up white intermittent or red phase, *if you do*, centrifuge again.

2. **IN FUME HOOD! Precipitate** the RNA from the aqueous phase: For each **ml of Tri-reagent add:**

   - **0.25ml** 2M NaAc, **pH 4 at -20** (ON BENCH),

   - **0.7ml Isopropanol (molecular grade) at -20**. (Found in yellow cabinet)

3. **Mix** thoroughly by overtaxing, store the final solution for **1-3 hours at -20 or O/N**

## Now Prepare:

Aliquot 3M NaAc in fume hood and put at -20

Aliquot 70 % EtOH in fume hood and put at -20

70% ETOH

17.5 ml ETOH

Make up to 25 ml $H_2O$

Aliquot 100 % EtOH in fume hood and put at -20

## DNase treat and Purify

- Turn on **hot plate** - **Get aliquoted RDD buffer to room temp**
- Pre heat **RNase free** $H_2O$ to 63 C

**Purify:**

4. **Collect** the precipitated RNA by centrifugation at
   - Maximum speed (17500 x*g*) for **15 minutes at 4°C** in a microfuge.
   - Pellet will form
   - Discard supernatant

5. **Wash** the pellet **twice** with RNase free **70% ethanol**

   – Add **1300ul** ethanol
   - Centrifuge 17500 x*g* for **15 minutes at 4°C**
   - Pipette out excess after centrifuge
   - **Add 300ul** ethanol wash
   - Centrifuge 17500 x*g* for **15 minutes at 4°C**
   - Pipette out excess after centrifuge
   - Give Pulse spin (about 5000 rpm)
   - Pipet out remaining ethanol
   - Store open on bench 1 – 3 mins (too long and dry will hinder pellet dissolving step!)

RNase free 70% ETOH

17.5 ml ETOH

Make up to 25 ml $H_2O$

6. **Add** 50-100µl of **RNase free $H_2O$**
   - **Add 87.5 µl**, (avoids having to adjust volume in next step)

7. Dissolve pellet:
   - Heating to 62 C for 1 -5 min
   - A **Very gentle** vortex to help dissolve, after vortex, give pulse spin to locate SDW on pellet and return to 62 C
   - Repeat Xn (pellet must be dissolved)

**DNase treatment:**

DNase 1 does not work on broken up DNA very well– so don't vortex before this step – after is fine

**Prepare:**

Get centrifuge to **12 C** for phenol step

8. Prepare for DNase treatment

- **ROOM TEMP 10µl RDD buffer (must add buffer first – aliquot out amount needed!)**
- Add 10 ul buffer to the sample, give quick mix flick and tap

(if not already, adjust total volume to **100µl** with **DEPC water**)

- Add the 12.5 ul mix to the sample give flick and quick centrifuge

9. Incubate at warm room temperature for **15 minutes and mix by gently.**

– **Must be 20 – 25 C. Hold in hand and gently rotate or put on rocker**

DNase can also be used on columns but with different amount of buffer

**Purify pure RNA**

Phenol Chloroform at R/T

Add aliquoted sigma water to bring volume to 500 ul – so 400 ul from the last step

- Add 500 ul Phenol Chloroform !!! **FOR RNA USE**

Ensure no upper phase is left in the tip by pipetting down into the phenol solution

- Shake vigorously until cloudy - **vortex for about 1 min**
- leave at R/T for 3 mins (over 10 mins can degrade DNA!)

Amounts = 480 ul into bubble

- Centrifuge at 11000 x*g* for 12 mins at 12 C
  - Collect aqueous phase to new 2 ml eppindorf
  - Avoid contaminants too near the interface

**Chloroform only step (fume hood):**

- Add aliquoted sigma water to bring volume to 500 ul…
- Add 500 ul Chloroform (use new pipettes as it melts plas
- Shake vigorously until cloudy (vortex for about 1 min)
- Centrifuge at 11000 x*g* for 10 mins at 12 C
  - Collect aqueous phase to new 2 ml eppindorf
  - Avoid contaminants too near the interface

This is required to remove phenol that can inhibit enzymatic reactions.

Amounts = 400 to bubble, then 30 ul from bubble

**Precipitate (all at -20)**

Aliquot 3M NaAc in fume hood and put at -20 ☐

Aliquot 100 % EtOH in fume hood and put at -20 ☐

- Add 1/10 volume 3M sodium acetate pH 5.2 **(supernatant / 100) X10)** i.e. 430 ul = 43 ul

And

- 2 volumes of 100% ethanol (stock at -20) **(twice the supernatant)** i.e. 430 ul = 860 ul

And

- Mix by inversion and place in -20 **IN PRECOOLED RACK overnight**

- Pre-cool centrifuge

- Pre heat RNase free H2O in 1 ml aliquots

**Pellet ( 2nd day, or 3rd day)**

- Centrifuge17500 x*g* for **13 minutes at 4°C**
- Carefully pipette out and discard supernatant - keep pellet

**Wash and store**

- 1 ml 70 % ethanol (-20) directly over pellet and finger tap to dislodge
- Centrifuge at max - 17500 rpm 15 mins 4C
- Pipette out supernatant

Aliquot 70 % EtOH in fume hood and put at -20

Repeat to ensure purity at least **X1** totally covering pellet (about 300 ul), then:

- Pulse spin
- Pipet out
- Air dry 3 – 5 mins

Turn on heat block to 62 C

- Dissolve pellet in 50 ul **(less will give higher concentration)** aliquated sigma distilled by:-

E170

- Heating to 62 C for 1 min
- Vortex to help dissolve, after vortex, give pulse spin to locate SDW on pellet and return to 62 C
- Repeat X3 (pellet must be dissolved)
- Nanodrop on ice put and straight to store at **-80**

Get ice

**DNase**

1500 kunits units stock dissolve in 550ul

So, 2.81 kunits units per ul

1 mg = 2000 Kunitz units

1000 ug = 2000 Kunitz units

So, 2 units per ug

1000/2000 X 100 = 50%

So,

50 % of 1500 is 750 ug or 0.75 mg. So we have a total of 750 mg DNas1 in stock solution.

So in our 550 ul stock we have 1.364 ug per ul.

**In our reaction we have 2.5 ul. So a total of 3.41 ug in 100 ul reaction volume. So 34.1 ng/ ul**

Column reaction has 10 ul / 80 ul so 175 ng/ul

RNase-Free DNase Set (50)

79254

## 8.5 Appendix E. Linearisation and riboprobe synthesis

E170

*Vortexing can shear DNA over 5 Kbp!

*RNA and ssDNA will remain in aqueous phase as Nitrogen bases can interact with $H_2O$.

**Digest (table overleaf)**

-Add to 1.5 ml RNase free eppindorf in the quantities listed in table **(make master mixes)**:

1, DEPC ddH20 (use aliquoted sigma water)

2, Buffer

3, DNA

**MIX and SPIN**

4, Enzyme in appropriate dilution buffer (keep on ice)

**MIX (DO NOT VORTEX!) and TAP/SPIN**

- Incubate at 37 deg (use heat bath). Can leave O/N, though may degrade DNA – check for linearization after 1 h, should be compete.

(from overleaf)…Add aliquoted sigma water to bring volume to 500 ul…

Phenol aliquoted in fume hood in 580 ul put at 4 deg in dark



- Add 500 ul Phenol Chloroform
  - Shake vigorously until cloudy (vortex for about 1 min)
  - leave at R/T for 3 mins (over 10 mins can degrade DNA!)

E41
C386X

- Centrifuge at 11000 x*g* for 9 mins at room temperature
  - Collect aqueous phase to new 2 ml eppindorf
  - Avoid contaminants too near the interface

E170

**Precipitate (ALL MUST BE AT -20, INCLUDING CENTRIFUGE)**

Aliquot 3M NaAc in fume hood and put at -20



- Add 1/10 volume 3M sodium acetate pH 5.2 **(supernatant / 100) X10)** i.e. 480 ul = 4
  And
- 2 volumes of 100% ethanol (stock at -20) **(twice the supernatant)** i.e. 480 ul = 960 ul
  And
- Mix by inversion and place in -20 for at least 1 hour **(PREFERABLY overnigh**

Aliquot 100 % EtOH in fume hood and put at -20



E41

- Pre-cool rotor and centrifuge
- Centrifuge 15000 rpm 15 mins 4C, carefully pipette out and discard **all** supernatant - keep pellet

**Wash and store**

- Totally cover with 70 % ethanol (-20) directly over pellet and finger tap to dis
- Centrifuge at 15000 rpm 15 mins 4C
    - pour of if pellet easily visible
    - Pulse spin
    - Pipet out
    - Air dry 3 – 5 mins

Aliquot 70 % EtOH in fume hood and put at -20

Turn on heat block to 62 C

- Dissolve pellet in 11 ul aliquated sigma distilled by:-
    - Heating to 62 C for 1 min
    - Vortex to help dissolve, after vortex, give pulse spin to locate SDW on pellet and return to 62 C
    - Repeat X3 (pellet must be dissolved)
    - Nanodrop on ice put and straight to store at -20

E170

Get ice

DNA = 15/x ng/ul = 47.5…
15/ **0.315 ng**/ul = 46 in min amount possible from midi prep

| | Reagent | 1: | 2: | 3: | 4: | 5: | 6: |
|---|---|---|---|---|---|---|---|
| 1 | **SDW** (make up to 75 ul) | | | | | | |
| | **Cut smart Buffer** (thaw on ice) | 7.5 | 7.5 | 7.5 | 7.5 | 7.5 | 7.5 |
| | **DNA (15 ug)** (thaw on ice) | | | | | | |
| | Restriction Enzyme **20 ul** in Diluent B or C – MIX GENTLY UP AND DOWN WITH 200 uL TIP (keep at -20 and on ice) | | | | | | |
| 2 | **Spe1** (T7) (Dil C) | | | | | | |
| | **Nco1** (Sp6) (Dil C) | | | | | | |
| | **PvuII** (Sp6) (Dil B) | | | | | | |
| | **EcoRV** (T3) (Dil B) | | | | | | |
| | **Mix and spin 75 ul (if required)** total and incubate at 37 C for 1.5 hours – GENTLY FINGER TAP | | | | | | |
| | Enzyme in Diluents (on ice):<br><br>Dilute 20 000 units/ml (20 u/ul) to 1000 u/ml (1 u/ul)<br>So, add **1 ul** enzyme to **19 ul** diluent eg. **2.5 ul** NcoI in **47.5** Diluent,<br>Then use 20 ul of this per reaction | | | | | | |

Must add at least 25 % as large pipetting error occurs

**1 = Prepare first**

**2 = Prepare last and add to first solution**

**POST LIN, Add 425 ul (to make up to 500 ul) SDW following reaction and proceed to phenol chloroform precipitation…**

**Probe synth**

| Reagents (ul) (Give thawed reagents mix and spin) | 1: | 2: | 3: | 4: | 5: | 6: | 7: |
|---|---|---|---|---|---|---|---|
| 5X Buffer (for 1X) (R/T) | 6 | 6 | 6 | 6 | 6 | 6 | 6 |
| SDW (R/T) | | | | | | | |
| DTT (100Mm for 10mM) (R/T) | 3 | 3 | 3 | 3 | 3 | 3 | 3 |
| Rnasin (30 units) (keep at -20 and on ice) | 1 | 1 | 1 | 1 | 1 | 1 | 1 |
| DIG Mix (10X for 1X) (Thaw on ice) | 3 | 3 | 3 | 3 | 3 | 3 | 3 |
| DNA Template (3 ug) | | | | | | | |
| Mix and Pulse Spin | | | | | | | |
| Polymerase Enzyme ALL 3 ul (30 – 60 U) (keep at -20 and on ice) | | | | | | | |
| Sp6 | | | | | | | |
| T7 | | | | | | | |
| T3 | | | | | | | |
| Gently Mix and Pulse Spin the 33.6 ul total and Incubate at 37 C for 2.25 hours | | | | | | | |

**Positive Control Protocol**

**Add the following components at room temperature in the order listed:**

- Transcription Optimized 5X Buffer 4µl
- DTT, 100mM 2µl
- Recombinant RNasin® Ribonuclease Inhibitor 20–40u
- rATP, rCTP, rGTP and rUTP (2.5mM each)
- (prepared by mixing 1 volume of each of
- the 10mM rNTP stocks supplied) 4µl

- **pGEM® Express Positive Control Template 1µg – 1ul (stock is 1ug/ul. So, add 3ul in reaction from MY protocol above)**
- **SP6, T3 or T7 RNA Polymerase 15–20u**
- Nuclease-Free Water to a final volume of 20µl

**Prducts: T7 = two bands 2346 and 1065**

**Sp6 = two bands 2566 and 1787**

Template + water = 17.6 ul

**Gel electrophoresis** (Standard 1 % Gel in TAE Buffer, with denaturing buffer conditions)

Take 5 ul from reaction and set up gel (keep reaction incubating until gel is running). Once gel is running the aliquot the probe in hybe buffer (next page).

**Gel:**

**DON'T FORGET TO RUN CONTROL**

- **5 ul** RNA
- **15 ul** RNA sample buffer (made by me)
- **5 ul** EtBr
- **4 ul** 6X loading buffer

- **67 C for 8 mins**
- **Load straight on to gel**

30/03/15

HALF ALL THESE AMOUNTS IN NEW ADAPTION TO PROTOCOL

**IMPORTANT GEL CONDITIONS (make gel during synthesis)**

- **Pre cool running buffer at 4 C**
- **Run gel at 5 V per cm (about 70 V)**
- **Turn off after dye has run 2/3 way down whole gel (about 1.5 hours)**

**RNA Ladder:**

**Thaw ladder on ice**

Gently mix when thawed

**4 ul** 2X RNA loading dye

**4 ul** Ladder

Briefly vortex

**67 C for 10 mins**

**Place on ice and load all on gel**

**Aliquot in Hybe** (aliquot whilst running gel)

- Use opened riboprobe aliquot hybe buffer from E161 -20

- **KEEP ALL ON ICE ALL DO ALL IN FUME HOOD** -

- Mix probe 1:1 with Hybe
    - 28.6 probe: 28.6 hybe
- Aliquot the 57.2 ul **using sterile screw caps** in:
    - 20 ul X1
    - 10 ul X3
    - 7.2 ul X1
    -
- Store in -80

30/03/15 NEW PROTOCOL

- Following probe synth add all 33.6 to column
- Following spin, add 20 ul
- Aliquot:
    - 3x18 ul into sealed screw caps
    - 2.5 ul for gel
    - Store at -20 in lab

## 8.6 Appendix F Western Blot

**Lysis buffer** (from pre made stocks)
1 ml buffer: Fridge E41
10 ul protease: -20 E41
2 ul phosphatase: Our -20

Found in: see above

**Harvesting for western**

- Rinse hearts in ICE cold PBS to remove excess blood
- Place into liquid nitrogen before storage at -80

**1** - Homogenise through needles in Lysis buffer

- Add 80 ul **lysis buffer** for 3 hearts (HH20), (200 ul for HH29)
- Keep on ice at all times when possible
- Briefly centrifuge to collect hearts at bottom of tube and homogenise (see below)
- Toward end centrifuge briefly again to collect hearts and homogenise further

Homogenise thoroughly by **NEDDLE HOMGENISATION – DEPRESS NEEDLE TO BOTTOM AT START TO EXPELL ALL AIR.**

Suck up and down until homogenous then change needle

- 1, Needle 21 (0.8 green)
- 2, Needle 23 (0.6 blue)
- **3**, Needle 25 (0.5 yellow) – **This is all needed up to HH25**
- Incubate on ice for 30 min total time on rocker

Following Hominization:

**2** - Centrifuge at **10,000 x g** (approximately 9700 rpm for rotors of a 9.5 cm radius) for **20 minutes** at **4°C** to pellet cell debris, and then transfer the supernatant to a fresh microfuge tube without disturbing the pellet.

(Protein should be in supernatant, but also test the re-suspended pellet by Bradford to be sure when optimising)

**3** - Samples can be:

- Frozen at -20 (-80°C for long-term storage), or be used for immediate Western blotting or immunoprecipitation.
  - Aliquot to avoid repeated freeze thaws
- 5 ul taken for Bradford assay (1.5 ul for HH29)

**4** - Determine protein concentration of the lysate by Bradford or BCA protein assay **(see next page).**

- Re-suspended pellet and 5 ul supernatant sample
- All in duplicate

**Bradford assay**

USE THE PROTEIN ASSAY DYE (BIORAD) FROM THE CLEAR BOTTLE **UNDILUTED (Bio-Rad Protein Assay Dye Reagent Concentrate, 450 ml #5000006)**

Found in: Our lab

**1** – Remove aliquoted 1x dye from 4°C storage to R/T (all solutions should be room temperature)

(Invert the 1x dye reagent a few times before use)

**2** – Prepare standards and unknown samples:

- Water – BSA or Unknown to 800 ul – Dye 200 ul (Protein assay dye from clear bottle)
- Gently vortex
- Incubate 10 – 45 min (10 works well - no longer than 45 min!) **light protected**

BSA 1 mg / ml in -20 Matt and KL protein box

**How to prepare:**

Blank + 6 standards + unknown (ideally in duplicate)

-Use **stock** solution **of 1 mg/ml**

- Six standards from 1.5 ug/ml to 10 ug/ml (1.5, 2, 4, 6, 8, 10 ug/ml)

| | BLANK | 1 | 2 | 3 | 4 | 5 | 6 |
|---|---|---|---|---|---|---|---|
| **BSA** | 0 | 1.5 | 2 | 4 | 6 | 8 | 10 |
| **WATER** | 800 | 798.5 | 798 | 796 | 794 | 792 | 790 |

- **Unknown samples optimisation**

Unknown samples must be optimised as conc. is not known, so do:

**1**, 2 ul sample

**2**, 4 ul sample

**3**, 8 ul sample

Once protein amount is determined in controls, use just one conc. mid-range in standards in duplicate

5 ul for 3 HH20 hearts

1.5 ul for 1 hh29 heart

Example.

STANDARD 1: 1000ug/ml (stock) x 2ul = 2ug/ml x 1000ul

STANDARD 2: 1000ug/ml x 4 = 4 ug/ml x 1000ul

The extinction coefficient indicates how much light a protein absorbs at a certain wavelength. It is useful to have an estimation of this coefficient for following a protein which a spectrophotometer when purifying it.

It has been shown that it is possible to estimate the molar extinction coefficient of a protein from knowledge of its amino acid composition. BSA contains many amino acids and can only give an estimate of the extinction coefficient

The Bradford assay is actually based on a shift in the absorbance of a dye, Coomassie Brilliant Blue G-250, from 465 nm to 595 nm when it binds a protein under acidic conditions. So if dye is all bound, no matter what the protein concentration, the absorbance will not alter.

If extinction coefficient were known then a standard curve would not be necessary. However, the type/amount of proteins is not known. Extinction co-efficients can only be taken from concentrations well within the range of the LINEAR line.

**Equation**

$$A = \varepsilon . c . l$$

We can use this equation to check that our Bradford assay line of best fit confers to beer lambert law – just use transportation:-

- **E** = c/a
- **C** =a/e

**(l is the path length that is 1 – so ignored)**

**My Antibodies needed**

1, HV11 from mouse – Secondary **ANTI-MOUSE GREEN**

2, GAPDH polyclonal Rabbit – Secondary **ANTI-RABBIT RED**

Can do protein precipitation to concentrate sample if need be. See thermo-scientific acetone protocol in notes

**Using the Bio-rad smart spec 3000**

**(Better to use standard machine in D40 – Louse Marinez-Pomares lab)**

- On switch is on back of machine
- Enter info into the machine:
  - Protein – Yes
  - Standard - Yes
  - Blank - Yes
  - 6 standards
- **Read blank**
- Add the conc. of standards for each one.
- Standard curve modification – No

  **- Easier to use normal absorbance spectrometer at 595/ Bradford assay setting –**

**Door codes**

**E41 = C179X**

**E84 = C3467X**

**D69 = C148YZ**

**Liaque phone No.**

**07400 161 903**

**New academic now running lab: Dr. Steve Alexander**

**LOADING TIP – to avoid edge effect, load the same volume of X1 loading buffer to the last protein filled well.**

X6 SDS solubilisation buffer in -20 E41

For Western blotting, mix sample with 6X SDS sample buffer to a final **dilution of 1X (see below)**. Heat the mixture to 95°C for 5 minutes before loading onto an SDS-PAGE gel

**(Some membrane proteins may require 37 C - membrane proteins can aggregate, some proteins with very strong tertiary structure may require 100 C)**

6X SDS and Sample (1ug / I ul) preparation (do on day – do not refreeze sample once mixed with SDS)

Eg.

6X x 0.5 ul = 1X x 3 ul total

This is for a 1 ug / ul stock for a total of 2.5 ug protein – **Double all for a 5 ug gel if enough sample**

- Warm up the heat block to **95** °C (37 - 100°C see below on temp)
- Remove the gel from caster/fridge and place into gel holder, making sure that the
- Make **50ml** 10x running buffer to final volume of **500ml** (1X Running buffer) in **Distilled $H_20$** and pour into the central reservoir between the two gel plates
- Make sure the wells are clean by rinsing with a pipette

X10 Running buffer in: On shelf in bottle E41 near

- Vortex the samples (before and after heating step)
- Denature the samples by placing them in a heat block for **5mins at 95°C** (after this you may wish to aliquot the sample however, they will need to be heated again)
- Vortex the samples (before and after heating step)
- **Spin** the samples in a centrifuge at **13000 rpm** for **1 min**

- Load the samples (**3 ul (or 5ul if enough sample**) onto the gel, including **1 ul** of Biorad precision plus protein dual colure molecular weight marker. Dip the tip in the buffer before placing in the well to remove excess sample on outside of tip
- Place the lid on the gel (black to black, red to red etc.)

Molecular marker in -20 E41

- Run the gel for approx. **35-110mins at 175V – longer for high molecular weight** (check bubbles have appeared in the tank as an indication that it is running) until the blue line has run off the bottom of the gel.

- Clean all glassware that will be needed for the next steps whilst gel is running

**Gel Transfer**

- Clean a plastic tray with: **ddH2O**, then **IMS**, then again with **ddH2O** (do this with all instruments).
- Fill tray with **transfer buffer**
    - Soak:
        - Filter paper X2
        - Nitrocellulose (blot) paper X1
        - Sponge X2
        - Cassette X1

Transfer buffer in cold room E94

Filter paper in E41

Blot paper in E41

Sponge in E41

**Assemble the transfer cassette:**

**(These steps can be reversed – so step 3 is assembled first with**

**cassette clear side facing down)**

**Step 1,** Before gel has finished assemble step 1.

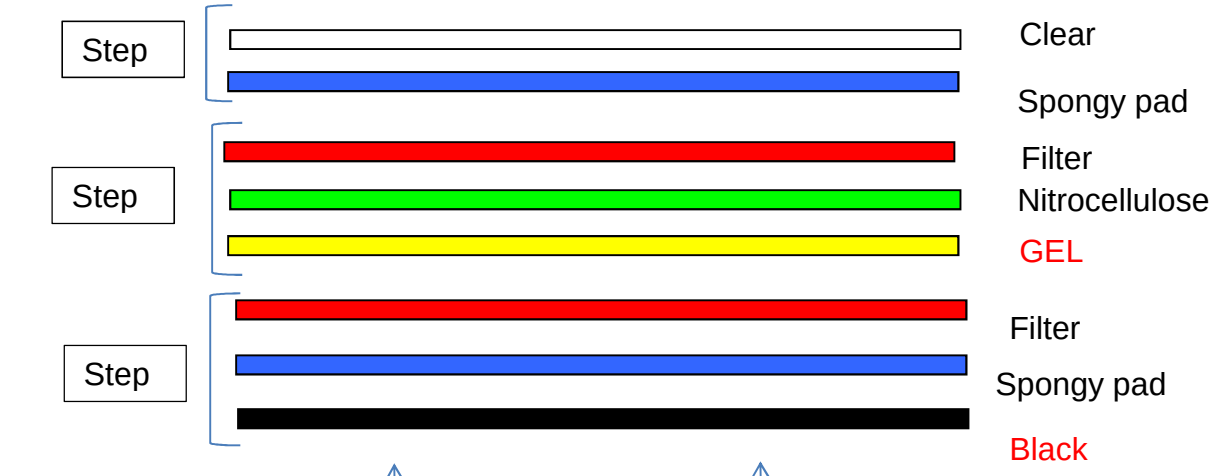
- Once finished, remove gel try and pore of buffer
- Open case with green Biorad tool
- Soak gel in transfer buffer for a few mins
- Remove stacking gel from top of gel
- wash in transfer buffer again

**Step 2,** Place gel on filter paper – gel side down

**(Reversed protocol: align ladder with top left on clear back – nitrocellulose MUST be in front of the gel with current (-) coming from behind)**

- Place each layer down on top of step 1 in order shown. **Ensure all bubbles** are **rolled out** before placing on the next layer

**Step 3,** Add final pad and close down cassette




- Place the assembled cassette in to the transfer holder (BLACK on BLACK)
- Place into tank (prongs in middle)
- Add ice pack directly to tank, and pack around with ice
- Fill with transfer buffer
- Put top on unit and run at **100 V** for **60 min** (check for bubbles when running)

**Check protein transfer**

- Once running is complete, carefully place nitrocellulose blot marker side up on a clean tray
- Add a few drops of PONCEAUS **(shelf on left E41 (red colour)** solution
  - Proteins will show on blot
  - Get picture on phone (if necessary mark areas you will need to cut)
- Remove solution by TBST wash
- Cut to shape (for antibody combinations etc.) and cut off corner under ladder so that the blot can easily be orientated later

**Tris-buffered saline tween** (TBST) in big white tank E41

Make 5 % BSA solution in TBST.

Filter the solution

BSA in our fridge

**Block**

- Place blot in 5 % BSA solution (BSA in TBST) for **60 mins** on shaker

Make Primary Antibody solution

Make 5 % BSA solution in TBST.
BSA in our fridge
HV11 = 1:1000
GAPDH = 1:1000

e.g 5 ul in 5 ml (depends on size of gel)

**Primary antibody**

- Make plastic seal pouch for blot:

  - Cut at end and seal at one end

  - Place blot and place centrally

  - Seal the longer sides (now just the top remains)

  - Add antibody solution to top with pipette

  - Remove bubbles as best you can

  - Seal top edge

  - Tape flat to glass plate ensuring even and free distributing of solution over the blot

  - Place on shaking platform overnight protected from light in cold room (but don't use foil as it seems to interfere with signal – blue tissue works well)

**NEXT DAY – Following overnight incubation**

**Washes at RT with TBST**

- Clean glass container
- Pour out antibody solution into falcon to be re-used (store at -20)
- With forceps place the blot into the new glass container and **RINSE X3** with **TBST**
- **Followed by additional washes:**
  - **X3 5 mins**
  - **X3 15 mins**

Make Secondary Antibody solution

Make 5 % BSA solution in TBST.

Secondary antibody 1:10,000 (Manufacturer recommends 1:10,000 – 40,000)

**3 ul in 30 ml**

HV11 = Anti Mouse
GAPDH = Anti rabbit

**Secondary antibody**

Following the final wash, add the prepared secondary

antibody solution to the glass tray and shake for 1 hour

37 C shaker in E41 (protected from light, but don't use

Foil as it seems to interfere with signal)

**Washes after secondary**

- Discard the secondary antibody solution
    - **Rinse X3 TBST**
    - **5 min X3 TBST**
    - **15 min X3 TBST**
    - **Rinse X1 DD$H_2O$**

**Scanning D69**

- Take to D69
    - Forceps
    - Blue tissue paper (white leaves particles)
    - Blot in tray/butter bowl
        - Keep moist with DD$H_2O$

- Moisten the scanner glass where the blot will be placed
- Place blot protein face down with ladder (trimmed edge to the left)
- Note the grid position of the blot
  Eg. 6 vertical (y) 4 horizontal (x)

Computer software for LI-COR

- Use your own log in and create folder in Z drive
- Open odyssey image studio from desktop
- Tick the 700 and 800 boxes
- µ = 84
- Q = lowest
- F = 0 for scanning blots
- Click on scan area
- Enter your x and y details by clicking on the scan area and dragging out the image box
- Press start

Adjust band contrasts

- …….

Crop to size

- ……

Shapes

- Draw rectangle

Manual

Western

Adjust lines over bands

Down load images

Instruments

Management

Down load scan

Type in picture number

Export

Single image view

Current image

(After quantitation)

Reduce noise

Analysis

Send to excel

Normalise by dividing by GAPDH